CAMBRIDGE MONOGRAPHS ON PARTICLE PHYSICS,
NUCLEAR PHYSICS AND COSMOLOGY

Nuclear Superfluidity

Pairing in Finite Systems

David M. Brink and
Ricardo A. Broglia

https://doi.org/10.1017/9781009401920 Published online by Cambridge University Press

Nuclear Superfluidity

Pairing in Finite Systems

Nuclear Superfluidity is the first modern text devoted exclusively to pair-correlations in nuclei. It begins by exploring pair-correlations in a variety of systems including superconductivity in metals at low temperatures and superfluidity in liquid ^{3}He and in neutron stars. The book goes on to introduce basic theoretical methods, symmetry breaking and symmetry restoration in finite many-body systems. The last four chapters are devoted to introducing new results on the role of polarization effects in the structure of both normal and exotic nuclei. Central to this discussion is the fact that while bare nucleon–nucleon interactions are essential for the production of pair-correlations in nuclei, the coupling of pairs of nucleons to low-energy nuclear collective excitations also plays an important role.

This book will be essential reading for researchers and students in both experimental and theoretical nuclear physics, and related research fields such as metal clusters, fullerenes and quantum dots. This title, first published in 2005, has been reissued as an Open Access publication on Cambridge Core.

DAVID M. BRINK obtained his first degree at the University of Tasmania in 1951 and his D.Phil. at Oxford University in 1955. Between 1958 and 1993 he held academic positions in the University of Oxford, including a Fellowship at Balliol College and the Moseley Readership in Theoretical Physics, and taught many branches of physics at graduate and undergraduate level. From 1993 to 1998 he was Professor of the History of Physics at the University of Trento in Italy. Professor Brink is a Fellow of the Royal Society and in 1982 was a recipient of the Rutherford Medal of the Institute of Physics. He has published several books including *Semi-classical Methods in Nucleus–Nucleus Scattering* (Cambridge University Press, 1985).

RICARDO A. BROGLIA earned his Ph.D. at the University of Cuyo, Argentina, in 1965. Following positions at the University of Buenos Aires, the Niels Bohr Institute and the University of Minnesota, he joined the staff of the Niels Bohr Institute in 1970, where he is now adjunct Professor. He has held visiting positions at the State University of New York at Stony Brook, Brookhaven National Laboratory, Los Alamos Scientific Laboratory and Oak Ridge National Laboratory. In 1985 he was called to occupy the chair of Nuclear Structure at the University of Milan. Professor Broglia's research interests include nuclear structure and nuclear reactions, the physics of metal clusters and fullerenes, and the folding and aggregation of proteins. He has published several books on these subjects including *Finite Quantum Systems* jointly with George Bertsch (Cambridge University Press, 1994).

CAMBRIDGE MONOGRAPHS ON PARTICLE PHYSICS NUCLEAR PHYSICS AND COSMOLOGY 24

General Editors: T. Ericson, P. V. Landshoff

1. K. Winter (ed.): *Neutrino Physics*
2. J. F. Donoghue, E. Golowich and B. R. Holstein: *Dynamics of the Standard Model*
3. E. Leader and E. Predazzi: *An Introduction to Gauge Theories and Modern Particle Physics, Volume 1: Electroweak Interactions, the 'New Particles' and the Parton Model*
4. E. Leader and E. Predazzi: *An Introduction to Gauge Theories and Modern Particle Physics, Volume 2: CP-Violation, QCD and Hard Processes*
5. C. Grupen: *Particle Detectors*
6. H. Grosse and A. Martin: *Particle Physics and the Schrödinger Equation*
7. B. Andersson: *The Lund Model*
8. R. K. Ellis, W. J. Stirling and B. R. Webber: *QCD and Collider Physics*
9. I. I. Bigi and A. I. Sanda: *CP Violation*
10. A. V. Manohar and M. B. Wise: *Heavy Quark Physics*
11. R. K. Bock, H. Grote, R. Frühwirth and M. Regler: *Data Analysis Techniques for High-Energy Physics, Second edition*
12. D. Green: *The Physics of Particle Detectors*
13. V. N. Gribov and J. Nyiri: *Quantum Electrodynamics*
14. K. Winter (ed.): *Neutrino Physics, Second edition*
15. E. Leader: *Spin in Particle Physics*
16. J. D. Walecka: *Electron Scattering for Nuclear and Nucleon Structure*
17. S. Narison: *QCD as a Theory of Hadrons*
18. J. F. Letessier and J. Rafelski: *Hadrons and Quark–Gluon Plasma*
19. A. Donnachie, H. G. Dosch, P. V. Landshoff and O. Nachtmann: *Pomeron Physics and QCD*
20. A. Hofmann: *The Physics of Synchrotron Radiation*
21. J. B. Kogut and M. A. Stephanov: *The Phases of Quantum Chromodynamics*
22. D. Green: *High P_t Physics at Hadron Colliders*
23. T. Hatsuda, K. Yagi and Y. Miake: *Quark–Gluon Plasma*
24. D. M. Brink and R. A. Broglia: *Nuclear Superfluidity*

Nuclear Superfluidity
Pairing in Finite Systems

DAVID M. BRINK and RICARDO A. BROGLIA

CAMBRIDGE
UNIVERSITY PRESS

Shaftesbury Road, Cambridge CB2 8EA, United Kingdom

One Liberty Plaza, 20th Floor, New York, NY 10006, USA

477 Williamstown Road, Port Melbourne, VIC 3207, Australia

314–321, 3rd Floor, Plot 3, Splendor Forum, Jasola District Centre, New Delhi – 110025, India

103 Penang Road, #05-06/07, Visioncrest Commercial, Singapore 238467

Cambridge University Press is part of Cambridge University Press & Assessment,
a department of the University of Cambridge.

We share the University's mission to contribute to society through the pursuit of
education, learning and research at the highest international levels of excellence.

www.cambridge.org
Information on this title: www.cambridge.org/9781009401876

DOI: 10.1017/9781009401920

First published 2005
First paperback printing 2010
Reissued as OA 2023

A catalogue record for this publication is available from the British Library.

ISBN 978-1-009-40187-6 Hardback
ISBN 978-1-009-40190-6 Paperback

For my family – DMB
For Angela, Donatella, Gianandrea and Bettina – RAB

Contents

https://doi.org/10.1017/9781009401920 Published online by Cambridge University Press

https://doi.org/10.1017/9781009401920 Published online by Cambridge University Press

https://doi.org/10.1017/9781009401920 Published online by Cambridge University Press

Preface

The present monograph aims to provide an account of the basic results obtained in the exploration of the subject of nuclear superfluidity, placing special emphasis on recent developments coming out from ongoing research, in particular medium polarization and pairing in exotic nuclei.

The marked mass dependence of the abundance of nuclear species testifies to the fact that nucleons in nuclei move essentially independently of each other in an average potential produced by the effect of all the other nucleons. Special stability is ascribed to the closing of shells in correspondence with magic numbers. Adding nucleons to a closed shell system polarizes the shells, leading eventually to deformations. The best studied of these phase transitions are associated with deformations in: (a) three-dimensional space (violating angular momentum conservation, i.e. rotational invariance), (b) gauge space (violating particle number conservation, i.e. gauge invariance).

The phenomenon of spontaneous symmetry breaking in gauge space (i.e. the fact that the Hamiltonian describing a system is symmetric with respect to gauge transformations while the state is not) is intimately connected with nuclear superfluidity. This is the subject of Chapters 1, 2 and 3.

While potential energy always prefers special arrangements and thus leads to the spontaneous symmetry-breaking phenomena, fluctuations favour symmetry, leading to collective modes (intimately connected with symmetry restoration): pairing rotations and pairing vibrations, analogues in gauge space to rotations in three-dimensional space of the system as a whole, as well as to (multipole) surface vibrations respectively. This is the subject of Chapters 4, 5, and 6. Pairing also plays a central role in phenomena like exotic decay, alpha decay and fission where a nucleus divides into two smaller subsystems. Some aspects of this important subject are taken up in Chapter 7.

Associated with spontaneous symmetry breaking the system acquires emergent properties not contained in the Hamiltonian describing it, nor in the particles

composing it, in particular, an order parameter and a generalized rigidity. The order parameter measures the magnitude of the distortion: e.g. the quadrupole moment (which measures the number of aligned single-particle orbitals) in the case of deformed nuclei in normal space, the pairing gap (which measures the 'binding energy' of pairs of nucleons moving in time-reversal states and forming Cooper pairs, the building blocks of fermion superfluidity) in the case of gauge deformations. Generalized rigidity indicates the fact that pushing a deformed nucleus at one of the tips (through, e.g. a time-dependent Coulomb field induced by the passage of a heavy ion), the push is propagated over the whole system and one can set the nucleus into rotation. Two-particle transfer reactions provide the push to set a superfluid nucleus into rotation in gauge space, as was first found by Josephson in connection with superconductivity in condensed matter. This brings us to the subtitle of the present monograph: pairing in finite systems.

Although one can draw many analogies between the behaviour of infinite and of finite many-body systems (FMBS), there are also major differences. In particular, while in transition between the normal and superfluid phase taking place in infinite systems, all particles moving close to the Fermi surface play a similar role, in the case of FMBS very few orbitals control the phenomenon, providing also most of the stability of the new phase. This fact provides the possibility, among other things, of studying superfluidity in terms of individual orbitals, both in the case of the (standard) s-wave pairing as well as in the case of d-wave pairing. At variance to the case of infinite systems where pairing vibrations are hard to observe, FMBS provide the framework to study the spectrum of pairing vibrations both in superfluid as well as in normal nuclei, their interweaving and resulting anharmonicity phenomena which are at the basis of the condensation of Cooper pairs and thus of superfluidity. The ubiquitous role played by pairing vibrations (Chapter 5) in nuclear structure (pairing phase transition, dealignment, nuclear masses, etc.) is discussed in detail in Chapters 6 and 8.

A microscopic calculation of superfluidity in nuclei starts from a mean-field calculation which provides the single-particle levels of the bare nucleons. Bouncing inelastically off the nuclear surface, nucleons can excite a collective vibration at a given instant of time and reabsorb it at a later time. Through this process the bare nucleons become dressed. Physically, this means that what one measures (the experimental single-particle energies, closely related to the effective mass of a nucleon inside the nucleus) is not the bare mass but something else which includes the effect of the virtual processes mentioned above.

Collective surface vibrations excited by a nucleon at a given time may also be reabsorbed by another nucleon at a later time. Such a process turns out to be of importance in renormalizing the bare nucleon–nucleon pairing interaction arising from the exchange of mesons, and is the subject of Chapters 8, 9 and 10.

Because halo nuclei (i.e. nuclei where the excess of one type of nucleons forces the least bound particles into very extended orbits) are highly polarizable,

they provide a particularly testing ground and novel framework to assess the role polarization effects play in pairing correlations in nuclei. This is the subject of Chapter 11.

A number of important themes are not covered in any detail by the present monograph: in particular, two-neutron transfer reactions and proton–neutron pairing. Concerning the first subject an extensive literature is available, including review papers and chapters of books. Concerning the second subject, although much theoretical work has been published on $T = 0$ p-n pairing, the experimental evidence remains, to date, circumstantial at best. There is an extensive literature on $T = 1$ n-p pairing, which includes several detailed review papers.

It could be remarked that the present treatise also does not cover all the work of large shell model studies of pairing in nuclei. This is true. One has to remember, however, that nuclear field theory (NFT) used in connection with the Bloch–Horowitz (perturbation theory) formalism, or with the Dyson equation, leads also to an (essentially) exact diagonalization of pairing as well as of mean field. What is accomplished in one approach (shell model) using very large configuration spaces, is obtained in the second approach (NFT) by accurately dressing the elementary modes of nuclear excitation (single-particle motion and collective vibrations) and the vertex controlling their mutual interweaving.

We feel uncomfortable about not including a chapter on pairing at finite temperature and on pairing in other FMBS, such as atomic clusters or quantum dots. However, this feeling is partially mitigated by the fact that the first subject is standard in any book on condensed matter physics, and the results can essentially be taken over to the case of atomic nuclei (see Brink (1994)). The second subject can be found among the topics covered by recently published books, written also by practitioners of nuclear physics (see e.g. Lipparini (2003), Broglia *et al*. (2004)).

Over the years we have received much illumination on the subject dealt with in the present monograph from a number of people. DMB would like to acknowledge stimulating discussions with physicists at the European Center for Theoretical Studies in Nuclear Physics and Related Areas (ECT*) in Trento, Italy and especially with Ben Mottelson, Renzo Leonardi, Sandro Stringari and Aage Winther. He also achieved a deeper understanding of nuclear structure as a result of discussions with George Bertsch in Seattle, Brian Buck in Oxford and members of the theory groups in many laboratories including Catania, Kyushu, Kyoto, Lund, MSU, Orsay, Milan. Padova, Pisa, Saclay, Sapporo, Surrey and Tokyo. RAB wishes to acknowledge the debt he owes to George Bertsch, Ole Hansen and Claus Riedel. The interaction and collaboration with Aage Bohr and Ben Mottelson, started in 1965 and continued through the years, has been a major source of inspiration. At that time, when he arrived at the Niels Bohr Institute of Copenhagen, the main foundations of nuclear superfluidity were already solidly established. Nonetheless pairing was again a major subject of research. In fact,

the exploration of the collective degrees of freedom was under way, triggered also, as has always happened in connection with major developments in nuclear physics, by the availability of new experimental data. This time, two-neutron transfer data came from the group of Ole Hansen and Ove Nathan. RAB was fortunate to participate closely in this exploration with Daniel Bes (teacher, collaborator and friend from whom he learned so much through the years) as well as with Ole Hansen. RAB wishes also to thank Ben Bayman, Gerry Brown, Bob Schrieffer, Peter Schuck, Vladimir Zelevinsky and Witek Nazariewicz for much illumination. His debt to Francisco Barranco is very large, and increases as each day goes by, as a consequence of our common striving to understand pairing in a variety of FMBS setups. Thanks are also due to Pier Francesco Bortignon and to Gianiuca Coló for advice and collaboration on particular subjects discussed in this book, and to Enrico Vigezzi for useful criticism. RAB also acknowledges a most fruitful, lifelong collaboration with Aage Winther. During the many versions of the book Francesco Marini has taken care of all the technical aspects of the manuscript. His help has been invaluable to us. Last but not least, thanks are also due to all the students of the fourth year course of 'Nuclear Structure Theory', which RAB has delivered since 1986 at the Department of Physics of the University of Milan, building on the wealth of experience gathered in previous years at the Niels Bohr Institute and at Stony Brook (State University of New York) in the presentation of particular subjects covered in the present book.

David Brink
Oxford, May 2004

Ricardo A. Broglia
Milan, May 2004

1
Introduction

1.1 Pairing in nuclei, superconductors, liquid ^{3}He and neutrons stars

If one sweeps a magnetic field through a metallic ring (e.g. a ring made out of lead) immersed in liquid helium ($T \sim 4\,\mathrm{K}$) it induces a current which does not show any measurable decrease for a year, and a lower bound of 10^5 years for its characteristic decay time has been established using nuclear resonance to detect any slight decrease in the field produced by the circulating current (File and Mills (1963)). If a torus-shaped vessel filled with liquid helium below the critical temperature $T_c = 2.17\,\mathrm{K}$ (known as He II) and packed with porous material, which provides very narrow capillary channels, is rotated around its axis of symmetry and then brought to rest, the liquid continues to flow (Reppy and Depatie (1964)), showing no reduction in the angular velocity over a twelve-hour period, and indicating that He II can flow without dissipation. Using an adiabatic cooling apparatus, Osheroff *et al.* (1972 a,b) found two anomalies in the pressure–time curve of liquid ^{3}He, when the volume was changed at a constant rate. At the critical temperature $T_c = 2.7\,\mathrm{mK}$ the slope of the curve suffered a discontinuity, and at about $T_c = 1.8\,\mathrm{mK}$ there was a singularity involving hysteresis (see also Osheroff (1997) and Lee (1997)). If a deformed nucleus in its ground state is set into a state of rotation by the action of a non-uniform, time-dependent Coulomb field, it displays rotational bands with a moment of inertia which is a fraction (between one-half to one-third) of the rigid moment of inertia (Belyaev (1959), Bohr and Mottelson (1975)). Rotating neutron stars (pulsars) display marked glitches, that is, sudden increases in the frequency of the emitted pulses of radiation (McKenna and Lyne (1990), McCullough *et al.* (1990), Flanagan (1990), Anderson *et al.* (1982)). All the above observations are examples of phenomena known as superconductivity and superfluidity.

From a microscopic point of view, helium atoms are structureless spherical particles interacting via a two-body potential. The attractive part of this potential,

arising from weak Van der Waals-type dipole, quadrupole, etc. forces, causes helium gas to condense, at normal pressure, into a liquid at temperatures of 3.2 K and 4.2 K for ^{3}He and ^{4}He respectively.

The striking difference in the behaviour of ^{3}He and ^{4}He at even lower temperatures, in particular the fact that the critical temperature for ^{3}He to become superfluid is roughly one thousandth of the transition temperature of ^{4}He, is a consequence of the fact that ^{3}He is composed of an odd number of fermions (two protons, one neutron and two electrons), and is thus also a fermion, while ^{4}He, containing one more neutron, is a boson. Since in a Bose system single-particle states may be multiply occupied, at low temperatures this system has a tendency to condense into the lowest-energy single-particle state (Bose–Einstein condensation). It is believed that the superfluid transition in ^{4}He is a manifestation of Bose–Einstein condensation (see e.g. Leggett (1989), Pitaevskii and Stringari (2003), Pethick and Smith (2002)).

The basic feature of the Bose condensate is its phase rigidity, i.e. the fact that it is energetically favourable for the particles to condense into a single-particle state of fixed quantum-mechanical phase, such that the global gauge symmetry is spontaneously broken. For three-dimensional (3D-) systems, macroscopic flow of the condensate is (meta) stable, giving rise to the phenomenon of superfluidity (frictionless flow).

In a Fermi system, on the other hand, the Pauli exclusion principle allows only single occupation of fermion states. In the simplest approximation the fermions move independently in an average potential and occupy the lowest available single-particle states up to a Fermi energy ε_{F}. Fermions with energy near ε_{F} are, in a variety of systems, subject to a pairing residual interaction. The associated pairing correlations are important for understanding the structure of the low-lying states of nuclei, the properties of neutron stars and those of metals and of liquid helium ^{3}He at low temperatures. The relevant fermions are nucleons in nuclei, and in neutron stars, electrons in superconductors and ^{3}He atoms in liquid helium.

The pairing interaction leads to pairs of fermions bound in states coupled to integer spin (zero or one). These pairs, whose structure is different for each physical system, behave like bosons, and can at low temperatures Bose-condense, the condensate being characterized by macroscopic quantum coherence leading to the superconducting or superfluid phase. The mechanism and the consequences of this condensation in the case of nuclei is the subject of the present monograph.

Particular emphasis is placed on the study of quantal-size-effects (QSE). These effects are due to the fact that the nucleus is a finite many-body system where the surface plays a paramount role. In fact, the nuclear surface is not only the source of space quantization and thus of the discreteness of the single-particle levels, but also, by vibrating as a whole, of the existence of collective surface modes. Furthermore, because the length at which Cooper pairs are correlated is much

larger than the nuclear dimension, the nuclear superfluid can be viewed as a zero-dimensional system. Because the number of pairs which build the condensate is small, fluctuations become very important.

1.2 Macroscopic wavefunction and phase rigidity

The central idea of the macroscopic quantum state is represented by assigning a macroscopic number of particles to a single wavefunction ($\tilde{\Psi}$) (see e.g. Anderson (1964, 1984), Mercerau (1969), Tilley and Tilley (1974), Bruus and Flensberg (2004)). These particles are assumed to have condensed into a single state. This condensation results in a macroscopic density of particles (ρ_s) sharing the same quantum phase (Φ). The resulting wavefunction is then $\bar{\Psi} = \Psi \exp(i\Phi)$. In this form $\rho_s = (\bar{\Psi}^* \bar{\Psi})$ is not the usual probability of finding a particle but, owing to the macroscopic number of particles involved, is actually the effective particle density. Both Ψ and Φ may be functions of space and time and their variations will therefore determine the motion of the quantum fluid.

In what follows we shall be more interested in understanding the consequences the r-dependence of Φ has on the behaviour of the system and somewhat neglect the r-dependence of Ψ. Since, by definition, the particles are in precisely the same state and must therefore behave in an identical fashion, the equations of motion for the macrostate must also be identical to the equations of motion for any single particle in this state. Because the phase is common to so many particles, its effects do not average out on a macroscopic scale, but remain to fundamentally determine the behaviour of the system.

Changes in the wavefunction are of course determined by the Schrödinger equation. In particular, the centre of mass velocity ($\vec{V}$) can be calculated for this wavefunction from the velocity operator ($\vec{v}$) common to all the particles

$$\vec{v} = -\frac{1}{m^*}(i\hbar\vec{\nabla} + e^*\vec{A})$$

where e^* and m^* are, respectively, the (effective) charge and mass of the particles and $\vec{A}$ is the vector potential. The centre of mass velocity is

$$\vec{V} = \tfrac{1}{2}\left\{\bar{\Psi}\vec{v}^{\,+}\bar{\Psi}^{\,+} + \bar{\Psi}^{\,+}\vec{v}\bar{\Psi}\right\} / \left(\bar{\Psi}^{\,+}\bar{\Psi}\right)$$

giving a current

$$\vec{J} = e^*\rho_s\vec{V} = \frac{e^*\rho_s}{m^*}\left(\hbar\vec{\nabla}\Phi - e^*\vec{A}\right). \tag{1.1}$$

By taking the curl of this equation one can derive another equation of significance, namely

$$\vec{\nabla} \times \vec{J} + \frac{\rho_s e^{*2}}{m^* c}\vec{B} = 0. \tag{1.2}$$

https://doi.org/10.1017/9781009401920 Published online by Cambridge University Press

This is the solution found by F. London and H. London (London, 1954) of the relation

$$\frac{\partial}{\partial t}\left(\vec{\nabla}\times\vec{J}+\frac{\rho_{\mathrm{s}}e^{*^2}}{m^*c}\vec{B}\right)=0. \tag{1.3}$$

This equation together with the Maxwell equation

$$\vec{\nabla}\times\vec{B}=\frac{4\pi}{c}\vec{J}, \tag{1.4}$$

characterizes a medium that conducts electricity without dissipation. In fact, in such circumstances, electrons under the effect of an electric field will be freely accelerated without dissipation so that their mean velocity $\vec{v}_{\mathrm{s}}$ will satisfy

$$m^*\frac{\mathrm{d}\vec{v}_{\mathrm{s}}}{\mathrm{d}t}=-e^*\vec{E}.$$

Since the current density carried by these electrons is $\vec{J}=-e^*v_{\mathrm{s}}\rho_{\mathrm{s}}$, the above equation can be written as

$$\frac{\mathrm{d}}{\mathrm{d}t}\vec{J}=\frac{\rho_{\mathrm{s}}e^{*2}}{m^*}\vec{E}. \tag{1.5}$$

The Fourier transform of this equation gives the ordinary AC conductivity for an electron gas of density ρ_{s} in the Drude model, when the relaxation time τ becomes infinitely large, that is,

$$\vec{J}=\sigma_{\mathrm{s}}(\omega)E(\omega)$$

where

$$\sigma_{\mathrm{s}}(\omega)=\lim_{\tau\to\infty}\sigma(\omega)$$

is the frequency dependent (or AC) conductivity

$$\sigma(\omega)=\frac{\sigma_0}{1-\mathrm{i}\omega\tau},$$

the zero-frequency conductivity being

$$\sigma_0=\frac{\rho_{\mathrm{s}}e^{*^2}\tau}{m^*}.$$

Substituting equation (1.5) into Faraday's induction law

$$\nabla\times\vec{E}=-\frac{1}{c}\frac{\partial\vec{B}}{\partial t},$$

one finds equation (1.3). In other words, $\vec{\nabla}\times\vec{J}+\frac{\rho_{\mathrm{s}}e^{*^2}}{m^*c}\vec{B}=C$ characterizes a non-dissipative electric medium. The more restrictive London equation, which

https://doi.org/10.1017/9781009401920 Published online by Cambridge University Press

specifically characterizes superconductors and distinguishes them from mere perfect conductors, requires in addition $C = 0$.

The reason for replacing (1.3) by (1.2) is that the latter equation leads directly to essential experimental facts, by forbidding currents or magnetic fields internal to the superconductor except within a layer of thickness $\Lambda = \left(\frac{m^*c^2}{4\pi\rho_s e^{*2}}\right)^{1/2} \approx 42\left(\frac{r_s}{a_0}\right)^{3/2}\left(\frac{\rho}{\rho_s}\right)^{1/2}$ (London penetration depth) of the surface, $r_0 = a_B r_s$ being the Wigner-Seit cell radius of the system under consideration, defining the density ρ ($r_0 = (4\pi\rho/3)^{-1/3}$). In fact, equations (1.2) and (1.4) imply

$$\nabla^2 \vec{B} = \frac{4\pi\rho_s e^{*2}}{m^*c^2}\vec{B},$$
$$\nabla^2 \vec{J} = \frac{4\pi\rho_s e^{*2}}{m^*c^2}\vec{J},$$

where the relation $\vec{\nabla} \times (\vec{\nabla}\times) = \vec{\nabla}(\vec{\nabla}\cdot) - \nabla^2$ was used. Assuming a semi-infinite superconductor occupying the half space $x > 0$,

$$B(x) = B(0)e^{-x/\Lambda},$$

and

$$J(x) = J(0)e^{-x/\Lambda}.$$

Thus, the London equation implies the Meissner effect, along with a specific picture of the surface currents that screen out the applied field. These currents occur within a surface layer of thickness $10^2 - 10^3$ Å. Within this same surface layer the field drops continuously to zero, predictions which are confirmed, among other things, by the fact that the field penetration is not complete in superconducting films as thin as or thinner than the penetration depth Λ.

Let us now return to equation (1.1). This relation can be obtained by minimizing the free energy of the system with respect to the phase Φ. In other words, subject to a phase gradient, the system minimizes its energy by carrying a current even in thermodynamical equilibrium, and such a current is always dissipationless. This is true both for charged systems (like, e.g., metals where $e^* = 2e$ and $m^* = 2m_e$), as well as for neutral systems (like, e.g., He II, where $e^* = 0$ and $m^* = m_4$).

Of course there is an energy cost for the system to carry the current, but as long as this cost is smaller than the alternative which is to go out of the superfluid or superconducting state, the current carrying state is chosen. The critical current is reached when the energies are equal (and equal to the value of the gap, see Sections 1.4 and 1.5 and Figs. 1.6 and 1.7), and then the superfluid or superconductor goes into the normal state (see equations (1.17) and (1.21), respectively).

Within this context, it should be noted that the appearance of the excitation gap is not the reason for the superfluidity or superconductivity itself, but a consequence of the spontaneous symmetry breaking of gauge invariance. In fact, gapless superconductors do exist (in this connection see Sections 5.3 and 6.2.1).

1.3 Broken symmetry and collective modes

In many phase transitions, such as that to the ferromagnetic state, or from the normal to the superconducting state, or again from a spherical to a deformed nucleus, the ground state of the low-temperature phase has a lower symmetry than the Hamiltonian used to describe the system. The situation is one of broken symmetry. In cases where the symmetry group that is broken is continuous (e.g. the rotation group), a new collective mode appears, whose frequency, in the absence of long-range forces, goes to zero in the long wavelength limit (Anderson Goldstone Nambu (AGN) mode (see Chapter 4)). For the ferromagnet, the elementary excitations required by Goldstone's theorem (Goldstone, 1961) are Bloch's spin waves (magnons), in which the magnetization precesses about its direction in the ground state (see Figs. 1.1 and 1.2).

Superconductors furnish an example of a system in which the excitations required by the symmetry-breaking process have a finite frequency in the

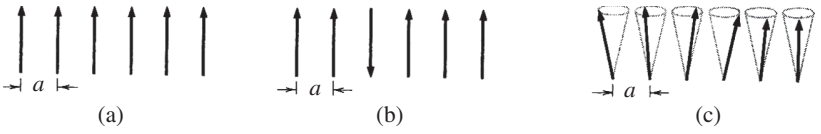

Figure 1.1. (a) Classical picture of the ground state of a simple ferromagnet; all spins are parallel. (b) A possible excitation; one spin is reversed. (c) The low-lying elementary excitations are spin waves. The ends of the spin vectors precess on the surfaces of cones, with successive spins advanced in phase by a constant angle (after C. Kittel (1968)). From *Introduction to Solid State Physics*, 7th edition, by Charles Kittel, Copyright 1995 John Wiley & Sons Inc. Reprinted with permission of John Wiley & Sons Inc.

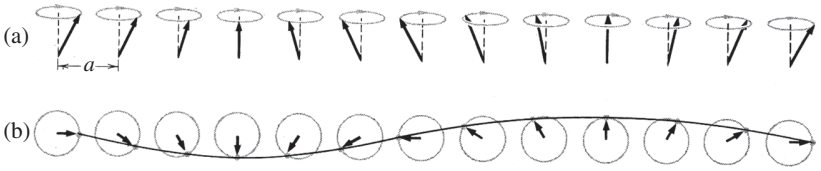

Figure 1.2. A spin wave on a line of spins. (a) The spins viewed in perspective. (b) Spins viewed from above, showing one wavelength. The wave is drawn through the ends of the spin vectors (after Kittel (1968)). From *Introduction to Solid State Physics*, 7th edition, by Charles Kittel, Copyright 1995 John Wiley & Sons Inc. Reprinted with permission of John Wiley & Sons Inc.

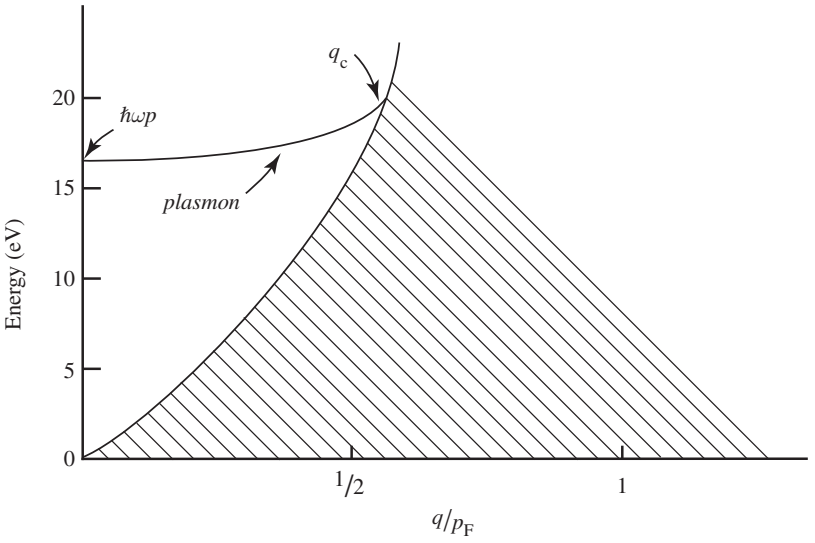

Figure 1.3. Excitation spectrum of density fluctuations in a quantum plasma with the density of Al, as calculated in the random phase approximation. Plasmons are essentially undamped (see also Section 8.3.4) for wavevectors less than q_c, and are strongly damped (Landau damping) beyond q_c by the single particle–hole excitations, whose energies lie within the hatched region (after Pines (1963)).

long wavelength limit (because of the infinite range of the Coulomb force): the corresponding Goldstone mode is the familiar plasma oscillation (see Fig. 1.3).

For a neutral fermion superfluid, on the other hand, the collective mode is the zero-sound mode proposed by Anderson (1958) and Bogoliubov (1958a), which has a vanishing frequency at long wavelengths (see Section 4.3.1).

An example of AGN boson in a neutral system is provided by the fourth sound in superfluid ^{3}He, which corresponds to the oscillatory motion of the superfluid phase in a confined geometry (superleak) where the normal fluid is clamped. For example, assume a porous medium. In it, the normal-fluid fraction (see equation (1.12)) is clamped by the scattering of quasiparticles with the surface of the very narrow channels. The superfluid fraction is barely affected by the confining walls, provided that the channel diameter is greater than the coherence length $\xi(T)$ (equation (1.32)), and thus may move freely. The oscillatory motion of the superfluid phase in such a confined geometry is called fourth sound (see Vollhardt and Wölfle (1990)). In the case of atomic nuclei, the very occurrence of collective rotational degrees of freedom may be said to originate in a breaking of rotational invariance, which introduces a 'deformation' that makes it possible to specify an orientation of the system (Bohr and Mottelson, 1975). Rotation (see Fig. 1.4) represents the collective mode associated with such a spontaneous

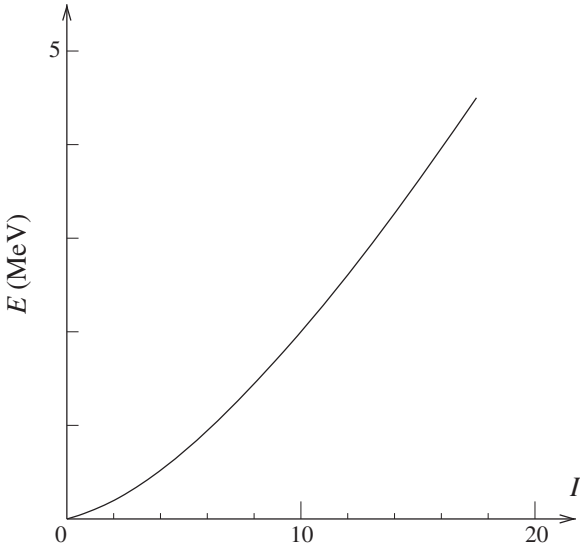

Figure 1.4. Schematic representation of the (discrete) energy levels of the (ground state) rotational band of a quadrupole deformed atomic nucleus as a function of the angular momentum I ($E = (\hbar^2/2\mathcal{I})I(I+1)$, where $\mathcal{I}$ is the moment of inertia).

symmetry breaking (AGN boson). The full degrees of freedom associated with rotations in three-dimensional space come into play if the deformation completely breaks the rotational symmetry, thus permitting a unique specification of the orientation. If the deformation is invariant with respect to a subgroup of rotations, the corresponding elements are part of the intrinsic degree of freedom, and the collective rotational modes of excitation are correspondingly reduced, disappearing entirely in the limit of spherical symmetry.

1.4 Superfluid ^{4}He (He II)

^{4}He becomes liquid under its own vapour pressure at 4.21 K. The liquid phase at this temperature, helium I, behaves like a normal liquid, but at 2.17 K it shows a further phase transition – to helium II. Helium II is a most peculiar liquid: it shows superfluidity, i.e. a lack of viscosity when flowing through a narrow slit or capillary. At 2.17 K the specific heat shows a very strong pronounced peak, resembling the Greek letter λ, whence Ehrenfest suggested the name λ-point for the transition point (see Fig. 1.5).

The theory developed by Landau (Landau (1941, 1947)) was constructed upon the basic idea that the equilibrium properties of liquid helium below the λ-point could be expressed in terms of the energy spectrum of the elementary

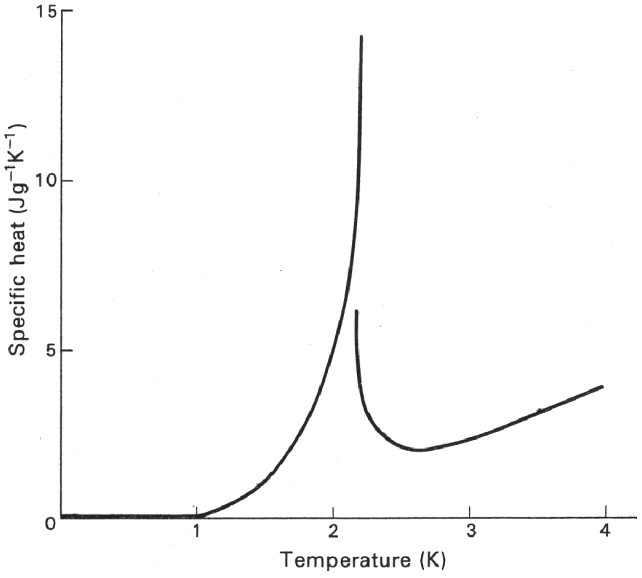

Figure 1.5. Specific heat of ^{4}He (after Atkins (1959)).

excitations possible in helium, namely phonons and rotons. Landau considers the quantization of liquids and reaches the conclusion that there are states possible in the liquid for which

$$\text{curl}\,\vec{v} = 0, \tag{1.6}$$

where $\vec{v}$ is the velocity of the liquid. Note that this relation is obtained from equation (1.1) for $e^* = 0$ (neutral system). Such states correspond to potential flow, as would be the case in classical hydrodynamics, because, just as there is no continuous transition in quantum mechanics between states with zero angular momentum and with non-vanishing angular momentum, in the same way there may be no continuous transition between states with curl $\vec{v} = 0$ and those with curl $\vec{v} \neq 0$. Consequently, one concludes that there will be an energy gap Δ between the lowest energy level corresponding to potential flow and the lowest energy level of vortex motion (curl $\vec{v} \neq 0$). In order that the liquid be superfluid, it is necessary that the vortex motions start at a higher energy than the potential flow motions.

The spectrum of helium II can thus be seen as a superposition of two continuous spectra: one corresponding to potential flow and one corresponding to vortex motion. The potential flow part of the spectrum corresponds to longitudinal waves, i.e. sound waves. The elementary excitations are thus phonons, the energy

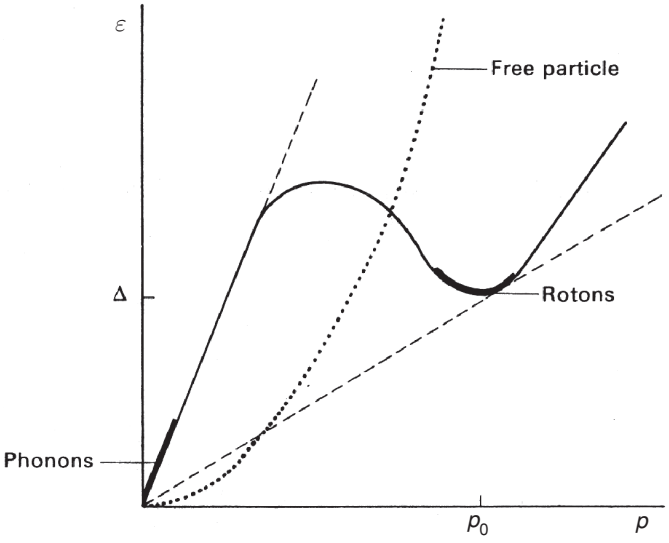

Figure 1.6. Phonon–roton spectrum suggested by Landau. Broken lines indicate superfluid critical velocities. Dotted line shows free-particle parabola for comparison.

spectrum of which is known to be (Fig. 1.6)

$$\varepsilon_{\mathrm{ph}} = c_{\mathrm{s}} p,$$

where p is the momentum of the excitation while c_{s} is the sound velocity.

The elementary excitations of the vortex motion were called rotons by Tamm. The roton spectrum is given by

$$\varepsilon_{\mathrm{r}} = \Delta + \frac{(p - p_0)^2}{2\mu}, \tag{1.7}$$

where Δ is the energy gap mentioned above while μ is the inertia of the rotons.

It should be emphasized that the above two equations (see also Fig. 1.6) give the energy of the excitation spectrum of the elementary excitations of the helium II and not the energy spectrum of the single helium atoms

$$\varepsilon_{\mathrm{sp}} = \frac{p^2}{2m_4}.$$

Note that given the dispersion relation shown in Fig. 1.6 it is difficult to speak strictly of rotons and phonons as qualitatively different types of excitations. It could be more correct to speak simply of the long wave (small p) and short wave (p in the neighbourhood of p_0) excitations. In any case, there is an essential difference between phonons and rotons. Phonons can have zero energy in the long wavelength limit and thus qualify as AGN modes (Anderson (1952, 1963), Nambu (1959, 1960)), while rotons have always an energy $\geq \Delta$ and can thus

never be an example of Goldstone's theorem (Goldstone (1961), Goldstone *et al.* (1962)).

At finite temperature and assuming it to be sufficiently low, one can consider the excitation of He II to be that of a perfect gas of phonons and rotons. This means that one neglects the interaction between the elementary excitations. If one assumes that the presence of excitations does not affect the spectrum of any new excitation, one can prove (see below) that new phonon and rotons cannot be excited if the liquid moves with $V < (V_c)_{\text{phon,rot}}$ (see equations (1.17) and (1.19)) through a capillary. However, the phonon and roton gas will not be superfluid. Landau showed indeed that this gas will stick to the walls and behave like an ordinary liquid. This leads to the conclusion that at finite, not too high, temperatures, part of the liquid behaves normally while the remainder shows superfluidity.

In other words in a quantum liquid such as helium both normal and superfluid motion can occur and while there is no real division of the liquid into two parts, such that some atoms belong to the superfluid liquid and others to the normal liquid, it is possible to assign to each of the two liquids its own mass. In fact, the density of the normal liquid at a given temperature can be defined as the effective mass of the roton and phonon gases.

To evaluate these masses, we consider the liquid moving at a velocity $\vec{V}$. Since the phonons are bosons, their distribution function is $\{\exp\beta[\varepsilon - (\vec{p}\cdot\vec{V})] - 1\}^{-1}$, where $\beta = 1/T$. The total momentum per unit volume is then

$$\vec{P}_{\text{ph}} = \frac{1}{(2\pi h)^3}\int \frac{\vec{p}\ \mathrm{d}^3 p}{\mathrm{e}^{\beta[\varepsilon - \vec{p}\cdot\vec{V}]} - 1}. \tag{1.8}$$

The effective phonon mass density ρ_{ph} can then be defined through the relation

$$\vec{P}_{\text{ph}} = \rho_{\text{ph}}\vec{V}. \tag{1.9}$$

For small $\vec{V}$ one can expand the denominator in the integral and retain only the linear term in $\vec{V}$. This leads to

$$\rho_{\text{ph}} = \frac{4}{3}\rho\frac{E_{\text{ph}}}{c_{\text{s}}^2}, \tag{1.10}$$

where ρ is the total density of the liquid and E_{ph} the energy of the phonon gas which is proportional to T^4.

One can evaluate the effective roton mass density ρ_{r} in a similar way. Having found ρ_{r} and ρ_{ph} one has determined the normal fluid density,

$$\rho_{\text{n}} = \rho_{\text{r}} + \rho_{\text{ph}}, \tag{1.11}$$

as well as the superfluid density

$$\rho_{\text{s}} = \rho - \rho_{\text{n}}. \tag{1.12}$$

Landau suggests that the λ-point can be defined as that for which the temperature is such that $\rho_n = \rho_s$.

The basic idea of Landau is thus that the equilibrium properties of He II can be expressed as a gas consisting of (non-interacting) phonons and rotons, and is based on the fact that the only system statistical mechanics can deal with satisfactorily is a perfect gas. In other words, for sufficiently low temperatures one may assume that the excitation of the liquid helium can be considered to be a gas of phonons and rotons and, moreover, a perfect gas of these elementary excitations.

Let us now consider the question of superfluidity at absolute zero temperature. One must show that when helium flows through a capillary at a constant velocity $\vec{V}$ it cannot be slowed down by exciting an elementary excitation, provided $\vec{V}$ is smaller than some critical velocity. In order to see this, let us find the energy necessary to create an excitation of momentum $\vec{p}$. Suppose a body of velocity $\vec{V}$ and mass M creates an excitation and ends up moving with velocity $\vec{V}'$. From momentum conservation

$$M\vec{V} = M\vec{V}' + \vec{p}, \tag{1.13}$$

so that the new kinetic energy of the body is

$$\frac{1}{2M}(MV')^2 = \frac{M}{2}V'^2 = \frac{1}{2M}(M\vec{V} - \vec{p})^2 = \frac{1}{2}MV^2 - \vec{V}\cdot\vec{p} + \frac{p^2}{2M}. \tag{1.14}$$

If $\varepsilon(\vec{p})$ is the energy of an elementary excitation of momentum $\vec{p}$, this excitation cannot be created unless

$$\frac{1}{2}MV^2 \geq \frac{1}{2}MV'^2 + \varepsilon(\vec{p}). \tag{1.15}$$

Consequently

$$\varepsilon(p) \leq \frac{1}{2}MV^2 - \frac{1}{2}MV'^2 = \vec{V}\cdot\vec{p} - \frac{p^2}{2M}. \tag{1.16}$$

For large M, $\varepsilon(p) \leq \vec{V}\cdot\vec{p}$. Thus, the critical velocity necessary to create an elementary excitation in He II is then derived by drawing a tangent to the dispersion relation $\varepsilon(p)$ versus p (see Fig. 1.6), i.e.

$$V_c = \frac{\varepsilon(p)}{p}. \tag{1.17}$$

There are two solutions of this relation. One occurs at the origin,

$$(V_c)_{phon} = c_s, \tag{1.18}$$

which indicates that the critical velocity for the creation of phonons is the velocity of first sound (239 m s^{-1}).

To find the second solution of (1.16), one draws the straight line which passes through the origin and touches the curve close to the roton minimum. This

leads to

$$(V_c)_{rot} \approx \frac{\Delta}{p_0} = 58\,\mathrm{m\ s^{-1}}. \tag{1.19}$$

Because $(V_c)_{rot} < (V_c)_{phon}$, $(V_c)_{rot}$ is the critical velocity for superfluidity.

Note also that the condition given in equation (1.17) for the case of the free-particle parabola (see Fig. 1.6) is

$$(V_c)_{sp} = 0. \tag{1.20}$$

A critical velocity of zero means that superfluidity is impossible in any system where free-particle motion can take place. Thus, it is the energy gap Δ, together with the lack of any other thermal excitation below the dispersion relation shown in Fig. 1.6, which ensures a finite value of the critical velocity in He II. Detailed calculations of the dispersion relations shown in Fig. 1.6 have been carried out starting from the classical papers of Feynman (1972), see also Belyaev (1958a, 1958b), Hugenholtz and Pines (1959), Brueckner and Sawada (1957a, 1957b), Alberico *et al*. (1976) and references therein.

1.5 Critical velocity for superconductors

The excitation spectrum of a superconducting metal worked out by Bardeen, Cooper and Schrieffer (Bardeen *et al*., 1957a,b; Chapter 3) is shown in Fig. 1.7.

The Landau criterion for superconductivity gives the critical velocity

$$(V_c)_{sc} = \frac{\Delta}{\hbar k_F}. \tag{1.21}$$

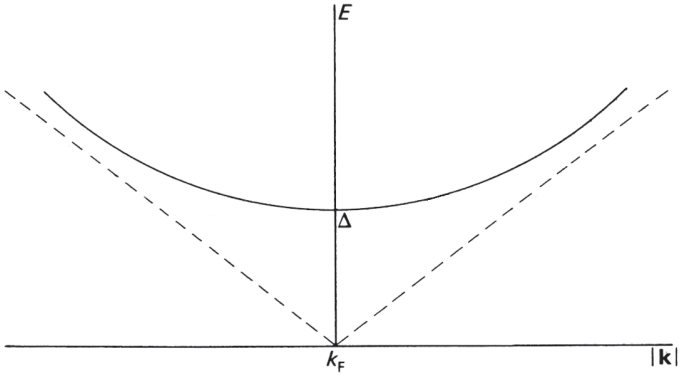

Figure 1.7. Sketch of the BCS excitation spectrum (full line) $E_k = \sqrt{(\varepsilon_k^2 + \Delta^2)}$, with the normal spectrum $|\varepsilon_k|$ (broken line). The normal spectrum is $\varepsilon_k = \hbar^2 k^2/2m_e - \hbar^2 k_F^2/2m_e$ which can be approximated by $\varepsilon_k = v_F'(|k| - k_F)$ with $v_F' = \hbar k_F/m_e$.

https://doi.org/10.1017/9781009401920 Published online by Cambridge University Press

Using the values for Sn

$$k_{\mathrm{F}} = 1.64 \times 10^{8}\ \mathrm{cm}^{-1}, \tag{1.22}$$

$$T_{\mathrm{c}} = 3.72\,\mathrm{K} = 0.32\ \mathrm{meV}, \tag{1.23}$$

and the BCS relation (Section 1.7)

$$\frac{2\Delta(0)}{T_{\mathrm{c}}} = 3.5, \tag{1.24}$$

one obtains

$$(V_{\mathrm{c}})_{\mathrm{sc}} = \frac{\Delta}{\hbar k_{\mathrm{F}}} = 51.2\ \mathrm{m\,s}^{-1} \tag{1.25}$$

where use was made of $\hbar c \approx 2 \times 10^{-2}$ meV cm and $c = 3 \times 10^{8}\ \mathrm{m\,s}^{-1}$. For the case of nuclei see Appendix K.

The use of Δ for both the (BCS) superconducting energy gap (see Fig. 1.7) and the roton energy minimum in neutral superfluids (see Fig. 1.6) is so well established in the literature that it is preferable to retain this double usage, at the risk (hopefully slight) of confusion.

1.6 Pairing in nuclei

The shell model potential is the average potential for a nucleon moving in a nucleus. It has a central and a spin-orbit component and, in a spherical nucleus, the individual nucleon states are specified by an orbital angular momentum l, a total angular momentum $j(= l \pm \frac{1}{2})$ and an eigenvalue m of j_z (Brink and Satchler, 1968). The nucleons interact through a strong, short-range, attractive nuclear force which contributes both to the shell model potential and to the residual interaction between nucleons. Two neutrons (or two protons) can best take advantage of the residual interaction to minimize their energy by moving in time-reversed orbits, i.e. states with the same j but equal and opposite m. The residual interaction (being time-reversal invariant) preserves the time-reversed motion because when such a pair of nucleons interact they scatter into time-reversed states. The total angular momentum of the pair is zero.

The ground state of a nucleus with an even number of neutrons and protons is obtained by coupling like nucleons in states with energies near the Fermi energy to form zero angular momentum pairs. Excited states are formed by breaking pairs, and the lowest states are constructed by breaking one pair. These states have an excitation energy of about 2Δ which is the pair binding energy (see Fig. 1.8).

https://doi.org/10.1017/9781009401920 Published online by Cambridge University Press

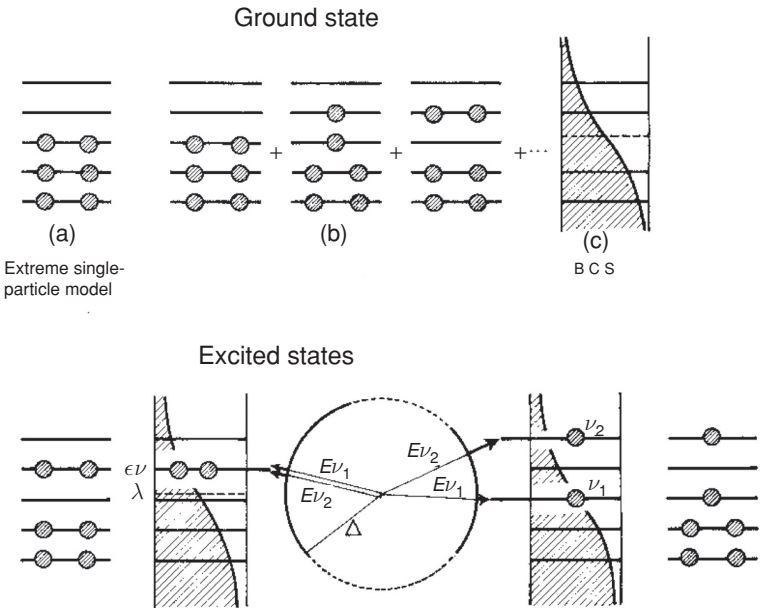

Figure 1.8. Schematic picture of the ground state and of the lowest excited states with angular momentum zero and positive parity in a system with an even number of fermions moving in a set of single-particle levels, assumed to be double degenerate.
Ground state: the ground state is obtained, in this extreme independent particle model, by filling the lowest orbitals compatible with the Pauli principle. The large energy gap observed in the nuclear spectrum is understood assuming a large energy loss not only to the breaking of a pair, but also to the lifting of pairs from one level to another; these two process are indicated in (b). That is, in the case where pairing correlations are taken into account, the ground state is a linear combination of pairs of particles in time-reversal states distributed over all the available levels. Thus the pair-correlated ground state consists of pairs scattering across the diffuse Fermi surface, a basic feature which is reflected in the occupation number shown to the far right (c).
Excited states: excited states can thus only be generated by breaking a pair of particles in any two levels, as shown in the lower part of the figure. Because the energy associated with each particle of the pair is $E_\nu = \sqrt{(\varepsilon_\nu - \lambda)^2 + \Delta^2}$, where ε_ν is the single-particle energy, λ is the Fermi energy and Δ the pairing gap, the minimum excitation energy is 2Δ, as shown. Note that the radius of the circle is the pairing gap, which measures the diffusivity of the Fermi surface. To the far left and right we show the extreme single-particle configurations associated with the two quasiparticle states shown close to the pairing gap circle, as well as the two-particle and two-quasiparticle excitation energy (after Nathan and Nilsson (1965)). Reprinted from *Alpha- Beta- and Gamma-Ray Spectroscopy*, Vol. 1, Nathan, H. and Nilsson, S. G., Editor Siegbahn, H., page 601, Copyright 1965, with permission from Elsevier.

The odd nucleon in a nucleus with an odd number of neutrons or protons must remain unpaired. One can obtain a qualitative description of the low states of such a nucleus in terms of the orbits available to the unpaired nucleon. In this approximation the degrees of freedom of the paired nucleons are neglected.

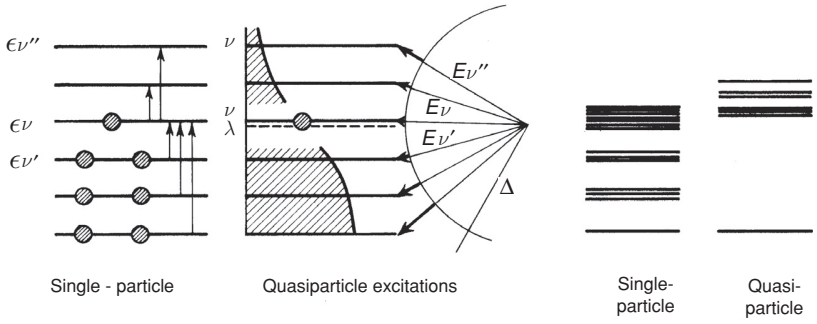

Figure 1.9. Ground state and excited states in the extreme independent single-particle model and in the pairing-correlated, superfluid model in the case of a system with an odd number of particles. In the first case, the energy of the ground state of the odd system differs from that of the even with one particle fewer by the energy difference $\varepsilon_\nu - \varepsilon_{\nu'}$, while in the second case by the energy $E_\nu = \sqrt{(\varepsilon_\nu - \lambda)^2 + \Delta^2} \approx \Delta$, associated with the fact the odd particle has no partner. Excited states can be obtained in the independent particle case by promoting the odd particle to states above the level ε_ν, or by exciting one particle from the state below to the state ε_ν or to one above it. To the left only a selected number of these excitations are shown. In the superfluid case excited states can be obtained by breaking of pairs in any orbit. The associated quasiparticle energy is drawn also here by an arrow of which the thin part indicates the contribution of the pairing gap and the thick part indicates the kinetic energy contribution, i.e. the contribution arising from the single-particle motion. Note the very different density of levels emerging from these two pictures, which are shown at the far left of the figure (after Nathan and Nilsson (1965)). Reprinted from *Alpha- Beta- and Gamma-Ray Spectroscopy*, Vol. 1, Nathan, H. and Nilsson, S. G., Editor Siegbahn, H., page 601, Copyright 1965, with permission from Elsevier.

When pairing correlations are taken into account this system in its ground state has an excitation energy of the order of Δ compared with the even system (see Fig. 1.9).

This effect leads to an odd–even staggering in nuclear masses and nucleon separation energies. If $B(N, Z)$ is the binding energy of a nucleus with Z protons and N neutrons then the energy required to separate the last neutron is

$$S_{\mathrm{n}}(N, Z) = B(N, Z) - B(N-1, Z). \tag{1.26}$$

Similarly the separation energy for the last proton is

$$S_{\mathrm{p}}(N, Z) = B(N, Z) - B(N, Z-1). \tag{1.27}$$

On average the neutron separation energy $S_{\mathrm{n}}(N, Z)$ should be larger for a nucleus with even N compared with a nucleus with odd N by the neutron pairing energy 2Δ. Fig. 1.10 shows the neutron separation energy for a sequence of nuclei

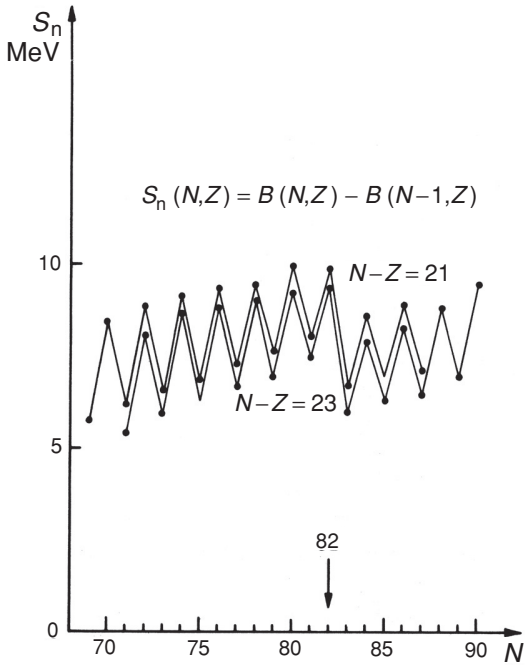

Figure 1.10. The neutron separation energies, S_n, are taken from the compilation by J. H. E. Mattauch, W. Thiele and A. H. Wapstra, Nuclear Phys. **67**, 1 (1965) (after Bohr and Mottelson (1969)).

with $N - Z = 21, 23$, i.e. in the neighbourhood of the $N = 82$ closed shell. There is a general tendency for S_n to increase as N increases but super-imposed on this trend there is a clear odd–even staggering effect due to pairing.

Values for the neutron pairing energy, known as the pairing gap, can be obtained from measured separation energies by using the formula

$$\begin{aligned}\Delta_n &= \tfrac{1}{4}\{2S_n(N,Z) - S_n(N+1,Z) - S_n(N-1,Z)\} \\ &= \tfrac{1}{4}\{B(N-2,Z) - 3B(N-1,Z) + 3B(N,Z) - B(N+1,Z)\}\,,\end{aligned} \tag{1.28}$$

where N is even. Similarly, the proton separation energy is given by

$$\begin{aligned}\Delta_p &= \tfrac{1}{4}\big\{2S_p(N,Z) - S_p(N,Z+1) - S_p(N,Z-1)\big\} \\ &= \tfrac{1}{4}\{B(N,Z-2) - 3B(N,Z-1) + 3B(N,Z) - B(N,Z+1)\}.\end{aligned} \tag{1.29}$$

Empirical values of the pairing energy parameters Δ_n and Δ_p are collected in Fig. 1.11. The general trend with mass number A can be fitted by the formula

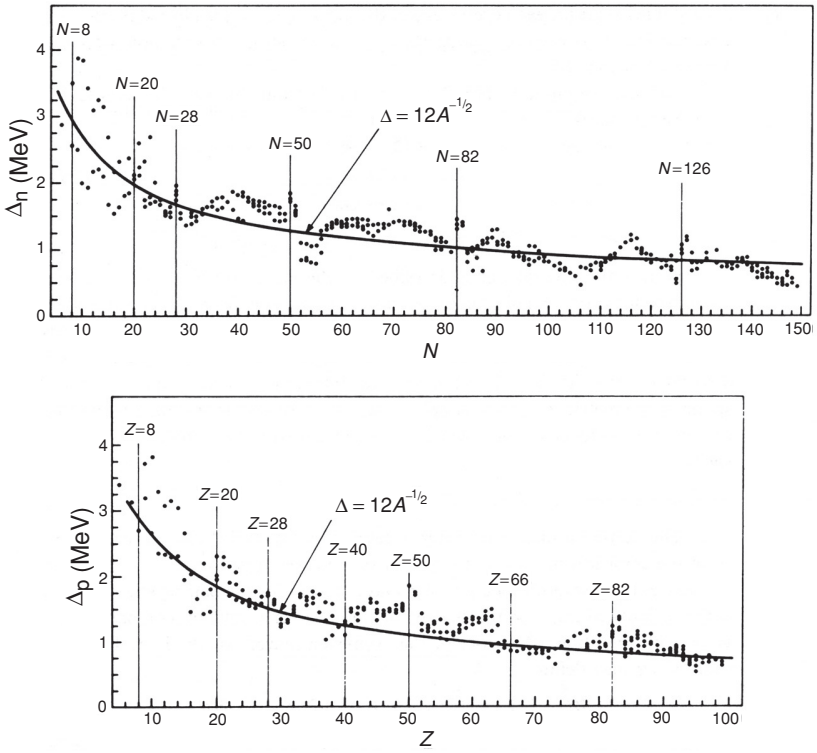

Figure 1.11. The odd–even mass differences for neutrons and protons are based on the analysis of Zeldes *et al.* (1967) (after Bohr and Mottelson (1969)).

(see Bohr and Mottelson (1969)).

$$\Delta \approx 12/A^{\frac{1}{2}}\ \text{MeV}. \tag{1.30}$$

Conspicuous local variations of the pairing gap with the number of neutrons or protons are observed, which cannot be fitted in detail by the smooth behaviour given by expression (1.30) (see e.g. Fig. 10.6). This A-dependence of Δ correlates, as a rule, with the collectivity displayed by low-lying surface vibrations of the different isotopes or isotones (see e.g. Fig. 10.7). This correlation testifies to the fact that, in addition to the bare nucleon–nucleon force, the exchange of collective surface vibrations between nucleons moving in time-reversal states close to the Fermi energy contributes to nuclear pairing correlations. The relative importance of this induced pairing interaction compared with the bare nucleon–nucleon interaction is a subject which is discussed in Chapters 8, 9, 10 and 11.

https://doi.org/10.1017/9781009401920 Published online by Cambridge University Press

1.7 Superconductivity

Electrons near the Fermi surface in a superconductor interact to form correlated pairs. This idea was first suggested by Cooper (1956) and the pairs are often called 'Cooper pairs'. Cooper pairs are constructed from states in which the two electrons have zero total spin and equal and opposite linear momentum $\mathbf{k}$ and $-\mathbf{k}$. The interaction which produces pairing correlations in a normal superconductor is a coupling between electrons via the positive ions of the crystal lattice. The electrons are coupled to the lattice by electrostatic forces. An electron moving through a crystal distorts the lattice and this distortion influences the motion of other electrons. Another way of expressing this is to say that an electron can emit or absorb a virtual phonon. The effective interaction between electrons is a result of the virtual emission of a phonon by one electron and its absorption by another. This interaction causes scattering of an electron pair from states $(\mathbf{k}, -\mathbf{k})$ to states $(\mathbf{k}', -\mathbf{k}')$ with an amplitude $V_{\mathbf{k}'\mathbf{k}}$ which depends on the electron–phonon coupling and on the phonon spectrum (see Fig. 1.12).

The interaction which produces pairing correlations in a normal superconductor is the result of a delicate balance between Coulomb repulsion screened by dynamical polarization effects of both electrons (plasmons) and ions (phonons). The screening of the Coulomb repulsion due to the exchange of plasmons (measured by the dimensionless parameter $\mu*$) plays an equally important role in determining the properties of superconductors as the effective interaction arising from the exchange of phonons (measured by the dimensionless parameter λ). Systems displaying small ($\ll 1$) values of $\mu*$ and large ($\gtrsim 0.3 - 0.4$) values of λ are expected to be normal or incipient high-T_c superconductors, such as

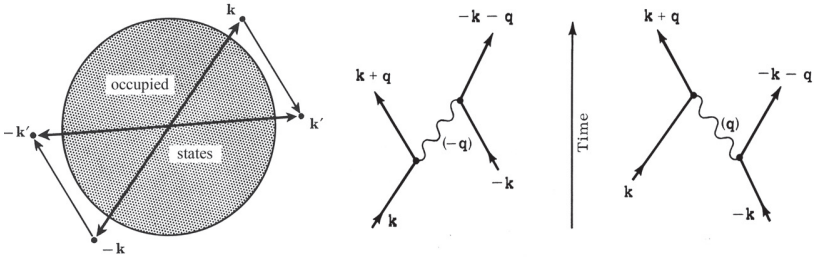

Figure 1.12. Schematic representation of the Cooper pair phenomenon. In (a) a transition is illustrated in which one pair of electrons moving in time-reversal states above the Fermi sea and carrying zero centre-of-mass momentum interact, exchanging momentum $\vec{q}$. The carriers of this interaction are the lattice phonons which are exchanged between the two electrons, as shown in (b).

https://doi.org/10.1017/9781009401920 Published online by Cambridge University Press

alkaline doped fullerides, i.e. materials made out of e.g. C_{60} fullerenes, in which case $\mu* \approx 0.3$ and $\lambda \approx 1$ (Gunnarsson (1997), (2004), Broglia *et al*. (2004)).

In the nuclear case the situation is quite different, as the strong force is (for relative distances $\gtrsim 0.75$ fm) attractive in the s-wave channel (see Figs. 8.2 and 8.5). Consequently, the main origin of nuclear pairing is due to the nucleon–nucleon strong force.

It is found, however, that the exchange of collective surface vibrations between pairs of nucleons moving in time-reversal states lying close to the Fermi energy seems to play a role which cannot be neglected in a quantitative description of pairing in nuclei (Chapters 8, 9, 10 and 11). The main differences between the phonon exchange in solids and in nuclei is that nuclear vibrations can be viewed as coherent motion of nucleons. To take care of Pauli principle violations as well as to avoid double counting of the same degrees of freedom, nuclear field theoretical methods have to be used in the calculation of the coupling of nucleons to nuclear surface vibrations leading to an induced pairing interaction (see Bes *et al*. (1976a,b), Bortignon *et al*. (1977), see also Appendix F).

Returning now to the case of superconductors, each Cooper pair has a binding energy 2Δ which is much smaller than the Fermi energy ε_F. The main components of the pair wavefunction come from electron states with energies ε within Δ of the Fermi energy,

$$\varepsilon_F - \Delta < \varepsilon < \varepsilon_F + \Delta. \tag{1.31}$$

The energy spread $\delta\varepsilon \approx 2\Delta$ corresponds to a momentum range $\delta p \approx 2\Delta/v_F$ where v_F is the Fermi velocity. The uncertainty relation $\delta x \approx \hbar/\delta p \approx \hbar v_F/2\Delta$ gives an estimate of the size of a Cooper pair. The quantity

$$\xi = \frac{\hbar v_F}{2\Delta} \tag{1.32}$$

is called the coherence length or correlation length of the superconductor, and is a measure of the size of a Cooper pair. The coherence length ξ is much larger than the crystal lattice spacing ($\sim$5 Å) in Type I superconductors. The Fermi velocity of electrons in these materials is normally large ($v_F \approx 10^6\,\mathrm{m\,s^{-1}}$) and the energy gap is small, leading to a large coherence length. For example $\xi \approx 10714$ Å for Sn and $\xi \approx 4615$ Å for Pb. Type II superconductors have a much smaller coherence length ($\xi \approx 50$ Å). This is partly because the electrons in these materials have a large effective mass and a small Fermi velocity ($v_F \approx 10^4\,\mathrm{m\,s^{-1}}$). Also, the energy gap is usually larger.

Bardeen, Cooper and Schrieffer (1957a,b) and Schrieffer (1964) developed a microscopic theory of superconductivity which incorporated the idea of Cooper pairs and gave a consistent treatment of the Pauli principle. The theory (called the BCS theory) has also been used to describe pairing in nuclei (Bohr, Mottelson

and Pines (1958)) and is discussed in Chapter 3 of this book. According to the BCS theory all electrons near the Fermi surface in the ground state of a superconductor form correlated Cooper pairs. Excited states are formed by breaking pairs and there is an energy gap 2Δ between the ground state and the lower excited states (Fig. 1.8). It is this energy gap which stabilizes the superconducting state. Thermal effects can break pairs, and in BCS theory the presence of unpaired electrons reduces the binding of those pairs which remain. Thus the gap parameter 2Δ is temperature dependent and decreases as T increases. At a critical temperature T_c the energy gap becomes zero, the pairs are broken and there is a phase transition from the superconducting phase into the normal phase. BCS theory predicts a definite relation between the transition temperature T_c and the energy gap $\Delta(0)$ at $T = 0$, namely,

$$\frac{2\Delta(0)}{T_c} = 3.51. \tag{1.33}$$

This relation can be checked experimentally because both $\Delta(0)$ and T_c can be measured. For most normal superconductors the ratio lies in the range 3.2–4.6 and is close to the BCS value.

These concepts have had also a profound influence on the theory of elementary particles. The Nambu–Jona-Lasinio model (1961a,b) was the first to pursue such matters, assuming that a kind of superconducting material occupied the whole Universe. This corresponds to the Higgs field introduced in later developments. In this world, particles and antiparticles, e.g. quarks and antiquarks, are the constituents of the Cooper pairs. Breaking one of these pairs produces a massive quark and a massive antiquark. Disturbing the distribution of the pairs creates waves (Anderson–Nambu–Goldstone modes) which can be interpreted as bosons, e.g. pions (see Chapter 4). The role which gauge invariance (charge conservation) plays in the BCS theory is played here by chiral invariance (invariance with respect to left-handedness and right-handedness operations).

Leggett (1989) points out that the Cooper pairs in the BCS theory of the superconducting state must all behave in exactly the same way, not only as regards their internal structure but also as regards their centre of mass motion. Each Cooper pair is made up of two fermions and therefore the pairs behave like bosons. From this point of view superconductivity is due to Bose condensation of the pairs. The analogy is not complete. In a Bose liquid such as ^{4}He the bosons exist even when they are not all condensed, while in the superconducting state either the Cooper pairs are condensed or they do not exist. Such a picture should, however, be modified for finite systems like nuclei, as well as for superconductors around the critical temperature and for superconducting metal clusters (see Section 1.9). In the nucleus, pairing vibrations (Chapter 5), i.e. collective modes which change the number of pairs, play an important role. They can be viewed as bound states

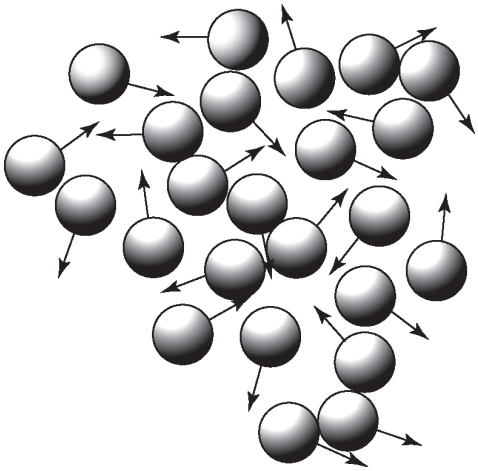

Figure 1.13. A system of independent Cooper pairs (Schafroth pairs). This situation corresponds to the incoherent solution of the many Cooper pair problem, the so called Fock state.

at the top of the Fermi surface (Anderson (1958), Högaasen-Feldman (1961), Bes and Broglia (1966)). In finite systems the presence of incipient Cooper pairs smooths out the sharp phase transition predicted by BCS theory.

There is another important fact to be considered in connection with the description of superconductors in terms of electron pairs. As pointed out by Schrieffer (1964) the pairs could be treated as independent if they were well separated (see Fig. 1.13), and Cooper's discussion would be appropriate for Schafroth (1955) pairs, see also Ogg (1946), Blatt and Butler (1955); note also the renewed interest in Schafroth pairs in connection with high T_c superconductivity (Alexandrov, 2003). However, actual superconductors differ in a fundamental manner from a bound-pair model in which the pairs are well separated in space and weakly interacting. The pairs overlap strongly and there are, in a superconducting metal, on average one million bound pairs (eliminating electrons deep in the Fermi sea) which have their centres of mass falling within the region occupied by a given pair wavefunction (see Fig. 1.14).

The study of Bose–Einstein condensation (BEC) has opened new interest on the study of the two, widely different, regimes schematically depicted in Figs. 1.13 and 1.14. In particular, with the possibility of studying ultracold Fermi gases of, for example, alkali metal atoms (Jochim *et al*. (2003), Greiner *et al*. (2003), Zwierlein *et al*. (2003), Regal *et al*. (2004)) like potassium or lithium, whose nucleus has an even integer spin but an odd number of protons and of neutrons ($^{40}_{19}K_{21}$, $^{6}_{3}Li_{3}$). A notable property of these atomic gases is the presence of scattering resonances, so called Feshbach resonances. A Feshbach resonance is an enhancement in the scattering amplitude of a particle incident on a

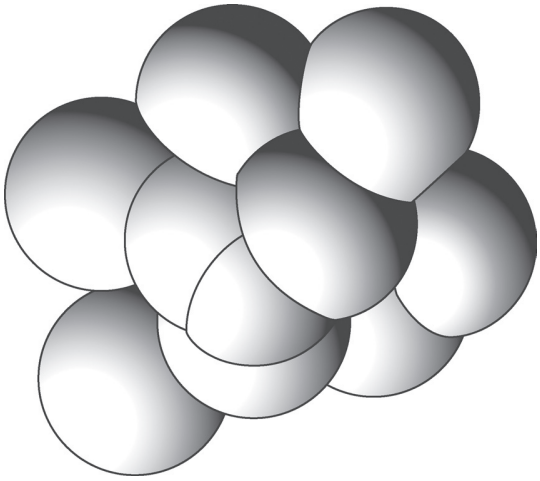

Figure 1.14. There are about 10^{18} Cooper pairs per cm^3 in a superconducting metal. A Cooper pair has a spatial extension of about 10^{-4} cm. Thus a given Cooper pair will overlap with 10^6 other Cooper pairs, leading to strong pair–pair correlation, as schematically shown. This solution corresponds to the coherent solution of the many Cooper pair problem (coherent state).

target – for instance, a nucleon scattering from a nucleus or an atom scattering from another atom – when it has approximately the energy needed to create a quasi-bound state of the two-particle system.

If a pair of ultracold atoms happens to have a bound state (molecular state) close to zero energy, then during collisions they will stick together for a while as they undergo a Feshbach resonance. While few molecules have a bound state near zero energy, Feshbach resonances can be produced using an external magnetic field (Zeeman tuning). The resonance is induced in the scattering between two atoms in different internal states, typical hyperfine states, and results in the divergence in the two-body s-wave scattering length α_F (the interaction between a pair of ultracold atoms is directly proportional to α_F). Feshbach resonances allow the experimental study of a Fermi gas at various interaction regimes. By varying the value of α_F (atoms repel if α_F is positive and attract if it is negative), one can explore different kinds of fermionic superfluidity, ranging from the BCS superfluidity, to BEC. Momentum correlations in Cooper-paired particles extend over long distances, whereas correlations in a molecule are short range. Consequently, the diatomic molecules do not constitute Cooper pairs. However, the molecules can be dissociated by moving the system back across the Feshbach resonance into the atomic regime. Interest in the transition from BEC-like behaviour to BCS-like behaviour was discussed, even before the discovery of Bose–Einstein condensation, by Leggett (1980).

Superconductors have unusual magnetic properties. When a sample of superconductor is placed in a magnetic field supercurrents are developed inside it which exclude the magnetic flux. Type I superconductors exclude the magnetic flux B completely for applied fields H less than a critical field H_c. This is the Meissner effect (Meissner and Ochsenfeld (1933)). Above H_c there is complete flux penetration and the normal state is restored. The Meissner effect is more complicated in a Type II superconductor in that there are two critical fields $H_{c1} < H_{c2}$. There is complete exclusion of flux if $H < H_{c1}$ and partial penetration for $H_{c1} < H < H_{c2}$ The critical field H_{c2} depends on temperature and goes to zero at the critical temperature T_c. Magnetic fields reduce or destroy superconductivity because they break time reversal invariance and reduce the binding of the Cooper pairs. When discussing magnetic effects it is important to make a distinction between the fields H and B. A number of conventions are possible depending on whether the supercurrent is regarded as an external current or a magnetization current. One convention which is commonly used is that H is generated by external currents and is unaffected by the presence of the superconductor. Supercurrents are considered to be magnetization currents which modify the flux B, but do not affect H.

The Ginzburg–Landau (1950) theory is a phenomenological theory of superconductivity which is based on Landau's theory of second order phase transitions (see e.g. Patashinskii and Pokrovskiĭ (1979) and refs. therein). Landau had argued that such a transition is characterized by an order parameter in a simple way. Ginzburg and Landau applied the method to superconductors. They introduced a complex order parameter ψ which could be interpreted as a kind of macroscopic wavefunction for the superconductor. In the presence of a magnetic field the free energy density is

$$f(\mathbf{r}) = f_0 + \alpha|\psi(r)|^2 + \frac{1}{2}\beta|\psi(r)|^4 + \frac{1}{2m^*}|(-\mathrm{i}\hbar\vec{\nabla}\psi - q\mathbf{A}\psi)|^2 + \frac{1}{2}\mu_0\mathbf{B}^2. \tag{1.34}$$

Here $\mathbf{A}$ is the vector potential of the magnetic field $\mathbf{B}$, q is the charge of the carriers of the supercurrent, and α and β are temperature-dependent constants. The Ginzburg–Landau theory is gauge-invariant provided that a gauge transformation of the vector potential is associated with a change in the phase of the order parameter. One can check that the gauge transformation

$$\psi' = \mathrm{e}^{\mathrm{i}\chi}, \quad \mathbf{A}' = \mathbf{A} + \hbar\vec{\nabla}\chi/q \tag{1.35}$$

leaves the free energy invariant. The electric current density is (see also Section 1.2)

$$\mathbf{J}(\mathbf{r}) = \frac{q\hbar}{2m^*\mathrm{i}}(\psi^*\vec{\nabla}\psi - \psi\vec{\nabla}\psi^* - 2\mathrm{i}q\mathbf{A}\psi^*\psi/\hbar), \tag{1.36}$$

https://doi.org/10.1017/9781009401920 Published online by Cambridge University Press

and is also invariant with respect to the gauge transformation given in equation (1.35). The quantity m^* is the effective mass of the carriers. The Ginzburg–Landau theory gives a good description of the magnetic properties of both Type I and Type II superconductors and predicts that magnetic flux is quantized in certain situations.

The magnetic flux trapped in a superconducting ring is quantized and the quantization condition can be derived from the form (1.36) of the supercurrent and the condition that the order parameter is single valued. There may be supercurrents in the surface of a ring enclosing magnetic flux but the current in the interior is zero. Also, the magnitude of the order parameter will be approximately constant in the interior of the material of the ring. If we write $\psi = |\psi|\exp(i\phi)$ then the condition that the current density (1.36) is zero gives

$$\hbar\nabla\phi - q\mathbf{A} = 0. \tag{1.37}$$

If ψ is single valued then ϕ can be changed by an integer multiple of 2π around the ring. Integrating equation (1.37) along a path C inside the ring gives the flux quantization condition

$$\Phi = \oint_C \mathbf{A}\cdot\mathbf{dl} = n2\pi\hbar/q \tag{1.38}$$

where n is an integer.

The quantum $2\pi\hbar/q$ of magnetic flux has been measured (Parks and Little (1964)) with the result that the charge of the carriers of the supercurrent is $|q| = 2e$, that is e^* (Section 1.2). This result indicates that the carriers of the supercurrent are the Cooper pairs of the BCS theory. The absence of electrical resistance in a superconductor is due to the binding energy 2Δ of the pairs. Because of this binding the electrons cannot scatter individually (note, however, the discussion at the end of Section 1.2).

The BCS theory describes a superconductor in equilibrium. An extension to include departures from equilibrium using the time-dependent mean-field approximation was made by Gor′kov (1960a,b) who established a connection between the BCS microscopic theory and the phenomenological Ginzburg–Landau theory. Gor′kov introduces a pair-field $\Delta(\mathbf{r})$ which in general is complex and position-dependent. In an equilibrium situation $2\Delta(\mathbf{r})$ is the BCS energy gap between the ground state and excited states. Gor′kov showed that the pair field $\Delta(\mathbf{r})$ is essentially the same as the order parameter $\psi(\mathbf{r})$ of the Ginzburg–Landau theory except for a constant factor due to the different normalization of ψ (see also Bes *et al*. (1970)).

1.8 Superfluidity of liquid ^{3}He

When the effective interaction $V_{\mathbf{k},\mathbf{k}'}$ for scattering of an electron pair from a state $(\mathbf{k}, -\mathbf{k})$ to a state $(\mathbf{k}', -\mathbf{k}')$ is independent of the angle between $\mathbf{k}$ and $\mathbf{k}'$

https://doi.org/10.1017/9781009401920 Published online by Cambridge University Press

then the Cooper pairs have zero orbital angular momentum and the pairing is called s-wave pairing. The Pauli principle requires that the pair wavefunction should be antisymmetric. As the orbital state is symmetric, the spin state must be antisymmetric and the pair must be in singlet state with spin $S = 0$. Most superconductors have s-wave pairing, but there could be a component of d-wave pairing due to crystal field effects. Pairing in nuclei is essentially s-wave pairing, although there is also evidence for d-wave pairing (Section 5.3 and Section 6.2.2). Furthermore, because of the presence of two types of fermions (protons and neutrons), the isospin dependence of pairing is important in nuclei (Bohr (1968), Nathan (1968), Bayman *et al*. (1969), Bes *et al*. (1977)).

The situation is different in the superfluid state of liquid ^{3}He because the interaction potential between ^{3}He atoms is strongly repulsive at small separations. This repulsion inhibits s-wave pairing and favours pairs with non-zero orbital angular momentum. Experimental and theoretical work has shown that p-wave pairing is important. In this case the orbital wave function of a pair of ^{3}He atoms is antisymmetric. Then the Pauli principle requires the spin of the pair to be symmetric with $S = 1$ and there is spin triplet pairing.

Triplet pairing is more complicated than singlet pairing. A pair has spin angular momentum $S = 1$ and orbital angular momentum $L = 1$ and there are several ways in which S and L can couple. The Ginzburg–Landau order parameter has nine complex components. It is for this reason that the superfluid phases of ^{3}He have a very rich structure. There are many superfluid phases. Two of them are the A-phase and the B-phase. In the A-phase the spin part of the wavefunctions is $|\uparrow\uparrow\rangle$ or $|\downarrow\downarrow\rangle$ while in the B-phase the pairing includes the combination $|\uparrow\downarrow\rangle + |\downarrow\uparrow\rangle$. The structure of the phases is anisotropic on a small scale due to various spin alignment correlations (see Vollhardt and Wölfle (1990) and refs. therein). The phase structure of ^{3}He was predicted by Leggett (1972) see also Anderson and Morel (1961), Balian and Werthamer (1963), Anderson and Brinkman (1973), (1975) and Ambegaokar and Mermin (1973)).

1.9 Comparison of pairing in nuclei with superconductivity

In this section we point out some of the differences between pairing properties of nuclei and superconductors. The coherence length in a superconductor is defined in equation (1.32). It measures the size of a Cooper pair. In both Type I and Type II superconductors the coherence length is large compared with the interatomic spacing in the material but small compared with the typical size of a piece of superconducting material. The situation is very different in a nucleus. Using the appropriate Fermi wave number ($k_{\mathrm{F}} \approx 1.36\,\mathrm{fm}^{-1}$) we get $\hbar\upsilon_{\mathrm{F}} = 54\,\mathrm{MeV\ fm}$. Then equation (1.32) gives a coherence length

$$\xi \approx \frac{27}{\Delta}\,\mathrm{fm}, \tag{1.39}$$

https://doi.org/10.1017/9781009401920 Published online by Cambridge University Press

the gap being in units of MeV. For a typical nucleus with $A = 140$, $\Delta \approx 1$ MeV, $\xi \approx 27$ fm. This compares with a nuclear radius $R = 1.2A^{1/3}$ fm ≈ 6.3 fm for medium heavy nuclei ($A \approx 120$). Thus the coherence length is larger than the nuclear radius. The same result holds for all nuclei in the periodic table. In a nucleus the size of a Cooper pair is given by the nuclear size rather than by the coherence length.

Quantum size effects can modify the properties of a superconductor if its dimensions are small enough. The first changes occur when the size is small compared with the coherence length but is still large in comparison with interatomic distances. In principle such a superconductor has the same properties as a bulk sample so long as it is not in a magnetic field. The behaviour in a strong field has interesting features. For example, the energy gap in the energy spectrum disappears at a certain value of the field. However, this field is not yet strong enough to break the Cooper pairs, and other properties of the superconducting state are retained. When the field is increased further there is a second-order phase transition to the normal state. These and other properties of small superconducting particles have been reviewed by Perenboom *et al*. (1981) (see also Kubo (1962), Black *et al*. (1996), Ralph *et al*. (1997), Farine and Schuck (2002)).

Properties of a sample of a superconductor depend on its dimension. A two-dimensional film or a one-dimensional wire behave differently from a three-dimensional sample. The meaning of a thin film is that the thickness is small compared with the coherence length. Similarly, a wire is effectively one-dimensional if its radius is small compared with the coherence length. Using the same criteria a nucleus should be regarded as a zero-dimensional superconductor (Chapter 4).

If the dimensions of a superconducting particle become much smaller than the coherence length other effects come into play. Anderson (1959) suggested that there is a lower limit in size for a particle still to be superconducting. A relevant parameter for this regime is the ratio of the mean spacing of single particle states δ with the same spin to the transition temperature T_c

$$\bar{\delta} = \frac{\delta}{T_c} = \frac{2}{\rho(\varepsilon_F)T_c}, \tag{1.40}$$

where $\rho(\varepsilon_F)$ is the density of states at the Fermi level. Mühlschlegel *et al*. (1972) and Lauritzen *et al*. (1993) have calculated the effects of thermal fluctuations on the superconducting phase transitions using Ginzburg–Landau theory, path integral methods plus RPA theory, respectively. They show that the fluctuations smooth out the discontinuity in the thermal capacity at the transition temperature. The smoothing is complete when $\bar{\delta} = 1$, but is already significant if $\bar{\delta} \approx 0.01$. This smoothing has been observed experimentally by Tsuboi and Suzuki (1977). They measured the electronic specific heat of small particles of Sn with an average diameter ranging from 25 nm up to 220 nm. Some of their results are shown in Fig. 1.15.

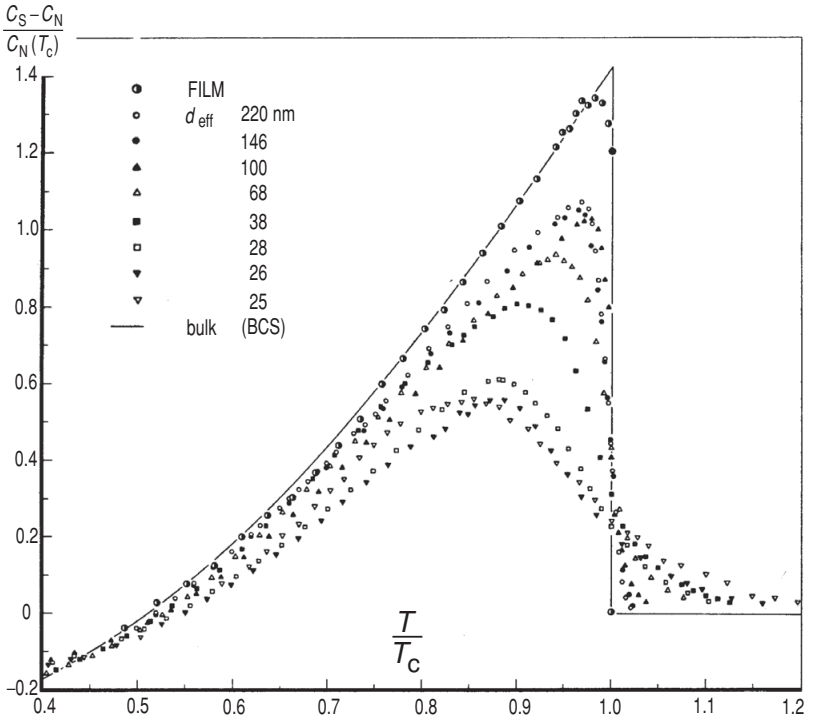

Figure 1.15. Measured normalized difference $(C_S - C_N)/C_N(T_c)$ of the specific heat in the superconductive and normal state respectively, for tin particles with different diameters, as a function of the reduced temperature. The measurements are normalized to $C_N(T_c) = \gamma T_c$, with $\gamma = 1.78 \times 10^{-3}\,\mathrm{JK}^{-2}\,\mathrm{mol}^{-1}$. The ensemble of tin particles, isolated from each other by an oxide layer, was prepared by depositing tin islands in vacuum and then oxidising their surfaces repeatedly. From Tsuboi and Suzuki (1977).

Quantum size effects are also significant in nuclei and no sharp pairing phase transition is expected. Pairing correlations should definitely become weaker as the excitation energy is increased but there will be no sudden transition (Chapter 6).

Mottelson and Valatin (1960) argued that there is a close formal correspondence between the equations of motion in a constant magnetic field and those in a rotating reference system. They suggested that critical magnetic field phenomena in superconductors should have their counterpart in the rotational spectra of nuclei. The Coriolis forces in a rotating nucleus tend to decouple pairs of particles in time-reversal states. When the angular velocity is sufficiently large then pairing correlations should be destroyed completely. Mottelson and Valatin estimated a critical angular velocity ω_c above which there would no longer be any pairing correlation. This is analogous to the critical magnetic field B_c for a superconductor.

https://doi.org/10.1017/9781009401920 Published online by Cambridge University Press

The correspondence between the effect of a magnetic field on a superconductor and the influence of rotations on pairing in a nucleus is not complete. The London penetration depth is destroyed by an applied magnetic field in two stages. In the absence of a magnetic field all the electrons are paired in the superconducting ground state. Excited states are formed by breaking pairs. The two-quasiparticle states have an excitation energy and so on. The magnetic field produces a Zeeman splitting of the excited states and reduces the energy gap. The splitting is largest in a quasiparticle state with maximum angular momentum. This is $k_{\mathrm{F}}R$, where R is the radius of the particle and k_{F} is the Fermi momentum. When the field has a strength B_1 given by:

$$\frac{e\hbar}{2m}(2k_{\mathrm{F}}R)B_1 = 2\Delta, \tag{1.41}$$

the lowest two-quasiparticle state becomes degenerate with the fully paired ground state. In these circumstances the field is strong enough to reduce the energy gap to zero but not strong enough to destroy the superconductivity. It is an example of gapless superconductivity (Perenboom *et al.* (1981)).

The two-quasiparticle state with highest angular momentum has a magnetic moment $(e\hbar/2m)2k_{\mathrm{F}}R$, while the largest magnetic moment of a four-quasiparticle state is almost twice that value. Thus, when the field increases slightly above B_1, the four-quasiparticle state becomes degenerate with the fully paired state. As the field increases further, more and more pairs are broken. The resultant blocking reduces the effective strength of the pairing interaction and eventually the pairing disappears. Calculations reviewed in Perenboom *et al.* (1981) based on the BCS theory with a Fermi gas density of states and including no shell effects, give the critical field as

$$B_{\mathrm{c}} = 2.6B_1. \tag{1.42}$$

The first of these size effects exists in rotating nuclei. As discussed in Brink (1994), the largest two-quasiparticle angular momentum is $j_1 + (j_1 - 1) = 2j_1 - 1$, where j_1 is the maximum single-particle angular momentum available near the Fermi level. Normally it corresponds to the intruder state with $j_{max} = l_{max} + 1/2$ which is pushed down from the next shell by the spin–orbit interaction. This two-quasiparticle state is split by the rotation and becomes degenerate with the fully paired state when

$$\hbar\omega_1 = \frac{2\Delta}{2j_1 - 1}. \tag{1.43}$$

Physically this size effect is associated with the band crossing (or 'backbend', see Chapter 6, Fig. 6.3) observed in rotating nuclei and ω_1 should be indentified with the band crossing frequency. The two quasiparticlcs align their angular momentum with the rotational axis of the nucleus.

Backbending is a striking effect which is observed in the rotational spectrum of many deformed nuclei. The corresponding effect is much more difficult to detect

in superconductors because the critical field B_1 (see equation (1.41)) depends on the radius of the sample and it is difficult to obtain grains of uniform size. As well as producing backbending, rotations tend to quench the pair correlations in a nucleus. There should be a phase transition to an unpaired state at a critical rotational frequency ω_c. Analogy with the superconducting case equation (1.42) suggests $\omega_c \approx 2.6\omega_1$. Making use of equation (1.43) with typical values of $\Delta \approx 1.2$ MeV and $j_1 \approx 13/2$ for medium heavy nuclei ($A \approx 150$), leads to $\hbar\omega_c \approx 0.5$ MeV.

As in the case of the critical temperature, finite size effects will smooth out any sudden phase transition. Pairing correlations should definitely be reduced as the angular velocity increases but they are unlikely to vanish suddenly at $\omega \approx \omega_c$.

Finite size effects in nuclei smooth out some of the striking effects associated with phase transitions in superconductors, but at the same time there are new phenomena associated with the finite size which are unknown in superconductors. Shell effects are a consequence of the finite size of nuclei. The spacing $\hbar w_0$ between major shells in a nucleus can be estimated from the formula (Bohr and Mottelson (1969))

$$\hbar w_0 \approx 41 A^{-1/3}\,\text{MeV} \approx \frac{49}{R}\,\text{MeV fm}, \tag{1.44}$$

where we have used $R = 1.2A^{1/3}$fm. Equations (1.39) and (1.44) give a relation

$$\frac{R}{\xi} \approx 1.8\frac{\Delta}{\hbar w_0}. \tag{1.45}$$

Thus the condition that the nuclear radius is small compared with the coherence length is related to a condition that the pairing strength 2Δ is less than the shell spacing $\hbar w_0$. Consequently, a phase transition from normal into superfluid states can take place at $T = 0$, as a function of particle number. In fact in closed shell nuclei $\Delta \ll \delta \approx 0.5\hbar w_0$ while in open shell nuclei $\Delta > \delta \approx \hbar w_0/10$. Spatial quantization in atomic nuclei leads to single-particle states with quite different angular momenta. Cooper pairs based on large angular momenta levels and lying close to the Fermi energy feel the action of nuclear rotation stronger than Cooper pairs based on low angular momenta levels. Consequently, the breaking of Cooper pairs takes place in atomic nuclei as a function of rotational frequency, stepwise. This interplay between pairing and shell effects is responsible for the band crossing or 'backbending' phenomena observed in rotating deformed nuclei (Stephens and Simon (1972), Bohr and Mottelson (1974, 1981), Broglia *et al.* (1974a), (1975)) (see Chapter 6).

1.10 Neutron stars

Atoms dissolve when ordinary matter is compressed to a very high density, namely when the separation of the nuclei is smaller than the atomic size. The

positive charged nuclei move in a plasma of free electrons. For such an assembly the lowest energy state is reached for a system of $^{56}_{26}$Fe nuclei because they are the nuclei with the largest binding energy. If the matter is compressed to a still higher density the electron Fermi energy increases and the electrons become relativistic. For a sufficiently large density it becomes energetically favourable for the electrons to combine with the bound nuclear protons to form neutrons by inverse β-decay. This moves the equilibrium nuclear composition away from $^{56}_{26}$Fe to more neutron-rich nuclei. Coulomb forces play a weaker role than in isolated atomic nuclei. When the density increases to $\sim 4 \times 10^{11}\,\mathrm{g\,cm^{-3}}$ (note that saturation nuclear density corresponds to $\rho = 2.8 \times 10^{4}\,\mathrm{g\,cm^{-3}}$), the ratio n/p reaches a critical level. Any further increase in the density leads to 'neutron drip', that is, a two-phase system in which electrons, nuclei, and free neutrons coexist and together determine the state of lowest energy. Increasing the density above $4 \times 10^{11}\,\mathrm{g\,cm^{-3}}$ leads to higher n/p ratios and more and more free neutrons. Finally, when the density exceeds about $4 \times 10^{12}\,\mathrm{g\,cm^{-3}}$, more pressure is provided by neutrons than by electrons (Shapiro and Teukolsky (1983)).

Pulsars are astronomical objects emitting periodic pulses of radio waves. It is thought that the objects are neutron stars. The near simultaneous discoveries of the Crab and Vela pulsars (Hewish *et al.* (1968), Gold (1969)), provided evidence for the formation of neutron stars in supernova explosions. At the relatively low temperatures ($\leq$keV) expected for all but the youngest neutron stars, one expects to find neutron superfluidity in the crust and interior (see Fig. 1.16). One also expects the remaining protons in the interior to be paired and hence

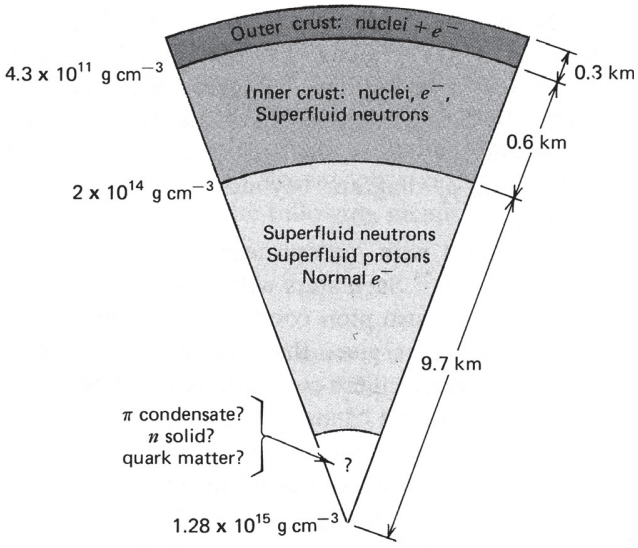

Figure 1.16. Cross-section of neutron stars (after Pines (1980)).

https://doi.org/10.1017/9781009401920 Published online by Cambridge University Press

superconducting (Shaham (1980)). It is unlikely, however, that the electrons are superconducting because the electron–phonon coupling is too weak.

Calculations suggest that at least three distinct hadronic superfluids exist inside a neutron star (Pines *et al*. (1980)):

1. In the inner crust ($4.3 \times 10^{11}\,\mathrm{g\,cm^{-3}} < \rho < 2 \times 10^{14}\,\mathrm{g\,cm^{-3}}$, the free neutrons may pair in a $^1S_0$ state to form a superfluid amid the neutron-rich nuclei.
2. In the quantum liquid regime ($\rho \geq 2 \times 10^{14}\,\mathrm{g\,cm^{-3}}$), where the nuclei have dissolved into a degenerate fluid of neutrons and protons, the neutron fluid is likely to be paired in a $^3P_2$ state.
3. The protons in the quantum liquid are expected to be superconducting in a $^1S_0$ state.

There are a number of important consequences of hadron superfluidity and superconductivity, which may lead to observational effects. In particular the cooling time scale of pulsars (Pizzochero *et al*. (2002)), as well as the sudden changes in the pulsar periods known as glitches (Anderson *et al*. (1982), Pines, Tamagaki and Tsuruta (1992)).

2

The pairing force and seniority

2.1 Evidence for pairing correlations

The nucleus ^{208}Pb is well described by the independent particle model in terms of closed shells in both neutrons and protons. The absence of low-lying states supports this hypothesis. The shell model would then describe the low-lying levels of ^{207}Pb in terms of the states of a single neutron hole. The observed energies, angular momenta and parities are in good accord with this picture, although small admixtures of more complicated configurations must be invoked to account for some fast electromagnetic decays (see Sections 9.1 and 9.2). The next step is to interpret the levels of ^{206}Pb in terms of two holes, which are combinations of the single-hole states of ^{207}Pb, interacting through a residual interaction. The dramatic effect of the internucleon force is shown by the fact that there is only one excited state below 1.2 MeV, compared with the five we would get in the independent hole approximation (see Fig. 2.1). This becomes even more striking in ^{204}Pb, where the independent hole picture predicts about thirty levels within 1 MeV of the ground state, whereas again only one is observed (Mottelson (1996)).

Another indication of the importance of the residual interaction among nucleon pairs is the well-known difference in physical properties between even and odd nuclei. For example, studies of cosmic abundances show that nuclei with even proton and neutron numbers are much more abundant, and thus more stable, indicating stronger binding energies.

Fig. 2.2 shows a typical trend in binding energies as a function of the number of nucleons (see also Fig. 1.10). The binding energies of the even nuclei ($N_0,\ N_0 \pm 2, \ldots$) give rise to the lower line and odd nuclei to the upper line. The ordinate is $E - \lambda\,(N - N_0)$ where E is the energy and λ is the chemical potential. The term $\lambda\,(N - N_0)$ subtracts the average dependence of the energy on the particle number so that the odd–even fluctuations show more clearly. The energy

https://doi.org/10.1017/9781009401920 Published online by Cambridge University Press

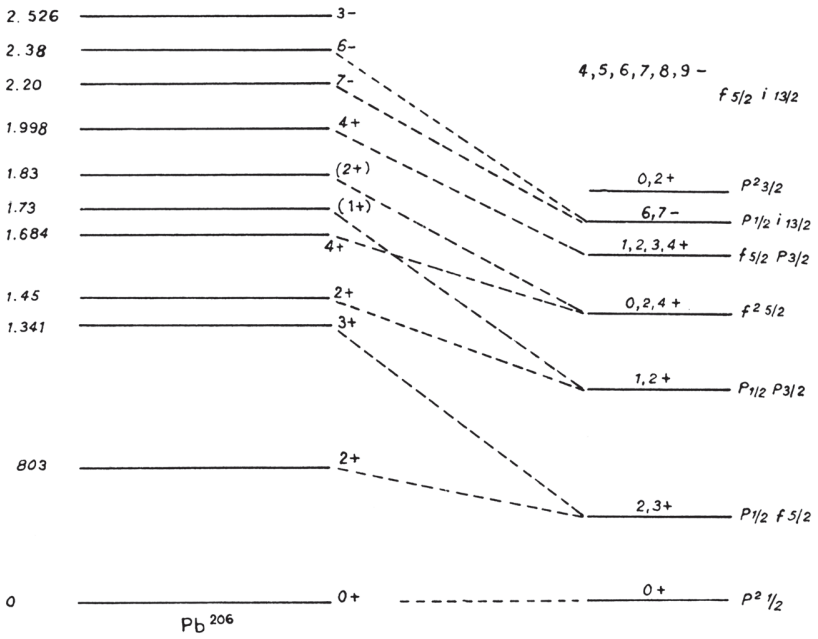

Figure 2.1. Level spectrum of ^{206}Pb. The experimental spectrum together with the observed spin and parities are shown on the left. On the right the different possible configurations $(j_1\, j_2)$ are drawn with excitation energies equal to $E(j_1) + E(j_2)$ as obtained from ^{207}Pb. The spin and parities of the different levels that can be obtained from coupling j_1 and j_2 connect these asignments with the appropriate levels in the observed spectrum (after Mottelson (1996)).

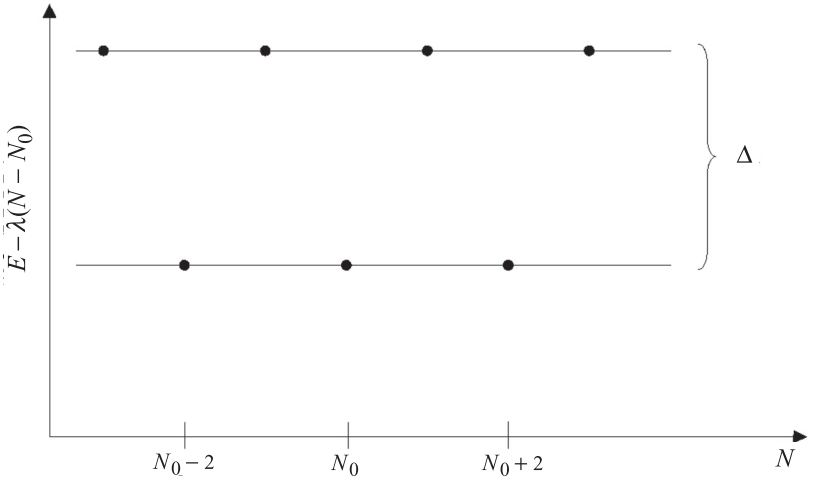

Figure 2.2. Binding energies $(-E)$ as a function of the number of neutrons. The quantity $-\lambda$ is the average binding energy per added neutron, that is λ = chemical potential.

https://doi.org/10.1017/9781009401920 Published online by Cambridge University Press

difference between the lines is Δ. Whether this quantity reflects the binding energy associated with a pair interaction between nucleons or not depends on its magnitude. This is because the quantization of the independent particle model also implies an extra binding energy for the even system compared with the odd system. The magnitude of this effect can be estimated in the Fermi gas model (see equations (2.4)–(2.7)).

The spacing d between states at the Fermi energy with the same spin and isospin quantum numbers can be written in terms of the total level density sum of the proton and neutron level densities $\rho = 3A/2\varepsilon_{\mathrm{F}}$ as

$$d = \frac{4}{\rho(\varepsilon_{\mathrm{F}})} = \frac{8\varepsilon_{\mathrm{F}}}{3A}. \tag{2.1}$$

The factor of 4 is due to the fact that each level can be occupied by two protons and two neutrons (with spin up and spin down). If the levels are equally spaced the total energy is

$$E(N) = \tfrac{1}{4}d(N-1)^2 - \tfrac{1}{4}d\ \delta(N, \text{even}), \tag{2.2}$$

for each type of particle, as can be seen from Fig. 2.3. Making use of the relations given in equations (1.28) and (2.2) and of the fact that $B(N) = -E(N)$, one finds

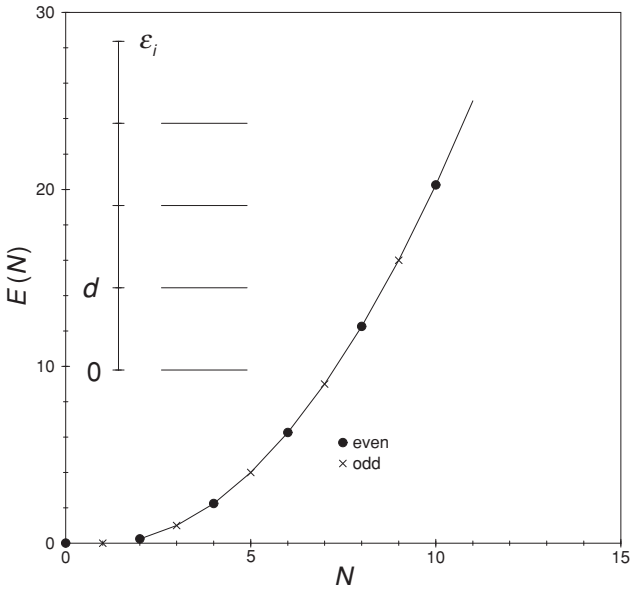

Figure 2.3. Energy $E(N) = \sum_{i=1}^{N} \varepsilon_i$ associated with the motion of N identical independent particles moving in the set of equidistant two-folded single-particle levels shown in upper left corner. Under close inspection, there is an odd–even staggering as described by equation (2.2). The dots and the crosses represent the even and odd systems respectively. The continuous curve corresponds to the expression given by equation (2.2).

https://doi.org/10.1017/9781009401920 Published online by Cambridge University Press

that the effective gap parameter in this model is (Bohr and Mottelson (1969))

$$(\Delta)_{\rm kin} \;=\; 2 \times \frac{d}{8} \;\simeq\; \frac{2\varepsilon_{\rm F}}{3A} \;\sim\; \frac{25}{A}{\rm MeV}. \tag{2.3}$$

The observed pairing energies are shown in Fig. 1.11 and can be parametrized according to equation (1.30). For a ^{160}Dy nucleus ($A = 160$) we have $(\Delta)_{\rm kin} \simeq 0.16\,{\rm MeV}$ and $\Delta \approx 0.95\,{\rm MeV}$. Thus Δ is almost an order of magnitude larger than $(\Delta)_{\rm kin}$ (see also Satula *et al*. (1998) and Rutz *et al*. (1999)).

The large observed odd–even effect may be described in terms of pairwise correlations of identical particles. These contribute an additional binding energy for each pair of nucleons near the top of the Fermi distribution coupled to angular momentum zero. This can be seen from the spectra shown in Fig. 2.1. Giving an extra binding energy to the $p^2_{1/2}(0^+)$ configuration is equivalent to moving up all the excited states by the same amount. In this way overall agreement between theory and experiment is obtained.

We conclude this section by collecting together some numerical values of Fermi gas parameters which will be used in this chapter and in other parts of the book. The average particle density of nuclear matter is taken to be

$$\rho(0) = 0.17 \;\; \text{nucleons fm}^{-3}, \tag{2.4}$$

i.e.

$$\rho(0) = 2.8 \times 10^{14}\,{\rm gm\,cm}^{-3}, \tag{2.5}$$

which corresponds to a nuclear radius $R = r_0 A^{\frac{1}{3}}$, with $r_0 = 1.1\,{\rm fm}$. The Fermi wave number is

$$k_{\rm F} = 1.36\,{\rm fm}^{-1}\,, \tag{2.6}$$

(an average value for neutrons and protons, $N = Z = A/2$) and the Fermi energy is

$$\varepsilon_{\rm F} = \frac{\hbar^2 k_{\rm F}^2}{2m} \simeq 37\,{\rm MeV}. \tag{2.7}$$

This value of $\varepsilon_{\rm F}$ has been used in equation (2.3).

2.2 The pairing interaction

The idea of a pairing interaction was already present in the early developments of the shell model (Mayer and Jensen (1955)). The purpose of this section is to identify two general properties of a pairing force interaction. The first is that it is short range and the second that it has a multipole expansion containing high angular momentum components (Belyaev (1959), Bayman (1960), Mottelson (1962)). Both of these properties are illustrated by the example of a delta function potential discussed at the end of this section and in Section 2.3. The second is important for understanding the induced pairing interaction in Chapters 8, 10 and 11.

https://doi.org/10.1017/9781009401920 Published online by Cambridge University Press

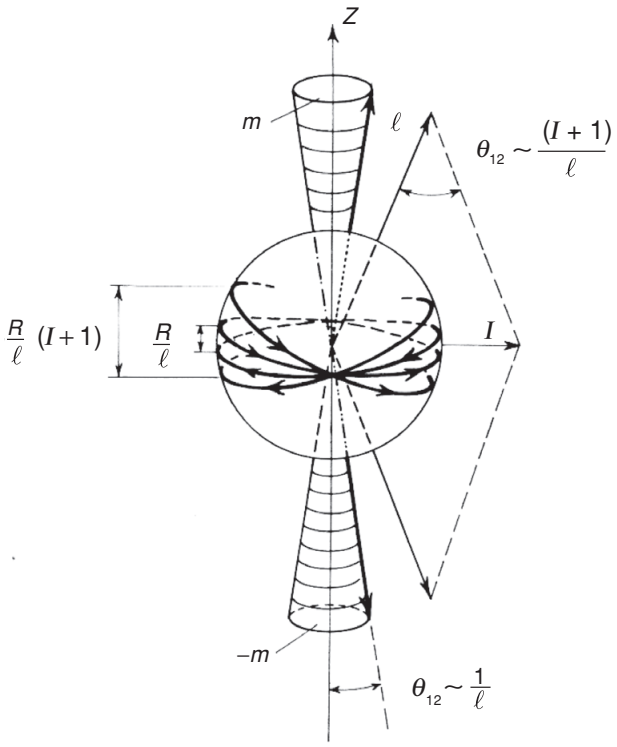

Figure 2.4. Schematic representation of two time-reversed orbits coupled to angular momentum $I = 0$ and $I \neq 0$. Two identical nucleons are assumed to move in time-reversal orbits labelled by the orbital angular momentum ℓ and the projection m. When the two particles are coupled to angular momentum zero their orbits wobble within an angle $\theta_{12} \sim 1/\ell$. This is required by the Heisenberg uncetainty principle within conjugated variables, in the present case $\Delta\ell_z \Delta\theta_{12} \gtrsim 1$. In a simple classical picture where the particles are concentrated at a radius R, such wobbling results in a typical distance between the two particles of the order of R/ℓ. The larger the angular momentum the closer is the system to the classical limit and larger will be the probability that the particles are on top of each other. When the relative motion of the particles are coupled to a finite value I of the total angular momentum, aside from the quantal wobbling, there will be a further tilting of the single-particle orbital proportional to I/ℓ. This will add, on average, a distance RI/ℓ between the two particles.

Consider two particles in the same ℓ-orbit coupled to various total angular momenta $L = 0, 1, 2, \ldots$. The radial dependence of the single-particle wavefunctions will, in most cases, describe particles moving in orbits with a radius of the order of the nuclear radius. The main degree of freedom available to the particles corresponds to different possible orientations of the orbital planes. The associated particle correlations are mainly correlations in angle. This is illustrated in Fig. 2.4. Two identical nucleons are assumed to move in time-reversed orbits labelled by the orbital angular momentum ℓ with projections m and $-m$. When the two particles are coupled to an angular momentum $L = 0$ their orbits

https://doi.org/10.1017/9781009401920 Published online by Cambridge University Press

wobble within an angle $\theta_{12} \sim 1/\ell$. This is required by the Heisenberg uncertainty relation for conjugate variables $\Delta\ell\ \Delta\theta_{12} \sim 1$. In a simple classical picture where the particles are located at a radius R such a wobbling results in a typical distance between the particles of the order of R/ℓ.

If we now consider a state of the ℓ^2 configuration with $I \neq 0$ (but still $I \ll l$) then the average angle θ_{12} between the particles will be larger. This will increase their average separation by a distance of the order of RI/ℓ, giving a total separation $\sim R(I+1)/\ell$. Consequently, if the range of the force is small compared with R/ℓ, the states with $I = 2$ will have an interaction energy which is a fraction ($\sim 1/3$) of that in the $I = 0$ state.

Let us now expand a general interaction in multipoles (Brink and Satchler (1968))

$$\begin{aligned} V(r_{12}) = V(|\vec{r}_1 - \vec{r}_2|) &= \sum_\lambda J_\lambda(r_1, r_2) \sum_\mu Y_{\lambda\mu}(\hat{r_1}) Y^*_{\lambda\mu}(\hat{r_2}) \\ &= \sum_\lambda \frac{2\lambda+1}{4\pi} J_\lambda(r_1, r_2) P_\lambda(\cos\theta_{12}) \\ &= \sum_\lambda V_\lambda(r_1, r_2) P_\lambda(\cos\theta_{12}). \end{aligned} \tag{2.8}$$

If particles 1 and 2 are in orbitals confined to a fairly restricted radial region, the dependence on $r_1,\ r_2$ may be ignored for a particular λ. The function P_λ drops from its maximum at $\theta_{12} = 0$ in an angular distance $1/\lambda$ (Fig. 2.5). Thus 1 and 2 interact through the component λ only if r_{12} in equation (2.8) fulfils $r_{12} < R/\lambda$,

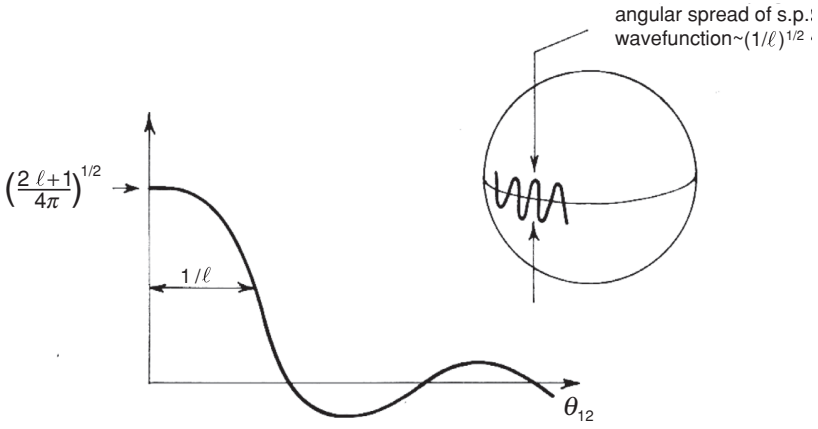

Figure 2.5. Schematic picture indicating the angular spread of the wavefunction of two particles coupled to angular momentum $I = 0$. Particle 1 is moving in an orbital with $m = \ell$ while particle 2 has $m = -\ell$. These one-particle states correspond to wavefunctions concentrated in the equatorial plane, but possessing an angular spreading $\sim (\ell)^{-1/2}$ due to quantal zero point fluctuations (after Mottelson (1962)). Copyright © Società italiana di Fisica.

https://doi.org/10.1017/9781009401920 Published online by Cambridge University Press

where R is the mean value of the radii $\vec{r}_1$ and $\vec{r}_2$. Thus, as λ increases, the effective forces range decreases. This leads to the expectation that the strength of the λ terms increases as the range of $V(r_{12})$ decreases. For a force of range much greater than the nuclear size, only the $\lambda = 0$ monopole part is important. At the other extreme, a δ-function force has coefficients $V_\lambda(r_1, r_2)$ that increase with λ, as can be seen from the relation

$$V_\lambda = \frac{(2\lambda + 1)}{4\pi r_1^2}\delta(r_1 - r_2). \tag{2.9}$$

Pairing force effects come from all the high λ terms, representing the short-range effects of $V(r_{12})$.

2.3 The δ-function nucleon–nucleon potential

As discussed in Section 2.2, the δ-function potential

$$V(r_{12}) = -4\pi V_0\, \delta(\vec{r}_1 - \vec{r}_2), \tag{2.10}$$

is a simple representation of a short-range attractive effective interaction between identical valence nucleons. Two identical nucleons in a shell model orbit with angular momentum j coupled to a total angular momentum I have a wavefunction $|jjIM\rangle$ and the interaction energy E_I is

$$E_I = \langle jjIM|V|jjIM\rangle.$$

The matrix element can be evaluated to give

$$E_I = -\frac{(2j+1)}{2} V_0\, I(j) |\langle I\ j\ 0\ \tfrac{1}{2}|\ j\ \tfrac{1}{2}\rangle|^2, \tag{2.11}$$

where

$$I(j) = \int R_j^4 r^2 \mathrm{d}r,$$

is an integral depending on the radial wavefunction R_j of the level j, and $\langle I\ j\ 0\ \frac{1}{2}|\ j\ \frac{1}{2}\rangle$ is a Clebsch–Gordon coefficient. The details of the derivation of equation (2.11) are given e.g. in Bayman (1960), Brink and Satchler (1968) de-Shalit and Talmi (1963), Lawson (1980) and Heyde (1990). When the total angular momentum $I = 0$, the energy E_0 in equation (2.11) simplifies to

$$E_0 = -\frac{(2j+1)}{2}\, V_0\, I(j). \tag{2.12}$$

The radial integral $I(j)$ can be estimated by assuming that R_j is constant inside the nuclear radius R_0 and is zero outside. Normalizing the wavefunction gives

$$R_j = \sqrt{3/R_0^3},$$

https://doi.org/10.1017/9781009401920 Published online by Cambridge University Press

and

$$I(j) \approx 3/R_0^3 \,.$$

If one corrects this estimate for the spillout of the nucleons (see Appendix D, Section D.2), one has to divide the result by $(1 + a/R)^3 \approx 1.4$, thus leading to

$$I(j) \approx 1.2\,\mathrm{fm}^{-3}/A, \tag{2.13}$$

if $R_0 = 1.2A^{\frac{1}{3}}\,\mathrm{fm}$. In the limit $j \gg I$ the Clebsch–Gordon coefficient in equation (2.11) can be estimated by using its semiclassical limit

$$\lim_{j\gg I} \langle j\ \tfrac{1}{2}\ I\ 0|\ j\tfrac{1}{2}\rangle \approx P_I(0) \ = \ \frac{(-1)^{I/2}\ \ I!}{2^I\ (I/2)!(I/2)!}. \tag{2.14}$$

Substituting $I = 0, 2, 4$ and 6 into equation (2.14) gives

$$E_2 \sim (1/4)\,E_0, \quad E_4 \sim (9/64)\ E_0, \quad E_6 \sim (25/256)E_0, \tag{2.15}$$

showing that pairing is much stronger for the state with $I = 0$ than for other values of I. The spectrum (2.15) is illustrated in Fig. 2.6.

The pairing force is an approximation to a short-range potential like the δ-function interaction, and is defined so that the energy E_I of a pair is large when $I = 0$ and is zero for $I \neq 0$. It can be expressed in second quantized form by using the pair-creation operator (see Appendix A)

$$P_j^\dagger = \sum_{m>0}(-1)^{j-m}a_{jm}^\dagger a_{j-m}^\dagger, \tag{2.16}$$

and the corresponding pair-annihilation operator

$$P_j = \sum_{m>0}(-1)^{j-m}a_{j-m}a_{jm}. \tag{2.17}$$

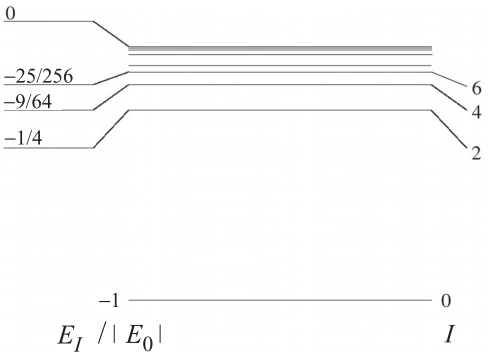

Figure 2.6. Spectrum of two particles moving in a single-j orbital coupled to angular momentum I and interacting through a contact nucleon–nucleon potential.

https://doi.org/10.1017/9781009401920 Published online by Cambridge University Press

The operator $P_j^\dagger$ creates a pair of identical nucleons (say neutrons) with total angular momentum $I = 0$ and the normalized pair state $|(jj)_0\rangle$ can be written as

$$|(jj)_0\rangle = \frac{1}{\sqrt{j+\frac{1}{2}}} P_j^\dagger |0\rangle. \tag{2.18}$$

The pairing force interaction potential is defined as

$$V = -G\ P_j^\dagger P_j, \tag{2.19}$$

and with this potential the interaction energy of a pair is

$$E_I = \begin{cases} -G(j+\frac{1}{2}) & \text{if } I = 0, \\ 0 & \text{if } I \neq 0. \end{cases} \tag{2.20}$$

The pairing potential can be generalized to the case where the nucleon pair can occupy one of several j-orbits. The generalization is

$$V = -\sum_{jj'} G(jj') P_j^\dagger P_{j'}. \tag{2.21}$$

To understand the physical properties of the pairing potential in another way we write

$$a_{jm}^\dagger = a_\nu^\dagger \quad \text{and} \quad (-1)^{j-m} a_{j-m}^\dagger = a_{\bar{\nu}}^\dagger \tag{2.22}$$

The operator a_ν^+ creates a nucleon in a single-particle state $|\nu\rangle = |jm\rangle$ and $a_{\bar{\nu}}^+$ creates an identical nucleon in the time-reversed state $|\bar{\nu}\rangle = (-1)^{j-m}|j\ -m\rangle$ (see Appendix A). The generalized pairing potential is

$$V = -\sum_{\nu\nu'>0} G_{\nu\nu'} P_\nu^\dagger P_{\nu'}, \tag{2.23}$$

where $P_\nu^\dagger = a_\nu^\dagger a_{\bar{\nu}}^\dagger$ and $P_\nu = a_{\bar{\nu}} a_\nu$. The sum in equation (2.23) is over $\nu > 0$ and $\nu' > 0$ which corresponds to m and m' positive. The pairing strength $G_{\nu,\nu'}$ is an amplitude for a nucleon pair in the state $|\nu'\rangle$ and the time-reversed state $|\bar{\nu}'\rangle$ to make a transition to the state $|\nu\rangle$ and its time-reversed state $|\bar{\nu}\rangle$. The pairing force potential produces correlations between pairs of nucleons in time-reversed states.

We finish this section by making an estimate of the pairing force strength parameter G. By comparing equations (2.12) and (2.20) we see that

$$G = V_0 I(j) \approx 1.2\,\text{fm}^{-3}\ V_0/A. \tag{2.24}$$

https://doi.org/10.1017/9781009401920 Published online by Cambridge University Press

To estimate V_0 we use the δ-function potential to relate V_0 to the strength of the shell model single-particle potential $U(r)$ by writing (see equation (A.28))

$$U(r) = -4\pi \int \mathrm{d}^3 r' V_0 \delta(\mathbf{r} - \mathbf{r}')\rho(r') = -4\pi V_0 \rho(r), \tag{2.25}$$

where $\rho(r)$ is the nucleon density inside a nucleus. If $\rho(r) = \rho_0$ is constant then

$$\rho_0 = A/(\frac{4\pi}{3} R_0^3) \simeq 0.17\,\mathrm{fm}^{-3}.$$

Hence

$$V_0 \approx -\frac{U_0}{4\pi\rho_0} = \frac{50\,\mathrm{MeV\ fm}^3}{4\pi \times 0.17} = \frac{294}{4\pi}\,\mathrm{MeV\,fm}^3, \tag{2.26}$$

and (see Section 2.5)

$$G \approx \frac{28}{A}\ \mathrm{MeV}. \tag{2.27}$$

This estimate should not be taken too seriously because the real nucleon–nucleon interaction is much more complicated than that defined in equation (2.10) (see Chapter 8, Section 8.1). We shall, however, see in the following sections that the estimate (2.27) is not unreasonable.

2.4 The degenerate model and quasi-spin

A simple shell model Hamiltonian for a number of identical nucleons outside a closed shell and interacting by a pairing force residual interaction can be written as

$$H = \sum_j N_j \varepsilon_j - \sum_{jj'} G_{jj'} P_j^\dagger\ P_{j'}, \tag{2.28}$$

where ε_j is the energy of the single-particle orbit j while $N_j = a_j^\dagger a_j$. There is a simple limiting case of this Hamiltonian for which the eigenvalues and eigenvectors can be found analytically. This is the degenerate model (see Appendix H), where all the single-particle energies are the same and all the pairing strengths are equal

$$\varepsilon_j = \varepsilon; \qquad G_{jj'} = G. \tag{2.29}$$

In this case several j-levels are degenerate and the total degeneracy is

$$\sum_j (2j+1) = 2\Omega.$$

The Hamiltonian (2.28) can be written as

$$H = \varepsilon N - G S_+ S_- = \varepsilon N - G P^\dagger P, \tag{2.30}$$

https://doi.org/10.1017/9781009401920 Published online by Cambridge University Press

where

$$S_+ = P^\dagger = \sum_{\nu=1}^{\Omega} a_\nu^\dagger a_{\overline{\nu}}^\dagger \quad \text{and} \quad S_- = P = \sum_{\nu=1}^{\Omega} a_{\overline{\nu}} a_\nu, \tag{2.31}$$

and $\hat{N}$ is the number operator for the total number of nucleons outside the closed shells

$$\hat{N} = \sum_{\nu=1}^{\Omega} (a_\nu^\dagger a_\nu + a_{\overline{\nu}}^\dagger a_{\overline{\nu}}). \tag{2.32}$$

The operators S_+, S_- and $\mathrm{S}_z = \frac{1}{2}(\hat{N} - \Omega)$ satisfy the commutation relation

$$\begin{aligned} [S_+, S_-] &= -2S_z = \Omega - \hat{N}, \\ [S_+, S_z] &= S_z, \qquad [S_-, S_z] = -S_z. \end{aligned} \tag{2.33}$$

These are the same as the commutation relation for the angular momentum operators J_+, J_- and J_z and for this reason they are called quasi-spin operators. The quasi-spin method was introduced by Anderson (1958) and used by Ichimura (1964), Lawson(1980) and others. Angular momentum methods can be used to find the eigenvalues and eigenvector of the simplified Hamiltonian (2.28). The operator

$$\mathbf{S^2} = S_+ S_- + S_z(S_z - 1), \tag{2.34}$$

which is the analogue of the square of the total angular momentum, commutes with S_+, S_- and also with H.

The Hamiltonian (2.28) can be written as

$$H = \varepsilon \hat{N} - G\Big(\mathbf{S^2} - S_z(S_z - 1)\Big), \tag{2.35}$$

and the eigenvalues are

$$\begin{aligned} E &= \varepsilon \hat{N} - G\Big(S(S+1) - S_z(S_z - 1)\Big) \\ &= \varepsilon \hat{N} - G(S + S_z)(S - S_z + 1). \end{aligned} \tag{2.36}$$

The standard convention is to write

$$S = \tfrac{1}{2}(\Omega - \upsilon)\,, \tag{2.37}$$

where the quantum number υ is called the seniority, a concept which was introduced by Racah (1942, 1943) in papers on the group theoretical classification of atomic wavefunctions (see de Shalit and Talmi (1963)). One can then write

$$(S + S_z) = \tfrac{1}{2}(\hat{N} - \upsilon) \qquad \text{and} \qquad (S - S_z) = \Omega - \tfrac{1}{2}(\hat{N} + \upsilon), \tag{2.38}$$

https://doi.org/10.1017/9781009401920 Published online by Cambridge University Press

and

$$E = \varepsilon N - E(N, \upsilon),$$

with

$$E(N, \upsilon) = -\tfrac{1}{4}G(N - \upsilon)(2\Omega - N - \upsilon + 2). \tag{2.39}$$

The combination $(S + S_z)$ must be an integer, hence $N - \upsilon$ is an even integer. It is useful to consider the cases where N is even and N is odd.

(i) *N-even*: The ground state has $\upsilon = 0$ and has energy

$$E(N, 0) = -\tfrac{1}{4}G(2N\Omega - N^2 + 2N). \tag{2.40}$$

The first excited state has $\upsilon = 2$ with excitation energy

$$\Delta E = G\Omega = 2\Delta. \tag{2.41}$$

High excited states have $\upsilon = 4, 6, \ldots$

(ii) *N-odd*: The ground state has $\upsilon = 1$ and energy

$$E(N, 1) = -\frac{G}{4}(N - 1)(2\Omega - N + 1), \tag{2.42}$$

and the first excited state has $\upsilon = 3$ again with excitation energy

$$\Delta E = G\Omega = 2\Delta. \tag{2.43}$$

This excitation energy is the pairing energy and the gap parameter Δ is analogous to the gap parameter appearing in the BCS theory of pairing to be discussed in Chapter 3 (see also Appendix G, in particular equation (G.10); see also Appendix H, equation (H.4)).

2.5 Pairing binding energy formula

The lowest eigenvalue of the pairing Hamiltonian (2.25) can be written as

$$E_{\mathrm{g}} = \varepsilon N + \tfrac{1}{4}GN(N - 1) - \tfrac{1}{4}G(2\Omega + 1)[N], \tag{2.44}$$

where

$$\begin{aligned} [N] &= N \quad \text{if} \quad N \text{ is even}, \\ [N] &= N - 1 \quad \text{if} \quad N \text{ is odd}. \end{aligned} \tag{2.45}$$

An accurate binding energy formula (Talmi (1972)) follows from (2.44) by adding an average interaction $\overline{E}$ between all pairs of nucleons. The result is

$$E_{\mathrm{g}} = \varepsilon N + \tfrac{1}{2}\alpha N(N - 1) + \tfrac{1}{2}\beta[N], \tag{2.46}$$

https://doi.org/10.1017/9781009401920 Published online by Cambridge University Press

where

$$\alpha = \tfrac{1}{2}G + \overline{E} \quad \text{and} \quad \beta = -\tfrac{1}{2}G(2\Omega + 1). \tag{2.47}$$

The last term in equation (2.47) is the pairing energy term found in the systematics of nuclear binding energies which depends on the evenness or oddness of the number of protons and neutrons. The large observed odd–even effect is a consequence of the pair correlations induced by the pairing force. Using the expression given in equation (1.28) to extract a pairing energy from equation (2.46), the terms proportional to ε and α cancel and there is a contribution only from the third term and we obtain

$$\Delta = -\tfrac{1}{2}\beta = \tfrac{1}{4}G(2\Omega + 1). \tag{2.48}$$

The empirical fit to Δ given in equation (1.30) can be used to obtain an estimate of the pairing force parameter G.

When Ω is large the value (2.48) for Δ obtained from the binding energy formula given in equation (2.46) is almost equal to the gap parameter (2.43) from excitation energies. They differ by a factor $(1 + 1/2\Omega)$ (see also equation (H.4)).

Lawson (1980) has fitted Talmi's formula to the binding energies of Ca isotopes and obtained

$$\beta = -3.23\,\text{MeV}, \quad \Delta = 1.62\,\text{MeV}. \tag{2.49}$$

Equation (1.30) gives $\Delta = 1.81$ MeV for $A = 44$, which is close to Lawson's number. Using $\Omega = j + \frac{1}{2} = 4$ for the $7/2$ shell, (2.48) and (2.49) yield a value of $G = 0.72$ MeV, which corresponds to a relation $G \approx 31/A$ MeV (see equation (2.27)).

2.6 Quasi-spin wavefunctions

States in a quasi-spin multiplet have the same value of S but different values of S_z. In other words, they have the same seniority but different particle number. The operator S_+ increases S_z by one unit and the particle number by two units without changing S or υ. In a similar way S_- conserves S and υ but reduces the particle number by 2 units.

We consider some special cases. When $\upsilon = 0$ the quasi-spin quantum number $S = \frac{1}{2}\Omega$. This case gives the ground state of even nuclei. The state $|0\rangle$ with $N = 0$ corresponds to $S_z = -S = -\frac{1}{2}\Omega$. The ground state with N nucleons and $\upsilon = 0$ is obtained by creating $N/2$ pairs with the pair-creation operator S_+,

$$|N, 0\rangle = A(N, 0)S_+^{N/2}|0\rangle, \tag{2.50}$$

where $A(N, 0)$ is a normalization constant. Next we consider the case where $\upsilon = 2$ and $S = \frac{1}{2}\Omega - 1$. A state with $S_z = -S$ has nucleon number $N = 2$ and

https://doi.org/10.1017/9781009401920 Published online by Cambridge University Press

the property

$$S_-|N=2,\upsilon=2\rangle=0. \tag{2.51}$$

This state is highly degenerate, because all two-nucleon states where the nucleons are not paired have this property. Each of the unpaired nucleon states leads to a sequence of states with the same seniority and different particle number. Thus the general state with seniority υ should be written as $|N,\upsilon,\alpha\rangle$ where the quantum number α distinguishes between states with the same particle number and the same seniority. The energies do not depend on α and the pair operators S_+ and S_- do not change α. The state with lowest seniority for any particular N and α has $N=\upsilon$ unpaired nucleons and

$$S_-|\upsilon,\upsilon,\alpha\rangle=0. \tag{2.52}$$

The state $|N,\upsilon,\alpha\rangle$ can be obtained from it by adding $(N-\upsilon)/2$ pairs

$$|N,\upsilon,\alpha\rangle=A(N,\upsilon)S_+^{(N-\upsilon)/2}|\upsilon,\upsilon,\alpha\rangle. \tag{2.53}$$

The following physical picture emerges from the arguments in this section. An eigenstate $|N,\upsilon,\alpha\rangle$ of the quasi-spin Hamiltonian has υ unpaired nucleons. The state of these nucleons is labelled by the quantum numbers α. The remaining $N-\upsilon$ nucleons form coherent pairs, with properties contained in the pair-creation operator S_+. The ground state in any nucleus is the state with the maximum number of pairs or alternatively the smallest number υ of unpaired nucleons.

From angular momentum theory (Brink and Satchler (1968)) the matrix elements of the ladder operator S_+ and S_- between normalized states are

$$\begin{aligned}\langle S,S_z+1|S_+|S,S_z\rangle&=\sqrt{(S-S_z)(S+S_z-1)},\\ \langle S,S_z-1|S_-|S,S_z\rangle&=\sqrt{(S+S_z)(S-S_z+1)}.\end{aligned} \tag{2.54}$$

In the following we write the matrix elements in terms of the particle number N and the seniority υ and replace the quasi-spin raising and lowering operators by the pair-creation and pair-annihilation operators $P^+=S_+$ and $P=S_-$ so that they become

$$\begin{aligned}\langle N+2,\upsilon,\alpha|P^\dagger|N,\upsilon,\alpha\rangle&=\tfrac{1}{2}\sqrt{(2\Omega-N-\upsilon)(N-\upsilon+2)},\\ \langle N-2,\upsilon,\alpha|P|N,\upsilon,\alpha\rangle&=\tfrac{1}{2}\sqrt{(N-\upsilon)(2\Omega-N-\upsilon+2)}.\end{aligned} \tag{2.55}$$

The matrix elements (2.55) are called pair-transfer matrix elements and involve the addition or removal of a correlated pair from the initial state. Transitions with large neutron pair-transfer matrix elements have large cross-sections in two-neutron transfer reactions, for example in (t, p) or (p, t) reactions. The cross-section is proportional to the square of the magnitude of the pair-transfer matrix element.

Pairing correlations enhance pair-transfer processes (Broglia *et al.* (1973)). Consider, for example, the pair-addition matrix element between states of seniority $\upsilon = 0$. The basic matrix element is between an initial state with $N = 0$ and a final state with $N = 2$. Its value from equation (2.55) is

$$\langle 2, 0|P^\dagger|0, 0\rangle = \sqrt{\Omega}. \tag{2.56}$$

The corresponding matrix element for adding a pair to the state with $N/2$ correlated pairs is

$$\langle N + 2, 0|P^\dagger|N, 0\rangle = \tfrac{1}{2}\sqrt{(2\Omega - N)(N + 2)}. \tag{2.57}$$

The enhancement of the transfer cross-section is given by

$$\left|\frac{\langle N + 2, 0|P^\dagger|N, 0\rangle}{\langle 2, 0|P^\dagger|0, 0\rangle}\right|^2 = \frac{(2\Omega - N)(N + 2)}{2\Omega} \approx \frac{N + 2}{2}, \tag{2.58}$$

when $2\Omega \gg N$. In this limit the enhancement is proportional to the number of pairs in the final state. The pair-transfer operators S_+ and S_- do not change the seniority. Hence pair-transfer cross-sections which involve a change in seniority should be small (see Chapter, 4, equation (4.52), Fig. 4.2).

2.7 Pairing rotations

The expression (2.39) for the energy in the degenerate pairing model can also be written in terms of the seniority and the number π of pairs missing or in excess of the middle of the shell. The energy eigenvalues in this representation are

$$E(\upsilon, \pi) = -\tfrac{1}{4}G(\Omega - \upsilon)(\Omega + 2 - \upsilon) + G\pi\,(\pi + 1)\,. \tag{2.59}$$

The dependence of the energy and of the transfer matrix element on υ and π exhibits a natural grouping of levels. States with the same seniority and different number of particles can be interpreted as members of a collective band. Their energy displays a smooth dependence on π and they are connected by enhanced and fairly constant matrix elements of the two-nucleon transfer operator. States belonging to different bands are widely separated in energy and are not connected by the pairing operator. In fact the bands resemble those of a rotor and we can call them pairing rotational bands (Bohr (1968), Bes and Broglia (1966), Belyaev (1972)). Later we shall see that they can be interpreted as rotational bands in gauge space (Chapter 4).

Because of nuclear shell structure, the j-shells are bunched together within a major shell, and a general tendency towards the degenerate pairing model is realized in some nuclei, especially in single closed-shell nuclei.

The main term in nuclear binding energies is linear in the number of particles and this must be subtracted before a comparison with pairing rotations can be

made. The experimental binding energies of some Sn-isotopes with this subtraction are displayed in Fig. 4.2 (see Bes and Broglia (1977)). They follow the rotational parabola closely. The available data on two-neutron transfer cross-sections is also given in the same figure. These should be proportional to the squares of the matrix elements of P^+. Two important features of the band description are well satisfied, namely (i) the cross-sections between ground states are much stronger than those linking ground and excited states and (ii) the ground state cross-sections are rather constant (see Appendix H, Section H.3).

2.8 Exact solution of the pairing Hamiltonian

Exact solutions of the pairing problem have been studied by a number of authors (Kerman *et al*. (1960), Lipkin (1960), Nogami (1963, 1964)). In what follows we will discuss an exact solution of the pairing force problem for a non-degenerate set of single-particle levels ε_j and a constant pairing strength $G_{jj'} = G$ (Richardson (1963, 1965, 1977), Richardson and Sherman (1964)). The method did not involve diagonalizing the pairing Hamiltonian, but instead led to a set of non-linear equations for parameters in the pairing wavefunctions. Recently there has been renewed interest in Richardson's method both for condensed matter and nuclear physics applications (Sierra *et al*. (2000), Dukelsky *et al*. (2002)). Also new and efficient algorithms for solving Richardson's equations have been developed. This section introduces Richardson's method and draws attention to some recent developments. Here we quote some of the important equations and refer to the original papers for details.

The Hamiltonian in question is

$$H = \sum_j N_j \varepsilon_j - G \sum_{jj'} P_j^\dagger P_j, \tag{2.60}$$

the exact eigenstates with n pairs being

$$\psi = \prod_\alpha^n \left[\sum_j \frac{1}{2\varepsilon_j - e_\alpha} P_j^\dagger \right] |0\rangle, \tag{2.61}$$

where $|0\rangle$ is a state without any paired particles. This wavefunction has a very interesting structure. It depends on the single-particle energies and on parameters e_α. For example, in a system with 8 pairs distributed among 16 pair levels Richardson's wavefunction for the ground state depends on only 8 parameters. On the other hand, the dimension of the shell model space for the seniority zero levels is about 12 000.

The quantities e_α in the above wavefunction are solutions of a set of n non-linear equations which can be written as

$$\sum_j \frac{d_j}{2\varepsilon_j - e_\alpha} + \sum_{\beta\neq\alpha}^{n} \frac{1}{e_\beta - e_\alpha} + \frac{1}{2G} = 0. \tag{2.62}$$

The parameters $d_j = (\nu_j - \Omega_j)/2$ depend on the pair degeneracies $\Omega_j = (2j + 1)/2$. The seniority ν_j is the number of unpaired particles in the level j. This condition allows for the blocking of single-particle levels by unpaired particles. The notation here is the one used by Dukelsky *et al.* (2002). The total energy of the state ψ is

$$E(e_\alpha) = \langle 0|H|0\rangle + \sum_\alpha e_\alpha. \tag{2.63}$$

In the ground state, pairs fill up the lowest available levels up to the Fermi level when the interaction strength G is zero. When the interaction strength is small the pair-occupation numbers for pair states below the Fermi level are almost unity and the occupation numbers of states above the Fermi level are small. When the interaction strength increases, the occupation numbers change smoothly from unity to zero as ε_j increases through the Fermi energy. The pair-occupation numbers are given by

$$n_j = \frac{\partial E(e_\alpha)}{\partial \varepsilon_j} = \sum_\alpha \frac{\partial e_\alpha}{\partial \varepsilon_j}. \tag{2.64}$$

Differentiating equation (2.62) with respect to ε_j yields a set of linear equations for the derivatives $\partial e_\alpha/\partial\varepsilon_j$ (Richardson (1977)).

The solutions e_α may be real or complex. Complex solutions occur in complex conjugate pairs. Until recently most numerical applications have focused on problems with doubly degenerate single-particle levels and have used Richardson's (1977) technique for solving the equations of the theory, but recently problems of more direct relevance to nuclear structure have been studied. Dukelsky *et al.* (2002) have solved the pairing force problem for ^{114}Sn and ^{116}Sn in a large basis of single-particle states ($d_{5/2}$, $g_{7/2}$, $s_{1/2}$, $d_{3/2}$ and $h_{11/2}$) and calculated the occupation numbers of the single-particle states as a function of the pairing strength G. Their calculations illustrate how the e_α move in the complex plane as G changes. As Richardson's method is exact the energies and occupation numbers vary smoothly with G. More recently Rombouts *et al.* (2004) have found a new method for solving Richardson's equations which is especially convenient for shell model applications where the single-particle levels are degenerate. The studies in these last two references provide interesting insights into the variation of the e_α with the coupling strength G. One disadvantage of Richardson's method is that the parameters e_α do not seem to have a

simple physical interpretation. Another is that, although physical quantities like energies and occupation numbers vary smoothly with the interaction strength G, the e_α can have a singular cusp-like behaviour for certain values of G. Ways of avoiding this problem have been developed by Rombouts *et al.* (2004).

In 1977 Richardson was able to show that his theory was equivalent to the BCS theory in a suitable large N limit by using an analogue with a two-dimensional electrostatic problem. The energy levels j were represented by a system of fixed negative charges d_j and positions ε_j on the y-axis and the e_α were represented by n movable positive charges with positions $x_\alpha,\ y_\alpha$ in the x–y plane equal to the real and imaginary parts of e_α. The attractive coupling strength G was represented by a uniform electric field $1/2G$ acting in the negative y-direction. The real and imaginary parts of the e_α correspond to the x- and y-coordinates of the charges. Equation (2.62) is the equilibrium equation for the forces acting on the positive charge α. The electrostatic potential energy of the movable charges corresponding to the force equation (2.62) is

$$U = \sum_j d_j \ln|2\varepsilon_j - e_\alpha| - \sum_{\alpha\neq\beta} \ln|e_\alpha - e_\beta| + \sum_\alpha e_\alpha/2G. \tag{2.65}$$

Stationary points of the electrostatic energy U are solutions of Richardson's equations. This electrostatic analogy was exploited by Dukelsky *et al.* (2002) in the solution of the pairing problem for ^{114}Sn and ^{116}Sn. It allows one to get a physical picture of the solutions of Richardson's equations. It also points to possible instabilties because the stationary points of U are saddle points rather than minima. Recently Volya *et al.* (2001) have developed a method based on quasi-spin for diagonalizing the Hamiltonian of a system with a constant pairing interaction. It is an alternative to solving Richardson's equations and can be extended to include other terms in the nuclear Hamiltonian (see Volya *et al.* (2002)).

2.8.1 The degenerate case

The pairing force problem for a set of degenerate single-particle levels was solved with the quasi-spin method in Section 2.4. Richardson's equations (2.62) also have a simple solution in this case. The solution gives the energy eigenvalues $E(e_\alpha)$ with seniority υ when there are n pairs in a level with degeneracy Ω. The total number of particles N is related to the number of pairs by $n = (N - \upsilon)/2$. If one takes the energy of the degenerate single-particle state to be $\varepsilon_0 = 0$, equation (2.62) reduces to

$$\frac{\Omega - \upsilon}{2e_\alpha} + \sum_{\beta\neq\alpha} \frac{1}{e_\beta - e_\alpha} + \frac{1}{2G} = 0. \tag{2.66}$$

https://doi.org/10.1017/9781009401920 Published online by Cambridge University Press

Multiplying by e_α and summing over α gives

$$E(e_\alpha) = \sum_1^n e_\alpha = -2G\left(\frac{n(\Omega-\nu)}{2} - \sum_{\beta\neq\alpha}\frac{e_\alpha}{e_\alpha - e_\beta}\right) \tag{2.67}$$

$$= -G\left(n(\Omega-\upsilon) - n(n-1)\right) \tag{2.68}$$

$$= -\frac{G}{4}(N-\upsilon)(2\Omega - N - \upsilon + 2), \tag{2.69}$$

which is identical to equation (2.39) in Section 2.4. In this example the Richardson wavefunction (2.61) does not depend on the individual e_α and reduces to the simple pairing force wavefunction in equation (2.50). When there is more than one single-particle level, as in the case of ^{116}Sn, the interplay between the different e_α and single-particle energies determines the structure of the pairing wavefunction.

https://doi.org/10.1017/9781009401920 Published online by Cambridge University Press

3
The BCS theory

3.1 The BCS wavefunction

To deal with realistic situations, the degenerate model of Section 2.4 has to be generalized for more realistic applications than those discussed in Chapter 2. We need to consider not only the case where several nucleons outside a closed shell occupy non-degenerate single-particle levels, but also the situation where the matrix elements $G_{\nu\nu'}$ of the pairing interaction are not necessarily equal. There is no analytical method for finding the energy levels and wavefunctions of the more general pairing Hamiltonian defined in equation (2.28) but the BCS method gives the solution to this problem in the mean-field approximation (Bardeen, Cooper and Schrieffer (1957a,b)).

One way to generalize the ground-state wavefunction of the degenerate model discussed in Chapter 2 is to define an operator

$$B^\dagger = \sum_\nu g_\nu a_\nu^\dagger a_{\bar{\nu}}^\dagger, \tag{3.1}$$

which creates a correlated pair of nucleons analogous to a Cooper pair. The coefficents g_ν specify its structure. In a spherical nucleus the binding is strongest for an s-pair with total angular momentum zero. In this case the pair-creation operator can be written in terms of the operators $P_j^\dagger$ defined in equation (2.16)

$$B^\dagger = \sum_j g_j \, P_j^\dagger. \tag{3.2}$$

A completely antisymmetric state Φ_n with n pairs outside a closed inert core $|0\rangle$ is approximated by

$$\Phi_n = N_n (B^\dagger)^n |0\rangle, \tag{3.3}$$

https://doi.org/10.1017/9781009401920 Published online by Cambridge University Press

where N_n is a normalization constant. The wavefunction (3.3) can be used as a trial wavefunction in a variational principle and the coefficients g_j treated as variational parameters (de Gennes (1966)). The wavefunction (3.3) is not very easy to work with. One can consider instead a generating function

$$\Phi = C\Pi_{\nu>0}(1 + e^{i\phi} g_\nu a_\nu^\dagger a_{\bar{\nu}}^\dagger)|0\rangle, \tag{3.4}$$

where C is chosen so that Φ is normalized. In equation (3.4) ν refers to the quantum numbers of the single-particle states $|j, m\rangle$ and $\bar{\nu}$ to the time-reversed states $(-1)^{j-m}|j\ -\ m\rangle$ (see Appendix A, Section A.2).

The product in equation (3.4) is over $\nu > 0$, where the notation indicates that only a single term is included for each pair of degenerate levels. For example, in a spherical nucleus the product is taken only over positive values of the magnetic quantum numbers m. Negative values of m are included automatically because $a_\nu^\dagger\, a_{\bar{\nu}}^\dagger$ creates a pair in the state ν and its time reverse $\bar{\nu}$. The state Φ is not an eigenstate of the particle number. However the state Φ_n can be projected out of Φ by picking out the coefficient of $\exp(in\phi)$ in the expansion of (3.4) (see equations (4.45), (4.46) and subsequent discussion).

The BCS wavefunction is obtained by writing Φ in a slightly different way by incorporating the normalization constant into the product (see Appendix G, Section G.4)

$$\Phi = \Pi_{\nu>0}\,(U_\nu + V_\nu\, a_\nu^\dagger\, a_{\bar{\nu}}^\dagger)|0\rangle, \tag{3.5}$$

with

$$V_\nu/U_\nu = e^{i\phi} g_\nu, \quad |U_\nu|^2 + |V_\nu|^2 = 1. \tag{3.6}$$

In general the coefficients U_ν and V_ν are complex but in Sections 3.2–3.7 they are taken to be real quantities restricted only by the normalization condition in equation (3.6), which ensures that Φ is normalized to unity. The phase ϕ will re-emerge in Section 3.8 and will play an important role as a gauge angle (see also Chapters 1, 4 and Appendix I). The wavefunction Φ was introduced by Bardeen, Cooper and Schrieffer (1957a) in their fundamental paper on superconductivity.

The wavefunction Φ does not have a definite number of particles, but it can be written as a linear combination of the normalized eigenstates Φ_n with the particle number $N = 2n$

$$\Phi = \sum_n a_n \Phi_n.$$

The average number of particles is

$$\langle N\rangle = 2\langle n\rangle = 2\sum_{\nu>0} |V_\nu|^2, \tag{3.7}$$

https://doi.org/10.1017/9781009401920 Published online by Cambridge University Press

and the width ΔN of the probability distribution $|a_n|^2$ is given by

$$(\Delta N)^2 = \langle N^2\rangle - \langle N\rangle^2 = 4\sum_{\nu>0} |U_\nu|^2|V_\nu|^2. \tag{3.8}$$

To estimate ΔN assume that the single nucleon states $|\nu\rangle$ (i.e. the states $|jm\rangle$ with positive m) have an average spacing d and are partially occupied over an energy range 2Δ. Then

$$(\Delta N)^2 \simeq 2\,\Delta/d \;\simeq\; \langle N_p\rangle \tag{3.9}$$

where $\langle N_p\rangle$ is the average number of particles occupying single-particle levels with energy lying in this energy range.

In a superconductor $\langle N_p\rangle \gg 1$ so that

$$\langle N\rangle > \langle N_p\rangle \gg \Delta N \gg 1. \tag{3.10}$$

Typical numbers are $\langle N_p\rangle \simeq 10^{16}$, $\Delta N \sim 10^8$. In these circumstances the probability distribution of the number of pairs has a very sharp maximum, but a_n still has a rather smooth dependence on n in the sense that

$$a_n \approx a_{n+p}, \tag{3.11}$$

if p is not too large. This result means that expectation values of simple operators can be calculated accurately with the wavefunction Φ. Suppose F conserves particle number. Then

$$\langle\Phi|F|\Phi\rangle = \sum |a_{N/2}|^2\langle N|F|N\rangle. \tag{3.12}$$

If $\langle N|F|N\rangle$ is slowly varying on the scale of ΔN, then N may be replaced by its average value $\langle N\rangle = N^*$, and the matrix element taken outside the summation so that

$$\langle\Phi|F|\Phi\rangle \approx \langle N^*|F|N^*\rangle, \tag{3.13}$$

In the same way if F acting on a state with N particles gives a state with $N+2$ particles then

$$\begin{aligned}\langle\Phi|F|\Phi\rangle &= \sum_N a^*_{(\frac{N+2}{2})}a_{(\frac{N}{2})}\langle N+2|F|N\rangle \\ &\approx \sum_N |a_{N/2}|^2\langle N^*+2|F|N^*\rangle \\ &\approx \langle N^*+2|F|N^*\rangle.\end{aligned} \tag{3.14}$$

The situation in a nucleus is different because in a typical case $\langle N_p\rangle \simeq 10$ and $\Delta N \sim 3$. The relations (3.10) are not very well satisfied and the

https://doi.org/10.1017/9781009401920 Published online by Cambridge University Press

formulae (3.13) and (3.14) are not so accurate. They are, however, still useful for making semi-quantitative estimates. If more accurate values are needed then there are two ways to proceed. Either the number projected wavefunctions Φ_n must be used, or the particle number fluctuations in Φ must be taken into account (see Chapter 4 and Appendix I, Section I.4, see also Appendix J). Both procedures lead to equivalent results (see Section 6.6). The number projected wavefunctions Φ_n have exactly the form of equation (3.3) with $g_\nu = V_\nu/U_\nu$ (see Section 4.2).

3.2 The energy

The best wavefunction Φ_n of the form (3.3) is obtained by minimizing the expectation value $\langle\Phi_n|H|\Phi_n\rangle$ with respect to the coefficients g_ν. When using the wavefunction Φ the procedure is different because the number of particles is not fixed. The expectation value $\langle\Phi|H|\Phi\rangle$ has to be minimized with a constraint that the average number of particles has a definite value. This can be done by minimizing

$$\langle\Phi|H - \lambda N|\Phi\rangle, \tag{3.15}$$

where λ is a Lagrange multiplier. Physically λ is the Fermi energy. The Hamiltonian H contains the single-particle term and the pairing interaction defined in equation (2.28) and is

$$H = \sum_{\nu>0} \varepsilon_\nu (a^\dagger_\nu a_\nu + a^\dagger_{\bar\nu} a_{\bar\nu}) - \sum_{\nu\nu'>0} G_{\nu\nu'} P^\dagger_\nu P_{\nu'}. \tag{3.16}$$

The expectation value of $H - \lambda N$ can be calculated in a straightforward way using equation (3.5) for Φ. The result is

$$\langle\Phi|H - \lambda N|\Phi\rangle = \sum_{\nu>0} 2V_\nu^2(\varepsilon_\nu - \lambda) - \sum_{\nu\nu'>0} G_{\nu\nu'} U_\nu V_\nu U_{\nu'} V_{\nu'} - \sum_{\nu>0} G_{\nu\nu} |V_\nu|^4. \tag{3.17}$$

Here we have used the relations

$$\langle\Phi|P^\dagger_\nu|\Phi\rangle = \langle\Phi|P_\nu|\Phi\rangle = U_\nu V_\nu, \tag{3.18}$$

where U_ν and V_ν are taken to be real and positive.

The last term proportional to $|V_\nu|^4$ in equation (3.17) is essentially a Hartree–Fock self-consistent field contribution to the single-particle energy. Its main effect is to give a small renormalization of the single-particle energies. It complicates the theory without giving any important physical effects and is usually neglected because the aim of the simple BCS theory is to focus on the effects of pairing (see Appendix G, Section G.3). We omit it in the subsequent

discussions. Any more general interaction would have other Hartree–Fock contributions.

The stationary condition with respect to variations of U_ν and V_ν

$$\delta\langle\Phi|H-\lambda|\Phi\rangle = 0$$

with the constraint $U_\nu\delta U_\nu + V_\nu\delta V_\nu = 0$, coming from the normalization condition on U_ν and V_ν, leads to the equation

$$2(\varepsilon_\nu - \lambda)U_\nu V_\nu \; - \sum_{\nu'>0} G_{\nu\nu'}(U_\nu^2 - V_\nu^2)U_{\nu'}V_{\nu'} = 0. \tag{3.19}$$

This equation can be simplified by setting

$$U_\nu = \sin\,\theta_\nu, \quad V_\nu = \cos\theta_\nu, \tag{3.20}$$

where $0 \le \theta_\nu \le \pi/2$ so that $U_\nu \ge 0$ and $V_\nu \ge 0$. This representation was used by Anderson (1958) in his paper on collective excitations in superconductors.

The normalization condition for U_ν and V_ν is satisfied automatically by this choice and

$$2U_\nu V_\nu = \sin 2\theta_\nu, \qquad |U_\nu|^2 - |V_\nu|^2 = \cos 2\theta_\nu. \tag{3.21}$$

Then the variational equations (3.17) reduce to

$$2(\varepsilon_\nu - \lambda)\tan 2\theta_\nu = \sum_{\nu'>0} G_{\nu\nu'}\sin 2\theta_{\nu'}. \tag{3.22}$$

Equation (3.22) can be written in the form

$$\tan 2\theta_\nu = \frac{\Delta_\nu}{\varepsilon_\nu - \lambda}, \tag{3.23}$$

with

$$\Delta_\nu = \frac{1}{2}\sum_{\nu'>0} G_{\nu\nu'}\sin 2\theta_{\nu'} = \sum_{\nu'>0} G_{\nu\nu'}U_{\nu'}V_{\nu'}. \tag{3.24}$$

The angles θ_ν are real and lie in the range $0 \le \theta_\nu \le \pi/2$. Hence the Δ_ν are real and positive if $G_{\nu\nu'} > 0$.

Equations (3.23) is equivalent to the relations

$$\sin\,2\theta_\nu = \frac{\Delta_\nu}{E_\nu}, \qquad \cos\,2\theta_\nu = \frac{(\varepsilon_\nu - \lambda)}{E_\nu}, \tag{3.25}$$

where

$$E_\nu = \sqrt{(\varepsilon_\nu - \lambda)^2 + \Delta_\nu^2} \; > 0. \tag{3.26}$$

We also have

$$|U_\nu^2| = \frac{1}{2}\left(1 + \frac{\varepsilon_\nu - \lambda}{E_\nu}\right), \qquad |V_\nu^2| = \frac{1}{2}\left(1 - \frac{\varepsilon_\nu - \lambda}{E_\nu}\right). \tag{3.27}$$

Note that $|V_\nu|^2 > \frac{1}{2}$ if the state ε_ν is below the Fermi level λ.
Inserting equations (3.25) into equations (3.24) leads to

$$\Delta_\nu = \frac{1}{2}\sum_{\nu'>0} \frac{G_{\nu'\nu}\Delta_{\nu'}}{\sqrt{(\varepsilon_{\nu'}-\lambda)^2+\Delta_{\nu'}^2}}\,. \tag{3.28}$$

These equations have to be solved simultaneously with

$$N = \langle N\rangle \approx \sum_{\nu>0}\left[1 - \frac{\varepsilon_\nu - \lambda}{\sqrt{(\varepsilon_\nu-\lambda)^2+\Delta_\nu^2}}\right], \tag{3.29}$$

which can be considered as an equation for the Fermi energy λ. This condition comes from the constraint that the mean number of particles in Φ should equal the actual number N in the system. The minimum value of the energy which corresponds to the above set of variational equations is

$$\langle E\rangle = \sum_{\nu>0} 2|V_\nu|^2\varepsilon_\nu - \frac{1}{4}\sum_{\mu\nu>0} G_{\mu\nu}\frac{\Delta_\mu}{E_\mu}\frac{\Delta_\nu}{E_\nu}. \tag{3.30}$$

An important special case is the constant pairing model, where the pairing matrix elements are $G_{\mu\nu} = G$ for single-particle states μ and ν lying in a certain range around the Fermi level, and are zero if μ or ν lie outside that range. In this case the $\Delta_\nu = \Delta$ are all equal and the set of equations (3.28) reduces to a single equation

$$1 = \frac{G}{2}\sum_{\nu>0}\frac{1}{\sqrt{(\varepsilon_\nu-\lambda)^2+\Delta^2}} = \frac{G}{2}\sum_\nu \frac{1}{E_\nu}. \tag{3.31}$$

This is the well-known gap equation which is the starting point of much of the theory of pairing in nuclei. The total energy equation (3.30) simplifies to

$$\langle E\rangle = 2\sum_{\nu>0}|V_\nu|^2\varepsilon_\nu - \frac{\Delta^2}{G}. \tag{3.32}$$

The mean square fluctuation in the nucleon number (3.8) is

$$(\Delta N)^2 = \sum_{\nu>0}\frac{\Delta^2}{E_\nu^2}. \tag{3.33}$$

An alternative approach to BCS theory is given in Appendix G.

3.3 Excited states and quasiparticles

The wavefunction Φ is a linear combination of states with an even number of particles and is appropriate as an approximation to the ground state of a system

https://doi.org/10.1017/9781009401920 Published online by Cambridge University Press

with N even. A possible trial wavefunction for an odd nucleus with a single nucleon in the state μ is

$$\Phi_\mu = \Pi_{\nu>0,\nu\neq\mu}(U_\nu + V_\nu a^\dagger_{\bar{\nu}} a^\dagger_\nu) a^\dagger_\mu |0\rangle. \tag{3.34}$$

The expectation value of $(H - \lambda N)$ in this state can be obtained from equation (3.17) by replacing the term $2\,|V_\nu|^2(\varepsilon_\mu - \lambda)$ in the sum over single-particle energies by $(\varepsilon_\mu - \lambda)$ and by omitting the terms with ν or ν' equal to μ in the potential energy terms. The result reduces to

$$\langle \Phi_\mu | H - \lambda N | \Phi_\mu \rangle - \langle \Phi | H - \lambda N | \Phi \rangle = E_\mu, \tag{3.35}$$

where E_μ is given by equation (3.26). It is the energy needed to place an odd particle in the state μ. The actual situation is more complicated because the argument assumes that adding the extra particle does not change Δ_ν or λ. In fact there are changes in both equation (3.28) and equation (3.29) which determine Δ_ν and λ. The term $\nu = \mu$ is omitted in equation (3.28), and in equation (3.29) N must be replaced by $N + 1$ and the term $\nu = \mu$ omitted in the sum on the right-hand side. For a system like a superconductor, where the fluctuations are small, the changes in λ and Δ_μ are negligible but in a nucleus they can be important. The changes in excitation energies and wavefunctions due to the fact that the state μ is occupied by a single nucleon are called 'blocking effects'.

If blocking effects are neglected, then the wavefunction Φ_μ defined in equation (3.34) can be written in another way by introducing quasiparticle creation and annihilation operators by the Valatin (1958)–Bogoliubov (1958a,b) transformations

$$\alpha^\dagger_\mu = U_\mu a^\dagger_\mu - V_\mu a_{\bar{\mu}}, \tag{3.36a}$$

$$\alpha^\dagger_{\bar{\mu}} = U_\mu a^\dagger_{\bar{\mu}} + V_\mu a_\mu, \tag{3.36b}$$

$$\alpha_{\bar{\mu}} = U_\mu a_{\bar{\mu}} + V_\mu a^+_\mu, \tag{3.36c}$$

$$\alpha_\mu = U_\mu a_\mu - V_\mu a^+_{\bar{\mu}}. \tag{3.36d}$$

In a spherical nucleus the coefficients (U_μ, V_μ) should depend on j but not on m. Using the phases introduced in equation (2.22), equation (3.36a) can be written as

$$\alpha^\dagger_{jm} = U_j a^\dagger_{jm} - V_j (-1)^{j-m} a_{j-m}. \tag{3.37a}$$

Equation (3.36b) becomes

$$(-1)^{j+m}\alpha^\dagger_{j-m} = (-1)^{j+m} U_j a^\dagger_{j-m} + V_j a_{jm}. \tag{3.37b}$$

These two equations are consistent for both positive and negative m.

The quasiparticle operators in equations (3.37) have the properties

$$\Phi_\mu = \alpha_\mu^+ \Phi \,, \tag{3.38a}$$

$$\alpha_\mu \Phi = 0 \,, \tag{3.38b}$$

$$\{\alpha_\mu, \alpha_\nu^+\} = \delta_{\mu\nu}. \tag{3.38c}$$

The operators $\alpha_\mu^\dagger$ and α_μ obey fermion commutation relations and are called quasiparticle creation and annihilation operators. Because of condition (3.38*b*) Φ is the quasiparticle vacuum state, and Φ_μ defined by equation (3.38*a*) is a one-quasiparticle state with a quasiparticle in the state μ. The quasiparticle energy is

$$E_\mu = \sqrt{(\varepsilon_\mu - \lambda)^2 + \Delta^2} \,, \tag{3.39}$$

its minimum value being Δ.

The wavefunction Φ gives an approximate description of the ground state of an even (open shell) nucleus. The one-quasiparticle state $\alpha_\mu^\dagger \Phi$ is an approximation to a state of an odd nucleus. The two-quasiparticle state

$$\Phi_{\mu\nu} = \alpha_\mu^\dagger \alpha_\nu^\dagger \Phi, \tag{3.40}$$

with excitation energy

$$E_\mu + E_\nu \geq 2\Delta, \tag{3.41}$$

is an approximation to an excited state of an even nucleus.

Thus BCS theory with constant pairing predicts that there is an energy gap of at least 2Δ between the ground state and the two-quasiparticle states. For a metal, this implies that electrons can move without resistance, provided the temperature is low so the probability of collisions with an energy exchange of 2Δ is low (see Chapter 1, see also discussion end Section 1.2). The system is then said to be in a superconducting state. In the nuclear case the relation (3.41) implies, for example, that the moment of inertia of a deformed system is considerably smaller than the rigid value, provided that the angular momentum is low so that the effect of the Coriolis force is smaller than 2Δ (see Chapter 6).

The concept of a quasiparticle state is simple only if blocking effects are neglected and the values of Δ and λ are kept constant for the ground state and for excited states. Blocking effects become more and more important as more quasiparticles are excited and in the end are responsible for the phase transition from the superconducting to the normal phase when the temperature, magnetic field or angular velocity are increased beyond critical values. As the temperature of a superconductor is increased, more and more quasiparticles are excited and the pairing gap 2Δ is reduced because of blocking. As the pairing gap is reduced it is easier to excite quasiparticles. At the critical temperature the blocking effects

are catastrophic, the pairing gap goes to zero and superconductivity disappears (see Fig. 1.15).

3.4 The mean-field Hamiltonian

The single-particle states in the Hartree–Fock theory are eigenstates of the mean-field Hamiltonian. The mean-field potential in this Hamiltonian describes the average interaction of a nucleon with all the other nucleons in the nucleus. In the same way it is possible to introduce a mean field to describe the average pairing interaction. In what follows we give a heuristic approach which is specific for the BCS model with a constant pairing strength.

The procedure is to introduce a pair-potential which is analogous to the Hartree–Fock self-consistent field (see also Appendix G)

$$V_{\text{pair}} = -\Delta(P^\dagger + P) \qquad \text{with} \qquad \Delta = G\langle P^\dagger\rangle = G\langle P\rangle. \tag{3.42}$$

In this equation $\langle P^\dagger\rangle$ is shorthand for $\langle\Phi_0|P^\dagger|\Phi_0\rangle$ and $P^\dagger$ is the pair-creation operator

$$P^\dagger = \sum_{\nu>0} a_\nu^\dagger a_{\bar{\nu}}^\dagger. \tag{3.43}$$

With the sign convention of Section 3.2, Δ and $\langle P^\dagger\rangle = \langle P\rangle^*$ are real and positive. A notable feature of the pair-potential (3.42) is that it does not conserve particle number. This is not unexpected because the BCS ground state does not have a good particle number in any case.

The mean-field Hamiltonian is

$$h' = \sum_{\nu>0}(\varepsilon_\nu - \lambda)(a_\nu^\dagger a_\nu + a_{\bar{\nu}}^\dagger a_{\bar{\nu}}) - \Delta(P^\dagger + P). \tag{3.44}$$

When h' is written in terms of the quasiparticle operators (3.36) it reduces to

$$h' = \sum_\nu E_\nu(\alpha_\nu^\dagger\alpha_\nu + \alpha_{\bar{\nu}}^\dagger\alpha_{\bar{\nu}}) + h_0, \tag{3.45}$$

where E_ν are the quasiparticle energies, $\alpha_\nu^\dagger$, α_ν are the quasiparticle creation and annihilation operators and h_0 is a constant. The quasiparticle operators (3.36) satisfy Fermi commutation relations. Hence (see (A.69))

$$[h', \alpha_\nu^\dagger] = E_\nu\alpha_\nu^\dagger \qquad \text{and} \qquad [h', \alpha_\nu] = -E_\nu\alpha_\nu. \tag{3.46}$$

Substituting the expression (3.44) for h' and (3.36) for $\alpha_\nu^\dagger$ we find that (3.44) and (3.45) are consistent provided U_ν and V_ν satisfy the matrix equations

$$\begin{pmatrix} \varepsilon_\nu - \lambda & \Delta \\ \Delta & -(\varepsilon_\nu - \lambda) \end{pmatrix} \begin{pmatrix} U_\nu \\ V_\nu \end{pmatrix} = E_\nu \begin{pmatrix} U_\nu \\ V_\nu \end{pmatrix}. \tag{3.47}$$

https://doi.org/10.1017/9781009401920 Published online by Cambridge University Press

The positive eigenvalue of equation (3.47) is the quasiparticle energy

$$E_\nu = \sqrt{(\varepsilon_\nu - \lambda)^2 + \Delta^2},$$

and the coefficients (U_ν, V_ν) satisfy

$$\Delta V_\nu = (E_\nu - (\varepsilon_\nu - \lambda))\, U_\nu.$$

Combining this with the normalization condition $(U_\nu^2 + V_\nu^2) = 1$ gives

$$U_\nu^2 - V_\nu^2 = \frac{2(\varepsilon_\nu - \lambda)}{\Delta} U_\nu V_\nu, \tag{3.48}$$

which is consistent with equations (3.21) and (3.25) (see Appendix G).

We conclude this section with some general remarks about mean-field potentials. Suppose h' includes a deformation potential as well as a pairing potential. A possible form is

$$h' = \sum_{\nu>0} (\varepsilon_\nu - \lambda)(a_\nu^\dagger a_\nu + a_{\bar\nu}^\dagger a_{\bar\nu}) - K\langle Q\rangle Q - G\big(\langle P^\dagger\rangle P + \langle P\rangle P^\dagger\big). \tag{3.49}$$

The first term in (3.49) contains the single-particle energies in a spherical potential. The second is a quadrupole deformation field proportional to a quadrupole moment operator Q of the nucleons in occupied orbitals. It arises from an effective quadrupole–quadrupole interaction between nucleons and is self-consistent in the sense that it is proportional to the average quadrupole moment of the nucleus (Bohr and Mottelson (1975)). The first two terms in (3.49) together correspond to the Nilsson shell-model potential for a deformed nucleus (Nilsson (1955), Nilsson and Ragnarsson (1995)). The third term is the pairing potential.

The total energy of a nucleus with mean-field Hamiltonian (3.49) is

$$\langle (H - \lambda N)\rangle = \sum (\varepsilon_\nu - \lambda)\langle N_\nu\rangle - \tfrac{1}{2} K\langle Q\rangle.\langle Q\rangle - G\langle P^\dagger\rangle\langle P\rangle. \tag{3.50}$$

The factor $\frac{1}{2}$ in the second term arises because the quadrupole–quadrupole force is a two-body effective interaction and the term $-K\langle Q\rangle.\langle Q\rangle$ counts the energy of each pair twice. A similar argument explains the relation between the coefficients of the pairing terms in the mean field and in the total energy.

3.5 The correlation energy

The pair-correlation energy of a many-particle system is the difference between the energies with and without pairing. If the pairing strength is constant, the energy including pair correlations is

$$E_{\rm p} = \sum_{\nu>0} 2|V_\nu|^2 \varepsilon_\nu - \Delta^2/G, \tag{3.51}$$

https://doi.org/10.1017/9781009401920 Published online by Cambridge University Press

while the energy without correlations is

$$E_0 = \sum_{\nu>0} 2|V_\nu^0|^2 \varepsilon_\nu. \tag{3.52}$$

The occupation probabilities $|V_\nu^0|^2$ in equation (3.52) are unity below the Fermi level and zero above. In both equations (3.51) and (3.52) the Fermi energy ε_F has to be chosen to give the correct number of particles. The correlation energy is

$$E_\mathrm{corr} = E_\mathrm{p} - E_0. \tag{3.53}$$

This energy must be negative if the pairing correlations are to be stable. The correlation energy can also be written as

$$E_\mathrm{corr} = E_\mathrm{s} - \Delta^2/G \tag{3.54}$$

where

$$E_\mathrm{s} = \sum_{\nu>0} 2(|V_\nu|^2 - |V_\nu^0|^2)\varepsilon_\nu. \tag{3.55}$$

The correlation energy can be estimated in a closed form when the single-particle levels which contribute to the pairing are uniformly spaced between $\varepsilon_\mathrm{F} - \Lambda$ and $\varepsilon_\mathrm{F} + \Lambda$ and the pairing strength is constant in this range and zero outside. We choose $\varepsilon_\mathrm{F} = 0$ and denote the single-particle level density by g. The level ν and its time reverse $\bar{\nu}$ are degenerate so the density of levels with $\nu > 0$ is $g/2$. Note that for a uniform level distribution $g/2 = 1/d$, where d is the energy difference between two successive levels (see Fig. 2.3). The gap equation (3.31) can be written as an integral equation

$$\frac{gG}{4} \int_{-\Lambda}^{\Lambda} \frac{\mathrm{d}\varepsilon}{\sqrt{\varepsilon^2 + \Delta^2}} = 1, \tag{3.56}$$

provided that the gap parameter Δ is large compared with the spacing of single-particle levels ($g\Delta \gg 1$). The integral can be evaluated to give

$$\frac{gG}{2} \sinh^{-1}(\Lambda/\Delta) = 1. \tag{3.57}$$

This equation yields a formula for the gap parameter

$$\Delta = \Lambda/\sinh(2/gG) \approx 2\Lambda \mathrm{e}^{-2/gG}, \tag{3.58}$$

where the last formula is valid in the weak coupling limit $2/gG \gg 1$ or $\Delta \ll \Lambda$. With the same approximation the single-particle part of the correlation energy

https://doi.org/10.1017/9781009401920 Published online by Cambridge University Press

is given by

$$E_s = \frac{g}{2}\left[\int_{-\Lambda}^{\Lambda}\left(1 - \frac{\varepsilon}{\sqrt{\varepsilon^2+\Delta^2}}\right)\varepsilon d\varepsilon - 2\int_{-\Lambda}^{0}\varepsilon d\varepsilon\right]$$
$$= \frac{g}{2}\left[\Lambda^2 - \Lambda\sqrt{\Lambda^2+\Delta^2}\right] + \Delta^2/G$$
$$\approx \Delta^2/G - g\Delta^2/4, \qquad \text{if} \qquad \Lambda \gg \Delta. \tag{3.59}$$

Substituting this expression in equation (3.54) gives the BCS expression for the correlation energy

$$E_{\text{corr}} = -g\frac{\Delta^2}{4}\,. \tag{3.60}$$

In the case of a uniform level ($g = 2/d$) distribution $E_{\text{corr}} = -\Delta^2/2d$.

At this stage we give some estimates of the parameters in equation (3.58). The total level density for neutrons and protons for a nucleus with $N = Z$ in the Fermi gas model is

$$g_n + g_p = \frac{3A}{2\varepsilon_F} \approx \frac{A}{25}\,\text{MeV}^{-1}, \tag{3.61}$$

making use of the Fermi energy $\varepsilon_F = 37$ MeV. Empirical evidence shows that the value given in equation (3.61) is an underestimate. A better estimate which takes surface effects into account (see Chapter 9 and Appendix B) is $g_n + g_p = A/16\,\text{MeV}^{-1}$ (see Bohr and Mottelson (1969), Bortignon, Bracco and Broglia (1998)). In this section we use

$$g_n = N/16\,\text{MeV}^{-1}, \qquad g_p = Z/16\,\text{MeV}^{-1}, \tag{3.62}$$

for the neutron and proton level densities (see Section 8.2).

The monopole pairing force constants used in the rare earth region to reproduce the empirical value of the pairing gap are (Nilsson and Ragnarsson (1995), see also equation (2.27))

$$G_n = 20.5/A\,\text{MeV}, \qquad G_p = 26/A\,\text{MeV}. \tag{3.63}$$

The parameter combination in the gap equation (3.58) is $2/gG$. In the rare earth region this combination does not have a strong A dependence and the values for neutrons and protons are

$$2/(g_nG_n) = 2.7, \qquad 2/(g_pG_p) = 2.9. \tag{3.64}$$

They are consistent with the weak coupling limit (3.58). Bohr and Mottelson (1975) choose $\Lambda = \hbar\omega_c$ where $\hbar\omega_c = 41A^{-1/3}$ MeV is the major shell spacing in the harmonic oscillator shell model. For a nucleus with $A = 160$ we have $\Lambda = 7.6$ MeV which leads to a gap parameter $\Delta_n = 1.0$ MeV for neutrons. The

https://doi.org/10.1017/9781009401920 Published online by Cambridge University Press

global empirical formula given in equation (1.28) gives $\Delta_n = 0.95\,\text{MeV}$ which is close to the value calculated from the gap equation.

For the same mass number the numerical values of the terms in (3.59) for one type of particle are

$$\Delta^2/G \approx 7.8\,\text{MeV}, \qquad g\Delta^2/4 \approx 1.5\,\text{MeV},$$

where the values of G_n and g_n from equations (3.63) and (3.62) have been used. In this last equation the empirical value $N = 0.6A$ was used.

The total pairing energy Δ^2/G is quite large but in the correlation energy it is partially cancelled by a similar term describing the fact that, in the BCS ground state, particles moving in levels close to the Fermi energy are partially excited across the Fermi surface, in keeping with the fact that V_ν^2 changes smoothly from 1 to 0 around λ, being equal to $\frac{1}{2}$ at the Fermi energy. The overall result $E_{\text{corr}} \approx -g\Delta^2/4 \approx -1.5\,\text{MeV}$, corresponds to a considerably smaller (in absolute value) contribution.

3.6 Pairing correlations in the wavefunction

If the nucleus has many nucleons outside closed shells the pairing interaction can produce strong correlations in the wavefunction. The matrix element

$$\alpha_0 = \langle \Phi | P^\dagger | \Phi \rangle \tag{3.65}$$

of the pair addition operator $P^\dagger$ is non-zero and gives a measure of the pair correlations in the BCS wavefunction. The operator $P^\dagger$ increases the number of particles by 2 and, according to the arguments in Section 3.1,

$$\alpha_0 = \langle \Phi | S_+ | \Phi \rangle \approx \langle N^* + 2 | P^\dagger | N^* \rangle. \tag{3.66}$$

The matrix element (3.65) can be easily calculated and the result is

$$\alpha_0 = \sum_{\nu>0} U_\nu V_\nu = \frac{\Delta}{2} \sum_{\nu>0} \frac{1}{E_\nu} = \frac{\Delta}{G}. \tag{3.67}$$

Because $U_\nu V_\nu$ is peaked at the Fermi energy, one can replace the state dependent value of this quantity by $\frac{1}{2}$. Consequently $2\alpha_0 = \Omega$.

Thus, the quantity α_0 can be used to give an estimate of the number of correlated pairs in the BCS ground state.

In the rare earth region ($A \sim 170$) $G_n \approx 0.12\,\text{MeV}$, $G_p \approx 0.15\,\text{MeV}$ and $\Delta_n \approx \Delta_p \approx 0.92\,\text{MeV}$ and the pairing-correlation parameters for neutrons and protons are estimated as

$$(\alpha_0)_n \approx 8, \qquad (\alpha_0)_p \approx 6. \tag{3.68}$$

Thus the number of correlated neutron and proton pairs is small, and pairing is a relatively weak effect in nuclei. Consequently, one expects that pairing fluctuations, which play a minor role in macroscopic systems, become important in nuclei (see Chapter 5 and Section 8.4).

https://doi.org/10.1017/9781009401920 Published online by Cambridge University Press

3.7 The degenerate model in the BCS approximation

The pairing model with degenerate single-particle levels was solved analytically by the quasi-spin method in Section 2.4. Expressions were given for the energy levels, wavefunctions, and pair-distortion matrix elements. In this section we test the accuracy of the BCS method by comparing the BCS approximation with the exact results of the quasi-spin approach (see also Appendix H).

The exact ground-state energy of a system with an even number of particles is given in equation (2.39) as

$$E_{\rm ex} = N\varepsilon - \tfrac{1}{4}GN(2\Omega - N + 2), \tag{3.69}$$

where 2Ω is the degeneracy of the level with energy ε. To obtain the BCS approximation to the ground-state energy we note that, as all the single-particle energies ε_ν are equal, the quasiparticle energies E_ν and occupation probabilities $|V_\nu|^2$ are independent of ν. The gap equation (3.31) reduces to a simple algebraic equation for the quasiparticle energy

$$E = \sqrt{(\varepsilon - \lambda)^2 + \Delta^2} = \tfrac{1}{2}\Omega G. \tag{3.70}$$

The constraint (3.7) on the total particle number gives the BCS occupation probability

$$V^2 = \frac{N}{2\Omega}. \tag{3.71}$$

The Fermi energy and gap parameter are given by

$$\varepsilon - \lambda = \tfrac{1}{2}G(\Omega - N), \quad \Delta^2 = \tfrac{1}{4}G^2N(2\Omega - N). \tag{3.72}$$

Using these in equation (3.32) for the BCS ground-state energy we get

$$E_{\rm BCS} = N\varepsilon - \tfrac{1}{4}GN(2\Omega - N). \tag{3.73}$$

To assess the accuracy of the BCS method one can look at the ratio

$$\frac{E_{\rm ex} - E_{\rm BCS}}{E_{\rm ex} - N\varepsilon} = \frac{2}{2\Omega - N + 2}. \tag{3.74}$$

As an example, one can consider the case of ^{116}Sn where there are $N = 16$ valence neutrons occupying the orbits $g_{7/2}$, $h_{11/2}$, $d_{5/2}$, $d_{3/2}$ and $s_{1/2}$ (see Fig. 10.2). If all these levels are assumed to be degenerate then $\Omega = 16$ and the ratio (3.74) is 0.11 or 11%.

The first excited states in the exact solution are the seniority $v = 2$ states while in the BCS method they are the two-quasiparticle states. The excitation energy is $\Delta E = G\Omega$ in both cases. The pair-transfer amplitude is the BCS pair-distortion parameter (3.67)

$$\alpha_0 = \Delta/G = \tfrac{1}{2}\sqrt{N(2\Omega - N)},$$

https://doi.org/10.1017/9781009401920 Published online by Cambridge University Press

which agrees well with (2.57) if N and Ω are reasonably large. For the ^{116}Sn example the ratio $\alpha_0/\langle N+2,0|P^+|N,0\rangle$ is equal to $(16/18)^{1/2}=0.94$, implying a 6% error of the BCS estimate. However, the measurable quantity is the ratio of the two-particle transfer cross-sections. In this case, the ratio is $16/18=0.89$, corresponding again to an 11% error. Note that if one considers the Hartree–Fock self-consistent field contribution in equation (3.17), (3.73) becomes $E_{\rm BCS}=NE-\frac{1}{4}GN(2\Omega-N+N/\Omega)$. The ratio (3.74) is equal to $(2-N/\Omega)/(2\Omega-N+2)$ (Lawson (1980)) which has the value 0.06 for $\Omega=N=16$.

3.8 Gauge invariance

There is a close analogy between the BCS wavefunction for a system with pairing and the Hartree–Fock wavefunction of a deformed nucleus (Bes and Broglia (1966)). In both cases there is a broken symmetry, which is the topic of discussion of the next chapter, and which is briefly touched upon in this section. First we recall some properties of a deformed Hartree–Fock wavefunction.

The Hartree–Fock method approximates the ground-state wavefunction of a nucleus by a Slater determinant which minimizes the expectation value of the Hamiltonian (see Appendix A). The nuclear Hamiltonian is rotationally invariant and its exact eigenstates are also eigenstates of angular momentum. On the other hand, in many cases, the Hartree–Fock state is deformed and is not an angular momentum eigenstate. Symmetry is broken because the Hartree–Fock wavefunction has a lower symmetry than the original Hamiltonian. Rotational symmetry is still present in the sense that there are many degenerate solutions of the Hartree–Fock equations. Rotating one solution yields another with the same energy. States with definite angular momentum, which are approximations to the states in the lowest rotational band of the nucleus, can be projected out of a deformed Hartree–Fock wavefunction. The Hartree–Fock state is called the intrinsic state of the rotational band (Nilsson (1955), Bohr and Mottelson (1975), see equation (3.50)).

The BCS wavefunction has analogous properties. The pairing Hamiltonian conserves particle number and if N is the particle number operator

$$[N,H]=0 \quad \text{or} \quad U^\dagger(\chi)HU(\chi)=1, \tag{3.75}$$

where the unitary gauge operator is defined as

$$U(\chi)=\mathrm{e}^{-\mathrm{i}N\chi/2}. \tag{3.76}$$

The relations (3.75) express the fact that H is invariant for rotations in gauge space. The general BCS wavefunction is

$$\Phi=\Pi_{\nu>0}(U_\nu+\mathrm{e}^{\mathrm{i}\phi}V_\nu a_\nu^\dagger a_{\bar\nu}^\dagger)|0\rangle, \tag{3.77}$$

https://doi.org/10.1017/9781009401920 Published online by Cambridge University Press

where U_ν and V_ν are chosen to be real. The gauge operator acting on Φ gives

$$U(\chi)\Phi = \Pi_{\nu>0}(U_\nu + e^{i(\phi-\chi)}V_\nu a_\nu^\dagger a_{\bar{\nu}}^\dagger)|0\rangle. \tag{3.78}$$

The BCS state Φ does not have a definite particle number and can be called a 'deformed state in gauge space'. The angle ϕ specifies the orientation of the BCS state Φ in gauge space and $U(\chi)$ rotates it through an angle χ in that space. Invariance of H for rotations in gauge space implies that the energy expectation value is independent of ϕ or χ. The BCS wavefunction (3.77) can be thought of as being deformed in gauge space. The α_0 in equation (3.65) gives a measure of the deformation. For this reason it is sometimes called the pair-distortion parameter.

As discussed in Section 3.1 the BCS state can be written as a linear combination of normalized states Φ_n with a definite number of pairs $n = N/2$,

$$\Phi = \sum a_n e^{in\phi}\Phi_n. \tag{3.79}$$

Projection of a state with definite particle number n means to pick out the component Φ_n from Φ. It is the term with coefficient proportional to $e^{in\phi}$ in the expansion (3.79).

The gauge angle χ is the conjugate variable to the number n of pairs. One can transform from a pair number to a gauge angle representation by making a Fourier transformation (see discussion after equation (4.46), Section 4.2)

$$\Phi(\chi) = \sum_n e^{in\phi}\Phi_n. \tag{3.80}$$

Then the gauge angle χ is a dynamical variable conjugate to the number of pairs n. In the gauge angle representation the operator can be written as

$$n = -i\frac{\partial}{\partial\chi}. \tag{3.81}$$

There is an uncertainty relation between χ and n

$$\Delta\chi\,\Delta n \sim 1, \tag{3.82}$$

which has to be understood with the same qualifications as for the angle – angular momentum uncertainty relation because χ is restricted to the range $0 \le \chi < 2\pi$. These subjects are taken up in further detail in the next chapter (see also Appendix I).

3.9 Matrix elements of one-body operators

Formulae for matrix elements of one-body operators in the BCS theory are derived in Lane (1964), Kisslinger and Sorensen (1963), Rowe (1970), Bes and Sorensen (1969), Ring and Schuck (1980), Bohr and Mottelson (1975). For completeness we summarize some of the important results here. In second

quantization the one-body operator $\hat{F}$ is

$$F = \sum_{\mu\nu} \langle \mu | F | \nu \rangle a_\mu^\dagger a_\nu. \tag{3.83}$$

Expressing the particle-creation and annihilation operators in terms of quasiparticle operators this equation becomes

$$\begin{aligned} F &= \sum_{\mu\nu} \langle \mu | F | \nu \rangle \left(U_\mu \alpha_\mu^\dagger + V_\mu \alpha_{\bar{\mu}} \right) \left(U_\nu \alpha_\nu + V_\nu \alpha_{\bar{\nu}}^\dagger \right) \\ &= F_{0\mathrm{qp}} + F_{1\mathrm{qp}} + F_{2\mathrm{qp}} + F_{2\mathrm{qp}}^\dagger. \end{aligned} \tag{3.84}$$

Here

$$\begin{aligned} F_{0\mathrm{qp}} &= \sum_{\nu} \langle \nu | F | \nu \rangle V_\nu^2, \\ F_{1\mathrm{qp}} &= \sum_{\mu\nu} \langle \mu | F | \nu \rangle \left(U_\mu U_\nu \alpha_\mu^\dagger \alpha_\nu - V_\mu V_\nu \alpha_{\bar{\nu}}^\dagger \alpha_{\bar{\mu}} \right), \\ F_{2\mathrm{qp}} &= \sum_{\mu\nu} \langle \mu | F | \nu \rangle U_\mu V_\nu \alpha_\mu^\dagger \alpha_{\bar{\nu}}^\dagger, \end{aligned} \tag{3.85}$$

where the Bogoliubov amplitudes U_ν and V_ν are real.

The operator $F_{0\mathrm{qp}}$ does not depend on the quasiparticle operators and may have a non-zero expectation value in the BCS vacuum state $|\mathrm{BCS}\rangle$. The $F_{1\mathrm{qp}}$ operator has matrix elements between one-quasiparticle states while the operators $F_{2\mathrm{qp}}$ and $F_{2\mathrm{qp}}^\dagger$ create and annihilate pairs of quasiparticles respectively.

When the operator F has the time-reversal properties $(\tau^{-1} F \tau)^\dagger = -cF$ then the analysis carried out in Appendix A, Section A.2 shows that

$$\langle \bar{\mu} | F | \bar{\nu} \rangle = -c \langle \nu | F | \mu \rangle \qquad \text{and} \qquad \langle \mu | F | \bar{\nu} \rangle = c \langle \nu | F | \bar{\mu} \rangle. \tag{3.86}$$

Using these relations we get

$$F_{0\mathrm{qp}} = \sum_{\nu>0} V_\nu^2 \left(\langle \nu | F | \nu \rangle + \langle \bar{\nu} | F | \bar{\nu} \rangle \right) = \sum_{\nu>0} V_\nu^2 (1 - c) \langle \nu | F | \nu \rangle. \tag{3.87}$$

The expression for $F_{1\mathrm{qp}}$ can be simplified by making a change of summation variables $\bar{\nu} \to \mu$ and $\bar{\mu} \to \nu$ in the second term. It reduces to

$$F_{1\mathrm{qp}} = \sum_{\mu\nu} \langle \mu | F | \nu \rangle \left(U_\mu U_\nu \alpha_\mu^\dagger \alpha_\nu + c V_\mu V_\nu \alpha_\nu^\dagger \alpha_\nu \right). \tag{3.88}$$

In a similar way

$$F_{2\mathrm{qp}} = \sum_{\mu>\nu} \left(U_\nu V_\mu - c U_\mu V_\nu \right) \langle \mu | F | \bar{\nu} \rangle \alpha_\mu^\dagger \alpha_\nu^\dagger. \tag{3.89}$$

Matrix elements of F between states with the same number of quasiparticles or with quasiparticle number differing by 2 can be calculated from these

https://doi.org/10.1017/9781009401920 Published online by Cambridge University Press

expressions. Pair correlations can enhance or suppress matrix elements depending on the time-reversal properties of the operator.

One example is the influence of pairing correlations on matrix elements of single-particle multipole operators in one-quasiparticle states in a spherical nucleus. The reduced matrix element of the operator $F_{\lambda\mu}$ in a quasiparticle state $\bar{j}$ is related to the corresponding single-particle reduced matrix element by

$$\langle \bar{j} \| F_\lambda \| \bar{j} \rangle = \left(U_j^2 + c V_j^2 \right) \langle j \| F_\lambda \| j \rangle. \tag{3.90}$$

The quadrupole operator $Q_{2\mu}$ is time-even and has $c = -1$. Hence quadrupole matrix elements in one-quasiparticle states are modified by a factor $\left(U_j^2 - V_j^2 \right)$. This factor is positive if the quasiparticle state is above the Fermi level and negative if it is below. On the other hand the magnetic moment operator $M_{1\mu}$ is time-odd, has $c = 1$ and the corresponding factor is $\left(U_j^2 + V_j^2 \right) = 1$. Thus the magnetic moment of a quasiparticle state is the same as for a particle state.

Another example is the effect of pairing on the moment of inertia of a deformed nucleus. The cranking moment of inertia in a nucleus with pairing is (Belyaev (1959), Migdal (1959), Bohr and Mottelson (1975))

$$\mathcal{I} = 2\hbar^2 \sum_{\mu\nu} \frac{|\langle \mu\nu | j_y | BCS \rangle|^2}{E_\mu + E_\nu}, \tag{3.91}$$

where the sum is taken over two-quasiparticle states. Using the relation between two-quasiparticle matrix elements and particle matrix elements we have

$$|\langle \mu\nu | j_y | BCS \rangle|^2 = |\langle \mu | j_y | \bar{\nu} \rangle|^2 \left(U_\mu V_\nu - U_\nu V_\mu \right)^2 \tag{3.92}$$

because j_y is a time-odd operator and $c = 1$. The cranking formula gives a moment of inertia equal to the rigid value when there are no pairing correlations. Pairing correlations reduce the moment of inertia partly because the energy denominators are increased (the quasiparticle excitation energies are larger than the corresponding particle excitations) and partly because the two-quasiparticle matrix elements of j_y are smaller than the corresponding particle matrix elements.

3.10 Pairing and isospin

An important nuclear symmetry property manifests itself in the conservation of isospin: a nuclear state is characterized by the total isospin quantum number as well as by the total angular momentum, the number of pairs of particles, etc. The existence of the isospin symmetry requires that the Hamiltonian describing the nuclear system should be invariant under rotations in isospace. The isospin symmetry is violated by a pairing interaction acting only between identical nucleons,

as was the case considered in the previous sections. Thus an invariant pairing force must, in addition to the nn and pp terms, contain pn components. One may distinguish between an isoscalar ($T = 0$) and an isovector ($T = 1$) pairing interaction. The isoscalar pairing interaction acts only between np pairs coupled to $T = 0$. The isovector interaction has equal matrix elements between pp, np and nn pairs coupled to $T = 1$ (see e.g. Bohr (1968), Nathan (1968), Bayman *et al*. (1969), Bes *et al*. (1977), Dussel *et al*. (1970), Garrido *et al*. (1999)).

Parikh (1965) gave an exact solution of the pairing problem for a system of neutrons and protons in a degenerate single-particle level interacting with an isovector pairing force by generalizing the quasi-spin methods using identical nucleons. The role of the seniority υ is played by two quantum numbers, namely the seniority itself and the reduced isospin t (which is the isospin of the unpaired nucleons). Within each representation (υ, t), the states are labelled by the total number of nucleons N, the total isospin T and its z-component T_z. The energy eigenvalues are given by

$$E(\upsilon, t; N, T) = -\frac{G_1}{2}\left[N\left(\Omega - \frac{N-6}{4}\right) - \upsilon\left(\Omega - \frac{\upsilon - 6}{4}\right) + t(t+1) - T(T+1)\right] \tag{3.93}$$

This expression reduces to equation (2.39) in the case of identical nucleons by putting $T = N/2$ and $t = \upsilon/2$. If $\upsilon = 0$ only even (odd) values of T are allowed if the number of pairs is even (odd).

3.10.1 $T = 0$ and $T = 1$ pairing co-existence

All the discussion in the previous sections of this chapter relate to isovector pairing. The strength of the two-body nucleon–nucleon interaction is comparable in $T = 0$ and $T = 1$ states so there is no *a priori* reason why pairing should be more important for isovector pairs than for isoscalar pairs. To give an idea of the issues involved we refer to a selection of the many papers written on this subject.

Engel *et al*. (1997) examined the possible co-existence of isovector and isoscalar pairing in an exactly solvable model. They considered a degenerate model with a Hamiltonian containing both isovector ($T = 1,\ S = 0$) and isoscalar pairing ($T = 0,\ S = 1$) pairing. The Hamiltonian contains a parameter x which fixes the relative strengths of the isovector and isoscalar pairing; $x = -1$ is pure isovector pairing, $x = 1$ is pure isoscalar while for $x = 0$ the isovector and isoscalar strengths are equal. They calculated the overlap between the exact ground state and the pure isovector spin-singlet paired state as a function of x in a $T = 0$ nucleus with an even number of pairs. They found that there is a

https://doi.org/10.1017/9781009401920 Published online by Cambridge University Press

relatively sharp phase transition as x increases through zero. The ground state is a rather pure isovector paired state for $x < 0$ and changes to an isoscalar paired state as x increases through zero. There is a strong mixing for $x = 0$ and for this value of x the Hamiltonian has Wigner SU(4) supermultiplet symmetry.

Goodman (1998) solved the isospin generalized BCS and Hartree–Fock–Bogoliubov equations for the ground states of even–even $N = Z$ nuclei with mass numbers $A = 76$–96. His calculations included both isovector and isoscalar pairing. He found a transition from isovector pairing at the beginning of the isotope sequence to isoscalar pairing near the middle of the sequence. These results indicate that $T = 0$ and $T = 1$ pairing can co-exist and that $T = 0$ pairing can be dominant in some nuclei. This result is consistent with the findings of Engel *et al*. (1997). In a recent paper Bes *et al*. (2000) found a more general class of solutions to the BCS equations in the presence of isovector and isoscalar pairing correlations.

One indication of np pairing comes from the Wigner energy. This is an additional binding energy of an $N = Z$ nucleus relative to its neighbours which appears as a spike in the isobaric mass parabola as a function of $T_3 = |N - Z|/2$. Satula *et al*. (1997a) used a standard form for the Wigner energy and extracted its parameters from experimental binding energies. Then they made shell model calculations in the s-d and p-f shells using standard interactions which include both $T = 1$ and $T = 0$ components. The parameters of the Wigner energy extracted from the shell model binding energies fit the experimental values (see also Goriely *et al*. (2001, 2002)). The authors repeated the shell model calculations with the $T = 0$ components removed. By comparing the results of the two calculations they found that most of the Wigner energy in the shell model calculations comes from the $T = 0$ neutron–proton interaction and that the interaction between deuteron-like ($J = 1$) and 'stretched' ($J_{\max}$) pairs are of comparable importance. Within this context, it may be possible to create a $T = 0$ nuclear vortex (see Appendix K, and Ramon Wyss, *Key Topics in Nuclear Structure*, Abstracts, Paestum 23–27 May 2004, p. 73, as well as Satula and Wyss (2001a) and Frauendorf and Sheikh (2000)).

Satula and Wyss (1997b) studied the competition between $T = 0$ and $T = 1$ pairing in $N \approx Z$ nuclei in a cranked mean field calculation (see also Satula and Wyss (2001b)). They found that the sudden phase transition between $T = 0$ and $T = 1$ pairing is a generic feature of the BCS approximation for $N = Z$ nuclei. This phase transition is smeared out if a good particle number is projected out by the Lipkin (1960), Nogami (1964) method. Then the $T = 0$ and $T = 1$ pairing correlations can co-exist even at non-zero rotational frequencies. For $N \neq Z$ nuclei $T = 0$ and $T = 1$ pairing correlations can co-exist even in the BCS approximation but are confined to a narrow region along the $N = Z$ line. The additional binding arising from these correlations can be viewed as a microscopic origin of the Wigner energy in even nuclei.

4

Spontaneous symmetry breaking

4.1 General background

As already mentioned in previous chapters, the nuclear structure exhibits many similarities with the electron structure of metals. In both cases, one is dealing with systems of fermions which may be characterized in a first approximation in terms of independent particle motion. However in both systems, important correlations in the particle motion arise from the action of the forces between particles. In particular, it is well established that nucleons moving close to the Fermi energy in time-reversal states have the tendency to form Cooper pairs which eventually condense (Bohr, Mottelson and Pines (1958), Bohr and Mottelson (1975)). This phenomenon, which has its parallel in low-temperature superconductivity, modifies the structure of nuclei in an important way. In particular it influences the occupation numbers of single-particle levels around the Fermi surface (Chapter 3), the moment of inertia of deformed nuclei (Chapter 3), the lifetime of alpha and cluster decay and fission processes (Chapter 7), the depopulation of superdeformed configurations (Chapter 6) and the cross-sections of two-nucleon transfer reactions (Chapter 5).

While one does not expect the transition between the normal and the superfluid phases of the atomic nucleus to be sharp because of finite size effects and the central role played by fluctuations (see Chapter 6), there is a strong analogy between phenomena in nuclei and the corresponding phenomena in bulk superconductors. Spontaneous symmetry breaking is important in both nuclei and superconductors. We focus our attention on one of the fingerprints of the broken symmetry, namely the consequences it has for the energy level spectra of the systems.

The phenomenon of spontaneous symmetry breaking had been known for a long time before the formulation of the BCS theory of superconductivity in 1957. An example is the Jahn–Teller effect in solid state physics; if the symmetry of

a crystal is such that ground-state degeneracy of electron states at a crystal site is not the Kramers minimum then it is energetically favourable for the crystal to distort in such a way as to lower the symmetry enough to remove the degeneracy. The same phenomenon is the origin of deformed shapes in nuclei (see Reinhardt and Otten (1984)). The Hartree–Fock single-particle states in a spherical potential for a nucleus with neutron and proton numbers far from closed shells are degenerate or almost degenerate. The energy is reduced by allowing the self-consistent potential to deform to remove the degeneracy. Even though the nuclear Hamiltonian is rotationally invariant the Hartree–Fock wavefunction of a deformed nucleus is not an eigenstate of angular momentum. The theory produces a nucleon density distribution which is deformed and has a definite orientation in space. A rotation applied to a Hartree–Fock state produces an equivalent state with the same energy as the original state. This idea is the basis of Bohr and Mottelson's (1953) and Nilsson's (1955) theory of deformed nuclei.

The situation is similar with Bardeen, Cooper and Schrieffer's (1957a,b) theory of superconductivity. The Hamiltonian of the BCS theory commutes with the electron number operator $\hat{N}$. The ground state of a finite superconductor should be an eigenstate of $\hat{N}$ but the BCS wavefunction does not have this property. A gauge transformation applied to the BCS ground state produces another, different, BCS state with the same ground-state energy. There are an infinite number of equivalent states connected by gauge transformations. The BCS theory predicts that there is an energy gap 2Δ between the ground state and excited two-quasiparticle states. Anderson (1958) investigated corrections to the BCS theory using the random phase approximation (RPA). He found a dispersion relation predicting a phonon-like collective mode related to zero sound with energies within the BCS energy gap. He related this collective excitation to the gauge symmetry breaking. Similar results were obtained by a different method at about the same time by Bogoliubov *et al*. (1958). His approach was based on a development of his quasiparticle theory (Bogoliubov (1958b)).

The connection between the gauge symmetry breaking and Anderson's collective states (Anderson (1958)) was studied in more detail by Nambu (1959). He argued that the phonon-like collective states are essential to the gauge-invariant character of the theory and that they are a necessary consequence of the gauge invariance. He showed that gauge invariance, the energy gap and the collective states are related to each other. In a subsequent paper Nambu (1960) extended his ideas to a γ_5-invariant theory with zero-mass fermions. There γ_5-symmetry breaking (or chiral symmetry breaking) leads to non-zero baryon masses (analogous to the BCS energy gap) and zero-mass pseudoscalar mesons (analogous to Anderson's collective states). Nambu's ideas were incorporated in the Nambu, Jona-Lasinio (1961a,b) model of baryons and mesons which was motivated by the BCS theory of superconductors.

Nambu's (1959) paper is based on a mean field generalization of the BCS theory with RPA corrections (see also Eguchi and Nisijima (1995)). Goldstone (1961) extended Nambu's work in a paper on symmetry breaking with the title 'Field theories with "superconductor" solutions'. He considered several simple covariant models and conjectured that, whenever the original Lagrangian has a continuous symmetry group and the new solutions have a reduced symmetry, then the theory must contain massless bosons. The models he considered were renormalizable, so that Goldstone's result might be very general, and apply not only to approximate mean field solutions, but also to exact solutions.

Goldstone's conjecture was put on a firmer footing by Goldstone, Salam and Weinberg (1962). They proved by three different methods that, if there is a continuous symmetry transformation under which the Lagrangian is invariant, then either the vacuum state is also invariant, or there must exist spinless bosons of zero mass. In particle physics these bosons are called Goldstone bosons. We refer to them as Anderson, Goldstone, Nambu (AGN) bosons because analogous excitations were discovered in theories of superconductivity by Anderson and Nambu and their relation to gauge symmetry breaking was recognized by those authors.

In the following discussion we distinguish between large and small systems, or more properly between three-dimensional (3D-) and zero-dimensional (0D-) systems. We make use of the random phase approximation treatment of pairing developed by Anderson (1958) for the case of a large neutral system and by Högaasen-Feldman (1961) and Bes and Broglia (1966) for the case of the atomic nucleus (see also Scadron (1985) and Broglia *et al*. (2000)).

4.1.1 Infinite systems and finite systems

As discussed in Section 1.7, in normal metals at low temperature the coherence length ξ is of the order of 10^3 Å. This quantity is much larger than the spacing between electrons ($r_s \approx 1$–3 Å) where

$$r_s = \left(\frac{3}{4\pi n}\right)^{1/3}, \tag{4.1}$$

is the Wigner–Seitz radius, while n is the electron density of the system. At the same time, the quantity ξ is also much smaller than the physical dimension L of a typical macroscopic sample. The inequalities $r_s \ll \xi \ll L$ are typical of three-dimensional (3D-) superconductors. In keeping with these results, within the region occupied by any given pair will be found the centre of mass of many (of the order of 10^6) pairs. In a superconductor the pair phase $\phi(\vec{r})$ (gauge angle) is approximately constant over spatial regions characteristic of the correlations in the superconducting phase, and a supercurrent with gauge-invariant velocity $\boldsymbol{v}_s = -\hbar/2m_e(\boldsymbol{\nabla}\phi - 2e/\hbar c\boldsymbol{A})$ where $\boldsymbol{A}$ is the vector potential, can be defined.

https://doi.org/10.1017/9781009401920 Published online by Cambridge University Press

It is obtained by multiplying the wavefunctions of all the effectively interacting particles by approximately the same phase factor. In an anisotropic superfluid such as ^{3}He-A the order parameter not only has a phase but also has an orientation, the preferred direction of $\boldsymbol{l}$, the relative orbital angular momentum of the $l = 1$ Cooper pairs. In this system the superfluid velocity depends not only on the spatial change of the phase ϕ, but also on that of $\boldsymbol{l}$. Parametrizing $\boldsymbol{l}$ by the azimuthal (β) and the polar (α) angles, $\boldsymbol{v}_s$ now takes the form $\boldsymbol{v}_s = \hbar/2m_3(\boldsymbol{\nabla}\phi - \cos\beta\boldsymbol{\nabla}\alpha)$, where m_3 is the mass of the ^{3}He atom (Vollhardt and Wölfle (1990)).

The situation is quite different in nuclei, where $\xi \approx 30$ fm (see equation (1.39)), a quantity which is much larger than the average distance between nucleons ($\approx$2 fm) (see Appendix C). On the other hand, pairs must be located inside the nucleus (radius $R \approx 5$–7 fm for medium heavy nuclei). Thus a nucleus can be viewed as a 0D-system, where the phenomenon of quantized superflow observed in infinite 3D-systems does not seem to have a counterpart. Superflow may, on the other hand, play an important role in the dynamics of nuclear matter occurring in neutron stars (see Section 1.10 and Ruderman (1972), Anderson *et al*. (1982), Pines *et al*. (1980), (1992) and references therein).

The BCS solution of the pairing problem in a finite nucleus has been presented in Chapter 3 and Appendix G. In the next section we will discuss the RPA (collective) modes which are built on it (see Appendices I and J) with special reference to spontaneous symmetry breaking. Then in Section 4.3 we will make a comparison with Anderson's (1958) derivation of collective modes in infinite 3D neutral superconductor and comment on the similarities and differences between the finite and infinite cases.

4.2 Pairing in atomic nuclei (0D systems; $\xi \gg R$)

The present section is concerned with gauge symmetry breaking in a system of neutrons or protons interacting with a pairing force. We begin it by dividing the Hamiltonian into a mean field part and a fluctuating part. The ground state of the mean field part is represented by a BCS wavefunction. The original Hamiltonian is invariant with respect to rotations in gauge space but the mean field Hamiltonian and the BCS wavefunction are not (see Section 3.8). There is a discussion of the transformation properties under rotations in gauge space. The next step is to derive the RPA equations for the fluctuations about the mean field wavefunctions. The RPA equations can be solved exactly for the simple pairing problem. The gauge invariance of the original Hamiltonian requires that the RPA equations must have a zero-frequency mode. This mode comes out automatically from the explicit solution of the RPA equations, but it can also be found by a general argument from gauge symmetry (Section 4.2.3). The zero-frequency mode is related to pair addition and removal processes (Section 4.2.4). The nucleon number dependence of the ground-state energy is contained in the Fermi

energy, which gives a linear dependence, and a 'moment of inertia' which gives a quadratic dependence. The arguments are illustrated by a simple schematic model in Section 4.2.5, and by Weinberg's (1996) discussion of symmetry breaking in macroscopic systems. Section 4.2.6 presents a comparison with experiment.

4.2.1 Deformation in gauge space: mean-field approximation

Our Hamiltonian describes the motion of independent particles interacting through a pairing force,

$$H = H_{\rm sp} + H_{\rm p}. \tag{4.2}$$

Here

$$H_{\rm sp} = \sum_{\nu>0} (\varepsilon_\nu - \lambda)(a^\dagger_\nu a_\nu + a^\dagger_{\bar\nu} a_{\bar\nu}), \tag{4.3}$$

is the single-particle Hamiltonian. The operator $a^\dagger_\nu$ creates a particle (fermion) with quantum numbers ν. For spherical nuclei, ν stands for n, l, j and m, i.e. the number of nodes, the orbital angular momentum, the total angular momentum and its projection, respectively. The state $|\bar\nu\rangle$ is obtained from the state $|\nu\rangle$ by the operation of time reversal. The condition $\nu > 0$ means $m > 0$, where m is the magnetic quantum number. The single-particle energies ε_ν are measured from the Fermi energy λ. The pairing Hamiltonian

$$H_{\rm p} = -G P^\dagger P, \tag{4.4}$$

is written in terms of the pair operator

$$P^\dagger = \sum_{\nu>0} a^\dagger_\nu a^\dagger_{\bar\nu}, \tag{4.5}$$

which creates a pair of particles in time-reversal states. In a spherical nucleus these are coupled to angular momentum zero. The BCS solution of this Hamiltonian provides a mean-field approximation to H, where the pairing gap parameter,

$$\Delta = G\alpha_0, \tag{4.6}$$

plays a central role in determining the properties of the system. The quantity

$$\alpha_0 = \langle {\rm BCS}| P^\dagger |{\rm BCS}\rangle \tag{4.7}$$

is the average value of the pair transfer operator in the pairing mean-field ground state $|{\rm BCS}\rangle$.

As a function of these parameters, the total Hamiltonian

$$H = H_{\rm MF} + H_{\rm fluct}, \tag{4.8}$$

https://doi.org/10.1017/9781009401920 Published online by Cambridge University Press

can be written as a sum of a mean field term

$$H_{\rm MF} = H_{\rm sp} - \Delta(P^\dagger + P) + \frac{\Delta^2}{G} \tag{4.9}$$

and a fluctuation term

$$H_{\rm fluct} = -G(P^\dagger - \alpha_0)(P - \alpha_0). \tag{4.10}$$

BCS theory assumes $\alpha_0 \gg (P^\dagger - \alpha_0)(P - \alpha_0)$ and solves the reduced Hamiltonian $H_{\rm MF}$ making an ansatz for $|{\rm BCS}\rangle$.

As in Chapter 3 we make a special choice of gauge and define a standard BCS wavefunction as

$$|{\rm BCS}\rangle_{\mathcal{K}} = \prod_{\nu>0}(U_\nu + V_\nu a_\nu^\dagger a_{\bar\nu}^\dagger)|0\rangle, \tag{4.11}$$

where U_ν and V_ν are real. This wavefunction does not have a fixed number of particles and selects a privileged orientation in gauge space. The Hamiltonian H (equations (4.2) or (4.8)) is invariant with respect to rotations in gauge space generated by the operator

$$\mathcal{G}(\phi) = {\rm e}^{-\frac{{\rm i}\hat N}{2}\phi}, \tag{4.12}$$

where $\hat N = \sum_\nu a_\nu^\dagger a_\nu$ is the particle number operator. The state

$$|{\rm BCS}\,(\phi)\rangle_{\mathcal{K}} = \mathcal{G}(\phi)\prod_{\nu>0}(U_\nu + V_\nu a_\nu^\dagger a_{\bar\nu}^\dagger)|0\rangle \tag{4.13}$$

$$= \prod_{\nu>0}(U_\nu + {\rm e}^{-{\rm i}\phi} V_\nu a_\nu^\dagger a_{\bar\nu}^\dagger)|0\rangle \tag{4.14}$$

is obtained from the standard state $|{\rm BCS}\rangle_{\mathcal{K}}$ by rotating it through an angle ϕ in gauge space. The new BCS state has the same energy and a similar structure as $|{\rm BCS}\rangle_{\mathcal{K}}$. The rotated state can be written in another way as

$$|{\rm BCS}\,(\phi)\rangle_{\mathcal{K}} = |{\rm BCS}\rangle_{\mathcal{K}'} = \prod_{\nu>0}(U_\nu + V_\nu a_\nu'^\dagger a_{\bar\nu}'^\dagger)|0\rangle, \tag{4.15}$$

in terms of rotated creation operators

$$\begin{aligned} a_\nu'^\dagger &= \mathcal{G}(\phi) a_\nu^\dagger \mathcal{G}^{-1}(\phi)\,, \\ &= {\rm e}^{-\frac{\rm i}{2}\phi} a_\nu^\dagger. \end{aligned} \tag{4.16}$$

This allows us to define an intrinsic (body-fixed) coordinate frame $\mathcal{K}'$ (see Fig. 4.1), in terms of the primed operators.

The state $|{\rm BCS}(\phi)\rangle_{\mathcal{K}}$ with gauge angle ϕ with respect to the laboratory coordinate system $\mathcal{K}$ has the angle $\phi = 0$ with respect to the intrinsic system $\mathcal{K}'$.

https://doi.org/10.1017/9781009401920 Published online by Cambridge University Press

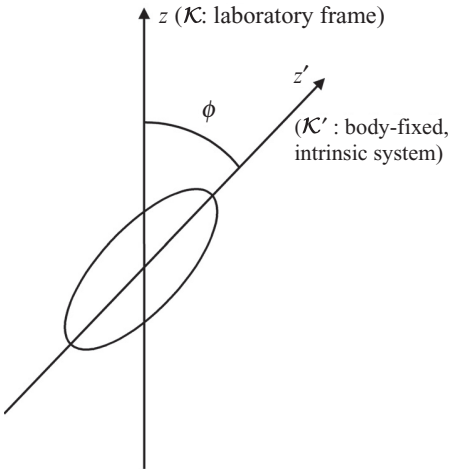

Figure 4.1. Schematic representation of a deformation in gauge space defining a privileged orientation z' in the two-dimensional space and thus an intrinsic, body-fixed, coordinate system of reference $\mathcal{K}'$, making an angle ϕ with the laboratory frame of reference $\mathcal{K}$.

The mean-field pairing Hamiltonian becomes diagonal in the quasiparticle basis, i.e.

$$H_{\mathrm{MF}} = U + H_{11}, \tag{4.17}$$

where

$$U = 2\sum_{\nu>0}(\varepsilon_\nu - \lambda)V_\nu^2 - \frac{\Delta^2}{G} \tag{4.18}$$

and

$$H_{11} = \sum_\nu E_\nu \alpha_\nu^\dagger \alpha_\nu. \tag{4.19}$$

The quasiparticle creation operator

$$\alpha_\nu^\dagger = U_\nu a_\nu^\dagger - V_\nu a_{\bar{\nu}} \tag{4.20}$$

is defined in terms of the BCS theory U_ν and V_ν occupation numbers, the state $|\mathrm{BCS}\rangle$ is the quasiparticle vacuum. The quasiparticle energy is

$$E_\nu = \sqrt{(\varepsilon_\nu - \lambda)^2 + \Delta^2}\,. \tag{4.21}$$

We shall see that restoration of symmetry is obtained by diagonalizing the residual interaction acting among the quasiparticles associated with the terms H_{p}'' in the expression (Anderson (1958), Bes and Broglia (1966), Broglia (1985))

$$H_{\mathrm{fluct}} = H_{\mathrm{p}}' + H_{\mathrm{p}}'' + C, \tag{4.22}$$

https://doi.org/10.1017/9781009401920 Published online by Cambridge University Press

where

$$H'_{\rm p} = -\frac{G}{4}\left(\sum_{\nu>0}(U_\nu^2 - V_\nu^2)(\Gamma_\nu^\dagger + \Gamma_\nu)\right)^2 \tag{4.23}$$

and

$$H''_{\rm p} = \frac{G}{4}\left(\sum_{\nu>0}(\Gamma_\nu^\dagger - \Gamma_\nu)\right)^2, \tag{4.24}$$

with

$$\Gamma_\nu^\dagger = \alpha_\nu^\dagger \alpha_{\bar{\nu}}^\dagger . \tag{4.25}$$

The term C in equation (4.22) stands for constant terms, as well as for terms proportional to the number of quasiparticles, and which consequently vanish when acting on the BCS ground state (see Appendices I and J). Neglecting terms proportional to the number of quasiparticles is an important approximation in the RPA and it has to be done consistently. The structure displayed by $H'_{\rm p}$ and $H''_{\rm p}$ is a consequence of the fact that, neglecting terms of type C, one can write

$$P^\dagger + P = \sum_{\nu>0}(U_\nu^2 - V_\nu^2)(\Gamma_\nu^\dagger + \Gamma_\nu) \tag{4.26}$$

and

$$P^\dagger - P = \sum_{\nu>0}(U_\nu^2 + V_\nu^2)(\Gamma_\nu^\dagger - \Gamma_\nu) = \sum_{\nu>0}(\Gamma_\nu^\dagger - \Gamma_\nu). \tag{4.27}$$

In other words, there are two fields which can create (annihilate) two quasiparticles, namely U_ν^2 and V_ν^2. These fields can be combined in a symmetric $(U_\nu^2 + V_\nu^2)$ and in an antisymmetric $(U_\nu^2 - V_\nu^2)$ fashion with respect to the Fermi surface.

Making use of the approximate commutation relation (see Appendix A, Section A.4)

$$[\Gamma_\nu, \Gamma_{\nu'}^\dagger] = \delta(\nu, \nu'), \tag{4.28}$$

which neglects terms proportional to the number of quasiparticles, the solutions of

$$\widetilde{H} = H_{\rm MF} + H'_{\rm p} + H''_{\rm p}, \tag{4.29}$$

in particular the collective modes, can be obtained in the harmonic approximation (RPA), through the equations of motion (see Appendix A)

$$[\widetilde{H}, \Gamma_n^\dagger] = \hbar\omega_n \Gamma_n^\dagger \tag{4.30}$$

and

$$[\Gamma_n, \Gamma_{n'}^\dagger] = \delta(n, n'), \tag{4.31}$$

where

$$\Gamma_n^\dagger = \sum_\nu (a_{n\nu}\Gamma_\nu^\dagger + b_{n\nu}\Gamma_\nu), \tag{4.32}$$

is the creation operator of the nth vibrational mode. Equations (4.30) and (4.31) lead to a dispersion relation and to the normalization condition of the eigenstates, which determine the frequencies $\omega_n = (C_n/D_n)^{1/2}$, the RPA energies $W_n = \hbar\omega_n$, and the zero point fluctuations $(\hbar/2\omega_n D_n)^{1/2}$ associated with the modes, and thus the restoring force (C_n) and inertia (D_n) parameters for the corresponding harmonic motion.

Note that to neglect C in equation (4.22) is equivalent to a quasi-boson approximation. In fact, defining the conjugate variables

$$q_\nu = \frac{1}{\sqrt{2}}(\Gamma_\nu^\dagger + \Gamma_\nu), \quad p_\nu = -\frac{\mathrm{i}}{\sqrt{2}}(\Gamma_\nu^\dagger - \Gamma_\nu),$$

fulfilling the condition (see equation (4.28))

$$[q_\nu, p_{\nu'}] = \mathrm{i}\delta(\nu, \nu'),$$

one can write

$$H_\mathrm{p}' + H_\mathrm{p}'' = -\frac{G}{2}\Big[\Big(\sum_{\nu>0}(U_\nu^2 - V_\nu^2)q_\nu\Big)^2 + \Big(\sum_{\nu>0} p_\nu\Big)^2\Big].$$

This is diagonalized by the transformation (equivalent to equations (4.30) and (4.31))

$$Q_n = \sum_{\nu'} \lambda_{n\nu'} q_{\nu'}, \quad P_n = \sum_{\nu'} \mu_{n\nu'} p_{\nu'},$$

so that

$$\widetilde{H} = \sum_n \Big(\frac{P_n^2}{2D_n} + \frac{C_n}{2}Q_n^2\Big)$$

and

$$[Q_n, P_{n'}] = \mathrm{i}\delta(n, n'), \quad [Q_n, \widetilde{H}] = \mathrm{i}\frac{P_n}{D_n}, \quad [P_n, \widetilde{H}] = -\mathrm{i}C_n Q_n,$$

implying that the eigenvalues are $W_n = \hbar(C_n/D_n)^{1/2}$.

4.2.2 Solution of the RPA equations

In what follows we do not diagonalize the full Hamiltonian $H_\mathrm{MF} + H_\mathrm{p}' + H_\mathrm{p}''$ but discuss two special cases (for the simultaneous diagonalization of H_MF, H_p' and H_p'' we refer the reader to Appendix J). As a first case we consider the Hamiltonian (see equations (4.17) and (4.23)) $H_\mathrm{MF} + H_\mathrm{p}'$ where the odd term H_p'

https://doi.org/10.1017/9781009401920 Published online by Cambridge University Press

in the interaction is antisymmetric with respect to the Fermi surface. The even term $H''_{\rm p}$ is neglected. Equation (4.30) leads, in this case, to the dispersion relation

$$\sum_{\nu>0} \frac{2E_\nu (U_\nu^2 - V_\nu^2)^2}{(2E_\nu)^2 - (W'_n)^2} = \frac{1}{G}. \tag{4.33}$$

Making use of the BCS relation

$$U_\nu^2 - V_\nu^2 = \frac{\varepsilon_\nu - \lambda}{E_\nu}, \tag{4.34}$$

which is equivalent to the BCS gap equation, it can be shown that the lowest energy solution of equation (4.33) is $W'_1 = \hbar\omega_1 = 2\Delta$. These pairing vibrations (Bes and Broglia (1966)) have been studied extensively through two-nucleon transfer processes (see e.g. Broglia *et al.* (1973) and references therein) and found to be weakly collective, a property also shared with the pairing vibration of a 3D-system (Anderson (1958)). However, they become very collective in the case of normal nuclei, where multiphonon pairing vibration states have been strongly excited through two-particle transfer reaction (see Chapter 5, see also Section 8.4). These modes have not been observed in normal infinite systems.

The second special case includes the even-interaction $H''_{\rm p}$ which is symmetric with respect to the Fermi surface and neglects the odd term $H'_{\rm p}$. The Hamiltonian is (see equations (4.17) and (4.24)) $H_{\rm MF} + H''_{\rm p}$. Equation (4.30) leads to

$$\sum_{\nu>0} \frac{2E_\nu}{(2E_\nu)^2 - (W''_n)^2} = \frac{1}{G}\,. \tag{4.35}$$

Using the gap equation

$$\sum_{\nu>0} \frac{1}{E_\nu} = \frac{2}{G}\,, \tag{4.36}$$

this reduces to

$$\sum_{\nu>0} \frac{1}{2E_\nu} \frac{(W''_n)^2}{(2E_\nu)^2 - (W''_n)^2} = 0. \tag{4.37}$$

The lowest energy solution of this equation is $W''_1 = 0$. The general amplitudes associated with the one-phonon amplitude (see equation (4.32)) are

$$a_{n\nu} = \frac{\Lambda''_n}{2E_\nu - W''_n}\,, \qquad b_{n\nu} = \frac{\Lambda''_n}{2E_\nu + W''_n}. \tag{4.38}$$

The normalization factor

$$\Lambda''_n = \frac{1}{2}\left(\sum_{\nu>0} \frac{2E_\nu \hbar\omega''_n}{\left((2E_\nu)^2 - (\hbar\omega''_n)^2\right)^2}\right)^{-1/2} \tag{4.39}$$

https://doi.org/10.1017/9781009401920 Published online by Cambridge University Press

is proportional to the zero-point fluctuation of the corresponding vibrational mode. In the case of the zero-frequency mode Λ_1'' is infinite. The amplitudes of the zero-frequency mode are $a_{1\nu} = b_{1\nu} \propto 1/E_\nu$ but cannot be normalized.

4.2.3 The zero-frequency mode

There is a more general way of looking at the zero-frequency mode. The operator $\hat{N}$ which counts the number of nucleons is

$$\hat{N} = \sum_\nu a_\nu^\dagger a_\nu = \sum_\nu \left(U_\nu \alpha_\nu^\dagger + V_\nu \alpha_{\bar{\nu}}\right)\left(U_\nu \alpha_\nu + V_\nu \alpha_{\bar{\nu}}^\dagger\right). \tag{4.40}$$

The RPA approximation $\tilde{N}$ for $\hat{N}$ can be written in terms of the quasiboson operators introduced in (4.25) as

$$\begin{aligned}\tilde{N} &= 2\sum_{\nu>0} U_\nu V_\nu (\Gamma_\nu^\dagger + \Gamma_\nu) + N_0 \\ &= \Delta \sum_{\nu>0} \frac{1}{E_\nu}(\Gamma_\nu^\dagger + \Gamma_\nu) + N_0,\end{aligned} \tag{4.41}$$

where $N_0 = 2\sum_{\nu>0} V_\nu^2$ is the average number of particles in the quasiparticle vacuum state. Terms proportional to the number of quasiparticles have been neglected. The operator $\hat{N}$ commutes with the exact Hamiltonian and it is easy to check that $\tilde{N}$ commutes with the RPA Hamiltonian defined in equation (4.29). In fact, because $[(\Gamma_\nu + \Gamma_\nu^\dagger), (\Gamma_{\nu'} + \Gamma_{\nu'}^\dagger)] = 0$, one can show that $[\mathrm{H}_\mathrm{p}', \tilde{N}] = 0$. Furthermore, because $2U_\nu \Delta_\nu = \Delta/E_\nu$ and the quasiparticle energies satisfy the gap equation (4.36) one can demonstrate that $[\mathrm{H}_{\mathrm{MF}} + \mathrm{H}_\mathrm{p}'', \tilde{N}] = 0$ (see Appendix I). There are two conclusions to be drawn from these results. One is that particle number conservation is restored, by taking into account the fluctuations of the pairing mean field around the static deformation α_0, in the RPA (in particular those associated with H_p''). The other is that the operator $(\hat{N} - N_0)$ is the creation operator of the zero-frequency mode of the RPA equation of motion (4.30).

In fact, the one-phonon state associated with the zero-frequency mode is

$$|1''\rangle = \Gamma_1^\dagger |0''\rangle \sim \Lambda_1'' \sum_{\nu>0} \frac{1}{2E_\nu}(\Gamma_\nu^\dagger + \Gamma_\nu)|0''\rangle \tag{4.42}$$

$$= \frac{\Lambda_1''}{2\Delta}(\hat{N} - N_0)|0''\rangle, \tag{4.43}$$

where $|0''\rangle$ is the ground state of the RPA Hamiltonian. The first line in the above equation is obtained from (4.38) by putting $W_1'' = 0$, and the second line is from equation (4.41). In equation (4.42) $\Gamma_1^\dagger$ is a boson creation operator and should be finite. On the other hand the normalization constant $\Lambda_1'' \to \infty$ for

https://doi.org/10.1017/9781009401920 Published online by Cambridge University Press

the zero energy mode. This is possible only if in (4.43) $(\tilde{N} - N_0) \to 0$ which is another demonstration that particle number conservation is restored in the RPA approximation. This, together with equation (4.45), are the basic equations which testify to the fact that gauge symmetry is being restored.

Because a finite (rigid) rotation in gauge space can be generated by a series of infinitesimal operations of the type defined in equation (4.12), i.e.

$$\mathcal{G}(\delta\phi) \approx 1 - \mathrm{i}\frac{\hat{N}}{2}\delta\phi \ , \tag{4.44}$$

the state $|1''\rangle$ in equation (4.43) is obtained by a gauge rotation of the ground state.

The zero-point amplitude associated with this state, proportional to the quantity Λ_1'', diverges (see equation (4.39)) but nonetheless defines a finite inertia for pairing rotations (see (I.34)). By a proper inclusion of these fluctuations (of the orientation angle in gauge space, see also discussion at the end of Appendix I) one can restore gauge invariance to the $|\mathrm{BCS}\rangle_{\mathcal{K}'}$ state. In fact the states,

$$\begin{aligned}
|N\rangle &\sim \int \mathrm{d}\phi \, \mathrm{e}^{\mathrm{i}\frac{N}{2}\phi} |\mathrm{BCS}\rangle_{\mathcal{K}'} \\
&= \left(\prod_{\nu>0} U_\nu\right) \int \mathrm{d}\phi \, \mathrm{e}^{\mathrm{i}\frac{N}{2}\phi} \\
&\qquad \times \left(1 + \mathrm{e}^{-\mathrm{i}\phi} \sum_{\nu>0} c(\nu) a_\nu^\dagger a_{\bar{\nu}}^\dagger + \mathrm{e}^{-2\mathrm{i}\phi} \left(\sum_{\nu>0} c(\nu) a_\nu^\dagger a_{\bar{\nu}}^\dagger\right)^2 + \cdots\right) |0\rangle \\
&\sim \left(\sum_{\nu>0} c(\nu) a_\nu^\dagger a_{\bar{\nu}}^\dagger\right)^{\frac{N}{2}} |0\rangle \ ,
\end{aligned} \tag{4.45}$$

where

$$c(\nu) = \frac{V_\nu}{U_\nu}, \tag{4.46}$$

are states with fixed number N of particles.* They are the members of a pairing rotational band (rotations in gauge space) (Bes and Broglia (1966), see also Belyaev (1972)). Examples of such a rotational band are provided by the ground state of even–even nuclei with many particles outside the closed shell (see Section 4.2.5 and Fig. 4.2). The operation carried out in equation (4.45) is number projection. It can be viewed as a change of representation between the conjugate variables N and ϕ, from the ϕ-representation to the N-representation (see Anderson (1964)).

* See Section 6.6 for a discussion of alternative techniques of projection devised to restore particle number conservation.

https://doi.org/10.1017/9781009401920 Published online by Cambridge University Press

The BCS wavefunction $|\mathrm{BCS}\rangle_{\mathcal{K}'}$ has a definite orientation in gauge space. The RPA ground state $|0''\rangle$ in equation (4.42) and the zero-frequency mode built on it has a uniform distribution in ϕ-space, corresponding to the RPA representation of the number projected states $|N\rangle$ given in equation (4.45).

The inertia associated with pairing rotational bands is obtained by recognizing that the normalization quantity Λ_n'' is also the particle-vibration coupling strength of the nth mode. Thus

$$\frac{D_1''}{\hbar^2} = 4\sum_{\nu>0}\frac{U_\nu^2 V_\nu^2}{E_\nu}. \tag{4.47}$$

This result is derived and discussed in Appendix I. It coincides with the cranking model moment of inertia (Ring and Schuck (1980), equation (3.91)).

$$\frac{\mathcal{J}}{\hbar^2} = 2\sum_{\nu>0}\frac{\left|\langle\nu\bar{\nu}|\hat{N}|\mathrm{BCS}\rangle\right|^2}{2E_\nu}. \tag{4.48}$$

We shall see that, although this moment of inertia is finite, the associated rotational energies are much smaller than typical quasiparticle energies, as expected for a collective mode.

4.2.4 Two-particle transfer reaction

The basic feature characterizing a family of states as belonging to a rotational (or vibrational) band is the fact that there exists an operator $\hat{O}$ whose matrix elements between members of the band, aside from displaying very simple relations, are conspicuosly enhanced with respect to the value of the same operator between pure particle states. Consequently, the (external) field associated with the operator $\hat{O}$ constitutes the specific probe to excite the band. In particular, in the case of rotations in normal space of quadrupole-deformed nuclei, it is the E2-operator which displays large matrix elements, while Coulomb excitation is the specific probe of dynamic and static nuclear deformations, and of the associated collective bands.

The specific probes of the pairing modes are two-nucleon transfer reactions (see e.g. Lane (1964), Mottelson (1977), Broglia (1985c), Broglia *et al*. (1985c)) and references therein). In fact, the existence of a large static pair deformation (pairing gap) manifests itself very directly in the pattern of two-particle transfer intensities, in keeping with the fact that

$$\langle\mathrm{BCS}|P^\dagger|\mathrm{BCS}\rangle = \frac{\Delta}{G}. \tag{4.49}$$

https://doi.org/10.1017/9781009401920 Published online by Cambridge University Press

Consequently, the two-particle cross-section between members of the pairing rotational band is

$$\sigma_{\rm rot} \sim \left(\frac{\Delta}{G}\right)^2 \sim \frac{A}{4}, \tag{4.50}$$

where use was made of the empirical values $\Delta \approx 12\,\text{MeV}/\sqrt{A}$ and $G \approx 25\,\text{MeV}/A$ (Bohr and Mottelson (1975)). The two-particle transfer cross-section associated with a typical two-quasiparticle state is

$$\sigma_{\rm 2qp} \sim \langle \nu\bar{\nu}|P^\dagger|\text{BCS}\rangle^2 = U_\nu^4 \approx 1\ . \tag{4.51}$$

From the ratio

$$\bar{R} = \frac{\sigma_{\rm rot}}{\sigma_{\rm 2qp}} \sim \frac{A}{4} \tag{4.52}$$

one expects that, in superfluid nuclei, a large fraction of the cross-section associated with the transfer of two nucleons in time-reversal states connects members of the same pairing rotational band.

Note that the total two-particle transfer cross-section, once Q-value effects are eliminated, is the same for a system of nucleons which move independently of each other in the mean field as it is for the same system of nucleons interacting via a pairing force; i.e. the same before and after the pairing interaction is switched on. The basic difference introduced by the presence of U and V factors in the corresponding cross-sections is that of concentrating a large fraction of the original strength on the ground-state transition (see Broglia *et al.* (1972a)).

4.2.5 A schematic model

Let us consider particles moving in a single j-shell with pair degeneracy $\Omega = (2j+1)/2$. The BCS occupation numbers can be written directly as (Appendix H, see also Section 3.7)

$$V = \left(\frac{N}{2\Omega}\right)^{1/2}, \quad U = \left(1 - \frac{N}{2\Omega}\right)^{1/2}, \tag{4.53}$$

and lead to a gap and a Fermi energy

$$\Delta = \frac{G}{2}\sqrt{N(2\Omega - N)} \tag{4.54}$$

and

$$\lambda = -\frac{G}{2}(\Omega - N), \tag{4.55}$$

https://doi.org/10.1017/9781009401920 Published online by Cambridge University Press

respectively. The quasiparticle energy is given by

$$E = \frac{G\Omega}{2}. \tag{4.56}$$

Typical superfluid nuclei, i.e. nuclei with many particles outside the closed shell and thus with a large number of 0^+ pairs (Cooper pairs) in the ground state, display a large pairing gap. Within the present simplified model, this situation corresponds to $N \approx \Omega$. In fact, the pairing gap given in equation (4.54) acquires its largest value $\Delta = G\Omega/2$ for $N = \Omega$. In what follows we shall have this situation in mind in discussing the properties of the excitation spectrum. The ground-state energy (see Appendices H, I) is

$$\begin{aligned} E_0 = U + \lambda N &= \lambda N + \frac{G}{4}N^2 \\ &= \lambda N + \frac{\hbar^2}{2\mathcal{J}}N^2, \end{aligned} \tag{4.57}$$

where $n = N/2$ is the number of pairs, and where the moment of inertia is determined by the relation

$$\frac{2\mathcal{J}}{\hbar^2} = \frac{4}{G}. \tag{4.58}$$

This result coincides with that obtained from equation (4.48) making use of the occupation numbers and quasiparticle energy provided by equations (4.53) and (4.56) respectively.

From the ratio,

$$\frac{\hbar^2/2\mathcal{J}}{2E} \approx \frac{1}{\Omega} \ll 1. \tag{4.59}$$

This indicates that the rotational excitations have an energy which is much smaller than that associated with the quasiparticle energies, the ratio approaching zero, as $N = \Omega \to \infty$. In this connection, it is illuminating to quote part of the discussion in Weinberg (1996) on spontaneously broken global symmetries, where he uses a chair as an example of a macroscopic system:

> spontaneous symmetry breaking actually occurs only for idealized systems that are infinitely large. The appearance of broken symmetry for a chair arises because it has a macroscopic moment of inertia $\mathcal{J}$, so that its ground state is part of a tower of rotationally excited states whose energies are separated by only tiny amounts, of the order of $\hbar^2/\mathcal{J}$. This gives the state vector of a chair an exquisite sensitivity to external perturbations; even very weak external fields will shift the energy much more than the energy difference of these rotational levels. In consequence, any rotationally asymmetric external field will cause the ground state or any other state of the chair with definite angular momentum rapidly to develop components with other angular momentum quantum numbers. The states of the

chair that are relatively stable with respect to small external perturbations are not those with definite angular momentum quantum numbers, but rather those with a definite orientation, in which the rotational symmetry of the underlying theory is broken.

Weinberg's arguments are true for an atomic nucleus only in the limit $N \to \infty$ when deformation and rotation are rigorously defined. Nevertheless when one observes a (pairing) rotational spectrum one can talk about a privileged direction in gauge space, which can be clamped down in a collision between two superfluid nuclei (see Broglia and Winther (1991)) resulting in the transfer of a Cooper pair (this is a Josephson-like phenomenon, see Anderson (1972), Anderson (1964) p. 134; see also Appendix L).

Broken symmetries in relativistic theories and in many-body systems imply an Anderson–Goldstone–Nambu (AGN) boson (zero-mass particle or phonon branch respectively). The analogous property in the case of the RPA description of pairing in atomic nuclei is the $\hbar\omega_1'' = 0$ solution (see Section 4.2 as well as equation (4.57)) and the associated pairing rotational band built out of the ground state of systems with N, $N \pm 2$, $N \pm 4, \ldots$, particles. As shall be seen in the next subsection, there exists strong experimental evidence which testifies to the validity of this picture.

4.2.6 Comparison with experiment

In Fig. 4.2 we summarize the experimental information concerning the ground-state energies of one of the longest sequences of isotopes of nuclei with many nucleons outside a closed shell, that associated with the Sn-isotopes ($^{A}_{50}$Sn) (Broglia *et al.* (1973), Broglia (1985c), Bes and Broglia (1977)). The data can be rather accurately fitted, after a linear term has been removed, with the parabola corresponding to an energy parameter $\hbar^2/2\mathcal{J} = 0.1\,\text{MeV}$, in overall agreement with the simple estimate provided by the prefactor of N^2 in equation (4.57) ($G/4 \approx 28/4A\,\text{MeV} \approx 0.07\,\text{MeV}$, $A \approx 100$, see equation (2.27) and Appendix H). Also displayed in Fig. 4.2 is systematic information on the transfer of two neutrons in time-reversal states (single Cooper pair transfer). The average value of $\bar{R} = 24.4$ is in overall agreement with the simple estimate provided by equation (4.52) ($\bar{R} = 25$ for $A \approx 100$, see also Appendix H).

The diagonalization of the total Hamiltonian $H = H_{\text{MF}} + H_{\text{p}}' + H_{\text{p}}''$ in the RPA has still a root at $\omega_1 = 0$ (corresponding to the $\omega_1'' = 0$ root of the Hamiltonian $H_{\text{MF}} + H_{\text{p}}''$), orthogonal to all the other two-quasiparticle like states (pairing vibrations), and which are somewhat modified by the Coriolis coupling associated with the rotation of the system in gauge space as a whole (see Appendix J). Pairing vibrations of superfluid nuclei correspond to the odd solution discussed by Anderson in his RPA treatment of superconductivity

https://doi.org/10.1017/9781009401920 Published online by Cambridge University Press

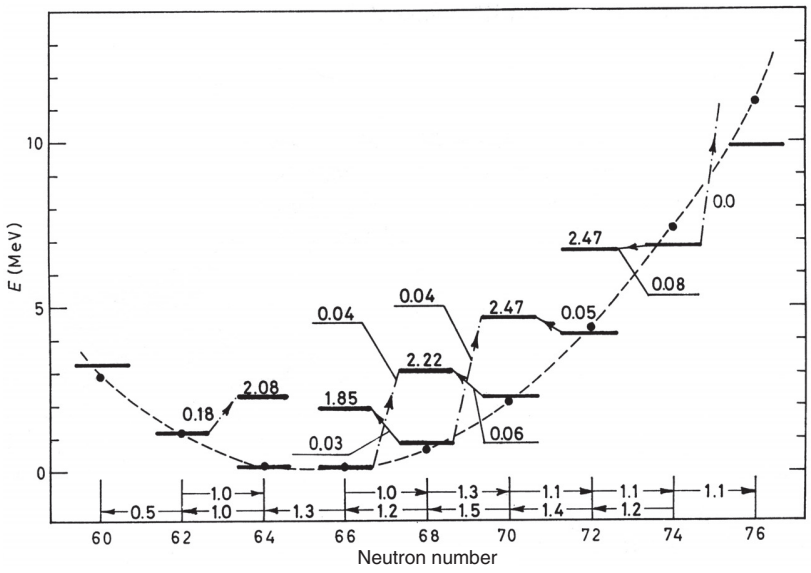

Figure 4.2. Experimental energies of the $J^\pi = 0^+$ states of the even Sn isotopes excited in two-particle transfer reactions ((t, p) and (p, t)). The heavy drawn lines represent the values of the expression $E = -B(\mathrm{Sn}) + E_{\mathrm{exc}} + 8.58N + 45.3\,(\mathrm{MeV})$, where the binding energies $B(A)$ (in MeV) are taken from Wapstra and Gove (1971). The dashed line represents the parabola $0.10(N - 65.4)^2$ Also displayed is the excited pairing rotational band associated with the pairing vibrational mode. In all cases where more than one $J^\pi = 0^+$ state has been excited below 3 MeV in two-neutron transfer processes, the energy $\sum_i \sigma(0_i)E(0_i^+)/\sum_i \sigma(0_i^+)$ of the centroid is quoted, as well as the corresponding cross-section $\sum_i \sigma(0_i^+)$. The quantity $\sigma(0_i^+)$ is the relative cross-sections with respect to the ground-state cross-sections. The numbers along the abscissa are the ground-state (p, t) and (t, p) cross-sections normalized to the $^{116}\mathrm{Sn} \leftrightarrow {}^{118}\mathrm{Sn(gs)}$ cross-section. The (t, p) and (p, t) data utilizing in constructing this figure were taken from Bjerregaard *et al.* (1968), Bjerregaard *et al.* (1969), Flynn *et al.* (1970), Flemming *et al.* (1970).

(Anderson (1958)), lying at the top of the pairing gap. These solutions are, as a rule, both in the 0D and in the 3D systems, almost pure two-quasiparticle states (see Broglia *et al.* (1977)). This is the reason why we should not refer to them further. As will be discussed in Chapter 5 pairing vibrations play an important role in closed shell (normal) nuclei.

4.3 Infinite 3D neutral superconductors ($\xi \ll L$)

In this section we follow Anderson (1958) and study the correlated two-quasiparticle excitations associated with the Hamiltonian

$$\mathcal{H} = \sum_{k,\sigma} \varepsilon_k a^\dagger_{k\sigma} a_{k\sigma} + \frac{1}{2} \sum_{k \neq k',q} \sum_{\sigma,\sigma'} V(\vec{k}, \vec{k}') a^\dagger_{k',\sigma'} a^\dagger_{-k'+q,\sigma} a_{-k+q,\sigma} a_{k,\sigma}\,. \tag{4.60}$$

https://doi.org/10.1017/9781009401920 Published online by Cambridge University Press

Here the (Galilean invariant) Coulomb and induced interactions have been lumped together in $V(k, k')$, while σ denotes the projection of the electron spin. Making use of the RPA equations of motion for the operators

$$\hat{b}_k^Q = a_{-k-Q\downarrow} a_{k\uparrow}, \tag{4.61}$$

$$\hat{\rho}_k^Q = a_{k+Q\uparrow}^\dagger a_{k\uparrow}, \tag{4.62}$$

and for the corresponding Hermitian, and time-reversal conjugate operators, Anderson (1958) obtains for the even solution of the Hamiltonian $\mathcal{H}$,

$$\begin{vmatrix} 1 - 2V_{\mathrm{D}} f & l \\ 2V_{\mathrm{D}} h & 1 - g \end{vmatrix} = 0\,, \tag{4.63}$$

where

$$f = \sum_k \frac{\omega_{kQ} n_{kQ}}{(\nu_k^Q)^2 - \nu^2}, \tag{4.64}$$

$$g = \sum_k \frac{(-V)\nu_k^Q \cos^2\left[\frac{1}{2}(\theta_k - \theta_{k+Q})\right]}{(\nu_k^Q)^2 - \nu^2}, \tag{4.65}$$

$$h = \sum_k \frac{(-V)(b_k + b_{k+Q})}{(\nu_k^Q)^2 - \nu^2}, \tag{4.66}$$

$$l = \sum_k \frac{\omega_{kQ}^2 (b_k + b_{k+Q})}{\nu^2 - (\nu_k^Q)^2}, \tag{4.67}$$

and where V_{D} indicates the 'direct', unscreened interaction. In the above equations one has used the definitions

$$b_k = \langle a_{-k\downarrow} a_{k\uparrow} \rangle = b_k^* = U_k V_k, \tag{4.68}$$

$$\omega_{kQ} = \varepsilon_{k+Q} - \varepsilon_k, \tag{4.69}$$

$$n_{kQ} = n_{k+Q} - n_k, \tag{4.70}$$

$$\nu_k^Q = E_k + E_{k+Q}, \quad \left(E_k = (\varepsilon_k^2 + \Delta_k^2)^{1/2}\right), \tag{4.71}$$

$$\cos\theta_k = U_k^2 - V_k^2. \tag{4.72}$$

The collective modes associated with the secular equation (4.63) have entirely different behaviour, depending on whether we consider the charged or neutral case. In the charged case, V_{D} is singular and large, and f determines the frequencies. In the neutral case the frequencies are mostly determined by g.

4.3.1 Neutral superconductor

Following Anderson (1958) we assume $V_{\mathrm{D}} = V$ as $Q \to 0$. Since $f \sim Q^2$, and thus $1 - 2V_{\mathrm{D}} f \approx 1$, equation (4.63) can be approximated as

$$1 - g = 2Vhl. \tag{4.73}$$

https://doi.org/10.1017/9781009401920 Published online by Cambridge University Press

Because also $l \sim Q^2$, in the limit $Q \to 0$ the dispersion relation reads (see (4.35))

$$\sum_k \frac{(-V)2E_k}{(2E_k)^2 - \nu^2} = 1\,, \tag{4.74}$$

where $2E_k \approx \nu_k^Q$. In keeping with the BCS gap equation, equation (4.74) admits a solution with $\nu = 0$.

In the following we use the approximation $\omega_{kQ}^2 \approx \frac{1}{3}\left(\frac{k_F Q}{m}\right)^2$. The factor $1/3$ comes from the average $\langle \cos^2 \gamma \rangle$ where γ is the angle between $\vec{k}$ and $\vec{Q}$. Expanding h and l to the lowest non-vanishing order in Q^2 and ν^2, and g to first order,

$$h \approx \sum_k \frac{(-V)2U_k V_k}{(2E_k)^2} = 2\Delta \sum_k \frac{(-V)}{(2E_k)^3}, \tag{4.75}$$

$$l \approx -\sum_k \frac{\omega_{kQ}^2 2U_k V_k}{(2E_k)^2} = -\frac{1}{3}k_F^2 \frac{Q^2}{m^2} \sum_k \frac{2U_k V_k}{(2E_k)^2}, \tag{4.76}$$

$$g \approx 1 + \nu^2 \sum_k \frac{(-V)}{(2E_k)^3} - \sum_k \frac{(-V)\omega_{kQ}^2}{(2E_k)^3}, \tag{4.77}$$

the dispersion relation equation (4.73) becomes

$$1 - \left(1 + \nu^2 \sum_k \frac{(-V)}{(2E_k)^3} - \sum_k \frac{(-V)\omega_{kQ}^2}{(2E_k)^3}\right) = 2V \left(2\Delta \sum_k \frac{(-V)}{(2E_k)^3}\right)\left(-\sum_k \frac{\omega_{kQ}^2 2U_k V_k}{(2E_k)^2}\right), \tag{4.78}$$

which can also be written as

$$\nu = \frac{1}{\sqrt{3}} v_F Q \left(1 + 4V\Delta \sum_k \frac{2U_k V_k}{(2E_k)^2}\right)^{1/2}, \tag{4.79}$$

where the assumption has been made that $\Delta_k = \Delta$. The AGN-phonon velocity $v_F/\sqrt{3}$ seems to be a kinematical 'ideal gas' effect, which has also been derived in a different way by Bogoliubov *et al.* (1958). It is curious that the term which modifies the 'ideal gas' velocity in equation (4.79) is related to the pairing moment of inertia (see Appendix H, equation (H.17) and Appendix I, equation (I.24)) and (4.47),

$$4V\Delta \sum_k \frac{2U_k V_k}{(2E_k)^2} = V\frac{\mathcal{I}}{\hbar^2} = V\frac{\partial N}{\partial \lambda}. \tag{4.80}$$

An example of an AGN boson in a neutral system is provided by the fourth sound in superfluid ^{3}He, which corresponds to the oscillatory motion of the

https://doi.org/10.1017/9781009401920 Published online by Cambridge University Press

superfluid phase in a confined geometry (superleak) where the normal fluid is clamped. The corresponding sound velocity $C_4^2 = C_1^2 \bar{\rho}_s/\rho$, where $\bar{\rho}_s$ is the superfluid density and ρ the total density of the system, is proportional to the first sound velocity (Vollhardt and Wölfle (1990)), $C_1^2 = \frac{1}{3} v_F^2 (1 + F_0^s)(1 + \frac{1}{3} F_1^s)$, where F_l^s are the spin symmetric $l = 0$ and $l = 1$ Landau parameters (see Section 10.5.1).

Let us now return to the main subject discussed above, namely the relation between the solutions of the dispersion relations given in equations (4.35) and (4.74) (see also equations (J.27) and (4.63))), solutions which look suggestively similar (see also equations (4.57) and (4.79)). It has been argued that in relativistic theory, as well as in 3D many-body systems, the $Q \to 0$ is a proper solution of the problem (zero-mass particle and phonon branch respectively), while in a 0D system like the nucleus, it is a spurious solution to be eliminated in terms of a pairing rotational band whose inertia is that of the $\omega_1 = 0$ root or spurious state (see equation (4.47)). To this line of reasoning one could argue that, had we used a more powerful technique than RPA to diagonalize the Hamiltonian $H = H_0 + H'_p + H''_p$, we would have obtained the modified two-quasiparticle-like states (pairing vibrations), and the pairing rotational band, without further ado.

For a discussion of these subjects which goes beyond the RPA, we refer the reader to Bes and Kurchan (1990).

https://doi.org/10.1017/9781009401920 Published online by Cambridge University Press

5
Pairing vibrations

When the strength G of the pairing interaction is greater than a critical value G_c, the gap equation has a non-zero solution for the gap parameter Δ and the BCS ground state of a system of nucleons is stable. Single nucleon levels are partially occupied in an energy range Δ around the Fermi energy λ. The BCS state is not an eigenstate of nucleon number and violates gauge invariance. Pairing vibrations, which are fluctuations about the BCS state, were studied in Chapter 4 and it was shown that gauge invariance was restored within the framework of the random phase approximation (RPA). In this chapter we study the question of pairing vibrations within a more general context, considering also pairing vibrations in normal nuclei which have pairing strengths $G < G_c$ and $\Delta = 0$. To a first approximation single-particle levels are occupied with unit probability up to the Fermi energy and with zero probability for states above the Fermi level. Pairing vibrations modify this simple picture and are associated with fields which change the number of particles by 2. They produce correlations which enhance or modify pair transfer amplitudes. Parts of this chapter is based on Broglia and Riedel (1967a,b) and Broglia *et al*. (1973) (see also Anderson (1958), Högaasen-Feldman (1961), Bes and Broglia (1966), Bohr and Mottelson (1975), Ring and Schuck (1980), Wölfle (1972, 1978), Schmidt (1972)).

5.1 The two-level model

The simplest model which displays fluctuations of the pairing gap contains two j-shells which may have the same or different degeneracy, and which are separated by a distance D. Pairs of particles are scattered in these orbitals by a pairing force with constant matrix elements. A solution of the two-level model was given by Högaasen-Feldman (1961). More generally the exact eigenstates for a pairing force with constant matrix elements distributed in an arbitrary number of levels was found by Richardson and Sherman (1964) (see Section 2.8).

The two-level model Hamiltonian can be written as

$$H = \frac{D}{2}(N_{j_2} - N_{j_1}) - \frac{1}{4}G(P^\dagger_{j_1} + P^\dagger_{j_2})(P_{j_1} + P_{j_2}), \tag{5.1}$$

where

$$P^\dagger_{j_1} = \sum_{m>0}(-1)^{j+m} a^\dagger_{jm} a^\dagger_{j-m} = -\sqrt{\Omega}[a^\dagger_j a^\dagger_j]^0_0\,,$$
$$N_j = \sum_m a^\dagger_{jm} a_{jm}, \qquad \Omega = \frac{2j+1}{2}, \qquad (j = j_1, j_2). \tag{5.2}$$

The two-level model does not have an analytical solution, although it allows for a rather simple numerical solution in the orthonormal basis

$$|m, n-m\rangle = M_m^{-1}(P^\dagger_{j_1})^m (P^\dagger_{j_2})^{n-m}|0\rangle, \tag{5.3}$$

n being the total number of pairs of particles in the system. The matrix element of the Hamiltonian (5.1) in this basis is

$$\begin{aligned}\langle m', n-m'|H|m, n-m\rangle &= \delta(m, m')\\ &\times [(n-2m)D - G(m(\Omega_1 + 1 - m) + (n-m)(\Omega_2 + 1 - n + m))]^{1/2}\\ &- \delta(m', (m-1))G[m(\Omega_1 + 1 - m)(n - m + 1)(\Omega_2 - n + m)]^{1/2}\\ &- \delta(m', (m+1))G[(m+1)(\Omega_1 - m)(n-m)(\Omega_2 + 1 - n + m)]^{1/2}.\end{aligned} \tag{5.4}$$

To obtain the solution of the model one has thus to diagonalize a codiagonal matrix.

As discussed in Chapters 2 and 3, two-particle transfer processes are the specific tools to study the pairing degrees of freedom, in particular pairing vibrations. The model operator which induces such processes is defined as

$$T = P^\dagger_1 + P^\dagger_2. \tag{5.5}$$

In the basis (5.3) the T operator has the following matrix elements

$$\begin{aligned}&\langle m', n+1-m'|T|m, n-m\rangle\\ &= \delta(m', m)[(n-m+1)(\Omega_2 - n + m)]^{1/2}\\ &\quad + \delta(m', (m+1))[(m+1)(\Omega_1 - m)]^{1/2}.\end{aligned} \tag{5.6}$$

The two-particle transfer cross-section can be shown to be proportional to the square of the matrix element (5.6) (see e.g. Broglia *et al.* (1973)).

From the commutation relation $[N_i, P^\dagger_j] = 2\delta(i, j)P^\dagger_j$ one can calculate the occupation number of the two orbits

$$\begin{aligned}\langle\alpha|N_1|\alpha\rangle &= 2\sum_m m|c_{n,m}|^2,\\ \langle\alpha|N_2|\alpha\rangle &= 2\sum_m (n-m)|c_{n,m}|^2,\end{aligned} \tag{5.7}$$

https://doi.org/10.1017/9781009401920 Published online by Cambridge University Press

where the eigenfunction of the total Hamiltonian is

$$|\alpha\rangle = \sum_m c_{n,m} |m, n-m\rangle. \tag{5.8}$$

For $\Omega_1 = \Omega_2 = \Omega$ there are two dimensionless parameters in the model. The first is chosen to be Ω (see equation (5.2)) and it gives a measure of the phase space which the particles have at their disposal to correlate. The second is

$$x = 2G\frac{\Omega}{D} \tag{5.9}$$

and measures the interplay between the pairing strength and the shell effects.

In Fig. 5.1 we display the energies, cross-sections and occupation amplitudes associated with a system $\Omega_1 = \Omega_2 = \Omega = 20$ and $x = 0.5$ and $x = 2.0$ as a function of the number of pairs n ($18 \leq n \leq 22$). When $n = \Omega$, the lower level is full and the upper level is empty in the limit $x \to 0$. In the case $x = 0.5$ the coupling is weak and there is only one characteristic energy, the spacing D between the two single-particle levels.

Any level lies at approximately an integer number of times this energy with respect to the ground state, forming a (harmonic) pairing vibrational band. The two-nucleon transfer cross-section associated with transitions between ground states is proportional to $|n - \Omega|$, i.e. to the absolute value of the number of pairs missing from or in excess of the closed shell. All the first-excited-state stripping cross-sections for $n - \Omega < 0$ are equal and their common value is close to $|\langle \text{gs}(n = 20)|T|\,\text{gs}(n = 19)\rangle|^2$. On the other hand, none of the lowest excited states with $n - \Omega \geq 0$ is populated in such reactions. This is also true for the second and higher excited states for $n - \Omega \leq 0$. A similar pattern is observed for two-nucleon pickup processes.

For the case of $x = 2$ the energy of the states follows a parabolic distribution (pairing rotational band, see Chapter 4) as a function of the number of particles. There are two characteristic energies, corresponding to interband and intraband spacing. The situation is very similar to the one encountered in the case of a single j-shell (see equation (4.57), also Appendix H). In this case, however, there is a finite cross-section to the excited states, although an order of magnitude smaller than between states lying in the same energy parabola. The situation for $x = 1.2$ is intermediate to the one observed for $x = 0.5$ and $x = 2$.

The probability amplitude $|c_{n,m}|^2$ associated with the ground state of the closed-shell system ($n - \Omega = 0$) is also given in Fig. 5.1 as a function of $n - m$. Note that a major change takes place in going from $x = 0.5$ to $x = 2.0$, indicating a change in the coupling scheme of the nucleons correlated through the pairing interaction. Similar results to those displayed in Fig. 5.1 are obtained for $\Omega_1 \neq \Omega_2$ (see Broglia and Sørensen (1968)). One can, however, distinguish in this case two typical energies and two basic two-particle transfer cross-sections,

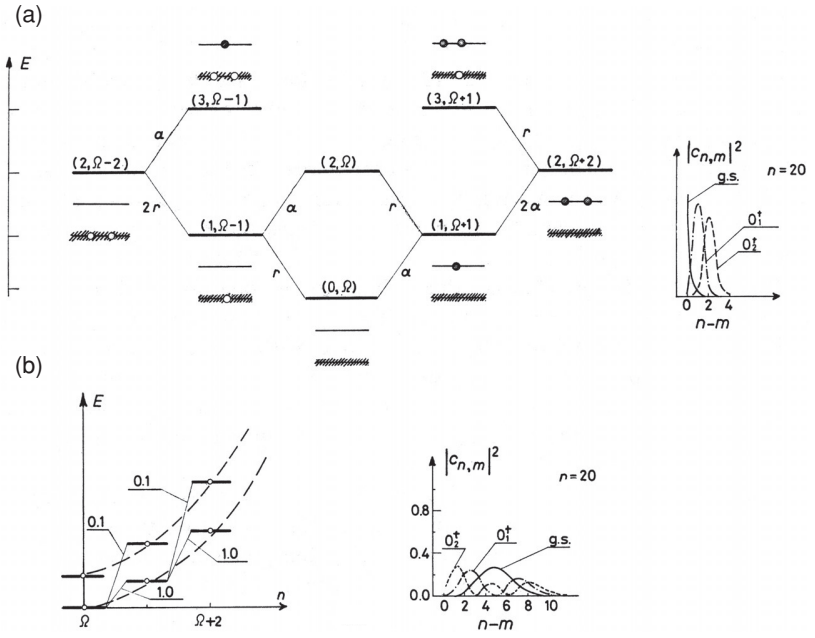

Figure 5.1. Schematic representation of the solution of the two-level model for $\Omega_1 = \Omega_2 = 20$ and for different values of x and n. In (a) the results for $x = 0.5$ are displayed. Because of the particular degeneracy of the model, the energy of the ground state of the system with $n = \Omega \pm 1$ pairs of particles is the same when measured with respect to the closed-shell system (see, however, Sections 5.2 and 8.4). All two-particle transition probabilities are measured in terms of $a = \sigma(\text{gs}(\Omega_1) \rightarrow \text{gs}(\Omega_1 + 1))$ and of $r = \sigma(\text{gs}(\Omega_1) \rightarrow \text{gs}(\Omega_1 - 1))$. Because of the particular symmetry of the model $a = r$. For each level of the spectrum, which is identified by the quantum numbers (N, n), a schematic representation of the main component of the wavefunction is shown. The corresponding square amplitudes $|c_{n,m}|^2$ (see equations (5.7) and (5.8)) associated with the ground state and low excited states of the $n = \Omega_1$ system are also shown. In (b) the energies and two-particle cross-sections for $x = 2.0$ associated with the ground and the first excited states of the systems with $n \geq \Omega_1$ are displayed. The quantities $|c_{n,m}|^2$ corresponding to the ground state and two lowest excited states are also displayed.

one associated with the removal of a pair and the other with the addition of a pair (see Figs. 5.5 and 8.17).

5.1.1 *Collective treatment of pairing vibrations; normal systems ($x < 1$)*

The different levels of the pairing spectrum obtained by diagonalizing the Hamiltonian defined in equation (5.1) for $x < 1$ and reported in Fig. 5.1 can be labelled by the number of pairs n and by a number N indicating their energy sequence in the spectrum. The lowest state corresponds to a closed-shell system and has $(N = 0, n = \Omega)$. The two lowest excited states have the same energy E and are labelled $(N = 1, n = \Omega + 1)$ and $(N = 1, n = \Omega - 1)$ respectively. The next

https://doi.org/10.1017/9781009401920 Published online by Cambridge University Press

excitation energy is $2E$ and corresponds to a triplet of states comprising the two states $(N = 2, n = \Omega \pm 2)$ and $(N = 2, n = \Omega)$. This spectrum is characteristic of a two-dimensional harmonic oscillator, where N indicates the number of phonons, while $\hbar n$ plays the role of the angular momentum in two dimensions. The values of the transfer cross-sections as well as the associated selection rules further confirm the harmonic structure of the spectrum. One of the degrees of freedom of the two-dimensional oscillator is associated with the change in the number of pairs in the shell above the Fermi surface (pair addition mode) and the other with the change in the number of pairs in the shell below the Fermi surface (pair removal mode).

It is thus natural to rewrite the Hamiltonian (5.1) as

$$H = (W_{\mathrm{a}}\Gamma_{\mathrm{a}}^{\dagger}\Gamma_{\mathrm{a}} + W_{\mathrm{r}}\Gamma_{\mathrm{r}}^{\dagger}\Gamma_{\mathrm{r}}), \tag{5.10}$$

where $\Gamma_{\mathrm{a}}^{\dagger}$ and $\Gamma_{\mathrm{r}}^{\dagger}$ are the creation operators of the pair addition and pair removal modes, which are expressed in terms of the operators $P_j^{\dagger}$ and P_j as

$$\begin{aligned} \Gamma_{\mathrm{a}}^{\dagger} &= a_2 P_2^{\dagger} + a_1 P_1^{\dagger}, \\ \Gamma_{\mathrm{r}}^{\dagger} &= r_1 P_1 + r_2 P_2. \end{aligned} \tag{5.11}$$

Note that the definition introduced in equation (5.10) is equivalent (in the quasi-beam approximation) to the relations $[H, \Gamma_{\mathrm{a}}^{\dagger}] = W_{\mathrm{a}}\Gamma_{\mathrm{a}}^{\dagger}$ and $[H, \Gamma_{\mathrm{r}}^{\dagger}] = W_{\mathrm{r}}\Gamma_{\mathrm{r}}^{\dagger}$ (see Appendix A, equation (A.68)).

Assuming the relation

$$[P_j, P_{j'}^{\dagger}] = (\Omega - N_j)\delta(j, j') \approx \Omega\delta(j, j') \tag{5.12}$$

to be valid for any state of the system under discussion, one obtains

$$a_2 = r_1 = -\frac{2G\sqrt{\Omega}}{(1-x)^{1/4}(2D - W)} \tag{5.13}$$

and

$$a_1 = r_2 = \frac{2G\sqrt{\Omega}}{(1-x)^{1/4}(2D + W)}, \tag{5.14}$$

where

$$W = W_{\mathrm{a}} = W_{\mathrm{r}} = 2D(1-x)^{1/2} \tag{5.15}$$

is the common energy of the pairing modes of excitation. The intensity with which the pair addition and pair removal modes are excited is

$$\begin{aligned} &|\langle n_{\mathrm{a}} = 1, n_{\mathrm{r}}|T|n_{\mathrm{a}} = 0, n_{\mathrm{r}}\rangle|^2 = (a_2 - a_1)^2\Omega^2 \\ &= |\langle n_{\mathrm{a}}, n_{\mathrm{r}} = 1|T|n_{\mathrm{a}}, n_{\mathrm{r}} = 0\rangle|^2 = (r_2 - r_1)^2\Omega^2 \\ &= \Omega(1-x)^{-1/2}. \end{aligned} \tag{5.16}$$

https://doi.org/10.1017/9781009401920 Published online by Cambridge University Press

The above results reproduce the main features of the exact calculations for $x < 1$. Acting with $\Gamma_a^\dagger$ and $\Gamma_r^\dagger$ on the vacuum state, one can build the whole pairing spectrum. A general state is given by

$$|n_a, n_r\rangle = \frac{1}{\sqrt{n_a! n_r!}} (\Gamma_a^\dagger)^{n_a} (\Gamma_r^\dagger)^{n_r} |n_a = 0, n_r = 0\rangle. \tag{5.17}$$

The RPA solution is valid for small values of x. As x increases, W decreases and the cross-sections associated with the two modes tend to ∞. The transition between the normal and the superfluid phase takes place for $x = 1$. Similar features to the one discussed above are also observed in the phase transition between spherical and quadrupole deformed nuclei. In this case the electromagnetic-transition probability plays the role of the two-nucleon transfer cross-section. The analogy between surface and pairing modes can be carried quite far as discussed in Broglia *et al*. (1973) (see also Belyaev (1972) and Schmidt (1972)). The theory of pairing vibrations can also be cast in terms of the collective variables α, ϕ as done in the case of pairing rotations. In fact, in these variables it is possible to formulate the problem of the pairing modes through a Hamiltonian which treats rotations and vibrations on an equal footing (see Bes *et al*. (1970)). For $\Delta \sim 0$, the energies associated with fluctuations in α and ϕ are comparable.

5.1.2 *Collective treatment of pairing vibrations; superfluid systems ($x > 1$)*

The main static effects of the pairing correlations for $x > 1$ can be taken into account through the quasiparticle transformation, which implies a complete hybridization of particles and holes, and thus an intrinsic system connected with the laboratory system through a rotation in gauge space (see Chapter 4 and Appendix I). As discussed in Chapter 3 and in Appendix G, the pairing Hamiltonian approximately reduces to the independent quasiparticle Hamiltonian

$$H_{11} = \sum_j E_j [\alpha_j^\dagger \alpha_j]_0^0, \tag{5.18}$$

where E_j are quasiparticle energies and $\alpha_{jm}^\dagger$, α_{jm} are quasiparticle creation and annihilation operators respectively. The symbol $[\ \ ]_0^0$ implies that these operators are coupled to angular momentum zero, and consequently also zero magnetic quantum number. In the present section we review the different types of collective modes generated by the residual interaction between the quasiparticles.

We consider the system $n = \Omega_1 = \Omega_2$, in which case $\lambda = 0$. The BCS occupation parameters are in this case

$$U_2^2 = V_1^2 = \frac{1}{2}\left(1 - \frac{1}{x}\right) \tag{5.19}$$

https://doi.org/10.1017/9781009401920 Published online by Cambridge University Press

and

$$U_1^2 = V_2^2 = \frac{1}{2}\left(1 + \frac{1}{x}\right), \tag{5.20}$$

while the quasiparticle energy is

$$E = G\Omega. \tag{5.21}$$

The two-level system displays a pairing distortion (gap) of magnitude

$$\begin{aligned}\Delta = G\langle 0|T|0\rangle &= G\Omega(U_1V_1 + U_2V_2)\\ &= G\Omega\left(1 - \frac{1}{x^2}\right)^{1/2},\end{aligned} \tag{5.22}$$

$|0>$ being the BCS ground state. Note that Δ is a collective deformation receiving contributions from all the pairs of particles, and thus is proportional to Ω. The expression given in equation (5.22) should coincide with the single j-shell expression given in equation (H.4) (for $N = \Omega$, see also Section 3.7) in the case $D = 0$. Note, however, that in this case the total degeneracy of the two degenerate shells is 2Ω, thus leading to $\Delta = G\Omega$.

The fluctuations around this equilibrium distortion are induced by the residual interaction among the quasiparticles $H'_{\rm p}$ and $H''_{\rm p}$ (see equations (4.23) and (4.24)) leading to the secular equation (see Appendix J, equation (J.31))

$$W_n^2\left[\left(W_n^2 - 4\Delta^2\right)A - B\right] = 0, \tag{5.23}$$

where

$$A = \left(\sum_i \frac{\Omega_i}{2E_i(4E_i^2 - W_n^2)}\right)^2, \tag{5.24}$$

$$B = \left(\sum_i \frac{\Omega_i f_i}{4E_i^2 - W_n^2}\right)^2 \tag{5.25}$$

and

$$f_i = U_i^2 - V_i^2. \tag{5.26}$$

The forward-going and backward-going RPA amplitudes are

$$a_{ni} = \frac{\Lambda_{1n} f_i + \Lambda_{2n}}{2E_i - W_n}\sqrt{\Omega_i}, \tag{5.27}$$

$$b_{ni} = \frac{-\Lambda_{1n} f_i + \Lambda_{2n}}{2E_i + W_n}\sqrt{\Omega_i}, \tag{5.28}$$

while

$$\frac{\Lambda_{2n}}{\Lambda_{1n}} = -\frac{\sum_i \frac{\Omega_i f_i}{4E_i^2 - W_n^2}}{W_n \sum_i \frac{\Omega_i}{2E_i(4E_i^2 - W_n^2)}} \tag{5.29}$$

and

$$\Lambda_{1n} = \frac{1}{2}\left[W_n \left(\sum_i \frac{f_i^2 2E_i \Omega_i}{(4E_i^2 - W_n^2)^2} \right) + \left(\sum_i \frac{f_i(4E_i^2 + W_n^2)\Omega_i}{(4E_i^2 - W_n^2)^2} \right) \frac{\Lambda_{2n}}{\Lambda_{1n}} + W_n \left(\sum_i \frac{2E_i \Omega_i}{(4E_i^2 - \Omega_i)^2} \right) \left(\frac{\Lambda_{2n}}{\Lambda_{1n}} \right)^2 \right]^{-1/2} . \tag{5.30}$$

The elements a_{11} and a_{22} in the 2×2 determinant (see equation (J.27)) correspond to the dispersion relations resulting from the linearization conditions $[H_{11} + H'_p, \Gamma'^{\dagger}_n] = W'_n \Gamma'^{\dagger}_n$ and $[H_{11} + H''_p, \Gamma''^{\dagger}_n] = W''_n \Gamma''^{\dagger}_n$, respectively, the corresponding collective modes being the pairing vibrations and the Anderson–Goldstone–Nambu (AGN) mode (see Chapter 4). Aside from the root at $W_n = 0$, all roots of (5.23) fulfil the condition $W_n \geq 2\Delta$. In fact, because A and B are positive quantities, the dispersion relation cannot be zero for $W_n < 2\Delta$. If $W_n = 2\Delta$ is a possible root, then the coupling term between the AGN and the pairing vibration, i.e. between the even and odd solutions of the pairing Hamiltonian, must be zero. Thus

$$\sum_i \frac{\Omega_i f_i}{4E_i^2 - W_n^2}\bigg|_{W_n = 2\Delta} = \sum_i \frac{\Omega_i}{4E_i(\varepsilon_i - \lambda)} = 0, \tag{5.31}$$

which holds true if there is a symmetric distribution of levels around the Fermi surface. This is the case in the model under discussion. Thus

$$W = 2\Delta \tag{5.32}$$

and

$$\Lambda_{2n}/\Lambda_{1n} = 0. \tag{5.33}$$

Utilizing the fact that $f_1 = -f_2 = -\varepsilon/G\Omega$, and equations (5.20), (5.21) and (5.30), we obtain

$$\Lambda_{1n} = \left[\frac{W_n}{2} \left(\sum_i \frac{2E_i \Omega_i f_i^2}{(4E_i^2 - W_n^2)^2} \right) \right]^{-1/2} = \varepsilon \sqrt{\frac{G}{2\Delta}} . \tag{5.34}$$

Thus

$$a_1 = -\frac{\varepsilon^2}{2(G\Omega - \Delta)} \sqrt{\frac{1}{2\Delta G\Omega}} = -b_1 . \tag{5.35}$$

https://doi.org/10.1017/9781009401920 Published online by Cambridge University Press

From this result and the expression of the two-body transfer operator

$$T = \sqrt{\Omega_j} U_j^2 \left(\sum_n a_{ni} \Gamma_n^\dagger - \sum_n b_{ni} \Gamma_n \right) + \sqrt{\Omega_j} V_j^2 \left(\sum_n a_{ni} \Gamma_n - \sum_n b_{ni} \Gamma_n^\dagger \right) + \Omega_j U_j V_j \,, \tag{5.36}$$

we obtain

$$\sigma_{\rm gs} = |\langle {\rm gs}(\Omega)|T|{\rm gs}(\Omega - 1)\rangle|^2 = \left(\sum_{j=1,2} \Omega_j U_j V_j \right)^2 = \left(1 - \frac{1}{x^2} \right) \Omega^2 \tag{5.37}$$

and

$$\sigma_1 = |\langle n = 1(\Omega)|T|{\rm gs}(\Omega - 1)\rangle|^2 = \left[\sum_j \sqrt{\Omega_j} (U_j^2 a_{nj} + V_j^2 b_{nj}) \right]^2 = \frac{\Omega}{2x^2 (1 - 1/x^2)^{1/2}} \,, \tag{5.38}$$

for intraband and cross-over two-particle cross-sections, respectively.

All pairs of particles participate in the transition between members of the ground-state rotational band, and the cross-section is proportional to Ω^2. This transition is very large compared with the transition to the pairing vibration. The corresponding ratio

$$\frac{\sigma_1}{\sigma_{\rm gs}} = \frac{1}{2x^2} \left(1 + \frac{3}{2} \frac{1}{x^2} \right) \frac{1}{\Omega} \tag{5.39}$$

is about 10^{-2} for $x = 2$ and $\Omega \approx 10$, which can be considered typical numbers for superfluid systems.

Thus, the pairing vibration, which can be viewed as a coherent transfer of quasiparticles across the Fermi surface, gives rise to a pairing rotational band weakly connected with the ground-state band (see Chapter 4, in particular Fig. 4.2).

5.1.3 Pairing phase transitions

In the case of the quadrupole surface modes of excitation, changes of coupling scheme from the spherical-phonon scheme to the deformed-rotational scheme take place in different regions of the mass table. This change in coupling scheme is usually referred to as a quadrupole phase transition (see, e.g. Bohr and Mottelson (1975)). The pairing order parameter can also be subjected to a 'macroscopic' change and the system undergoes a phase transition from the normal (pairing vibrational) to the superconducting (pairing rotational) state. In both cases the polarization effects of particles outside closed shells give rise to a static field

https://doi.org/10.1017/9781009401920 Published online by Cambridge University Press

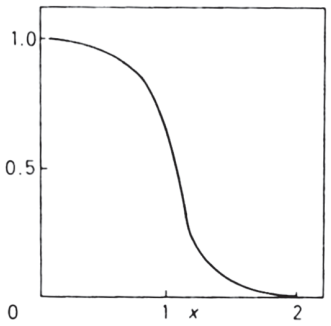

Figure 5.2. Ratio $|< n = 1(\Omega)|T|\mathrm{gs}(\Omega - 1) >|^2 / |< \mathrm{gs}(\Omega)|T|\mathrm{gs}(\Omega - 1) >|^2$ calculated by utilizing the exact functions of the two-level model ($\Omega = 20$) as a function of x.

which violates, in one case, rotational invariance and, in the other, particle number conservation, leading to a privileged orientation in normal and in gauge space. The associated fluctuations which restore rotational and gauge invariance give rise to quadrupole (see Bohr and Mottelson (1975)) and to pairing rotational bands (Bes and Broglia (1966), Chapter 4). The specific probes to study quadrupole phase transitions are Coulomb excitation and inelastic scattering. In a similar way, (t, p) and (p, t) reactions are the specific probes to study the change in the pairing coupling elements.

The most conspicuous feature associated with a pairing phase transition is the behaviour of the ratio $\sigma_1/\sigma_{\mathrm{gs}}$. Equation (5.16) shows that $\sigma_1/\sigma_{\mathrm{gs}} \approx 1$ for the normal phase while equation (5.39) shows that it tends to zero in the superfluid phase. The exact variation of this ratio as a function of x for the two-level model is displayed in Fig. 5.2. Both the RPA pairing vibration scheme for $x < 1$ (equation (5.16)) and the BCS for $x > 1$ (equation (5.38)) diverge at $x = 1$, while the exact calculation predicts a smooth transition. The approximate results are in good agreement with the exact ones for $x \lesssim 0.5$ and for $x \gtrsim 1.5$.

The variation of the two-particle transition intensities have been studied as a function of the number n of pairs in Broglia *et al.* (1968b). The cross-section σ_{gs} from the ground state of the initial nucleus to the ground state of the final nucleus has a rather smooth variation with n and increases as the strength x of the pairing interaction increases. The cross-section σ_1 associated with the pair addition mode to the first excited state is strongly affected by the pairing phase transition. For $x > 1.4$, the crossing of the closed shell at $n = \Omega$ is smooth while for $x < 1.2$ there is a sudden drop in σ_1 at $n = \Omega$. This is because, in the normal phase, the pairing vibration is a two-phonon state, whereas, in the superfluid case, it is a one-phonon type of excitation, the closed shell being defined as the state containing no phonons. In both cases, the two-body transfer operator can change the number of phonons in one.

There is a pairing phase transition in high spin states of deformed nuclei which is induced by the nuclear rotation. The Coriolis field plays the role of an external magnetic field in a superconductor. This phenomenon will be discussed in Chapter 6 of this book.

5.2 Applications

In what follows we apply the concepts developed above to the case of pairing vibration in closed- and in open-shell nuclei.

5.2.1 Normal systems (Pb isotopes)

The nucleus ^{208}Pb provides the best example of a closed-shell nucleus. There is a neat separation between particles and holes. In fact $D \approx 3\,\text{MeV}$ and $2G\,\Omega \approx 0.2 \times 5 \approx 1.0\,\text{MeV}$ ($G \approx 21.5/A\,\text{MeV}$, $j_1 = p_{1/2}$, $j_2 = g_{9/2}$, see Table 5.1), which results in $x \approx 0.3$.

Systematic (t, p) and (p, t) experiments carried out in this region show a well-developed monopole pairing vibrational band (see Fig. 5.5) which encompasses states with up to three phonons of the same type (gs(^{202}Pb)) or of different type

Table 5.1. *Forward-going and backward-going amplitude (5.51) describing the motion of two particles* (^{210}Pb) *and two holes* (^{206}Pb) *around* ^{208}Pb. *A coupling constant* $G = 21.4/A$ MeV *was utilized to reproduce the extra binding energy (5.46) of* ^{210}Pb, *while the corresponding quantity (5.45) for* ^{206}Pb *was reproduced for* $G = 21.7/A$ MeV *(see also Fig. 8.17).*

Single-particle states		^{206}Pb		^{210}Pb
0 $h_{9/2}$	$r_1(\gamma)$	0.11	$a_1(\gamma)$	0.09
1 $f_{7/2}$		0.14		0.10
0 $i_{13/2}$		0.27		0.16
2 $p_{3/2}$		0.24		0.10
1 $f_{5/2}$		0.41		0.14
2 $p_{1/2}$		0.84		−0.10
1 $g_{9/2}$	$r_1(\omega)$	0.13	$a_1(\omega)$	0.82
0 $h_{11/2}$		0.11		0.44
0 $j_{15/2}$		0.11		0.35
2 $d_{5/2}$		0.06		0.20
3 $s_{1/2}$		0.03		0.09
1 $g_{7/2}$		0.06		0.17
2 $d_{3/2}$		0.04		0.11

https://doi.org/10.1017/9781009401920 Published online by Cambridge University Press

(excited state in ^{206}Pb). The identification of 0^+ states excited in either (t, p) or (p, t) reactions is rather simple due to the well-developed diffraction pattern of the associated angular distribution (see Broglia *et al.* (1973)). Two quantum numbers are needed to classify the different states of this two-dimensional harmonic oscillator. We utilize (n_r, n_a) which indicate the number of pair removal and pair addition modes in each state.

The energy of the (1, 1) state in ^{208}Pb predicted by the pairing vibrational model is

$$\begin{aligned} W(1,1) &= (B(208) - B(206)) - (B(210) - B(208)) \\ &= (14.110 - 9.123)\,\text{MeV} = 4.987\,\text{MeV}, \end{aligned} \tag{5.40}$$

where $B(A)$ is the binding energy of the Pb isotope with mass A.

For pedagogical purposes we require the pair addition and pair subtraction modes to have the same energy. Thus

$$W = W(0,1) = W(1,0) = 2.494\,\text{MeV}. \tag{5.41}$$

The excitation energy of any state of the model can be then written as

$$W(n_r, n_a) = (n_a + n_r)2.494\,\text{MeV}. \tag{5.42}$$

The experimental magnitude to be compared is

$$E(N) = (B(^{208}\text{Pb}) - B(N)) + 5.808(N - 126)\,\text{MeV}. \tag{5.43}$$

The linear term ensures $E(124) = E(128)$, which corresponds to the condition (5.41). The different transitions associated with these states are given in terms of the basic cross-section

$$a = \sigma(\text{gs}(^{208}\text{Pb} \rightarrow \text{gs}(^{210}\text{Pb}))) \qquad \text{and} \qquad r = \sigma(\text{gs}(^{208}\text{Pb} \rightarrow \text{gs}(^{206}\text{Pb}))). \tag{5.44}$$

The experimental data associated with (t, p)–(p, t)-reactions on the Pb isotopes around ^{208}Pb are displayed, in term of these elements, in Fig. 5.5.

A microscopic description of the pair addition and pair subtraction modes is obtained by diagonalizing the pairing Hamiltonian in the RPA. The particles and holes are allowed to move in the six levels below and the seven levels above the Fermi surface which are experimentally known (see Table 5.1). The discussion here follows Broglia and Riedel (1967a) and Broglia (1985c). The strength of the coupling constant is determined by fitting the extra binding energy $E(124) = E(128)$, which corresponds to the condition (5.41).

The pairing energies of the two holes and two particles are

$$\begin{aligned} \Delta(206) &= 2[B(208) - B(207)] - [B(208) - B(206)] \\ &= 14.750\,\text{MeV} - 14.110\,\text{MeV} = 640\,\text{keV} \end{aligned} \tag{5.45}$$

https://doi.org/10.1017/9781009401920 Published online by Cambridge University Press

and

$$\Delta(210) = 2[B(210) - B(208)] - [B(209) - B(208)]$$
$$= 9123\,\text{MeV} - 7886\,\text{MeV} = 1237\,\text{keV}. \tag{5.46}$$

The pair addition and pair removal creation operators can be written as

$$\Gamma_n^\dagger(\beta = 2) = \sum_\omega a_n(\omega)\Gamma^\dagger(\omega) + \sum_\gamma a_n(\gamma)\Gamma(\gamma) \tag{5.47}$$

and

$$\Gamma_n^\dagger(\beta = -2) = \sum_\gamma r_n(\gamma)\Gamma^\dagger(\gamma) + \sum_\omega r_n(\omega)\Gamma(\omega), \tag{5.48}$$

where

$$\Gamma^\dagger(\omega) = a^\dagger(\omega)a^\dagger(\bar{\omega}),$$
$$\Gamma^\dagger(\gamma) = a(\bar{\gamma})a(\gamma), \tag{5.49}$$

and n labels the states according to their energy. The indices ω and γ are the shell model quantum numbers of single-particle orbits above and below the Fermi surface, while $\beta = 2$ refers to pair addition and $\beta = -2$ to pair removal modes, β being the transfer quantum number. The RPA equations are the same as those given in equations (5.10)–(5.14) but now for a general distribution of single-particle levels. The energy W_n obtained by linearizing the pairing Hamiltonian is the nth root of the dispersion relation

$$\frac{1}{G(\pm 2)} = \sum_\omega \frac{1}{2\varepsilon(\omega) \mp W_n(\beta = \pm 2)} + \sum_\gamma \frac{1}{2\varepsilon(\gamma) \pm W_n(\beta = \pm 2)}. \tag{5.50}$$

The coefficients a_n and r_n are equal to (see Table 5.1, as well as Fig. 8.17)

$$a_n(\omega) = \frac{\Lambda_n(\beta = 2)}{2\varepsilon(\omega) - W_n(\beta = 2)}, \quad a_n(\gamma) = -\frac{\Lambda_n(\beta = 2)}{2\varepsilon(\gamma) - W_n(\beta = 2)},$$
$$r_n(\omega) = -\frac{\Lambda_n(\beta = -2)}{2\varepsilon(\omega) - W_n(\beta = -2)}, \quad r_n(\gamma) = \frac{\Lambda_n(\beta = -2)}{2\varepsilon(\gamma) - W_n(\beta = -2)}, \tag{5.51}$$

where

$$< 0|\Gamma(\beta = \pm 2)H_p a^\dagger(j)a^\dagger(\bar{j})|0 >= \Lambda_n(\beta = \pm 2)$$
$$= \left[\pm \sum_\omega [2\varepsilon(\omega) \mp W_n(\beta = \pm 2)]^{-2} \right.$$
$$\left. \mp \sum_\gamma [2\varepsilon(\gamma) \mp W_n(\beta = \pm 2)]^{-2} \right]^{-1/2}, \tag{5.52}$$

https://doi.org/10.1017/9781009401920 Published online by Cambridge University Press

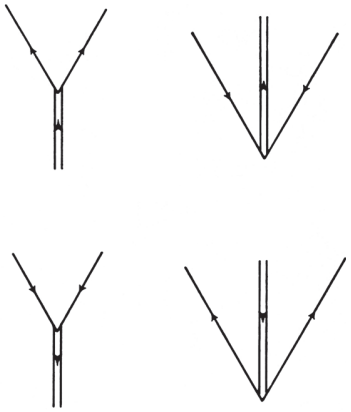

Figure 5.3. Graphical representation of the forward-going and backward-going amplitudes (5.51) of the pairing modes. The vertex strength is equal to $\Lambda_n(\beta = \pm 2)$ (see equation (5.52)). The pairing boson is represented by a double arrowed line, while a single arrowed line represents a fermion.

is the normalization constant of the phonon wavefunction as well as the strength with which a pair of particles in time-reversed states couples to the pairing mode.

Note that the amplitudes (5.51) are obtained by dividing the normalization constants $\Lambda_n(\beta = 2)$ and $\Lambda_n(\beta = -2)$ by the corresponding energy denominators (see Fig. 5.3). This is a common feature of separable forces. The central role played by $\Lambda_n(\beta)$ in the study of the interplay between the different modes of excitation will become apparent in the following sections. The cross-section associated with the transfer of two particles starting from the $N_0 - 2$ ground-state system and leading to the closed-shell (N_0) ground state is

$$r \equiv \sigma^{(0s)}((1,0) \rightarrow (0,0)) \propto \Lambda_1^2(\beta = -2). \tag{5.53}$$

For the cross-section leading to the pair addition mode one obtains

$$a \equiv \sigma^{(0s)}((0,0) \rightarrow (0,1)) \propto \Lambda_1^2(\beta = 2). \tag{5.54}$$

The values of the pairing strengths obtained by fitting the energy of the 206 and 210 ground states are $G(2) = 0.10\,\text{MeV}$ and $G(-2) = 0.14\,\text{MeV}$. The resulting absolute cross-sections are reproduced within a factor of 2. Details of the calculations of the two-particle transfer cross-section are given in Broglia and Riedel (1967a), Broglia *et al*. (1973) and Broglia (1985c). By utilizing the microscopic results it is possible to give a measure of the collectivity of the pair addition and pair removal modes by expressing the corresponding cross-sections in terms of absolute two-particle units. Typical enhancements

$$\varepsilon = \sigma_{\text{exp}}/\sigma_{2\text{p}}, \tag{5.55}$$

https://doi.org/10.1017/9781009401920 Published online by Cambridge University Press

of order 12 are obtained, where σ_{2p} is the average value of the two-particle cross-section to pure two-particle states (see Broglia *et al.* (1971d)). This number can be compared with the value of 10 B_{sp} which is typical of the B(E2) transition rate connecting the lowest 2^+ with the ground state of spherical nuclei.

Note that the contributions of all the different two-particle and two-hole components of the microscopic wavefunction to the corresponding transfer amplitudes associated with the excitation of the $n = 1$ mode are constructively coherent.

5.2.2 Superfluid systems (Sn isotopes)

The Sn isotopes are probably the best example of superfluid spherical nuclei, with a large number of particles outside the closed shell and a large value of the pairing parameter Δ (≈ 1.4 MeV). (t, p) and (p, t) data is shown in Fig. 5.4 (see also Fig. 4.2). The ground-state transition dominates the spectrum, the interband-to-intraband ratio never becoming larger than 0.18. The behaviour of the (t, p) and (p, t) intensities is rather asymmetric, indicating a competition between pairing and shell effects, as shown below. We discuss first the reaction ^{118}Sn(t, p)^{120}Sn.

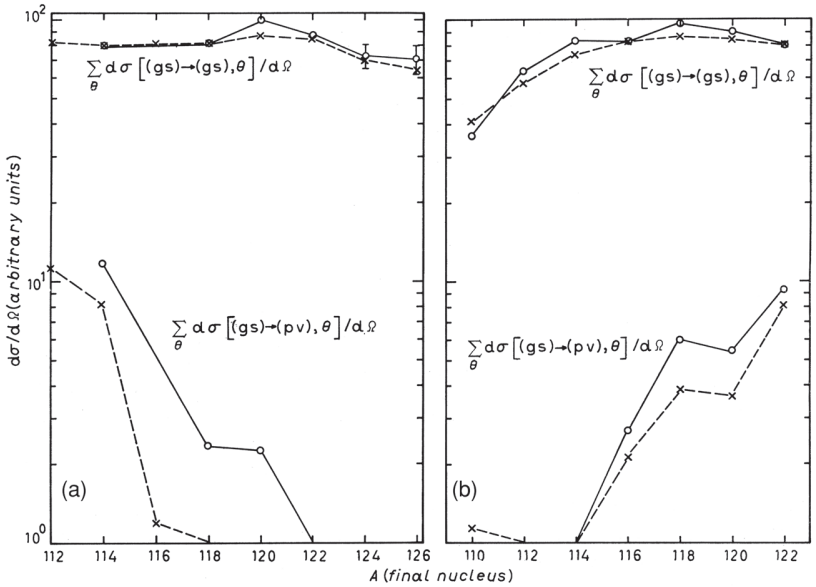

Figure 5.4. Experimental (Bjerregaard *et al.* (1968, 1969), Flynn *et al.* (1970) Fleming *et al.* (1970)) (solid line and open circles) and theoretical (dashed line and crosses) cross-sections corresponding to the $J^\pi = 0^+$ states below 3 MeV excited in the reactions (a) $^{A+2}$Sn(p, t) and (b) $^{A-2}$Sn(t, p). When more than one excited state was observed, the numbers reported are the centroid energy and the summed cross-section. The normalization between theory and experiment was done in both cases to the ^{118}Sn(p, t) $\to$ ^{120}Sn(p, t) reactions.

https://doi.org/10.1017/9781009401920 Published online by Cambridge University Press

Table 5.2. *Wavefunctions (see equations (5.27) and (5.28))) and energies associated with the lowest $J^\pi = 0^+$ states of ^{118}Sn. The valence particles were allowed to move in the five single-particle states displayed. The corresponding BCS occupation parameter U is also given for each single-particle state.*

		$2d_{5/2}$	$1g_{7/2}$	$3s_{1/2}$	$2h_{11/2}$	$2d_{3/2}$
U		0.2449	0.3489	0.4438	0.7861	0.8494
0_1^+	a	−0.0143	−0.0278	−0.0212	0.4340	0.9003
$W = 2.61$ MeV	b	0.0122	0.0155	0.0075	−0.0034	−0.0005
0_2^+	a	−0.1903	−0.4773	−0.7384	−0.4128	0.1638
$W = 2.73$ MeV	b	0.0163	0.0160	0.0039	0.0629	−0.0450
0_3^+	a	−0.1768	−0.7429	0.6243	−0.1605	0.0666
$W = 3.24$ MeV	b	0.0050	0.0029	−0.0013	0.0458	−0.0313

The Hamiltonian $H = H_{11} + H'_{\rm p} + H''_{\rm p}$ (see Section 4.2.1 and Appendix J) was diagonalized in the RPA. A coupling constant $G = 23/A$ MeV was utilized, determined by fitting the ^{118}Sn pairing gap ($\Delta_n = 1.39$ MeV). This procedure yields the occupation parameters, energies and wavefunctions given in Table 5.2 (see also Broglia *et al*. (1968a)).

Making use of these wavefunctions the following enhancement factors (see equation (5.55)) were obtained,

$$\varepsilon = 220 \ \ (\text{gs}), \qquad \varepsilon = 4 \ \ (0_1^+), \qquad \varepsilon = 4 \ \ (0_2^+) \, . \tag{5.56}$$

The square root of the value associated with the ground state gives a measure of the number of twofold degenerate levels contributing to the static pairing distortion Δ. This number is ≈ 15 (see (3.68)). Thus, all the levels considered in solving the BCS equation contribute to the ground-state transition (in fact $\sum_j (j + 1/2) = 18$). The enhancement factor $\varepsilon(\text{gs}) = 220$ associated with an interband transition should be compared with the enhancement factors obtained for the $E2$ decay of the 2^+ member of the ground-state rotational band in quadrupole deformed nuclei. Typical numbers are 200 $B_{\rm sp}$ implying that about $\sqrt{200} \approx 14$ twofold degenerate levels contribute to the quadrupole static deformation Q_0.

The systematic comparison between the intensities predicted by the pairing vibrational model and the experimental data is carried out in Fig. 5.4. A rather considerable change of the order parameter $\Delta/<\delta\varepsilon>$ takes place through Sn isotopes. The quantity $<\delta\varepsilon>$ is the average distance between the levels around the Fermi surface. Thus $\Delta/<\delta\varepsilon>$ plays a similar role to that played by x in the case of the two-level model (see Section 5.1, equation (5.9)). It may be approximated by the number $n_\Delta(A)$ of double degenerate single-particle levels

https://doi.org/10.1017/9781009401920 Published online by Cambridge University Press

in the interval $\Delta(A)$ around $\lambda(A)$. We obtain (see also equation (3.68))

$$n_\Delta(^{112}\mathrm{Sn}) = 8, \qquad n_\Delta(^{116}\mathrm{Sn}) = 3 \tag{5.57}$$

and

$$n_\Delta(^{120}\mathrm{Sn}) = 8. \tag{5.58}$$

These changes in $\Delta / <\delta\varepsilon>$ give rise to a partial distinction between particles and holes and, consequently, to two collective transitions similar to the case of normal systems, in particular for the case of ^{114}Sn.

5.3 Multipole pairing vibrations

In the previous sections we have concentrated our attention in the monopole pairing modes. Thus, we have restricted the distortions and vibrations of the Fermi surface to be isotropic. The condensation in p-wave observed in the case of ^{3}He gives an example, at the macroscopic scale, of non-isotropic distortions of the Fermi surface, produced by a pairing interaction acting in an $l = 1$ state of relative motion (see Chapter 1). In fact, the three superfluid phases corresponding to $\uparrow\uparrow$, $\downarrow\downarrow$ and $\uparrow\downarrow$ ($m = \pm 1, 0$) have been observed (see e.g. Vollhardt and Wölfle (1990)). Experimental evidence indicates that high-T_c superconductors (cuprates) display a mixture of s- and d-pairing (see, e.g. Tinkham (1996) Section 9.6). In nuclei the only component of the short-range part of the residual interaction which gives rise to a condensate is the monopole pairing force. It is, however, expected that multipole vibrations, which change the number of particles by two, can play an important role in the dynamics of the nuclear spectrum (see also Section 8.4).

5.3.1 Normal systems (Pb isotopes)

There is specific evidence for the existence of multipole pairing vibrations provided by the strong $L = 2, 4$ and 6 cross-sections associated with (t, p) and (p, t) transitions in the Pb isotopes (Bjerregaard *et al*. (1966b), Igo *et al*. (1971), Landford and McGrory (1973)). A microscopic description of these modes can be obtained as in the case of the monopole pairing vibration, in the framework of the random-phase approximation, allowing the particles to correlate through the schematic interaction (Bes and Broglia (1971))

$$H(2\lambda) = -\frac{\pi G_\lambda}{2\lambda + 1} \sum_\mu P^\dagger_{\lambda\mu} P_{\lambda\mu}, \tag{5.59}$$

where

$$P^\dagger_{\lambda\mu} = \sum_{j_1 j_2} < j_1 || Y_\lambda || j_2 > [a^\dagger_{j_1} a^\dagger_{j_2}]^\lambda_\mu \, . \tag{5.60}$$

https://doi.org/10.1017/9781009401920 Published online by Cambridge University Press

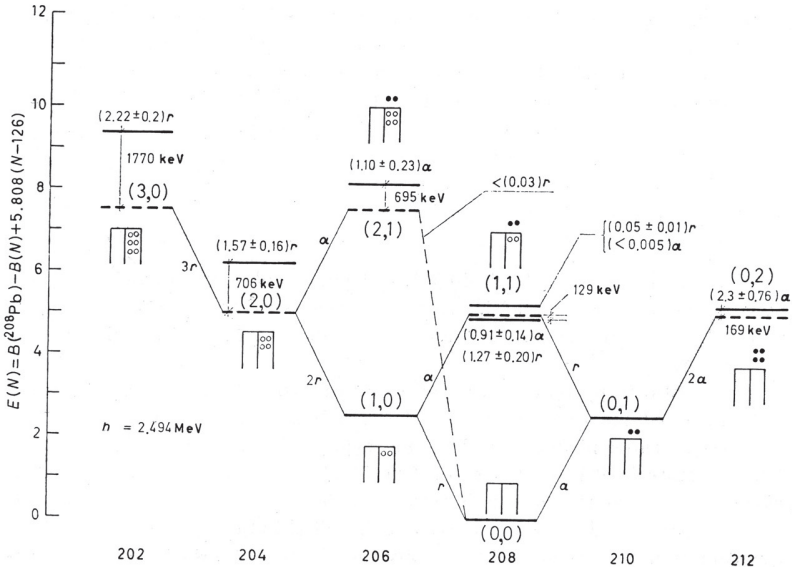

Figure 5.5. The many-phonon pairing spectrum around ^{208}Pb. The energies predicted by the pairing vibrational model are displayed as dashed horizontal lines. The harmonic quantum numbers (n_r, n_a) are indicated for each level. A schematic representation of the many-particle many-hole structure of the state is also given. The transitions predicted by the model are indicated in units of r and a (see equation (5.44)). The corresponding experimental numbers are also given together with their errors, above each level. The dashed line between the states (0, 0) and (2, 1) indicates that the ^{208}Pb(p, t)^{206}Pb reaction to the three-phonon state in ^{208}Pb was carried out and an upper limit of $0.03r$ for the corresponding cross-section was determined (see Flynn *et al*. (1972) Broglia *et al*. (1973), also Landford and McGrory (1973)).

The coupling constant G_λ can be determined through dispersion relations similar to that shown in equation (5.50), by fitting the binding energy of the two-particle and two-hole system, respectively. The resulting values corresponding to the multipolarities $\lambda = 0, 2, 4$ and 6 and to both ^{206}Pb (pair-removal modes) and ^{210}Pb (pair-addition modes) are very similar to each other and equal to (see Broglia *et al*. (1974b))

$$G_\lambda \approx 27/A \text{ MeV}. \tag{5.61}$$

Using the corresponding wavefunctions one obtains the (t, p) and (p, t) cross-sections displayed in Table 5.3.

The quadrupole transition probability between the lowest 2^+ and the ground state of ^{210}Pb is given in the present model by

$$B(E2; 0 \to 2^+) = (e_{\text{eff}})^2 \left[2 \sum_{j_1 j 2} a(j_1 j_2; 2^+) a(j_1^2; \text{gs}) \frac{< j_2 || r^2 Y_2 || j_1 >}{\sqrt{2j_1 + 1}} \right]^2 . \tag{5.62}$$

https://doi.org/10.1017/9781009401920 Published online by Cambridge University Press

Table 5.3. *Ratio of experimental (Landford and McGrory (1973), Bjerregaard et al. (1966a), Igo et al. (1971)) and theoretical (Broglia et al. (1974b)) cross-sections associated with the reactions* ^{208}Pb(t, p)^{206}Pb *leading to the lowest states of each spin and parity.*

	^{208}Pb(p, t) ^{206}Pb(J^π)		^{208}Pb(t, p) ^{210}Pb(J^π)	
J^π	E (MeV)	$\frac{[d\sigma(J^\pi)/d\Omega]_{exp}}{[d\sigma(J^\pi)/d\Omega]_{th}}$	E (MeV)	$\frac{[d\sigma(J^\pi)/d\Omega]_{exp}}{[d\sigma(J^\pi)/d\Omega]_{th}}$
0^+	0.000	0.94	0.000	1.47
2^+	0.803	0.75	0.795	0.78
4^+	1.684	0.88	1.094	1.21
6^+	3.253	0.49	1.193	0.77

Using the calculated amplitudes and the experimental data ($B(E2)_{206} = 7B_{sp} = 0.5B(E2)_{210}$), one obtains for the effective charges (see Bohr and Mottelson (1975) and references therein)

$$e_{eff}(^{206}\text{Pb}) = 0.98, \qquad e_{eff}(^{210}\text{Pb}) = 1.03. \tag{5.63}$$

These values are consistent with the effective charges obtained from transitions among single-particle states in ^{207}Pb and ^{209}Pb (see Bohr and Mottelson (1975) and references therein). This result provides further support for the description of the 2_1^+ of ^{210}Pb as a pairing vibration of ^{208}Pb.

The existence of a $\mu = 0$ quadrupole pairing force of strength approximately equal to (5.61) has been shown (Ragnarsson and Broglia (1976)) to play a basic role in the 0^+ spectrum of the actinide nuclei (see next section). As discussed in Hamamoto (1977), the $\mu = 1$ component of the quadrupole pairing force plays an important role in determining the value of the moment of inertia of deformed nuclei (see also Migdal (1959) and Belyaev (1961)).

5.3.2 Superfluid systems (heavy deformed nuclei)

In normal spherical nuclei the Hamiltonian (5.59) generates the $\alpha \pm 2$ modes, but has no systematic effect on the particle–hole states, i.e. states with transfer quantum number $\alpha = 0$. The part of the nuclear interaction which generates isoscalar surface vibrations can be written schematically as (see also Section 3.4)

$$H(0\lambda) = -\frac{\kappa_\lambda}{2} \sum_\mu Q^\dagger_{\lambda\mu} Q_{\lambda\mu}, \tag{5.64}$$

https://doi.org/10.1017/9781009401920 Published online by Cambridge University Press

where

$$Q_{\lambda\mu} = -\frac{1}{\sqrt{2\lambda+1}} \sum_{a_1 a_2} < a_1 || r^\lambda Y_\lambda || a_2 > [a_1^\dagger a_2]^\lambda_\mu. \tag{5.65}$$

In superfluid nuclei, because the distinction between particles and holes is lost, the two-quasiparticle states $(\lambda, \pi = (-1)^\lambda)$ are correlated by both the multipole pairing and the particle–hole interaction. Note that while the correlations generated by (5.59) specifically enhance two-nucleon transfer reactions, (5.65) enhances inelastic scattering and Coulomb excitation processes (see Broglia *et al.* (1971d), (1973)). Consequently, the presence of both particle–hole and multipole pairing interaction lead to ground-state correlations (zero point fluctuations) which, being opposite to each other (blocking effects), stabilize low-lying vibrations displaying both enhanced $B(E\lambda)$ as well as (t, p) and (p, t) cross-sections. The consequences of the interplay between multipole particle–hole and pairing (particle–particle) correlations in the nuclear spectrum is still an open question (see e.g. Volya *et al.* (2001, 2002), Zelevinsky and Volya (2004)).

Because of the conservation of angular momentum, the BCS pairing gap, which can be related to the odd–even mass difference, is determined by the monopole pairing interaction. This is also true, as discussed above, for the fluctuations of the gap giving rise to two-quasiparticle 0^+ pairing vibrational states.

For deformed nuclei this restriction is no longer valid. The pairing gap now receives contributions from different pairing multipoles, i.e.

$$\Delta_i = \Delta_0 + \sum_{\lambda>0} \Delta_\lambda Q_i^{(\lambda)}, \tag{5.66}$$

where

$$Q_i^{(\lambda)} = < i || Y_\lambda || i >, \tag{5.67}$$

$$\Delta_0 = G_0 \sum_i U_i V_i \tag{5.68}$$

is the standard (monopole) pairing gap and

$$\Delta_\lambda = \sqrt{\frac{\pi}{2\lambda+1}} G_\lambda \sum_i < i || Y_\lambda || i > U_i V_i \tag{5.69}$$

measures the multipole distortion (departure from anisotropy) of the Fermi surface (see Broglia *et al.* (1969a)). The index i labels Nilsson single-particle levels. Specialized to the case of $\lambda = 2$, the pairing matrix elements are equal to

$$\langle i\tilde{i} | (H(2,0) + H(2,2)) | j\tilde{j} \rangle = -G_0 - G_2 Q_i Q_j, \tag{5.70}$$

where we have used $Q_i = Q_i^{(2)}$. The violation of both angular momentum and particle number conservation brings a new dimension to the role that multipole pairing correlations play in nuclear structure (Bes *et al.* (1972)).

https://doi.org/10.1017/9781009401920 Published online by Cambridge University Press

In particular, the gap (5.66) can become very small for certain levels as well as the matrix element (5.70). This phenomenon is analogous to the phenomenon of gapless superconductivity in solid-state physics. There, an impurity traps a magnetic field which is larger than the critical magnetic field H_c, thus giving rise to some quasiparticles for which $\Delta_i \approx 0$. In nuclei, it is the shell structure which acts as impurity, displaying particular signs of the quadrupole moment for particular values of the angular momentum (see Sections 6.2.1 and 6.2.2).

One can distinguish two different types of pairing matrix elements: (i) those that are related with the scattering of particles between pairs of single particles having the same sign of the quadrupole moment, i.e.

$$G_{oo} = < i_o \bar{i}_o | H(20) + H(22) | i'_o \bar{i}'_o > = -G_o - G_2 Q_{i_o} Q_{i'_o}, \quad (5.71)$$

$$G_{op} = < i_p \bar{i}_p | H(20) + H(22) | i'_p \bar{i}'_p > = -G_o - G_2 Q_{i_p} Q_{i'_p}, \quad (5.72)$$

and (ii) those between pairs of orbitals with opposite sign of the quadrupole moment, i.e.

$$G_{pp} = < i_p \bar{i}_p | H(20) + H(22) | i'_p \bar{i}'_p > = -G_o + G_2 | Q_{i_p} Q_{i'_p} |. \quad (5.73)$$

The label o denotes oblate orbitals which have a negative sign of Q, while p stands for prolate orbitals corresponding to a positive sign.

In general,

$$|G_{oo}| \approx |G_{pp}| \gg |G_{op}|. \quad (5.74)$$

In this case we can distinguish, as in the case of closed-shell system, between two groups of single-particle levels which are uncoupled from each other. In the closed-shell system $< i\bar{i} | H(20) | i'\bar{i}' >$ has similar values for the scattering of any pair of particles. However, if $i > i_F$, $i' < i_{F'}$, the scattering amplitude $G_0/\Delta\varepsilon$ becomes very small, $\Delta\varepsilon$ being twice the single energy gap (for Pb, $\Delta\varepsilon \approx 7$ MeV and $G \approx 0.1$ MeV). There is thus a static decoupling between the single-particle levels.

In the case of deformed nuclei, on the other hand, the single-particle levels are closely spaced and $\Delta\varepsilon$ is of order of G (e.g. the average spacing of the single-particle levels of ^{234}U around the Fermi energy shown in Fig. 5.6 is 360 keV). However, because of the inequality (5.74), the scattering amplitude between oblate and prolate single-particle orbitals can become very small. In this case there is a dynamical decoupling between the single-particle levels due to the correlations among the particles.

Let us consider the effect of the monopole plus quadrupole pairing force acting on a system of particles moving in the single-particle levels displayed in Fig. 5.6. Around the Fermi surface there is a predominance of prolate levels, while ≈ 0.7 MeV below the Fermi surface there is a group of oblate single-particle levels.

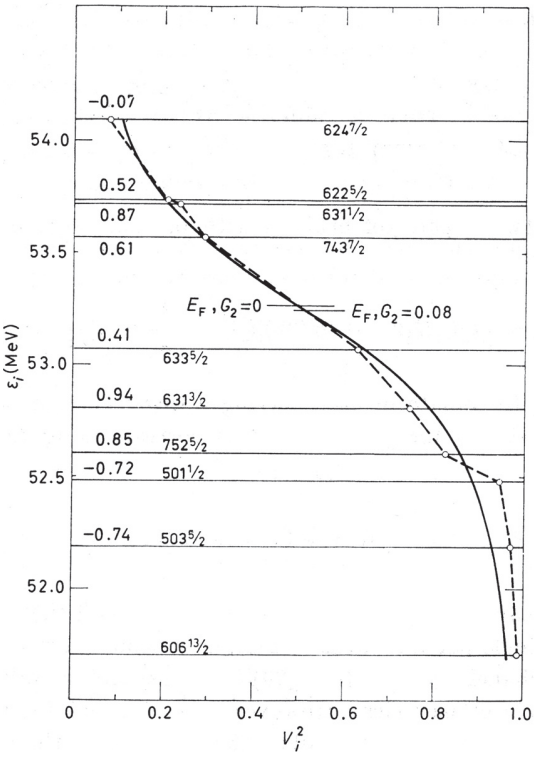

Figure 5.6. The occupation probability V_i^2 for levels around the Fermi surface E_F of ^{234}U for $G_2 = 0.08$ MeV (dashed line). For each level the asymptotic quantum numbers are given as well as the value of the single-particle quadrupole moment in fm^2.

When the residual monopole and quadrupole pairing interactions are switched on, one can construct essentially two ground states. The ground state of nucleus A, based on the levels around the Fermi surface, and the ground state of the $A-2$ system (pair-removal mode), based on the states with negative value of the quadrupole moment. Thus, this latter state has a similar relation to its ground state as the $N_0 - 2$ system has to the closed N_0 system ground state. Note that all the different terms which contribute to the two-nucleon transfer amplitude of the excited state can produce constructive coherence and still be orthogonal to the ground state, because the two states have components appreciably different from zero on different single-particle orbitals and thus are orthogonal *ab initio*.

Although the deformed nucleus ^{234}U is superfluid, the quadrupole pairing correlations allow for the existence of real particles ($V_i \approx 1$), almost uncoupled from the superfluid ground state and moving rather close to the Fermi surface. Because of the non-conservation of the number of particles, the states based on the oblate orbitals become an excited state of the A-system, namely an isomeric

https://doi.org/10.1017/9781009401920 Published online by Cambridge University Press

pairing state with a rather differerent average value of the gap parameter than the ground state.

The existence of a pairing isomer in a pairing deformed nucleus is evidenced by the unusually large two-nucleon transfer cross-section to excited 0^+ states, in a similar way that a shape isomer in a quadrupole deformed nucleus displays a very retarded electromagnetic-transition probability. Giving the same weight to the different configurations, we get, for the ground-state (t, p) and (p, t) cross-sections,

$$\sigma(\text{gs} \rightarrow \text{gs}) = \left(\sum_i U_i V_i \right)^2 = (\Delta / G)^2. \tag{5.75}$$

The corresponding cross-sections to an excited 0^+ state are given by

$$\sigma^{(\text{p,t})}(\text{gs} \rightarrow 0^+) \approx \left(2 \sum_i a_i V_i^2 \right)^2 \tag{5.76}$$

and

$$\sigma^{(\text{t,p})}(\text{gs} \rightarrow 0^+) \approx \left(2 \sum_i a_i U_i^2 \right)^2, \tag{5.77}$$

where a_i denotes the two-quasiparticle component (forward-going amplitude) of the single-particle state i.

In the actinide region a typical value for (5.75) is 100, while (5.76) and (5.77) depend strongly on the amplitude a_i. If the first excited state is below the smallest two-quasiparticle energy $2E_i$ and is mainly generated by vibrations of the monopole pairing gap, all the a_i below the Fermi surface have one sign and all those above the opposite sign. This sign change is necessary for the excited state to be orthogonal to the ground state. If $G_2 = 0$, the low-lying excited states will mainly be built out of the states close to the Fermi surface (with $U_i \approx V_i \approx 0.5$), which means that (5.77) and (5.78) will be about equal and of the order of unity because of cancellations from states below and above the Fermi surface.

The pairing isomer ($G_2 \approx 0.1$), on the other hand, is mainly built out of the oblate levels below the Fermi surface and is, from the start, orthogonal to the ground state which has very small components on these single-particle levels. For these oblate levels, $V_i^2 \approx 1 (\varepsilon_i < \varepsilon_\text{F})$ and the different contributions to (5.77) add with the same sign resulting in a large (p, t) cross-section.

In a schematic model where the 0^+ state has equal amplitudes on configurations built out of the five oblate orbitals, we find

$$\sigma^{(\text{p,t})}(\text{gs} \rightarrow 0^+) \approx \left(2 \sum_{i=1}^{5} \sqrt{\frac{1}{5}} \right)^2 = 20, \tag{5.78}$$

https://doi.org/10.1017/9781009401920 Published online by Cambridge University Press

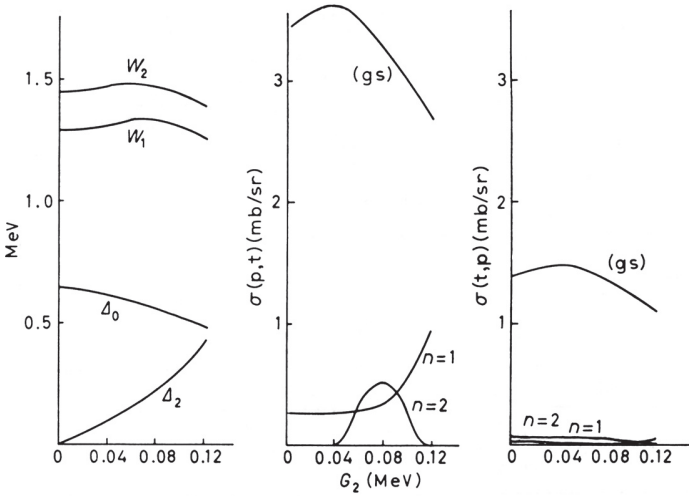

Figure 5.7. Dependence of the different parameters associated with the monopole and quadrupole pairing degree of freedom as a function of G_2, and for the nucleus ^{234}U. The labels $n = 1$ and $n = 2$ indicate the first and the second 0^+ excited state, respectively.

while the (t, p) cross-section is essentially zero ($U_i \approx 0$)($\varepsilon_i < \varepsilon_F$) . Moreover, as the oblate single-particle levels have a small average value of Δ, the quasiparticle energies $E_i = \sqrt{(\varepsilon_i - \lambda)^2 + \Delta^2}$ will be relatively small implying that the pairing isomer will be found at a low excitation energy.

In Fig. 5.7 we display the change of the different physical magnitudes (W, σ(t, p), σ(p, t), Δ_0 and Δ_2) as a function of G_2 for fixed values of G_0 and of K_2. According to the discussion connected with the results displayed in Table 5.3, one should choose $G_2 = G_0$. For this value of G_2 we display in Table 5.4 the results of the model discussed above for nuclei in the actinide region, in comparison with the experimental data (see also Casten *et al.* (1972)).

Before concluding this section it is interesting to mention the results of a recent ^{160}Gd(p, t)^{158}Gd experiment by Lesher *et al.* (2002), in which 13 excited 0^+ states with energy below 3.2 MeV have been observed. Calculations making use of both particle–hole and pairing multipole interactions seem to be able to explain the presence of so many low-lying 0^+ states (N. Lo Giudice, A. V. Sushkov and N. Yu. Shirikova, *Key Topics in Nuclear Structure*, Paestum 23–27 May 2004, abstracts, p. 76). While none of these states is found to lead to collective electromagnetic transition probabilities, some of them are found to display collectivity in the pairing channel. Note that Zamfir *et al.* (2002) are able to account for essentially all of the 0^+ states observed within a basis

Table 5.4. *The experimental (Maher et al. (1970) excitation energies, relative* (p, t) *cross-sections and* $X = \rho^2 e^2 R_0^4 / B(E2; 2 \rightarrow 0)$ *values associated with the low-lying* 0^+ *states are compared with the theoretical calculations (Ragnarsson and Broglia (1976)) for the actinide region.*

	Excitation energy (keV)		$\frac{\sigma(\text{excited } 0^+)}{\sigma(\text{g.s. } 0^+)}$		X	
Nucleus	Experimental	Theoretical	Experimental	Theoretical	Experimental	Theoretical
^{228}Th	830		18		(0.83)	
		930		13.4		0.33
^{230}Th	636		18		0.22 ± 0.10	
	1590		3			
		1040		16.8		0.35
		1270		4.4		0.39
^{232}U	695		13		0.17 ± 0.04	
		930		8.5		0.37
^{234}U	812		13		0.50 ± 0.08	
		1020		16.5		0.41
		1250		2.0		0.46
^{236}U	920		13			
		950		11.7		0.39
		1220		2.1		0.35
		1760		1.6		0.97
^{240}Pu	862		15		0.05 ± 0.01	
	1091		10			
		1070		6.0		0.41
		1260		1.5		0.40
		1450		2.6		
^{242}Pu	956		24			
		1100		9.0		0.39
		1210		13.7		0.24
		1610		5.9		
^{246}Cm	1176		11			
		1180		4.8		0.42
		1300		5.2		0.24
		1610		11.1		

which include s, d and f bosons. This result seem sensible in keeping with the fact that if one adds a g boson to the basis, the calculations would be essentially equivalent to those of Lo Giudice *et al*. mentioned above; see Broglia (1981).

6
Phase transitions

In the present chapter we shall discuss the consequences the finite number of particles have in the phenomenon of pairing phase transition in atomic nuclei. Finite size effects give rise to fluctuations of the pairing gap and thus of the correlation length (order parameter) ξ. Because ξ is much larger than the size of the nucleus, it comes as no surprise that in describing the phase transition in the small-particle superconductors one doesn't need the non-analytic functions necessary to account for the condensation in infinite systems. On the other hand, the phenomena in both systems are closely related and, in a system like the nucleus, we have the possibility of studying the transition in terms of the spectrum of individual states. Thus the transition from a pair-correlated to a normal system with increasing angular momentum involves the coupling between rotational bands associated with the ground state and with excited (few quasiparticle) states.

Because all the transitions we shall treat are connected with level crossings at zero temperature, it is more appropriate to talk about quantal phase transitions (see Sachdev (1999)).

The variation of the moment of inertia $\mathcal{I}$ of rotational bands with angular momentum provides one clue to the variation of the pairing gap with angular momentum. This is because the moment of inertia has a simple monotonic dependence on Δ. In characterizing a superfluid nucleus the moment of inertia $\mathcal{I}$ of the rotational bands and the energy of the lowest non-collective excitations $2E_\nu$ play a central role. Bohr and Mottelson (1975, equation (4.128)) have given a qualitative estimate of the effect of pair correlations on the moment of inertia which depends on a dimensionless parameter $x \sim \beta_2 \hbar\omega_0/2\Delta$ where β_2 is the quadrupole deformation of the system, $\hbar\omega_0 \sim 41/A^{1/3}$ MeV is the energy between major shells in the single-particle potential, and Δ is the pairing gap. Their expression for the relation between the rigid moment of inertia $\mathcal{I}_{\text{rig}}$ and the actual moment of inertia of a deformed nucleus is $\mathcal{I} = \mathcal{I}_{\text{rig}}(1 - g(x))$

https://doi.org/10.1017/9781009401920 Published online by Cambridge University Press

where

$$g(x) \approx \frac{\ln\left(x + \sqrt{1+x^2}\right)}{x\sqrt{1+x^2}}.$$

The moment of inertia tends to the rigid value when the pairing is weak and decreases as Δ increases ($x \approx \beta_2 \hbar\omega_0/2\Delta$). For typical cases ($A = 160$, $\beta_2 \sim 0.3$, $\hbar\omega_0 \sim 7.5$, $\Delta \sim 0.9$ MeV) one obtains $x \sim 1.25$, and $g(x) \sim 0.5$. However, both $\mathcal{I}$ and E_ν are strongly dependent on the shape of the nucleus, which is modified by the rotation of the system as a whole, making it difficult to extract the order parameter from the changes observed in these quantities.

A better probe is the transfer of two nucleons as a function of the angular momentum. In fact, as already discussed in Chapters 4 and 5, the ratio of the two-nucleon transfer differential cross-section between the ground states of superfluid nuclei, normalized with respect to the DWBA differential cross-section calculated making use of a form factor describing the motion of two uncorrelated particles in a single j-orbit typical of the mass region, is approximately given by $(\Delta/G)^2$ where G is the pairing coupling constant.

New possibilities have been opened by the observation of tunnelling between different minima of the potential-energy surface, which displays a very strong dependence on the rotational frequency. The tunnelling probability depends exponentially on the pairing gap, making such measurements extremely sensitive to changes of Δ as a function of I. The tunnelling probability from a deformed to a superdeformed configuration (see Section 6.5) can be written in the WKB approximation, assuming the barrier is well described by an inverted parabola as a function of the deformation, as (see Chapter 7)

$$P \sim \exp\left[-\frac{2\pi(E_\mathrm{B} - E)}{\hbar\sqrt{C/D}}\right].$$

The quantity E_B is the height of the barrier, E the (zero point) energy of the system in the deformed minimum, while D and C are the tunnelling mass parameter of the system and the curvature of the parabola. In Section 7.1.1 it will be shown that $D \propto \Delta^{-2}$ for a superfluid nucleus.

In Sections 6.1–6.5 we discuss the general properties of the pairing phase transition as a function of I, paying special attention to the energies, alignments (derivative of the energies with respect to angular momenta) and moments of inertia. The dependence of the moment of inertia on pair correlations is discussed in Section 6.2.1 to obtain an estimate of the critical angular momentum for pair collapse. In Section 6.5 we discuss the role played by pairing in the tunnelling between superdeformed and normal deformed nuclei, while in the

last section we discuss the role that pairing fluctuations play in the rotation of nuclei.

6.1 The experimental situation

There are two mechanisms by which the nucleus can generate high angular momentum: single-particle alignment along a common axis or by a collective rotation of the nucleus as a whole. This is illustrated in Fig. 6.1, where level schemes of ^{158}Er and ^{147}Gd are shown. The ^{158}Er scheme is quite regular and the dominant behaviour is collective rotation of a body displaying prolate deformation. The spectrum of ^{147}Gd is very irregular, with complicated decay pathways and isomeric states. Its dominant behaviour is very likely single-particle alignment.

In spite of differences, both of these schemes contain elements of the other type of behaviour. In particular, there are irregularities in the ^{158}Er rotational pattern at spins around 16 and 26. In fact, as the nucleus de-excites from a high

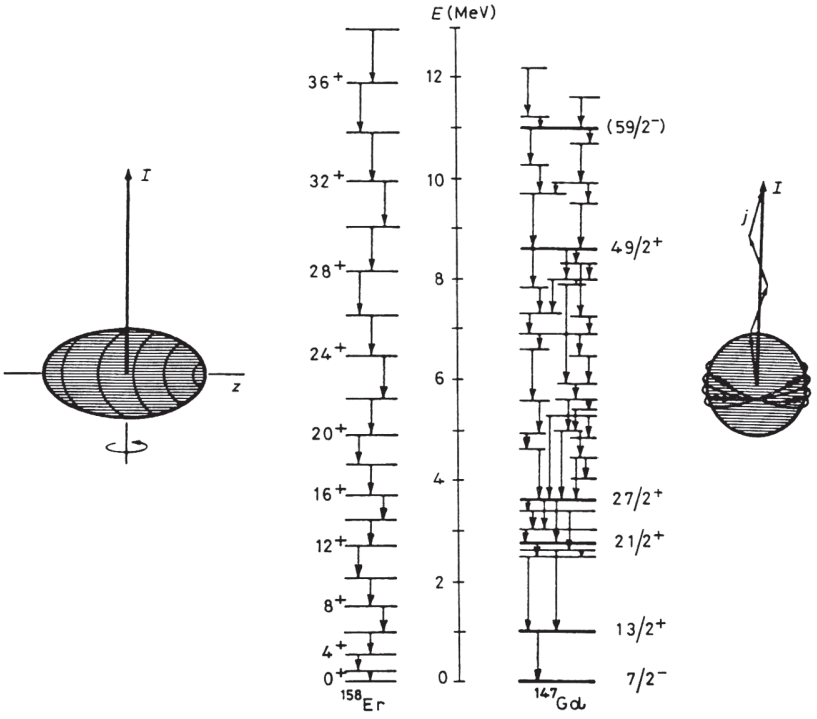

Figure 6.1. Level scheme for ^{158}Er and ^{147}Gd, together with illustrations of the dominant source of angular momentum for each case (from Stephens (1985)).

https://doi.org/10.1017/9781009401920 Published online by Cambridge University Press

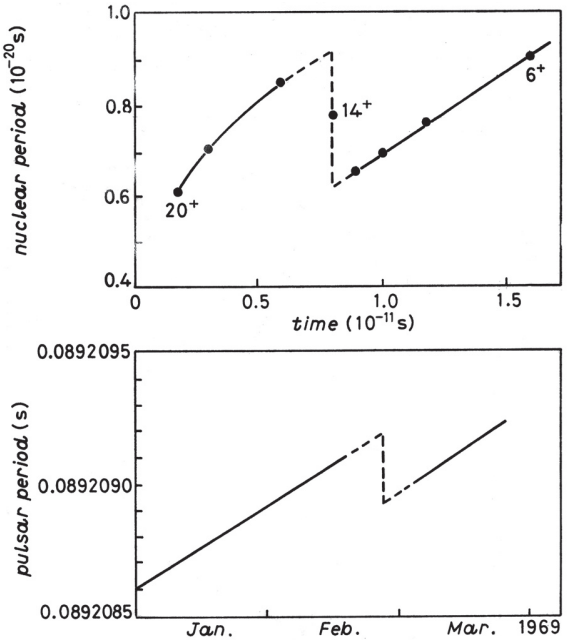

Figure 6.2. Plots of the rotational period against time for the nucleus ^{158}Er (top) and the pulsar Vela (bottom) (from Stephens (1985)).

initial spin, the regular increase of the nuclear period (slowing-down) is interrupted occasionally by rather marked decreases. These correspond to internal rearrangements, 'nuclear quakes', and are generally called 'backbends'. One may compare them to another type of quakes – 'star-quakes'. Neutron stars or 'pulsars' are also rapidly rotating systems that are slowing down (Chapter 1). Occasionally they too display sudden speed ups of the rotational motion called 'glitches' (see Anderson *et al.* (1982), Ruderman (1972), Shapiro and Teukolsky (1983), Pines *et al.* (1992)).

It is quite common for rapidly rotating objects to modify their internal structure and thus their moments of inertia, and that these modifications revert back, often in sudden jumps of the rotational period, as the system slows down. The interesting question for each system has to do with the nature of the internal modification. The slowing-down of the nucleus ^{158}Er below spin 20 is compared with the pulsar Vela in Fig. 6.2. The behaviours are quite similar, though the percentage change in the nuclear case is much larger. The pulsar glitches are not too well understood at present – early explanations had to do with a sudden breaking of the solid crust on the neutron star, but more recent ones involve vortices in the flow pattern (see e.g. Epstein and Baym (1988), Pizzochero *et al.* (1997), Alpar (1977, 1998), Donati and Pizzochero (2003)). The nuclear glitch

is due to the sudden pairing of two high-j particles. In the case of this first backbend in ^{158}Er, the particles are $i_{13/2}$ neutrons. Above $I \sim 14$ this pair of aligned particles contributes $10\hbar$ along the rotation axis, but this is lost below $I \sim 14$ when the particles suddenly couple to spin nearly zero (decoupling) and begin to participate in the pairing correlations. The angular momentum has to be made up by the collective rotation, which must speed up, thereby decreasing the period.

Such a behaviour is now well studied in nuclei around ^{158}Er, and the change described above corresponds to a crossing of two rotational bands (Stephens and Simon (1972)). A band with two aligned $i_{13/2}$ neutrons crosses the ground-state band, which has all particles participating in the pairing correlations (pairing vacuum). Thus the discontinuity actually corresponds to a shift into another band, though the mixing between these bands gives collective enhancement to the transition connecting the bands, often to the point where they are stronger than the 'in-band' transitions at the crossing. The energy of the aligned band relative to the ground band gradually decreases with increasing spin because of the Coriolis interaction. Just as a gyroscope will attempt to align its rotation axis with that of its rotating frame, so a pair of high-j particles tends to align its rotation axis (angular momentum) with that of the rotating nucleus, thereby decreasing its energy relative to a band without such an alignment.

The shift in angular momentum between the orbital motion of individual particles and the collective rotation of the nucleus is illustrated in Fig. 6.3, where the top figure is the moment of inertia plotted against angular frequency ($\hbar\omega = E_\gamma/2$) for a nucleus ^{158}Er. The sharp increases in the moment of inertia due to the alignments are apparent, the first one giving rise to a 'backbending' as the sequence shifts bands and the second to an 'upbend'. In the centre of Fig. 6.3, spin is plotted against angular frequency. The members of the three different bands fall rather clearly on separate lines, and the difference in spin between the lines at a given frequency represents the difference in aligned angular momentum, Δi, between the bands at that frequency. The $i_{13/2}$ band has about $10\hbar$ units on angular momentum aligned relative to the ground band of ^{158}Er. The next higher band has two more particles aligned (four-quasiparticle state), which are believed to be $h_{11/2}$ protons, and the additional Δi is about $7\hbar$. Both the spin and the angular frequency in Fig. 6.3 are directly measurable quantities. Another is the interaction of the two bands as they cross. A strong interaction means heavy mixing of the bands and a 'smoothed-out' crossing, whereas weak interactions are associated with sudden sharp crossings. The crossing of rotational bands is illustrated in Fig. 6.4 where the energy levels of ^{160}Yb are plotted against spin. In addition to the two bands crossing along the yrast sequence, there are many band crossings in the levels above. In the case of ^{158}Er there are three band crossings in the first few MeV of excitation. The crossing points occur near the backbends or upbends in Fig. 6.3.

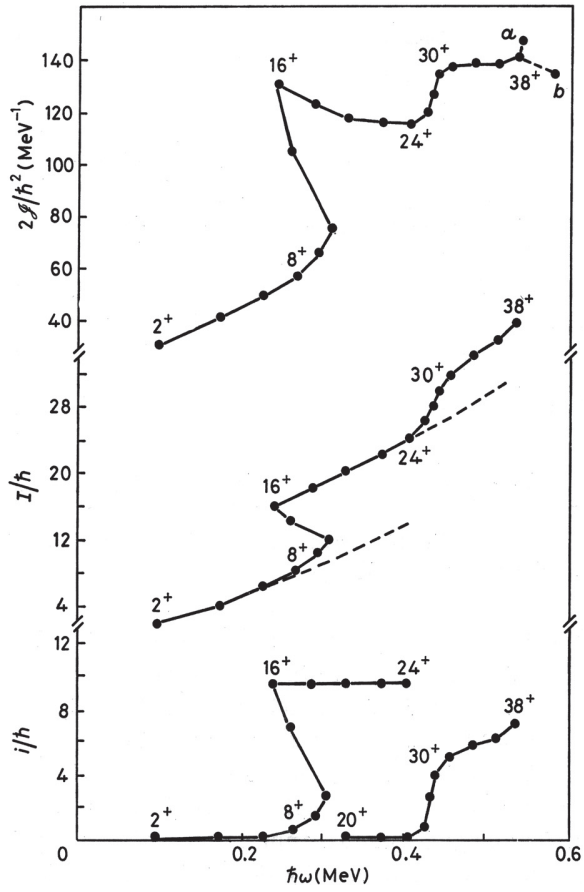

Figure 6.3. Plots of the moment of inertia (top), spin (middle) and spin alignment (bottom) against the rotational frequency for the yrast sequence in ^{158}Er (Yrast states are the states with lowest energy for each angular momentum). The angular velocity is obtained from the measured γ-ray energies in the collective rotational band by $2\hbar\omega = E_\gamma$. The moment of inertia is defined by $\mathcal{I} = I/\omega$. The experimental alignment in the lower part of the figure is defined by $i(\omega) = I - I_s(\omega)$ where $I_s(\omega)$ is the angular momentum of a reference band indicated by the dashed curves in the middle part of the figure. It is fitted to the smoothly varying parts of the curve of angular momentum $I(\omega)$ (after Stephens (1985)).

6.2 Static pairing correlations: the BCS theory of pairing phase transitions in strongly rotating nuclei

The nucleon orbitals in a static deformed potential are twofold degenerate, corresponding to a time reversal of their motion (Kramers degeneracy). This situation for an axially symmetric prolate nucleus is illustrated at the top of Fig. 6.5. The angular momentum, j, of the nucleon has projections $\pm\Omega$ along the symmetry axis and, when occupied by two nucleons, results in total angular momentum

https://doi.org/10.1017/9781009401920 Published online by Cambridge University Press

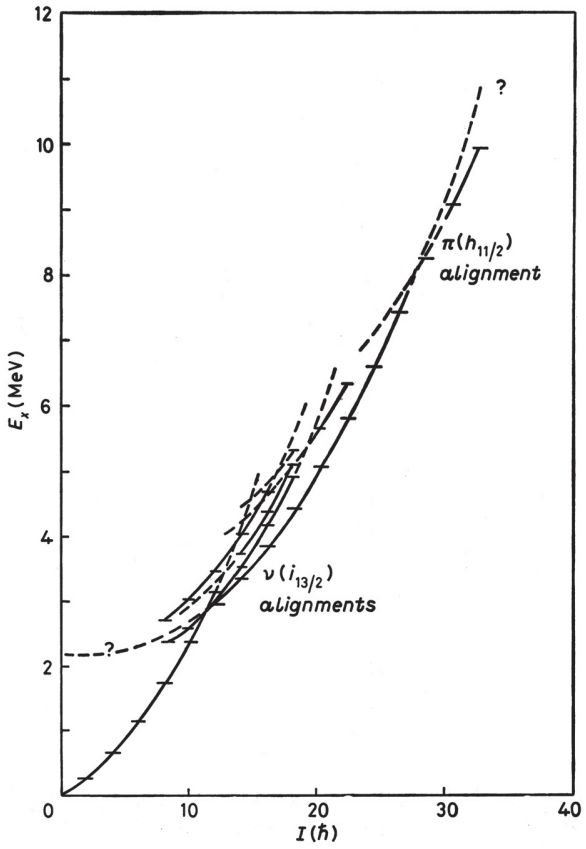

Figure 6.4. Rotational-band trajectories on an E against I plot for the levels of ^{160}Yb. The observed levels are indicated by the horizontal marks (after Stephens (1985)).

zero. Every orbital, characterized by j, Ω, can give rise to such a spin-zero pair. The nucleons in a filled orbital near the Fermi level can scatter as a pair into a nearby empty orbital, and the coherent scattering pattern that develops comprises the nuclear pairing correlation.

These pairing correlations affect the ability of the nucleus to generate angular momentum. In fact, insofar as the pairs are coupled to spin zero, they can contribute nothing towards generating angular momentum. This causes a reduction factor of 2–3 in the nuclear moment of inertia, which is given reasonably well by the BCS model (equation (3.91)). It follows that angular momentum will tend to weaken the pairing correlations, thus increasing the moment of inertia and reducing the rotational energy.

The mechanism of this weakening is the Coriolis force, which acts oppositely on the two members of the pair, lifting their degeneracy. Ultimately the Coriolis

https://doi.org/10.1017/9781009401920 Published online by Cambridge University Press

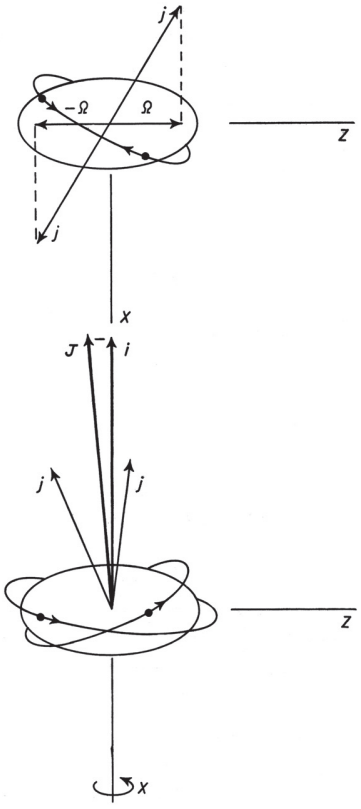

Figure 6.5. The two important coupling schemes in deformed nuclei. In the absence of rotation (top) particles with angular momentum j are in time-reversed orbits with projections $\pm\Omega$ along the symmetry (z)-axis. At high rotational frequencies the particles couple to a J, aligned as well as possible with the rotation (x)-axis, along which they have projection i (from Stephens (1985)).

force will align the particle angular momentum as well as possible with the rotation axis, as illustrated at the bottom of Fig. 6.5. This process is analogous to the effect of a magnetic field on the paired electrons in a superconductor.

6.2.1 Estimate of crossing frequency: gapless superconductivity

Pair correlations lead to a decrease in the rotational moment of inertia and, hence, to an increase in the rotational energy for given I. Thus, for sufficiently large rotational frequencies, the gain in energy associated with the pair correlation is upset by the increased rotational energy, and one expects (Mottelson and Valatin (1960), Bohr (1977)) a phase transition to normal nuclear matter (see Fig. 6.6).

https://doi.org/10.1017/9781009401920 Published online by Cambridge University Press

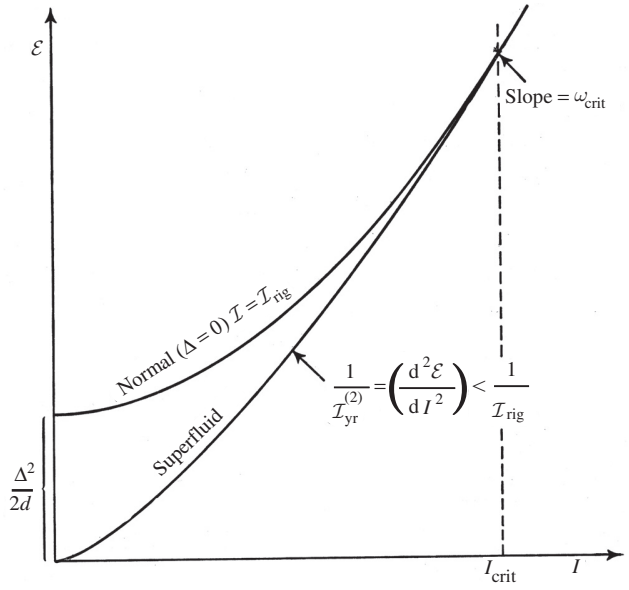

Figure 6.6. Schematic comparison between yrast lines for superfluid and normal systems (from Bohr and Mottelson (1981)). The quantity $\Delta^2/2d$ is the pairing correlation energy (see Section 3.5).

With pairing included, single-particle motion in a rotating potential can be described by a Hamiltonian of the form

$$H' = H_{\text{sp}} + V_{\text{pair}} - \lambda\hat{N} - \hbar\omega j_x, \tag{6.1}$$

with

$$H_{\text{sp}} - \lambda\hat{N} = \sum_{\nu>0} 2(\varepsilon_\nu - \lambda)a^\dagger_\nu a_\nu, \tag{6.2}$$

$$V_{\text{pair}} = -\Delta \sum_{\nu>0} (a^\dagger_\nu a^\dagger_{\bar{\nu}} + a_{\bar{\nu}} a_\nu), \tag{6.3}$$

$$j_x = \sum_{\nu_1\nu_2} \langle \nu_2 | j_x | \nu_1 \rangle a^\dagger_{\nu_2} a_{\nu_1}, \tag{6.4}$$

where ν labels the eigenstates of H_{sp} and $\bar{\nu}$ is the time reverse of ν. The number operator is denoted by $\hat{N}$. The pair potential includes only the monopole term that creates and annihilates pairs of particles moving in single-particle states conjugate under time reversal. Additional terms in the pair potential may be present. The strength of the pair potential, as well as the shape of the nucleus, is a function of ω characterizing the equilibrium for given rotational frequency.

The Hamiltonian (6.1) is a bilinear form in the particle creation and annihilation operators $a^\dagger, a$ and can be brought to diagonal form by a linear

https://doi.org/10.1017/9781009401920 Published online by Cambridge University Press

transformation to quasiparticle operators

$$\alpha_i^\dagger = \sum_\nu (U_{i\nu} a_\nu^\dagger - V_{i\nu} a_{\bar{\nu}}), \tag{6.5}$$

leading to

$$H' = \text{const} + \sum_i E_i' \alpha_i^\dagger \alpha_i. \tag{6.6}$$

The transformation (6.5) is a generalization of the more familiar one which applies to time-reversal-invariant potentials (Bohr and Mottelson (1974), Bohr (1977)). Essential new features are that the quasiparticle states no longer have the twofold degeneracy and that the quasiparticle energies E' can be smaller than Δ (in analogy to the situation in gapless superconductors (Goswami *et al.* (1967))).

We can see the new features most easily for a nucleus rotating about the symmetry axis. In this case, the eigenstates ν of H_{sp} are also eigenstates of j_x (with eigenvalue Ω). The quasiparticle transformation is now the usual one as for τ-invariant potentials

$$\begin{cases} \alpha_\nu^\dagger = U_\nu a_\nu^\dagger - V_\nu a_{\bar{\nu}}, \\ a_\nu^\dagger = U_\nu \alpha_\nu^\dagger + V_\nu \alpha_{\bar{\nu}}, \end{cases} \tag{6.7}$$

which leaves the operator j_x diagonal

$$j_x = \sum_\nu \Omega a_\nu^\dagger a_\nu = \sum_\nu \Omega \alpha_\nu^\dagger \alpha_\nu, \tag{6.8}$$

and the quasiparticle energies are

$$E_\nu' = \left((\varepsilon_\nu - \lambda)^2 + \Delta^2\right)^{1/2} - \hbar\omega\Omega. \tag{6.9}$$

The quasiparticle spectrum (6.9) is illustrated schematically in Fig. 6.7. For an even number of particles, the quasiparticle vacuum ($v = 0$) is the lowest state for rotational frequencies that are smaller than the value for which the sum of the two lowest quasiparticle energies vanishes. For larger ω, this two-quasiparticle state becomes the lowest (so called 'yrast' state, i.e. the set of states that have the lowest energy for each angular momentum), until the next pair of quasiparticles has zero energy, after which the four-quasiparticle state moves to the yrast line, etc. The characteristic frequency ω_1 for the first of these crossings is of order

$$\omega_1 \sim \frac{\Delta}{\Omega_{\max}}, \tag{6.10}$$

https://doi.org/10.1017/9781009401920 Published online by Cambridge University Press

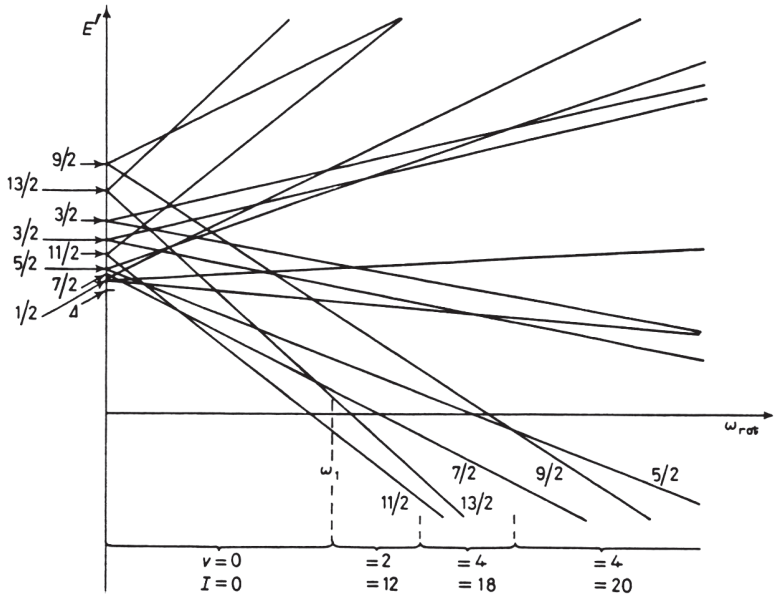

Figure 6.7. Quasiparticle energies E' corresponding to a schematic single-particle spectrum (from Bohr (1977)). Copyright © Società italiana di Fisica.

where $\Omega_{\max}(= j_{\max})$ is the largest single-particle angular momentum near the Fermi surface. Systematics obtained from experimental data are fitted well by an empirical relation (see equation (1.43))

$$\hbar\omega_1 \approx \frac{1.67\Delta}{j_1}.$$

Estimates for band crossings for some high-j shells are found in Garrett *et al.* (1988). Note that the empirical estimate is always larger than the limiting theoretical value. This is because band crossing occurs in deformed nuclei and the limiting value (6.10) assumes a spherical system.

The possibility of negative-energy quasiparticle excitations appears as a general feature of pairing in rotating potentials. In fact, the rotational-alignment effect implies that quasiparticles carry a non-vanishing component Ω_x of angular momentum; thus the excitation of a quasiparticle, for fixed I, is associated with a decrease in the collective rotational energy, corresponding to the last term in (6.9). When the sum of two quasiparticle energies vanishes, one expects a band crossing on the yrast line. For example, in an even–even nucleus, a $v = 2$ band with a large value of $\langle j_1\rangle + \langle j_2\rangle$ may cross the $v = 0$ band.

For nuclei with mass around $A \sim 150$, the first pairs of particles which align are those associated with the $i_{13/2}$ orbital. Making use of standard values of

https://doi.org/10.1017/9781009401920 Published online by Cambridge University Press

$\Delta \sim 1.2$ MeV for this mass region, one expects the frequency of the first crossing to be $\hbar\omega \sim 1.2\,\text{MeV}/6 \sim 0.2\,\text{MeV}$. This rough estimate is consistent with the observed values. The estimate of Garrett *et al.* (1988) given by the equation above for ^{158}Er leads to $\hbar\omega_1 \approx 0.3$ MeV (see Fig. 6.3).

An estimate of the critical angular momentum for total pairing collapse can be obtained making use of Fig. 6.6. Accordingly

$$\begin{aligned} \tfrac{\Delta^2}{2d} &\approx (E_{\text{rot}})_S - (E_{\text{rot}})_N \sim \left(\tfrac{\hbar^2}{2\mathcal{I}_\Delta} - \tfrac{\hbar^2}{2\mathcal{I}_{\text{rig}}}\right) I_c^2 \\ &\approx \left(\tfrac{1}{60} - \tfrac{1}{120}\right) I_c^2\,\text{MeV} \approx \left(I_c^2/120\right)\text{MeV}, \end{aligned} \tag{6.11}$$

where the values for the moments of inertia were taken from Fig. 6.3. Note that $\mathcal{I}_{\text{rig}}/\hbar^2 \sim 60$ coincides with the value extracted from the analysis of γ–γ correlation (Garrett, Hagemann and Herskind (1986)). Making use of $\Delta \sim 1.2$ MeV and of a standard value $d \sim 0.3 - 0.2$ MeV, one obtains

$$I_c \approx 20\hbar. \tag{6.12}$$

Making use of the semiclassical relation $\mathcal{I}\omega_c = I_c$ (see (6.45)), where $\hbar^2/2\mathcal{I} \approx (1/80)$ MeV, one obtains $\hbar\omega_c \approx 0.5$ MeV (see Section 1.9 and Fig. 6.3).

Note that relation (6.11) is equivalent to that used in superconductivity in bulk matter to determine the critical magnetic field.

6.2.2 Pairing in D-states

In Fig. 6.8 the aligned angular momentum i (measured by the difference in angular momentum between the band under consideration and a reference band) of two $i_{13/2}$ neutrons in nuclei around mass 160, is plotted against rotational frequency (approximately half the rotational γ-ray energy) for three bands. The critical frequency is about 0.26 MeV and the aligned angular momentum is $\sim 10\hbar$ ($12\hbar$ is the maximum for two $i_{13/2}$ neutrons). The dashed lines are for two bands in the nucleus ^{163}Yb with one additional neutron located in an orbital labelled either E or F. These orbitals comprise a time-reversed pair at zero rotational frequency and are not very pure shell model states, though their dominant component is $h_{9/2}$. In the even–even nucleus ^{162}Yb, this pair of states (E, F) is available for the pairing correlations, and, in particular, a pair of $i_{13/2}$ neutrons can scatter into it. On the other hand, in ^{163}Yb it is blocked by the odd nucleon for the bands based on either E or F. The pairing correlations are thereby weaker in general, and in particular for a pair of $i_{13/2}$ neutrons. It is easier to unpair and align the $i_{13/2}$ neutrons, and this occurs at a lower rotational frequency, $\sim$0.22 MeV, as seen in Fig. 6.8. This shift can be related to the change in the pairing correlations involved and turns out to correspond to a $(20 \div 30)\%$ reduction in pairing. Thus we learn that blocking just one orbital near the Fermi level reduces the pairing correlations

https://doi.org/10.1017/9781009401920 Published online by Cambridge University Press

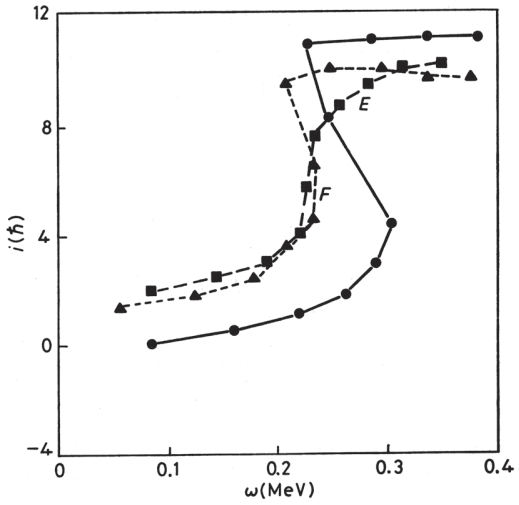

Figure 6.8. The aligned angular momentum, i, is plotted against rotational frequency, ω, for the first backbend ($i_{13/2}$ alignment) region of the lowest-lying (yrast) sequence in ^{162}Yb (continuous line) and for two bands in ^{163}Yb (labelled E and F). The midpoint of the sharp rise is approximately the crossing frequency (after Stephens (1985), Garrett *et al*. (1986)).

appreciably, a result that is confirmed by other kinds of experiments like transfer of pairs of nucleons and directly from the odd–even mass difference. Pairing correlations although playing an extremely important role in the structure of nuclei close to the ground state are weak, and two to three blocked levels of either type (protons or neutrons) are enough to destroy the correlations for that nucleon type.

Conspicuous deviations from the systematic discussed above have been observed (see Fig. 6.9) in specific nuclei. In fact, in ^{161}Er, for example, the crossing of the rotational band based on the $[521]3/2^-$ level shows the effect but not the band based on the $[505]11/2^-$ state. In fact, the $\delta(\hbar\omega)$ associated with the $[521]3/2^-$ orbit is ~ 40 keV, while $\delta(\hbar\omega) \sim 0$ for $[505]11/2^-$.

Both orbitals are close to the Fermi surface at rotational frequency $\omega = 0$. However, the $[521]3/2^-$ orbital has an intrinsic quadrupole moment $q_\nu > 0$, as all the rest of levels in this energy region, while the $[505]11/2^-$ orbital has $q_\nu < 0$ (see Fig. 6.10).

This has important consequences as the nucleus displays quadrupole pairing correlations, aside from monopole pairing correlations. The pairing gap is in this case state dependent (Bes *et al*. (1972), Van Rij and Kahana (1972) and Shimizu *et al*. (1989)), and can be written as (see Section 5.3)

$$\Delta_\nu = G_0 \sum_{\nu'>0} U_{\nu'} V_{\nu'} + G_2 q_\nu \sum_{\nu'>0} U_{\nu'} V_{\nu'} q_{\nu'}. \tag{6.13}$$

https://doi.org/10.1017/9781009401920 Published online by Cambridge University Press

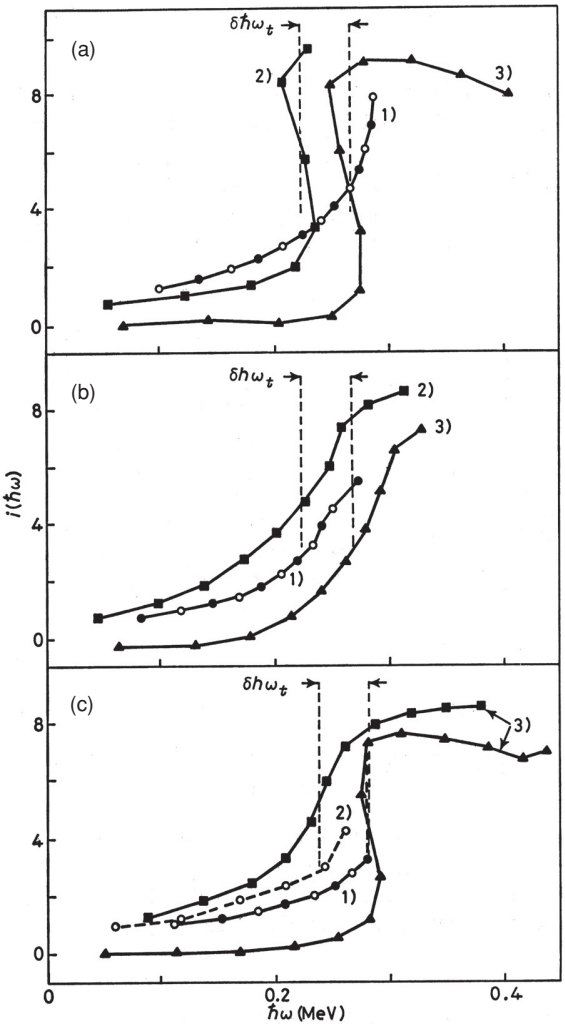

Figure 6.9. Alignment plot for selected decay sequences of rotational states illustrating the observed shifts in crossing frequency: (a) curve 1) ^{181}Os $(7/2^-[514])$, curve 2) ^{181}Os $(7/2^-[521])$, curve 3) ^{182}Os (yrast); (b) curve 1) ^{173}W $(5/2^-[512])$, curve 2) ^{173}W $(1/2^-[521])$, curve 3) ^{172}W (yrast); (c) curve 1) ^{161}Er $(11/2^-[505])$, curve 2) ^{161}Er $(3/2^-[521])$, curve 3) ^{162}Er (yrast). The crossing frequencies are shown by the vertical dashed lines for the ground-state decay sequences in both even- and odd-N isotopes. Signature zero and $1/2$ decay sequences are indicated by solid sysmbols, and the $\alpha = -1/2$ sequence is indicated by open symbols. Reprinted from *Physics Letters* B, Vol. 118, Garrett *et al*., 'Configuration dependent pairing from band crossing frequencies', page 298, Copyright 1982, with permission from Elsevier.

https://doi.org/10.1017/9781009401920 Published online by Cambridge University Press

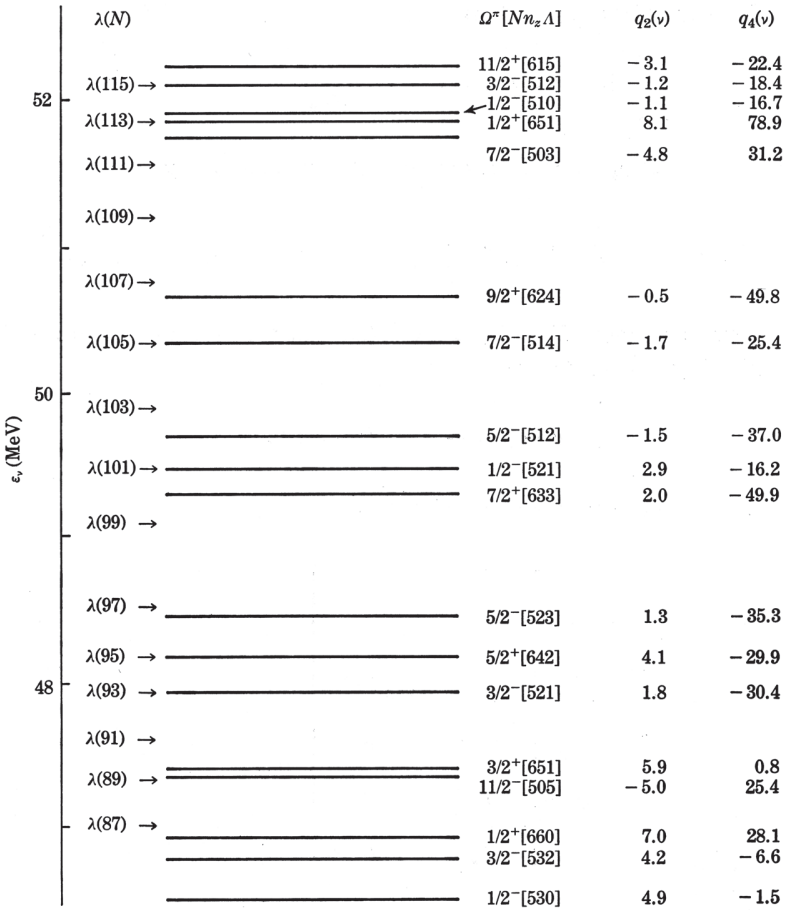

Figure 6.10. Spectrum of neutron Nilsson orbits, identified by the quantum numbers N, n_z and λ (see Nilsson and Ragnarsson (1995)), for rare-earth nuclei calculated assuming $\beta_2 = 0.25$. The position of the Fermi surface, λ, for $\omega = 0.90$ MeV is also indicated for odd neutron numbers. The asymptotic quantum numbers and the quadrupole and hexadecapole moments, $q_2(\nu)$ and $q_4(\nu)$, in units of fm^2 and fm^4, respectively, are indicated for each configuration (from Garrett *et al*. (1982)).

Blocking the orbital ν_b leads to a change in Δ_ν measured by

$$\delta\Delta_\nu(\nu_b) = \Delta_\nu - \Delta_\nu(\nu_b) = GU_{\nu_b}V_{\nu_b}(1 + q_\nu q_{\nu_b}) \approx \frac{G}{2}(1 + q_\nu q_{\nu_b}), \qquad (6.14)$$

where we have assumed $U_{\nu_b} \approx V_{\nu_b} \approx 1/\sqrt{2}$ (correct for levels close to the Fermi surface). Making use of the fact that (Nilsson and Ragnarsson (1995))

$$q \sim (3n_z - N)/(N + 3/2),$$

https://doi.org/10.1017/9781009401920 Published online by Cambridge University Press

we obtain for the case under discussion

$$\left.\begin{array}{ll}[660]\ 1/2^+ & 1.6\\ [651]\ 3/2^+ & 1.2\\ [642]\ 5/2^+ & 0.8\end{array}\right\}\ 1.2,$$

$$\left.\begin{array}{ll}[521]\ 3/2^- & 0.15\\ [530]\ 1/2^- & 0.6\end{array}\right\}\ 0.4,$$

$$[505]\ 11/2^- \quad -0.8.$$

Setting $G \approx 27/A$ MeV, one obtains

$$\delta\Delta_{i_{13/2}}([521]3/2^-) \approx \frac{1}{2}\left(\frac{27}{161}\text{MeV}\right) \times (1 + 1.2 \times 0.4) \approx 130 \text{ keV},$$
$$\delta\Delta_{i_{13/2}}([505]11/2^-) \approx \frac{1}{2}\left(\frac{27}{161}\text{MeV}\right) \times (1 - 1.2 \times 0.8) \approx 0 \text{ keV}. \quad (6.15)$$

This result implies that two particles moving in time-reversal states in the orbital $[505]11/2^-$ do not feel they are in a superfluid nucleus and thus do not contribute to the pairing gap.

The correlation between the shape of a valence quasi-neutron orbital and the shift in band crossing frequencies between neighbouring odd- and even-N isotopes is shown in Fig. 6.11.

6.2.3 Time-reversal violation due to rotation (the $i_{13/2}$ model)

In this subsection we discuss some aspects of the phenomenon of pairing collapse under the influence of strong rotations within a pure $i_{13/2}$ model (Broglia *et al.* (1985a)). We assume the system under study to display axial symmetry around the z-axis, and moreover symmetry with respect to the (x, y)-plane.

The axis of rotation is chosen to be perpendicular to the symmetry axis, which leads to collective rotations. The motion of the particles is controlled by the Nilsson Hamiltonian. The associated single-particle Routhian reads

$$h^{\omega}_{\text{sp}} = h_{\text{N}}(\varepsilon) - \omega j_x, \quad (6.16)$$

with

$$h_{\text{N}}(\varepsilon) = Q j_x^2, \quad (6.17)$$

where Q is proportional to the quadrupole moment of the system. The Hamiltonian h^{ω}_{sp} is invariant under space reflection (parity) and under rotations through 180° about the x-axis, i.e. rotations induced by the operator

$$R_x = \exp[-\text{i}\pi j_x]. \quad (6.18)$$

https://doi.org/10.1017/9781009401920 Published online by Cambridge University Press

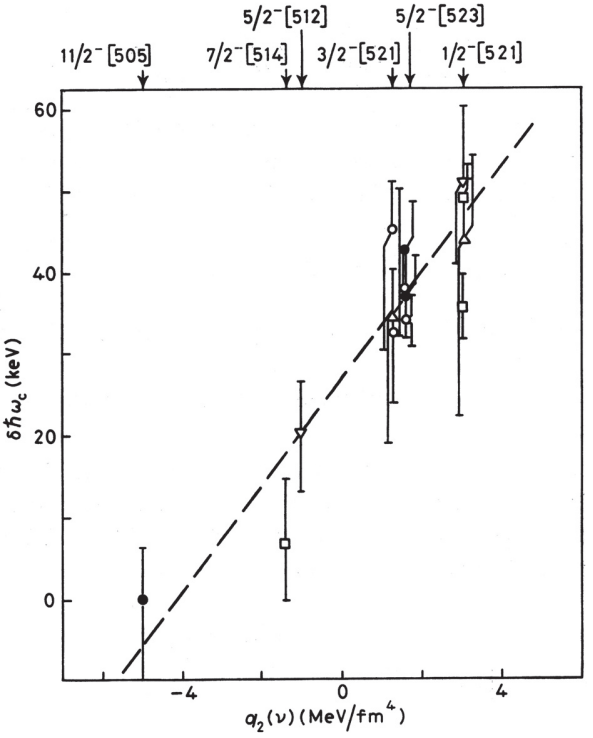

Figure 6.11. Correlation between $\delta\hbar\omega_c$ (see equation (6.15)) and the quadrupole moment, $q_2(\nu)$, of the orbit of the valence quasi-neutron ν: • Er, ○ Yb, △ Hf, ▽ W, □ Os (see Fig. 6.10). The asymptotic quantum numbers of the various configurations are given at the top of the figure. The dashed line is drawn only to guide the eye. Reprinted from *Nuclear Physics*, Vol. A400, Garrett *et al*., 'The structure of rotating deformed nuclei,' page 113, Copyright 1982, with permission from Elsevier.

The eigenvalues ε_ν^ω and the eigenstates $|\nu^\omega\rangle$ of the cranking Hamiltonian

$$h_{\rm sp}^\omega|\nu^\omega\rangle = \varepsilon_\nu^\omega|\nu^\omega\rangle \ , \tag{6.19}$$

can thus be labelled by the parity of the state and by the signature quantum number (Bohr and Mottelson (1974)), which is intimately related to the eigenvalues of the operator (6.18).

Let us denote by $|\nu, \Omega_\nu\rangle$ the eigenstates of the Nilsson Hamiltonian $h_{\rm N}^\omega(\varepsilon)$ and adopt the following phase convention

$$\begin{cases} R_x|\nu, \Omega_\nu\rangle = {\rm i}(-1)^{\Omega_\nu - 1/2}|\nu, \tilde{\Omega}_\nu\rangle, \\ R_x|\nu, \tilde{\Omega}_\nu\rangle = {\rm i}(-1)^{\Omega_\nu + 1/2}|\nu, \Omega_\nu\rangle, \end{cases} \tag{6.20}$$

where $|\nu, \tilde{\Omega}_\nu\rangle$ is the time-reversal state to $|\nu, \Omega_\nu\rangle$, while Ω_ν is the magnetic quantum number of the state.

https://doi.org/10.1017/9781009401920 Published online by Cambridge University Press

The states

$$|\chi\rangle = \frac{1}{\sqrt{2}}\{(-1)^{\Omega_\nu+1/2}|\nu, \Omega_\nu\rangle + |\nu, \tilde{\Omega}_\nu\rangle\} \tag{6.21}$$

and

$$|\tilde{\chi}\rangle = \frac{1}{\sqrt{2}}\{-|\nu, \Omega_\nu\rangle + (-1)^{\Omega_\nu-1/2}|\nu, \tilde{\Omega}_\nu\rangle\}, \tag{6.22}$$

which are still related by the time-reversal operation, are eigenstates of R_x with eigenvalues

$$R_x|\chi\rangle = -\mathrm{i}|\chi\rangle \tag{6.23}$$

and

$$R_x|\tilde{\chi}\rangle = \mathrm{i}|\tilde{\chi}\rangle. \tag{6.24}$$

The state (6.21) is said to have signature $\alpha = +\frac{1}{2}$, while the state (6.22) has signature $\alpha = -\frac{1}{2}$.

In the basis $|\chi, \tilde{\chi}\rangle$ the eigenvalue equation (6.19) is block-diagonal, i.e.

$$\begin{pmatrix} h_{\mathrm{N}} - j_x\omega & 0 \\ 0 & h_{\mathrm{N}} + j_x\omega \end{pmatrix}\begin{pmatrix} G \\ H \end{pmatrix} = \varepsilon^{\omega}\begin{pmatrix} G \\ H \end{pmatrix}. \tag{6.25}$$

The resulting eigenstates can be written as

$$|j\rangle = |\pi, \alpha = \tfrac{1}{2}\rangle = \sum_{\chi} G^j_\chi|\chi\rangle \tag{6.26}$$

and

$$|\hat{j}\rangle = |\pi, \alpha = -\tfrac{1}{2}\rangle = \sum_{\chi} H^{\hat{j}}_{\tilde{\chi}}|\tilde{\chi}\rangle. \tag{6.27}$$

Note that the states $|j\rangle$ and $|\hat{j}\rangle$ are related by the operation of time reversal only at $\omega = 0$ (zero rotational frequency). The violation of time-reversal symmetry is measured by the deviation from 1 of the pairing matrix element

$$\langle j\,\hat{j}'|P^\dagger|0\rangle = \sum_{\chi\chi'} G^j_\chi H^{\hat{j}'}_{\chi'}\langle\chi\,\chi'|P^\dagger|0\rangle, \tag{6.28}$$

where

$$P^\dagger = \sum_{\nu_\alpha>0,\nu_\beta>0}\langle\tilde{\nu_\beta}|\tau|\nu_\alpha\rangle a^\dagger_{\nu_\alpha}a^\dagger_{\tilde{\nu_\beta}} \tag{6.29}$$

and

$$\langle\chi\,\chi'|P^\dagger|0\rangle = \langle\chi'|\tau|\chi\rangle = \Delta(\chi', \tilde{\chi}), \tag{6.30}$$

https://doi.org/10.1017/9781009401920 Published online by Cambridge University Press

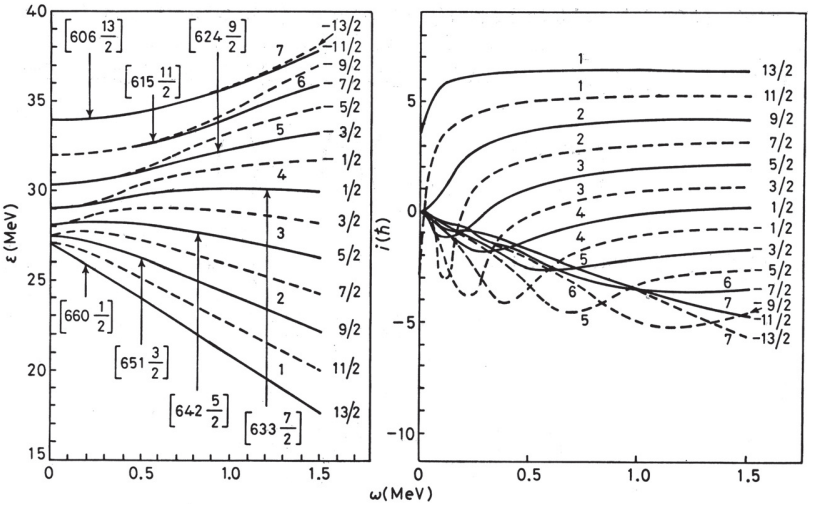

Figure 6.12. Eigenvalues ε_ν^ω and alignments i_ν^ω associated with the eigenstates of the cranked Hamiltonian, for the case of a $1i_{13/2}$ orbital. The eigenvalues are defined through equation (6.25), while the alignment is given by equation (6.32).

the time-reversal operator having been denoted by τ (see Appendix A). Note that the pair field (6.29) coincides with the transfer operator which creates two particles in time-reversal state. From the result (6.30) one obtains

$$M_{j\hat{j}'} = \langle j\hat{j}'|P^\dagger|0\rangle = \sum_\chi G_\chi^j H_{\tilde{\chi}}^{\hat{j}}. \tag{6.31}$$

The fact that the pairing field only connects states of different signature can be understood by the fact that at $\omega = 0$, $|j\rangle \to |\chi\rangle$ and $|\hat{j}\rangle \to |\tilde{\chi}\rangle \sim \tau|\chi\rangle$, which are time-reversal states.

In Fig. 6.12 we display the energies ε_ν^ω associated with the diagonalization of $h_{\rm sp}$ in the $i_{13/2}$ single-particle orbital as a function of rotational frequency. In the same figure we also give the alignments

$$i = -\frac{\mathrm{d}\langle h_{\rm sp}^\omega\rangle}{\mathrm{d}\omega} = \langle j_x\rangle \tag{6.32}$$

associated with each level.

The square of the pairing matrix elements or pairing overlaps are shown in Fig. 6.13 for a variety of configurations. The most conspicuous features displayed by these quantities can be summarized as follows (see also Broglia (1985c), Nikam and Ring (1987), Nikam *et al.* (1986, 1987), Vigezzi *et al.* (1988)):

https://doi.org/10.1017/9781009401920 Published online by Cambridge University Press

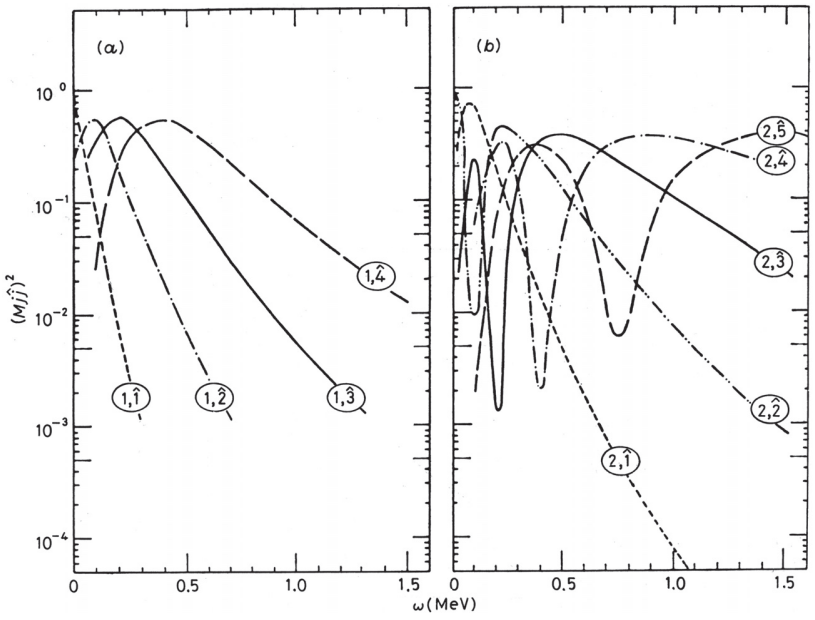

Figure 6.13. Square of the pairing matrix elements as defined in equation (6.31) connecting different eigenstates of the cranking Hamiltonian, as a function of the rotational frequency.

(a) Matrix elements that start being 1 at $\omega = 0$ decrease with increasing values of ω, the opposite being true for those matrix elements which are zero at $\omega = 0$. Many of them become zero again at $\omega \to \infty$ displaying a maximum for finite values of ω.

(b) Aside from the matrix elements $\langle 1, \hat{j}|P_2^\dagger|0\rangle$ all other matrix elements oscillate. The first property can be understood making use of the sum rule

$$\sum_{jj'} \langle j\,\hat{j}'|P^\dagger|0\rangle^2 = \Omega, \tag{6.33}$$

where $\Omega = j + 1/2$ is the number of pairs one can place in the shell, and from the fact that at $\omega = 0$ the twofold degenerate Nilsson states are time-reversal partners, while for $\omega j_x \gg h_{\rm N}(\varepsilon)$, where m_x is a good quantum number, the time-reversal states are those associated with the values $\pm\Omega_x$ of the magnetic quantum number j_x.

6.2.4 *Detailed numerical calculations*

In Fig. 6.14 self-consistent calculations (Shimizu *et al.* (1989)) of the BCS neutron pairing gap and of the alignment as a function of the rotational frequency are shown for the nucleus ^{168}Yb.

https://doi.org/10.1017/9781009401920 Published online by Cambridge University Press

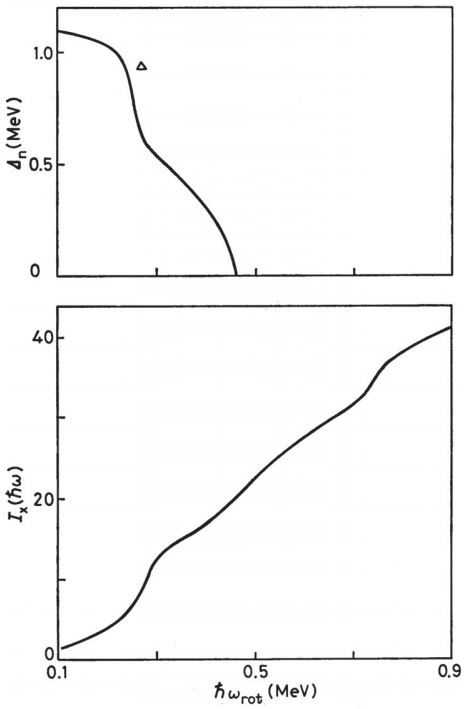

Figure 6.14. The static (BCS) neutron pair gap Δ and the alignment of the lowest $(\pi, \alpha) = (+, 0)$ configuration of $^{168}_{98}$Yb. Reprinted with permission from Shimizu *et al.*, *Rev. Mod. Phys.* **61**:131 (1989). Copyright 1989 by the American Physical Society.

A significant decrease, of the order of 400 keV, is predicted at the frequency of the first crossing ($\sim$0.26 MeV). From here on the pairing gap decreases rather smoothly until, at $\omega_{\rm rot}$ $\sim$0.45 MeV it goes to zero.

A simple estimate of the crossing frequencies and of the critical value $\omega_{\rm c}$ based on equations (6.10) and (6.11) is shown in Table 6.1 and demonstrates overall agreement with the detailed calculations.

From the above discussions and the present results, one can conclude that pairing collapse under the influence of rotation is controlled by the progressive splitting of signature partners and the associated reduction of the pairing matrix elements (time-reversal overlaps). For definite frequencies these overlaps become so small that the corresponding state $(j\,\hat{j}')$ is blocked, and does not contribute to the sum appearing in the BCS equations of the pairing gap. At the frequency where two to three signature pairs are blocked, these equations lead to the trivial solution $\Delta = 0$.

The phenomenon of pairing collapse can be also viewed in terms of the crossing of 2, 4 . . . quasiparticle bands with the original ground-state band. This is a

https://doi.org/10.1017/9781009401920 Published online by Cambridge University Press

Table 6.1. *Alignments and crossing frequencies for particles moving in a variety of orbitals of* ^{168}*Yb. The average value* $\langle j_x \rangle = ((l + 1/2) + (l - 1/2))/2$ *was used to estimate an average crossing frequency through equation (6.10). From the analysis of the irregularities in the* $I - \omega$ *relation associated with the first band crossing in the rare-earth nuclei (*$i_{13/2}$ *alignment), it is found that the alignment is less (*$\sim$*25%) than the maximun value* $i = j = 13/2$*. The particle retains a strong coupling to the symmetry axis, and it is only the component of angular momentum along this symmetry axis that can easily be aligned. The quantity* $\overline{j_x} = \langle j_x \rangle - 25\%$ *was used to obtain somewhat more realistic estimates* $\overline{\omega_1}$ *of the crossing frequencies (see discussion following equation (6.10)).*

	$\langle j_x \rangle(\hbar)$	$\langle \omega_1 \rangle$(MeV)	$\overline{j_x}(\hbar)$	$\overline{\omega_1}$(MeV)
i	6	0.20	4.5	0.27
h	5	0.24	3.8	0.32
g	4	0.30	3.0	0.40
f	3	0.40	2.3	0.50

valid interpretation to the extent that one does not require that all bands have a strict existence at all rotational frequencies. In fact, in the case under discussion only the first crossing is clearly seen experimentally.

6.3 Pairing fluctuations

For rotational frequencies ω smaller than the critical frequency ω_c, where the BCS gap becomes zero, the pairing contribution to the ground-state energy is proportional to the square of the number of particles. That is, $E_0 \sim GN^2$, typical of a pairing rotational band (see Chapters 4 and 5). The contribution to E_0 of the zero-point fluctuations associated with the pairing modes is $E_{\rm gsc} \sim GN$, leading to a ratio $r \sim E_{\rm gsc}/E_0 \sim N^{-1}$. For rotational frequencies $\omega > \omega_c$, that is for normal systems, $E_{\rm gsc} \sim GN$ as before, while $E_0 \sim GN$ typical of pairing vibrational bands. The ratio r is in this case of order 1. It is thus expected that the effects of zero-point fluctuations associated with pairing vibrations will be much more important at rotational frequencies $\omega \gtrsim \omega_c$ than at $\omega < \omega_c$.

In the present subsection we study some of the consequences these fluctuations have on a variety of properties of strongly rotating nuclei. We carry out our investigations for high rotational frequencies $\omega > \omega_c$, i.e. for normal systems. The calculations are done in the framework of the cranked shell model treating the

pairing vibrations of the normal system in the RPA. By decreasing ω, but keeping it always larger than ω_c, we gradually approach the pairing phase transition. That is, we study the onset of the normal to superfluid phase transition at zero temperature, taking into account the fluctuations induced by pairing vibrations (see Barranco *et al*. (1987)).

The equations determining the properties of pairing vibrations in normal systems, i.e. in systems with fixed number of particles, are, in the random-phase approximation (Broglia *et al*. (1986), Shimizu *et al*. (1989)),

$$\sum_n(\beta = +2) = \frac{1}{G}, \tag{6.34}$$

$$\sum_n(\beta = +2) = \sum_{k\hat{k}'} \frac{M^2_{k\hat{k}'} U^2_k U^2_{\hat{k}'}}{e_k + e_{\hat{k}'} - W_{+2}(n)} + \sum_{i\hat{i}'} \frac{M^2_{i\hat{i}'} U^2_i U^2_{\hat{i}'}}{e_i + e_{\hat{i}'} + W_{+2}(n)} \tag{6.35}$$

and

$$\sum_{k\hat{k}'} X^2_{k\hat{k}'}(+2, n) - \sum_{i\hat{i}'} Y^2_{i\hat{i}'}(+2, n) = 1. \tag{6.36}$$

The amplitudes X and Y are defined as

$$\begin{cases} X_{k\hat{k}'}(+2, n) = \dfrac{\Lambda_{+2}(n) M_{k\hat{k}'} U^2_k U^2_{\hat{k}'}}{e_k + e_{\hat{k}'} - W_{+2}(n)}, \\ Y_{i\hat{i}'}(+2, n) \ = \dfrac{\Lambda_{+2}(n) M_{i\hat{i}'} U^2_i U^2_{\hat{i}'}}{e_i + e_{\hat{i}'} + W_{+2}(n)}, \end{cases} \tag{6.37}$$

the quantity $\Lambda_{+2}(n)$ being the particle-vibration coupling strength determined from the normalization condition (6.36). The quantities $M_{i\hat{i}'}$ are the pairing matrix elements connecting states with different signatures, while e_i and $e_{\hat{i}'}$ are the associated single-particle energies measured from the Fermi energy. The pairing vibrations are labelled by the transfer quantum number $\beta = \pm 2$. The quantities U^2 and V^2 are either 1 or 0 according to the occupancy of the state. The equations above thus describe the pair addition modes, i.e. vibrations which increase the number of particles by 2. The index n indicates whether the solution of equation (6.35) one considers corresponds to the state with lowest energy ($n = 1$), next to lowest ($n = 2$), etc.

Similar equations describe the pair removal modes, i.e. vibrations which diminish the number of particles by two units. It is noted that all quantities in equation (6.35), with the exception of the pairing coupling constant G, depend on the rotational frequency ω. This is, of course, an oversimplification of the problem, in view of the fact that a non-negligible contribution to G arises from the exchange of collective vibrations between pairs of nucleons forming Cooper pairs (see Chapters 8–10).

https://doi.org/10.1017/9781009401920 Published online by Cambridge University Press

The Mottelson–Valatin (1960) critical rotational frequency for which the BCS equations have a solution $\Delta = 0$ coincides with the frequency for which the energy of the pair-addition and pair-removal modes of the normal system goes to zero, i.e.

$$(W_{+2}(n))_{\omega_c} = (W_{-2}(n))_{\omega_c} = 0. \tag{6.38}$$

In fact, in this case equation (6.35) is equivalent to the BCS gap equation if one interprets the energies e_j as quasiparticle energies.

The influence of pairing fluctuations on different nuclear properties can be calculated in the RPA. In particular, the contribution to the energy of a given configuration of parity π and signature α is given by (see Section 8.4)

$$E_{\rm gsc}(\pi, \alpha) = \frac{1}{2} \sum_{\beta=\pm 2, n} W_\beta(\pi\alpha; n) - \frac{1}{2} \sum_{jj'} (e_j + e_{\hat{j}'}), \tag{6.39}$$

which is the sum of the energies of the pair-addition and subtraction modes measured from the energy of the unperturbed two-particle poles $(e_j + e_{\hat{j}'})$. With j we indicate both levels above $(j > k)$ and below $(j < i)$ the Fermi energy. The quantity $E_{\rm gsc}$ is thus equal to the sum of the correlation energies of all pair-addition and pair-subtraction modes.

The total energy of the variety of configurations calculated in the rotating frame ('Routhian') is

$$e(\pi, \alpha) = \langle h^{\omega}_{\rm sp} \rangle + E_{\rm gsc}. \tag{6.40}$$

The average angular momentum associated with these configurations along the axis of rotation can be written as

$$i_x(\pi, \alpha) = -\frac{\partial e(\pi, \alpha)}{\partial \omega} = \langle j_c \rangle - \frac{\partial E_{\rm gsc}}{\partial \omega}. \tag{6.41}$$

Examples of the quantities, again for ^{168}Yb, are shown in Fig. 6.15. The bands have different parity signature quantum numbers (π, α).

The ease with which the $(+, 0)$ configuration reacts to pairing correlations, leading to smaller alignments, reflects the fact that in this configuration the lowest levels of both even and odd parity are filled with an even number of particles. Consequently the configuration $(+, 0)$ is the analogue to the BCS vacuum at $\omega > \omega_c$.

The configuration $(-, 0)$ or $(-, 1)$ is associated with situations where one has an odd number of particles in both even- and odd-parity levels. They thus correspond to two-quasiparticle configurations at $\omega < \omega_c$, relative to the $(+, 0)$ configuration. This implies that the $(-, 0)$ and $(-, 1)$ configurations are affected by a high degree of blocking. Consequently, pairing vibrations typical of normal systems can develop at a lower frequency than in the case of the $(+, 0)$ configurations. That is, one needs only moderate values of ω to achieve the situation in which the fluctuations of the pairing gap are as large as its average value.

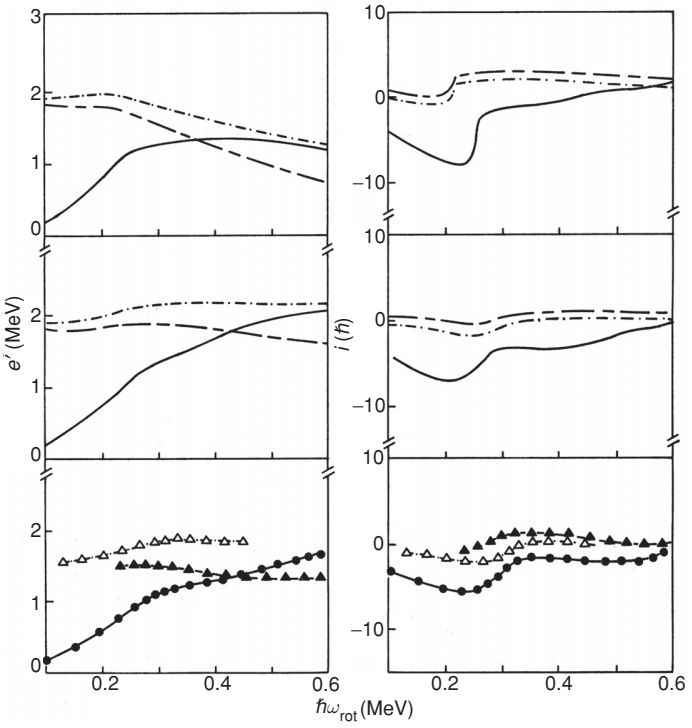

Figure 6.15. Comparison of calculated Routhians, with fluctuations (middle portion) and without fluctuations (top portion), and experimental Routhians (bottom portion), e' (left-hand side), and alignments, i (right-hand side), for various configurations in $^{168}_{92}$Yb. The $(+, 0)$ configuration is denoted by solid lines and solid dots, $(-, 0)$ by dot-dashed lines and open triangles and $(-, 1)$ by double-dashed lines and solid triangles. The calculated and experimental values are referred to reference configurations with constant moment of inertia of $62\hbar^2\,\mathrm{MeV}^{-3}$ and $66\hbar^2\,\mathrm{MeV}^{-1}$, respectively. Reprinted with permission from Shimizu *et al*., *Rev. Mod. Phys.* 61:131 (1989). Copyright 1989 by the American Physical Society.

6.4 Moments of inertia

As a consequence of the interplay between collective and single-particle motions, there are a variety of moments of inertia one can measure and compare with detailed calculations (Broglia *et al*. (1985b), Szymanski (1985)). The first distinction to be made is between kinematic and dynamic values (Bohr and Mottelson (1974)).

The moment of inertia defined as the first derivative of the rotational energy with respect to spin

$$\frac{\mathcal{I}^{(1)}}{\hbar^2} = I\left(\frac{\mathrm{d}E}{\mathrm{d}I}\right)^{-1} = \frac{I}{\hbar\omega} \tag{6.42}$$

is the so-called 'kinematic' moment of inertia, because it has to do with the motion of the system, the ratio of angular momentum to angular frequency. It is

https://doi.org/10.1017/9781009401920 Published online by Cambridge University Press

also apparent that the second derivative leads to the definition

$$\frac{\mathcal{I}^{(2)}}{\hbar^2} = \left(\frac{\mathrm{d}^2 E}{\mathrm{d}I^2}\right)^{-1} = \frac{\mathrm{d}I}{\mathrm{d}(\hbar\omega)}, \tag{6.43}$$

where $\mathcal{I}^{(2)}$ is called the 'dynamic' moment of inertia, because it has to do with the way the system will respond to a force.

In general $\mathcal{I}^{(1)}$ and $\mathcal{I}^{(2)}$ are different in rotating nuclei, because of the effect of the Coriolis term $\sim I \cdot j$.

A simple approximation for the rotational energy is

$$E(I) = E_0 + \frac{(I - i_0)^2}{2\mathcal{I}}, \tag{6.44}$$

where $\mathcal{I}$ is identified as the second moment of inertia. The quantity i_0 is related in some general way to the part of angular momentum carried out by the single-particle motion. It should not, however, be confused with the actual particle alignment, as can be seen from Fig. 6.16.

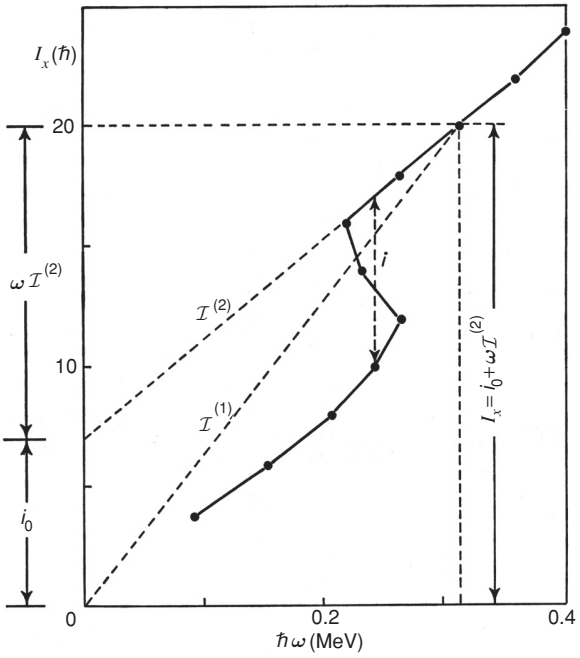

Figure 6.16. Illustration of apparent alignment i_0. Apparent alignment (i_0), the $\omega = 0$ intercept of an extrapolation of the local dynamic moment of inertia, $\mathcal{I}^{(2)}$, can be defined as the difference between the kinematic, $\mathcal{I}^{(1)}$, and dynamic moments of inertia. The various quantities entering this definition are indicated in the figure. The $I_x(\omega)$ data are for the ground-state, $(-, 1/2)$ configuration of $^{159}_{91}$Er. Reprinted with permission from Shimizu *et al.*, *Rev. Mod. Phys.* 61:131 (1989). Copyright 1989 by the American Physical Society.

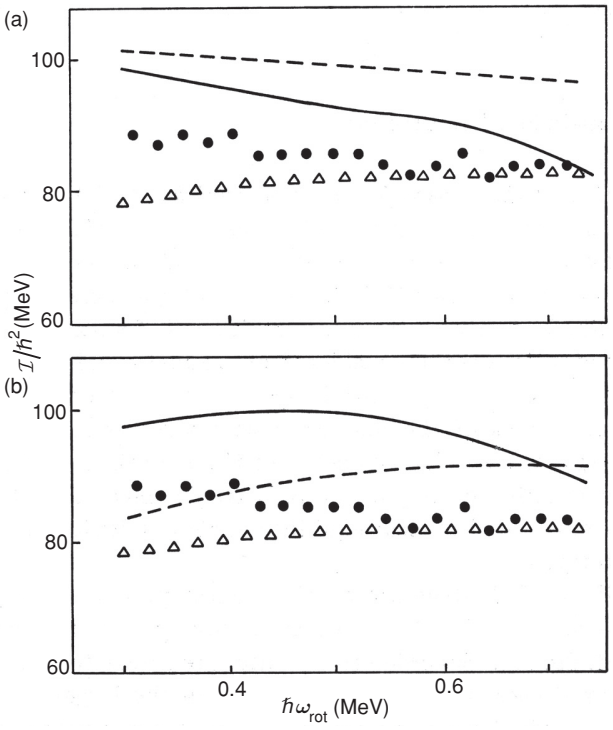

Figure 6.17. The kinematic and the dynamic moment of inertia, $\mathcal{I}^{(1)}$ and $\mathcal{I}^{(2)}$, associated with the superdeformed band of ^{152}Dy (see Fig. 6.18) as functions of the rotational frequency (for a quadrupole deformation parameter) ($\varepsilon_2 = 0.58$): (a) results without taking into account pairing fluctuations, (b) results including pairing fluctuations: theory: $-\mathcal{I}^{(2)}$, $---\ \mathcal{I}^{(1)}$; experiment: $\bullet\bullet\bullet\ \mathcal{I}^{(2)}$, $\triangle\triangle\triangle\ \mathcal{I}^{(1)}$. The absolute value of $\mathcal{I}$ is overestimated because the Strutinsky renormalization of the angular momentum was left out. Reprinted from *Physics Letters* B, Vol. 198, Shimizu *et al*., 'Role of static and dynamic pairing correlations in the superdeformed band of ^{152}Dy, page 35, Copyright 1987, with permission from Elsevier.

The parametrization (6.44) arises from the cranking model where the canonical frequency ω, which determines the magnitude of the rotational perturbation, is approximately given by

$$\omega = \frac{1}{\mathcal{I}_0}(I - i_0) \sim \frac{R}{\mathcal{I}_0}, \tag{6.45}$$

where R is the angular momentum of the collective rotation and $\mathcal{I}_0$ the moment of inertia of the rotor in the particle-rotor model.

Examples of the role played by pairing fluctuations in the behaviour of $\mathcal{I}^{(1)}$ and $\mathcal{I}^{(2)}$ with rotational frequency are shown in Fig. 6.17 for the case of the superdeformed band of ^{152}Dy.

6.5 Condensation-induced tunnelling

The interplay between collective degrees of freedom and single-particle motion common to all many-body systems is encountered in the study of nuclear structure in a particular concrete form. This is because of the possibility of detailed studies of individual quantum states, as carried out, for example, in the case of the nuclear potential energy considered as a function of the shape. While the general features of this 'potential-energy function' can be described in terms of bulk properties of the nuclear matter such as surface tension and electrostatic energy, the specific geometry of the quantized orbits of the individual nucleons contributes important anisotropic effects; a striking consequence is the occurrence of nuclear-equilibrium shapes deviating strongly from spherical symmetry.

The effect of the shell structure on the nuclear potential energy has come into perspective in the study of superdeformed bands, the first one observed (see e.g. Nolan and Twin (1988)) being that of the nucleus ^{152}Dy (see Fig. 6.18, see also Åberg (1987)). Superdeformed states are associated with quadrupole deformed nuclear shapes, where the ratio between the larger and the smaller

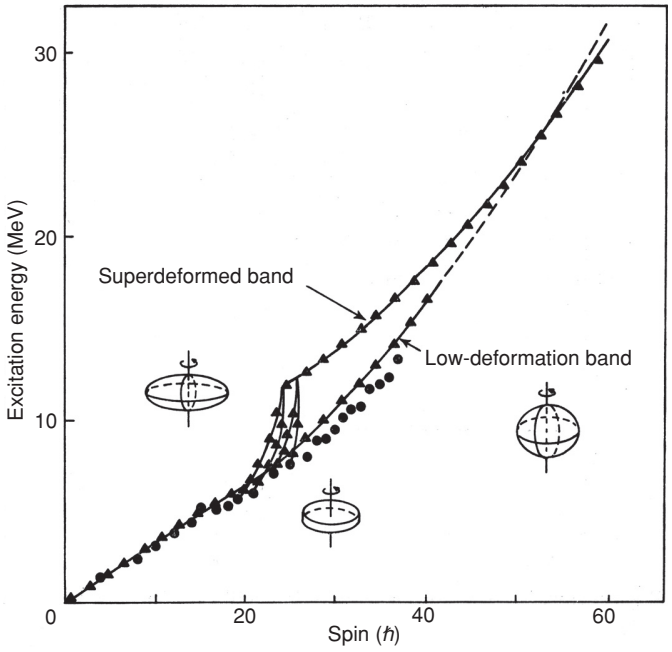

Figure 6.18. The experimental knowledge about ^{152}Dy includes states at three different deformations: non-collective oblate states, a collective low-deformation band (presumably prolate) and a collective superdeformed band. Some typical decay paths de-exciting the superdeformed band to oblate states are illustrated (dots). Reprinted, with permission, from the *Annual Review of Nuclear Science*, Volume 23 © 1973 by Annual Reviews www.annualreviews.org

https://doi.org/10.1017/9781009401920 Published online by Cambridge University Press

radii is 2 : 1. This is probably the largest deformation a nucleus can hold without fissioning, hence the name. The microscopic basis for the appearance of superdeformed configurations reflects a special stability associated with the shell structure, and is intimately connected with that found for the existence of fission isomers (Michaudon (1973)).

The nature of these shells can be understood in a simple manner by reference to one-particle motion in a spheroidal deformed harmonic-oscillator potential. As illustrated in Fig. 6.19, the degeneracies of the isotropic oscillator are removed by the deformation, but new major shells (degeneracies) reappear when the oscillator frequencies in the different directions have rational ratios.

Especially large effects occur for a deformation with the frequency ratio $\omega_\perp : \omega_3 = 2:1$, and the associated nucleon numbers for closed shells are $N = 80, 110, 140, \ldots$. The nuclear potential differs from the harmonic oscillator in the radial dependence and in the occurrence of a large spin-orbit coupling. The inclusion of these effects leaves intact the main features of the oscillator shell structure in the 2 : 1 potential, but modifies the closed-shell numbers to $N = \ldots, 86, 116, \ldots$ (Bohr and Mottelson (1973)).

Once the superdeformed yrast band of ^{152}Dy is populated with a spin $I \sim 60\hbar$, the nucleus remains in it through eighteen collective $E2$ transitions (Twin *et al.* (1986)) until suddenly at spin $I = 24\hbar$ and about 5 MeV above the yrast line it terminates within an angular interval $\Delta I \sim (2 \div 4)\hbar$. This observation requires that a mechanism be identified which within a narrow range of $2 \div 4$ units of $\hbar$ can change the tunnelling probability between the superdeformed and the normal minimum by about six orders of magnitude.

Although the barrier between the superdeformed and the normal minima changes with spin, all calculations predict a smooth variation of it (Ragnarsson and Åberg (1986)) (see Fig. 6.20).

The sudden transition out of the superdeformed minimum at spin $I = 24\hbar$ is likely to be related to the onset of pairing caused by the disalignment of the lowest pair of $j_{15/2}$ quasiparticles, taking place at frequency ~0.3 MeV (Shimizu *et al.* (1987)) (see Section 6.2), although other mechanisms may play a role (see, e.g. Åberg (1999), Andreoiu *et al.* (2003), Sergeant *et al.* (2002)). This change in the pairing gap strongly reduces the inertial parameter D (see equations (7.6) and (7.8)), leading to a large increase of the tunnelling probability, as shown in Fig. 6.21. It is likely that these results are the clearest indication to date of a pairing collapse taking place in nuclei as a function of the angular momenta. The discussion of this subject is continued in Chapter 7.

6.6 Response function technique to calculate RPA fluctuations

In the present section we shall study the behaviour of the pairing correlation energy, and of the pairing gap of a superfluid, for deformed strongly rotating

https://doi.org/10.1017/9781009401920 Published online by Cambridge University Press

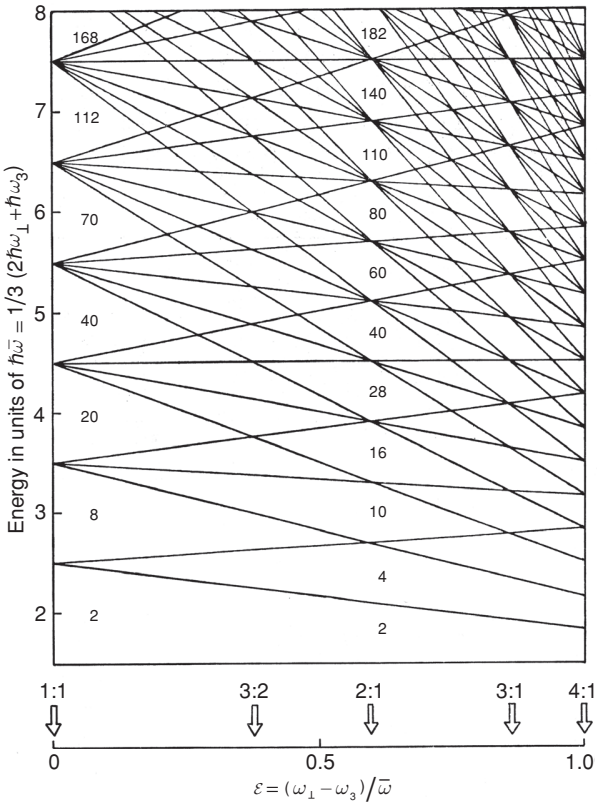

Figure 6.19. Shell structure in anisotropic harmonic-oscillator potential. This figure shows the single-particle energy levels, as a function of deformation, in a prolate axially symmetric oscillator potential. $V = (1/2)M(\omega_\perp^2(x_1^2 + x_2^2) + \omega_3^2 x_3^2)$, $E = \hbar\omega_\perp(n_\perp + 1) + \hbar\omega_3(n_3 + 1/2)$. The frequencies ω_3 and $\omega_\perp$ refer to motion parallel and perpendicular to the symmetry axis, while $\overline{\omega}$ is the mean frequency. The single-particle states can be specified by the number of quanta n_3 and $n_\perp$, and each energy level has a degeneracy $2(n_\perp + 1)$, due to the spin and the degeneracy in the motion perpendicular to the axis. Additional degeneracies leading to the formation of major shells may occur when the ratio of the frequencies $\omega_\perp : \omega_3$ is equal to the ratio between integers. The deformations corresponding to the most prominent shell structure effects are indicated by the arrows labelled by the corresponding frequency ratio. For the shells with frequency ratio 1 : 1 (spherical shape) and 2 : 1, the figure gives the particle numbers for closed-shell configurations (from Bohr and Mottelson (1973)). Reprinted, with permission, from the *Annual Review of Nuclear Science*, Volume 23 © 1973 by Annual Reviews www.annualreviews.org

nuclei as a function of the rotational frequency, taking into account pairing fluctuations in the RPA.

In the quasiparticle basis, the correlation energy takes the form

$$E_{\text{corr}}^{\text{RPA}} = \frac{1}{2}\Big[\sum_n \omega_n - \sum_{\alpha<\beta} E_{\alpha\beta}\Big], \tag{6.46}$$

https://doi.org/10.1017/9781009401920 Published online by Cambridge University Press

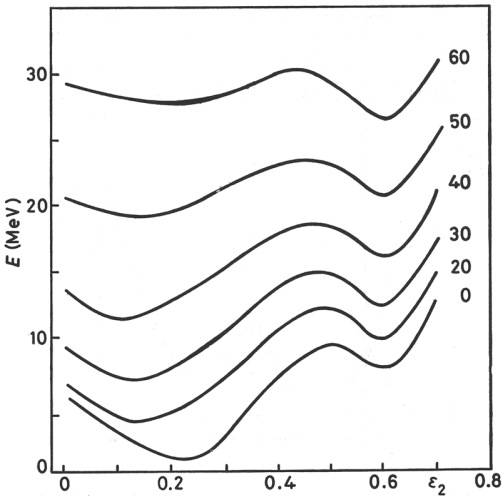

Figure 6.20. Potential energy of ^{152}Dy as a function of deformation parameter ε_2 for different values of the angular momentum.

where ω_n are the RPA eigenfrequencies, $E_{\alpha\beta} \equiv E_\alpha + E_\beta$ being the unperturbed two-quasiparticle energies. Because the different RPA modes contribute democratically to $E_{\rm corr}^{\rm RPA}$, to calculate this quantity one needs to determine very many, closely spaced, RPA eigenmodes. This is particularly true in the case where symmetries of the mean field are spontaneously broken, such as in the case of superfluid and deformed nuclei, where the detailed computation of the contribution of every single RPA root to $E_{\rm corr}^{\rm RPA}$ becomes unfeasible. To avoid this problem, Shimizu *et al*. (1989) developed a method to calculate the correlation energy, making use of response function techniques, and applied it to the study of pairing correlations in rapidly rotating nuclei. The essence of the method consists in expressing the RPA correlation as an integral in terms of the RPA response function, which can be calculated without explicitly solving the RPA eigenvalue problem. These techniques have been extended to deal with the Anderson–Goldstone–Nambu modes (Donati *et al*. (1999a)), and to calculate the nucleon effective mass in superfluid, deformed, rotating nuclei (Donati *et al*. (1999b)). An equivalent method was developed by Dönau *et al*. (1999).

Following Shimizu *et al*. (2000), we start from the Hamiltonian,

$$H = H_0 + V, \tag{6.47}$$

where H_0 is the unperturbed one-body (mean-field) Hamiltonian and V is the residual two-body interaction, which is assumed to be of multi-separable form,

$$V = -\frac{1}{2}\sum_\rho \chi_\rho Q_\rho Q_\rho, \tag{6.48}$$

https://doi.org/10.1017/9781009401920 Published online by Cambridge University Press

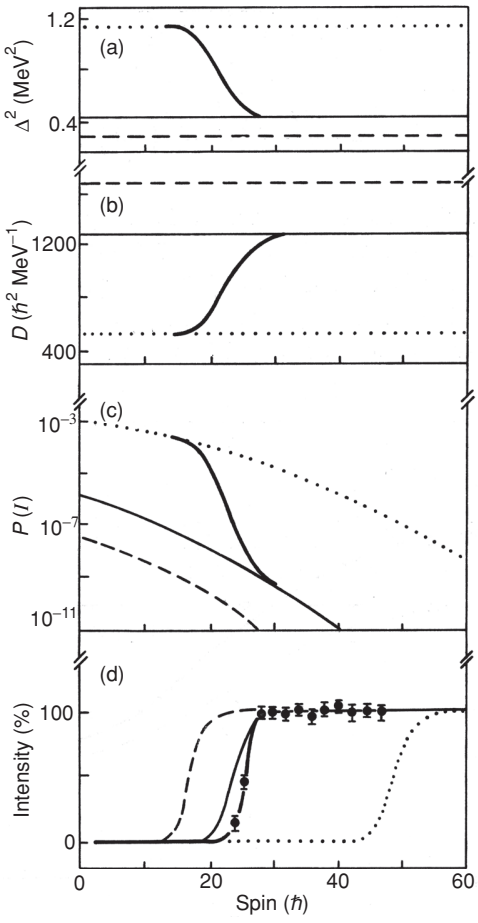

Figure 6.21. Four different possibilities for the variation of the square of the pairing gap with angular momentum are considered. (a) illustrates its influence on the barrier penetrability. Shown in graphs (b) and (c) is the associated variation of the inertial-mass parameter D and the penetrability factor $P(I)$. In (d) the relative intensity of the superdeformed band is shown as a function of the angular momentum in comparison with the experimental datum in comparison with the experimental data. Reprinted with permission from Herskind *et al.*, *Phys. Rev. Lett.* **59**: 2416–19 (1988). Copyright 1988 by the American Physical Society.

with Q_ρ being a one-body Hermitian operator while χ_ρ is the strength of the interaction in channel ρ. The associated ground-state energies and state vectors of H_0 and H are denoted E_0, $|\Phi_0\rangle$ and E, $|\Psi\rangle$, respectively. Turning on the interaction adiabatically, the correlation energy can be written as (Fetter and Walecka (1971))

$$E_{\text{corr}} \equiv E - E_0 = \int_0^1 \mathrm{d}\lambda \, \langle \Psi(\lambda) | V | \Psi(\lambda) \rangle. \tag{6.49}$$

https://doi.org/10.1017/9781009401920 Published online by Cambridge University Press

In this equation $|\Psi(\lambda)\rangle$ is the ground state of the λ-scaled Hamiltonian $H(\lambda) \equiv H_0 + \lambda V$. Within the RPA approximation, the above expression can be rewritten by making use of a contour integration as

$$E_{\rm corr}^{\rm RPA} = -\frac{1}{2}\int_0^1 {\rm d}\lambda \sum_{\rho,n} \chi_\rho \mathcal{Q}_{\rho,n}^{(\lambda)*} \mathcal{Q}_{\rho,n}^{(\lambda)}$$
$$= -\frac{1}{4\pi {\rm i}} \int_0^1 {\rm d}\lambda \oint_C {\rm d}z \sum_\rho \Big[\mathcal{R}_{\rho\rho}^{(\lambda)}(z)\chi_\rho\Big], \tag{6.50}$$

in terms of the λ-scaled RPA response function (matrix),

$$\mathcal{R}_{\rho\sigma}^{(\lambda)}(\omega) \equiv \sum_n \Big[\frac{\mathcal{Q}_{\rho,n}^{(\lambda)*}\mathcal{Q}_{\sigma,n}^{(\lambda)}}{\omega_n^{(\lambda)} - \omega} + \frac{\mathcal{Q}_{\rho,n}^{(\lambda)}\mathcal{Q}_{\sigma,n}^{(\lambda)*}}{\omega_n^{(\lambda)} + \omega}\Big], \tag{6.51}$$

where $\mathcal{Q}_{\rho,n}^{(\lambda)} = \langle n(\lambda)|Q_\rho|\Psi(\lambda)\rangle_{\rm RPA}$, and the contour C encloses all the positive λ-scaled RPA eigenvalues $z = \omega_n^{(\lambda)}$ clockwise. Note that $\mathcal{R}_{\rho\sigma}^{(\lambda)}(\omega)$ can be calculated as

$$\mathcal{R}^{(\lambda)}(\omega) = \big[1 - R(\omega)\ \chi\lambda\big]^{-1} R(\omega), \tag{6.52}$$

in terms of $\chi = (\Delta_{\rho\sigma}\chi_\rho)$ and the unperturbed response function (matrix), $R_{\rho\sigma}(\omega)$, which is defined by replacing $\mathcal{Q}_{\rho,n}^{(\lambda)}$ and $\omega_n^{(\lambda)}$ in equation (6.51) with unperturbed quantities, $q_{\rho,\alpha\beta} = \langle\alpha\beta|Q_\rho|0\rangle$ and $E_{\alpha\beta}$.

By choosing a common contour C for all values of $0 < \lambda < 1$, one may exchange the order of integration in equation (6.50) (Pines (1963), Appendix C). The selected path is the one shown in Fig. 6.22 passing through the origin of the complex z-plane in keeping with the presence of (non-normalizable) zero-energy modes (the symmetry-recovering or Anderson–Goldstone–Nambu modes, Chapter 4) in the RPA spectrum ($\omega_{n=\rm AGN} \to 0$ as $\lambda \to 1$). In this case the λ-integration in equation (6.50) converges because $|\mathcal{Q}_{\rho,n=\rm AGN}^{(\lambda)}|^2 \sim 1/\sqrt{1-\lambda}$ as $\lambda \to 1$. After performing the λ-integration analytically, one obtains

$$E_{\rm corr}^{\rm RPA} = \frac{1}{4\pi {\rm i}} \oint_{C_{1a}} F(z){\rm d}z, \tag{6.53}$$

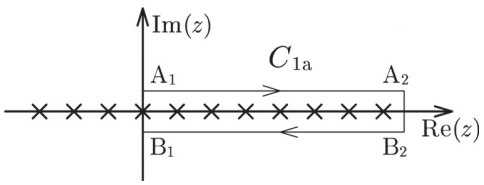

Figure 6.22. An illustration of the integration contour in the complex z-plane used in equation (6.53). Crosses denote the positions of all the λ-scaled RPA roots for arbitrary values of $0 < \lambda < 1$, i.e. $\mathrm{Re(A_2)} = \mathrm{Re(B_2)} > \max_{n,\lambda}\{\omega_n^{(\lambda)}\}$.

https://doi.org/10.1017/9781009401920 Published online by Cambridge University Press

where

$$F(z) \equiv -\int_0^1 \mathrm{Tr}\Big[\mathcal{R}^{(\lambda)}(z)\chi\Big]\mathrm{d}\lambda = \log\big(\det\big[1 - R(z)\chi\big]\big). \tag{6.54}$$

Rewriting the determinant as a function of the RPA and unperturbed energies, one obtains

$$F(z) = \sum_n \Big[\log(z - \omega_n) + \log(z + \omega_n)\Big] - \sum_{\alpha<\beta}\Big[\log(z - E_{\alpha\beta}) + \log(z + E_{\alpha\beta})\Big]. \tag{6.55}$$

Thus, equation (6.53) is the sum of integrals of the complex multi-valued logarithmic functions of type $\log(z - p)$, where the real value p (in our case ω_n or $E_{\alpha\beta}$) indicates a branch point. Here the principal branch of the logarithmic function should be taken in accordance with the choice of path C_{1a}, i.e. $-\pi < \arg\log(z - p) \leq \pi$, and the segment of the real axis with $z < p$ is the branch-cut. One can now integrate equation (6.53) around all the branch points within C_{1a} by deforming the path and using for each of them a clockwise circular path C_p centred at the point itself, i.e.

$$\int_{C_p} \log(z - p)\,\mathrm{d}z = 2\pi\mathrm{i}\,R_p, \tag{6.56}$$

where R_p is the radius of the circle C_p. Considering that R_p is ω_n or $E_{\alpha\beta}$, it can be shown that equation (6.53) leads to the original expression given in equation (6.46). The contribution associated with the zero mode vanishes in keeping with the fact that in this case the path of integration becomes a semicircle. This can also be seen by direct evaluation of the integral in equation (6.56) in the case where C_p is a semicircle centred at zero with $R_{p=0} \to 0$.

Making use of a limiting procedure and the following properties of the function $F(z)$,

$$[F(z)]^* = F(-z^*), \quad F(-z) = F(z), \tag{6.57}$$

$$F(z) \to o(1/z^2) \quad \text{as} \quad |z| \to \infty, \tag{6.58}$$

it can be shown that equation (6.53) can be written as

$$E_{\mathrm{corr}}^{\mathrm{RPA}} = \frac{1}{2\pi}\lim_{\varepsilon\to 0+}\int_0^\infty \mathrm{Im}\big[F(\omega + \mathrm{i}\varepsilon)\big]\mathrm{d}\omega, \tag{6.59}$$

which is the formula utilized in (Shimizu *et al.* (1989)). To obtain this result one deforms the path shown in Fig. 6.22 taking the part A_2 and B_2 to infinity and A_1B_1 infinitely close to the origin ($\varepsilon \to 0$). In this case the contributions from segments A_2B_2 and A_1B_1 vanish, those arising from A_1A_2 and B_1B_2 being equal.

https://doi.org/10.1017/9781009401920 Published online by Cambridge University Press

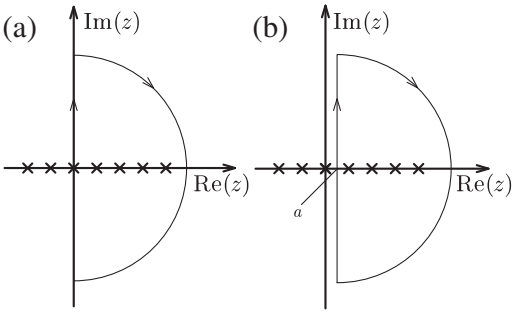

Figure 6.23. Modified integration contour from Fig. 6.22 found to be more suitable to calculate the RPA correlation energy. Taking the limit of infinite radius of the semicircle, the corresponding contribution vanishes.

In order to present a more efficient way to evaluate the RPA correlation energy, the integration path in Fig. 6.22 is modified to the one shown in Fig. 6.23a. Then the contribution from the semicircle vanishes as its radius goes to infinity because of the asymptotic property given in equation (6.58). Using also the properties given in equation (6.57), we obtain

$$E_{\rm corr}^{\rm RPA} = \frac{1}{2\pi}\int_0^\infty {\rm Re}\big[F({\rm i}\omega)\big]{\rm d}\omega. \tag{6.60}$$

Note that the modification of the path of integration from one parallel to the real axis into one parallel to the imaginary axis is quite useful for making the numerical calculations efficient. This is because ${\rm Im}F(z)$ is an oscillating function of ${\rm Re}(z)$ on the path shown in Fig. 6.22, while ${\rm Re}F(z)$ is a monotonically decreasing function along the imaginary axis on the path shown in Fig. 6.23a. Consequently, the number of mesh points needed in the calculation is strongly reduced after a suitable transformation of the integration variable.

In Shimizu *et al*. (1989) and Shimizu and Broglia (1990), pairing correlations in rapidly rotating nuclei have been studied using the general method discussed above. In these references, in addition to the RPA correlation energy, another measure of pairing correlations was introduced, namely the RPA pairing gap, $\Delta_{\rm RPA}$ (called the 'effective' pairing gap). It is defined as

$$\Delta_{\rm RPA} \equiv \sqrt{\Delta^2 + \tfrac{1}{2}G^2\, S_0({\rm RPA})}, \tag{6.61}$$

with

$$S_0({\rm RPA}) \equiv \sum_{n\neq {\rm AGN}} \Big[|\langle n|P|0\rangle|^2 + |\langle n|P^\dagger|0\rangle|^2\Big]_{\rm RPA}, \tag{6.62}$$

where $\Delta = G\,\langle 0|P^\dagger|0\rangle_{\rm HB}$ is the standard, static BCS pairing gap (the order parameter of mean field), while G is the pairing force strength. The non-energy

https://doi.org/10.1017/9781009401920 Published online by Cambridge University Press

weighted sum rule S_0(RPA) describes the contribution of pairing fluctuations, associated with the monopole pair-transfer operator, $P^\dagger = \sum_{i>0} a_i^\dagger a_{\bar{i}}^\dagger$, to the effective (RPA) gap. Note that $\sum_{n\neq \mathrm{AGN}}$ means that the divergent contribution from the zero energy mode (pairing rotation) is to be excluded, in keeping with the fact that its contribution to equation (6.61) is included through the static (BCS) pairing gap Δ. In Shimizu *et al*. (1989), S_0(RPA) was calculated making use of the expression

$$S_0(\mathrm{RPA}) \approx \frac{1}{\pi}\int_{\omega_{\mathrm{cut}}}^{\infty} \mathrm{Im}\,\mathrm{Tr}\big[\mathcal{R}(\omega + \mathrm{i}\varepsilon)\big]\mathrm{d}\omega, \tag{6.63}$$

where $\mathcal{R}(\omega) \equiv \mathcal{R}^{(\lambda=1)}(\omega)$ is the RPA response function, whose dimension is 2 corresponding to $Q_1 = (P^\dagger + P)/\sqrt{2}$ and $Q_2 = \mathrm{i}(P^\dagger - P)/\sqrt{2}$. A finite value of ε and a low-energy cutoff ω_{cut} are used to get rid of the AGN mode contribution numerically. This is the same approximation as that used in calculating the RPA correlation energy, and can then be avoided using the path shown in Fig. 6.23(b). In this way one avoids the singularity associated with an eventual zero mode, as

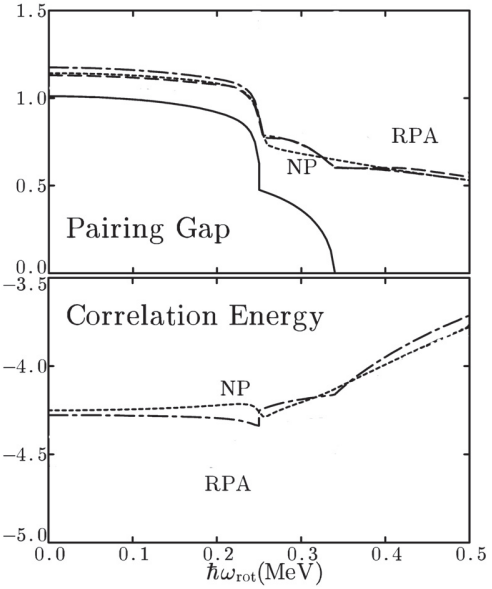

Figure 6.24. RPA pairing gap (upper panel) and RPA correlation energy (lower panel) for neutrons in ^{164}Er as a function of the rotational frequency. Both quantities are in MeV. The dash-dotted curves denote the results of calculations with $\varepsilon = 200$ keV and $\hbar\omega_{\mathrm{cut}} = 400$ keV. The value of the static (mean-field) pairing gap Δ, which vanishes at $\hbar\omega_{\mathrm{rot}} = 0.34$ MeV, is also displayed in the upper panel (continuous curve). The results of the number-projection (NP) calculations are shown as dotted curves.

https://doi.org/10.1017/9781009401920 Published online by Cambridge University Press

in this case $\mathcal{R}(z)$ has a second-order pole at the origin (see Donati *et al*. (1999a)):

$$S_0(\mathrm{RPA}) = \frac{1}{\pi}\int_0^\infty \mathrm{Re}\,\mathrm{Tr}\big[\mathcal{R}(a+\mathrm{i}\omega)\big]\mathrm{d}\omega. \tag{6.64}$$

Since the function $\mathrm{Tr}\big[\mathcal{R}(z)\big]$ has poles as singularities, the integral is independent of the choice of a. Summing up, making use of equations (6.60) and (6.64), both the RPA correlation energy and the RPA pairing gap can be exactly evaluated in a numerically efficient way.

In Fig. 6.24 we compare the results of the exact and approximate calculations of both $E_{\mathrm{corr}}^{\mathrm{RPA}}$ and Δ_{RPA} in the case of deformed, superfluid nuclei as a function of the rotational frequency. The average correlation energy is -4 MeV. This is much larger than the BCS pair correlation energy (≈ -1.5 MeV) calculated in Section 3.5. The difference is the RPA correlation energy (see also Section 8.4).

There is another method which allows us to go beyond mean-field approximation, namely the number-projection (NP) (see e.g. Ring and Schuck (1980), see also Section 4.2.2, in particular equation (4.45)). In Fig. 6.24 we also included the NP results for comparison. The NP correlation energy is defined as the energy difference between the NP and mean field (Hartree–Bogoliubov), $E_{\mathrm{corr}}^{(\mathrm{NP})} \equiv E_{\mathrm{NP}} - E_{\mathrm{HB}}$ (the exchange energy is included in E_{NP}). Although RPA leads to larger values of the correlations, especially in the superfluid phase, the rotational frequency dependences are quite similar. The advantage of the NP method over the RPA is to lead to smooth functions for both the correlation energy and the pairing gap at the pairing phase-transition point.

Pairing vibrations in the RPA framework have also been considered in the phase transition of metallic clusters as a function of temperature (see Fig. 1.15 and Mühschlegel *et al*. (1972), Lauritzen *et al*. (1993)). Within this context, it is of interest to consider the effect the dynamical pairing gap (see also Dang and Arima (1998, 2003)) may have on the width of the giant dipole resonance at low temperature (see N. Dinh Dang and A. Arima, *Key Topics in Nuclear Structure*, Paestum, 23–27 May, 2004, abstracts, p. 63).

7

Plastic behaviour of nuclei and other finite systems

In some circumstances the nucleus acts as a liquid and in others like an elastic solid. In general it responds elastically to sudden forces, and it flows plastically over longer periods of time (Bertsch (1980, 1988)). Examples of this behaviour are giant resonances and low-lying collective surface vibrations respectively. In the first case, as we shall see in Section 8.3, pairing plays no role, at least in the case of nuclei lying along the valley of stability. The nuclear single-particle states change their shape but the occupation numbers do not change. The energy of a giant resonance in a nucleus is of the order of the energy difference between major shells ($\hbar\omega \approx 41/A^{1/3}$ MeV, ≈ 7 MeV, for medium heavy nuclei), a quantity which is much larger than the pairing gap $\Delta \approx$ 1–1.5 MeV. Giant resonances are fast modes, the collective motion is dominated by mean-field effects and the rigidity is provided by the mean field (Bortignon, Bracco and Broglia (1998)). On the other hand, low-energy surface modes are associated with particle–hole excitations which are of the order of the pairing gap. Pairing plays a dominant role and the collective states are coherent linear combinations of two-quasiparticle excitations. The situation is, however, different in the case of exotic nuclei, where the last nucleons are very weakly bound. Nucleon spill out makes these systems particularly polarizable leading to 'pigmy resonances', whose properties can be influenced by pairing (Frascaria *et al*. (2004), see also last paragraph of Chapter 6).

In any case, both giant resonances and surface vibrations can be treated in the harmonic approximation, and viewed as phonon excitations (see Chapter 8). Consequently, as in the case of the harmonic oscillator, associated with each degree of freedom of the vibrations there is a zero-point motion. In other words, the surface of a nucleus fluctuates in its ground state. The amplitude of these fluctuations is particularly important for low-lying quadrupole and octupole vibrations and somewhat less but still consistent for low-lying vibrations with multipolarity $\lambda = 4$ and $\lambda = 5$ (see Appendix C). In general these fluctuations

https://doi.org/10.1017/9781009401920 Published online by Cambridge University Press

will be out of phase. However there is a finite although small probability that the fluctuations act coherently, allowing the system to probe large deformations. The presence of such deformations in the ground-state wavefunction is rather difficult to establish, as they act as virtual states which renormalize the properties of the ground state (see, however, Section 8.4).

7.1 Exotic decay

There are, however, exceptions to this situation, namely, in the case where the fluctuations lead to shapes corresponding to two daughter nuclei in a touching configuration, for which the Q-value associated with the division of the system is positive. In what follows we shall discuss an example of such a situation (see Fig. 7.1), namely the so-called exotic decay $^{223}\mathrm{Ra} \rightarrow {}^{14}\mathrm{C} + {}^{209}\mathrm{Pb}$, a situation where pairing plays a central role in determining the inertia of the system.

A theory for the decay envisages two stages. In the first stage the nucleus evolves from a state with a moderate deformation to a cluster configuration like the one shown in Fig. 7.1 of touching parent–daughter nuclei. During this process pairs of nucleons change their states and the initial A-particle wavefunction ϕ_0 evolves through local minima described by wavefunctions ϕ_i, until it reaches the touching configuration described by the wavefunction ϕ_n. In the deformation process the twofold degenerate single-particle levels (assuming axially symmetric deformation) will change their energy, those with wavefunctions along the poles decreasing their energy, while those along the equator will increase in energy as illustrated in the lower part of Fig. 7.2. At each crossing of an empty downsloping energy level and an occupied upsloping level two particles will

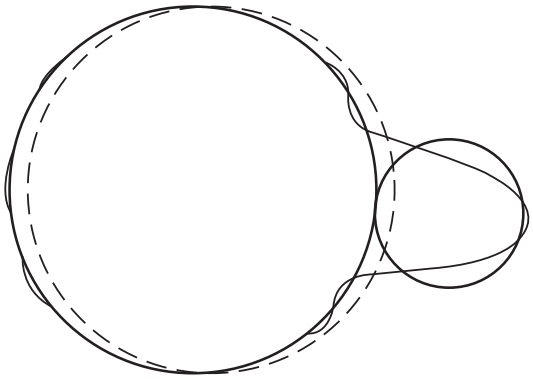

Figure 7.1. Shape transitions for the decay $^{223}\mathrm{Ra} \rightarrow {}^{209}\mathrm{Pb} + {}^{14}\mathrm{C}$. The original nucleus is shown dashed; the touching daughter nuclei as heavy solid lines. The transformation described in the text carries the initial shape to the one shown by the light solid line (after Bertsch (1988), Barranco *et al*. (1990)).

https://doi.org/10.1017/9781009401920 Published online by Cambridge University Press

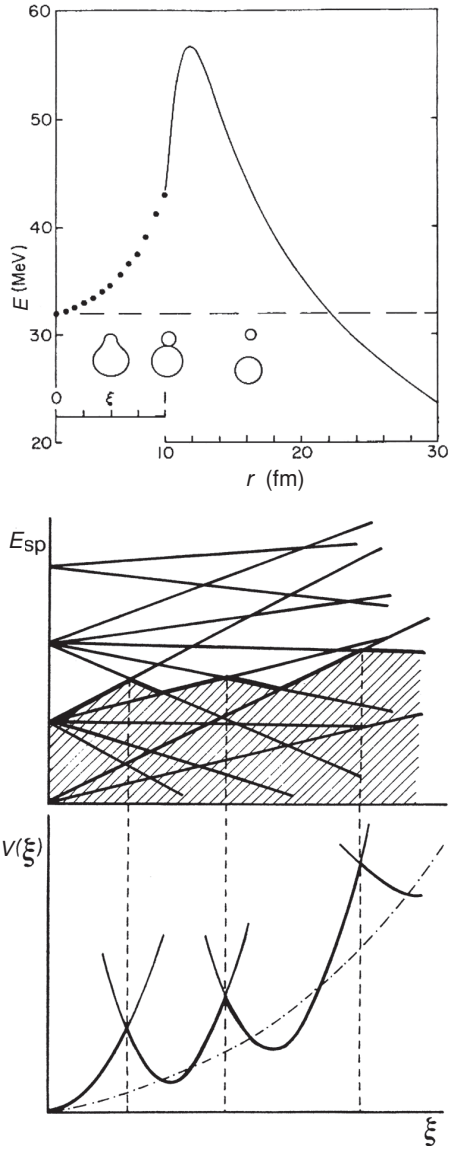

Figure 7.2. (Top) Potential energy curve for the decay ^{223}Ra $\rightarrow$ ^{209}Pb $+^{14}$C. The outside potential is a combination of Coulomb and nuclear heavy ion potentials. The dots show the assumed Hartree–Fock states describing the shape change in the internal region. (Middle) Schematic representation of the occupancy of the single-particle levels. (Bottom) Local Hartree–Fock potential energies as a function of the deformation parameter ξ. Reprinted with permission from Barranco *et al.*, *Phys. Rev. Lett.* **60**:507–10 (1988a). Copyright 1988 by the American Physical Society.

https://doi.org/10.1017/9781009401920 Published online by Cambridge University Press

change levels, under the action of the residual nuclear interaction, i.e. the part of the nuclear interaction not used in producing the mean field.

We assume that the wavefunction describing the evolution from the initial state ϕ_0 to the final touching state ϕ_n is

$$\Phi = \sum_{i=1}^{n} a_i \phi_i, \tag{7.1}$$

where the ϕ_i are wavefunctions with pair correlations, like e.g. BCS wavefunctions, but with a number-projection so that there is a definite number of pairs in the upsloping levels and in the downsloping levels (see equation (4.45)). The suffix n indicates the number of pairs transferred from the upsloping to the downsloping levels. The wavefunction ϕ_i describes the ith local minima in the potential energy diagram in Fig. 7.2 (bottom). The pairing interaction connects wavefunctions ϕ_i where the number of pairs changes from i to $i \pm 1$. Consequently, the equation determining the ground-state wavefunction is the lowest-energy solution of the equation

$$\begin{bmatrix} \ddots & \vdots & \vdots & \vdots & \vdots \\ \cdots & E_{i-1} & v & \cdots & \cdots \\ \cdots & v & E_i & v & \cdots \\ \cdots & \cdots & v & E_{i+1} & \cdots \\ \vdots & \vdots & \vdots & \vdots & \ddots \end{bmatrix} \begin{bmatrix} \cdots \\ a_{i-1} \\ a_i \\ a_{i+1} \\ \cdots \end{bmatrix} = E \begin{bmatrix} \cdots \\ a_{i-1} \\ a_i \\ a_{i+1} \\ \cdots \end{bmatrix}. \tag{7.2}$$

The connection between equation (7.2) and a Schrödinger equation describing collective motion,

$$\left(-\frac{\hbar^2}{2D} \frac{\mathrm{d}^2}{\mathrm{d}\xi^2} + V(\xi) \right) \psi(\xi) = \mathcal{E}(\xi), \tag{7.3}$$

can be made discretizing equation (7.3) on a grid of step $\Delta\xi = 1/n$ in the interval $0 < \xi < 1$, using

$$\frac{\mathrm{d}^2\psi}{\mathrm{d}\xi^2} \approx \frac{\psi(\xi_{i-1}) + \psi(\xi_{i+1}) - 2\psi(\xi_i)}{\Delta\xi^2}.$$

Assuming that the deformation variable ξ takes the value $\xi = 0$ for $\Phi = \phi_0$ (^{223}Ra in its configuration of minimum energy), and $\xi = 1$ for $\Phi = \phi_n$ (^{209}Pb and ^{14}C at touching distance), one can write

$$M \begin{bmatrix} \cdots \\ \psi\,(\xi_{i-1}) \\ \psi\,(\xi_i) \\ \psi\,(\xi_{i+1}) \\ \cdots \end{bmatrix} = \mathcal{E} \begin{bmatrix} \cdots \\ \psi\,(\xi_{i-1}) \\ \psi\,(\xi_i) \\ \psi\,(\xi_{i+1}) \\ \cdots \end{bmatrix}, \tag{7.4}$$

https://doi.org/10.1017/9781009401920 Published online by Cambridge University Press

where M is the matrix

$$\begin{bmatrix} \vdots & \vdots & \vdots \\ V(\xi_{i-1}) + \frac{\hbar^2}{D\Delta\xi^2} & -\frac{\hbar^2}{2D\Delta\xi^2} & \cdots \\ -\frac{\hbar^2}{2D\Delta\xi^2} & V(\xi_i) + \frac{\hbar^2}{D\Delta\xi^2} & -\frac{\hbar^2}{2D\Delta\xi^2} \\ \cdots & -\frac{\hbar^2}{2D\Delta\xi^2} & V(\xi_{i+1}) + \frac{\hbar^2}{D\Delta\xi^2} \\ \vdots & \vdots & \vdots \end{bmatrix}. \tag{7.5}$$

Comparing equations (7.2) and (7.5) one finds that the inertia of the system is

$$D = -\frac{\hbar^2}{2v} n^2. \tag{7.6}$$

To use the above equation as a calculational tool we need to know the number of level crossings n (see also Section 7.3) and the matrix element v. Before calculating the value of these parameters we note that the structure of this relation is quite plausible. The inertia is larger the larger the number of particles that have to be moved around in the motion. On the other hand, the larger the interaction, the smaller is the inertia, because it is easier to make a pair of particles jump at a crossing.

7.1.1 Inertia

It is fair to assume that the pairing residual interaction plays a central role in the process in which pairs of particles moving in time-reversal states change their state of motion. This is because pairing correlations lead to minimal friction. The pairing force Hamiltonian is

$$H_{\mathrm{p}} = -GP^{\dagger}P = -G\left(P_{\mathrm{u}}^{\dagger} + P_{\mathrm{d}}^{\dagger}\right)\left(P_{\mathrm{u}} + P_{\mathrm{d}}\right).$$

The transition matrix element between two successive states is

$$v = \langle \phi_{i+1} \left| H_{\mathrm{p}} \right| \phi_i \rangle = -G \langle \phi_{i+1} \left| P_{\mathrm{d}}^{\dagger} P_{\mathrm{u}} \right| \phi_i \rangle,$$

because a pair moves from an upsloping (u) level to a downsloping (d) level. It was shown in Chapter 3 that such transfer matrix elements can be estimated by mean values in BCS wavefunctions so that

$$\begin{aligned} v &\approx -G \langle \mathrm{BCS} \left| P_{\mathrm{d}}^{\dagger} \right| \mathrm{BCS} \rangle \langle \mathrm{BCS} \left| P_{\mathrm{u}} \right| \mathrm{BCS} \rangle \\ &\approx -\frac{G}{4} \langle \mathrm{BCS} \left| P \right| \mathrm{BCS} \rangle^2 = -\frac{1}{4} \frac{\Delta^2}{G}, \end{aligned} \tag{7.7}$$

where we have assumed that

$$\langle \mathrm{BCS} \left| P_{\mathrm{d}}^{\dagger} \right| \mathrm{BCS} \rangle = \tfrac{1}{2} \langle \mathrm{BCS} \left| P^{\dagger} \right| \mathrm{BCS} \rangle = \frac{\Delta}{2G}.$$

https://doi.org/10.1017/9781009401920 Published online by Cambridge University Press

We can state the result given in equation (7.7) in another way: a pairing force acting among all the downsloping and upsloping levels will give a matrix element which is the product of three factors: (i) the pairing force constant G, (ii) the probability (equal to $1/4$) that the initial states are occupied and the final is empty and (iii) the pairing enhancement factor $(\Delta/G)^2$. When both neutron and proton contributions are taken into account, equation (7.7) is modified to

$$v = -\left(\frac{\Delta_\nu^2 + \Delta_\pi^2}{4G}\right). \tag{7.8}$$

This same result has been derived in another way by Barranco *et al.* (1990). Employing the standard values $G = 25/A$ MeV, and $\Delta_\nu = \Delta_\pi = 12/\sqrt{A}$ MeV, one obtains

$$v = -2.9 \text{ MeV}. \tag{7.9}$$

To calculate D we need now to know n, i.e. the number of pairs of particles which have to be moved around in ^{223}Ra, to emit a ^{14}C. Because the centre of mass of the total system has to remain at rest, fourteen particles have to be moved in one direction and fourteen in the opposite. Consequently, a fair estimate of n is the reduced mass number of the process, i.e. $n \approx 13$. Finally,

$$D = -\frac{\hbar^2 n^2}{2v} = 29.1\ \hbar^2 \text{ MeV}^{-1}. \tag{7.10}$$

We now proceed to estimate the potential energy V.

7.1.2 Potential energy

Assuming that the energies of the different local minima lie on a parabola (see Fig. 7.2 (bottom)), one can write

$$V(\xi) = \tfrac{1}{2} C \xi^2. \tag{7.11}$$

An expression for the potential at $\xi = 1$ can be read off from the sketch in the upper part of Fig. 7.2

$$V(\xi = 1) + Q = U_{aA}^{c}(R_0) + U_{aA}^{N}(R_0), \tag{7.12}$$

where R_0 is the distance at which the two densities barely touch, i.e. $R_0 = R_a + R_A + a$, R_i being the radius of ^{14}C ($i = a$) and of ^{209}Pb ($i = A$). The diffusivity of the ion-ion potential U_{aA}^{N} is denoted by a, while U_{aA}^{c} is the Coulomb potential acting between the ions. Finally, the quantity $Q = 31.9$ MeV is the Q-value of the decay process.

The decay rate is very sensitive to the parameters of the potential barrier outside the touching radius. Here we follow Barranco *et al.* (1988a, 1990), and

https://doi.org/10.1017/9781009401920 Published online by Cambridge University Press

use the Christensen–Winther potential (Broglia and Winther (1991))

$$U_{aA}^{N} = S_0 \bar{R}_{aA} \exp\left(-\frac{r-R}{a}\right), \tag{7.13}$$

which gives a good description of heavy ion elastic scattering and fusion reactions. The radius parameters R and $\bar{R}_{aA}$ in (7.13) are defined by

$$\bar{R}_{aA} = \frac{R_a R_A}{R_a + R_A}, \quad R = R_a + R_A. \tag{7.14}$$

where R_a and R_A of the two nuclei are parametrized according to

$$R_i = (1.233 A_i^{1/3} - 0.98 A_i^{-1/3}) \text{ fm}, \tag{7.15}$$

and the values $S_0 = -50\,\text{MeV fm}^{-1}$, $a = 0.63$ fm are used. Substituting the numerical values into equation (7.13) one obtains

$$U_{aA}^{N}(r) = -94 \exp\left(-\frac{r-9.7}{0.63}\right) \text{MeV}, \tag{7.16}$$

and

$$V(\xi = 1) = U_{aA}^{c}(10.5) + U_{aA}^{N}(10.5) - 31.6\,\text{MeV} = 9.2\,\text{MeV} \tag{7.17}$$

leading to

$$C = 18.4 \text{ MeV}. \tag{7.18}$$

7.1.3 Formation probability

The wavefunction describing the ground state of the harmonic oscillator is

$$\psi(\xi) = \left(\frac{\alpha}{\sqrt{\pi}}\right)^{1/2} \mathrm{e}^{-\frac{1}{2}\alpha^2\xi^2}, \tag{7.19}$$

where

$$\alpha^2 = \frac{D\omega}{\hbar} = \sqrt{\frac{DC}{\hbar^2}} = \sqrt{\frac{C}{2|v|}} n \approx 23.2. \tag{7.20}$$

Consequently, the formation probability is

$$P = |\psi(\xi = 1)|^2 = \frac{\alpha}{\sqrt{\pi}} \mathrm{e}^{-\alpha^2} = 2.4 \times 10^{-10}. \tag{7.21}$$

That is, the ground state of ^{223}Ra acquires shapes resembling the touching configuration of ^{209}Pb and ^{14}C with the probability (7.21).

https://doi.org/10.1017/9781009401920 Published online by Cambridge University Press

7.1.4 Decay constant

Once the ^{14}C is formed, the decay process can be described in terms of the standard Gamow theory, i.e. in terms of a knocking rate f and a tunnelling factor T, the associated decay constant being

$$\lambda = PfT. \tag{7.22}$$

Before proceeding to the calculation of f and T, we want to make a short remark on the standard theory of alpha decay, where one assumes $P = 1$. The reason why this approach to alpha decay is able to provide an overall account of the experimental findings is because in this case the preformation factor is of the order of 1 ($P \approx 10^{-1}$), and the tunnelling probability T (or γ in the standard language) is a very sensitive function of the input parameters. Any uncertainty in P can be compensated by a small change in the radius and height of the Coulomb barrier.

7.1.5 Knocking rate

To estimate f one makes the standard assumption of motion of a particle of inertia D in the ground state of a harmonic well. Then

$$\omega = \sqrt{\frac{C}{D}} = 1.2 \times 10^{21}\mathrm{s}^{-1} \tag{7.23}$$

and

$$f = \frac{\omega}{2\pi} \approx 2 \times 10^{20}\mathrm{s}^{-1}. \tag{7.24}$$

7.1.6 Tunnelling probability

We have to calculate the probability for tunnelling the Coulomb barrier starting from the touching distance $R_0 \approx 10.3$ fm. A convenient analytic formula is obtained neglecting the nuclear potential (Tonozuka and Arima (1979)):

$$T = \frac{kR_0}{F_0^2(kR_0) + G_0^2(kR_0)}, \tag{7.25}$$

in terms of the regular and irregular Coulomb functions. In equation (7.25) k is given by

$$k = \sqrt{\frac{2M_{aA}}{(E_\mathrm{B} - Q)}\hbar^2}. \tag{7.26}$$

https://doi.org/10.1017/9781009401920 Published online by Cambridge University Press

The height of the Coulomb barrier is given by (Broglia and Winther (1991))

$$E_{\mathrm{B}} = \frac{Z_a Z_A e^2}{r_{\mathrm{B}}}(1 - \frac{0.63}{r_{\mathrm{B}}}) \approx 58 \text{ MeV}, \tag{7.27}$$

where the associated radius is given by

$$r_{\mathrm{B}} = 1.07(A_a^{1/3} + A_A^{1/3}) + 2.72 \text{ fm} \approx 11.6 \text{ fm}. \tag{7.28}$$

One finally obtains from equation (7.25)

$$T \approx 10^{-26}. \tag{7.29}$$

7.1.7 Comparison to experiment

Making use of the relation (7.22) and of the quantities (7.21), (7.24) and (7.29), one obtains the theoretical value

$$\lambda_{\mathrm{th}} \approx 10^{-16} \text{ s}^{-1}, \tag{7.30}$$

to be compared with the experimental value (Rose and Jones (1984)) of

$$\lambda_{\mathrm{exp}} = 4.3 \times 10^{-16} \text{ s}^{-1}. \tag{7.31}$$

One has to keep in mind that no calculation can predict a decay constant with an accuracy better than 1–2 orders of magnitude.

The theory presented here is based on the idea that the parent nucleus evolves from an initial state with a moderate deformation to a cluster configuration by a series of level crossings. The calculated preformation factor is $P \approx 10^{-10}$. Other theories suppose that the cluster structure exists in the parent nucleus so that the preformation factor $P = 1$. Theories with widely different preformation factors are able to fit the data because of the extreme sensitivity of the penetration factor to the barrier parameters. For example Buck and Merchant (1989) use a potential with a barrier height of 63.9 MeV and radius 10.2 fm for the cluster decay of ^{223}Ra instead of the Christensen and Winther values $E_{\mathrm{B}} = 58$ MeV and $r_{\mathrm{B}} = 11.6$ fm. An increase of the barrier height of 6 MeV decreases the penetration factor by a factor of 10^{10} and compensates for the increase in the penetration factor. They have also been able to fit many other exotic decays. Buck *et al*. (2000) have a method for predicting the cluster structure of a nucleus by relating it to the decay Q-value. One argument in favour of the approach in the present chapter is that the Christensen-Winther potentials fit heavy ion elastic scattering data. This aspect has not been studied for the potentials used by Buck and his collaborators. Another argument is that the superfluid tunnelling model discussed in the present chapter can also be applied to other processes.

Table 7.1. *The four decay modes of* ^{234}U *(after Broglia et al. (1993)).*

Decay	$\lambda_{exp}(s^{-1})$	$\lambda_{th}(s^{-1})$	n
^{4}He	$9. \times 10^{-14}$	$2. \times 10^{-14}$	4
^{24}Ne	6.3×10^{-26}	$1. \times 10^{-28}$	19
^{28}Mg	$2. \times 10^{-26}$	$2. \times 10^{-28}$	23
spont. fission	$(8.6 \pm 1.8) \times 10^{-24}$	$5. \times 10^{-24}$	52

7.2 A variety of applications

The superfluid tunnelling model has been applied to a variety of problems involving the evolution of the nuclear system between two minima. In particular:

(1) To the calculation of alpha and exotic decay as well as fission, where the model provides an overall account of the data over twenty orders of magnitude (Barranco *et al*. (1990)); in particular a quantitative picture of the four decay modes of ^{234}U (see Table 7.1) (Barranco *et al*. (1989)), as well as the correction of the chart of nuclides regarding the lifetime quoted for the spontaneous fission of ^{232}U. The model predicts in fact an exotic decay branch $^{232}\text{U} \rightarrow {}^{208}\text{Pb} + {}^{24}\text{Ne}$ which is close to the experimental value (Bonetti *et al*. (1990)), and to the 1990 'fission' value. The prediction of the model ($\lambda_{SF} = 5 \times 10^{-24}$ s^{-1}) of the spontaneous fission decay rate was found to be in agreement with experiment (Bonetti *et al*. (2000)).

(2) To the decay of superdeformed bands (Herskind *et al*. (1988)). Although the superdeformed minimum lies, as a rule, above the normal deformed minimum for spins less than 50 $\hbar$, its population is not affected down to spin of about 24 $\hbar$, where the sudden transition out of the superdeformed band observed in experiment can be related to the onset of pairing caused by the disalignment of the lowest pair of high-j particles (see Section 6.5).

(3) To the restoration of parity conservation in octupole deformed nuclei (Barranco *et al*. (1988b,c)). The potential energy surface of a superfluid nucleus with an even multipole deformation has, as a rule, a single absolute minimum as a function of the deformation. For odd multipole deformations, there will be two minima with mirror image wavefunctions. This is a basic requirement of quantum mechanics as the physical states must be eigenstates of the parity operator. In an octupole deformed nucleus, this is achieved by a tunnelling of the system between the minima. This tunnelling is connected with the interaction between odd- and even-parity rotational bands. In the particular case of ^{222}Ra it is experimentally found that the excitation of the first negative parity state is at $\Delta E = 242$ keV above the positive 0^+ ground state. The model predicts a value of ΔE lying between 150 and 500 keV, depending on the potential energy

surface used. In fact, in this case, because the number of steps is small, the result is rather sensitive to the details of the calculation.

(4) To the calculation of the lifetime of high K-isomer states in rotating nuclei (Bengtsson *et al.* (1989)), such as ^{182}Os. There is overwhelming experimental evidence which testifies to the fact that cold, deformed nuclei display axially symmetric quadrupole deformations. Therefore the projection of the angular momentum on the body-fixed symmetry axis is a conserved quantity, and its value K is a good quantum number (Bohr and Mottelson (1975)). In keeping with this fact, excited states with high K-values are often isomeric, decaying only by virtue of small admixtures of lower-K components. A consequence of the K-selection rule is that the decay from the high K-states takes place preferentially stepwise, and degrees of K-forbiddeness vary from 5 to 100 for each step $\Delta K = 1$. The decay of an isometric state with $I^{\pi} = 25^{+}$ has been observed in ^{182}Os, directly populating the state of the yrast band ($K = 0$), with a hindrance factor of 10^{-8}. One single transition thus changes K dramatically, and with an isomeric lifetime that is relatively short.

Interpreting the isomer as a rotation around the symmetry axis, i.e. where all the angular momentum is contributed by the particles (see Fig. 6.1 (right)), one has to deal with a tunnelling in the gamma degree of freedom (Bohr and Mottelson (1975)). Estimates making use of the superfluid tunnelling model lead to a hindrance factor of the order of 10^{-6}–10^{-9}, where the uncertainty is connected with poor knowledge of the potential around the K-isomer minimum.

(5) To the calculation of the deformation and of the energy of coexistence states (four-particle–four-hole excitations) in ^{16}O and ^{40}Ca (Bertsch (1980)). The evolution of the system from one local minimum to the next implies a change in the deformation such that the energy associated with the lowest 2p–2h excitation becomes zero. That is, a deformation leading to a crossing between the lowest empty and the lowest occupied single-particle state. In the case where the deformation has quadrupole multipolarity, and is axially symmetric, the relation between the number of level crossings n_2 and the deformation β_2 in a nucleus of mass number A is given by $\beta_2 = 2(12\pi/5)^{1/2} n_2/A$ (see equation (7.35)). Because each level is twofold degenerate, to produce a 4p–4h excitation one needs a deformation corresponding to $n_2 = 2$. This implies $\beta_2 = 0.7$ for ^{16}O and $\beta_2 = 0.3$ for ^{40}Ca, compared with the values of 0.84 and 0.27 deduced from the experimental evidence. A rough estimate of the energy can be obtained by calculating the change in surface tension associated with these deformations. Making use of the liquid drop model (see equation (7.32)), this change is $\Delta E = 1/2 C_2 \beta_2^2 \approx 2\beta_2^2 R_0^2 S$, where $R_0 = 1.2A^{1/3}$ fm is the nuclear radius, $S = 0.95\,\mathrm{MeV\,fm^{-2}}$ is the surface tension and the Coulomb correction to C_2 has been neglected. From this relation and the above deformation parameters one obtains 8 and 3 MeV respectively, compared with the experimental values of 6.1 and 3.4 MeV.

7.3 Low-lying surface vibrations

In most cases the lowest excited states of even–even nuclei have a quadrupole or octupole character (Bohr and Mottelson (1969, 1975)). Although these states carry a small fraction (5–10%) of the energy weighted sum rule (see Section 8.3.2), the associated transition probabilities are much larger than that of single-particle states. Furthermore, they are excited with large cross-section by projectiles which are absorbed at the nuclear surface. They are known as collective surface vibrations, and are intimately connected with the plastic behaviour of the atomic nucleus.

Consequently, we shall use, in the calculation of the frequencies of these modes, the same scheme used to discuss exotic decay in Section 7.1 (Broglia *et al.* (1994)). The two parameters entering the model are the restoring force C_L and the inertia D_L of the mode. Because we are dealing with the plastic behaviour of the system one can use the liquid drop model to calculate C_L. In fact, in a vibrational motion where the surface fluctuates with a frequency of the order of $10^{21}\ \mathrm{s}^{-1}$, the detailed motion of the nucleons associated with frequencies almost two orders of magnitude larger must be quite irrelevant. Consequently, the surface tension $S\ (\approx 0.95\ \mathrm{MeV\ fm}^{-2})$ is sufficient to characterize the deformation energy of the system, and the restoring force parameter can be written as (Bohr and Mottelson (1969, 1975)),

$$C_L = S(L-1)(L+2){R_0}^2 - \frac{3}{2\pi}\frac{L-1}{2L+1}\frac{e^2Z^2}{R_\mathrm{c}}\,. \tag{7.32}$$

The two radii in the expression are the nuclear and the Coulomb radii, $R_0 = 1.2A^{1/3}$ fm and $R_\mathrm{c} = 1.25A^{1/3}$ fm, respectively, A being the mass number. The quantity Z indicates the proton number of the system. In what follows we shall use the approximate relation $Z \approx A/2.4$ (see Section 3.5). In this way one obtains

$$\frac{C_L}{A^{2/3}} = \begin{cases} 5.4(1-0.003A)\,\mathrm{MeV} & (L=2), \\ 13.5(1-0.002A)\,\mathrm{MeV} & (L=3), \\ 38(1-0.0005A)\,\mathrm{MeV} & (L=5). \end{cases} \tag{7.33}$$

For the inertia we use

$$\frac{D_L}{\hbar^2} = -\frac{1}{2v}\left(\frac{\mathrm{d}n}{\mathrm{d}\beta_L}\right)^2, \tag{7.34}$$

where $v = -2.9\,\mathrm{MeV}$ and $\mathrm{d}n/\mathrm{d}\beta_L$ is the density of level crossings per unit deformation. In Section 7.1, where the phenomenon of exotic decay has been discussed, we have used a simplified version $\mathrm{d}n/\mathrm{d}\beta_L$ which, in that case is determined by the reduced mass number of the exotic decay products. In the present case we do not have any direct experimental input to calculate $\mathrm{d}n/\mathrm{d}\beta_L$, and have to work it out theoretically.

The quantity $\mathrm{d}n/\mathrm{d}\beta_L$ can be estimated quite accurately by realizing that the Fermi distribution in momentum space is spherical for each local minimum (Bertsch (1980, 1988)). Between crossings, the Fermi surface gets distorted. In fact, it elongates in correspondence to a spatial reduction of the nuclear radius and it retracts when the nuclear radius becomes larger. Each time the volume outside the original Fermi sphere contains two nucleons, it is possible to fill the depopulated momentum zones below the Fermi energy and restore spherical symmetry. This means that the system has moved from a local minimum to the nearest one, and that a pair of nucleons have changed orbital. Making use of such a model one obtains for $L \lesssim 5$ the approximate expression (Bertsch (1988))

$$\frac{\mathrm{d}n}{\mathrm{d}\beta_L} \approx \frac{1}{4}\sqrt{\frac{2L+1}{3\pi}}A. \tag{7.35}$$

We are now in a position to calculate the inertia of the modes

$$\frac{D_L}{\hbar^2} \approx (2L+1)10^{-3}A^2\,\mathrm{MeV}\,. \tag{7.36}$$

The basic frequencies associated with the low-lying collective vibrations $L = 2, 3, 4$ and 5 are thus

$$\hbar\omega_L = \sqrt{\frac{\hbar^2 C_L}{D_L}} \approx \sqrt{\frac{(L-1)(L+2)}{(2L+1)}}(1-0.001A)\frac{35}{A^{2/3}}\,\mathrm{MeV}\,. \tag{7.37}$$

In Figs. 7.3 and 7.4 we show the function given in equation (7.37) for $L = 2$ and $L = 3$ in comparison with the experimental findings. Although large fluctuations

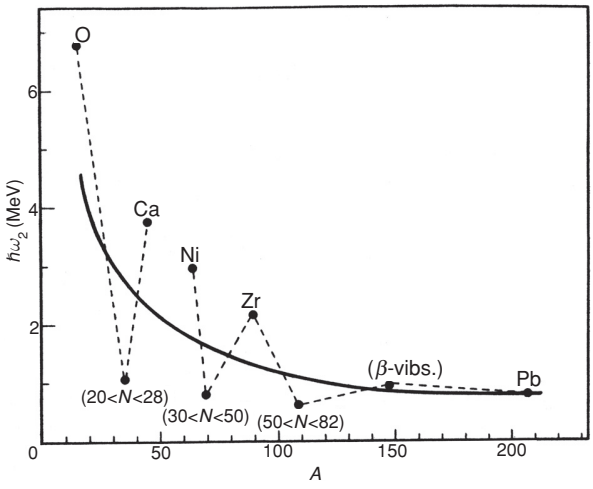

Figure 7.3. Average energy of the lowest 2^+ state in nuclei as a function of the mass number. The data are taken from Bohr and Mottelson (1969), Table 2.17 p. 196. The dashed line is to guide the eye. The continuous curve was calculated making use of equation (7.37) setting $L = 2$.

https://doi.org/10.1017/9781009401920 Published online by Cambridge University Press

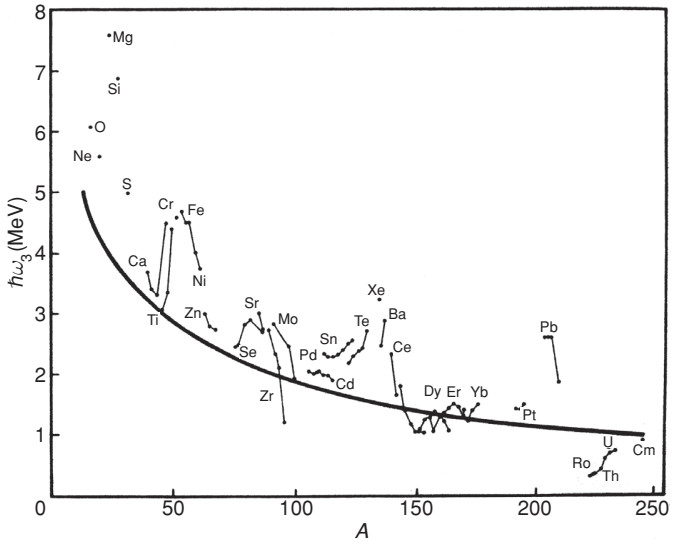

Figure 7.4. The same as in Fig. 7.3, but for $L = 3$. The data are taken from Bohr and Mottelson (1975) Fig. 6.40 p. 560.

about the theoretical value are observed, because shell effects greatly affect pairing correlations in nuclei (see also Chapter 10, Figs. 10.6–10.8), the result given in equation (7.37) provides an overall account of the experimental findings.

The amplitude of the zero-point motion associated with these modes is given by

$$\frac{\beta_L}{\sqrt{2L+1}} = \sqrt{\frac{\hbar\omega_L}{2C_L}} = \frac{3.6A^{-2/3}}{\left[(L-1)(L+2)(2L+1)\right]^{1/4}}. \tag{7.38}$$

From the above equation and from equation (7.35) one can estimate that the number of crossings associated with the vibrational modes of energy given in equation (7.37) is

$$n \approx \left(\frac{(2L+1)^3}{(L-1)(L+2)}\right)^{\frac{1}{4}} 0.3A^{1/3} \approx 0.5A^{1/3}. \tag{7.39}$$

Making use of $A^{1/3} \approx 5$ for medium-heavy nuclei, one obtains $n \approx 3$, an estimate which provides a quantitative justification for the use of a large amplitude description for low-lying surface vibrations of atomic nuclei. A detailed account of the low-lying collective surface vibrations taking into account shell effects is provided by the quasiparticle random phase approximation (QRPA) (see equation (8.47)).

7.4 Fission in metal clusters

Metal clusters have been investigated systematically during the past years. They are aggregates of metallic atoms, displaying clear shell structure. In particular, microclusters of sodium atoms can be viewed as a system of delocalized electrons, moving in single-particle orbits. An approximation for the description of the clusters is provided by the jellium model where the positive charge of the ions is assumed to be uniformly distributed over the cluster volume. The motion of the electrons can be described by a single-particle potential, arising from the interplay between the attractive jellium background, the Hartree–Fock potential and the correlation energy calculated in the local density approximation (LDA). In particular the shell closures, which in the case of Na clusters start with the magic numbers 8, 20 and 40, are well reproduced (see de Heer and Knight (1988), Broglia *et al*. (2004)).

Based on this picture one can explore analogies between metal clusters and nuclei. One example is the fission of a metal cluster, called a Coulomb explosion. The reason for this name is that clusters with almost any number of electrons can be made to fission, by charging them positively (see Eckhardt (1984)). Local-spin-density molecular dynamics calculations (Saunders (1990), Barnett *et al*. (1991)) predict the asymmetric fission of small doubly charged sodium (Na) clusters to occur predominantly via $\mathrm{Na}_n^{+2} \rightarrow \mathrm{Na}_{n-3}^{+} + \mathrm{Na}_3^{+}$, for $4 \leq n \leq 12$. For n less than or equal to 6, no fission barrier is present, while fission of larger clusters involves a barrier. The largest barrier for the range of clusters investigated is in the case of the process

$$\mathrm{Na}_{10}^{+2} \rightarrow \mathrm{Na}_7^{+} + \mathrm{Na}_3^{+}, \tag{7.40}$$

and is associated with the closed shell produced by eight electrons. The mean lifetime τ calculated by Saunders (1990) is

$$\tau \approx 2 \times 10^{-12}\ \mathrm{s}. \tag{7.41}$$

The deformation of clusters involves the electronic and phononic response of the system characterized by the times 10^{-15} s (≈ 1 eV) and 10^{-13} s (≈ 10 meV). Both these times are shorter than τ implying that one can use the Born–Oppenheimer (adiabatic) approximation for the description of a Coulomb explosion. The path to fission is determined by electronic level crossings rather than the inertia of the atomic nuclei. The fission decay rate for Na_{10}^{+2} clusters is given by equation (7.22) with a preformation factor P, a knocking rate f and a barrier penetration T. However, in this particular case, it is easier to calculate the product PT than to calculate the factors separately. In other words $P(n = 3)$ (see below) provides a situation where the two clusters Na_7^{+} and Na_3^{+} are beyond the fission barrier, i.e. a quantity that also contains T.

Within the framework of the model discussed in the previous section one expects to find $n = 3$ level crossings in the process. From the potential energy surface displayed in Fig. 1 of Saunders (1990), and dividing the interval between the ground states and scission (≈20 Å) into three equal parts, one can calculate the restoring force in the harmonic approximation

$$\tfrac{1}{2}C\xi^2 = 0.1 \text{ eV} \quad \left(\xi = \tfrac{1}{3}\right), \tag{7.42}$$

leading to

$$C \approx 2 \text{ eV}. \tag{7.43}$$

The inertia of the motion is given by

$$\frac{D}{\hbar^2} = \frac{n^2}{2|v|} = \frac{4.5}{|v|}, \tag{7.44}$$

where v is the matrix element responsible for the jump of two electrons from an occupied to an empty orbital, measured in eV.

Using $\omega = \sqrt{C/D}$ the knocking rate is determined by

$$f = \frac{\omega}{2\pi} \approx 0.16\sqrt{|v|}10^{15}\,\text{s}^{-1}. \tag{7.45}$$

The formation probability of the outgoing cluster on the surface of the parent cluster is determined by the parameter α^2 (see equation (7.21)) which in the present case is given by

$$\alpha^2 = \sqrt{\frac{C}{2|v|}}n = \frac{3}{\sqrt{|v|}}, \tag{7.46}$$

so that

$$P \approx \frac{1}{|v|^{1/4}} \exp\left(-\frac{3}{\sqrt{|v|}}\right). \tag{7.47}$$

The lifetime is then given by (see the discussion after equation (7.41) above)

$$\tau = (fP)^{-1} = \frac{\exp\left(\frac{3}{\sqrt{|v|}}\right)}{|v|^{1/4}} \times 6 \times 10^{-15}\,\text{s}. \tag{7.48}$$

Setting this quantity equal to (7.41) one obtains $|v| \approx 0.3$ eV. Matrix elements of the order of 0.3 eV are typical for interaction among electrons. It is still an open question to what extent such matrix elements are related to pairing in clusters (Snider and Sorbello (1984), Mottelson (1992), Barranco *et al*. (1992), a subject which is closely related to that discussed in connection with equation (2.3) (see Satula *et al*. (1998)).

8

Sources of pairing in nuclei

In general the two-body pairing force is parametrized in terms of: (a) an interaction with constant matrix elements of magnitude $G \approx 25/A$ MeV, (b) a contact interaction of strength $\frac{294}{4\pi}$ MeV fm^2, (c) an effective two-body force (Gogny (1975), Skyrme (1959)) whose parameters were adjusted so as to reproduce nuclear observables.

Although these calculations have shed much light on the workings of pairing correlations in nuclei, they say little concerning the relative importance of the bare nucleon–nucleon interaction and of the many-body renormalization effects taking place in the atomic nucleus. To gain insight into this question one has to proceed in several steps, starting with the bare nucleon–nucleon interaction, adding the renormalization effects afterwards. It has to be remembered that the results are not expected to be a simple sum of the different contributions, as the problem is highly non-linear. Making use of an analogy one can think of a metal, and of the non-linear effects associated with the simultaneous treatment of the bare Coulomb interaction, the coupling of electrons to plasmons (screening) and the coupling of electrons to phonons (Cooper pair formation) (see, e.g. Broglia *et al*. (2004)).

In the following three chapters we shall show that the nuclear surface plays a central role in the pairing phenomenon. This is due to the renormalization effects arising from the coupling of nucleons to low-lying collective surface vibrations. The most important effects are: the dressing of particles leading to an effective mass, and the exchange of vibrations among nucleons, giving rise to an induced pairing interaction. By taking all these effects into account on equal footing with the bare nucleon–nucleon interaction a consistent picture of pairing in nuclei is obtained (see Section 10.4 and Chapter 11).

The present chapter is an introduction to the renormalization problem. The contribution of the bare nucleon–nucleon (NN) interaction to the pairing gap is discussed in Sections 8.1 and 8.2. Calculations with a local single-particle

https://doi.org/10.1017/9781009401920 Published online by Cambridge University Press

potential give a pairing gap in agreement with experiment, but non-local effects reduce this by a factor of 2 (see Figs. 8.6 and 8.9). This is because the effective k-mass $m_k \sim 0.7m$ increases the spacing of single-particle levels near the Fermi surface. The role of the non-local effects is analysed in Section 8.2 (see Appendices B and E and H, Section H.4) with the conclusion that coupling of single-particle motion to low-energy collective modes must lead to important renormalization effects. Section 8.3 contains an introduction to particle-vibration coupling (see Appendices D and H, Section H.4) and the microscopic description of both low-energy and high-energy (giant resonances) collective modes.

Chapter 9 is concerned with the dynamical shell model. Coupling of single-particle motion to surface vibrations gives a time-dependent component to the nucleon–nucleus interaction which manifests itself as an energy dependence in the shell model potential. This energy dependence can be incorporated in the ω-mass $m_\omega > m$ which modifies the effects of the k-mass, and also of the occupation factors (see Appendix E and Section H.4).

The remaining contribution of the particle-vibration coupling is included in an effective interaction due to the exchange of surface phonons. The renormalized interaction is studied in Chapter 10 for the case of nuclei lying along the stability valley and in Chapter 11 for halo (exotic) nuclei.

8.1 The bare nucleon–nucleon potential and the pairing interaction

While one does not know how to work out a reliable nucleon–nucleon interaction at the level of quarks and gluons, phenomenological nucleon–nucleon interactions exist which describe quite accurately the variety of phase shifts obtained from the analysis of scattering processes in isolated two-nucleon systems (e.g. np and pp systems) and arising from the exchange of mesons, the carriers of the strong interaction. In the present context we are interested in the $^{2S+1}L_J = {}^1S_0$ phase shift, observed in the s-wave channel in the scattering of two identical ($T = 1$) nucleons in a singlet spin state.

This phase shift, shown in Fig. 8.1, is large and positive (implying an attractive interaction) at low relative momenta (typical, in the case of the atomic nucleus, of the surface region). It decreases as the relative momenta increase becoming zero and eventually negative (repulsive interaction) at relative momenta typical of nuclear saturation density.

Conventional models of the NN interaction are based on non-relativistic protons and neutrons interacting via a two-body potential. Typical NN potentials contain a strong short-range repulsion, an intermediate-range attraction, and a long-range one-pion-exchange (OPE) part (see Fig. 8.2(a)). One knows that such an approach is a great simplification over reality. Nucleons are composite systems with a rich resonance structure, which can be attributed to constituent quarks interacting by gluon exchange. Ideally a model of the NN interaction

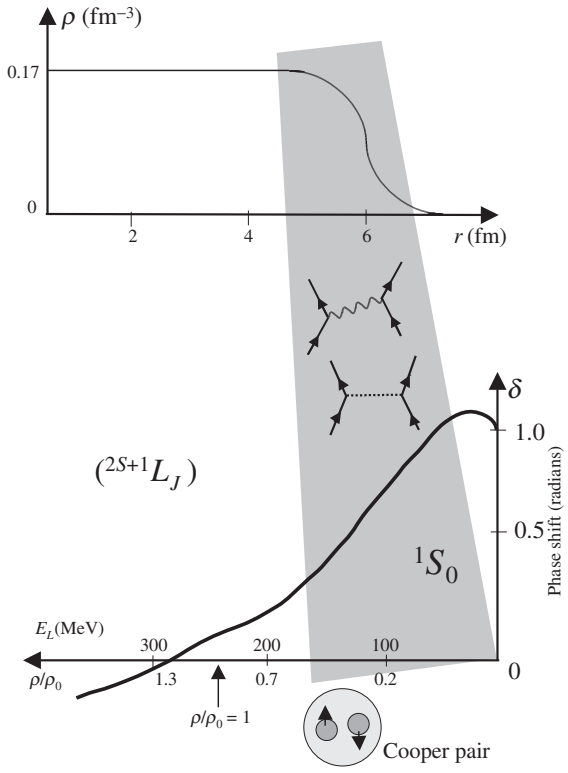

Figure 8.1. (Top) Schematic representation of the nuclear density ρ in units of fm^{-3} plotted as a function of the distance r (fm) from the centre of the nucleus. (Bottom) Phase shift δ associated with the elastic scattering of two nucleons moving in a singlet state of spin zero. Positive values of δ imply an attractive interaction, negative a repulsive one. For kinetic energies E_L associated with low relative velocities, i.e. around the nuclear surface where the density is low, the $^1S_0$ phase shift arising from the exchange of mesons (for example pions, represented by a horizontal dotted line in the scattering diagrams) between nucleons (represented by upward pointing arrowed lines) is attractive, and nucleons moving in time-reversal states form Cooper pairs which eventually condense leading to nuclear superfluidity. This effect is further accentuated because of the exchange of collective surface vibrations (wavy line in the scattering process) between the members of the Cooper pair.

would start with a field theoretical description of quark–quark interactions, but no satisfactory theory has yet been developed.

The Argonne v_{14} potential (Wiringa *et al.* (1984)) provides a convenient parametrization of the NN interaction to be used in nuclear structure calculations. It has the form

$$v_{14}(ij) = \sum_{p=1,14} [v_\pi^p(r_{ij}) + v_{\rm I}^p(r_{ij}) + v_{\rm s}^p(r_{ij})]O_{ij}^p, \tag{8.1}$$

https://doi.org/10.1017/9781009401920 Published online by Cambridge University Press

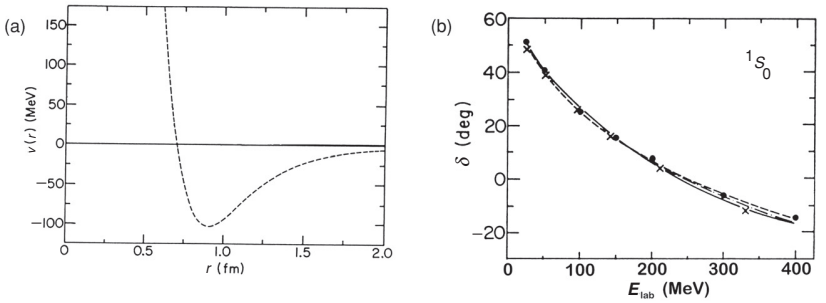

Figure 8.2. (a) $T = 1$, $S = 0$ central potential associated with the v_{14} NN interaction. (b) $T = 1$, $S = 0$ $^1S_0$ phase shifts: solid lines and dots are the energy-dependent and energy-independent phases of Arndt and Roper (1985). The dashed curve is the v_{14} model phase shift. Reprinted with permission from Wiringa *et al.*, *Phys. Rev.* **C29**: 1207–21 (1984) Copyright 1984 by the American Physical Society.

where

$$O_{i,j}^{p=1,14} = 1, \vec{\tau}_i \cdot \vec{\tau}_j, \vec{\sigma}_i \cdot \vec{\sigma}_j, (\vec{\sigma}_i \cdot \vec{\sigma}_j)(\vec{\tau}_i \cdot \vec{\tau}_j), S_{ij}, S_{ij}(\vec{\tau}_i \cdot \vec{\tau}_j), (\vec{L} \cdot \vec{S}), (\vec{L} \cdot \vec{S})(\vec{\tau}_i \cdot \vec{\tau}_j), \vec{L}^2, \vec{L}^2(\vec{\tau}_i \cdot \vec{\tau}_j), \vec{L}^2(\sigma_i \cdot \sigma_j), \vec{L}^2(\vec{\sigma}_i \cdot \vec{\sigma}_j)(\vec{\tau}_i \cdot \vec{\tau}_j), (\vec{L} \cdot \vec{S})^2, (\vec{L} \cdot \vec{S})^2(\vec{\tau}_i \cdot \vec{\tau}_j). \quad (8.2)$$

Here

$$S_{ij} = 3(\sigma_i \cdot \hat{r}_{ij})(\sigma_j \cdot \hat{r}_{ij}) - \vec{\sigma}_i \cdot \vec{\sigma}_j \quad (8.3)$$

is a tensor operator, $\vec{L}$ is the relative orbital angular momentum, and $\vec{S}$ is the total spin of the pair.

The first eight operators of equation (8.2) are the standard ones required to fit singlet and triplet S- and P-wave data. The 14 operators provide sufficient freedom to characterize the 14 singlet and triplet S, P, D and F states. The three radial components include the long-range OPE part v_π^p, and phenomenological intermediate-range and short-range parts $v_I^p(r)$, $v_s^p(r)$. As an example we show in Fig. 8.2(a) the $T = 1$, $S = 0$ central potential. The Argonne v_{14} $^1S_0$ phase shift fits for the experimental data (see Fig. 8.2(b)) are quite good with only one short-range functional form.

8.1.1 Calculation of the pairing properties of ^{120}Sn

Hartree–Fock–Bogoliubov-like calculations (Thouless (1961a,b), Ring and Schuck (1980)) of the pairing properties of the semi-magic nucleus $^{120}_{50}Sn_{70}$ have been carried out by Barranco *et al.* (1997), allowing the neutrons to move in the single-particle states of a Saxon–Woods potential (with parameters $V^0 = -55$ MeV, $r_0 = 1.2$ fm, $a = 0.65$ fm) and interacting through a v_{14}

https://doi.org/10.1017/9781009401920 Published online by Cambridge University Press

NN interaction. By solving the matrix equation

$$\begin{pmatrix} \varepsilon_i - \lambda & \Delta \\ \Delta & -(\varepsilon_i - \lambda) \end{pmatrix} \begin{pmatrix} U_i \\ V_i \end{pmatrix} = E_i \begin{pmatrix} U_i \\ V_i \end{pmatrix} \tag{8.4}$$

self-consistently with the constraint

$$N = 2 \sum_{a_1 > 0} {V_i}^2, \tag{8.5}$$

which fixes the average number of particles of the system and the Fermi energy λ, one obtains the quasiparticle energies E_i and occupation amplitudes V_i and U_i. The state-dependent pairing gap

$$\Delta_{a_1 a_2} = -\frac{1}{2} \sum_{b_1 b_2} \sum_i U^i_{b_1} V^i_{b_2} \langle a_1 \tilde{a}_2 | v_{14} | b_1 \tilde{b}_2 \rangle, \tag{8.6}$$

with $a_1 \equiv (n_1(l_1 1/2) j_1, m_1)$, where n_1, l_1, j_1 and m_1 are the number of modes, the orbital, the total angular momentum and its projection respectively of the state $|a_1\rangle$, depends on the matrix elements between two-particle states with the same or different number of nodes. The state $|\tilde{a}_2\rangle$ is obtained from the state $|a_2\rangle$ by the operation of time reversal.

As seen from the expression for the quasiparticle energy

$$E_{a_1} = \sqrt{(\varepsilon_{a_1} - \lambda)^2 + \Delta^2_{a_1 a_1}},$$

the quantity $\Delta_{a_1 a_2}$ is an energy gap in the spectrum of quasiparticles in the case of a continuous spectrum. For a discrete spectrum, it is meaningful to speak of a gap only for values of $\Delta_{a_1 a_2}$ which are greater than the distances between the single-particle energies ε_{a_1}.

Equations (8.4) and (8.5) always have a trivial solution, namely $\Delta_{a_1 a_2} = 0$ and $U_{a_1} = 1$, $V_{a_1} = 0$ for $\varepsilon_{a_1} > \lambda$ and $U_{a_1} = 0$, $V_{a_1} = 1$ for $\varepsilon_{a_1} < \lambda$. However, if the inequality

$$-\frac{1}{2} \sum_{b_1 b_2} \frac{\langle a_1 \tilde{a}_2 | v_{14} | b_1 \tilde{b}_2 \rangle}{\sqrt{|\varepsilon_{b_1} - \lambda||\varepsilon_{b_2} - \lambda|}} > 1 \tag{8.7}$$

is fulfilled, then there is also a non-trivial ($\Delta_{a_1 a_1} \neq 0$) solution of equations (8.4) and (8.5). This is possible only if the pairing component of the NN potential has a coherent character for sufficiently many states. In other words, the matrix elements $\langle a_1 \tilde{a}_2 | v_{14} | b_1 \tilde{b}_2 \rangle$ must have the same sign for a sufficiently broad region of states. If this is not the case cancellations will occur and coherence will be lost (Belyaev (1959)).

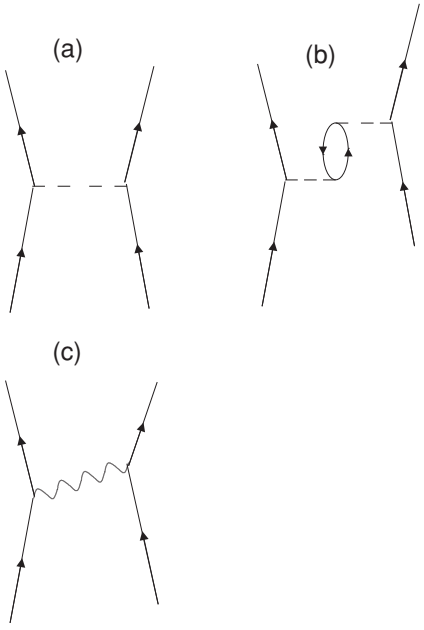

Figure 8.3. (a) NN scattering process through a bare interaction (horizontal dashed line; nucleons are drawn as arrowed lines). (b) Renormalization of the bare NN interaction due to core polarization (single particle–hole excitation, bubble). (c) NN interaction arising from the exchange of a collective vibration (resulting from bubble process summed to all orders (RPA), see Section 8.3).

Expanding the two-body interaction potential in spherical harmonics (see Fig. 8.3)

$$v_{14}(|\vec{r}_1 - \vec{r}_2|) = \sum_L v^L(r_1, r_2) P_L(\cos\theta_{12}),$$

helps to understand which parts of the NN interaction contribute to a coherent pairing interaction (see also Section 2.2). The spherically symmetric or monopole part of the interparticle interaction contributes to the self-consistent field. The single-particle levels in this field are degenerate and characterized by the value of the angular momentum j. Let us consider the particles in the same level j and neglect the interaction with the particles in other shells. The low-multipolarities ($L \lesssim 3$–5) are not expected to contribute to the pairing interaction in any substantial way, because they connect the levels with similar magnetic quantum numbers $|m_{a_1} - m_{b_1}| \leq L \approx 3$–5 and do not contribute in a significant way to the inequality equation (8.7). Therefore, the main contribution to the pairing interaction associated with the bare interaction comes from the high harmonics of the NN potential. This is the standard argument made in connection with pairing in nuclei (see e.g. Belyaev (1959), Mottelson (1962, 1996)).

https://doi.org/10.1017/9781009401920 Published online by Cambridge University Press

On the other hand, low multipolarities give essential contributions to the mean field. In particular $L = 2$, 3 and 4 can lead to spheroidal, octupole and hexadecapole static or dynamic (surface vibration) distortions. The low multipole components of the bare NN interaction give a small contribution to the pairing force, but the renormalization effects arising from core excitation (polarization) processes (Fig. 8.3(b)) are expected to be important (Bohr and Mottelson (1975), Section 6-5f). This is because such processes receive coherent contributions from all orders of perturbation (many-bubble processes), leading to collective surface vibrations of low energy which couple strongly to the nucleons (see Fig. 8.3(c)).

To obtain convergence of the solutions to equations (8.4) and (8.6), jumps of pairs of nucleons to single-particle orbitals lying as high as 600 MeV from ε_{F} have to be included in the calculations. For this purpose the continuum is discretized by placing the nucleus in a box. The size of the box is to be changed until convergence of the results is obtained. In the case of ^{120}Sn this is achieved for $R_{\mathrm{box}} \geq 12$ fm.

The large value of the energy associated with the two-particle scattering processes contributing to $\Delta_{a_1 a_2}$ is essentially due to the strong repulsion of the $T = 1$, $S = 0$ central potential (see Fig. 8.2) and not to the fact that the most important contribution to Cooper pair formation is connected with the high multipoles of the residual interactions, as discussed in connection with the condition given in equation (8.7). In fact, as seen from the single-particle valence spectrum of ^{120}Sn (see Fig. 8.4), levels with total spin as high as 11/2 and 9/2 are already present in this subspace, thus allowing the particles to profit from the v_{14} pairing correlations within this restricted subspace. This fact can be better appreciated from Fig. 8.5 where typical examples of the pairing matrix elements $\langle (a_1 a_2)_0 | v_{14} | (b_1 b_2)_0 \rangle$ are shown as a function of the energy associated with the (NN) scattering process. The negative (attractive) matrix elements are all concentrated at low energies (<20 MeV), associated essentially with scattering processes among valence single-particle orbits.

In Fig. 8.6 we show the diagonal part of the neutron pairing gap Δ_{a_k} ($\equiv \Delta_{a_k a_k}$) associated with the single-particle states of the system (Barranco *et al.* (1997)). The results have been averaged over an energy interval of ≈ 1 MeV to smooth out fluctuations associated with particular shells. The value of the pairing gap at the Fermi energy is $2.2^{+0.4}_{-0.8}$ MeV, the 'errors' reflecting the conspicuous state dependence of Δ. This value is of the same order of magnitude as that extracted from the odd–even mass difference, namely 1.4 MeV. One would then be tempted to conclude that the bare NN potential explains, even quantitatively, the values of the odd–even mass difference observed experimentally, and thus pairing superfluidity in nuclei. As we shall show below, this conclusion is not correct.

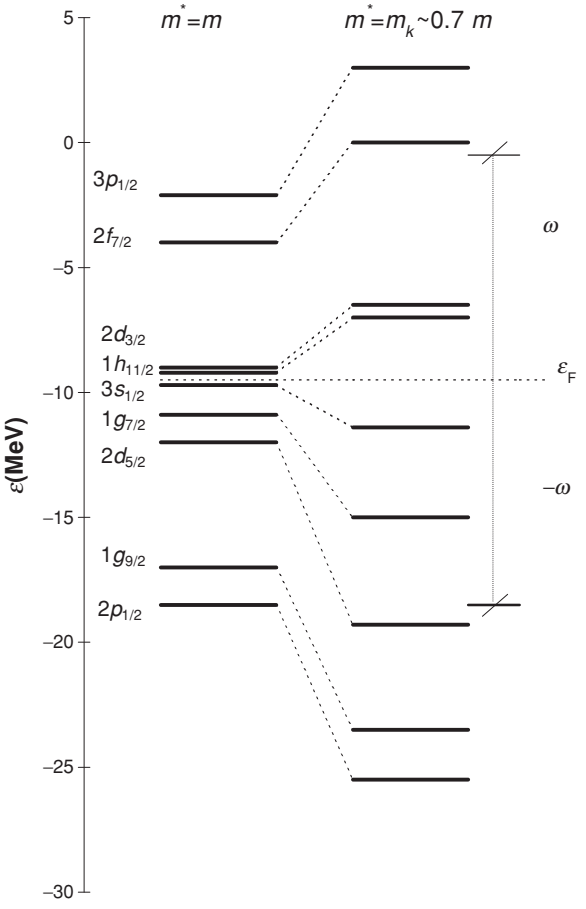

Figure 8.4. Valence single-particle levels used in the calculation of the pairing parameters of ^{120}Sn, determined using a Saxon–Woods potential with parameters given in equations (8.13)–(8.16) ($V = V^0 = -55$ MeV), and two effective k-masses (see equations (8.19) and (8.20)). The value of the Fermi energy $\varepsilon_F(\equiv \lambda)$ was obtained by solving the BCS number and gap equations with $N = 70$. Also indicated is the energy interval $\pm\omega$ around the Fermi energy over which the density of levels $N(0)$ is calculated (see the discussion following equation (8.20)).

8.2 Mean-field theory

Both in previous chapters as well as in solving the matrix eigenvalue relation given in equation (8.4), the assumption has been made that nucleons move in a local single-particle potential. This is, however, not correct. The equations which have to be solved to determine the single-particle energies and the occupation amplitudes consistently, are the integro-differential Hartree–Fock–Bogoliubov

https://doi.org/10.1017/9781009401920 Published online by Cambridge University Press

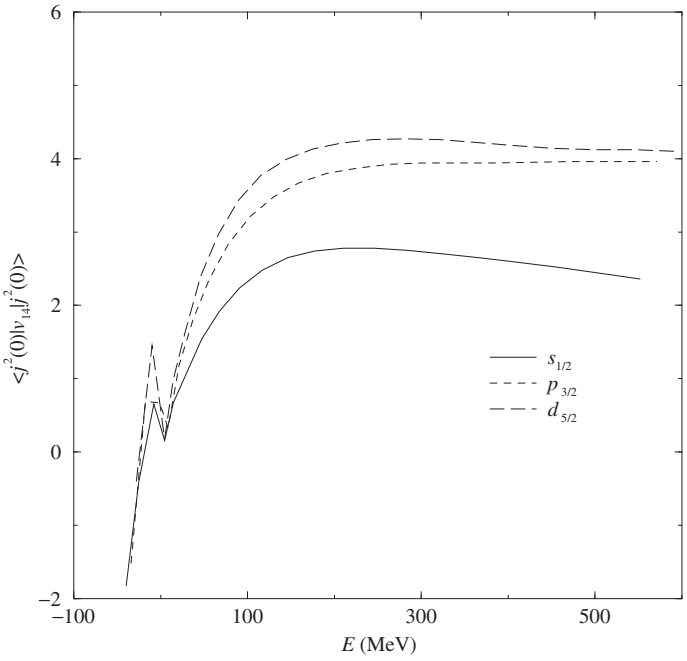

Figure 8.5. Diagonal matrix elements $\langle (n_1 l_1 j_1, n_2 l_1 j_1) 0^+ | v_{14} | (n_1 l_1 j_1, n_2 l_1 j_1) 0^+ \rangle$ of the v_{14} NN potential associated with $s^2(0)$, $p^2(0)$ and $d^2(0)$ configurations of ^{120}Sn, as a function of the energy involved in the scattering process. The negative values are associated with states involving low relative momentum and thus feeling mainly relative distances $r \gtrsim 0.8$ fm. Those associated with positive values are associated with states involving high relative momenta and thus probing the repulsive core (see Fig. 8.2(a)) (This figure is due to F. Barranco and E. Vigezzi).

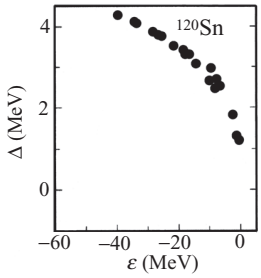

Figure 8.6. The state-dependent diagonal pairing gap of ^{120}Sn calculated making use of equations (8.4) and (8.5) and of the v_{14} matrix elements of the type shown in Fig. 8.5. The relation given in equation (8.5) for $N = 70$ fixes the Fermi energy at $\varepsilon_F = -7.2$ MeV.

https://doi.org/10.1017/9781009401920 Published online by Cambridge University Press

equations, containing both a local (Hartree) and a non-local (Fock) potential. In other words, equation (8.4) has to be supplemented so as to be able to calculate self-consistently the single-particle energies ε_i. In the following we derive the corresponding equations.

Mean-field theory is a very useful approximation in the study of the many-particle system. In the mean-field method one replaces the many-particle Schrödinger equation,

$$\left(-\sum_{i=1}^{A}\frac{\hbar^2}{2m}\nabla_i^2+\sum_{i<j=1}^{A}v(|\vec{r}_i-\vec{r}_j|)\right)\Psi_n(\vec{r}_1\ldots\vec{r}_A)=E_n\Psi_n(\vec{r}_1\ldots\vec{r}_A), \quad (8.8)$$

by a single-particle Schrödinger equation,

$$\left(-\frac{\hbar^2}{2m}\nabla^2+U(r)\right)\varphi_{\nu_j}(\vec{r})+\int \mathrm{d}^3\vec{r}\,' U_x(\vec{r},\vec{r}\,')\varphi_{\nu_j}(\vec{r}\,')=\varepsilon_{\nu_j}\varphi_{\nu_j}(\vec{r}) \quad (8.9)$$

and the total wavefunction $\Psi_n(\vec{r}_1\ldots\vec{r}_A)$ by the normalized determinant constructed out of the single-particle wavefunctions $\varphi_i(\vec{r})$.

The two potentials appearing in equation (8.9) are the Hartree (direct) potential,

$$U(\vec{r})=\int \mathrm{d}^3\vec{r}\,'\varrho(\vec{r}\,')v(|\vec{r}-\vec{r}\,'|), \quad (8.10)$$

where

$$\varrho(\vec{r})=\sum_{\nu_i\le\nu_\mathrm{F}}|\varphi_{\nu_i}(\vec{r})|^2$$

is the total density of the system, and the Fock (exchange) potential

$$U_x(\vec{r},\vec{r}\,')=-\sum_{\nu_i\le\nu_\mathrm{F}}\varphi^*_{\nu_i}(\vec{r}\,')v(|\vec{r}-\vec{r}\,'|)\varphi_{\nu_i}(\vec{r}). \quad (8.11)$$

This last term is directly connected with the fact that nucleons are fermions and thus satisfy the Pauli principle. In particular, the exchange potential ensures that nucleons do not interact with themselves (see Appendix A).

The total energy of the system in the Hartree–Fock ground state $|0\rangle_\mathrm{HF}=\frac{1}{\sqrt{A!}}\det(\varphi_{\nu_1}(\vec{r}_1)\ldots\varphi_{\nu_A}(\vec{r}_A))$ is given by

$$\begin{aligned}E={}_\mathrm{HF}\langle 0|H|0\rangle_\mathrm{HF}&=\sum_{\nu_i\le\nu_\mathrm{F}}\langle\nu_i|T|\nu_i\rangle+\frac{1}{2}\sum_{\nu_i,\nu_{i'}\le\nu_\mathrm{F}}\langle\nu_i\nu_{i'}|v|\nu_i\nu_{i'}\rangle_a\\&=\sum_{\nu_i\le\nu_\mathrm{F}}\varepsilon_i-\frac{1}{2}\sum_{\nu_i,\nu_{i'}\le\nu_\mathrm{F}}\langle\nu_i\nu_{i'}|v|\nu_i\nu_{i'}\rangle_a, \quad (8.12)\end{aligned}$$

where ν_F labels the Fermi level lying, by definition (zero temperature situation), halfway between the last occupied and the first unoccupied orbitals. In writing

https://doi.org/10.1017/9781009401920 Published online by Cambridge University Press

up the last term of the above equation the self-consistency relation

$$\langle \nu_2|T|\nu_1\rangle + \sum_{\nu_i \le \nu_F} \langle \nu_i \nu_2|v|\nu_i \nu_1\rangle_a = \langle \nu_2|T + U + U_x|\nu_1\rangle = \varepsilon_{\nu_1}\delta(\nu_1, \nu_2),$$

i.e. the matrix expression of equation (8.9), has been used. Note that the subindex a in the matrix element indicates the antisymmetrized matrix element, i.e. $\langle \nu_i \nu_k|v|\nu_i \nu_k\rangle_a = \langle \nu_i \nu_k|v|\nu_i \nu_k\rangle - \langle \nu_i \nu_k|v|\nu_k \nu_i\rangle$, and thus gives rise to both the direct and exchange potentials (see equation (A.16)). The factor $\frac{1}{2}$ in the last term of equation (8.12) reflects the fact that the two-particle interaction contributes to the average potential for both of the interacting particles and is thus counted twice, if one sums the single-particle energies for the filled orbitals (see equation (3.50)).

8.2.1 Effective mass (k-mass)

There is extensive experimental evidence showing that single-particle motion in nuclei is well described by a potential of Saxon–Woods type,

$$U(r, E) = V_0(E) f(r), \tag{8.13}$$

where

$$f(r) = \frac{1}{1 + \exp(\frac{r - R_0}{a})}, \tag{8.14}$$

to which a spin-orbit potential, proportional to $\frac{\partial f(r)}{\partial r}$, is added (see Bohr and Mottelson (1969)). The radius and the diffuseness parameters have the values

$$R = r_0 A^{\frac{1}{3}} \text{ fm}, \quad r_0 = 1.2 \text{ fm}, \quad a = 0.65 \text{ fm}, \tag{8.15}$$

and, for levels around the Fermi energy (valence orbitals), the strength $V_0(E)$ is a constant. On the other hand, the differential elastic scattering cross-section and the total nucleon–nucleus cross-section can be accurately described by

$$V = V_0(E) = V^0 + V_1 \frac{N - Z}{A} + \gamma E, \tag{8.16}$$

with $V^0 = -55$ MeV, $\gamma = 0.3{-}0.4$ and $V_1 \approx 30$ MeV, provided that one adds to the potential given in equation (8.13) an imaginary component (see Appendix B). The same parametrization describes the deeply bound states as shown in Fig. 8.7.

The relation given in equation (8.16) is valid for $|E| > 10$ MeV, where the single-particle energy E ($= \varepsilon - \varepsilon_F$) is measured from the Fermi energy. The valence orbitals ($|E| \le 5$ MeV) of nuclei around closed shells are well reproduced by the Saxon–Woods potential defined by equations (8.13)–(8.15) but in this case with $V \approx -55$ MeV, independent of energy.

https://doi.org/10.1017/9781009401920 Published online by Cambridge University Press

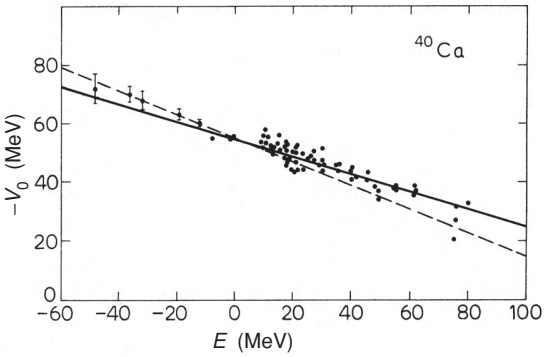

Figure 8.7. Dependence upon proton-bombarding energy of the depth V_0 of the potential well (defined in equation (8.13)) which reproduces the ^{40}Ca(p, p) differential cross-section for $E > 10$ MeV, and the experimental single-proton energies for $E < 0$ MeV. The full straight line corresponds (in MeV) to $V = V_0(E) = -55 + 0.3E$, and the dashed straight line to $V = V_0(E) = -55 + 0.4E$ (adapted from Bauer *et al.* (1982)).

The Schrödinger equation (8.9) can, for many purposes, be rewritten to a good approximation as (Mahaux *et al.* (1985))

$$\left(-\frac{\hbar^2}{2m_k}\nabla^2 + \tilde{U}(r)\right)\varphi_j(\vec{r}) = \varepsilon_j\varphi_j(\vec{r})\,, \tag{8.17}$$

where the k-effective mass m_k, which takes into account many of the effects associated with the non-local Hartree–Fock potential, has been introduced, and where the depth of the potential $\tilde{U}(r)$ is

$$\tilde{V}^0 = \frac{m}{m_k}V^0. \tag{8.18}$$

As shown in Appendix B (note that m_k may depend on r),

$$m_k = m\left(1 + \frac{m}{\hbar^2 k}\frac{\partial V(k)}{\partial k}\right)^{-1}, \tag{8.19}$$

where $V(k)$ is the Fourier transform of the Fock potential given in equation (8.11).

In Hartree–Fock theory, contributing to the energy dependence of the single-particle potential are the non-locality of $U_x(\vec{r}, \vec{r'})$, equivalent to a dependence on the linear momentum of the particle, and, in many cases, the genuine velocity-dependence of the two-body interaction. Equation (8.19) with the parametrization given in equation (8.16) leads to an effective mass $m^* = m_k$, known as the k-mass, which is considerably smaller than the bare nuclear mass. In fact,

$$m_k \approx 0.6m \rightarrow 0.7m. \tag{8.20}$$

Consequently, Hartree–Fock theory is able to accurately predict the sequence of the single-particle levels around the Fermi energy (i.e. $|E| \leq 10$ MeV), but not its

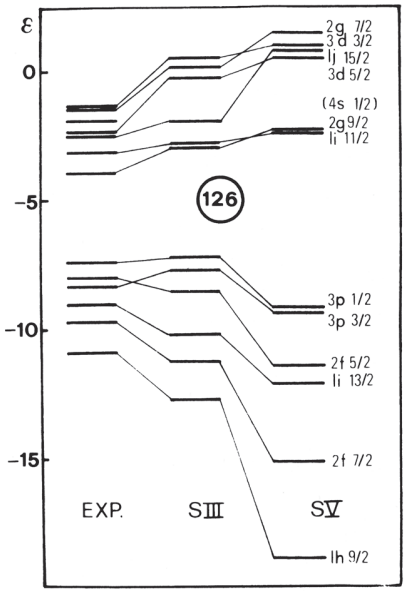

Figure 8.8. Comparison between the experimental single-neutron energies in the valence shells of ^{208}Pb and the values calculated in the Hartree–Fock approximation with a Skyrme III (SIII, middle) and a Skyrme V (SV, right) interaction (taken from Quentin and Flocard (1978)).

density. This is exemplified in Fig. 8.8 (see also Fig. 8.4), where the experimental values of the single-particle neutron energies of the valence orbitals of ^{208}Pb are compared with Hartree–Fock results calculated by making use of a particular parametrization of the effective two-body interaction (all displaying an effective k-mass smaller than the bare mass).

Making use of the k-mass given in equation (8.20) to calculate the single-particle energies appearing in equations (8.4), i.e. the solution of equation (8.17) with $m_k \approx 0.7m$ and with $\tilde{U}(r) = \tilde{V}^0 f(r)$, one obtains $\Delta_{a_1} \approx 0.5\,\text{MeV}$ (Barranco *et al*. (2004); see Fig. 8.9). This result, compared with the result shown in Fig. 8.6, can be understood by studying the dependence of the gap on the density of levels. For this purpose we make use of the results of the single j-shell. In this case the pairing gap has a simple expression in term of the pairing coupling constant G, the number of particles N and the pair dependency $\Omega = (2j+1)/2$. For a half-filled shell ($N = \Omega$) (see Appendix H)

$$\Delta = \frac{1}{2} G\Omega \approx \frac{G}{2} N(0)\omega, \tag{8.21}$$

where $N(0) = 2\Omega/2\omega$ is the density of levels at the Fermi energy, and where 2ω is the range of energy around the Fermi energy where pairs of particles

https://doi.org/10.1017/9781009401920 Published online by Cambridge University Press

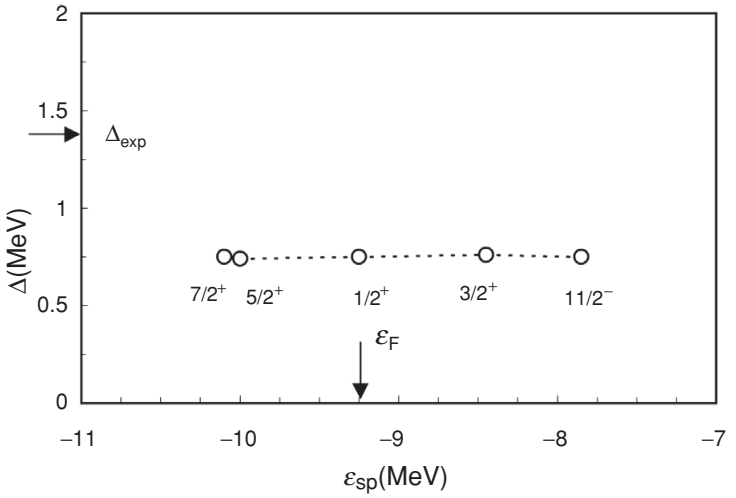

Figure 8.9. The state-dependent pairing gap of ^{120}Sn for the levels close to the Fermi energy obtained using BCS theory with the v_{14} Argonne potential (after Barranco *et al.* (2004)).

coupled to angular momentum zero are allowed to correlate through the pairing interaction. In the case under discussion and making use of a typical value of $\omega = 8\,\text{MeV}$ (see Fig. 8.4), the density of levels (for one spin orientation) changes from $N(0) = 3.4\,\text{MeV}^{-1}$ ($m^* = m$) to $N(0) = 1.6\,\text{MeV}^{-1}$ ($m^* = m_k = 0.7m$) (see (3.61) and (3.62)). Thus, the simple relation given in equation (8.21) predicts a decrease of a factor of 2 in the pairing gap. Among the limitations of Hartree–Fock theory to describe the nuclear structure one can mention: low density of levels, unrealistic occupation factors with values of either 1 or 0, single-particle states with infinite lifetimes (neglecting electromagnetic decay). These limitations are connected with the fact that HF is a static approximation to the many-body problem. That is, an approximation where fluctuations of the different (order) parameters characterizing the mean field are neglected (see e.g. equation (4.8) and subsequent discussion).

The presence of a mean field defines a surface which can vibrate. The vibrations renormalize (by coupling to the nucleons) their properties, giving rise to an effective mass (so-called ω-mass m_ω), to occupation factors $Z_\omega = (m/m_\omega)$ as well as to a splitting of the single-particle strength. The corresponding energy spread Γ_ω determines the lifetime $(\hbar/\Gamma_\omega)$ of the single-particle levels. These phenomena affect pairing correlations in an important, and sometimes opposite way. In particular, particles which have to carry a phonon for part of the time become effectively heavier than free particles. This leads to levels which are closer to the Fermi energy, and to an increase of the level density over that of HF theory (see Chapter 9 and Appendix B). The increase of the level density leads to an increase of the pairing gap. On the other hand, the fact that nucleons are

for part of the time in configurations containing a phonon means that the bare nucleon–nucleon interaction is less effective, leading to a decrease of the pairing correlations. This decrease is accentuated due to the fact that single-particle levels acquire an effective width due to the coupling to phonons (see equation (9.41)).

A phonon need not be reabsorbed by the same nucleon which has virtually excited it, but can be exchanged between pairs of nucleons. If these two nucleons move in time-reversal states, this exchange leads to an effective pairing interaction and thus to an increase of the pairing gap, because the degrees of freedom of the nucleons and of the collective vibrations overlap to some extent and one has to eliminate processes which are due to overcompleteness of the basis (see e.g. Appendix F).

Summing up, the interweaving of particles and vibrations affects pairing correlations in nuclei in a subtle way. This subject is discussed in Chapters 10 and 11.

In what follows we develop the tools to carry out this discussion. That is, we work out the particle-vibration coupling Hamiltonian. The general rules needed to calculate the variety of processes arising from the interweaving of nucleons and vibrations are discussed in Chapter 9 and Appendix D.

8.3 Random phase approximation

In solving the Hartree–Fock equations one has to specify the shape of the nucleus. The absolute minimum of the energy of a closed-shell system is associated with a spherical configuration. For nuclei with a number of nucleons outside the closed shell, or a number of holes in the closed shell, the absolute minimum may correspond to a deformed configuration. In either case there can be vibrations about the equilibrium shape which couple to the single-particle motion. The present section introduces the theory of particle-vibration coupling when the mean field is spherical. This leads to a microscopic description of the low-energy surface vibrations in the random phase approximation. The approach in this section is based on the one developed by Bohr and Mottelson (1975).

There is a simple parametrization of the nuclear radius which can account for the variety of situations. It is given by

$$R = R_0 \left(1 + \sum_{\lambda\mu} \alpha_{\lambda\mu} Y^*_{\lambda\mu}(\hat{r}) \right), \tag{8.22}$$

with the multipolarity $\lambda \geq 2$ and where $\alpha_{\lambda\mu}$ are deformation parameters while $Y_{\lambda\mu}$ are spherical harmonics. An adequate parametrization of the potential is still provided by equation (8.14), but with R_0 replaced by R. In the case of axially symmetric quadrupole deformations, the only deformation parameter different from zero is α_{20}. The Nilsson model used to describe the single-particle motion

https://doi.org/10.1017/9781009401920 Published online by Cambridge University Press

in quadrupole deformed nuclei is closely related to this potential (see Nilsson (1955) and Nilsson and Ragnarsson (1995)).

Let us now expand the single-particle potential to first order in the deformation parameters ($\alpha^2 \ll \alpha$). One obtains

$$U(r, R) = U(r, R_0) + \delta U(r), \tag{8.23}$$

where

$$\delta U(r) = -R_0 \frac{\partial U}{\partial r} \sum_{\lambda\mu} \alpha_{\lambda\mu} Y^*_{\lambda\mu}(\hat{r}). \tag{8.24}$$

It is well established that the nuclear surface can vibrate in certain normal modes. In this case the quantities $\alpha_{\lambda\mu}$ can be viewed as the coordinates of the harmonic oscillator Hamiltonian associated with the normal modes, i.e.

$$H_\alpha = \frac{\hat{\Pi}^2_\alpha}{2D_\alpha} + \frac{C_\alpha}{2}\hat{\alpha}^2, \tag{8.25}$$

where

$$\hat{\alpha} = \sqrt{\frac{\hbar\omega_\alpha}{2C_\alpha}}(\hat{\Gamma}^\dagger_\alpha + \Gamma_\alpha), \tag{8.26}$$

and $\hat{\Pi}_\alpha$ is the momentum variable conjugate to $\hat{\alpha}$. The quantities $\Gamma^\dagger_\alpha$ and Γ_α are boson creation and annihilation operators (Dirac (1935)) of the vibrational modes. Here $\omega_\alpha = \sqrt{C_\alpha/D_\alpha}$ and the quantity $\sqrt{\hbar\omega_\alpha/2C_\alpha}$ is the amplitude of the zero-point fluctuations in the ground state (the boson vacuum state $|0\rangle_{\rm B}$). The one-phonon state is

$$|\alpha\rangle = \Gamma^\dagger_\alpha |0\rangle_{\rm B}, \tag{8.27}$$

(see Appendix A). Consequently, the term δU leads to a coupling between the single-particle motion described in terms of the coordinate $\vec{r}$, and the collective vibrations, described in terms of the collective coordinates $\hat{\alpha}$, which we write as

$$\delta U = -\kappa \hat{\alpha} \hat{F}, \tag{8.28}$$

where κ is a coupling strength,

$$\hat{F} = \sum_{\nu_1\nu_2} \langle \nu_1 | F | \nu_2 \rangle a^\dagger_{\nu_1} a_{\nu_2}, \tag{8.29}$$

and $a^\dagger_{\nu_1}$ and a_{ν_2} are creation and annihilation operators of single-particle states. The dimensionless quantity

$$F = \frac{R_0}{\kappa}\frac{\partial U}{\partial r} Y^*_{\lambda\mu}(\hat{r}) \tag{8.30}$$

https://doi.org/10.1017/9781009401920 Published online by Cambridge University Press

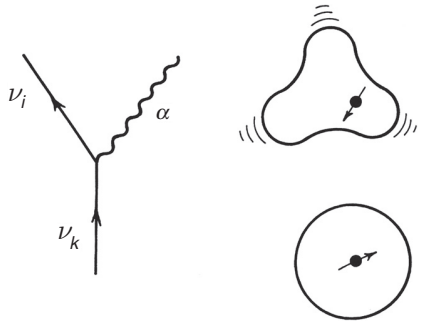

Figure 8.10. Graphical representation of the process by which a fermion, bouncing inelastically off the surface, sets it into vibration. Particles are represented by an arrowed line, while the vibration is shown by a wavy line. The black dot represents a nucleon moving in a spherical mean field of which it excites an octupole vibration after bouncing inelastically off the surface.

is a single-particle field peaked at the nuclear surface. In a normal self-sustained mode, there should be a consistency between variations of the density and of the potential. This is a generalization of the self-consistent condition existing between potential and density in the static case (see equation (8.10)) As we shall see in Sections 8.3.1 and 8.3.3, the quantity κ is the proportionality constant between these two variations.

Here we are treating angular momentum in a very cavalier way. This is done in order to be able to discuss the main physical consequences of the particle-vibration coupling Hamiltonian defined in equation (8.28) in simple terms. We refer the reader to Bohr and Mottelson (1975) and Bortignon *et al.* (1977) for the detailed expressions containing the proper angular momentum coupling coefficients (see also Chapter 10 and Appendix D).

The basic process described by the particle-vibration coupling Hamiltonian δU is that of a particle scattering inelastically off the surface and setting it into vibration, as shown in Fig. 8.10. The ease with which the process takes place is measured by the matrix element between the single-particle state $|\nu_k\rangle$ and the state $|\alpha\nu_{k'}\rangle$ representing a single particle coupled to a phonon

$$V(\nu_k, \nu_{k'}; \alpha) = \langle \alpha\nu_{k'}|\delta U|\nu_k\rangle = \Lambda_\alpha \langle \nu'_k|\hat{F}|\nu_k\rangle. \tag{8.31}$$

Here

$$\Lambda_\alpha = -\kappa\sqrt{\frac{\hbar\omega_\alpha}{2C_\alpha}} = \frac{-\kappa\beta_{\lambda\alpha}}{\sqrt{2\lambda_\alpha + 1}} \tag{8.32}$$

is the strength with which the particle couples to the vibration, and

$$\langle \nu'_k|\hat{F}|\nu_k\rangle = \int \mathrm{d}^3r\ \varphi^*_{\nu'_k}(\vec{r})F(\vec{r})\varphi_{\nu_k}(\vec{r}), \tag{8.33}$$

https://doi.org/10.1017/9781009401920 Published online by Cambridge University Press

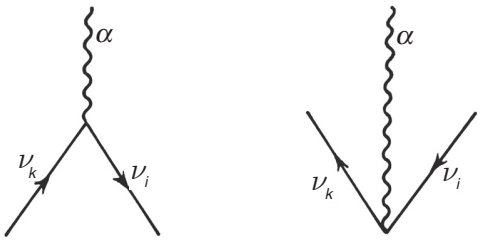

Figure 8.11. Graphical representation of two matrix elements of δU.

where $\varphi_{\nu_k}(\vec{r})$ and $\varphi_{\nu'_k}(\vec{r})$ are the single-particle wavefunctions, solutions of equations (8.17)–(8.20).

The quantity $\beta_{\lambda\alpha}$ is associated with the deformation parameters introduced in equation (8.22). In particular, for $\lambda = 2$ and $\mu = 0$, we have $\alpha_{20} = \beta_2/\sqrt{5}$. A similar matrix element can be obtained when the fermion, instead of a particle above the Fermi surface, is a hole in the Fermi sea (see Appendix A, equations (A.47), (A.48), for a discussion of the relation between the corresponding matrix element and the matrix element (8.31)). Aside from these matrix elements, the particle-vibration coupling Hamiltonian allows for two other matrix elements (see Fig. 8.11)

$$\langle\alpha|\delta U|\nu_k(\nu_i)^{-1}\rangle = \Lambda_\alpha\langle\tilde{\nu}_i|\hat{F}|\nu_k\rangle, \tag{8.34}$$

and

$$\langle\alpha\,\nu_k(\nu_i)^{-1}|\delta U|0\rangle = \Lambda_\alpha\langle\tilde{\nu}_i|\hat{F}|\nu_k\rangle^*, \tag{8.35}$$

where the symbol $|\nu_i^{-1}\rangle$ denotes a hole state while $|\tilde{\nu}_i\rangle$ is the state time-reversed to the state $|\nu_i\rangle$ (equation (A.41)). The first matrix element corresponds to the process in which a particle falls into a hole giving its energy and angular momentum to a vibrational state $|\alpha\rangle$. The matrix element (8.35) is associated with the process by which the vacuum becomes virtually excited through the simultaneous presence of a particle, a hole and a vibration.

8.3.1 RPA dispersion relation

Equation (8.28) for δU describes the coupling of single-particle motion to a vibrational mode with collective coordinate α. In the random phase approximation (RPA) a collective vibration can be viewed as a correlated particle–hole excitation, which, in the independent particle basis, corresponds to a linear combination of particle–hole excitations. A separable version of the RPA can be derived by recognizing the dual character of equation (8.28) for δU in the sense that the collective mode can be excited through the field $\hat{\alpha}$ as well as through the field $\hat{F}$ (see Fig. 8.12 and Appendix C, Section C.2). More explicitly we impose

https://doi.org/10.1017/9781009401920 Published online by Cambridge University Press

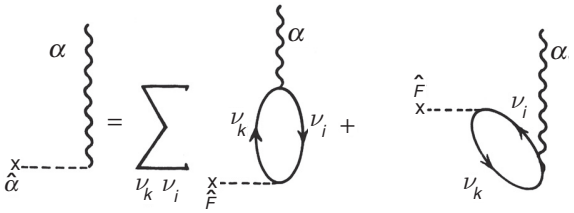

Figure 8.12. Excitation of the collective vibration in terms of the operators $\hat{\alpha}$ and $\hat{F}$. After Bohr and Mottelson (1975).

a self-consistency condition that the transition amplitude,

$$\langle\alpha|\hat{\alpha}|0\rangle = \sqrt{\frac{\hbar\omega_\alpha}{2C_\alpha}}, \tag{8.36}$$

should be equal to (see Fig. 8.12)

$$\langle\alpha|\hat{F}|0\rangle = \sum_{\nu_k,\nu_i}\left\{\frac{\langle\alpha|\delta U|\nu_k\nu_i^{-1}\rangle\langle\nu_k\nu_i^{-1}|\hat{F}|0\rangle}{\hbar\omega_\alpha - (\varepsilon_{\nu_k} - \varepsilon_{\nu_i})} + \frac{\langle\alpha|\hat{F}|\nu_k\nu_i^{-1};\alpha\rangle\langle\nu_k\nu_i^{-1};\alpha|\delta U|0\rangle}{-(\hbar\omega_\alpha + (\varepsilon_{\nu_k} - \varepsilon_{\nu_i}))}\right\}. \tag{8.37}$$

This expression for the transition matrix element can be expressed in terms of RPA amplitudes as

$$\langle\alpha|\hat{F}|0\rangle = -\sum_{\nu_k,\nu_i}(X_\alpha(\nu_k\nu_i) + Y_\alpha(\nu_k\nu_i))\langle\tilde{\nu}_i|\hat{F}|\nu_k\rangle,$$

where

$$\left.\begin{matrix}X_\alpha(\nu_k\nu_i)\\ Y_\alpha(\nu_k\nu_i)\end{matrix}\right\} = \pm\frac{\Lambda_\alpha\langle\tilde{\nu}_i|\hat{F}|\nu_k\rangle}{(\varepsilon_{\nu_k} - \varepsilon_{\nu_i}) \mp \hbar\omega_\alpha}. \tag{8.38}$$

For simplicity, the matrix element $\langle\tilde{\nu}_i|\hat{F}|\nu_k\rangle$ has been assumed to be real. Equating the relations given in equations (8.36) and (8.37) one obtains the RPA dispersion relation

$$W(\hbar\omega_\alpha) = \sum_{\nu_k,\nu_i}\frac{2(\varepsilon_{\nu_k} - \varepsilon_{\nu_i})|\langle\tilde{\nu}_i|\hat{F}|\nu_k\rangle|^2}{(\varepsilon_{\nu_k} - \varepsilon_{\nu_i})^2 - (\hbar\omega_\alpha)^2} = \frac{1}{\kappa}. \tag{8.39}$$

Equation (8.39) can be solved numerically for values of $\hbar\omega_\alpha$ as illustrated in Fig. 8.13.

https://doi.org/10.1017/9781009401920 Published online by Cambridge University Press

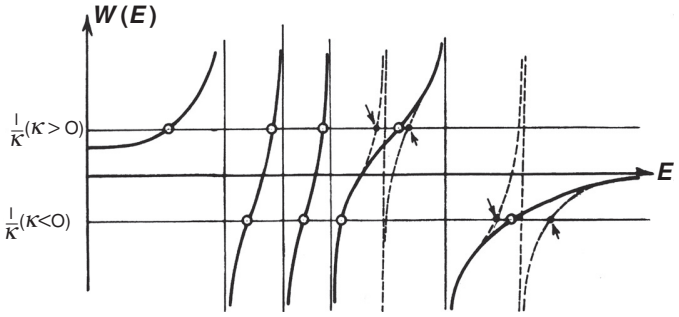

Figure 8.13. Graphical solution of the RPA dispersion relation, equation (8.39).

In keeping with the relation given in equation (8.37) one can write the phonon creation operator as

$$\Gamma_\alpha^\dagger = \sum_{\nu_k,\nu_i} X_\alpha(\nu_k,\nu_i)\Gamma^\dagger_{\nu_k\nu_i} + Y_\alpha(\nu_k,\nu_i)\Gamma_{\nu_k\nu_i}, \tag{8.40}$$

where $\Gamma^\dagger_{\nu_k\nu_i} = a^\dagger_{\nu_k} a_{\nu_i}$ and $\Gamma_{\nu_k\nu_i} = (a^\dagger_{\nu_k} a_{\nu_i})^\dagger$ are creation and annihilation operators of pairs of fermions which are assumed to display boson commutation relations as $\Gamma^\dagger_\alpha$ and Γ_α do (see Appendix A, Section A.4). This is the essence of the so-called random phase approximation (RPA). Consequently,

$$1 = [\Gamma_\alpha, \Gamma_\alpha^\dagger] = \sum_{\nu_k,\nu_i}(X^2_\alpha(\nu_k,\nu_i) - Y^2_\alpha(\nu_k,\nu_i)), \tag{8.41}$$

a relation which ensures that the one-phonon state $|\alpha\rangle = \Gamma^\dagger_\alpha|0\rangle_{\mathrm{B}}$ is normalized. Equation (8.41) provides the following microscopic expression for the square of the particle-vibration coupling strength

$$\begin{aligned}\Lambda^2_\alpha &= \left\{2\hbar\omega_\alpha \sum_{\nu_k,\nu_i} \frac{2(\varepsilon_{\nu_k} - \varepsilon_{\nu_i})|\langle\tilde{\nu}_i|\hat{F}|\nu_k\rangle|^2}{[(\varepsilon_{\nu_k} - \varepsilon_{\nu_i})^2 - (\hbar\omega_\alpha)^2]^2}\right\}^{-1} \\ &= \left(\frac{\partial W(E)}{\partial E}\Big|_{E=\hbar\omega_\alpha}\right)^{-1}.\end{aligned} \tag{8.42}$$

Because $(\Lambda_\alpha/\kappa)^2 = (\hbar\omega_\alpha/2C_\alpha)$, the above relation also provides the value of the transition probability $\langle\alpha|\hat{F}|0\rangle^2$.

Making use of the relation given in equation (8.41) and of the corresponding relations obtained from $[\Gamma_\alpha, \Gamma_\alpha] = [\Gamma^\dagger_\alpha, \Gamma^\dagger_\alpha] = 0$, one can invert the equation (8.40) obtaining

$$\Gamma^\dagger_{\nu_k\nu_i} = \sum_\alpha X_\alpha(\nu_k,\nu_i)\Gamma^\dagger_\alpha - Y_\alpha(\nu_k,\nu_i)\Gamma_\alpha. \tag{8.43}$$

https://doi.org/10.1017/9781009401920 Published online by Cambridge University Press

The dispersion relation (8.39) and the expression (8.42) for the normalization constant Λ_α can also be obtained with a separable interaction

$$\delta U_{\rm s} = -\kappa \hat{F}\hat{F}^{+}, \tag{8.44}$$

with

$$\hat{F} = \sum_{\nu_k,\nu_i} \langle \nu_k|F|\nu_i\rangle \Gamma^{\dagger}_{\nu_k\nu_i} + \langle \tilde{\nu_i}|F|\nu_k\rangle \Gamma_{\nu_k\nu_i}. \tag{8.45}$$

Let us comment on the general features of the graphical solutions of equation (8.39), as schematically displayed in Fig. 8.13. The poles of the dispersion relation $W(E)$ correspond to the values of the particle–hole excitation energies. Each root $\hbar\omega_\alpha$ is, in general, bound by two poles and there are as many states $|\alpha\rangle$ as particle–hole states $|\nu_k\nu_i^{-1}\rangle$. The collectivity of a state $|\alpha\rangle$ is measured by the normalization constant Λ_α^2 given in equation (8.42) which is equal to the inverse of the derivative of the dispersion relation $W(E)$ with respect to E at the value $E = \hbar\omega_\alpha$. Consequently, roots which are bound by two poles with similar energies will display little collectivity, as the associated derivative at the corresponding root is very large. Because of this, a single amplitude $X_\alpha(\nu_k, \nu_i)$ will dominate the microscopic structure of the associated wavefunction (see equations (8.27), (8.38) and (8.40)). Collective modes are possible when there is a gap in the particle–hole excitation spectrum. This can happen either at low excitation energies ($\leq$ 3–4 MeV), in connection with the spin–orbit splitting of single-particle levels in medium-heavy nuclei, or at high excitation energies in connection with the energy separation between major shells.

From equation (8.36) and the RPA self-consistency condition (see Appendix C, equation (C.5)), the transition amplitude is given by the relation

$$\langle \alpha|\hat{F}|0\rangle = (\hbar\omega_\alpha/2C_\alpha)^{1/2} = \frac{\beta_\alpha}{\sqrt{(2\lambda_\alpha+1)}}. \tag{8.46}$$

Typical values of β_α associated with these collective states are $\beta_\alpha \approx 0.08$–$0.1$. The corresponding excitation energies are 1–2 MeV for low-lying surface vibrational states, and 10–15 MeV for high-lying states (giant resonances).

An interesting feature of the spectrum emerging from the dispersion relation given in equation (8.39) is the fact that the nucleus displays collective states with low and high frequencies, compared with the energy difference $\hbar\omega_0 (\approx 41A^{-1/3}$ MeV) between major shells. The low-frequency modes are intimately connected with deformations (plastic behaviour, Chapter 7). High-frequency giant resonances are, on the other hand, related to the small amplitude oscillations (elastic behaviour, see Section 8.3).

To study giant resonances in nuclei lying along the valley of stability, the independent particle model is quite adequate. For a description of the low part of the spectrum, the independent particle model breaks down completely. One

must at least include the pairing interaction in the dynamics of the system (the same seems to be true in the case of giant resonances in exotic (halo) nuclei, in connection with the so-called 'pygmy' resonances (see, e.g. Frascaria *et al.* (2004)). The corresponding theory is called quasiparticle random phase approximation (QRPA, see Section 3.9 and Appendix J), The QRPA dispersion relation corresponding to equation (8.39) is

$$\sum_{\bar{\nu}\nu'} \frac{2(E_\nu + E_{\nu'})|\langle \nu'\bar{\nu}|\hat{F}|0\rangle|^2}{(E_\nu + E_{\nu'})^2 - (\hbar\omega_\alpha)^2} = \frac{1}{\kappa}, \tag{8.47}$$

where $\langle \nu'\bar{\nu}|\hat{F}|0\rangle$ is the matrix element of the interaction operator between the BCS vacuum state $|0\rangle$ and the two-quasiparticle state $\left|\nu'\bar{\nu}\right\rangle$. The solutions of the QRPA dispersion relation associated with the high-lying part of the spectrum (giant resonances) essentially coincide with those of equation (8.39). The low-energy part is, however, strongly modified. This is because for levels ν and ν' lying close to the Fermi energy the matrix element $\langle \nu'\bar{\nu}|\hat{F}|0\rangle$ contains U,V-factors which differ strongly from the independent particle model values of 0 or 1. The two-quasiparticle energy $E_\nu + E_{\nu'}$ depends on the pairing gap and is larger than the particle–hole excitation energy $\varepsilon_{\nu_k} - \varepsilon_{\nu_i}$. For simple estimates one can use the liquid drop model to calculated the restoring force and the pair hopping model to work out the inertia of the system, as already explained in Section 7.3.

8.3.2 Sum rules

The random phase approximation provides a diagonalization of the particle-vibration coupling Hamiltonian within the harmonic approximation. It is then natural that, as stated before, the number of states $|\alpha\rangle$ is equal to the number of particle–hole states $|\nu_k\nu_i^{-1}\rangle$ coupled to the quantum numbers of the vibration which form the basis states. Provided that the interaction among the fermions is velocity independent, the product of the energy of these states and the square of matrix elements between a particle and a hole state of any one-body operator which only depends on the spatial coordinate is a model-independent quantity, reflecting very general properties of the system as a whole. This result is known as an energy weighted sum rule (EWSR). In the case of dipole excitations it is proportional to the total number of charged particles of the system, being also proportional to the photoabsorption cross-section. One of the basic conditions to be fulfilled by any theoretical treatment used to diagonalize the residual interaction between particle–hole states should be to conserve the corresponding sum rule.

The importance of sum rules in the study of vibrational motion is that they are connected to basic operator identities which restrict the possible matrix elements

in a physical system. Also, through the use of sum rules it is possible to assess the collectivity of a given excitation. Furthermore, sum rules provide an upper limit to the energy that can be transferred to a nucleus under the action of an external field (Broglia and Winther (1991)). The subject of sum rules is quite general and in what follows we will only touch upon it. In particular we will discuss sum rules associated with spatially dependent single-particle fields.

It is simple to prove the EWSR in the form

$$\sum_n |\langle 0|\hat{F}|n\rangle|^2(E_n - E_0) = \tfrac{1}{2}\langle 0|[\hat{F}, [H, \hat{F}]]|0\rangle, \tag{8.48}$$

where n labels the complete set of eigenstates of the Hamiltonian H, E_n are the corresponding eigenvalues and $|0\rangle$ is the exact ground-state wavefunction. An extension of the energy weighted sum rule to the RPA was proved by Thouless (1961a). It has the same form as equation (8.48), but the meaning of the terms is different. The operator $\hat{F}$ is restricted to be a single-particle operator and the factors $(E_n - E_0)$ and $\langle 0|\hat{F}|n\rangle$ are RPA excitation energies and transition amplitudes. The matrix element on the right-hand side should be evaluated with the Hartree–Fock self-consistent ground-state wavefunction. There is an analogous generalization to the quasiparticle RPA. The proof of the RPA sum rule (8.48) in Thouless (1961a) holds when the potential V is a sum of two-body density-independent interactions. Problems which arise with density dependent forces have been discussed by Blaizot and Gogny (1977).

The right-hand side of eq.(8.48) can be simplified if $\hat{F} = \Sigma_k F(\vec{r}_k)$ is a one-particle operator, depending only on the spatial coordinates, and the potential energy terms in the Hamiltonian $H = T + V$ are local functions of the coordinates. Then $[V, F] = 0$ and the double commutator has contributions only from the kinetic energy part of the Hamiltonian. The double commutator can be expressed in terms of derivatives of F so that

$$\begin{aligned}\tfrac{1}{2}\langle 0|[\hat{F}, [H, \hat{F}]]|0\rangle &= \tfrac{1}{2}\langle 0|[\hat{F}, [T, \hat{F}]]|0\rangle \\ &= \langle 0|\sum_k \frac{\hbar^2}{2m}(\vec{\nabla}_k \hat{F}(\vec{r}_k))^2|0\rangle,\end{aligned} \tag{8.49}$$

where the last term implies the diagonal matrix element in the ground state. The average in equation (8.49) can be replaced by an integral over the density $\rho(r)$

$$\sum_n |\langle 0|\hat{F}|n\rangle|^2(E_n - E_0) = \frac{\hbar^2}{2m}\int \mathrm{d}^3 r\ |\vec{\nabla}\hat{F}|^2 \varrho(\vec{r}). \tag{8.50}$$

There is an analogous classical result for the reaction of a system in equilibrium to an impulsive field which gives each particle a momentum $\vec{\nabla}\hat{F}$. On average, the particles start at rest so their average energy after the sudden impulse is $\hbar^2|\vec{\nabla}\hat{F}|^2/2m$. This result is consistent with the fact that the energy weighted sum

https://doi.org/10.1017/9781009401920 Published online by Cambridge University Press

rule does not depend on the interactions acting among the nucleons, because the energy is absorbed in a very short time. On the other hand the nuclear forces accelerate the nucleons, and a longer time is required to produce a change in their velocities. Equation (8.48) also holds in the RPA provided that the factors on the left-hand side are interpreted as RPA energies and transition amplitudes (see, e.g. Bortignon *et al*. (1998)).

The energy weighted sum rule most often used for finite systems is associated with multipole fields, $F(\vec{r}) = r^L Y_{LM}(\hat{r})$. When the density $\rho(r)$ is spherically symmetrical the integral on the right-hand side of equation (8.50) can be simplified and

$$\sum_n |\langle 0|r^L Y_{LM}|n\rangle|^2 (E_n - E_0) = \frac{\hbar^2}{2m}\frac{(2L+1)L}{4\pi}\int \mathrm{d}^3 r\, r^{2L-2}\varrho$$
$$= \frac{\hbar^2}{2m} L(2L+1)\frac{A}{4\pi}\langle r^{2L-2}\rangle. \qquad (8.51)$$

8.3.3 Frequency of the giant quadrupole resonance

The mean energy of the giant quadrupole resonance in a spherical nucleus can be calculated from the dispersion relation (8.39). In a self-sustained vibration the changes in the density should be proportional to the changes in the potential. The coupling constant κ in equation (8.28) provides this proportionality factor. As discussed in Section 8.3.1 (see Fig. 8.12) and also in Appendix C, the operators $\hat{\alpha}$ and $\hat{F}$ can be viewed as the collective and the single-particle representation of the same field. In other words, equation (8.28) can also be thought of in terms of a separable two-body residual interaction (see equation (8.44))

$$v(\vec{r}, \vec{r'}) = -\kappa \hat{F}(\vec{r})\hat{F}^+(\vec{r'}). \qquad (8.52)$$

The appropriate choice of $\hat{F}(\vec{r})$ for a quadrupole resonance is the quadrupole field

$$\hat{F}(\vec{r}) \equiv F_{2M}(\vec{r}) = r^2 Y_{2M}(\hat{r}).$$

In the case of an isoscalar giant resonance the coupling constant κ can be estimated by an argument which has two parts (Bertsch and Broglia (1994)). The first is the assumption that the time-dependent displacements associated with this field are those of an irrotational incompressible fluid with a velocity potential $F_{2M}(\vec{r})$

$$\vec{u}(\vec{r}, t) = \alpha(t)\vec{u}_0(\vec{r}),$$

with

$$\vec{u}_0(\vec{r}) = \vec{\nabla} F_{2M}(\vec{r}).$$

https://doi.org/10.1017/9781009401920 Published online by Cambridge University Press

The time-dependence of $\vec{u}(\vec{r}, t)$ is carried by the collective coordinate $\alpha(t)$. The incompressibility follows from the relation

$$\vec{\nabla} \cdot \vec{u} = \alpha \nabla^2 F_{2M}(\vec{r}) = 0. \tag{8.53}$$

The second assumption is that the transition potential must be consistent with the change in the single-particle density, i.e. they should be generated by the same velocity field $\vec{u}(\vec{r}, t)$. This requirement is an extension to the dynamical case of the self-consistent relation between mean field and ground-state density in Hartree–Fock theory.

Let us carry out the calculations for a generic field $F_{LM} = r^L Y_{LM}$ and then particularize it for $L = 2$. The transition density and potential associated with the velocity field $\vec{u}$ are

$$\delta\varrho = \varrho(\vec{r} + \vec{u}) - \varrho(\vec{r}) = \alpha(t)\vec{u}_0(\vec{r}) \cdot \vec{\nabla}\varrho = \alpha(t)\vec{\nabla}F_{LM} \cdot \vec{\nabla}\varrho, \tag{8.54}$$

$$\delta\mathcal{U} = \vec{u} \cdot \vec{\nabla}\mathcal{U} = \alpha(t)\vec{\nabla}F_{LM} \cdot m\omega_0^2\vec{r} = \alpha(t)m\omega_0^2 L F_{LM}. \tag{8.55}$$

In this estimate, the harmonic oscillator potential has been used to describe the static field, i.e. $\mathcal{U}(r) = \frac{1}{2}m\omega_0^2 r^2$. The transition potential can also be calculated in terms of the convolution of the transition density and the two-body interaction using equation (8.10),

$$\delta\mathcal{U} = -\kappa_L F_{LM}(\vec{r}) \int \mathrm{d}^3r' \; F^*_{LM}(\vec{r'})\delta\varrho. \tag{8.56}$$

Equating the results of equations (8.55) and (8.56) one obtains

$$\kappa_L = -\frac{L\alpha(t)m\omega_0^2}{\int d^3r' F^*_{LM}(\vec{r'})\delta\varrho}. \tag{8.57}$$

The integral in this equation can be simplified using Gauss' theorem and the incompressibility condition equation (8.53)

$$\begin{aligned}\alpha(t) \int \mathrm{d}^3r' \; F^*_{LM}\vec{\nabla}F \cdot \vec{\nabla}\varrho &= -\alpha(t) \int \mathrm{d}^3r' \; |\nabla F|^2\varrho \\ &= -L(2L+1)\alpha(t) \int \mathrm{d}r \; r^{2L-2}\varrho \\ &= -L(2L+1)\alpha(t)\frac{A}{4\pi}\langle r^{2L-2}\rangle\end{aligned}$$

Inserting the result into equation (8.57) the factor $\alpha(t)$ cancels and the coupling parameter κ_L is

$$\kappa_L = \frac{4\pi m\omega_0^2}{(2L+1)A\langle r^{2L-2}\rangle}. \tag{8.58}$$

https://doi.org/10.1017/9781009401920 Published online by Cambridge University Press

For $L = 2$ the coupling parameter is

$$\kappa_2 = \frac{4\pi m\omega_0^2}{5A\langle r^2\rangle}.$$

Giant quadrupole excitations are produced by promoting particles from an occupied shell with principal quantum number N (harmonic oscillator) to unoccupied shells with principal quantum numbers $N+2, N+4$, etc. This is because the parity of the single-particle states is $(-1)^N$. Because in the harmonic oscillator the only non-diagonal matrix elements of the field r^2Y_{2M} are

$$\langle N'|r^2|N\rangle \propto \delta(N', N \pm 2),$$

the particle–hole excitation energy associated with quadrupole modes is $\varepsilon_{\nu_k} - \varepsilon_{\nu_i} = 2\hbar\omega_0$. The dispersion relation given in equation (8.39) can be written as

$$\frac{\sum_{\nu_k,\nu_i} 2(\varepsilon_{\nu_k} - \varepsilon_{\nu_i})|\langle\tilde{\nu}_i|r^2Y_2|\nu_k\rangle|^2}{(2\hbar\omega_0)^2 - (\hbar\omega_{\rm Q})^2} = \frac{1}{\kappa_2}.$$

Making use of the quadrupole energy weighted sum rule (see equation (8.51))

$$\sum_{\nu_k,\nu_i}(\varepsilon_{\nu_k} - \varepsilon_{\nu_i})|\langle\tilde{\nu}_i|r^2Y_2|\nu_k\rangle|^2 = \frac{5}{4\pi}\frac{\hbar^2}{m}A\langle r^2\rangle, \tag{8.59}$$

the factor $\langle r^2\rangle$ cancels and one obtains

$$\hbar\omega_Q = \sqrt{(2\hbar\omega_0)^2 - 2(\hbar\omega_0)^2} = \sqrt{2}\hbar\omega_0 = \frac{58}{A^{\frac{1}{3}}}\ \text{MeV}. \tag{8.60}$$

In Fig. 8.14 we display the systematics of centroids of the giant quadrupole as a function of mass number. The results are well parametrized by the function

$$\hbar\omega_Q \approx \frac{63}{A^{\frac{1}{3}}}\ \text{MeV}, \tag{8.61}$$

which is quite close to the theoretical result given in equation (8.60).

8.3.4 Damping of giant vibrations

One can view giant vibrations as a correlated particle–hole excitation built out of a particle above the Fermi surface and a hole in the Fermi sea. A first estimate of the damping width of giant vibrations can be obtained by assuming that the particle and the hole couple to a more complicated configuration acquiring a width. Then the total width is the sum of individual widths. Because in the damping process we deal with real processes, i.e. processes where the energy is conserved, the energy of the resonance has to be shared between the particle and the hole. The simplest expression one can write for the giant resonance damping

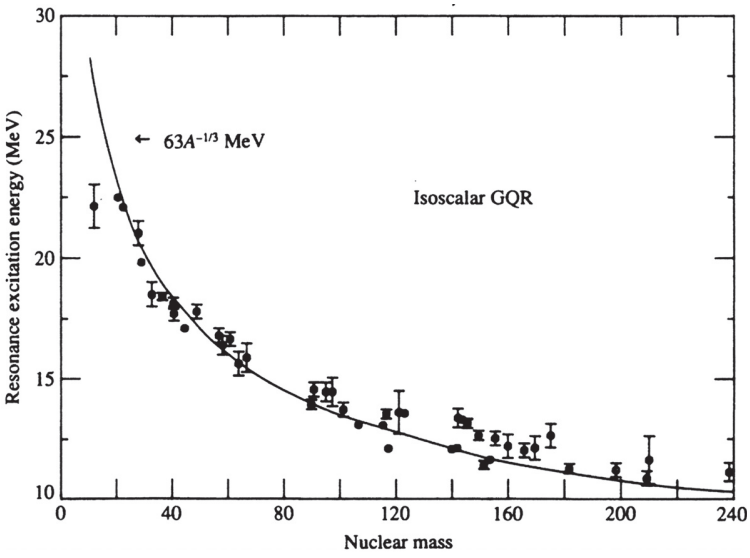

Figure 8.14. Energy systematics of the giant quadrupole resonance (GQR). (from Bertsch and Broglia (1994))

width is then

$$\begin{aligned}\Gamma^{\downarrow}_{\mathrm{GR}}(\hbar\omega_{\mathrm{GR}}) &= \Gamma^{\downarrow}_{p}\left(\tfrac{\hbar\omega_{\mathrm{GR}}}{2}\right) + \Gamma^{\downarrow}_{h}\left(\tfrac{\hbar\omega_{\mathrm{GR}}}{2}\right) \\ &\approx 0.5\hbar\omega_{\mathrm{GR}},\end{aligned} \tag{8.62}$$

where the expressions for $\Gamma^{\downarrow}_{p}$ and $\Gamma^{\downarrow}_{h}$ given in equation (9.15) have been used.

Making use of the expression $\hbar\omega_{Q} \approx 63A^{-1/3}$ MeV, the above equation leads to

$$\Gamma^{\downarrow}_{Q} \approx \frac{30}{A^{\frac{1}{3}}}\,\mathrm{MeV} \tag{8.63}$$

for the damping width of the giant quadrupole resonance. This expression is shown in Fig. 8.15 compared with the experimental findings. The simple estimate overpredicts the experimental findings by roughly 50%.

As will be shown below, the relation given by equation (8.62) neglects important correlation effects between the particle and the hole (Bortignon and Broglia (1981), Bortignon *et al.* (1983), Bertsch *et al.* (1983)). In fact, this relation implies that either the particle or the hole of the correlated particle–hole pair which constitutes a resonance can not only excite a surface vibration, which is true, but also reabsorb the phonon they have excited. This of course is not correct, in that a surface vibration excited by the inelastic scattering of the particles off the nuclear surface can be absorbed at a later time by the hole, and vice versa. In other words, the expression (8.62) takes care only of the (self-energy)

https://doi.org/10.1017/9781009401920 Published online by Cambridge University Press

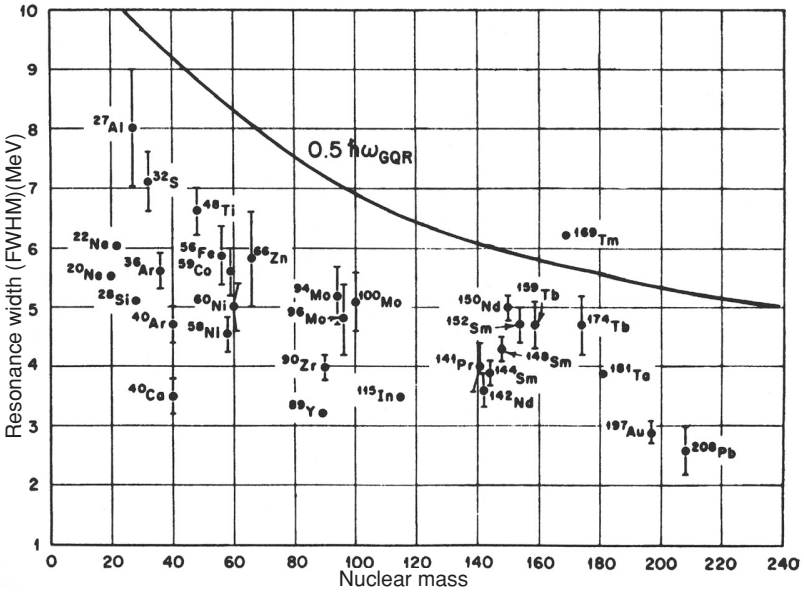

Figure 8.15. Damping width of the giant quadrupole vibration (see Satchler (1977)). The continuous curve corresponds to the estimate given in equation (8.63). Copyright © Società italiana di Fisica.

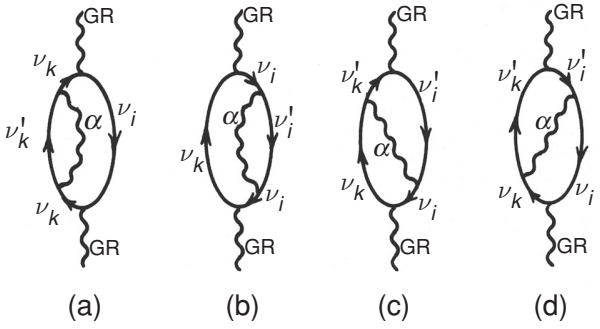

Figure 8.16. Lowest-order processes by which a resonance (GR) couples to a two-particle–two-hole intermediate state (doorway state) containing an uncorrelated particle–hole excitation and a surface vibration.

processes (a) and (b) of Fig. 8.16. We shall see that (vertex correction) processes (c) and (d), where a phonon is exchanged between the fermions, act as a glue between the particle and the hole, preventing, to a large extent, the decay of the resonance, and reducing the contributions (a) and (b) to the damping width. In fact, the self-energy correction to the giant vibration implied by the process of

https://doi.org/10.1017/9781009401920 Published online by Cambridge University Press

Fig. 8.16(a) is

$$\Sigma^{p}_{\text{self-en}}(\text{GR},\omega) = \sum_{\nu_k,\nu_i,\nu_{k'},\lambda} X^2_{\text{GR}}(\nu_k,\nu_i)\frac{V^2(\nu_k,\nu_{k'};\lambda)}{\hbar\omega - ((e_{\nu_{k'}} - e_{\nu_i}) + \hbar\omega_\lambda)}$$
$$= \sum_{\nu_k,\nu_i} X^2_{\text{GR}}(\nu_k,\nu_i)\Sigma(\nu_k,\omega + e_{\nu_i}), \tag{8.64}$$

i.e. it is the sum of the contributions of the self-energy of each particle participating in the linear combination of particle–hole excitations describing the resonance. In other words, it is the weighted average of the single-particle self-energies of all the particle–hole configurations. The weighting factor is the probability that the giant vibration will be in a given configuration. The particle self-energies are calculated at an energy $(\hbar\omega + e_{\nu_i})$, i.e. at an energy lower than the energy of the giant resonance by the amount e_{ν_i} $(= \varepsilon_{\nu_i} - \varepsilon_{\text{F}} < 0)$, which is the energy taken up by the hole of the different particle–hole excitations. A similar expression is obtained for the decay of the hole (see Fig. 8.16(b)), i.e.

$$\Sigma^{\hbar}_{\text{self-en}}(\text{GR},\omega) = \sum_{\nu_k,\nu_i} X^2_{\text{GR}}(\nu_k,\nu_i)\Sigma(\nu_i,\omega - e_{\nu_k}) \tag{8.65}$$

where now $e_{\nu_k} = \varepsilon_{\nu_k} - \varepsilon_{\text{F}} > 0$.

Making the ansatz that (a) the giant resonance is a very correlated state such that one can approximate the amplitudes by $|X| \sim \frac{1}{\sqrt{N}}$, N being the dimension of the particle–hole basis where the RPA solution of the giant vibration has been calculated, and (b) the particle-vibration coupling matrix elements are independent of the configuration, one can write, for both of the expressions given in equations (8.64) and (8.65),

$$\Sigma^{\nu}_{\text{self-en}}(\text{GR},\omega) \approx \Sigma(\nu,\omega - |e_{\nu'}|), \tag{8.66}$$

where ν is either a particle or a hole and ν' a hole or a particle respectively. The imaginary part of the above equation leads to the relation (8.62).

The self-energy associated with the process (d) of Fig. 8.16 is

$$\Sigma_{\text{vertex}}(\text{GR},\omega) = \sum_{\nu_k,\nu_i,\nu_{k'},\nu_{i'}} X_{\text{GR}}(\nu_k\nu_i)X_{\text{GR}}(\nu_{k'}\nu_{i'})$$
$$\times \frac{\langle\nu^{-1}_{i'}|\hat{F}|\nu^{-1}_{i}\rangle\langle\nu_{k'}|\hat{F}|\nu_k\rangle^2\Lambda^2_\lambda}{\hbar\omega - ((e_{\nu_{k'}} - e_{\nu_i}) + \hbar\omega_\lambda)}, \tag{8.67}$$

where $|\nu^{-1}_i\rangle$ represents a state of a hole and $|\nu_i\rangle$ that of a particle moving in the same single-particle state. The matrix elements between hole states are related to those between particle states according to

$$\langle\nu^{-1}_{i'}|\hat{F}|\nu^{-1}_{i}\rangle = c\langle\nu_{i'}|\hat{F}|\nu_i\rangle, \tag{8.68}$$

https://doi.org/10.1017/9781009401920 Published online by Cambridge University Press

where c is a phase (i.e. $c^2 = 1$) defined through the relation (see equation (A.49))

$$(\tau \hat{F} \tau^{-1})^{\dagger} = -c\hat{F}. \tag{8.69}$$

Here τ stands for the time-reversal operator and the dagger identifies Hermitian conjugation. Because an average $\langle \nu_{i'}|F|\nu_i\rangle$ and $\langle \nu_{k'}|F|\nu_k\rangle$ have the same order of magnitude one can approximate the last expression by

$$\Sigma_{\text{vertex}}(\text{GR}, \omega) \approx c \sum_{\nu_k, \nu_i, \nu_{k'}} (X_{\text{GR}}(\nu_k \nu_i)^2 \frac{V^2(\nu_{k'}, \nu_k; \lambda)}{\hbar\omega - ((e_{\nu_{k'}} - e_{\nu_i}) + \hbar\omega_\lambda)}. \tag{8.70}$$

A similar expression is obtained for the process depicted in Fig. 8.16(c). Consequently,

$$\frac{\Sigma_{\text{vertex}}}{\Sigma_{\text{self-en}}} \approx c\ . \tag{8.71}$$

Because the single-particle field $\hat{F}$ is a spin-isospin independent field, $c = -1$. The physical reason for the minus sign in the phase relating processes (a) and (d) of Fig. 8.16 is associated with the fact that the multipole moments of a particle and a hole have different sign, in keeping with the fact that closed-shell systems are spherical.

Under the approximation leading to equation (8.70), there would be a complete cancellation between the different processes contributing to the self-energy operator of the giant resonance, and eventually to its damping width. This result is intimately connected with Furry's theorem of quantum electrodynamics (Furry (1937)), as well as with general arguments on particle conservation (Ward (1950), Takahashi (1957), see also Bortignon *et al*. (1983)). The fact that the subspaces available to the particles (ν_k) and to the holes (ν_i) are different makes the approximations used above not quantitatively accurate although they are qualitatively sound. The cancellation implied by equation (8.71), although conspicuous, is not complete (see also discussion following equation (3.90)).

Numerical calculations indicate that the cancellation discussed above implies a reduction of the contributions stemming from particle- and hole-decay of the order of 30–50%, bringing theory into overall agreement with the experimental findings.

8.4 Correlation energy contribution to nuclear masses

In the present section we discuss some of the consequences that the zero-point fluctuations associated with pairing and surface vibrations have in the nuclear binding energies. Let us start by briefly commenting on the accuracy modern mass formulae have in accounting for the experimental findings.

https://doi.org/10.1017/9781009401920 Published online by Cambridge University Press

The best account of the experimental data based on mean-field theory provides a fitting to the 2135 measured masses with $N, Z > 8$ with a r.m.s. (root mean square) error of 0.674 MeV (Goriely *et al*. (2002)). This has been achieved by means of Hartree–Fock–Bardeen–Cooper–Schrieffer (HFBCS) calculations which employ a Skyrme-type zero-range effective force in the mean-field channel, supplemented by a zero-range pairing interaction. The 14-parameter set is named BSk2. As a reference point for the work of Baroni *et al*. (2004) we discuss below, they have considered a parameter set of almost equal quality, denoted by MSk7, where the r.m.s. error is 0.738 MeV (see also Goriely *et al*. (2001)).

Nuclei display both single-particle and collective degrees of freedom. Consequently, the corresponding ground states and associated nuclear masses reflect the effect of the zero-point fluctuations (ZPF) associated with these modes. While mean-field theory includes fluctuations associated with quasiparticles, it is only time-dependent mean-field theory which takes into account the zero-point fluctuations associated with collective vibrations. The need to consider their effect was put forward by Bertsch and Hagino (2001). Realistic calculations for the quadrupole degree of freedom have been performed for light nuclei (Stetcu and Johnson (2002)) and for a few selected isotopes within the so-called generator coordinate method (GCM) (Bender *et al*. (2004)).

Making use of random phase approximation (RPA) Baroni *et al*. (2004) calculated the ground-state correlation energies associated with both surface (quadrupole and octupole modes) and pairing vibrations for the Ca and Pb isotopes. Because pairing vibrations have a collective character only around closed-shell nuclei (being essentially pure two-quasiparticle states lying on top of twice the pairing gap in superfluid systems, see Section 5.2), one expects the associated ZPF (see e.g. Fig. 5.3, (right)) to lead to important corrections to the mass formula of Goriely *et al*. (2002). This is in keeping with the fact that the largest deviations from experiment found in this mass formula are observed in closed-shell systems.

To derive the particle–hole RPA equations, use can be made of the quasi-boson approximation where the RPA ground-state energy is given by (see e.g. Ring and Schuck (1980) see also Sections 6.3 and 6.6)

$$E_{\mathrm{RPA}} = E_{\mathrm{HF}} - (2\lambda + 1) \sum_{\alpha, n} \hbar\omega_{\alpha}(n) \sum_{ki} \left| Y^{\alpha}_{ki}(n) \right|^2 , \tag{8.72}$$

This relation reflects the fact that the amplitudes $Y^{\alpha}_{ki}(n)$ are directly related to the ground-state correlations induced by the corresponding vibrational modes. The second term of the right-hand side is called the correlation energy.

We now proceed to discuss the expected contributions to the nuclear mass arising from monopole and multipole pairing vibrations in Pb isotopes. Let us start by discussing the monopole pairing-vibration contributions.

https://doi.org/10.1017/9781009401920 Published online by Cambridge University Press

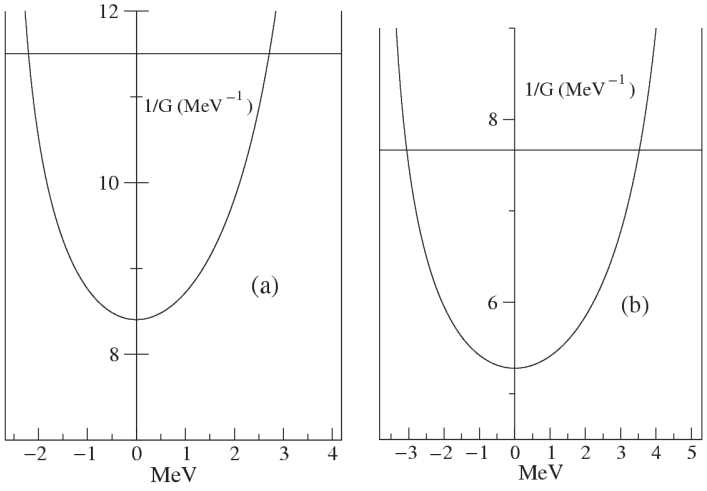

Figure 8.17. Monopole pairing–vibration dispersion relation for (a) neutrons and (b) protons for the nucleus ^{208}Pb. This figure is due to S. Baroni.

Fig. 8.17 shows the dispersion relations given in equation (5.50) calculated for ^{208}Pb for both protons and neutrons (see Section 5.2.1), making use of the valence orbitals of this nucleus. Making use of the fact that the sum of the pairing binding energies of ^{206}Pb and ^{210}Pb (see equations (5.45) and (5.46)) as well as in ^{206}Hg and ^{210}Po are ≈ 2 MeV (in this last case one has to take into account the Coulomb repulsion between the two protons, see e.g. Bortignon *et al.* (1977)), one obtains the values of 2.7 MeV and 2.2 MeV for the neutron pair-addition and pair-removal energies,* the corresponding values for the proton channel being 3.5 MeV and 3.1 MeV respectively. The contributions of the lowest ($n = 1$) pair-addition and pair-subtraction modes have been considered in the calculations because, as a rule, the $n \neq 1$ modes are much less collective.

Inserting the results mentioned above in equation (8.72) and the corresponding Y amplitudes ($= a_1(\omega)$ for ^{208}Pb and $r_1(\omega)$ for ^{206}Pb; see Table 5.1, and equations (6.34)–(6.37)), one obtains the ground-state correlation energy values -0.399 MeV (neutrons) and -0.449 MeV (protons) respectively. Making use of similar quantities associated with pairing vibrations with multipolarity $\lambda \neq 0$ (see Section 5.3.1), in particular quadrupole and hexadecapole pairing vibrations, the corresponding contributions have also been calculated.

In Table 8.1 we show these contributions to the ground-state energy (i.e. E_{RPA} as defined in equation (8.72)) associated with the monopole, quadrupole and

* Note that the condition introduced in equation (5.41) (and corresponding to the situation $x = 0.5$ in the two-level model of Fig. 5.1, see Section 5.2) to simplify the discussion of the energy spectrum is here not applicable.

https://doi.org/10.1017/9781009401920 Published online by Cambridge University Press

Table 8.1. *Ground-state correlation energies, arising from the neutron* (n) *and proton* (p) *monopole, quadrupole and hexadecapole pairing vibrations in* ^{208}Pb.

0^+		2^+		4^+	
n	p	n	p	n	p
−0.399	−0.449	−0.609	−0.244	−0.189	−0.092

Table 8.2. *Ground-state correlation energies for the* Pb *isotopes.*

	^{204}Pb	^{206}Pb	^{208}Pb	^{210}Pb	^{212}Pb
p–h vibrations	−2.793	−2.709	−2.237	−2.801	−3.173
Pairing vibrations	−0.785	−0.785	−1.981	−0.785	−0.785

hexadecapole pair-addition and pair-removal modes for both neutrons and protons associated with ^{208}Pb, the summed contribution amounting to −1.981 MeV ($\approx$ −1.196 MeV −0.785 MeV).

In Table 8.2 we collect the corresponding contribution for a number of Pb isotopes. As mentioned above, pairing vibrations are collective modes only around closed-shell nuclei, where particles and holes can be clearly distinguished. Consequently (see Chapter 5) we have considered the contribution of neutron pairing vibrations only for the closed-shell system (while the proton pairing vibrations were taken into account for all isotopes). Also shown in Table 8.2 are the contribution to E_{RPA} arising from the low-lying collective particle–hole vibrations calculated by making use of the MSk7 interaction to determine the single-particle states and the particle–hole correlated modes. Quadrupole and octupole vibrations with energy $<$7 MeV, and exhausting $\geq$2% of the non-energy weighted sum rule were included in the calculation of E_{RPA}. These conditions essentially select the lowest (one or two) states displaying correlated wavefunctions (see Section 7.3).

Similar calculations were repeated for the calcium isotopes $^{40-48}$Ca. In Table 8.3 the corresponding results are shown, together with the contribution of the particle–hole vibrational modes. When adding the results of Tables 8.2 and 8.3 to the HFBCS MSk7 mass formula of Goriely *et al*. (2001), the parameters of the Skyrme interaction should be refitted in order to provide the best reproduction of experimental masses. This should be done on a large sample of isotopes, a scope which was beyond the purpose of the paper of Baroni *et al*. (2004). If one restricts oneself to Ca isotopes (Pb isotopes) the results in Table 8.4

Table 8.3. *Ground-state correlation energies for the* Ca *isotopes.*

	^{40}Ca	^{42}Ca	^{44}Ca	^{46}Ca	^{48}Ca
p–h vibrations	−0.886	−1.418	−1.606	−1.391	−0.547
pairing vibrations	−4.761	−2.978	−3.239	−3.500	−5.823

Table 8.4. *(first column) Root mean square error associated with the HFBCS MSk7 mass formula of Goriely et al. (2001) and (second column) r.m.s.e. associated with HFBCS MSk7 mass formula (with sligthly adjusted parameters) plus the correlation contributions associated with surface and pairing vibrations calculated in the RPA. The quantity* $\bar{\sigma} = \left(\frac{\sigma_{\mathrm{Ca}}^2+\sigma_{\mathrm{Pb}}^2}{2}\right)^{1/2}$ *is shown in the last line.*

	σ (MeV)	
Pb	0.646	0.543
Ca	1.200	0.466
$\bar{\sigma}$	0.964	0.505

are obtained. Averaging the r.m.s. deviations associated with Ca and Pb isotopes leads to a value of 0.505 MeV compared with the value of 0.964 MeV obtained by making use of the results of Goriely *et al*. (2002). Although a global readjustment of the mean-field parameters should be envisaged, the fact that the locally extracted r.m.s. deviations have been reduced by a factor of approximately 2 can be considered meaningful, highlighting the important role that pairing vibrations play in the ground-state nuclear energies.

https://doi.org/10.1017/9781009401920 Published online by Cambridge University Press

9
Beyond mean field

The Hartree–Fock mean field is represented by a static potential. Non-locality may be approximated by a momentum dependence but the potential is energy independent. In general, independent particle motion is renormalized by coupling to more complicated degrees of freedom. Such couplings often involve a time delay and introduce an energy dependence into the single-particle motion. For example the effective interaction of two nucleons mediated by coupling to a surface vibration has an energy dependence related to the frequency of the vibrational mode.

The state of motion of a nucleon in a nucleus may change by a core polarization process where it promotes a nucleon from a state in the Fermi sea to a state above the Fermi surface as illustrated in Fig. 9.1 (see also Fig. 8.3(b)), or by an inelastic collision as illustrated in Fig. 8.10. This is an example of the doorway phenomenon, the states containing a nucleon and a vibration being the doorway states. The original formulation of the concepts of doorway state can be found in Block and Feshbach (1963). The review by Feshbach (1974) contains details of subsequent developments.

9.1 Doorway states

Through the coupling introduced in equation (8.24) a particle can set the nuclear surface into vibration. Such process can be repeated, the particle interacting a second time with the surface and reabsorbing the vibration (see Fig. 9.2). In this way the particle becomes dressed and the properties characterizing the nucleon, such as mass, charge, mean free path, occupation number, etc., are modified due to this coupling.

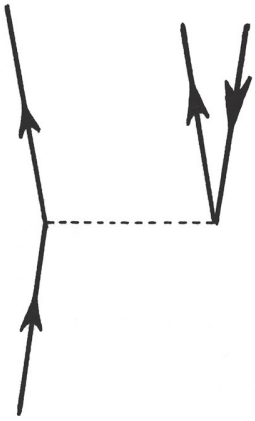

Figure 9.1. Collision between nucleons where a particle changes state of motion by inducing a particle–hole core excitation.

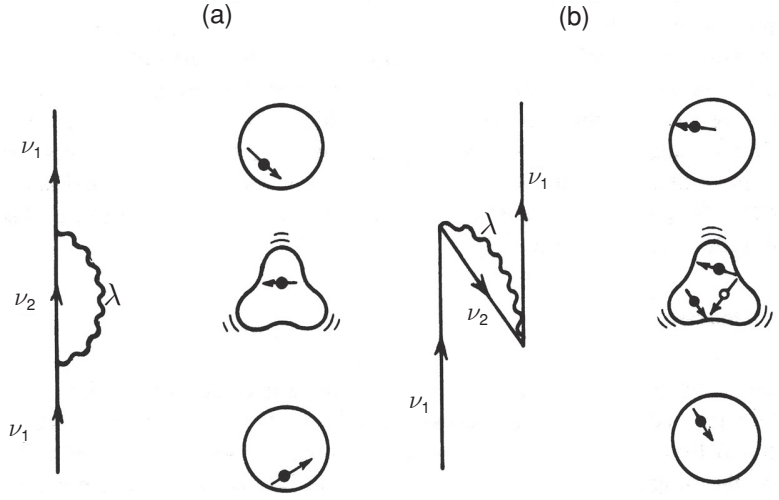

Figure 9.2. The lowest-order process by which the single-particle motion is renormalized by the coupling to the nuclear surface. In (a) the particle excites the vibration by bouncing inelastically off the surface. In (b) the vibration is excited by a virtual process (vacuum fluctuation). Particles are represented by an upwardgoing arrowed line (by a solid dot) while holes are pictured as a downwardgoing arrowed line (open circle). The surface vibration is drawn as a wavy line.

9.1.1 The dynamical shell model

The self-energy Σ of a nucleon in a nucleus is the renormalization of single particle or single hole energies due to coupling of single-particle motion to more complicated degrees of freedom. The present chapter will focus on the

https://doi.org/10.1017/9781009401920 Published online by Cambridge University Press

self-energy due to the coupling of single-particle motion to nuclear surface vibrations (the coupling to pairing vibrations in rotating nuclei was discussed in Chapter 6, in particular in Sections 6.3 and 6.4). The relevant processes in lowest order are illustrated in Fig. 9.2. The corresponding perturbation expression of the self-energy operator for a particle state is

$$\Sigma(\nu_1, \omega) = \sum_{\lambda, \varepsilon_2 > \varepsilon_F} \frac{V^2(\nu_1, \nu_2; \lambda)}{\omega - (\varepsilon_2 + \omega_\lambda)} - \sum_{\lambda, \varepsilon_2 < \varepsilon_F} \frac{V^2(\nu_1, \nu_2; \lambda)}{-\omega + (\varepsilon_2 - \omega_\lambda)}, \tag{9.1}$$

where the minus sign in the second term arises because of fermion exchange (Pauli principle). Each term of this expression has the typical structure of an energy correction in second-order perturbation theory, i.e. a square matrix element divided by an energy denominator. In equation (9.1) ω is the energy of the initial single-particle state $|\nu_1\rangle$. The phonons associated with the surface vibrations have energy ω_λ and multipolarity λ. The quantities $V(\nu_1, \nu_2; \lambda)$ are the particle-vibration coupling matrix elements which were defined in equation (8.31). The energy denominators are the energy differences between the initial and the intermediate states. The first term in equation (9.1) corresponds to the polarization graph in Fig. 9.2(a). The energies of both the initial single-particle state and the intermediate particle state ε_2 are both greater than the Fermi energy ε_F. The second term illustrated by the graph in Fig. 9.2(b) is associated with core correlations and the intermediate state $|\nu_2^{-1}\rangle$ is a hole state with energy $\varepsilon_2 < \varepsilon_F$.

Some general conclusions can be drawn from the structure of equation (9.1). The first term is negative for particle states with energies relative to the Fermi energy which are lower than the phonon energy, $\varepsilon_1 - \varepsilon_F < \hbar\omega_\lambda$. There is a cancellation between negative and positive contributions for high-energy single-particle states $\varepsilon_1 - \varepsilon_F \gg \hbar\omega_\lambda$. The second term is always positive because $\varepsilon_1 - \varepsilon_2 > 0$ and $\omega_\lambda > 0$. The net result is that low-energy single-particle states have a negative self-energy and are shifted towards the Fermi level. This shift has a maximum when $\varepsilon_1 - \varepsilon_F \approx \hbar\omega_\lambda$ and decreases or even changes sign for high single-particle states. The self-energy has the opposite sign for hole states and the resulting effect is to narrow the energy gap between particle states and hole states. A number of calculations starting from that of Bertsch and Kuo (1968) support these conclusions (see Mahaux *et al*. (1985) and references therein).

Both terms in equation (9.1) are important for an initial state $|\nu_1\rangle$ near the Fermi level and, in a Fermi gas model, the self-energy $\Sigma(\nu_1) \approx 0$ at the Fermi level due to a cancellation between the two terms. The first term in equation (9.1) is more important for an initial state $|\nu_1\rangle$ away from the Fermi level because the energy denominators are smaller. In the following we will make a simple estimate of the quantity $\Sigma(\nu_1)$ neglecting the second term. The first term can be written

more explicitly as

$$\Sigma(\nu_1) = \sum_{\nu_2,\lambda} \frac{V^2(\nu_1, \nu_2, \lambda)}{\varepsilon_1 - (\varepsilon_2 + \hbar\omega_\lambda)}$$
$$= \sum_{\nu_2\lambda} \frac{{\beta_\lambda}^2}{(2j_2+1)(2\lambda+1)} \frac{\langle j_2|R_0\frac{\partial U}{\partial r}|j_1\rangle^2 \langle l_2 j_2||Y_\lambda||l_1 j_1\rangle^2}{\varepsilon_1 - (\varepsilon_2 + \hbar\omega_\lambda)}, \qquad (9.2)$$

where the statistical factors and reduced matrix element of the spherical harmonic $Y_{\lambda\mu}$ associated with angular momentum coupling are shown explicitly (see Appendix D). There is a parity constraint and $l_1 + l_2 - \lambda$ is restricted to being even.

When $\nu_2 = \nu_1$ the phonon multipolarity λ must be even because of the parity constraint. Assuming furthermore that $j_1 \gg \lambda$, one can use the asymptotic form of the $3j$-symbols and write (see Appendix D)

$$\langle l_1 j_1||Y_\lambda||l_1 j_1\rangle^2 \approx 0.1(2j_1+1), \quad \text{when } \lambda \text{ is even.} \qquad (9.3)$$

The squared matrix element coupling the nucleon with the vibration can then be expressed as

$$V^2(\nu_1, \nu_1; \lambda) = \frac{0.1{\beta_\lambda}^2}{(2\lambda+1)} \langle j_1|R_0\frac{\partial U}{\partial r}|j_1\rangle^2, \qquad (9.4)$$

and the quantity $\Sigma(\nu_1)$ becomes

$$\Sigma(\nu_1) \approx \sum_\lambda \Sigma^\lambda(\nu_1), \qquad (9.5)$$

where

$$\Sigma^\lambda(\nu_1, \omega) = -\frac{V^2(\nu_1, \nu_1; \lambda)}{\hbar\omega_\lambda}. \qquad (9.6)$$

The numerators of all the factors appearing in the above equations have a similar magnitude for both low-lying collective surface vibrations and for high-lying modes. Because the energy $\hbar\omega_\lambda$ is much smaller for low-lying modes than for giant resonances, we shall consider only the coupling to low-lying vibrational states. In what follows we will estimate (9.6) for the low-lying quadrupole vibration of ^{208}Pb.

Single-particle levels can be clearly identified in closed-shell nuclei. The nucleus $^{208}_{82}$Pb is a paradigm of such systems, the single-particle gap for neutrons ($N = 126$), i.e. the energy difference between the last occupied $3p_{1/2}$ orbital and the first empty state $2g_{9/2}$ is 3.1 MeV. Making use of equations (7.37) and (7.38) we obtain $\hbar\omega = 0.7$ MeV and $\beta_2 = 0.11$. An estimate for the radial matrix element derived in Appendix D is $\langle j|R_0\partial U/\partial r|j\rangle \approx -50$ MeV. Substituting into

https://doi.org/10.1017/9781009401920 Published online by Cambridge University Press

equation (9.4) one obtains

$$V^2(\nu_1, \nu_1; \lambda = 2) = 0.6\,\mathrm{MeV}^2 \tag{9.7}$$

and

$$\Sigma^{\lambda=2}(\nu_1) = -0.9\,\mathrm{MeV}. \tag{9.8}$$

The estimate given in equation (9.8) is very sensitive to the parameters used. In particular a more realistic value of $\hbar\omega_2$ as well as of β_2 will reduce it considerably.

On the other hand the contribution of $\lambda = 4$ phonons and other j-values in the intermediate state would increase the estimate for the level shift. We retain the value $\Sigma(\nu_1) \approx -0.9\,\mathrm{MeV}$ for the purposes of the present section. The self-energy of a hole level has a similar magnitude but with opposite sign so the spacing between the occupied and unoccupied neutron levels would be reduced by 1.8 MeV. The ansatz that this reduction leads to the experimental value of 3.1 MW implies that the single-particle gap predicted by HF theory is 4.9 MeV (see Section 8.2). Because the density of levels is inversely proportional to the mass of the particle (see Appendix B) the above result corresponds to an effective mass (called ω-mass, see next section)

$$\frac{m^*}{m} \approx \frac{4.9}{3.1} = 1.6. \tag{9.9}$$

It could be argued that the relation $\mathrm{d}\varepsilon/\mathrm{d}k \sim 1/m^*$ was obtained for a uniform system. To bridge the gap between infinite nuclear matter and the case of potential wells of finite range let us consider a particle of mass m in a one-dimensional harmonic oscillator, which provides a sensible parametrization of the Saxon–Woods potential (see Fig. 9.3). It would be argued that in this case the density of levels is inversely proportional to the square root of the mass of the particle, in keeping with the fact that $\hbar\omega_0 = \hbar(C/m)^{1/2}$, C being the restoring force of the system. This is not the case as can be seen by writing the above relation in terms of the unit length parameter $b = (\hbar/m\omega_0)^{1/2}$, namely $\hbar\omega_0 = \hbar^2/mb^2$. Requiring the ground-state wavefunction $\Psi_0(r) \sim \exp(-r^2/2b^2)$ to have the same radial spread ($b = \text{const.}$) when one replaces the mass of the particle m by $m^* > m$, the density of levels turns out thus to be proportional to the effective mass, as in the infinite system discussed in Appendix B.

9.1.2 Motion of a particle in a complex potential

There is extensive experimental evidence showing that a nucleon moving in an orbital close to the Fermi energy has a mean free path which is large compared with the nuclear dimensions and it is effectively in a stationary state. Consequently the wavefunction can be written as $\varphi_1(\vec{r}, t) = \varphi_1(\vec{r})\mathrm{e}^{-\mathrm{i}\omega t}$. For single-particle levels progressively removed from the Fermi energy, the probability of finding states

https://doi.org/10.1017/9781009401920 Published online by Cambridge University Press

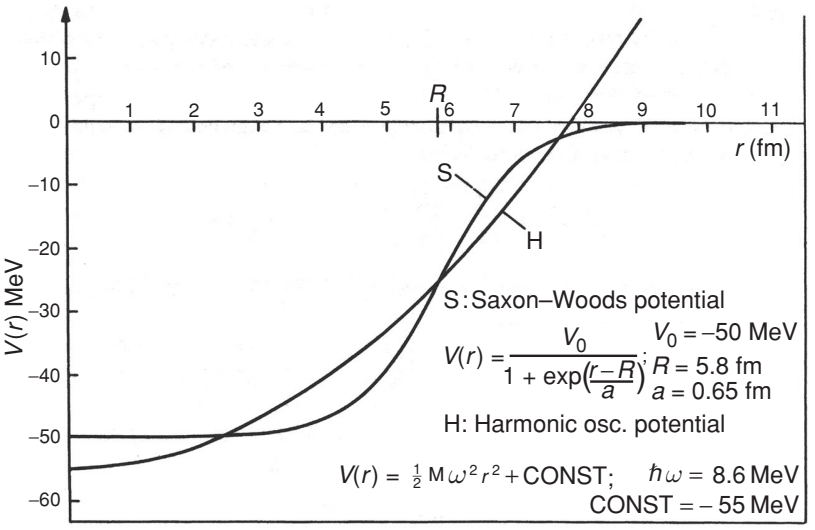

Figure 9.3. Comparison of a typical Saxon–Woods shell model potential and of a harmonic oscillator potential whose frequency has been chosen in order to fit the Saxon–Woods potential. (From Bohr and Mottelson (1969))

with the same energy as the single-particle state becomes sizable, in particular, states built out of a single particle and a collective surface vibration. Under these circumstances, the single-particle levels acquire a width and the associated wavefunction can be written as $\varphi_1(\vec{r}, t) = \varphi_1(\vec{r})\mathrm{e}^{-\mathrm{i}\omega t}\mathrm{e}^{-\frac{\Gamma}{2\hbar}t}$. Consequently, the probability of finding the state 1 occupied by a particle at time t, when it was occupied with probability 1 at time $t = 0$ decays exponentially with time, $\int \mathrm{d}^3 r \ |\varphi_1(\vec{r}, t)|^2 = \exp^{-\frac{\Gamma}{\hbar}t}$. The associated lifetime of the state is connected to the width Γ by Heisenberg's uncertainty relation,

$$\tau = \frac{\hbar}{\Gamma}. \tag{9.10}$$

The width Γ is associated with the imaginary part of the self-energy of a particle. When the energy of the intermediate state $\varepsilon_2 + \hbar\omega_\lambda$ coincides with the energy ε_1 of the initial state the first term in the expression for the self-energy diverges. The divergence can be avoided by making an energy average, replacing ω by $\omega + \mathrm{i}\frac{I}{2}$, where I represents the energy interval over which averages are carried out. The self-energy operator can then be written as

$$\Sigma(1, \omega + \mathrm{i}I) = \Delta E(1, \omega + \mathrm{i}I) - \frac{\mathrm{i}}{2}\Gamma(1, \omega + \mathrm{i}I), \tag{9.11}$$

the sum of a real and an imaginary term. The final result, obtained by taking the limit of $\Sigma(1, \omega + \mathrm{i}I)$ as $I \to 0$, should not depend on the averaging process.

https://doi.org/10.1017/9781009401920 Published online by Cambridge University Press

It is illuminating to calculate the imaginary part of the self-energy, i.e.

$$\Gamma(1,\omega) = \sum_{2,\lambda} V^2(1,2;\lambda) \frac{I}{(\omega - (\varepsilon_2 + \omega_\lambda))^2 + (\frac{I}{2})^2}. \tag{9.12}$$

Taking the limit of this function as $I \to 0$ one obtains

$$\Gamma(1,\omega) = 2\pi \sum_{2,\lambda} V^2(1,2;\lambda)\delta(\omega - (\varepsilon_2 + \omega_\lambda)). \tag{9.13}$$

Approximating $V(1,2;\lambda)$ by its average value V leads to the formula

$$\Gamma(1,\omega) = 2\pi V^2 \varrho(\omega), \tag{9.14}$$

where the quantity $\varrho(\omega) = \sum_{2,\lambda} \delta(\omega - (\varepsilon_2 + \omega_\lambda))$ is the density of final states per unit energy, into which the particle state can decay. This is just the Golden Rule and is the basic expression used to describe the decay width of a quantal state. For scattering states, the quantity $-\frac{1}{2}\Gamma$ can be identified with the imaginary part of the optical potential.

A simple empirical parametrization of the damping width is provided by the relation (see Fig. 9.4)

$$\Gamma^{\downarrow}_{\rm sp} \approx 0.5\hbar\omega, \tag{9.15}$$

where $\hbar\omega$ is the single-particle energy measured from the Fermi energy ($\hbar\omega = |\varepsilon_1 - \varepsilon_{\rm F}|$). This parametrization is supported by detailed calculations: Bortignon

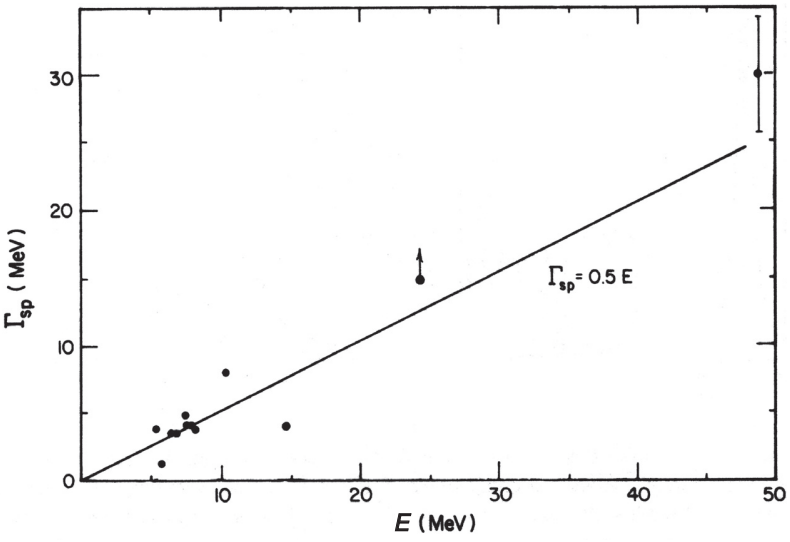

Figure 9.4. Full width at half maximum of the strength function associated with deep hole states, bound states and scattering states in a variety of nuclei. (From Bortignon *et al.* (1998))

https://doi.org/10.1017/9781009401920 Published online by Cambridge University Press

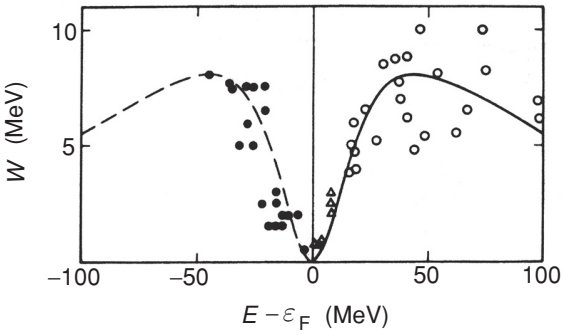

Figure 9.5. Dependence upon $\omega = E - \varepsilon_F$ of the imaginary part of the optical potential for nuclei with mass number $12 \leq A \leq 60$. (After Mahaux *et al.* (1985))

et al. (1986), Donati *et al.* (1996). Inserting the estimate given in equation (9.7) of the square of the particle-vibration coupling matrix elements and the empirical expression equation (9.15) into equation (9.14), we get an estimate for the density of intermediate states,

$$\varrho(\omega) = \frac{0.5}{2\pi}\frac{\hbar\omega}{V^2} \approx 0.13(\hbar\omega)\,\text{MeV}, \tag{9.16}$$

where $\hbar\omega$ is the single-particle energy measured from the Fermi energy expressed in MeV. In order that the single-particle state $|\nu\rangle$ can undergo a real transition into states composed of a particle and a vibration, the density of states should be sufficiently large ($\varrho(\omega) \gtrsim 1\,\text{MeV}^{-1}$). Thus damping will become important when $\hbar\omega \gtrsim 7$ MeV. On the other hand, for single-particle levels lying far away from the Fermi energy the virtual processes become unimportant and the effective mass of the nucleon coincides with the k-mass, while real processes give a damping width to these states (see Fig. 9.5).

9.2 Effective mass (ω-mass)

As the graphical perturbation expansion of the single-particle self-energy suggests (see Fig. 9.2 and equation (9.11)), the Hamiltonian describing the single-particle motion reads (see also equation (8.9)),

$$H_{\text{s.p.}} = \left[-\frac{\hbar^2}{2m}\nabla^2 + \tilde{V}(k) + \Delta E(\omega) \right] + U(r) + \mathrm{i}W(\omega), \tag{9.17}$$

where $\Delta E(\omega)$ is the real part of the self-energy and $W = -\frac{1}{2}\Gamma$ is the imaginary part of the optical potential. The dependence of $\tilde{V}(k)$ on the momentum of the particle is associated with the non-locality arising from the Pauli principle, and has been discussed in Section 8.2.1. The dependence of $\Delta E(\omega)$ on the frequency is associated with the non-locality in time generated by the coupling to a surface

https://doi.org/10.1017/9781009401920 Published online by Cambridge University Press

vibration excited by the particle at a given time and reabsorbed at a different time (virtual, off the energy shell-processes). Effects associated with real, on the energy shell-processes are described by W(ω).

For many purposes it is possible to rewrite the term in square brackets in equation (9.17) as a kinetic energy term with an effective mass m^* (see e.g. Mahaux *et al*. (1985)). In fact, requiring that (in keeping with the fact that one is calculating an inertia, see Appendix B)

$$\frac{\mathrm{d}\hbar\omega}{\mathrm{d}k} = \frac{\hbar^2 k}{m^*},$$

and calculating

$$\frac{\mathrm{d}\hbar\omega}{\mathrm{d}k} = \frac{\hbar^2 k}{m} + \frac{\partial \tilde{V}(k)}{\partial k} + \frac{\partial \Delta E(\omega)}{\partial \hbar\omega}\frac{\mathrm{d}\hbar\omega}{\mathrm{d}k}, \tag{9.18}$$

which is equivalent to

$$\frac{\mathrm{d}\hbar\omega}{\mathrm{d}k} = \frac{\hbar^2 k}{m}(1 - \frac{\partial \Delta E}{\partial \omega})^{-1}(1 + \frac{m}{\hbar^2 k}\frac{\partial \tilde{V}(k)}{\partial k}), \tag{9.19}$$

one obtains

$$\frac{m^*}{m} = \frac{m_k}{m}\frac{m_\omega}{m}. \tag{9.20}$$

In this equation the ω- and k-masses are given by

$$\frac{m_\omega}{m} = (1 - \frac{\partial \Delta E(\omega)}{\partial \hbar\omega}), \qquad \frac{m_k}{m} = \left(1 + \frac{m}{\hbar^2 k}\frac{\partial \tilde{V}(k)}{\partial k}\right)^{-1}, \tag{9.21}$$

where the ω-derivative is to be calculated at the Fermi energy, while m_k/m coincides with the k-mass defined in Section 8.2.1. Consequently,

$$H_{\mathrm{s.p.}} = -\frac{\hbar^2}{2m^*}\nabla^2 + \tilde{U} + \mathrm{i}\widetilde{W}, \tag{9.22}$$

which is the optical-model Hamiltonian with $\tilde{U} = (m/m^*)U$ and $\widetilde{W} = (m/m^*)W$. Note that m^* can have a radial dependence ($m^*(r)$).

In Fig. 9.6 we display results of calculations of the ω-mass for the single-particle and single-hole states of ^{208}Pb (see also equation (9.9)). The quantity m_ω/m has a peak as a function of the single-particle energy centred around ε_{F}, such that

$$\frac{m^*}{m} = \frac{m_\omega}{m}\frac{m_k}{m} \approx 1.4 \times 0.7 \approx 1.$$

The associated FWHM is approximately 10 MeV, i.e. the ω-mass increase over the bare mass happens in the interval of energy between -5 MeV and $+5$ MeV

https://doi.org/10.1017/9781009401920 Published online by Cambridge University Press

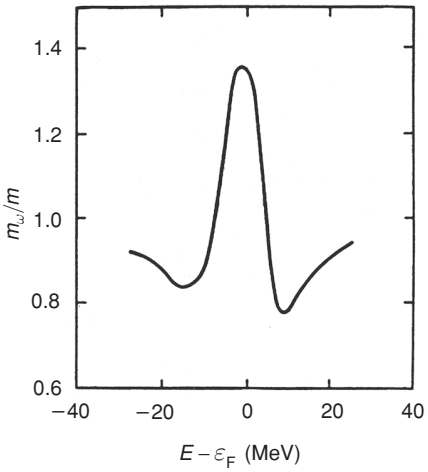

Figure 9.6. The ratio m_ω/m of the ω-mass of a nucleon in ^{208}Pb to the bare nucleon mass as a function of the energy of the particle measured with respect to the Fermi energy, calculated within the particle-vibration coupling model. (After Mahaux *et al*. (1985))

around the Fermi energy. This width is controlled by the frequency of collective surface vibrations which, in ^{208}Pb, correspond to an energy of the order of a few MeV. Consequently, for frequencies of the single particle much higher than this value, the phonons cannot dress the particle in an efficient way any more. Within the same interval of energy around the Fermi energy for which $m_\omega/m > 1$, the imaginary part of the self-energy (see Fig. 9.5 and equation (9.15)) is essentially zero. This is because no real transitions exist in this energy interval ($\varrho(\omega) < 1\,\mathrm{MeV}^{-1}$, see equation (9.16)). Furthermore, the result that the ω-mass is larger than the bare mass has the consequence that the density of levels around the Fermi energy is larger than that predicted by Hartree–Fock theory, in accordance with the experimental findings (see Fig. 8.8).

From these results one can understand why the empirical evidence concerning the energy of single-particle levels around the Fermi energy is well described by the motion of nucleons in a real, energy-independent, average potential, with a mass equal to the bare nucleon mass. However, there is a basic difference between this simple model and the results expressed by equation (9.17). In fact, in the empirical independent particle model the occupation of each level is either 1 or 0. The situation is more subtle here. Owing to its coupling to the nuclear surface, a particle which starts in a pure single-particle configuration is forced into more complicated states of motion. Consequently, the probability of finding a particle in a single-particle state below the Fermi level is different from 1. Similarly, unoccupied states at the level of the pure independent particle model become partially occupied as the particle jumps to these states by exciting a

surface mode. In fact, the quantity

$$Z_\omega = (m_\omega/m)^{-1} \tag{9.23}$$

is the single-particle spectroscopic factor at the Fermi energy (quasiparticle strength, see Appendix E, equation (E.18)).

The fact that the 'more complicated' states to which the particle states couple can be at a higher energy than the original energy available to the particle presents no contradiction, as these are virtual states, i.e. states which last a finite amount of time (off the energy shell-processes). Because of Heisenberg's relations, energy does not need to be conserved within a range which becomes larger the shorter the time the intermediate state is virtually excited. However, an external field, such as that produced by a proton, can provide the necessary energy to make the process real and eventually pick up a neutron in the reaction $A(p, d)B$ from states above the Fermi energy. Results of calculations of the occupation number

$$n_j = \begin{cases} 1 + \frac{\mathrm{d}\Delta E'}{\mathrm{d}E} & j = \text{occ. orbit}, \\ -\frac{\mathrm{d}\Delta E'}{\mathrm{d}E} & j = \text{empty orbit} \end{cases} \tag{9.24}$$

are given in Fig. 9.7. In the above equation, the quantity $\Delta E'$ is the contribution associated with Fig. 9.2(b) arising from ground-state correlations.

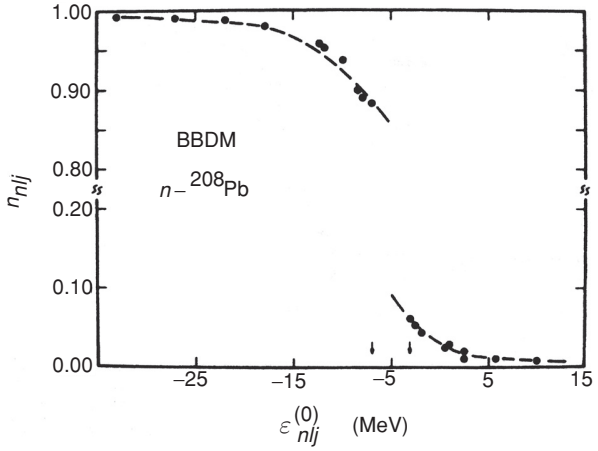

Figure 9.7. Occupation probability of neutron orbits in the correlated ^{208}Pb nucleus plotted against the single-particle energy ε_{nlj} computed in the Skyrme III-Hartree–Fock approximation. The calculation is based on equation (9.24). The dots correspond to the $1f_{7/2}$, $2p_{1/2}$, $1g_{7/2}$, $1h_{11/2}$, $1h_{9/2}$, $2f_{7/2}$,$2f_{5/2}$, $1i_{13/2}$, $3p_{3/2}$ and $3p_{1/2}$ hole states, and to the $2g_{9/2}$, $1i_{11/2}$, $1j_{15/2}$, $3d_{5/2}$, $2g_{7/2}$, $4s_{1/2}$, $3d_{3/2}$, $2h_{11/2}$ and $2h_{9/2}$ particle states. The dashed curve has been drawn to guide the eye through the calculated dots in order to exhibit their trend. The arrows show the location of $\varepsilon_{\mathrm{F}}^- = \varepsilon_{3p_{1/2}}$ and $\varepsilon_{\mathrm{F}}^+ = \varepsilon_{2g_{9/2}}$ (After Mahaux *et al.* (1985))

https://doi.org/10.1017/9781009401920 Published online by Cambridge University Press

The physics which is at the basis of the results displayed in Figs. 9.5 and 9.6 finds a compact expression in the dispersion relation (Mahaux *et al*. (1985))

$$\Delta E(\omega) \approx \frac{P}{\pi} \int \frac{W(\omega')}{\omega - \omega'} \mathrm{d}\omega'.$$

In this equation, P stands for the principal part integral for the real and imaginary parts of an analytic function (see equation (9.11)), i.e.

$$P \int_a^b f(x)/(x - x_0)\mathrm{d}x = \lim_{\delta \to 0^+} \left[\int_a^{x_0 - \delta} + \int_{x_0 + \delta}^b \right]$$

Because energy-conserving, on-the-energy shell processes are easier to calculate than virtual, off-the-energy shell processes, the dispersion relation above can be used in calculating the real potential from a known imaginary potential (see (9.17)).

9.3 The ω-mass and the induced interaction

In this section we obtain an expression for the ω-mass in a simplified version of the particle-vibration coupling model and show how it is related to the induced pairing interaction between nucleons resulting from the exchange of surface phonons. The self-energy of a nucleon is due to the emission and absorption of a virtual phonon as illustrated in Fig. 9.2 while the induced interaction is represented by Fig. 8.3(c). The general particle-vibration coupling model is simplified by considering coupling with only one type of phonon with frequency ω_λ and by assuming that the single nucleon levels are uniformly distributed around the Fermi level. A more systematic discussion of the induced nucleon–nucleon interaction due to phonon exchange will be presented in the next chapter.

The single-particle self-energy expression given in equation (9.1) is the sum of a polarization term $\Sigma^{(\mathrm{p})}(\omega)$ (Fig. 9.2(a)) and a core correlation term $\Sigma^{(\mathrm{c})}(\omega)$ (Fig. 9.2(b)) They give equal contributions to the ω-mass at the Fermi level in the simplified model considered here. The polarization term is

$$\Sigma_\nu^{(\mathrm{p})}(\omega) = \Delta E^{(\mathrm{p})}(\omega) = \sum_{\nu'} \frac{V^2(\nu, \nu'; \lambda)}{\omega - (e_{\nu'} + \hbar\omega_\lambda)}, \tag{9.25}$$

where $e_{\nu'} = \varepsilon_{\nu'} - \varepsilon_{\mathrm{F}}$ and $\omega = e_\nu - \varepsilon_{\mathrm{F}}$. At the Fermi energy $\omega = 0$ and

$$\begin{aligned} \left. \frac{\partial \Delta E_\nu^{(\mathrm{p})}(\omega)}{\partial \omega} \right|_{\omega=0} &= -\sum_{\nu'} \left. \frac{V^2(\nu, \nu'; \lambda)}{(\omega - (e_{\nu'} + \hbar\omega_\lambda))^2} \right|_{\omega=0} \\ &= -\sum_{\nu'} \frac{V^2(\nu, \nu'; \lambda)}{(e_{\nu'} + \hbar\omega_\lambda)^2}. \end{aligned} \tag{9.26}$$

https://doi.org/10.1017/9781009401920 Published online by Cambridge University Press

If the sum is approximated by an integral assuming a density of single-particle states of one-spin orientation at the Fermi level $N(0)$ ($g/2$ in equation (3.58), $1/d$ and $3A/8E_F$ in equation (2.1)) and constant single-particle matrix elements V we get

$$\left.\frac{\partial \Delta E_\nu^{(p)}(\omega)}{\partial \omega}\right| \approx -N(0)\int_0^\infty \frac{V^2 \mathrm{d}e}{(e+\hbar\omega_\lambda)^2} = -N(0)\frac{V^2}{\hbar\omega_\lambda}. \tag{9.27}$$

The core correlation part of the self-energy gives an equal contribution so that the total value is

$$\left.\frac{\partial \Delta E_\nu(\omega)}{\partial \omega}\right| = -2N(0)\frac{V^2}{\hbar\omega_\lambda}. \tag{9.28}$$

Consequently the ω-mass defined in equation (9.21) is

$$m_\omega = m\left(1 - \frac{\partial \Delta E_\nu^{(p)}(\omega)}{\partial \omega}\right) = m(1+\lambda_{\text{p-v}}). \tag{9.29}$$

The quantity $\lambda_{\text{p-v}}$ is defined by

$$\lambda_{\text{p-v}} = N(0)\frac{2V^2}{\hbar\omega_\lambda} = N(0)g_{\text{p-v}}, \tag{9.30}$$

where

$$g_{\text{p-v}} = \frac{2V^2}{\hbar\omega_\lambda}, \tag{9.31}$$

is a particle-vibration coupling parameter. The factor $(1+\lambda_{\text{p-v}})$ is known as the mass enhancement factor.

The vibration excited by a nucleon interacting with the surface can be absorbed by a second nucleon as shown in Fig. 8.3(c), giving rise to an induced interaction. In this section we are interested in the induced interaction which contributes to pairing. Nucleons in time-reversed states $|\nu\rangle$ and $|\bar{\nu}\rangle$ with energies ε exchange a phonon and make a transition to final states $|\nu'\rangle$ and $|\bar{\nu}'\rangle$ with energies ε' as illustrated in the inset of Fig. 10.1. The transition matrix element is

$$v_{\nu\nu'} = \frac{2V^2(\nu,\nu';\lambda)}{\varepsilon_\nu - (\varepsilon_{\nu'}+\hbar\omega_\lambda)}. \tag{9.32}$$

The factor 2 arises because there are two possible processes each giving the same matrix element: the phonon may be emitted by the state $|\nu\rangle$ and absorbed by $|\bar{\nu}\rangle$, and vice versa. The matrix element is not symmetric in the initial and final state.

A symmetrized form can be obtained by interchanging the initial and final states and averaging

$$v_{\nu\nu'} = \frac{V^2(\nu, \nu'; \lambda)}{\varepsilon_\nu - (\varepsilon_{\nu'} + \hbar\omega_\lambda)} + \frac{V^2(\nu, \nu'; \lambda)}{\varepsilon_{\nu'} - (\varepsilon_\nu + \hbar\omega_\lambda)} \tag{9.33}$$

$$= \frac{2\hbar\omega_\lambda V^2(\nu, \nu'; \lambda)}{(\varepsilon_\nu - \varepsilon_{\nu'})^2 - (\hbar\omega_\lambda)^2}. \tag{9.34}$$

For $\varepsilon_\nu \approx \varepsilon_{\nu'} \approx \varepsilon_{\mathrm{F}}$ and assuming a constant particle-vibration coupling matrix elements V, one obtains

$$v_{\nu\nu'} = -\frac{2V^2}{\hbar\omega_\lambda} = -g_{\text{p-v}}. \tag{9.35}$$

Making use of typical values of $\lambda_{\text{p-v}} \approx 0.6$ (see equation (9.9) and Fig. 9.6) and $N(0) \approx 3.4\,\mathrm{MeV}^{-1}$ (e.g. ^{120}Sn, see Fig. 8.4 and discussion following (8.21)) one obtains from equations (9.30) and (9.35) $\bar{v} = -0.2\,\mathrm{MeV}$ (see also Section 10.2, discussion in paragraph before equation (10.20)).

The bare nucleon–nucleon interaction is essential for the production of pair correlations in nuclei, but the induced interaction due to phonon exchange also contributes. In order to assess the importance of the induced interaction we make an estimate of the pairing gap, neglecting the bare interaction completely. The pairing gap equation with the interaction $v_{\nu\nu'} = -g_{\text{p-v}}$ is

$$\Delta = g_{\text{p-v}} \sum_{\nu>0} \frac{\Delta}{2E_\nu}. \tag{9.36}$$

By approximating the sum by an integral this relation can be written as

$$1 = g_{\text{p-v}} N(0) \int_{-\omega_D}^{\omega_D} \mathrm{d}e \frac{1}{\sqrt{e^2 + \Delta^2}} \approx g_{\text{p-v}} N(0) \sinh^{-1}\left(\frac{\omega_D}{\Delta}\right), \tag{9.37}$$

where $N(0)$ is the density of levels at the Fermi energy for one-spin orientation, and ω_D is a typical energy associated with surface vibrations. From the relation above one obtains

$$\Delta = \omega_D \left(\sinh\left(\frac{1}{\lambda_{\text{p-v}}}\right)\right)^{-1}. \tag{9.38}$$

In the case in which $\lambda_{\text{p-v}} \ll 1$ (weak coupling limit) one can write (see (3.58))

$$\Delta = 2\omega_D \exp\left(-\frac{1}{\lambda_{\text{p-v}}}\right), \tag{9.39}$$

while

$$\Delta = \omega_D \lambda_{\text{p-v}} \tag{9.40}$$

https://doi.org/10.1017/9781009401920 Published online by Cambridge University Press

in the case in which $\lambda_{\text{p-v}} \gg 1$ (strong coupling limit).

Making use of typical values of $\lambda_{\text{p-v}} \approx 0.6$ (see (9.9)) and $\omega_D \approx 1$–2 MeV, one expects from equation (9.39) the induced interaction arising from the exchange of low-lying collective surface vibrational states to give rise to pairing gaps of the order of 0.4–0.8 MeV, i.e. pairing gaps which are of the order of 50% of the empirical value $12/\sqrt{A}$ MeV.

The above treatment of the consequences the fermion–boson (particle–vibration) coupling has on the properties of the single-particle states neglects two major effects (see Sections 9.1 and 9.2, see also Schrieffer (1964) equation (7.83); note that $Z(p_\Delta)$ is the inverse of Z_ω). Firstly, the single-particle strength is reduced from the value of 1 to a smaller value Z_ω (see equation (9.23)). Secondly, the single-particle states acquire a finite width $\Gamma(\omega)$. These effects can change quantitatively the estimates given in Equations (9.39) and (9.40). In particular, considering only the effect of the width, i.e. setting $Z_\omega = 1$, Morel and Nozières (1962) found, for the case of an infinite system,

$$\Delta(\vec{k}) = \int V\left(\vec{k} - \vec{k}'\right) \frac{\Delta(k')}{2E_{k'}} \left[\frac{2}{\pi} \tanh^{-1}\left(\frac{E_{k'}}{\Gamma_{k'}}\right)\right] \frac{\mathrm{d}^3k'}{(2\pi)^3} \tag{9.41}$$

where $\vec{k}$ is the momentum of the single particle and $V(\vec{k} - \vec{k}')$ is the (state dependent) two-body interaction. The effect of the bracketed factor is to cut off the integral when the imaginary part Γ_k reaches the same magnitude as E_k, thus reducing the prefactor appearing in equations (9.39) and (9.40) (see also Baldo *et al*. (2002)).

The fact that there is an explicit relation between the value of the induced pairing interaction, of the ω-mass, of the occupation number Z_ω and of the damping width $\Gamma(\omega)$ is closely connected to sum rule arguments (Ward identities) relating self-energy and vertex correction processes to particle conservation (see Section 8.3.4 and Fig. 8.16) (see also Mahan (1981)).

Note that one has also neglected some of these relations and effects when discussing the results displayed in Fig. 8.6 and 8.9. They are taken up in Section 10.4, in connection with the results displayed in Fig. 10.16 (see also Appendix H, Section H.4, as well as Terasaki *et al*. (2002a, 2002b)).

Let us close this section by relating equation (9.40) to the single j-shell equation (H.30). Because $N(0) = \sum_j \Omega_j/2\omega_D = \Omega/2\omega_D$, where $\Omega_j = (2j+1)/2$, equation (9.40) can also be written as

$$\Delta = \frac{1}{2} g_{\text{p-v}} \Omega. \tag{9.42}$$

https://doi.org/10.1017/9781009401920 Published online by Cambridge University Press

10
Induced interaction

As discussed in the last section of Chapter 9 a pair of nucleons can interact with each other through the nuclear surface in a process in which one nucleon excites a vibrational mode which is then absorbed by the other nucleon (see inset Fig. 10.1). This process leads to a renormalization of the nucleon–nucleon interaction which, for nucleons close to the Fermi energy, is controlled by the exchange of low-lying surface collective vibrations. This is because low-energy surface vibrations match the frequencies of these nucleons and are very collective. This argument is the same as that used to explain the central role of surface vibrations in renormalizing the single-particle motion. The contribution of surface vibrations to the single-particle self-energy and to the ω-mass was analysed in Chapter 9 and a simplified version of the particle-vibration coupling model was introduced in Section 9.3. It gave explicit expressions for both the ω-mass and the induced pairing interaction and pairing gap due to phonon exchange. They both have a simple dependence on the coupling strength $g_{\text{p-v}}$ which is defined in equation (9.31). The present chapter extends the discussion of the induced interaction and presents the results of microscopic calculations. Section 10.3 presents results in a slab model, where the simplicity of the infinite system is retained (absence of shell structure), without losing surface effects.

10.1 Simple estimates

Estimates of the induced pairing interaction due to phonon exchange were obtained in Section 9.3 in a model with constant matrix elements and a uniform distribution of single-particle levels. The present section extends that discussion by including shell effects (Broglia *et al.* (2001)). The starting point is a perturbation expression for the induced interaction written in terms of (j, j) coupled

https://doi.org/10.1017/9781009401920 Published online by Cambridge University Press

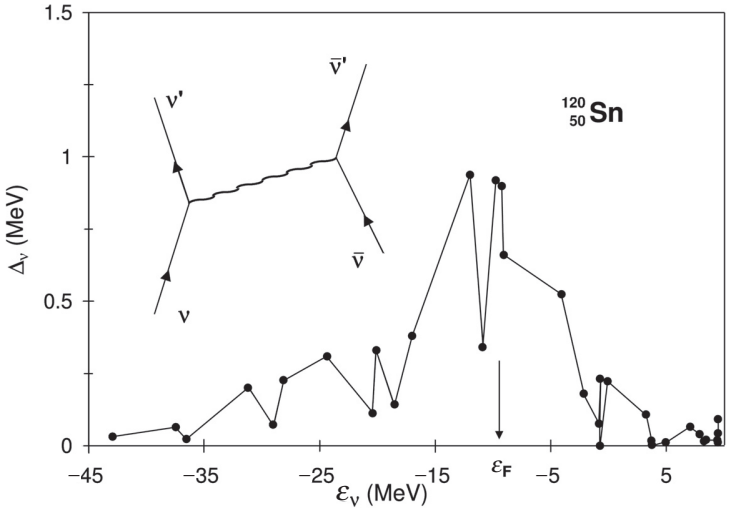

Figure 10.1. State-dependent pairing gap Δ_ν for the nucleus ^{120}Sn, calculated by making use of the induced interaction (see inset, where particles are represented by arrowed lines and phonons by a wavy line) (after Barranco *et al*. (1999)). Reprinted with permission from Barranco *et al*., *Phys. Rev. Lett.* **83**: 2147–50 (1999). Copyright 1999 the American Physical Society.

matrix elements

$$v_{jj'} \equiv \langle (jj)_0 | v | (j'j')_0 \rangle = \sum_\lambda v^\lambda_{jj'}, \tag{10.1}$$

where

$$v^\lambda_{jj'} = \frac{2}{\sqrt{(2j+1)(2j'+1)}} \frac{V^2\left(j, j'; \lambda\right)}{D_\lambda}. \tag{10.2}$$

Here $v_{jj'}$ is the induced matrix element for scattering of a pair of nucleons from the state j with energy ε_j to the state j' with energy $\varepsilon_{j'}$. The nucleons are coupled to a total angular momentum zero in both the initial and final states (see Appendix D, equations (D.11)–(D.14)). The matrix element $v_{jj'}$ is a sum of components $v^\lambda_{jj'}$ corresponding to the exchange of phonons with different multipolarities λ and energies $\hbar\omega_\lambda$. The $V^2\left(j, j'; \lambda\right)$ are the square of particle-vibration coupling matrix elements

$$V^2\left(j, j', \lambda\right) = \frac{\beta^2_\lambda}{2\lambda+1} \langle j' | R_0 \frac{\partial U}{\partial r} | j \rangle^2 \langle l'j' || Y_\lambda || lj \rangle^2, \tag{10.3}$$

introduced in Section 8.3 and defined in Appendix D (equation (D.9)). They were used in equation (9.6) for the calculation of single-particle self-energies. The quantity β_λ is the root mean square fluctuation of the collective coordinate

https://doi.org/10.1017/9781009401920 Published online by Cambridge University Press

of the phonon of multipolarity λ in the ground state and $\langle j'|R_0\partial U/\partial\lambda|j\rangle$ is a radial coupling matrix element. The energy denominator D_λ in equation (10.2) can be approximated in different ways. In Section 9.3 (equation (9.34)) it was written as

$$\frac{1}{D_\lambda} \approx \frac{\hbar\omega_\lambda}{\left(\varepsilon_i - \varepsilon_j\right)^2 - (\hbar\omega_\lambda)^2},$$

which reduces to $D_\lambda \approx -\hbar\omega_\lambda$ when $\varepsilon_i = \varepsilon_j$. The microscopic calculations presented in the next section use a more accurate energy denominator from Bloch–Horowitz perturbation theory (Bloch and Horowitz (1958))

$$D_\lambda = E_0 - (\hbar\omega_\lambda + e_j + e_{j'}), \tag{10.4}$$

used in Barranco *et al.* (1999) for calculating the contribution of phonon exchange to pairing in nuclei. Here $e_j = |\varepsilon_j - \varepsilon_{\rm F}|$ are single-particle energies measured from the Fermi energy and E_0 is a (negative) BCS correlation energy.

The diagonal ($j = j'$) induced matrix elements can be estimated from

$$\begin{aligned} v^\lambda_{jj} &= -\frac{2\beta_\lambda^2}{2\lambda+1}\frac{\langle j|R_0\frac{\partial U}{\partial r}|j\rangle^2}{(2j+1)}\frac{\langle j||Y_\lambda||j\rangle^2}{\hbar\omega_\lambda} \\ &\approx -\frac{0.2\beta_\lambda^2}{2\lambda+1}\frac{(50\,\text{MeV})^2}{\hbar\omega_\lambda}, \end{aligned} \tag{10.5}$$

with the approximations $D_\lambda \approx -\hbar\omega_\lambda$ for the energy denominator and $\langle j||Y_\lambda||j\rangle^2 \approx 0.1\,(2j+1)$) for the square of the reduced matrix element, as well as $\langle j|R_0\partial U/\partial r||j\rangle \approx -50$ MeV (Appendix D). Only even values of λ contribute when $j = j'$ because of the parity selection rule contained in the reduced matrix elements $\langle j||Y_\lambda||j\rangle$. There is also an angular momentum constraint $\lambda \leqslant 2j$. For ^{120}Sn, $\beta_2 = 0.119$ and $\hbar\omega_2 = 1.171$ MeV (Beer *et al.* (1970)), while an RPA estimate of the corresponding parameters for $\lambda = 4$ leads to $\beta_4 = 0.07$ and $\hbar\omega_4 = 1.2$ MeV (Gori (2002)). Making use of these values one obtains

$$v^2_{jj} = -1.2\,\text{MeV}, \quad v^4_{jj} = -0.2\,\text{MeV}, \quad v_{jj} = -1.4\,\text{MeV}, \tag{10.6}$$

a number which is also consistent with the result given in equation (9.8) (note the difference of a factor of 2 between self-energy and induced interaction; see equations (9.6) and (9.35) respectively). The same factor occurs in equations (10.2) and (10.5). It has its origin in the two possible time orderings in the phonon exchange diagram shown in Fig. 8.3(c) (see inset to Fig. 10.1).

The (typical) matrix element $v_{jj} = \langle (jj)_0|v|(j'j')_0\rangle$ ($= -1.4$ MeV) induced interaction reported in equation (10.6) is found to be of the same order of magnitude or even larger than the (attractive) bare interaction matrix elements reported in Fig. 8.5 (i.e. $-1.8 \lesssim \langle j^2(0)|v_{14}|j^2(0)\rangle \leq 0$, $j = s_{1/2}, p_{3/2}, d_{5/2}$). The fact that 'The polarization interaction resulting from the coupling to the low frequency

modes may be considerably larger than the bare force...' was discussed by Bohr and Mottelson (1975) in Section 6-5f p.432 (see also Broglia, Paar and Bes (1971a,b)).

Let us compare the induced interaction with the strength of the typical pairing force with constant matrix elements $G\,(\approx 25/A\,\text{MeV})$ tailored to reproduce the empirical value of the pairing gap $\Delta \approx 12/\sqrt{A}\,\text{MeV}$. The pairing strength G is a matrix element between uncoupled pair states and to make the comparison the states $|\,(jj)_0\rangle$ with total angular momentum zero have to be written in terms of uncoupled m-states

$$|\,(jj)_0\rangle = \sum_m \frac{(-1)^{j-m}}{\sqrt{2j+1}}|jm,\, j-m\rangle = \sum_m \frac{1}{\sqrt{(2j+1)}}|jm,\, \widetilde{jm}\rangle,$$

where $|\widetilde{jm}\rangle$ is the time reverse of the state $|jm\rangle$. The expression for the matrix element $v_{jj'}$ becomes

$$v_{jj'} = \langle (jj)_0\,|v|\,\left(j'j'\right)_0\rangle = \sum_{mm'} \frac{1}{\sqrt{(2j'+1)\,(2j+1)}}\langle jm,\, \widetilde{jm}|v|j'm',\, \widetilde{j'm'}\rangle.$$

Assuming that the matrix elements in the m-scheme are all equal, an induced pairing interaction strength can be defined by

$$G_{\text{ind}} = -\overline{\langle jm,\, \widetilde{jm}|v|j'm',\, \widetilde{j'm'}\rangle},$$

and one obtains (cf. equation (D.15))

$$\overline{\langle (jj)_0\,|v|\,(j'j')_0\rangle} = -\frac{\sqrt{(2j+1)\,(2j'+1)}}{2}G_{\text{ind}}. \tag{10.7}$$

Consequently, for $j = j'$,

$$G_{\text{ind}} = -\frac{2v_{jj}}{(2j+1)}. \tag{10.8}$$

The single neutron states near to the Fermi energy in ^{120}Sn are $d_{5/2}$, $h_{11/2}$, $s_{1/2}$, $g_{7/2}$ and $d_{5/2}$, corresponding to an average $\bar{j} = 7/2$. Making use of this value, the relation (10.8) and the estimate given in equation (10.6) one obtains $G_{\text{ind}} = 0.35\,\text{MeV}$. This number should be compared with the empirical pairing strength $G = (25/A) \approx 0.21\,\text{MeV}$. In spite of the over-simplifications of this estimate it surely indicates that the induced pairing interaction due to particle–phonon coupling can account for a significant fraction of the total pairing interaction.

The estimates of β_λ and $\hbar\omega_\lambda$ in Section 7.1 have a simple A-dependence ($\beta_\lambda \propto A^{-2/3}$ and $\hbar\omega_\lambda \propto A^{-2/3}$). Thus the matrix element

$$v^\lambda_{jj} \approx -\frac{185\,\text{MeV}}{(\lambda-1)(\lambda+2)}\frac{(1+0.001A)}{A^{2/3}} \tag{10.9}$$

https://doi.org/10.1017/9781009401920 Published online by Cambridge University Press

is approximately independent of j. The A-dependence of the induced pairing interaction strength given in equation (10.8) can be estimated by using this relation and the average degeneracy $\overline{(2j+1)}$ of a j-orbit near the Fermi level. This quantity can be calculated in terms of the mean value $\bar{k}_F = (2/3)k_F$ of the Fermi momentum ($k_F = 1.36\,\mathrm{fm}^{-1}$) and of the nuclear radius $R = 1.2A^{1/3}\,\mathrm{fm}$ ($j \approx \bar{k}_F R$) leading to $\overline{(2j+1)} \approx 2.2A^{1/3}$. Using this estimate and equations (10.1), (10.8) and (10.9) ($\lambda = 2$ and 4) we get

$$G_{\mathrm{ind}} \approx \frac{29}{A}\,\mathrm{MeV}. \tag{10.10}$$

This has the same A-dependence as the empirical pairing strength but is somewhat too large.

The following three sections present the results of detailed microscopic calculations of the induced interaction. The first is a self-consistent calculation of the pairing gap for the semi-magic nucleus ^{120}Sn as well as for Ca and Ti isotopes and the second is for a slab-model where shell effects are suppressed. Both of these calculations use Bloch–Horowitz energy denominators (10.4) which are always larger than the value $\hbar\omega_\lambda$ used for the estimates in this section. In Section 10.4 a calculation is presented based on the Dyson equation, which takes into account, aside from the bare nucleon–nucleon potential, the induced pairing interaction, on equal footing to the self-energy and vertex corrections. All of these microscopic theories give induced pairing strengths which are considerably smaller by a factor of about 2 than the estimate given in equation (10.10).

10.2 Microscopic calculations

In this section the results of a calculation of the state-dependent pairing gap associated with the induced interaction will be presented. The discussion is based on Broglia *et al.* (2001), Barranco *et al.* (1999). In the following ν refers to the pair state $|(j_\nu j_\nu)_0\rangle = |j_\nu^2(0)\rangle$ with total angular momentum zero and the matrix element (see Appendix D, equation (D.15))

$$G_{\nu\nu'} = -v_{\nu\nu'} = -\frac{2\langle j_\nu^2(0)|v|j_{\nu'}^2(0)\rangle}{\sqrt{(2j_\nu+1)(2j_{\nu'}+1)}}\,, \tag{10.11}$$

so that the normalization of $G_{\nu\nu'}$ is the same as the normalization of the induced interaction in equation (10.8), and can be directly compared with the pairing coupling constant and G ($\approx 25/A$ MeV) introduced in defining the BCS pairing Hamiltonian (Chapter 3).

The calculation of the matrix elements uses the perturbation method of Bloch and Horowitz (1958). The application of this method to nuclear problems is explained in Appendix B of Bes *et al.* (1976a). In the Bloch–Horowitz approach, the exchange of phonons (vibrations) is iterated to infinite order, by the

self-consistent solution of the set of coupled equations

$$G_{\nu\nu'} = -\sum_{\lambda n} \frac{4\beta_\lambda^2(n)}{(2j_\nu+1)(2j_{\nu'}+1)(2L+1)} \frac{\langle j_{\nu'}|R_0\frac{\partial U}{\partial r}|j_\nu\rangle^2 \langle j_{\nu'}||Y_\lambda||j_\nu\rangle^2}{E_0 - [e_\nu + e_{\nu'} + \hbar\omega_\lambda(n)]}\,, \tag{10.12}$$

with

$$E_0 = U - E_{\text{unp}}. \tag{10.13}$$

The energy E_0 in equation (10.13) is the pair-correlation energy and is the difference between the ground-state energy U including pairing correlations and the unperturbed ground state energy E_{unp}. The energies U and E_{unp} are defined explicitly in the following paragraph (see also Appendix G). The sum in equation (10.12) is taken over all multipolarities λ. The sum over n allows for the possibility that there may be several phonons with the same multipolarity. Equation (10.12) differs from (10.2) and (10.5) in several respects. The normalization is different because of the normalization (10.11) of $G_{\nu\nu'}$. In Bloch–Horowitz perturbation theory the energy denominator is the difference between the final energy of the system E_0 and the energy of the, unperturbed, intermediate state (see Fig. 10.1) $e_\nu + e_{\nu'} + \hbar\omega_\lambda(n)$. The dependence on E_0 is a feature of the Bloch–Horowitz perturbation method. The e_ν and $e_{\nu'}$ are magnitudes of single-particle energies of the states ν and ν' measured from the Fermi energy. As the correlation energy E_0 is negative, the denominator in the last factor in equation (10.12) is always negative and each term contributing to $G_{\nu\nu'}$ is positive. The expression for $G_{\nu\nu'}$ (equation (10.12)) is automatically symmetric in the initial and final states ν and ν'. Thus it is not necessary to make the *ad hoc* symmetrization as in equations (9.33), (9.34).

The unperturbed ground-state energy in equation (10.13) is

$$E_{\text{unp}} = \sum_{\substack{j_\nu \\ \varepsilon_\nu < \varepsilon_{\text{F}}}} (2j_\nu+1)(\varepsilon_\nu - \varepsilon_{\text{F}})\,. \tag{10.14}$$

where ε_ν are single-particle energies and ε_{F} is the Fermi energy. The perturbed energy is

$$U = \sum_{j_\nu} (2j_\nu+1)(\varepsilon_\nu - \varepsilon_{\text{F}})\,V_\nu^2 - \sum_{j_\nu j_{\nu'}} \frac{(2j_\nu+1)(2j_{\nu'}+1)}{4}\frac{G_{\nu\nu'}}{4}\frac{\Delta_{j_\nu}\Delta_{j_{\nu'}}}{E_{j_\nu}E_{j_{\nu'}}}. \tag{10.15}$$

Thus $E_0 = U - E_{\text{unp}}$ is the ground-state correlation energy. The gap parameters Δ_ν satisfy the gap equation

$$\Delta_{j_\nu} = \sum_{j_{\nu'}} \frac{2j_{\nu'}+1}{2}\frac{G_{\nu\nu'}\Delta_{j_{\nu'}}}{2E_{j_{\nu'}}}, \tag{10.16}$$

where the quasiparticle energies are given by

$$E_{j_\nu} = \sqrt{\left(\varepsilon_{j_\nu} - \varepsilon_{\mathrm{F}}\right)^2 + \Delta_\nu^2}\,. \tag{10.17}$$

The BCS occupation probabilities are defined by

$$V_{j_\nu}^2 = \frac{1}{2}\left(1 - \frac{\varepsilon_{j_\nu} - \varepsilon_{\mathrm{F}}}{E_{j_\nu}}\right),$$

and the Fermi energy ε_{F} is fixed by the condition

$$N = 2\sum_{j_\nu} V_{j_\nu}^2. \tag{10.18}$$

By using the gap equation (10.16) the second term in equation (10.15) can be written as a single sum

$$\sum_{j_\nu j'_\nu} \frac{(2j_\nu + 1)(2j_{\nu'} + 1)}{4} \frac{G_{\nu\nu'}}{4} \frac{\Delta_{j_\nu}\Delta_{j_{\nu'}}}{E_{j_\nu}E_{j_{\nu'}}} = \sum_{j_\nu} \frac{(2j_\nu + 1)}{2} \frac{\Delta_{j_\nu}^2}{2E_{j_\nu}} \tag{10.19}$$

The basic ingredients needed in solving these equations are the single-particle energies ε_ν and the corresponding wavefunctions $\phi_\nu(\vec{r})$, as well as the phonon energies $\hbar\omega_\lambda(n)$ and the transition probabilities

$$B\left(E\lambda : 0 \to \lambda(n)\right) = \left(\frac{3}{4\pi} ZeR^\lambda\right)^2 \beta_\lambda^2$$

of the vibrational modes. The quantities ε_ν and $\phi_\nu(\vec{r})$ are calculated assuming nucleons to move in an average field containing a spin-orbit term and parametrized in terms of a Saxon–Woods potential, with standard parameters. The vibrations are calculated in the quasiparticle random phase approximation (see equation (8.47)), adjusting the coupling constant to reproduce the energy and transition probabilities of lowest-lying vibrational states. The resulting values are, as a rule, quite close to the self-consistent value relating the potential variation to the density variation in a self-sustained normal mode of oscillation.

In Fig. 10.1 we show the calculated state-dependent pairing gap for the nucleus ^{120}Sn. The matrix elements $G_{\nu\nu'}$ are shown in Fig. 10.2 and Table 10.1. The corresponding state dependence of Δ_ν is closely connected with the strong state dependence of $G_{\nu\nu'}$. This dependence reflects the fact that scattering processes implying spin-flip are essentially possible only because of quantal fluctuations.

In any case, the average value of these matrix elements associated with states lying close to the Fermi energy is $\bar{G} = \sum_{\nu\geq\nu'} G_{\nu\nu'}/15 \approx 0.11$ MeV (see Section 9.3, discussion following equation (9.35), note that $\bar{G}$ is to be compared to $|\bar{v}|$), while the pairing-correlation energy is $E_0 \approx 4$ MeV. The value of $\bar{G}$ can be compared with the value $G \approx 0.2$ MeV of the standard parametrization $G = 25/A$ MeV. It is seen from Fig. 10.1 that the pairing gap around the Fermi energy

https://doi.org/10.1017/9781009401920 Published online by Cambridge University Press

Table 10.1. *Matrix elements $G_{\nu\nu'}$ of the induced interaction as shown in Fig. 10.2; The corresponding average value is $\bar{G} = \sum_{\nu' \geq \nu} G_{\nu\nu'}/15 = 0.11$ MeV (after Gori (2002)).*

	$d_{5/2}$	$g_{7/2}$	$s_{1/2}$	$h_{11/2}$	$d_{3/2}$
$d_{5/2}$	0.08	0.016	0.182	0.158	0.109
$g_{7/2}$	0.016	0.08	0.05	0.022	0.143
$s_{1/2}$	0.182	0.05	0	0.124	0.272
$h_{11/2}$	0.158	0.022	0.124	0.179	0.032
$d_{3/2}$	0.109	0.143	0.272	0.032	0.167

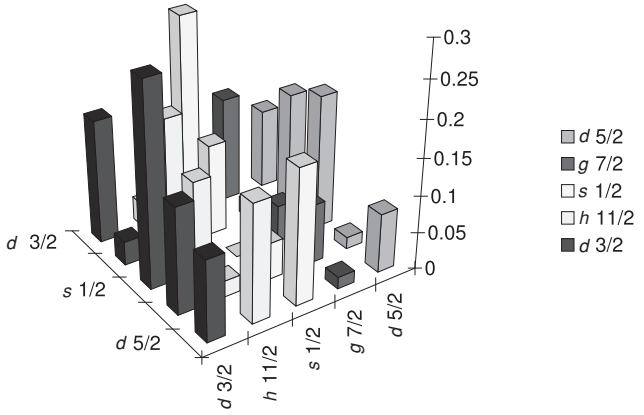

Figure 10.2. Matrix elements $G_{\nu\nu'}$ of the induced interaction defined in equations (10.11)–(10.12) used in the calculation of the state-dependent pairing gap of ^{120}Sn (equation (10.16)) shown in Fig.10.1 for levels lying close to the Fermi energy ε_F ($\varepsilon_{d_{5/2}} = -12.0$ MeV, $\varepsilon_{g_{7/2}} = -10.9$ MeV, $\varepsilon_{s_{1/2}} = -9.7$ MeV, $\varepsilon_{h_{11/2}} = -9.21$ MeV, $\varepsilon_{d_{3/2}} = -9.0$ MeV, $\varepsilon_{f_{7/2}} = -4.0$ MeV, $\varepsilon_F = -9.2$ MeV). The values on the ordinates are in MeV (after Gori (2002)).

is of the order of 0.8 MeV, which is an appreciable fraction of the empirical value of 1.4 MeV, obtained from the mass table (Audi and Wapstra (1995)) making use of the relation

$$\Delta = \tfrac{1}{2}\left[B\left(N-2, Z\right) + B\left(N, Z\right) - 2B\left(N-1, Z\right)\right], \tag{10.20}$$

where $B(N, Z)$ is the binding energy of the nucleus with N neutrons and Z protons.

Fig. 10.3 shows the value of the state-dependent pairing gap averaged over levels lying in an energy interval of the order of $\pm 2\Delta$ around the Fermi energy, for a number of Sn isotopes, in comparison with the corresponding empirical

https://doi.org/10.1017/9781009401920 Published online by Cambridge University Press

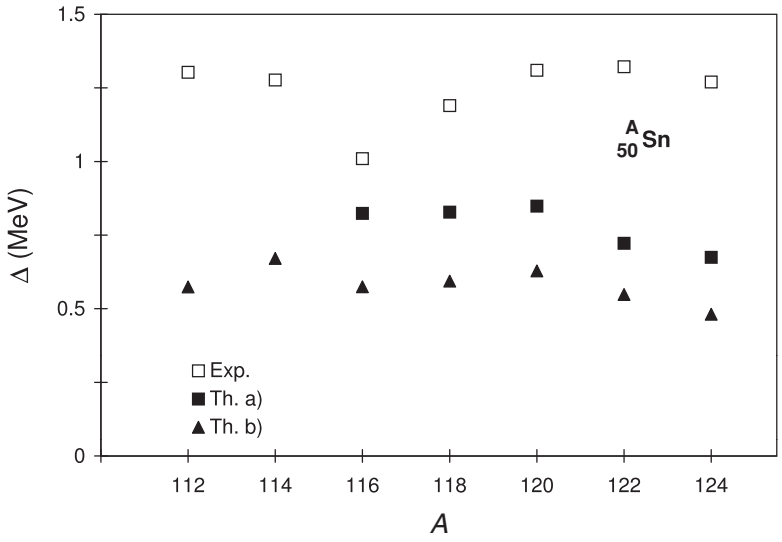

Figure 10.3. Average value of the state dependent pairing gap associated with levels lying close to the Fermi energy of $^{A}_{50}$Sn isotopes, calculated making use of the induced pairing interaction $G_{\nu\nu'}$ (equations (10.11)–(10.12)), in comparison with the empirical pairing gap (see equation (10.20)). The results of two calculations are shown, associated with RPA solutions which fit two different sets of transition probabilities associated with the low-lying quadrupole and octupole surface vibrations. The first set (also used to obtain the results reported in Fig. 10.1) was taken from Beer *et al*. (1970), Th. a). The second set is from Jonsson *et al*. (1981), Th. b). Reprinted with permission from Barranco *et al*., *Phys. Rev. Lett.* **83**:2147–50 (1999). Copyright 1999 by the American Physical Society.

values obtained from equation (10.20) and mass table. In all cases, theory accounts for a consistent fraction of the empirical values of the pairing gaps. If one were to reproduce this empirical value of Δ, one would need to add to $G_{\nu\nu'}$ an approximately constant quantity, which changes only slightly from isotope to isotope, and whose average value is $G_0 \approx 0.06\,\text{MeV}$. This corresponds to a parametrization $G_0 = X/A\,\text{MeV}$ with $X \approx 7$.

The main contribution to the state-dependent pairing gap defined in equation (10.16) arises from the exchange of low-lying surface collective modes. In fact, repeating the calculation of Δ_ν but this time including only the lowest-lying surface vibrations ($n = 1, \lambda^\pi = 2^+, 3^-, 4^+, 5^-$), one obtains results which coincide, within 20%, with those obtained from the full calculation. The main contributions arise from the exchange of low-lying quadrupole and octupole vibrations. These results are closely connected with the difference in matrix elements associated with low-lying collective surface vibrations and with giant resonances. In fact the average value of $G_{\nu\nu'}$ resulting from the coupling to vibrational states with energy $\hbar\omega_\lambda(n) \leq 7\,\text{MeV}$ is 0.08 MeV (see Fig. 10.4 and

Table 10.2. *Induced matrix elements* $(G_{\nu\nu'})_{\text{low}}$ *(in MeV) (see Fig. 10.4) (after Gori (2002)).*

	$d_{5/2}$	$g_{7/2}$	$s_{1/2}$	$h_{11/2}$	$d_{3/2}$
$d_{5/2}$	0.059	0.01	0.156	0.124	0.07
$g_{7/2}$	0.01	0.062	0.028	0.015	0.12
$s_{1/2}$	0.156	0.028	0	0.074	0.258
$h_{11/2}$	0.124	0.015	0.074	0.162	0.02
$d_{3/2}$	0.07	0.12	0.258	0.02	0.162

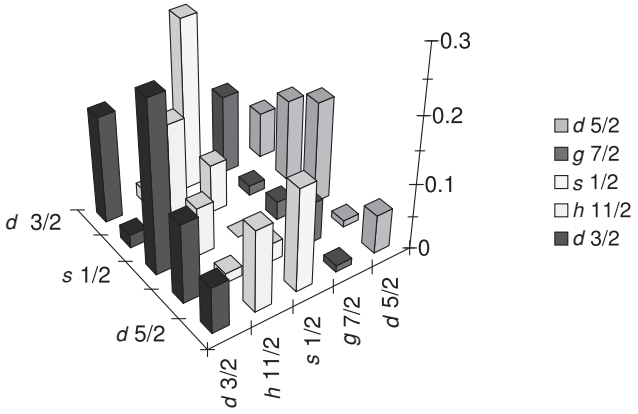

Figure 10.4. Induced interaction matrix elements $(G_{\nu\nu'})_{\text{low}}$ (in MeV) associated with the exchange between nucleons moving in time-reversal states close to the Fermi energy ε_{F} of ^{120}Sn of low-lying ($\hbar\omega(n) \leq 7\,\text{MeV}$) surface vibrations ($\lambda^{\pi} = 2^{+}, 3^{-}, 4^{+}, 5^{-}$) (after Gori (2002)).

Table 10.2), while that associated with the coupling to vibrational states with $\hbar\omega_{\lambda}(n) > 7\,\text{MeV}$ is 0.03 MeV (see Fig. 10.5 and Table 10.3). One expects that this small average value would become even smaller by considering the fact that giant resonances are not sharp states but display a damping width.

Because low-lying surface vibrations are built, to some extent, by the same valence nucleons which participate in the Cooper pair formation, one would expect that the values of $(G_{\nu\nu'})_{\text{low}}$ shown in Fig. 10.4 (and thus the total value $G_{\nu\nu'} = (G_{\nu\nu'})_{\text{low}} + (G_{\nu\nu'})_{\text{high}}$ shown in Fig. 10.2 as well as Δ_{ν} (Fig. 10.1) will be somewhat modified by Pauli principle corrections. In fact, it is found that these corrections modify (reduce), as a rule, the value of Δ_{ν} by about 10% from the value obtained by making use of equation (10.12) (Appendix F). This correction is expected to be larger in the case of light, halo nuclei (see next chapter).

https://doi.org/10.1017/9781009401920 Published online by Cambridge University Press

Table 10.3. *Matrix elements* $(G_{\nu\nu'})_{\text{high}}$ *(in MeV) as shown in Fig. 10.5 (after Gori (2002)).*

	$d_{5/2}$	$g_{7/2}$	$s_{1/2}$	$h_{11/2}$	$d_{3/2}$
$d_{5/2}$	0.026	0.007	0.04	0.044	0.048
$g_{7/2}$	0.007	0.025	0.025	0.009	0.036
$s_{1/2}$	0.04	0.025	0	0.064	0.046
$h_{11/2}$	0.044	0.009	0.064	0.042	0.016
$d_{3/2}$	0.048	0.036	0.046	0.016	0.027

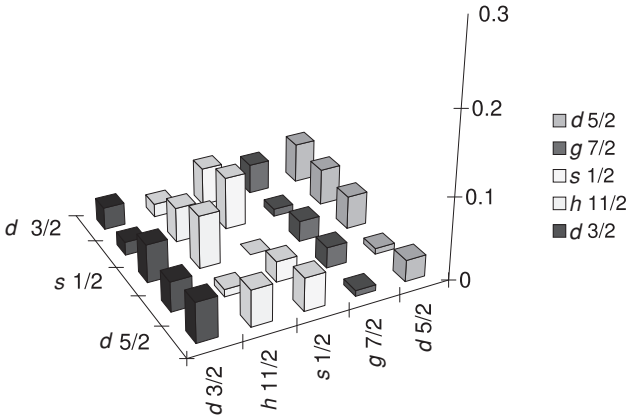

Figure 10.5. Induced matrix elements $(G_{\nu\nu'})_{\text{high}}$ (in MeV) associated with the exchange of high-lying vibrations (essentially giant resonances) with $\hbar\omega_\lambda(n) > 7\,\text{MeV}$ and ($\lambda^\pi = 2^+, 3^-, 4^+$ and 5^-) between nucleons moving in time-reversal states close to the Fermi energy ε_F of ^{120}Sn (after Gori (2002)).

In Fig. 10.6 the results of calculations of the pairing gap carried out as explained above for the isotopes ^{A}Ca and ^{A}Ti are shown compared with the empirical values obtained with the help of equation (10.20). The average value of $G_{\nu\nu'}$ associated with levels lying close to the Fermi energy is, in this case, of the order of 0.2 MeV, while E_0 is of the order of -3 MeV. The induced interaction leads to pairing gaps which again, in these cases, account for a consistent fraction of the empirical value. The results furthermore display a similar dependence on A to that displayed by the experimental values, a dependence which reflects the shell dependence of the collective surface modes. In particular, the low predicted value of Δ in ^{50}Ca compared with ^{42}Ca is due to the fact that the 'core' ^{48}Ca is more rigid than the core ^{40}Ca, as can be seen from Fig. 10.7 where the β_2 and β_3 values associated with the different Ca-isotopes are reported.

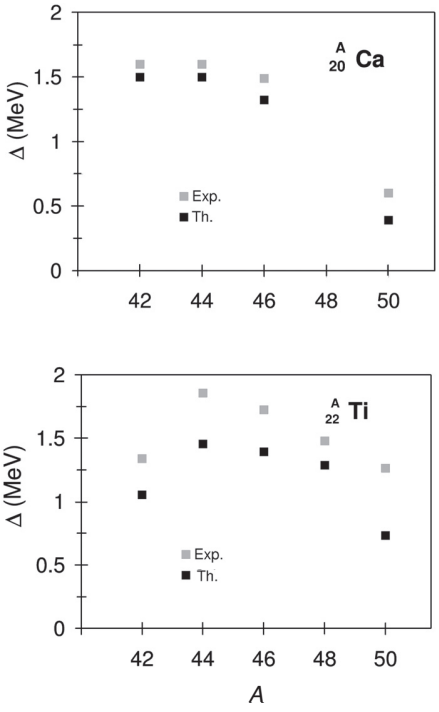

Figure 10.6. Average value of the state-dependent pairing gap associated with levels lying close to the Fermi energy of the ^{A} Ca- and the ^{A}Ti-isotopes, compared with the experimental data calculated by making use of the relation $\Delta = \frac{1}{2}[B(N-2, Z) + B(N, Z) - 2B(N-1, Z)]$, where $B(N, Z)$ is the binding energy of the nucleus with N protons and Z neutrons, after Gori (2002).

Within this context it is interesting to note that the corresponding quantities for the Sn-isotopes are essentially constant as a function of A (see Fig. 10.8)), a fact which is intimately connected with the essential constancy, as a function of A, observed in the gap of the Sn-isotopes (see Fig. 10.3).

The results discussed in this section may provide, at the microscopic level, insight into the success found by surface and density-dependent pairing interactions used in the literature to describe the low-energy nuclear structure (Green and Mozkowski (1965), Faessler (1968), Bertsch and Esbensen (1991)).

Let us conclude this section by noting that, because collective vibrations couple democratically to all nucleons, regardless of their isospin quantum number, the induced pairing-force mechanism is expected to lead to a consistent proton–neutron pairing correlation, as well as to multipole (in particular quadrupole) pairing correlations. Although the field has not been explored, calculations carried out in ^{42}Sc (Barranco *et al.* (1999)) indicate this to be the case.

https://doi.org/10.1017/9781009401920 Published online by Cambridge University Press

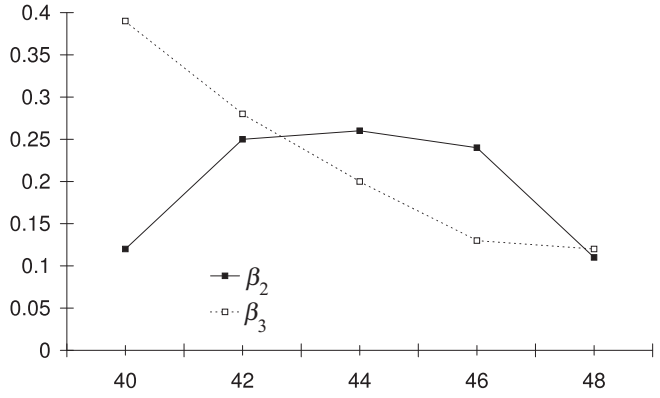

Figure 10.7. Value of the deformation parameters β_2, β_3 for the Ca-isotopes (after Gori (2002)).

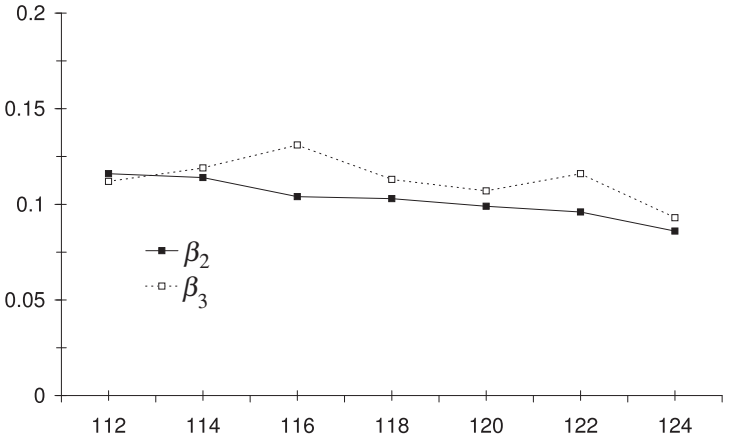

Figure 10.8. Value of the deformation parameters β_2, β_3 for the Sn-isotopes (Jonsson *et al.* (1981)) (after Gori (2002)).

10.3 Slab model

To assess the universality of the results presented in the previous section, we shall study the induced pairing interaction in a system free of shell effects, but retaining the properties associated with the confinement of nucleons by an elastic surface. For this purpose we use the slab model for semi-infinite nuclear matter proposed by Esbensen and Bertsch (1984a,b) and Bertsch and Esbensen (1985). In the present section the aim is to study the induced interaction between nucleons due to coupling with surface modes. The discussion here is based on the work of Giovanardi *et al.* (2002). The collective response of the nuclear surface is approximated by the RPA response function and the coupling of the nucleon motion to the surface vibrations is calculated self-consistently.

https://doi.org/10.1017/9781009401920 Published online by Cambridge University Press

In the theory of Esbensen and Bertsch (1984a,b) the nucleons are confined in the half-space $z < 0$ by the one-dimensional Fermi-like potential

$$V(z) = V_0(1 + e^{-z/a})^{-1}. \tag{10.21}$$

The single-particle wavefunctions in the potential (10.21) can be written as

$$\Phi_\nu(\vec{r}) = \mathrm{e}^{\mathrm{i}\vec{k}_{\nu\mathrm{p}}\cdot\vec{r}_\mathrm{p}}\phi_\nu(z). \tag{10.22}$$

The corresponding energy eigenvalues and momentum parallel to the surface are $\varepsilon_\nu = \frac{\hbar^2 k_{\nu\mathrm{p}}^2}{2m} + \varepsilon_{\nu z}$ where $\vec{k}_{\nu\mathrm{p}} = (k_{\nu x}, k_{\nu y}, 0)$. The vector $\vec{r}_\mathrm{p}$ is parallel to the plane of the surface of the slab $(x, y, 0)$. The wavefunctions $\phi_\nu(z)$ are solutions of the single-particle Schrödinger equation

$$\left(\frac{-\hbar^2}{2m}\frac{\mathrm{d}^2}{\mathrm{d}z^2} + V(z)\right)\phi_\nu(z) = \varepsilon_{\nu z}\phi_\nu(z), \tag{10.23}$$

normalized so that, for $z \to -\infty$,

$$\phi_\nu(z) = \sqrt{2}\cos(k_{\nu z}z + \theta_\nu), \tag{10.24}$$

where $k_{\nu z}$ is the asymptotic wavenumber and θ_ν a phase.

The next step in the calculation of the induced interaction consists in determining the vibrational modes of the system. For this purpose one diagonalizes the surface-peaked separable interaction

$$v(\vec{r}, \vec{r}') = k_0 g(|\vec{r}_\mathrm{p} - \vec{r}'_\mathrm{p}|)V'(z)V'(z'), \tag{10.25}$$

in a particle–hole basis and in the harmonic approximation (RPA). The quantity $V'(z)$ is the derivative of the potential defined in equation (10.21). The finite-range Yukawa interaction acting in the x, y-direction,

$$g(|\vec{r}_\mathrm{p} - \vec{r}'_\mathrm{p}|) = \frac{e^{|\vec{r}_\mathrm{p} - \vec{r}\,'_\mathrm{p}|/a_r}}{2\pi a_r |\vec{r}_\mathrm{p} - \vec{r}'_\mathrm{p}|}, \tag{10.26}$$

with $a_r = 1\,\mathrm{fm}$, has been chosen so as to give a realistic value of the nuclear surface tension ($1\,\mathrm{MeV/fm^2}$). The coupling strength κ_0 is determined by the relation

$$\kappa_0^{-1} = \int \mathrm{d}z\rho_0'(z)V'(z), \tag{10.27}$$

which expresses the self-consistent condition existing between density and potential fluctuations associated with the normal modes. Diagonalizing the interaction given in equation (10.26) in the harmonic approximation (RPA) one can construct the linear response function

$$R^{\mathrm{RPA}}(K, \hbar\omega) = \frac{R^0(K, \hbar\omega)}{1 - \kappa_0\tilde{g}(K)R^0(K, \hbar\omega)}. \tag{10.28}$$

https://doi.org/10.1017/9781009401920 Published online by Cambridge University Press

It is written in terms of the unperturbed response $R^0(K, \hbar\omega)$ which, in the slab model, can be accurately parametrized by an oscillator response function

$$R^0(K, \hbar\omega) = \frac{N}{\hbar}\left(\frac{1}{(\omega-\omega_0)+\mathrm{i}\gamma/2} - \frac{1}{(\omega+\omega_0)+\mathrm{i}\gamma/2}\right). \tag{10.29}$$

The energy centroid $\hbar\omega_0(K)$, the width $\hbar\gamma(K)$ and normalization strength $N(K)$ are functions of K. The function

$$\tilde{g}(K) = \frac{1}{\sqrt{1+(a_r K)^2}} \tag{10.30}$$

is the kernel of the two-dimensional Fourier transform

$$g(|\vec{r}_\mathrm{p} - \vec{r}\,'_\mathrm{p}|) = \int \frac{\mathrm{d}^2K}{(2\pi)^2}\, \mathrm{e}^{\mathrm{i}\vec{K}(\vec{r}_\mathrm{p}-\vec{r}\,'_\mathrm{p})}\, \tilde{g}(K).$$

The unperturbed strength function is proportional to the imaginary part of $R^0(K, \hbar\omega)$,

$$S_0(K, \hbar\omega) = -\frac{1}{\pi}\,\mathrm{Im}\, R^0(K, \hbar\omega). \tag{10.31}$$

It is a symmetric function of K and is antisymmetric in ω.

The RPA strength function is an even function of K and an odd function of ω. It can be expressed in terms of the unperturbed response as

$$S^\mathrm{RPA}(K, \hbar\omega) = \left(\frac{S_0(K, \hbar\omega)}{\left(1+\kappa\,\mathrm{Re}\, R^0(K, \hbar\omega)\right)^2 + (\kappa\pi S_0(K, \hbar\omega))^2}\right), \tag{10.32}$$

where $\kappa(K) = \kappa_0\tilde{g}(K)$. Esbensen and Bertsch showed that the denominator in equation (10.32) vanishes when $\omega = 0$ and $K = 0$ because of the self-consistency condition (10.27). When ω and K are small

$$S^\mathrm{RPA}(K, \hbar\omega) \propto \frac{\omega}{\omega^2 + \alpha K^2}, \tag{10.33}$$

where α depends on the parameters in S_0 and $\tilde{g}(K)$.

Now we consider the process in which pairs of nucleons moving in time-reversal states exchange the eigenmodes of equation (10.28). We shall denote by $k_{\nu\mathrm{p}}$ and $k_{\nu'\mathrm{p}}$ the momentum of the single-particle states in the initial and in the final channels respectively, in a plane parallel to that of the surface while $k_{\nu z}$ and $k_{\nu' z}$ denote the asymptotic momentum along the z-direction. The wavenumber $\vec{K}$ of the exchanged phonon is fixed by the relation expressing the parallel momentum conservation, i.e.

$$\vec{K} = \vec{k}_{\nu\mathrm{p}} - \vec{k}_{\nu'\mathrm{p}}.$$

https://doi.org/10.1017/9781009401920 Published online by Cambridge University Press

The equation corresponding to (10.12) for the induced pairing matrix element in the microscopic calculation in Section 12.2 can be written as

$$G_{\nu\nu'}(K) = 2(\kappa_0 \tilde{g}(K))^2 M^2_{\nu\nu'} \times \int_0^\infty \mathrm{d}\hbar\omega \, \frac{S^{\mathrm{RPA}}(K, \hbar\omega)}{E_0 - (|e_\nu| + |e_{\nu'}| + \hbar\omega)}. \quad (10.34)$$

The single-particle energies are defined by $e_j \equiv \varepsilon_j - \varepsilon_{\mathrm{F}}$ $(j = \nu, \nu')$, where ε_{F} is the Fermi energy while

$$\varepsilon_\nu \equiv \varepsilon_{\nu\mathrm{p}} + \varepsilon_{\nu z} = \frac{\hbar^2 k^2_{\nu\mathrm{p}}}{2m} + \varepsilon_{\nu z}, \quad (10.35)$$

$$\varepsilon_{\nu'} \equiv \varepsilon_{\nu'\mathrm{p}} + \varepsilon_{\nu' z} = \frac{\hbar^2}{2m} \left(\vec{k}_{\nu\mathrm{p}} - \vec{K}\right)^2 + \varepsilon_{\nu' z}. \quad (10.36)$$

The surface interaction matrix element is

$$M_{\nu\nu'} = \int \mathrm{d}z \, \phi^*_{k_{\nu' z}}(z) V'(z) \phi_{k_{\nu z}}(z). \quad (10.37)$$

and E_0 is the pair-correlation energy. Equation (10.34) has the same Bloch–Horowitz energy denomination as the induced pairing interaction in Section 10.2.

The total number of particles in the slab is

$$A = 2V \int \frac{\mathrm{d}^3 k}{(2\pi)^3} V^2(\vec{k}), \quad (10.38)$$

where V is the volume of the system. It is related to the surface area S and the thickness d of the slab by

$$V = S \cdot d.$$

This relation can be used to make a connection with finite nuclei. Putting $V = \frac{4}{3}\pi R^3$ and $S = 4\pi R^2$ in the surface area, one obtains

$$d = 0.4 \, A^{1/3}. \quad (10.39)$$

In the framework of Bloch–Horowitz perturbation theory, the BCS number and gap equations

$$N = 2V \int \frac{\mathrm{d}^2 k}{(2\pi)^3} V^2(k), \quad (10.40)$$

$$\Delta(\vec{k}_\nu) = 2d^{-1} \int \frac{\mathrm{d}^3 k_{\nu'}}{(2\pi)^3} \frac{G_{\nu\nu'}(K)}{2} U(\vec{k}_{\nu'}) V(\vec{k}_{\nu'}) \quad (10.41)$$

are solved self-consistently. The induced pairing matrix element $G_{\nu\nu'}(K)$ diverges when $K = 0$ because of the $1/\omega$ singularity in the unperturbed strength function. The approximation (10.33) for S^{RPA} which holds for small values of

https://doi.org/10.1017/9781009401920 Published online by Cambridge University Press

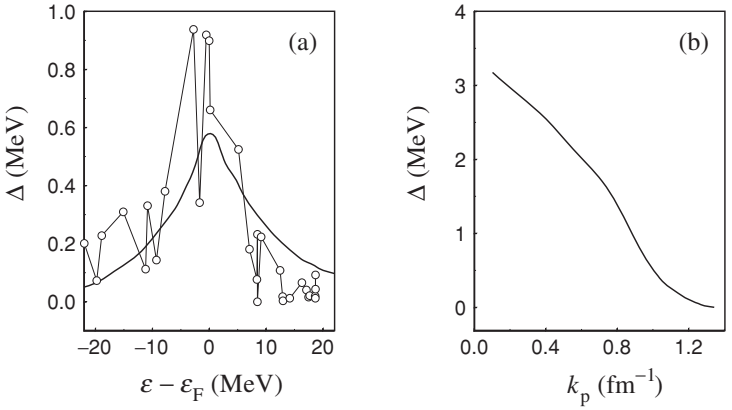

Figure 10.9. (a) Pairing gap of particles as a function of the particle energy $\varepsilon - \varepsilon_F = (\hbar k_\nu)^2/(2m) - \varepsilon_F$, for $R = 6$ fm. For each energy value, the pairing gap Δ has been calculatd as an average over the gaps of particles having the same k_ν^2. Detailed results for the nucleus ^{120}Sn are also shown (open dots, see Fig. 10.1). (b) The pairing gap of a particle at the Fermi energy as a function of the momentum component parallel to the surface of the slab. The gap goes to zero when $(k_\nu)_p = 1.337\,\text{fm}^{-1}$, corresponding to the case of particles moving in a plane parallel to the surface of the slab ($k_z = 0$). Reprinted with permission from Giovanardi *et al*., *Phys. Rev.* **C65**: 041304 (R) (2002). Copyright 2002 by the American Physical Society.

ω and K shows that $G_{\nu\nu'}(K)$ diverges as $\ln|K|$ for small K. Because this divergence is only logarithmic the integral in the gap equation converges. Equation (10.31) shows that $g(K) = 1$ for a zero-range interaction ($a_r = 0$) and that $g(K) \propto 1/(a_r K)^2$ for large K for a finite range interaction. Hence, because of the factor $g(K)$ in equation (10.34), the finite-range Yukawa interaction suppresses the high K contributions to $G_{\nu\nu'}(K)$. This corresponds to the high multipolarity surface vibrations in finite nuclei.

In the remainder of this section we discuss numerical results obtained by Giovanardi *et al*. (2002). They take the depth of the potential in equation (10.21) to be $V_0 = -45$ MeV with a diffusivity $a = 0.75$ fm. Because of the finite thickness of the slab the pairing gap $\Delta(\vec{k}_\nu)$ is not an isotropic function of $\vec{k}_\nu$. An energy-dependent pairing gap can be defined by averaging $\Delta(\vec{k}_\nu)$ over all the single-particle states with the same single-particle energy. This state-dependent pairing gap is shown in Fig. 10.9(a) as a function of $\varepsilon - \varepsilon_F = (\hbar k_\nu)^2/(2m) - \varepsilon_F$ for $R = 6$ fm ($A \approx 120$). The results for the nucleus ^{120}Sn from Section 10.2 are also shown (see Fig. 10.1). As expected, the pairing gap peaks at the Fermi surface, the associated FWHM reflecting the frequency distribution of the linear response of the system. In Fig. 10.9(b) we display the pairing gap associated with a particle at the Fermi energy as a function of the momentum component k_ν lying in the (x, y)-plane parallel to the surface of the slab. The marked decrease

https://doi.org/10.1017/9781009401920 Published online by Cambridge University Press

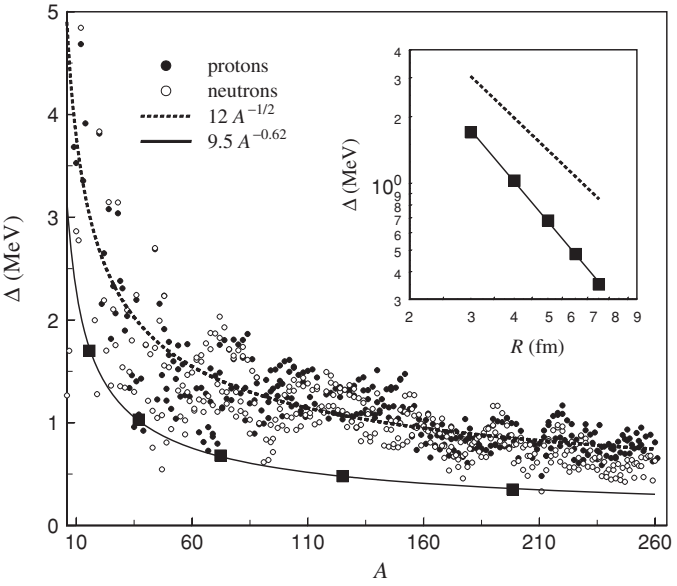

Figure 10.10. The experimental pairing gap of neutrons (open dots) and protons (solid dots) as a function of the mass number A, calculated from the nuclear binding energies (see equation (10.20)) are described, on average, by the function $12A^{-1/2}$ MeV (dotted curve) (Bohr and Mottelson (1969)). The solid squares show the results of the self-consistent solution of equations (10.34)–(10.41), results which are well fitted by the expression $\Delta = 9.5A^{-0.62}$ MeV. In the inset, the same results are displayed as a function of the nuclear radius R in a log-log scale, to emphasize the different behaviour of the two power laws. Reprinted with permission from Giovanardi *et al*., *Phys. Rev.* **C65**: 041304 (R) (2002). Copyright 2002 by the American Physical Society.

of Δ as a function of k_v testifies to the surface origin of the induced pairing interaction $G_{vv'}$ (equation (10.34)).

Following equations (10.41) and (10.40) the pairing gap should scale according to $A^{-1/3}$. This is, however, altered by the averaging and by the discrete spectrum of energies ε_{v_z} associated with motion in the z-direction.

In Fig. 10.10 we show the pairing gap Δ_{slab}, obtained by solving equations (10.34)–(10.41), and averaging $\Delta(k_v)$ over single-particle states with energy $|\varepsilon_v - \varepsilon_{\text{F}}| \leq 4$ MeV. The results are well fitted by the power law

$$\Delta_{\text{slab}} \approx \frac{9.5}{A^{0.62}} \text{ MeV}, \tag{10.42}$$

where the exponent of the mass number A is quite close to 2/3, typical of surface phenomena. In keeping with the fact that the experimental values are reproduced, on average, by the standard expression given in equation (1.30), i.e.

$$\Delta_{\text{exp}} \approx 12/\sqrt{A}\ , \tag{10.43}$$

https://doi.org/10.1017/9781009401920 Published online by Cambridge University Press

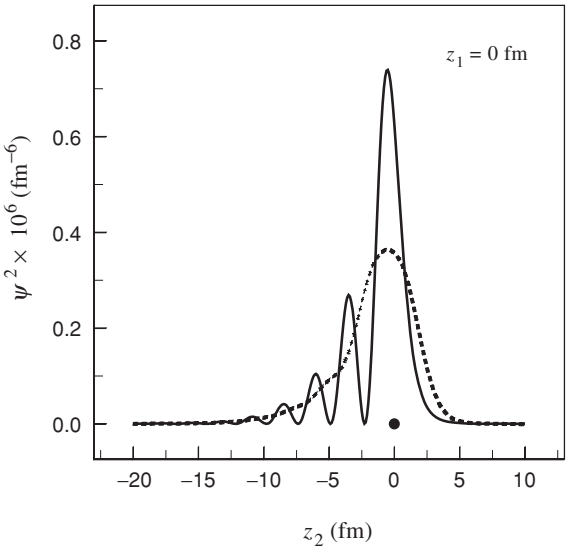

Figure 10.11. Plot of ψ^2 (equation (10.44)), for $R = 6$ fm and for particles with zero relative parallel coordinate ($R_\mathrm{p} = 0$), obtained fixing the coordinate of one particle (z_1, solid dot), as a function of the coordinate of the second particle (z_2). The surface of the slab is located at $z = 0$. Also shown is the value of ψ^2 averaged over an interval of ≈ 5 fm (dashed curve). Reprinted with permission from Giovanardi *et al*., *Phys. Rev.* **C65**: 041304 (R) (2002). Copyright 2002 by the American Physical Society.

one concludes that $\Delta_\mathrm{slab} \approx (0.45 \pm 0.04)\Delta_\mathrm{exp}$. In other words, the induced pairing interaction leads to pairing gaps which are of the order of 50% of those experimentally observed, a result which is similar to that obtained in the case of detailed calculations in finite nuclei.

To account for the experimental pairing gap, one needs to add to the interaction $G_{\nu\nu'}$ an extra contribution which we shall parametrize as G_0/A. One finds that $G_0 \approx (0.4 \pm 0.1)G$, where G/A is the strength of the pairing interaction which reproduces the experimental data (see Fig. 10.10, dotted curve). In particular, in the case of $R = 7$ fm, i.e. $A = 200$, one obtains $G = 27$ MeV, while $G_0 = 17$ MeV.

The results shown in Figs. 10.11 and 10.12 provide further insight into the role that the surface of a confined Fermi liquid has in the formation of Cooper pairs. In Fig. 10.11, the modulus squared of the anomalous density (closely connected with the Cooper pair wavefunction)

$$\psi(z_1, z_2, R_\mathrm{p}) = \int \frac{\mathrm{d}k_\mathrm{p}}{2\pi} k_\mathrm{p} J_0(k_\mathrm{p} R_\mathrm{p}) \int \frac{\mathrm{d}k_z}{2\pi} \phi_{k_z}(z_1)\phi_{k_z}(z_2) \times U(k_\mathrm{p}, k_z)V(k_\mathrm{p}, k_z), \tag{10.44}$$

https://doi.org/10.1017/9781009401920 Published online by Cambridge University Press

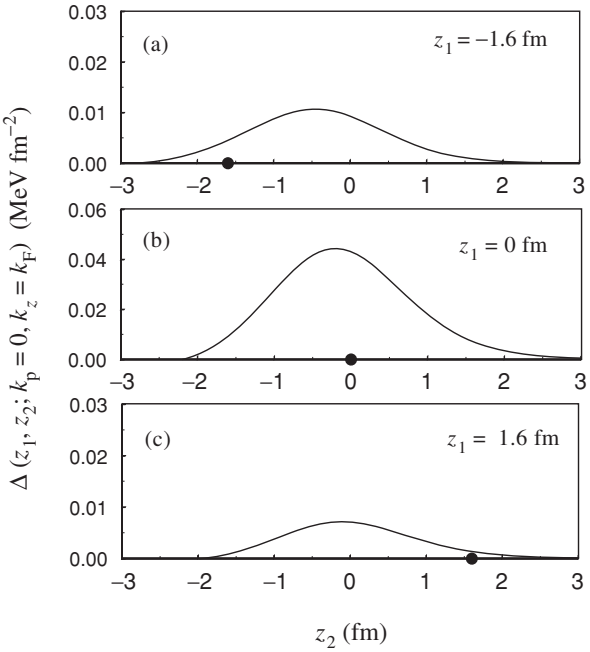

Figure 10.12. Pairing gap calculated, for $R = 6$ fm, as the product of the anomalous density ψ (equation (10.44)) and the induced interaction v (equation (10.45)), as a function of the z-coordinate of one of the two particles (z_2), giving the coordinate of the other particle (z_1) fixed values. Reprinted with permission from Giovanardi *et al*., *Phys. Rev.* **C69**: 041304 (R) (2002). Copyright 2002 by the American Physical Society.

is shown as a function of the coordinate z_2 of one of the particles, fixing the coordinate $z_1(= 0)$ of the other particle on the surface. In the above equation, J_0 is a Bessel function and R_p is the distance between particles in the direction parallel to the surface of the slab. Making use of the function ψ we have calculated the mean square radius $< r^2 >^{1/2} = \left(\int d^3r\ r^2|\psi|^2 / \int d^3r|\psi^2|\right)^{1/2}$ of the Cooper pair, obtaining 22 fm. This quantity is closely connected with the coherence length $\xi = \hbar v_F/\pi\Delta$ of the pair. Because $\varepsilon_F \approx 36$ MeV and $\Delta \approx 0.6$ MeV at the Fermi energy, one obtains, from this simple estimate, $\xi = 28$ fm.

The pairing gap $\Delta(z_1, z_2, R_p) = G_{\nu\nu'}(z_1, z_2, R_p) \times \psi(z_1, z_2, R_p)$ is obtained by multiplying the anomalous density by the induced interaction, defined in equation (10.34), a quantity which depends on e_ν and $e_{\nu'}$. For single-particle levels lying close to the Fermi energy we can neglect this dependence and write

$$G(z_1, z_2, R_p) = 2 \int \frac{d^2K}{2\pi^2} k_0^2 \tilde{g}(K) \frac{V'(z_1)V'(z_2)}{d^2} e^{iKR_p} \times \int d\hbar\omega \frac{\mathrm{Im}R^{RPA}(K, \omega)}{E_0 - \hbar\omega}. \quad (10.45)$$

https://doi.org/10.1017/9781009401920 Published online by Cambridge University Press

In Fig. 10.12, the Fourier transform $\Delta(z_1, z_2, k_\mathrm{p})$ of the quantity $\Delta(z_1, z_2, R_\mathrm{p})$, in a plane parallel to the surface, and setting $k_\mathrm{p} = 0$, is shown as a function of the z_2-coordinate of one of the two particles, and the other coordinate z_1 is given a fixed value. As expected, the probability that the two partners of a Cooper pair are close together, and thus that the associated pairing gap is large, is higher at the surface of the slab than elsewhere.

10.4 Induced pairing interaction, effective mass and vertex correction processes

As discussed in Section 9.3 there is an intimate relation between the self-energy process renormalizing the mass of the nucleons (ω-mass) and the pairing gap arising from Cooper pair formation through the exchange of surface vibrations between nucleons moving in time-reversal states close to the Fermi surface. In the above calculations the ω-dependence of the effective mass has been neglected. While this approximation is the same as that employed in the standard treatment of pairing leading to BCS number and gap equations (see Chapter 3), its range of validity is an open question. This is because setting $m^* = m$ implies that the occupation probability of the single-particle states is either 1 ($\varepsilon_\nu \leq \varepsilon_\mathrm{F}$) or 0 ($\varepsilon_\nu > \varepsilon_\mathrm{F}$). Consequently, they can fully participate in the processes leading to pair formation and thus to nuclear superfluidity. On the other hand, in the case in which $m^* = \frac{m_\omega m_k}{m} \approx m$, although apparently identical to the previous one, the spectroscopic factor associated with single-particle states lying close to the Fermi energy is $Z_\omega \approx (m_\omega/m)^{-1}$ (see equation (9.23)). Because $m_\omega/m > 1$, $Z_\omega < 1$, implying that the nucleons spend part of their time in more complicated configurations, configurations which make use also of empty states within the independent-particle approximation leading to an effective reduction of the space available to the particles to correlate ($\Omega_\mathrm{eff} < \Omega$). Consequently, these single-particle states can participate less effectively in producing the nuclear condensate, a handicap which is further accentuated by taking into account the splitting of the single-particle strength (see equation (9.41) and Section H.4).

10.4.1 Solution of the Dyson equation for normal and abnormal densities

Barranco *et al*. (2004) have investigated these questions in the case of a typical superfluid nucleus, i.e. ^{120}Sn. The formalism used is based on the Dyson equation (Terasaki *et al*. (2002a,b), Van der Sluys *et al*. (1993)). It gives a consistent description of the dressed, single-particle state $\tilde{a}$ of an odd nucleon renormalized by the (collective) response of all the other nucleons (Figs. 10.13(a)–10.13(d)), the renormalization of the energy $\hbar\omega_\nu$ (Figs. 10.14(a)–10.14(b)) and of the transition probability B(Eλ) (Figs. 10.14(c)–10.14(f)) of the collective vibrations of the even system (correlated particle–hole excitations), and the induced interaction

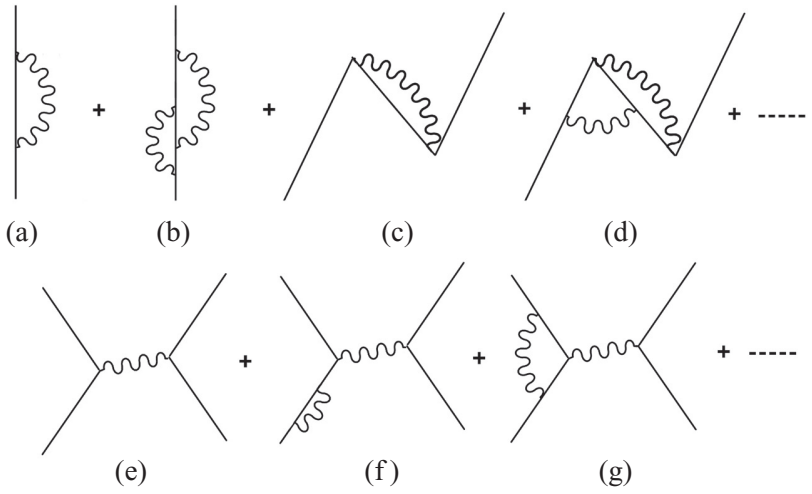

Figure 10.13. Renormalization processes arising from the particle-vibration coupling phenomenon. A line indicates quasiparticles obtained from BCS theory, making use of the mean-field single-particle states of the Skyrme parametrization Sly4 and the nucleon–nucleon v_{14} Argonne potential. The wavy line indicates the vibrational states (after Broglia *et al*. (2004)).

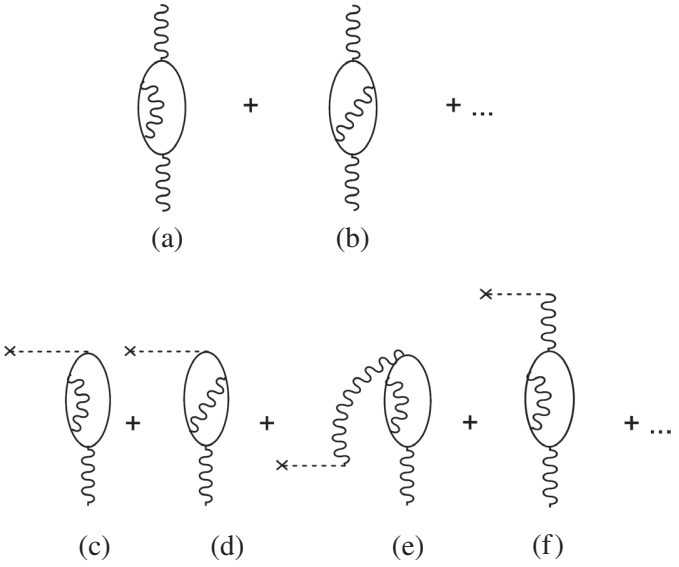

Figure 10.14. Most relevant processes taken into account in the renormalization of the energy of the phonon (a,b) and of the associated transition strength (c–f).

https://doi.org/10.1017/9781009401920 Published online by Cambridge University Press

due to the exchange of collective vibrations between pairs of nucleons, moving in time-reversal states close to the Fermi energy (Figs. 10.13(e)–10.13(g)). It includes both self-energy and vertex correction processes. Within this framework, the self-consistency existing between the dynamical deformations of the density and of the potential sustained by 'screened' particle-vibration coupling vertices leads to renormalization effects which stabilize the collectivity and the self-interaction of the elementary modes of nuclear excitation, in particular of the low-lying surface vibrational modes. This procedure produces a rather accurate description of experimental findings, in terms of very few parameters, namely: the k-mass m_k (equations (8.19) and (8.17)) and the particle-vibration coupling vertex $V(j, j' : \lambda)$ (see equation (8.31)).

A Skyrme interaction (Sly4 parametrization, with $m_k \approx 0.7m$) was used to determine the properties of the bare single-particle states, while the resulting particles were allowed to interact through the Argonne V_{14} nucleon–nucleon interaction, as well as to exchange phonons.

As seen from Fig. 10.15, Hartree–Fock theory is not able to account for the experimental quasiparticle energies of the low-lying states. Diagonalizing the

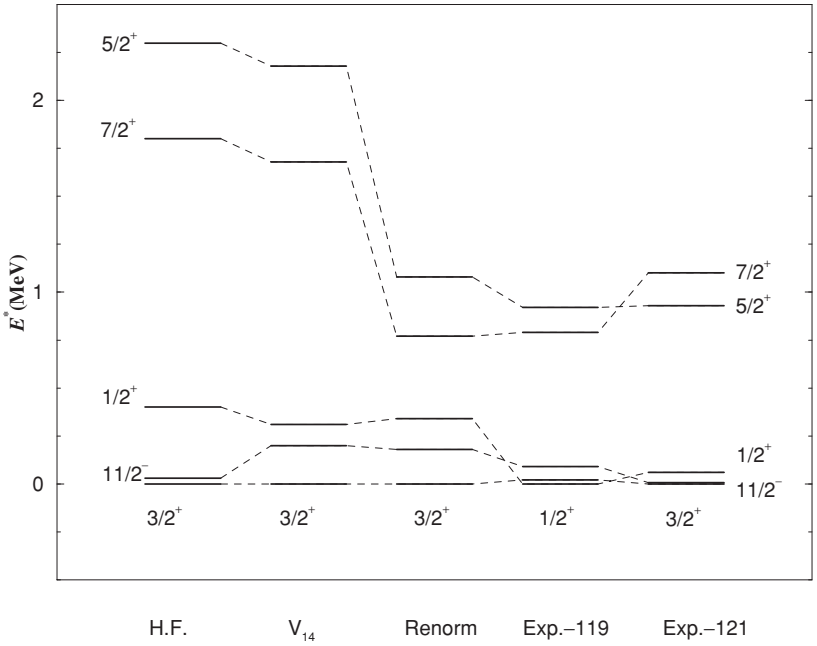

Figure 10.15. The spectra of the lowest quasiparticle states in ^{120}Sn calculated using Hartree–Fock theory, BCS with the Argonne V_{14} potential, and after renormalization, are compared with the experimental levels in the odd neighbouring nuclei ^{119}Sn and ^{121}Sn (after Barranco *et al*. (2004)).

https://doi.org/10.1017/9781009401920 Published online by Cambridge University Press

Table 10.4. *The energy and reduced E2 transition strength of the low-lying 2^+ state, calculated according to different theoretical models, are compared to the experimental values (Stelson et al. (1970)) (after Barranco et al. (2004)).*

	$\hbar\omega_{2+}$ (MeV)	B(E2 ↑) (e^2 fm^4)
RPA (Gogny)	2.9	660
RPA (Sly4)	1.5	890
RPA + renorm	0.9	2150
Exp.	1.2	2030

Argonne V_{14} nucleon–nucleon potential in the Hartree–Fock basis, within the framework of the BCS approximation including scattering states up to 800 MeV above the Fermi energy (to achieve convergence, repulsive core) in a spherical box of radius equal to 15 fm, one obtains the state-dependent pairing gap shown in Fig. 8.9 (labelled V_{14}). The resulting pairing gap (average value for levels around the Fermi energy) accounts for about half of the empirical pairing gap value (≈ 1.4 MeV) obtained from the odd–even mass difference. In keeping with this result, the quasiparticle spectrum (see Fig. 10.15), although being slightly closer to the experimental findings than that predicted by Hartree–Fock theory, displays large discrepancies with observations. The situation is rather similar concerning the low-lying quadrupole vibration of ^{120}Sn calculated in the QRPA with standard effective nucleon–nucleon interactions like Gogny or Skyrme forces. While energy is predicted too high, which may not be very important, the B(E2) value is too small by about a factor of 3 (see Table 10.4), a result which calls for a better theory.

In fact, renormalizing the energy and the transition strength of the 2^+ phonon, i.e. considering couplings of the type depicted in Fig. 10.14, couplings which have been shown to be essential in determining, for example, the width of giant resonances (see Fig. 8.16), one obtains an increase of the B(E2) transition probability which brings theory essentially in agreement with experiment (see Table 10.4). The most important processes which renormalize the energy of the phonon are shown in Figs. 10.14(a) and (b). Other graphs which are also of fourth order in the particle-vibration coupling vertex, but contain intermediate states with more than four quasiparticle states, lead to very small contributions. This is because these terms not only involve larger denominators, but also, because of their higher degree of complexity, give rise to contributions with 'random' phases which tend to cancel each other. This is a consequence of the fact that, while cancellation between the contribution associated with graphs (a) and (b) of Fig. 10.14 is strong in the particle–hole channel, the opposite is

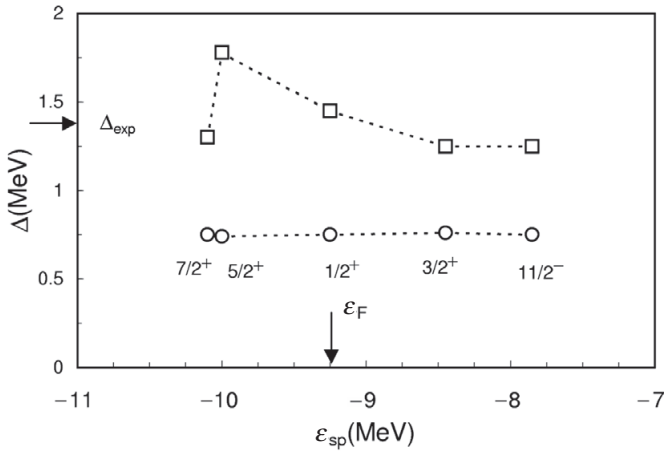

Figure 10.16. The state-dependent pairing gap for the levels close to the Fermi energy obtained using BCS theory with the v_{14} Argonne potential (circles) is compared with the result obtained by also including renormalization effects (squares) (after Barranco *et al*. (2004)).

true in the particle–particle channel (see equations (A.49) and (A.50)), and that the phonons are calculated in a Bogoliubov–Valatin-quasiparticle basis. In keeping with the above discussion, the most important processes renormalizing the B(E2) transition probability are those shown in Figs. 10.14(c),(d),(e) and (f).

Solving the Dyson equation by making use of phonons which account for the experimental findings, the state-dependent pairing gap shown in Fig. 10.16 was obtained. The average value of the resulting state-dependent pairing gap of ^{120}Sn is now close to the value $\Delta_{\rm exp} = 1.4$ MeV derived from the odd–even mass difference. In Fig. 10.15 the energy centroid of the peaks carrying the largest quasiparticle strength are shown, for the orbitals around the Fermi energy. These results provide an overall account of the lowest quasiparticle states measured in the odd systems ^{119}Sn and ^{121}Sn. In the case of $d_{5/2}$ orbital, the associated quasiparticle strength is strongly fragmented, and displays three low-energy peaks which collect less than 40% of the single-particle strength. Figures 10.15 and 10.16 show, respectively, the energy and the pairing gap associated with the lowest of these three peaks.

The results discussed in this section seem to be in contradiction with the results discussed in connection with Figs. 8.6 and 8.9. In fact, from these two figures one could expect that essentially the full effect associated with the increase of the pairing gap arising from the polarization processes, examples of which are shown in Fig. 10.13, are associated with effective mass processes like those displayed in Fig. 10.13(a) (see also equation (8.21)), leaving a negligible role to induced interaction processes like those shown in Fig. 10.13(e). The resolution of such an apparent contradiction is to be found in the fact that effective mass

processes simultaneously renormalize the density of levels $N(0)$ and the pairing interaction G. However, while $(N(0))_{\text{dressed}} \sim N(0)/Z_\omega$, $(G)_{\text{dressed}} \sim Z_\omega^2 G$, the overall effect being $(GN(0))_{\text{dressed}} \sim Z_\omega(GN(0))$. Because $Z_\omega < 1$, effective mass effects lead to a decrease of the pairing gap, decrease which is corrected to the value to be compared to the experimental data, by the contribution $Z_\omega^2 v_{\nu\nu'}$ arising from the induced interaction (see equation (9.33)). In fact, a further decrease of $N(0)$ is associated with fragmentation of the single-particle strength arising from renormalization processes like the one shown in Fig. 10.13(a) and measured by the (state dependent) width $\Gamma(j, \omega)$ (see Sections 9.1.2 and 9.3, equation (9.41)).

For a detailed account of these effects we refer to Morel and Nozières (1962), Schrieffer (1964), Mahan (1981) and Baldo *et al*. (2002). Also to Combescot (1999). A simple estimate of the relative importance of the different processes is given in Appendix H (Section H.4).

10.5 Superfluidity in the inner crust of neutron stars

There exists considerable experimental evidence which testifies to the fact that pulsars are rotating neutron stars (Pines *et al*. (1992)). It is believed that the crust of a neutron star is, in its outer part (10^6 g cm$^{-3} < \rho < 10^{11}$ g cm^{-3} and a few hundred metres thick), made out of nuclei arranged in a Coulomb lattice and of a nearly homogeneous background of relativistic electrons. As one goes deeper into the crust, because of the rising electron Fermi energy, the nuclear species become progressively more neutron-rich, beginning as ^{56}Fe and going through ^{118}Kr at mass density $\rho_d = 4.3 \times 10^{11}$g cm^{-3}, at which point neutrons are barely bound (Negele and Vautherin (1973)). At this density, known as the 'neutron drip density', nuclei have become so neutron-rich that, with increasing density, the neutron states lying in the continuum begin to be filled and the lattice of neutron-rich nuclei becomes permeated by a sea of free neutrons.

The region of densities $\rho_d < \rho < 0.7\rho_0$ (where $\rho_0 = 0.17$ nucleons per fm$^3 \approx 3 \times 10^{14}$ g cm^{-3} corresponds to saturation density, and where $\rho_d = 4.3 \times 10^{11}$ g cm^{-3} is the 'neutron drip' density) is the so-called 'inner crust' (thickness about one kilometre), where a Coulomb lattice of neutron-rich nuclei is permeated by a sea of free neutrons. In keeping with the fact that the nuclear interaction is, in this range of densities, attractive for pairs of nucleons moving in time-reversal states ($^1S_0$ neutron–neutron scattering, see Fig. 8.1) and because of the relatively low temperatures ($\leq$0.1 MeV) associated with all but the youngest of neutron stars, the free neutrons are believed to pair and form an isotropic s-wave superfluid. A proper understanding of the superfluidity properties of neutron-rich nuclei embedded in a sea of free neutrons (Wigner–Seitz cell) is of importance to determine the thermal properties of the neutron star crust, which is expected to play a central role in the early stages ($\approx 10^2$ years since formation) of the cooling

of neutron stars (Yakovlev and Pethick (2004), Pizzochero *et al*. (2002)). This knowledge is also important for the understanding of the vortex motion in the neutron superfluid within the solid crust of the neutron star, believed to be the origin of observed sudden decrease of the rotational period (spinup), or glitches (see Fig. 6.2) observed, for example, in the Crab ($|\Delta P|/P \approx 10^{-8}$) and Vela ($|\Delta P|/P \approx 2 \times 10^{-6}$) pulsar periods P (Alpar (1977), (1998), Anderson and Itoh (1975), Epstein and Baym (1988), Link and Epstein (1991), Pizzochero *et al*. (1997), Donati and Pizzochero (2003)).

Much effort has been concentrated in describing superfluidity of a uniform neutron star system using realistic nucleon–nucleon interactions (see e.g. Kennedy (1968), Sauls (1989), Takahara *et al*. (1994), Chen *et al*. (1986), Takatsuka (1984), Baldo *et al*. (1990), (1991), Chen *et al*. (1993), Wambach *et al*. (1993), Delion *et al*. (1995), Schulze *et al*. (1996), Lombardo and Schulze (2001), and references therein). However, in all the calculations, the role of impurities represented by nuclei in the sea of free neutrons has been neglected. In keeping with the fact that the pairing gap depends strongly on baryon density, a proper treatment of superfluidity in the neutron star crust should take into account the simultaneous presence of the free neutrons as well as the neutrons bound in the atomic nuclei (see also Delion *et al*. (1995)). To this purpose, theory should be able to provide, making use of a realistic interaction, equally reliable results for the uniform infinite system, as for the isolated atomic nucleus, limiting situations in which the results can be compared with a variety of calculations and with experimental data respectively. A unified description of these limiting situations will lend confidence to the results associated with finite atomic nuclei embedded in a sea of free neutrons. Contributions to carry out this programme are found in Barranco *et al*. (1997) and Gori *et al*. (2004b) (see also Sandulescu *et al*. (2004)).

The quantum mechanical calculations of the pairing gap in the inner crust of neutron stars were carried out by solving the Hartree–Fock–Boguliubov (HFB) equations (see Barranco *et al*. (1997), Barranco *et al.* (1998) and Section 8.1.1 equations (8.4)–(8.6); see also Dobaczewski *et al*. (2002), Dobaczezwski and Nazariewicz (1998)).

In Barranco *et al*. (1997) the single-particle states $|a_k\rangle = |n_k(l_a 1/2) j_a m_a\rangle$ describing the motion of nucleons in the mean fields calculated by Negele and Vautherin (1973) for each Wigner–Seitz cell density with a nucleus at the centre, and parametrized in terms of a Saxon–Woods potential, are labelled by the quantum numbers specifying the number of nodes n_k, the orbital angular momentum l_a, the total angular momentum j_a and its third component m_a, as well as the parity $(-1)^{l_a}$. The states $|\tilde{a_1}\rangle$ are obtained from the original states by the operation of time reversal. The quantities $U^i_{a_k}$ and $V^i_{a_k}$ are the occupation amplitudes of the single-particle states while E_i is the quasiparticle energy. The Argonne v_{14} potential was used in the calculation of the matrix elements

https://doi.org/10.1017/9781009401920 Published online by Cambridge University Press

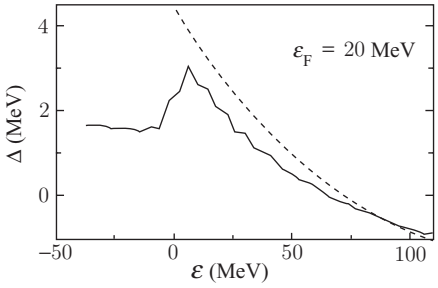

Figure 10.17. The pairing gaps obtained in a Wigner–Seitz cell of radius equal to 15 fm, and $\varepsilon_F = 20$ MeV, containing the nucleus Sn whose bound states are described in terms of a Saxon–Woods potential with a radius of 6.26 fm and a depth of 45.5 MeV, are shown by a solid and dashed curve, respectively for a diffusivity $a = 0.67$ fm and $a = 0$ fm. The gaps obtained for the discrete states have been averaged over 4 MeV. The gaps obtained for uniform neutron matter are shown by the dashed line (from Barranco *et al.* (1997)). Reprinted from *Physics Letters* B, Vol. 390, Barranco *et al.*, 'Role of finite nuclei on the pairing gap of the inner crust of neutron stars', page 15, Copyright 1997, with permission from Elsevier.

$\langle a_1 \tilde{a}_2 | v | b_1 \tilde{b}_2 \rangle$ (see Section 8.1). The quantity ε_F is the Fermi energy of the system and thus determines the average number of nucleons. To obtain convergence of the HFB equations, single-particle states lying as high as 600 MeV have to be included in the calculations. To this purpose the continuum is discretized by placing the nucleus in a box. For $\varepsilon_F > 0$, the radius of the box R_{box} coincides with the Wigner–Seitz cell radius R_{WS} as calculated by Negele and Vautherin (1973). For $\varepsilon_F < 0$, R_{box} should be varied until convergence of the results is achieved.

A number of situations corresponding to the densities discussed in this reference have been worked out. Particularly illustrative is the system composed of a nucleus containing 50 protons placed in the centre of a Wigner–Seitz cell of radius $R_{WS} = 15$ fm. Setting the Fermi energy at $\varepsilon_F = 20$ MeV ($\rho = 0.18\rho_0$), the Wigner–Seitz cell contains 600 neutrons. That is, we can view the system as a gigantic neutron-rich nucleus $^{600}_{50}$Sn. The selected density leads to the largest value of the pairing gap at the Fermi energy for the system under discussion (see Fig. 10.18).

Note that the large value of the pairing gap obtained in this calculation is connected with the fact that the single-particle energies were determined by making use of the bare nucleon mass and not the k-mass (see in this connection Figs. 8.6 and 8.9 as well as Sections 8.2 and 10.4). The same comment applies to Fig. 10.17, in which we display the diagonal part of the neutron pairing gap Δ_{a_k} ($\equiv \Delta_{a_k a_k}$) associated with the single-particle states of the system, obtained by solving equations (8.4)–(8.6) with $\varepsilon_F = 20$ MeV. The results have been averaged over an energy interval of 4 MeV to smooth out fluctuations associated with particular shells. The quantity Δ_{a_k} has a peak that corresponds to single-particle levels just barely unbound ($\varepsilon_{a_1} \approx 0$ MeV). It decreases as ε_{a_1} increases,

https://doi.org/10.1017/9781009401920 Published online by Cambridge University Press

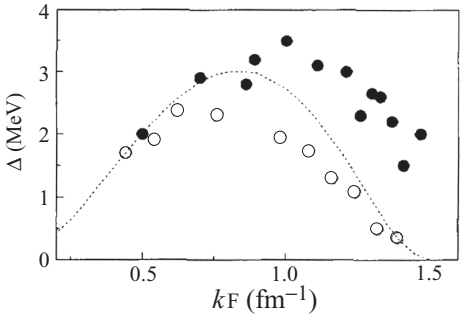

Figure 10.18. The dashed curve shows the pairing gaps at the Fermi energy in neutron matter as a function of the Fermi momentum. The solid dots show the pairing gaps of bound levels close to the Fermi energy, for different negative Fermi energies in the Saxon–Woods potential (with $a = 0.65$ fm) used in connection with Fig. 8.6 to describe ^{120}Sn. The Fermi momentum is referred to the bottom of the well. The open dots show the pairing gaps of levels close to the Fermi energy for positive values of ε_F and for the Wigner-Seitz cell discussed in connection with Fig. 10.17. Reprinted from *Physics Letters* B, Vol. 390, Barranco *et al*., 'Role of finite nuclei on the pairing gap of the inner crust of neutron stars', page 15, Copyright 1997, with permission from Elsevier.

in keeping with the fact that the content of relative momentum associated with such configurations also increases (see e.g. Baldo *et al*. (1990)). The pairing gap also decreases for bound neutron levels, because the density inside the nucleus is higher than outside it. The fact that the pairing gap does not vanish for bound levels ($\varepsilon_{a_1} < 0$), i.e. levels inside the nucleus, highlights the role the nuclear surface plays in the pairing phenomenon in atomic nuclei. We also show in Fig. 10.17 the pairing gap $\Delta(k)$ associated with uniform neutron matter as a function of the energy $\varepsilon = \hbar^2 k^2/2m$, calculated again setting $\varepsilon_F = 20$ MeV. From these calculations one concludes that the presence of the nucleus in the sea of free neutrons leads to an overall reduction of the pairing gap in the energy range $0 < \varepsilon < 100$ MeV, and the appearance of a broad bump near the edge of the single-particle potential well.

Results of calculations of the pairing gap for uniform neutron matter as a function of neutron Fermi wavenumber k_{F_n} (as a measure of density) for six models of crustal superfluidity are shown in Fig. 10.19 (from Lombardo and Schulze (2001)). The model labelled BCS is the simplest in which the pairing interaction is taken to be the neutron–neutron interaction in free space (see also Fig. 10.18). The five others – C86 (Chen *et al*. (1986)), C93 (Chen *et al*. (1993)), A (Ainsworth *et al*. (1989)), W (Wambach *et al*. (1993)), and S (Schulze *et al*. (1996)) include medium polarization effects which weaken the pairing. While all curves exhibit the same qualitative behaviour, there are also important differences. The BCS model is oversimplified, since it does not take into account effects of the medium.

https://doi.org/10.1017/9781009401920 Published online by Cambridge University Press

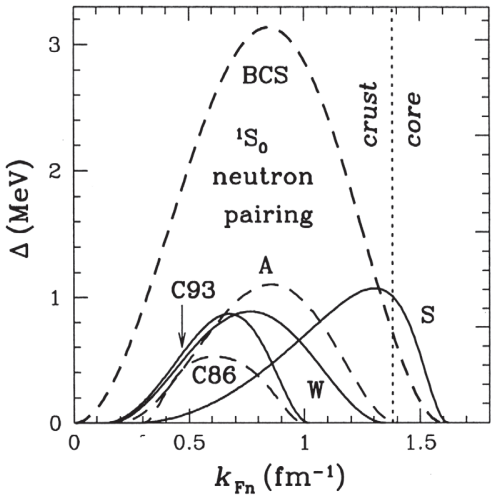

Figure 10.19. Energy gaps (left vertical axis) for various models of crustal neutron pairing as a function of neutron Fermi wavenumber. The vertical dotted line marks the crust–core interface (after Lombardo and Schulze (2001)).

Concerning the other results, one observes large variations in the predictions for the upper density at which neutron superfluidity disappears. While the reason for these differences is unclear, that the neglect of pairing fluctuations, fluctuations which become quite important when the mean-field pairing gap goes to zero, is likely to be one of the causes (see Section 6.6, Fig. 6.24).

In an infinite (3D) medium (i.e. a system where $r_s \ll \xi \ll L$ see Section 4.1.1, equation (4.1) and subsequent discussion) the gap is affected mainly by exchange of spin fluctuations, which reduce fluctuations, just as they do in metals. This is very different from what is found in the case of a finite (0D) medium ($r_s < L \ll \xi$), where density modes have a dominant role. The difference in the relative role played by density and magnetic modes in 0D and 3D systems is at the basis of the fact that medium polarization enhances the pairing gap in finite nuclei while it quenches it in the inner crust of neutron stars (see e.g. Figs. 10.16 and 10.19). This point is taken up in the next section.

10.5.1 Interplay between density and magnetic modes

In this section we discuss the mechanism which is at the basis of the seemingly contradictory results, namely the fact that while medium effects increase the nuclear pairing gap, they reduce it in the case of the inner crust of neutron stars. We shall show that these results are a natural consequence of the different (relative) collectivity displayed by density $S = 0$ (mainly surface) and $S = 1$ spin (mainly volume) modes in (infinite) neutron matter and in (finite) atomic nuclei

https://doi.org/10.1017/9781009401920 Published online by Cambridge University Press

(Gori *et al*. (2004b), see also Schrieffer (1994), Gor′kov and Melik-Barkhudrov (1961), Bortignon *et al*. (1983)). Strictly speaking, in the case of atomic nuclei, spin is not a good quantum number with which to identify the polarization quanta, because of the strong spin-orbit term present in these systems. We have thus adopted the criterion of distinguishing between natural ($\pi = (-1)^J$) and non-natural ($\pi = -(-1)^J$) parity modes, where J indicates the total angular momentum of the quanta. The classification reduces to that of $S = 0$ and $S = 1$ modes in the limit of no spin-orbit interaction.

In the following we address the question on hand within the scenario provided by the paradigmatic (superfluid) open-shell nucleus ^{120}Sn. The starting point corresponds to the calculation of the mean-field potential and associated quasiparticle properties within the framework of Hartree–Fock plus BCS theory using the SkM* force (Bartel *et al*. (1982)). The polarization quanta were worked out within the framework of quasiparticle random phase approximation (QRPA) (see e.g. Coló and Bortignon (2001)) making use of the particle–hole interaction

$$\begin{aligned} v_{\rm ph}(\vec{r},\vec{r}') &= \frac{\delta^2 E_{\rm HF}}{\delta\rho(\vec{r})\delta\rho(\vec{r}')} \qquad (10.46)\\ &= \left\{\left[F_0 + F_0'\vec{\tau}\cdot\vec{\tau}'\right] + \left[\left(G_0 + G_0'\vec{\tau}\cdot\vec{\tau}'\right)\vec{\sigma}\cdot\vec{\sigma}'\right]\right\}\delta(\vec{r}-\vec{r}')\,. \end{aligned}$$

In what follows we shall only consider the diagonal part of the $\vec{\tau}\cdot\vec{\tau}$ terms, in keeping with the fact that we are here interested in the neutron–neutron pairing interaction. Off-diagonal terms are associated with charge-exchange modes. Thus, in lowest order, they do not contribute to the neutron–neutron interaction, but are expected to be of relevance in the discussion of the proton–neutron pairing interaction.

The functions $F_0(\vec{r})$, $F_0'(\vec{r})$, $G_0(\vec{r})$ and $G_0'(\vec{r})$ (see also Section 4.3, discussion following equation (4.80)), generalized Landau–Migdal (Landau (1959), Migdal (1967)) parameters controlling the isoscalar and isovector (spin-independent and spin-dependent) channels are displayed in Fig. 10.20.

Vibrations of multipolarity $J = 2$, 3, 4 and 5 of both natural and unnatural parity were worked out. Those having energy $\leq$30 MeV were used in the calculation of the induced interaction (see Fig. 10.21(a)). The associated transition densities are

$$\begin{aligned} \delta\rho_\alpha^i(r) = &\frac{1}{\sqrt{2J+1}}\sum_{1,2}(X_{1,2}(i,\alpha) + \beta Y_{1,2}(i,\alpha))\\ &\times (U_1V_2 - cU_2V_1)\times\langle j_1||\hat{O}_\alpha||j_2\rangle\varphi_1(r)\varphi_2(r), \qquad (10.47) \end{aligned}$$

where one can have $\alpha = J$, $\beta = +1$, $\hat{O}_\alpha = Y_J$ or $\alpha = JL$, $\beta = -1$, $\hat{O}_\alpha = [Y_L \times \sigma]_J$ (concerning c, see Eq. (3.89)). The index i labels the different vibrational modes of a given spin and parity in order of increasing energy, while X and Y are the forwardsgoing and backwardsgoing QRPA amplitudes of the corresponding modes.

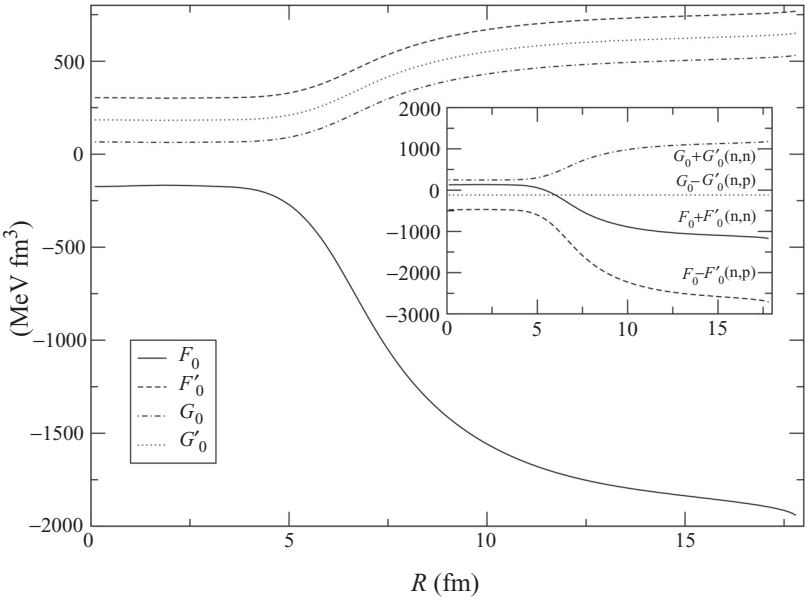

Figure 10.20. Generalized Landau parameters associated with the interaction SkM* defining the strength of the particle-hole interaction in the isoscalar (F_0), isovector (F'_0), spin isoscalar (G_0) and spin isovector (G'_0) channels. In the inset the functions $F_0 + F'_0$ (n–n interaction), $F_0 - F'_0$ (n–p), $G_0 + G'_0$ (n–n) and $G_0 - G'_0$ (n–p) are also shown. After Gori *et al.* (2004b).

We now calculate the induced pairing matrix elements associated with the exchange of polarization quanta between pairs of neutrons moving in time-reversed states. For this purpose the particle (neutron)-vibration coupling matrix elements are worked out:

(a) spin independent

$$\langle j'm', JM|\left[F_0(r) + F'_0(r)\vec{\tau}\cdot\vec{\tau}'\right]\delta(\vec{r}-\vec{r}')|jm\rangle \sim \int \mathrm{d}r\varphi_{j'}[(F_0+F'_0)\delta\rho^i_{Jn} + (F_0-F'_0)\delta\rho^i_{J\mathrm{p}}]\varphi_j, \qquad (10.48)$$

$\delta\rho^i_{Jn}$ and $\delta\rho^i_{Jp}$ being the neutron and proton contributions to the transition densities defined in equation (10.47),

(b) spin dependent

$$\langle j'm', JM|\left[G_0(r) + G'_0(r)\vec{\tau}\cdot\vec{\tau}'\right]\vec{\sigma}\cdot\vec{\sigma}'\delta(\vec{r}-\vec{r}')|jm\rangle \sim \int \mathrm{d}r\varphi_{j'}[(G_0+G'_0)\delta\rho^i_{JLn} + (G_0-G'_0)\delta\rho^i_{JL\mathrm{p}}]\varphi_j. \qquad (10.49)$$

These particle-vibration coupling matrix elements, together with the energies of the modes and the HF single-particle energies are the basic ingredients needed to

https://doi.org/10.1017/9781009401920 Published online by Cambridge University Press

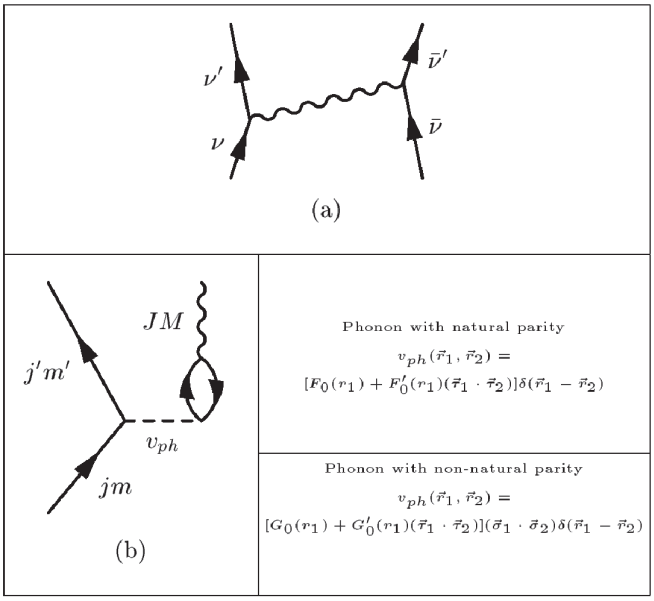

Figure 10.21. (a) Diagram depicting the pairing interaction induced by the exchange of phonons; (b) particle-vibration coupling vertex making explicit the dominant part of the particle–hole interaction giving rise, through the sum of bubble diagrams, to the corresponding QRPA modes (wavy line).

calculate the pairing induced interaction v_{ind} (see Fig. 10.21(a)). For non-natural parity modes, only the matrix elements (10.49) contribute. For natural parity modes, the matrix elements (10.48) are the dominant ones, and one can show that they are the only ones contributing to the diagonal matrix elements, which are displayed in Fig. 10.22. In this case it is thus possible to distinguish between the contributions associated with the exchange of $S = 0$ (density) and $S = 1$ (spin) vibrations. From Fig. 10.22 we can see that the exchange of spin fluctuations gives rise to repulsive matrix elements, while the exchange of density fluctuations leads to attractive matrix elements, the net result being predominantly attractive (in any case around the Fermi energy).

The resulting state-dependent pairing gap obtained by solving the BCS gap and number equations making use of the (total) induced pairing matrix elements ($S = 0$ (density) plus $S = 1$ (spin) modes) is depicted in Fig. 10.23(a). For states close to the Fermi energy they account for a consistent fraction of the experimental value (1.4 MeV). If one solves the BCS equations considering only the exchange of density modes (i.e. neglecting the contributions from equation (10.49)), one obtains values which are, on average, larger (see Fig. 10.23(b)). In fact, the exchange of $S = 1$ modes quenches the pairing gap arising from the exchange of only $S = 0$ modes by roughly 30%.

https://doi.org/10.1017/9781009401920 Published online by Cambridge University Press

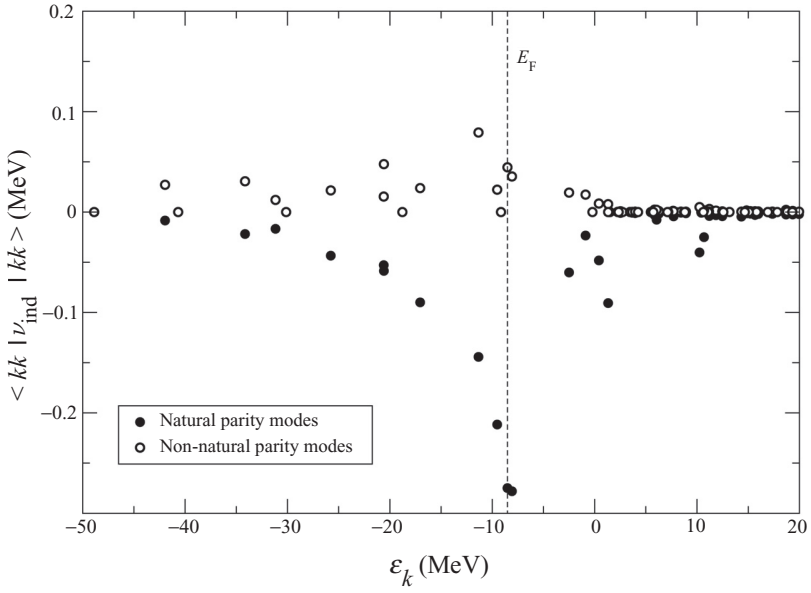

Figure 10.22. Diagonal induced pairing matrix elements resulting from the exchange of phonons with natural parity (solid circles) and those resulting from the exchange of phonons with non-natural parity vibrations (open circles), displayed as a function of the energy of the single-particle state ε_k. Note that the induced matrix elements in this figure can be directly compared with the empirical constant $G = 25/A(\approx 0.2\,\text{MeV}, A = 120)$ used to describe pairing correlations in nuclei within the framework of the BCS theory and a (pairing) force of constant matrix elements (after Gori *et al*. (2004b)).

To gain insight into what one would expect from these results in the case of infinite systems, we study the radial dependence of the particle-vibration coupling vertices shown in Fig. 10.21(b). The $S = 0$ modes associated with induced pairing matrix elements have a clear surface character. In particular, this is the case for the most attractive pairing matrix element which is associated with the $1h^2_{11/2}(0)$ ($\varepsilon_{1h_{11/2}} = -8.07\,\text{MeV}$, $\varepsilon_F = -8.50\,\text{MeV}$) configuration (see Fig. 10.22). Because of its large centrifugal barrier, the wavefunction of this single-particle state is mainly concentrated at the nuclear surface. The main contribution to the corresponding induced pairing matrix element arises from the exchange of a 2^+ phonon (of energy 1.5 MeV) between the two nucleons moving in time-reversal states in the $h_{11/2}$ orbital. The associated proton and neutron transition densities depicted in Fig. 10.24(a) testify to the fact that this phonon has the character of a surface vibration. Concerning the most repulsive matrix elements, we have found that the corresponding $S = 1$ phonons are volume modes. In particular, the largest (positive) matrix element is associated with the $2d^2_{3/2}(0)$ configuration ($\varepsilon_{2d_{3/2}} = -8.52\,\text{MeV}$). Because of the low angular momentum, one

https://doi.org/10.1017/9781009401920 Published online by Cambridge University Press

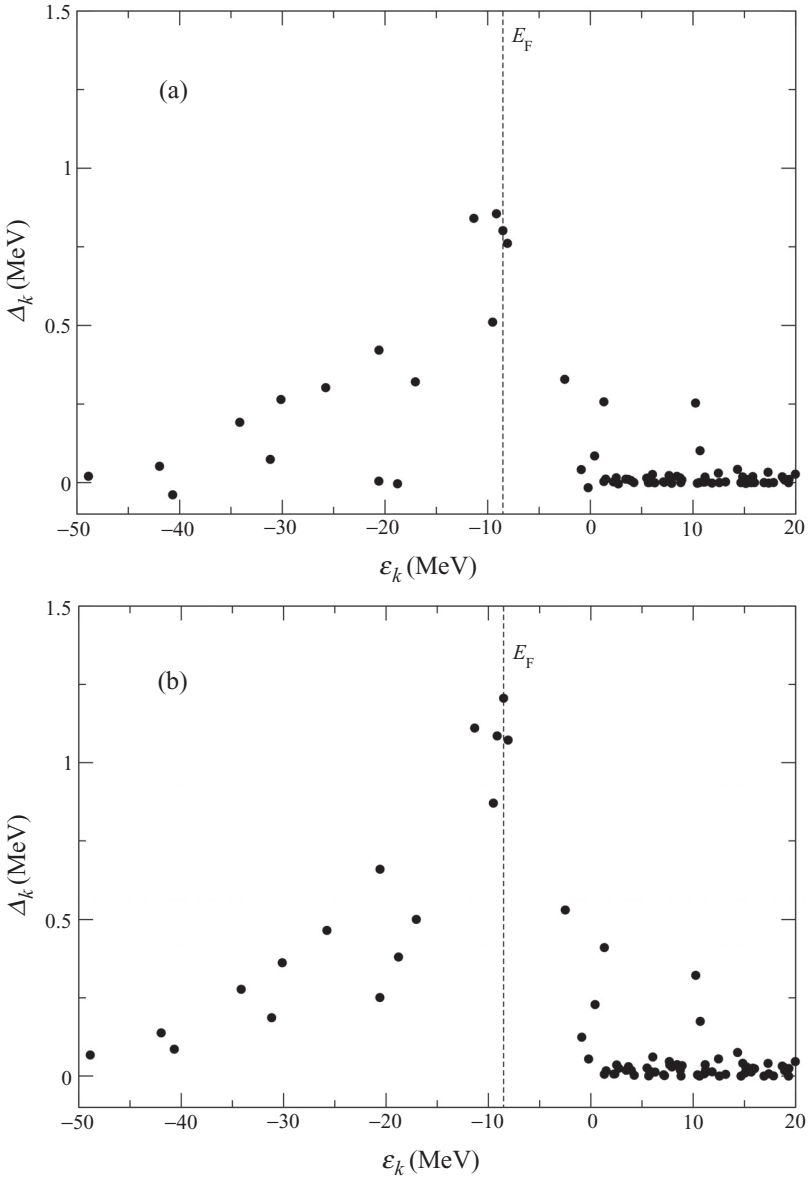

Figure 10.23. (a) The state-dependent pairing gap as a function of the single-particle energies obtained by solving the BCS equations associated with the total $(S = 0) + (S = 1)$ induced interaction matrix elements; (b) same as (a) but for the induced interaction matrix elements produced only by exchange of density modes $(S = 0)$ (after Gori *et al*. (2004b)).

https://doi.org/10.1017/9781009401920 Published online by Cambridge University Press

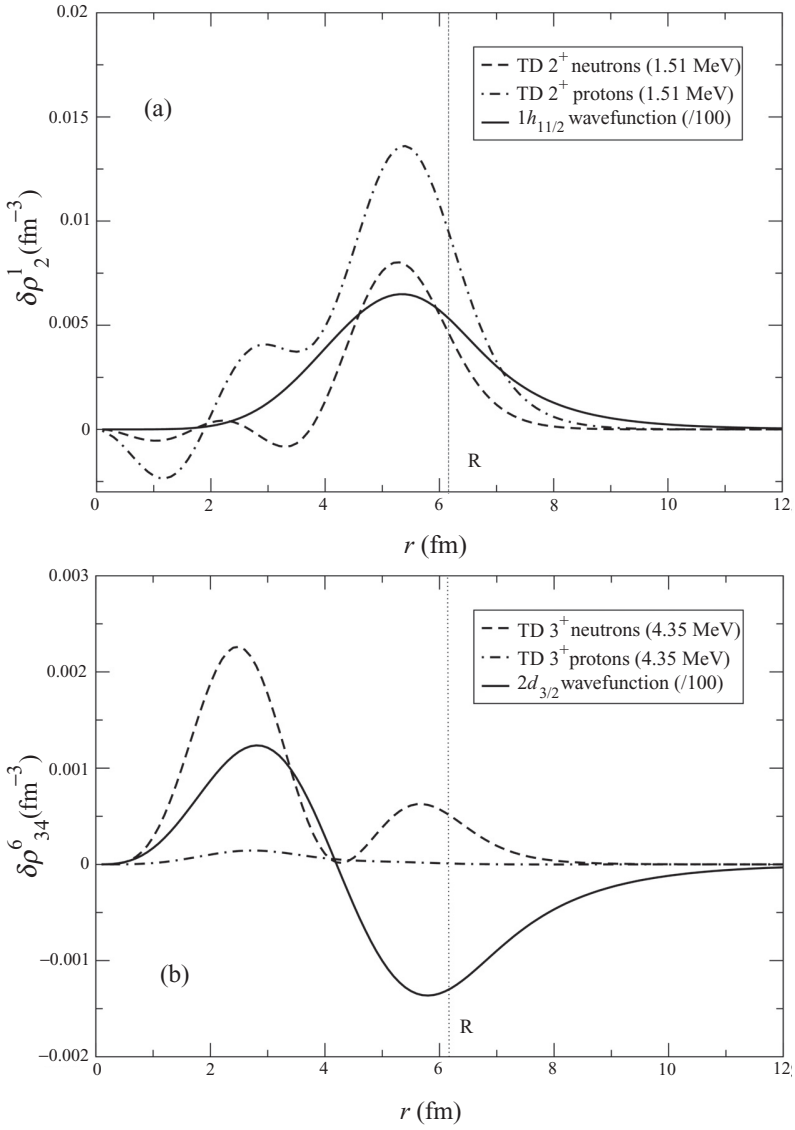

Figure 10.24. (a) The dashed and dot-dashed curves are respectively the neutron and proton transition densities associated with the 2^+ phonon with energy 1.5 MeV while the solid curve is the wavefunction of the $1h_{11/2}$ state (in arbitrary units). (b) The same as (a) but for the 3^+ phonon with energy 4.35 MeV and the $2d_{3/2}$ state (after Gori *et al*. (2004b)).

finds that a consistent fraction of the corresponding wavefunction is concentrated in the interior of the nucleus. This state can thus couple efficiently with phonons of volume character. In fact, the major contribution to the corresponding matrix element is due to the exchange of the 3^+ vibration (with energy at 4.35 MeV)

https://doi.org/10.1017/9781009401920 Published online by Cambridge University Press

which is a mode with a large volume component as testified by the corresponding proton and neutron transition densities shown in Fig. 10.24(b). One can conclude that states lying close to the Fermi energy with high j and thus localized at the surface mainly feel the (attractive) coupling arising from the exchange of $S = 0$ phonons. Because the contributions of these states to the gap equation are larger (statistically) than those associated with low-l states (lying also close to the Fermi energy), the resulting induced pairing interaction in nuclei is attractive. The situation is expected to be quite different in the case of infinite neutron matter. In fact, in going from the finite to the infinite system the collectivity of the $S = 0$, mainly surface modes will be strongly reduced, while not much is expected to happen to the $S = 1$, mainly volume modes.

Furthermore, in going from nuclear ($N = Z$) to neutron matter ($N = A$), many attractive contributions vanish. In fact, if we turn off the neutron–proton interaction contributing to the basic vertices shown in Fig. 10.20, a strongly net repulsive induced interaction is obtained (see Fig. 10.25), a situation which much resembles the neutron star case. This result can be understood by realizing that, while the function $F_0 + F_0'$ (corresponding to the particle–phonon coupling mediated by $\delta\rho^i_{Jn}$) has a node at the nuclear surface (see inset to Fig. 10.20),

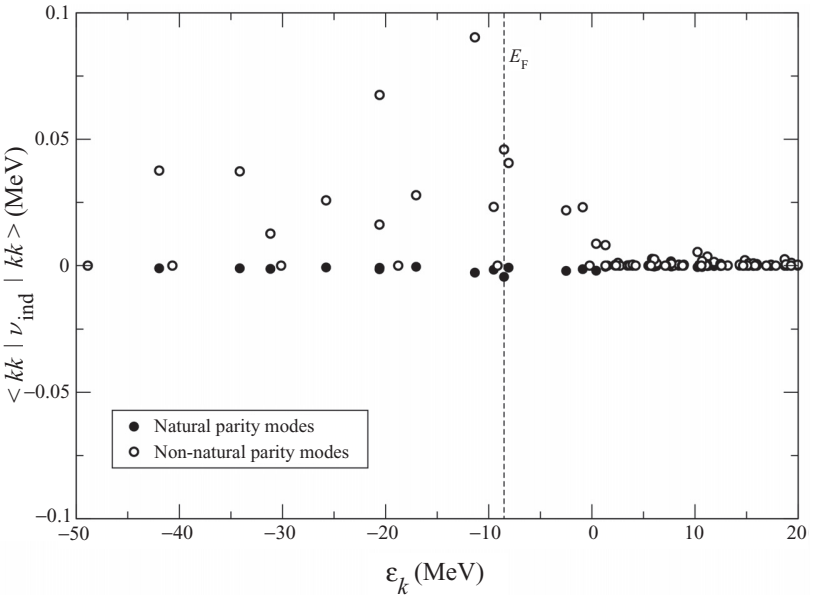

Figure 10.25. The diagonal matrix elements produced by the exchange of phonons with natural parity (filled circles) and those produced by the exchange of phonons with non-natural parity (empty circles) when the proton part of the phonon wavefunction is not included in the calculation, are displayed as a function of the energy of the single-particle state ε_k (after Gori *et al*. (2004b)).

https://doi.org/10.1017/9781009401920 Published online by Cambridge University Press

$G_0 + G'_0$ (corresponding to the particle-phonon coupling mediated by $\delta\rho^i_{JLn}$) is large and positive.

Summing up, the exchange of low-lying vibrations (in which neutrons and protons participate on equal footing) between pairs of nucleons moving in time-reversal states close to the Fermi energy leads to a sizeable attractive pairing interaction which accounts for about 70% of the pairing gap. The inclusion of spin (volume) modes, reduces that contribution by 30% in the case of finite nuclei, bringing the induced pairing contribution to the pairing gap to a value of the order of $\approx$50%, the other half coming from the bare nucleon–nucleon force. Spin modes overwhelm density modes when the coupling to surface (namely $S = 0$) modes as well as the proton–neutron coupling are neglected, a situation which mimics neutron matter.

https://doi.org/10.1017/9781009401920 Published online by Cambridge University Press

11
Pairing in exotic nuclei

Much of the recent research in nuclear structure focuses on nuclei near the neutron and proton drip lines. These are the *loci* in the chart of nuclides of the isotopes and isotones which are stable against neutron and proton emission and which have the largest number of neutrons and protons respectively. The most exotic of these nuclei, which have been produced in the laboratory, are light nuclei lying just within the drip lines. The nucleus $^{11}_{3}\mathrm{Li}_8$, containing three protons and eight neutrons, is bound by only a few hundred keV and is one of the best-studied examples of a 'halo' nucleus to date.

According to the shell model, two of the six neutrons in the ^{9}Li nucleus occupy the lowest $s_{1/2}$ orbital while the remaining four neutrons fill the $p_{3/2}$ orbital. The separation energy of the last neutron in ^{9}Li is $S_n \sim 4$ MeV which is typical for a light nucleus. The halo nucleus ^{11}Li has two neutrons outside a ^{9}Li core and the simple shell model predicts that they should fill the $p_{1/2}$ orbital. A special feature of ^{11}Li is that the last two neutrons are bound by only 290 keV, while the last neutron in ^{10}Li is not bound. A consequence of the small binding energy of the last two neutrons in ^{11}Li is that the radius of the orbital they occupy is much larger than the radius of the ^{9}Li core. They form a low-density cloud or 'halo' around the core.

In simple versions of the shell model the $s_{1/2}$ level from the *s–d* shell has an energy which is significantly larger than the $p_{1/2}$ level but in light neutron-rich nuclei the energy difference between these two levels decreases and there is evidence that in ^{10}Li the $s_{1/2}$ level lies below the $p_{1/2}$ level. In that case the last two neutrons in ^{11}Li might occupy the $s_{1/2}$ level. Consequently, the ^{11}Li ground state has a more complicated structure than that predicted by the pure independent particle model, which involves both the $s_{1/2}$ and the $p_{1/2}$ orbitals. The self-energy due to the neutron–phonon interaction is a possible mechanism for the change in the relative energies of the $s_{1/2}$ and $p_{1/2}$ levels.

https://doi.org/10.1017/9781009401920 Published online by Cambridge University Press

It is still an open question which mechanisms provide the glue needed to bind the two halo neutrons to the tightly bound $^{9}_{3}\mathrm{Li}_6$ core. To some extent, this problem seems to be similar to that of the instability of the normal state of an electron system at zero temperature, solved by Cooper, a solution which is at the basis of BCS theory of superconductivity. The main difference with the present case is associated with the shell structure of the system, implying a threshold in the intensity of the attractive interaction needed to produce a bound state (see Chapters 1 and 8). The bare nucleon–nucleon interaction is attractive in the $^{1}S_0$ channel and, if it was strong enough, it could bind the last two neutrons in ^{11}Li. Owing to the fact that the angular momentum content of the space available to the two 'halo' neutrons to correlate is low (essentially one s, p and d-orbitals are involved), the system can hardly profit from the large pairing component of the nucleon–nucleon potential (see Section 8.1), as, for example, nucleons in ^{120}Sn can (see Figs. 8.4 and 8.9). On the other hand, ^{11}Li is highly polarizable displaying a soft dipole mode, as well as collective quadrupole vibrations. As discussed in Chapter 10 there is an induced neutron–neutron interaction due to phonon exchange and there is evidence that the enhancement of the pairing force due to the induced interaction is necessary to bind the ^{11}Li nucleus.

Phenomena similar to those mentioned in connection with $^{10}_{3}$Li and $^{11}_{3}$Li have also been found in the case of $^{11}_{4}$Be and $^{12}_{4}$Be. The main difference with respect to the case of ^{11}Li is that both $s_{1/2}$ and $p_{1/2}$ neutron orbitals are bound in $^{11}_{4}\mathrm{Be}_7$, while they are resonant states in $^{10}_{3}\mathrm{Li}_7$. Thus, larger overlaps between the s^2, p^2 with the d^2 two-neutron configurations are found in ^{12}Be compared with ^{11}Li. The role of the $d_{5/2}$ configuration in the ground state of ^{12}Be is consequently quantitatively different than in the case of ^{11}Li. Furthermore, no soft dipole mode has been observed in ^{12}Be. Renormalization effects are, in this case, due to quadrupole vibrations.

The focus of this chapter is on the contribution of neutron–phonon coupling to the neutron single-particle energies in ^{10}Li and ^{11}Be and the binding of ^{11}Li and ^{12}Be. Our discussion is based on results of a study by Barranco *et al*. (2001), Broglia *et al*. (2002) and Gori *et al*. (2004a), results which are to be compared with those of Zukhov (1991, 1993), Esbensen *et al*. (1997), Bertsch and Esbensen (1991), Bertsch (1994) and Sagawa *et al*. (1993).

11.1 The halo nucleus ^{11}Li

The basic experimental facts which characterize ^{11}Li and which are also of particular relevance in connection with pairing in this system are (see Table 11.1): (a) $^{9}_{3}\mathrm{Li}_6$ and $^{11}_{3}\mathrm{Li}_8$ are stable, $^{10}_{3}\mathrm{Li}_7$ is not; (b) the two-neutron separation energy in ^{11}Li is only $S_{2n} = 0.294 \pm 0.03$ MeV (Tanihata (1996)) compared with values of 10 to 30 MeV in normal stable nuclei; (c) ^{10}Li displays s- and p-wave resonances

https://doi.org/10.1017/9781009401920 Published online by Cambridge University Press

Table 11.1. *Single-particle energies associated with the states s and p in* ^{10}Li. *Two-neutron separation energy* S_{2n}, *amplitude of the* s^2- *and of the* p^2-*configurations in the ground-state wavefunctions, mean square radius* $\langle r^2\rangle^{1/2}$ *of* ^{11}Li *and full width* $\Delta p_\perp = \sigma_\perp$ *of the momentum distribution of the neutrons emitted in the direction perpendicular to the beam during the breakup of* ^{11}Li *(after Barranco et al. (2001); see also Broglia et al. (2002)).*

			Theory	
		Exper.	Particle-vibration $+v_{14}$	Mean field
	s	0.1–0.2 MeV	0.2 MeV (virtual)	∼1 MeV (virtual)
$^{10}_{3}$Li$_7$ (not bound)	p	0.5–0.6 MeV	0.5 MeV (res.)	−1.2 MeV (bound)
	S_{2n}	0.294 ± 0.03 MeV	0.330 MeV	2.4 MeV
$^{11}_{3}$Li$_8$	s^2, p^2	50%, 50%	40%, 58%	0%, 100%
(bound)	$\langle r^2\rangle^{1/2}$	3.55 ± 0.1 fm	3.75 fm	
	$\sigma_\perp$	$48 \pm 10 \frac{\text{MeV}}{\text{c}}$	$55 \frac{\text{MeV}}{\text{c}}$	

at low energy, their centroids lying within the energy range 0.1–0.25 MeV and 0.5–0.6 MeV respectively (Zinser *et al*. (1995)), while these orbitals are well bound in nuclei of the same mass lying along the stability valley; (d) the mean square radius of ^{11}Li, $\langle r^2\rangle^{1/2} = 3.55 \pm 0.10$ fm (Kobayashi *et al*. (1989), Al-Khalili and Tostevin (1996), Hansen (1996)), is very large compared with the value 2.32 ± 0.02 fm of the ^{9}Li core, and testifies to the fact that the neutron halo must have a large radius ($\approx$ 6–7 fm); (e) the momentum distribution of the halo neutrons is very narrow, its FWHM is $\sigma_\perp = 48 \pm 10$ MeV/c for the (perpendicular) distribution observed in the case of the break-up of ^{11}Li on ^{12}C and is of the order of one-fifth of that measured during the break-up of normal nuclei (Kobayashi (1993), Tanihata (1996)); (f) the ground state of ^{11}Li is a mixture of configurations where the two-halo nucleons move around the ^{9}Li core in s^2- and p^2-configurations with almost equal weight (Aoi *et al*. (1997), Simon *et al*. (1999)). The wavefunctions of two-particle-like normal nuclei can be strongly mixed but are, as a rule, dominated by a single two-particle configuration (see e.g. Table 5.1 where the ground-state wavefunctions of ^{210}Pb and ^{206}Pb are given).

Two-neutron halo nuclei are commonly described as three-body systems consisting of two valence neutrons interacting with each other and with a structureless core (see Esbensen *et al*. (1997) and reference therein).

https://doi.org/10.1017/9781009401920 Published online by Cambridge University Press

The three-body Hamiltonian can be written as

$$H = \frac{p_1^2}{2m} + \frac{p_2^2}{2m} + V_{\rm nc}(1) + V_{\rm nc}(1) + V_{\rm nn} + \frac{\left(\vec{p}_1 + \vec{p}_2\right)^2}{2A_{\rm c}m}.$$

It includes the kinetic energy of each neutron, their interaction $V_{\rm nc}$ with the core, the interaction between the two valence neutrons, and the recoil kinetic energy of the core, which has the mass number $A_{\rm c}$.

The single-particle Hamiltonian for a neutron interacting with the core is

$$h_{\rm nc} = \frac{p^2}{2\mu} + V_{\rm nc}(r),$$

where $\mu = mA_{\rm c}/(A_{\rm c}+1)$ is the reduced mass.

The three-body Hamiltonian then takes the form

$$H = h_{\rm nc}(1) + h_{\rm nc}(2) + V_{\rm nn} + \frac{\vec{p}_1 \cdot \vec{p}_2}{A_{\rm c}m}. \tag{11.1}$$

This Hamiltonian is to be diagonalized in the space of 0^+ two-neutron states with wavefunctions

$$\Phi_{nn'lj}\left(\vec{r}_1, \vec{r}_2\right) = \left[\phi_{nlj}(\vec{r}_1)\phi_{n'lj}(\vec{r}_2)\right]_{00},$$

constructed from the eigenstates

$$\phi_{n\ell jm}\left(\vec{r}\right) = R_{n\ell}(r)\left[Y_\ell\left(\hat{r}\right)\chi(\sigma)\right]_{j\ell}$$

of the single-particle Hamiltonian $h_{\rm nc}$. To do this, one needs to calculate the matrix elements of $V_{\rm nn}$ and of $\vec{p}_1 \cdot \vec{p}_2/A_{\rm c}m$ between all 0^+ two-particle states. Note that $\vec{p}_1 \cdot \vec{p}_2/A_{\rm c}m \sim \vec{\nabla}_1 \cdot \vec{\nabla}_2$. Consequently, the matrix elements of the recoil term are intimately connected with the matrix element of the operator (see Appendix in Esbensen *et al.* (1997))

$$\hat{r}_1 \cdot \hat{r}_2 = \sum_m Y_{1m}(\vec{r}_1)Y^*_{1m}(\vec{r}_2).$$

The recoil term, needed to eliminate the spurious centre of mass motion of the system, is intimately connected to an (isoscalar) dipole–dipole field. In fact, the self-consistent value of the dipole–dipole residual interaction needed to describe the giant dipole resonance in the sum-rule conserving RPA leads to a zero-energy isoscalar dipole mode.

A central issue connected with this model is how accurately one must treat the various terms appearing in the Hamiltonian given in equation (11.1).

The ground state of ^{11}Li has been studied in several Faddeev and Faddeev-like three-body calculations (Zhukov (1991, 1993)) which make use of a shallow neutron core potential $V_{\rm nc}$ and a simple Gaussian interaction $V_{\rm nn}$ acting between the valence neutrons (see Table 11.2, lines 1 and 2). Calculations with the same $V_{\rm nc}$ but using for $V_{\rm nn}$ a density-dependent (to quench the interaction inside the core)

Table 11.2. *Comparison of the ground-state properties of* ^{11}Li *as calculated by making use of different approaches. Line 5 contains results of nuclear field theory calculations (NFT) discussed in Section 11.1. These results are compared with results published in the literature: (I) obtained with a technique based on a density-dependent, cutoff, contact interaction between the valence neutrons including (lines 3 and 6, Esbensen et al. (1997)) and neglecting (lines 4 and 7, Bertsch and Esbensen (1991)) recoil effects, (II) obtained by making use of a Faddeev approach based on realistic interactions (lines 1, 2 (Zhukov (1991), Ian Thompson, see Esbensen et al. (1997)) and 8 (Zhukov (1993))). The basic quantities that characterize the low-energy* nn *scattering are the scattering length* a_{nn} *and the effective range* r_{nn}. *They are the parameters in the expansion of* $k\cot\delta$ *in powers of the relative momentum* k ($k\cot\delta \approx -1/a_{nn} + \frac{1}{2} r_{nn} k^2$), *where* δ *is the* s*-wave phase-shift. The empirical values are* $a_{nn} = -18.5 \pm 0.5$ fm *and* $r_{nn} = 2.8 \pm 0.1$ fm *(Bertsch and Esbensen (1991), Zinser et al. (1997)).*

The results reported in lines 1 and 2 were obtained by making use of a shallow neutron-core potential ($V_{nc}(r) = -7.8\ \exp[-(r/2.55)]$ MeV), *which does not support any bound states, and a single Gaussian interaction* ($V_{nn}(r_{12}) = -3(\exp[-(r_{12}/1.8)^2]$ MeV), *leading to* s*-wave phase shifts which are in good agreement with the empirical values. The results quoted in lines 3 and 4 also made use of the shallow neutron–core potential and a density-dependent contact interaction in the* $T = 1$, $S = 0$ *channel (quenched inside the core). The two-halo neutrons are allowed to move in a radial box of 40* fm *with a cutoff of 25* MeV *(line 3) and 15* MeV *(line 4) respectively. The results in line 6 are based on a stronger core–neutron interaction (potential) in even-parity states producing an* s*-wave scattering length of* $a_{n0} = -5$ fm. *The results shown in line 7 were obtained in the non-recoil limit, with a neutron–core* $p_{1/2}$ *resonance at 800* keV. *A particular set of Faddeev results, based on a* $p_{1/2}$ *resonance at 200* keV *and realistic* nn*-interaction is shown in line 8. In column 3 we display the low-energy* nn*-scattering length* a_{nn}, *in column 4 the two neutron separation energy* S_{2n}, *in column 6 the neutron separation* $\langle r^2_{n,n}\rangle^{1/2} = \langle \Phi_{g.s} || \vec{r}_1 - \vec{r}_2|^2 | \Phi_{g.s}\rangle^{1/2}$, *in column 5 the dineutron core distance* $\langle r^2_{c,2n}\rangle^{1/2} = \langle \Phi_{g.s} | (\vec{r}_1 + \vec{r}_2)^2 | \Phi_{g.s}\rangle^{1/2}$, *while in column 7 we display the mean square radius* $\langle r^2\rangle_A^{1/2} = \left(\delta\langle r^2\rangle + \frac{A_c}{A}\langle r^2\rangle_{A_c}\right)^{1/2}$ *where* $\delta\langle r^2\rangle = \frac{1}{A}\left(\frac{2A_c}{A}\langle r^2_{c,2n}\rangle + \frac{1}{2}\langle r^2_{n,n}\rangle\right)$ *(Bertsch and Esbensen (1991)). In columns 8 and 9 we display the probability of the two-particle configurations to appear in the ground-state wavefunction.*

Line	Comments	a_{nn} (fm)	S_{2n} (keV)	$\langle r^2_{c,2n}\rangle^{1/2}$ (fm)	$\langle r^2_{n,n}\rangle^{1/2}$ (fm)	$\langle r^2\rangle_A^{1/2}$ (fm)	$(s_{1/2})^2$ %	$(p_{1/2})^2$ %
1	HMM[a]	−18.5	300	5	7.8	3.59	98.4	
2	Faddeev[a]	−18.5	318	5.3	7.9	3.66	95.1	
3	Esbensen[a]	−15	318	5.2	7.9	3.64	91.1	
4	Bertsch[a]	−15	318	5.0	8.2	3.63	94.4	
5	NFT	−18.5	330	5.1	8.6	3.75	40	58
6	Esbensen[b]	−15	295	5.1	6.8	3.52	23.1	61.0
7	Bertsch[b]	−15	200	4.9	6.2	3.42	6.1	76.9
8	Q9[b]	−18.5	295	4.6	6.7	3.41		

[a.] Table I Esbensen *et al*. (1997).
[b.] Table IV Esbensen *et al*. (1997).

https://doi.org/10.1017/9781009401920 Published online by Cambridge University Press

contact pairing interaction have also been published (see lines 3 and 4, Table 11.2) (Esbensen *et al*. (1997), Bertsch and Esbensen (1991), Bertsch (1994)). Note that the density-dependent interaction can simulate three-body forces. These forces have been found, in the most refined many-body calculations of light nuclei avaliable in the literature (see e.g. Pudliner (1995)), to play an important role in obtaining the correct binding energy.

In lines 6, 7 and 8 of Table 11.2, the results of contact interactions and realistic force Faddeev calculations are reported, where the parameters of $V_{\rm nc}$ and $V_{\rm nn}$ were adjusted so as to ensure the observed position of the $p_{1/2}$ and $s_{1/2}$ resonances and of the $^1S_0$ phase shifts.

It is seen that in all cases the observed two-neutron separation energy of ^{11}Li is adequately reproduced. The associated mean square radii are in reasonable agreement among each other. Larger variation among the results of the different calculations is found for the amplitude with which the $s^2_{1/2}(0)$ and $p^2_{1/2}(0)$ two-particle configurations enter the ground state of ^{11}Li. To be able to obtain a sizeable $s^2_{1/2}(0)$ component as required by the experimental findings (Aoi *et al*. (1997), Simon *et al*. (1999)) (see line 6 of Table 11.2) one is forced to use a different $V_{\rm nc}$ interaction for even and for odd single-particle states so as to place both the $p_{1/2}$ annd the $s_{1/2}$ resonances at the observed values (Esbensen *et al*. (1997)).

None of the above calculations was concerned with the influence that core polarization effects may have in the properties of the system. In Nuñes *et al*. (1996) the three-body model was extended to include explicitly certain core degrees of freedom and the model was applied to ^{12}Be where sizeable effects were found (see Section 11.2).

While the calculations discussed in this section provide an overall account of the experimental findings, they depend on a number of parameters, in particular those associated with $V_{\rm nc}$ (and determing the position of the resonant single-particle state), parameters which are likely to change from case to case, thus reducing the predictive power of the realistic calculations.

It is likely that much of this ambiguity can be eliminated by properly taking into account the influence of core polarization effects. In other words, by generalizing the models discussed above, in particular that of Bertsch and Esbensen (1991) and Esbensen *et al*. (1997), allowing the two neutrons to feel not only the $\vec{p}_1 \cdot \vec{p}_2/A_{\rm c}m$, dipole–dipole like interaction, but also to couple to the vibrations of the core of multipolarities different from $L = 1$, vibrations which are also strongly modified by the presence of halo neutrons. This constitutes the essence of the paper of Barranco *et al*. (2001) which we discuss in the next section.

11.1.1 Single-particle states in ^{10}Li: effective mass processes

Nuclear field theory (NFT) provides a systematic description of the nuclear spectrum in terms of the motion of the nucleons, of the collective vibrations of the system and of their interweaving. While (dressed) single-particle states

https://doi.org/10.1017/9781009401920 Published online by Cambridge University Press

and collective excitations are directly related to the experimental observations, all the degrees of freedom of the nucleus are already exhausted by the single-particle degrees of freedom. Consequently, overcompletness and Pauli principle correction processes are essential in the NFT description of the nuclear structure (Bes *et al*. (1976a), (1976b), Bortignon *et al*. (1977)).

This treatment is, to a large extent, equivalent to a full shell model calculation. As in the case of such calculations, the mean-field single-particle levels are used and the coupling to core excitations give rise, through self-energy and Pauli (blocking) effects, to parity inversion (Sagawa *et al*. (1993)) (inversion in the sequence between $s_{1/2}$ and $p_{1/2}$ states (resonances)).

Before discussing the sources of pairing correlations in ^{11}Li, one needs to determine the single-particle resonant spectrum of ^{10}Li. The basis of (bare) single-particle states used is determined by calculating the eigenvalues and eigenfunctions of a nucleon moving in the mean field of the ^{9}Li core, for which one can use a Saxon–Woods potential (Bohr and Mottelson (1969)), of depth $U_0 = -(51 - 30(N - Z)/A)\text{MeV} = -41\,\text{MeV}$. The continuum states of this potential are calculated by solving the problem in a box of radius equal to 40 fm, chosen to make the results stable. Arising mainly from Pauli principle effects (Fock potential, see Section 8.2.1) the k-mass is expected to be dependent on the density of the system. While in nuclei along the stability valley $m_k \approx 0.7\, m$, it is expected that in 'halo' nuclei $0.8 \lesssim m_k/m \lesssim 1$.

While mean-field theory predicts the orbital $p_{1/2}$ to be lower than the $s_{1/2}$ orbital (see Fig. 11.1, I(a)), experimentally the situation is reversed. Similar parity inversions have been observed in other isotones of $^{10}_{3}\text{Li}_7$, such as $^{11}_{4}\text{Be}_7$ (see Section 11.2). Shell model calculations have indicated that the effect of core excitation, in particular of quadrupole type, plays a central role in this inversion (Sagawa *et al*. (1993), see also Vinh Mau (1995)). Within the framework of Chapters 8 and 9, it is important to study the effect of the coupling of the $p_{1/2}$ and $s_{1/2}$ orbitals of ^{10}Li to quadrupole vibrations of the ^{9}Li core on the properties of the $1/2^+$ and $1/2^-$ states of this system. Monopole an*d* dipole vibrations have no low-lying strength in this nucleus and their coupling to the single-particle states of ^{10}Li lead to negligible contributions. The quadrupole vibrational state of ^{9}Li can be calculated by diagonalizing, in the random phase approximation (RPA), a quadrupole–quadrupole separable interaction (see e.g. (8.39)) taking into account the contributions arising from the excitation of particles into the continuum states. A natural choice of the coupling constant is the self-consistent value introduced in equations (8.58) and (10.27). A similar calculation carried out using this value for the neighbouring nucleus, ^{10}Be, yields good agreement with the experimentally known transition probability of the quadrupole low-lying vibrational state (Ajzenberg-Selove (1988, 1990), Raman *et al*. (1987)).

In the calculation of the renormalization effects of the single-particle resonances of ^{10}Li due to the coupling to vibrational states one has to consider not only the effective-mass-like diagrams (upper part graph of Fig. 11.1, I(b))

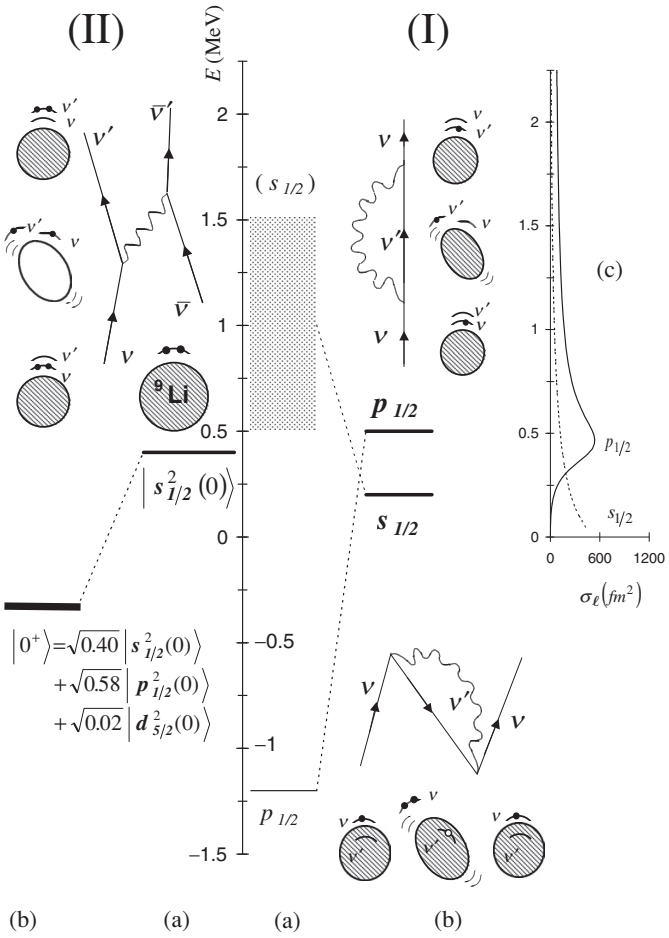

Figure 11.1. (I) Single-particle neutron resonances in ^{10}Li. In (a) the position of the levels $s_{1/2}$ and $p_{1/2}$ calculated using mean-field theory is shown (dotted area and thin horizontal line respectively). The coupling of a single-neutron (upward-pointing arrowed line) to a vibration (wavy line) calculated using the Feynman diagrams shown in (b) (schematically depicted also in terms of either solid dots (neutron) or open circles (neutron hole) moving in a single-particle level around or in the ^{9}Li core (hatched area)), leads to conspicuous shifts in the energy centroid of the $s_{1/2}$ and $p_{1/2}$ resonances (shown by thick horizontal lines) and eventually to an inversion in their sequence. In (c) we show the calculated partial cross-section σ_l for neutron elastic scattering off ^{9}Li. (II) The two-neutron system ^{11}Li. We show in (a) the mean-field picture of ^{11}Li, where two neutrons (solid dots) move in time-reversal states around the core ^{9}Li (hatched area) in the $s_{1/2}$ resonance leading to an unbound $s^2_{1/2}(0)$ state where the two neutrons are coupled to zero angular momentum. The exchange of vibrations between the two neutrons shown in the upper part of the figure leads to a density-dependent interaction which, added to the nucleon–nucleon interaction (v_{14} Argonne), correlates the two-neutron system leading to a bound state $|0^+\rangle$, where the two neutrons move with probability 0.40, 0.58 and 0.02 in the two-particle configurations $s^2_{1/2}(0)$, $p^2_{1/2}(0)$ and $d^2_{5/2}(0)$ respectively (after Barranco *et al*. (2001)).

https://doi.org/10.1017/9781009401920 Published online by Cambridge University Press

Table 11.3. *RPA wavefunction of the collective low-lying quadrupole vibration of* ^{9}Li *(X and Y are the forward-going and backward-going amplitudes respectively, equation (8.38)), calculated using a separable quadrupole–quadrupole interaction (equation (3.50), see also equation (8.44)) and allowing particles to move in the levels of the Saxon–Woods potential discussed in the text. The self-consistent value* ($\kappa_2 = 0.013\,\mathrm{MeV}^{-1}$*; see equation (8.58)) of the coupling constant has been adopted. The energy of this state is* $E_{2+} = 3.3\,\mathrm{MeV}$. *All the listed amplitudes refer to neutron transitions, except for the last two columns. The resulting value for the quadrupole transition probability corresponds to the deformation parameter* $\beta_2 = 0.66$. *A calculation of the low-lying quadrupole transition in the neighbouring nucleus* ^{10}Be *with the same coupling constant yields the value* $\beta_2 = 0.9$, *close to the experimental value* $\beta_2 = 1.1$ *(Raman et al. (1987)).*

	$1p_{3/2}^{-1}1p_{1/2}$	$1p_{3/2}^{-1}8f_{7/2}$	$1p_{3/2}^{-1}9f_{7/2}$	$1s_{1/2}^{-1}d_{5/2}$	$1p_{3/2}^{-1}p_{1/2}\,(\pi)$	$1s_{1/2}^{-1}1d_{5/2}\,(\pi)$
X_{ph}	1.02	0.07	0.08	0.07	0.15	0.09
Y_{ph}	0.28	0.05	0.06	0.06	0.09	0.07

leading to attractive (negative) contributions to the single-particle energies, but also those couplings leading to ground-state correlation (repulsive) corrections associated with diagrams containing two particles, one hole and a vibration in the intermediate states (lower part diagram of Fig. 11.1, I(b) (see Section 9.1, and Fig. 9.2). Because of such ground-state correlation processes, the $p_{1/2}$ state experiences an upward shift in energy. This arises from the coupling of this orbital to the $p_{3/2}$ hole-state through quadrupole vibrational states resulting from the exchange of the odd particle state $p_{1/2}$ with that participating in the vibration, in keeping with the fact that the $(p_{1/2}p_{3/2}^{-1})$ particle–hole excitation constitutes an important component of the quadrupole vibration wavefunction (see Table 11.3). As a consequence, the $p_{1/2}$ state becomes unbound, turning into a low-lying resonance with centroid $E_{\mathrm{res}} \approx 0.5\,\mathrm{MeV}$. Owing to the coupling to the vibrations the s-state is instead shifted downwards. There are essentially no (repulsive) contributions arising from the ground state correlation-correction processes for the s-state.

On the other hand (attractive) effective-mass-like processes with intermediate states consisting of one particle plus a vibrational state of the type $(d_{5/2} \times 2^+)$ lead to a virtual state with $E_{\mathrm{virt}} = 0.2\,\mathrm{MeV}$ (see Fig. 11.1, I(b)). The above results provide an overall account of the s- and p-resonances observed experimentally. The important difference between the distribution of the single-particle strength associated with the resonant state $p_{1/2}$ and the virtual state $s_{1/2}$ can be observed

in Fig. 11.1, I(c), where the partial cross-section σ_l for neutron elastic scattering off ^{9}Li is shown. While σ_p displays a clear peak at 0.5 MeV, σ_s is a smoothly decreasing function of the energy. A small increase in the depth of the potential felt by the s-neutron will lead to a (slightly) bound state, hence the name of virtual resonance.

11.1.2 ^{11}Li and the Cooper pair problem

In the infinite system bound Cooper pairs exist for an arbitrarily weak interaction (see Section 1.7), while in the nuclear case this phenomenon occurs only if the strength of the nucleon–nucleon potential is larger than a critical value related to the spacing of single-particle levels in the nuclear spectrum (see Section 1.9). In fact, calculations carried out using v_{14} Argonne NN potential (see Chapter 8) show that the nuclear forces are able to bind Cooper pairs in open-shell nuclei like, for example, ^{120}Sn leading to sizeable pairing gaps (see Figs. 8.6 and 8.9), but not in closed-shell nuclei.

The situation is quite different in the case of ^{11}Li where the NN-Argonne potential, is not able to bind the last two neutrons. To calculate the spectrum of ^{11}Li one places two neutrons in the continuum of levels associated with the $s_{1/2}$ and $p_{1/2}$ resonances as well as in the $d_{5/2}$ states, and diagonalizes the v_{14} NN potential. The calculations show that the bare nucleon–nucleon interaction is not able to bind the two last neutrons to the ^{9}Li core. The low-lying states resulting from the diagonalization of the Argonne nucleon–nucleon force are dominated by one of the configurations $|s^2_{1/2}(0)>$, $|p^2_{1/2}(0)>$ or $|d^2_{5/2}(0)>$. The v_{14} NN potential produces almost no mixing between s-waves, p-waves and d-waves, and only shifts the energy of the unperturbed (resonant) configurations $s^2_{1/2}(0)$ and $p^2_{1/2}(0)$ by about 80 keV without giving rise to a bound system. The $d^2_{5/2}(0)$ configurations are essentially not shifted. Making use of the same single-particle levels and the same matrix elements of the nucleon–nucleon potential to solve the BCS gap equations, one obtains no solution other than the trivial one of zero pairing gap ($\Delta_\nu = 0$). At the basis of this negative result is the fact that the most important single-particle states which contribute to correlations between the halo neutrons of ^{11}Li are the $s_{1/2}$, $p_{1/2}$ and $d_{5/2}$ orbitals. In this low angular momentum phase space, the two neutrons are not able to profit fully from the strong force-pairing interaction associated with the v_{14} NN potential (see equation (8.7)). This is because only the components of multipolarity $L = 0$, 1 and 2 of this force are effective in ^{11}Li because of angular momentum and parity conservation rules.

This negative result together with the fact that ^{11}Li displays strongly collective, low-lying vibrations suggests that the exchange of these vibrations between the two outer neutrons of ^{11}Li is likely to be the main source of pairing correlations in that nucleus (see Fig. 11.2). This effect has been studied by Barranco *et al.* (2001). The $L = 0$, 1 and 2-vibrational spectrum of ^{11}Li needed to calculate the

https://doi.org/10.1017/9781009401920 Published online by Cambridge University Press

Table 11.4. *RPA wavefunction of the collective low-lying quadrupole phonon in* ^{11}Li*, of energy* $E_{2+} = 5.05$ MeV. *All the listed amplitudes refer to neutron transitions, except for the last column. The self-consistent value* ($\kappa_2 = 0.013\,\text{MeV}^{-1}$) *for the coupling constant was used. The resulting value for the deformation parameter is* $\beta_2 = 0.5$.

	$1p^{-1}_{3/2}1p_{1/2}$	$2s^{-1}_{1/2}5d_{3/2}$	$1p^{-1}_{1/2}6p_{3/2}$	$2s^{-1}_{1/2}3d_{5/2}$	$2s^{-1}_{1/2}5d_{5/2}$	$1p^{-1}_{3/2}1p_{1/2}$ (π)
X_{ph}	0.824	0.404	0.151	0.125	0.126	0.16
Y_{ph}	0.119	0.011	−0.002	−0.049	−0.011	0.07

matrix elements of this induced interaction was determined in much the same way as in ^{9}Li, i.e. making use of the RPA (see Table 11.3) with the same value of the quadrupole coupling constant. Because the calculations are carried out on the physical (correlated) ^{11}Li ground state, the particle–hole transitions associated with the vibrational states involving the $p_{1/2}$ and the $s_{1/2}$ states are to be calculated with the energies and corresponding occupation numbers resulting from the full diagonalization. The strength of the separable dipole–dipole interaction can be adjusted to provide an overall account of the experimental dipole response in ^{11}Li. Unperturbed particle–hole excitations up to 70 MeV have been included and phonon states up to 50 MeV have been considered. Within this space there are of the order of 10^2 states, exhausting the associated energy-weighted sum rule (Section 8.3). The calculated soft dipole response is shown in Fig. 11.3 (see also Fig. 11.2). The low-lying quadrupole response is concentrated in a single peak, whose wavefunction is shown in Table 11.4. A Skyrme-type effective interaction (SLy4) was instead used to calculate the monopole linear response. The corresponding solutions were obtained in coordinate space making use of a mesh extending up to a radius of 80 fm. The monopole response exhausts 94% of the EWSR considering the summed contributions up to 40 MeV of excitation energy (see Fig. 11.3(c)).

All the resulting vibrational states were coupled to the single-particle states making use of the corresponding transition densities (formfactors, see Fig. 11.3(b) and (d)) and associated particle–vibration coupling strengths. In the monopole case, the response function was discretized in bins of 300 keV.

These calculations, which form the basis of the results shown in Fig. 11.1 and Table 11.1, allowed the two outer neutrons of ^{11}Li both to exchange phonons (induced interaction, Fig. 11.1, II(a)), as well as to emit and later reabsorb them (self-energy correction, Fig. 11.1, I(b)). It was found that the last two neutrons in ^{11}Li form a bound (Cooper) pair, the lowest eigenstate of the associated secular matrix being $E_{\text{gs}} = -0.270$ MeV. This result is mostly due to the exchange of the low-lying dipole vibrations shown in Fig. 11.3(a) with associated wavefunction

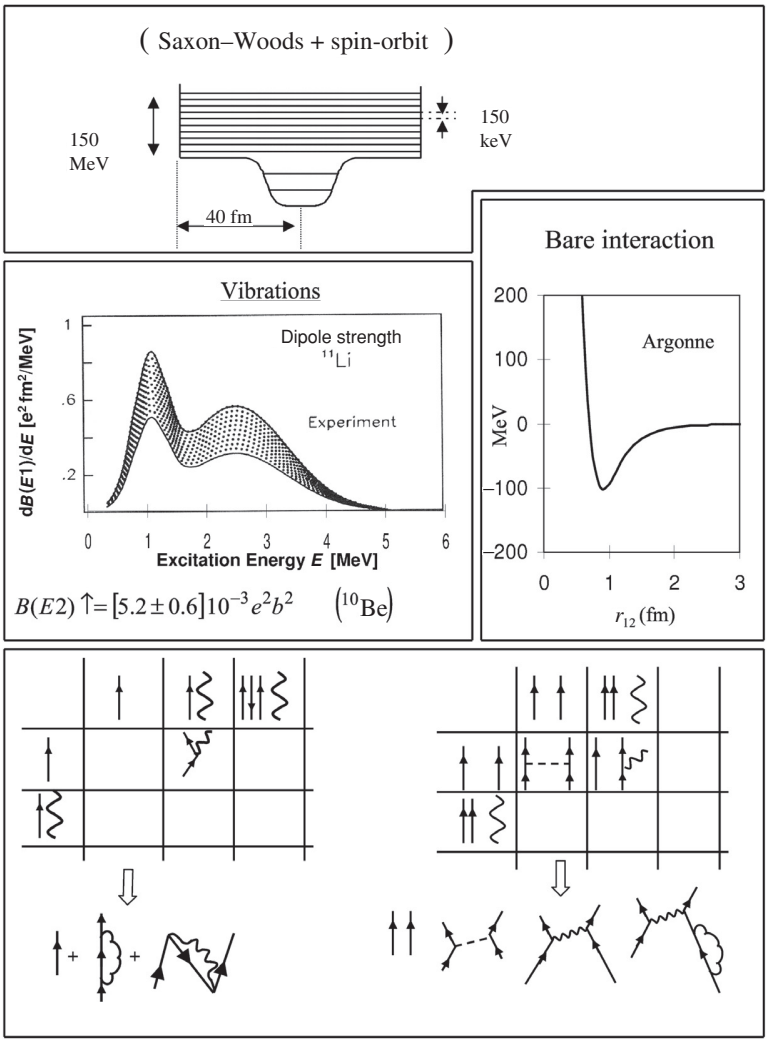

Figure 11.2. In the upper part of the figure, the single-particle potential used to describe the single-particle motion in Li is schematically shown. In the middle left part, the experimental elements used to calculate the strength of the dipole and quadrupole separable interactions are shown, while at the right the dependence of the $T = 1$, $S = 0$ v_{14} Argonne potential on the relative distance r_{12} is displayed. Scattering events up to 200 MeV are to be considered due to the repulsive core of v_{14}. In the lower part of the figure, a schematic representation of the matrices associated with the coupling of neutrons (arrowed lines) through the v_{14} potential (dashed line) and through surface vibrations (wavy lines) for ^{10}Li (left) and ^{11}Li (right) are displayed. The last row shows the basic processes taken into account to all orders in the diagonalization of the corresponding matrices.

https://doi.org/10.1017/9781009401920 Published online by Cambridge University Press

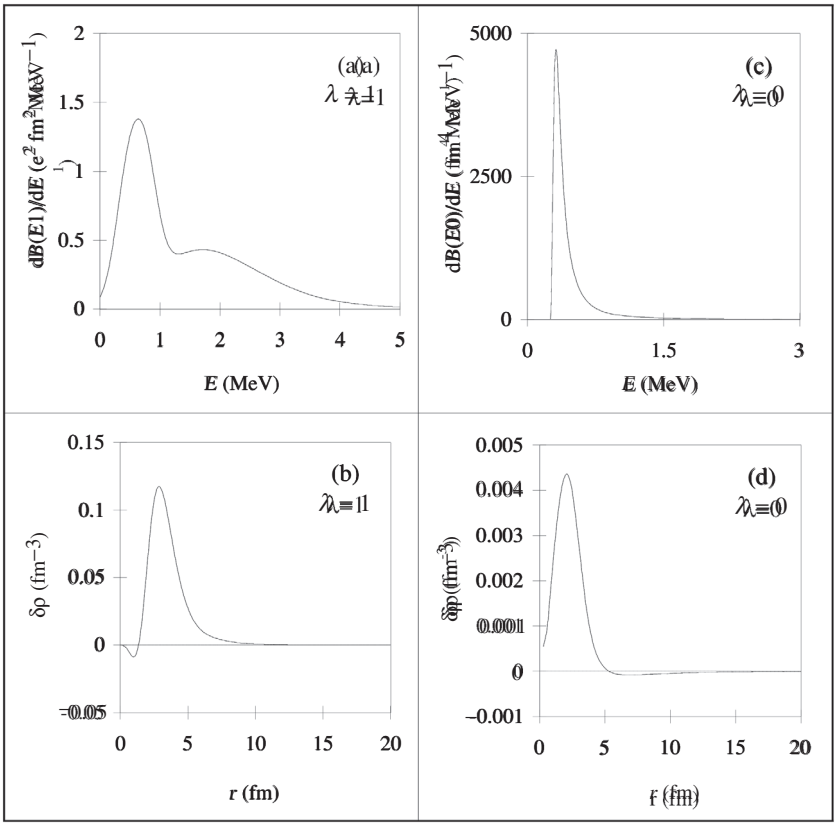

Figure 11.3. Dipole and monopole linear response functions and transition densities of ^{11}Li calculated in the RPA. The dipole response ($\lambda^\pi = 1^-$) was determined making use of the multipole–multipole separable interaction $H = t_z \kappa_1 (F_1(\vec{r}_1) \cdot F_1(\vec{r}_2))_0$, with $F_{1M}(\vec{r}) = r \frac{\partial U}{\partial r} Y_{1M}$. The coupling constant was fixed to provide an overall account of the experimental findings. For simplicity we show in (a) the overall strength function (coarse mesh representation) and not the individual states (about 100). The transition density associated with the state close to the peak, at $E_{1^-} = 0.75$ MeV is shown in (b) (see equation (10.47)). The corresponding wavefunction is shown in Table 11.5. No experimental information exists concerning the monopole modes. An effective Skyrme interaction (SLy4) was used to determine the strength function shown in (c). The transition density at the peak ($E_{0^+} \approx 0.5$ MeV) is shown in (d) (after Barranco *et al.* (2001)).

collected in Table 11.5. Adding to the induced interaction the nucleon–nucleon v_{14} Argonne potential one obtains $E_{\rm gs} = -0.330$ MeV, and thus a two-neutron separation energy quite close to the experimental value. Measured from the unperturbed energy of a pair of neutrons in the lowest state calculated for ^{10}Li, namely the s-resonance ($E_{\rm unp} = 2E_{s_{1/2}} = 400$ keV, see Fig. 11.1, I(b)), it leads to a pairing correlation (Section 3.5) energy $E_0 = E_{\rm unp} - E_{\rm gs} = 0.730$ MeV (see Fig. 11.1, II(b)).

https://doi.org/10.1017/9781009401920 Published online by Cambridge University Press

Table 11.5. *RPA wavefunction of the strongest low-lying dipole vibration of* ^{11}Li *($E_{1-} = 0.75$ MeV), contributing most importantly to the pairing induced interaction (Fig. 11.1 II). All the listed amplitudes refer to neutron transitions. The value $\kappa_{1-} = 0.0043\,\mathrm{MeV}^{-1}$ for the isovector coupling constant has been used. It was determined in order to get a good agreement with the experimental findings. Note that this value is quite similar to the self-consistent value of* $0.0032\,\mathrm{MeV}^{-1}$. *The resulting strength function (see Fig. 11.3(a)) integrated up to* 4 MeV *gives 7% of the Thomas–Reiche–Kuhn energy weighted sum rule (equation (8.51) with $L = 1$), to be compared with the experimental value of 8% (Zinser et al. (1997)).*

	$1p^{-1}_{1/2}2s_{1/2}$	$1p^{-1}_{1/2}3s_{1/2}$	$1p^{-1}_{1/2}4s_{1/2}$	$1p^{-1}_{1/2}1d_{3/2}$	$1p^{-1}_{3/2}5d_{5/2}$	$1p^{-1}_{3/2}6d_{5/2}$	$1p^{-1}_{3/2}7d_{5/2}$
X_{ph}	0.847	−0.335	0.244	0.165	0.197	0.201	0.157
Y_{ph}	0.088	0.060	0.088	0.008	0.165	0.173	0.138

From the associated two-particle ground-state wavefunction $\Psi_0(\vec{r}_1, \vec{r}_2)(\equiv \langle \vec{r}_1, \vec{r}_2|0^+\rangle)$, Barranco *et al*. (2001) obtain a momentum distribution (whose FWHM is $\sigma_\perp = 56$ MeV/c, for ^{11}Li on ^{12}C) and ground-state occupation probabilities of the two-particle states $s^2_{1/2}(0)$, $p^2_{1/2}(0)$ and $d^2_{5/2}(0)$ (0.40, 0.58 and 0.02 respectively, see Fig. 11.1, II(b)), which provide an overall account of the experimental findings. The radius of the associated single-particle distribution is 7.1 fm. Adding to this density that of the core nucleons one obtains the total density of ^{11}Li. The associated mean square radius (3.9 fm) is somewhat larger than the experimental value.

Within the framework of the above discussion it is unlikely that one can obtain a good description of the medium polarization effects in ^{11}Li by coupling the two-halo neutrons to vibrations of ^{9}Li. In fact, this model gives very different results to those obtained by coupling the vibrations of ^{11}Li to the two-halo neutrons, correcting for Pauli principle violations (Appendix F) (in this connection see Kuo *et al*. (1997)).

Also in this connection, we note that Hamamoto and Mottelson (2003) have studied pairing correlations in weakly bound neutron systems by solving the HFB equations in coordinate space with the correct asymptotic boundary conditions. These are systems where the pair field provides a significant coupling between neutron pairs in the bound state and neutrons moving in the low-energy continuum. Making use of a local pair field of either volume type (that is, $\Delta(r) \sim f(r)$, see equation (8.14) or surface type $\Delta(r) \sim r\mathrm{d}f(r)/\mathrm{d}r$) they found that $s_{1/2}$ neutrons with small binding energies are nearly decoupled from the main pair field. Because $s_{1/2}$ neutrons play a central role in halo nuclei, Hamamoto and Mottelson conclude that the HFB approximation is inadequate to describe these nuclei.

Although the question is quite open, it is likely that this result is another example of the limitations of static mean-field theories discussed at the end of

Section 8.2. These limitations are, at least partially, removed by the dynamic shell model (Mahaux (1985)), taking also into account, in a self-consistent manner, the induced pairing interaction arising from polarization effects.

In fact, the exchange of vibrations with a long tail form factor (see Fig. 11.3(b)) give rise to pairing fields which extend far beyond that associated with the density of the core which is closely connected with the formfactor $f(r)$ (see Barranco *et al*. 2001 as well as Figs. 11.4 and 11.5).

11.1.3 Spatial structure of the Cooper pair

The spatial structure of the Cooper pair described by the wavefunction $\Psi_0(\vec{r}_1, \vec{r}_2)$ is shown in Fig. 11.4. The mean square radius of the centre of mass of the two neutrons is $\langle r^2_{\rm cm}\rangle^{1/2} = 5.4$ fm. This result demonstrates the importance that the correlations have in collecting the small (enhanced) amplitudes of the uncorrelated two-particle configuration $s^2_{1/2}(0)$ in the region between 4 and 5 fm, a region in which the $p^2_{1/2}(0)$, helped by the centrifugal barrier, shows a somewhat larger concentration (see Fig. 11.5). From the above results, it emerges that the exchange of vibrations between the least bound neutrons leads to a (density-dependent) pairing interaction acting essentially only outside the core (see also Bertsch and Esbensen (1991)). Note that the long wavelength behaviour of these vibrations is connected with the excitation of the neutron halo, the large size of which not only makes the system easily polarizable but also provides the elastic medium through which the loosely bound neutrons exchange vibrations with each other. Because the vibrational states of ^{11}Li are built out of excitations which occupy, to some extent, the same particle states occupied by the loosely bound neutrons being studied, the corresponding particle-vibration matrix elements have to be corrected because of Pauli violating contributions (see Appendix F) following the nuclear field theory rules (Bes *et al*. (1976a,b), Bes and Broglia (1977), Bortignon *et al*. (1977))). In particular, the reduction factors of the particle–vibration coupling Hamiltonian $H_{\rm c}$ (see Appendix F) associated with the matrix elements $< s_{1/2} \times 1^- | H_{\rm c} | p_{1/2} >$, $< s_{1/2} \times 0^+ | H_{\rm c} | s_{1/2} >$ and $< p_{1/2} \times 0^+ | H_{\rm c} | p_{1/2} >$ are 0.68, 0.25 and 0.25 respectively.

The average mean square distance between the halo neutrons is $\langle r^2_{12}\rangle^{1/2} \approx 9.2$ fm, a result which is consistent with the fact that the coherence length associated with Cooper pairs in nuclei is larger than the nuclear dimensions thus preventing the possibility of a nuclear supercurrent. On the other hand, this value of $< r^2_{12} >$ does not prevent the two correlated neutrons being close together, the corresponding (small) probability (see Fig. 11.4) being much larger than that associated with the uncorrelated neutrons (see Fig. 11.5).

Similar results to those reported above are obtained solving the BCS equation for the two-neutron system making use of the matrix elements used in the diagonalization, the sum of those of the nucleon–nucleon v_{14} Argonne

https://doi.org/10.1017/9781009401920 Published online by Cambridge University Press

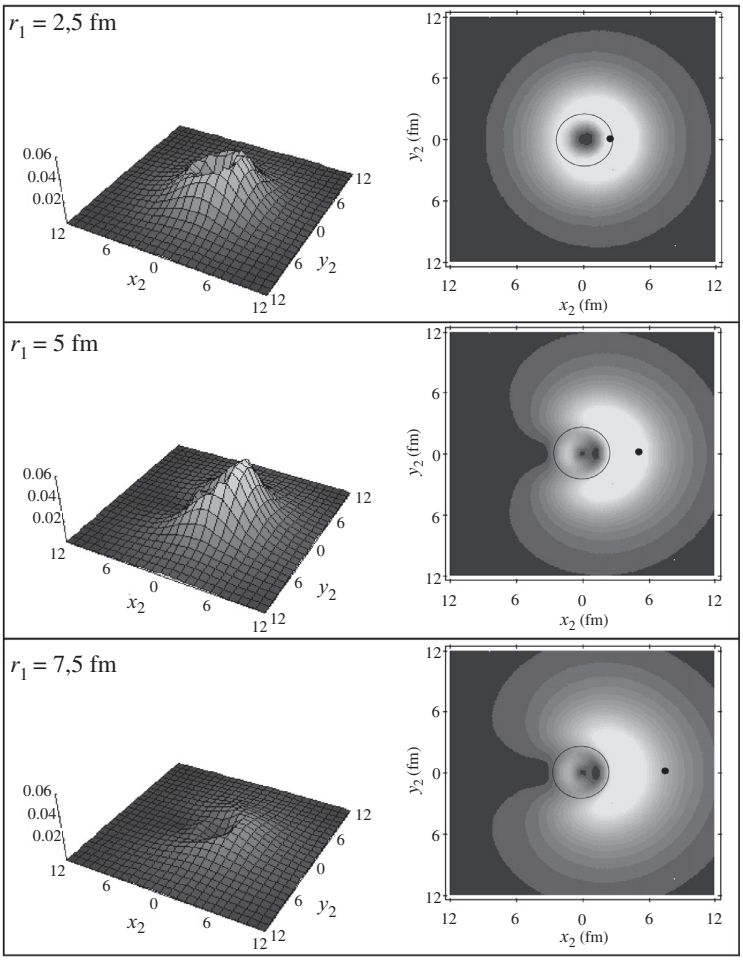

Figure 11.4. Spatial structure of two-neutron Cooper pair. The modulus squared wavefunction $|\Psi_0(\vec{r}_1, \vec{r}_2)|^2 = |\langle \vec{r}_1, \vec{r}_2 | 0^+ \rangle|^2$ (see Fig. 11.1, II (b)) describing the motion of the two-halo neutrons around the ^{9}Li core (normalized to unity and multiplied by $16\pi^2 r_1^2 r_2^2$) is displayed as a function of the cartesian coordinates $x_2 = r_2 \cos(\theta_{12})$ and $y_2 = r_2 \sin(\theta_{12})$ of particle 2, for fixed value of the position of particle 1 ($r_1 = 2.5, 5, 7.5$ fm) represented in the right panels by a solid dot, while the core ^{9}Li is shown as a solid curve circle. The numbers appearing on the z-axis of the three-dimensional plots displayed on the left side of the figure are in units of fm^{-2} (after Barranco *et al*. (2001)).

potential and those of the induced interaction. In this case, the correlation energy is $E_0 = -0.7$ MeV, the separation energy of the two neutrons becoming $S_{2n} = 0.360$ MeV. The radial structure of the projected BCS wavefunctions $\sum_{\nu>0}(V_\nu/U_\nu)\varphi_\nu(\vec{r}_1)\varphi_\nu(\vec{r}_2)$ displays a spatial structure quite similar to $\Psi_0(\vec{r}_1, \vec{r}_2)$, the admixture of s- , p- and d- two-particle configurations being now 46%, 51%

https://doi.org/10.1017/9781009401920 Published online by Cambridge University Press

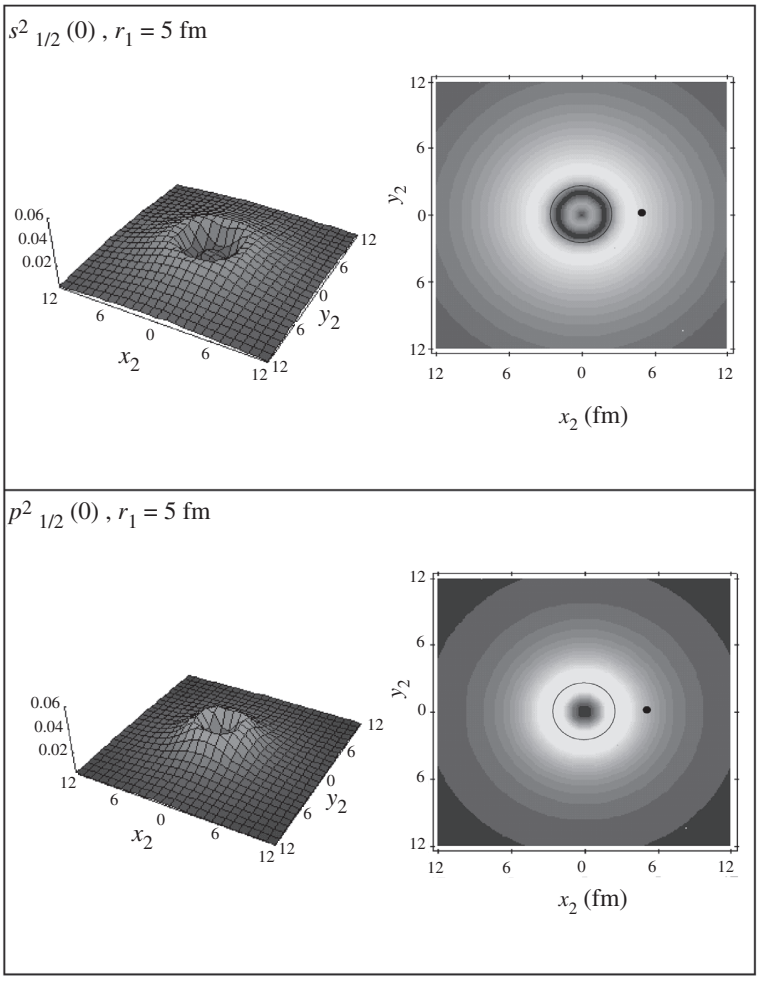

Figure 11.5. Spatial distribution of the pure two-particle configurations $s^2_{1/2}$ (0) and $p^2_{1/2}$(0) as a function of the x- and y-coordinates of particle 2, for a fixed value of the coordinate of particle 1 ($r_1 = 5$ fm). For more details see the caption to Fig. 11.4 (after Barranco *et al.* (2001)).

and 3% respectively. The coherence length ξ, i.e. the mean square distance between the two neutrons forming the Cooper pair, is in this case $\langle r^2_{12} \rangle^{1/2} = 7.8$ fm.

11.1.4 Transfer reactions

The specific probe of pairing correlations is two-particle transfer reactions (see e.g. Broglia *et al.* (1973) and references therein). Combined with single-particle

https://doi.org/10.1017/9781009401920 Published online by Cambridge University Press

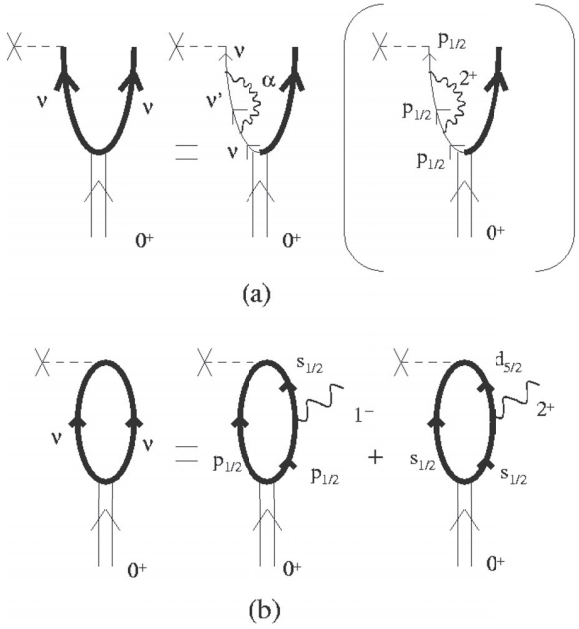

Figure 11.6. (a) Field theoretical representation of the process ^{11}Li$(p, d)^{10}$Li. A double arrowed line indicates the two-halo neutron Cooper pair, while a single arrowed heavy drawn curve indicates a nucleon dressed through its coupling to a vibration (wavy line). In parentheses a specific contribution to the dressing process is shown. (b) Field theoretical representation of the two-neutron pick-up process ^{11}Li$(p, t)^{9}$Li.

stripping and pick-up reactions (see Fig. 11.6) they can provide a stringent test of the main (microscopic) predictions that nuclear field theory makes concerning ^{10}Li and ^{11}Li, namely

$$|\tilde{s}_{1/2}\rangle = a|s_{1/2}\rangle + b|d_{5/2} \times 2^+; \tfrac{1}{2}^+\rangle + c|p_{1/2} \times 1^-; \tfrac{1}{2}^+\rangle + \ldots, \quad (11.2)$$

$$|\tilde{p}_{1/2}\rangle = A|p_{1/2}\rangle + B|p_{1/2} \times 2^+; \tfrac{1}{2}^-\rangle + C|s_{1/2} \times 1^-; \tfrac{1}{2}^-\rangle + \ldots, \quad (11.3)$$

and

$$|0^+\rangle = \alpha|s^2_{1/2}(0)\rangle + \beta|p^2_{1/2}(0)\rangle + \gamma|d^2_{5/2}(0)\rangle + \delta|\left(s_{1/2}, d_{5/2}\right) 2^+ \times 2^+; 0\rangle + \gamma|\left(s_{1/2}, p_{1/2}\right) 1^- \times 1^-; 0\rangle + \ldots . \quad (11.4)$$

In what follows we shall discuss the one-particle spectroscopic factors associated with (d, p) and (p, d) reactions and spectroscopic amplitudes associated with (t, p) and (p, t) reactions. The measurement of these quantities could be, in principle, attempted by making use of inverse kinematics techniques.

https://doi.org/10.1017/9781009401920 Published online by Cambridge University Press

11.1.5 Spectroscopics factors

Quite generally the $^{9}\mathrm{Li}(d,\,p)^{10}\mathrm{Li}$ reaction may provide information on

$$|\langle\tilde{\nu}|a_{\nu}^{+}|gs\,(^{9}\mathrm{Li})\rangle|^{2}=\begin{cases}a^{2} & \nu=s_{1/2},\\ A^{2} & \nu=p_{1/2},\end{cases} \tag{11.5}$$

and $^{11}\mathrm{Li}(p,\,d)^{10}\mathrm{Li}$ (see Fig. 11.6 (a)) on

$$|\langle\tilde{\nu}|a_{\nu}|0^{+}\rangle|^{2}=\begin{cases}(\alpha a)^{2} & \nu=s_{1/2},\\ (\beta A)^{2} & \nu=p_{1/2}.\end{cases} \tag{11.6}$$

11.1.6 B-coefficients

The spectroscopic amplitudes associated with the two-particle process $^{11}\mathrm{Li}(p,\,t)^{9}\mathrm{Li}$ is given by (see Fig. 11.6 (b))

$$B_{\nu}\left(0^{+}\right)=\langle^{9}\mathrm{Li}(gs)|\,[a_{\nu}a_{\nu}]_{0}\,|0^{+}\rangle=\begin{cases}\alpha & \nu=s_{1/2},\\ \beta & \nu=p_{1/2},\\ \gamma & \nu=d_{5/2}.\end{cases} \tag{11.7}$$

The two-particle transfer cross-section is

$$\sigma(p,\,t)\sim\left(\sum_{\nu}B_{\nu}\left(0^{+}\right)\right)^{2}\approx(\alpha+\beta+\gamma)^{2}\,. \tag{11.8}$$

11.2 The halo nucleus ^{12}Be

In what follows we shall study the nuclei $^{11}_{4}\mathrm{Be}_{7}$ and $^{12}_{4}\mathrm{Be}_{8}$, allowing the nucleons to interact through a nucleon–nucleon realistic potential (Argonne v_{14}) taking also into account the coupling between single-particle motion and collective vibrations of the system as was done in the previous section for the case of ^{11}Li and ^{12}Li. Special emphasis will be made, in the present case, on the calculation of the spectroscopic factors of ^{12}Be which, together with the ground-state occupation probabilities of the two-particle configurations s^{2}, p^{2} and d^{2}, provide the most sensitive predictions for a detailed comparison with the experimental findings (Gori *et al*. (2004a)).

We start by considering the system $^{11}_{4}\mathrm{Be}_{7}$ described as one neutron moving around the core $^{10}_{4}\mathrm{Be}_{6}$, in keeping with the fact that the value of the neutron separation energy in ^{10}Be is 6.813 MeV compared with the value of 0.504 MeV in ^{11}Be. The single-particle levels are determined by solving the Schrödinger equation

$$\left(-\frac{\hbar^{2}}{2m_{k}}\nabla_{r}^{2}+U'(r)\right)\phi_{j}(r)=\epsilon_{j}\phi_{j}(r), \tag{11.9}$$

https://doi.org/10.1017/9781009401920 Published online by Cambridge University Press

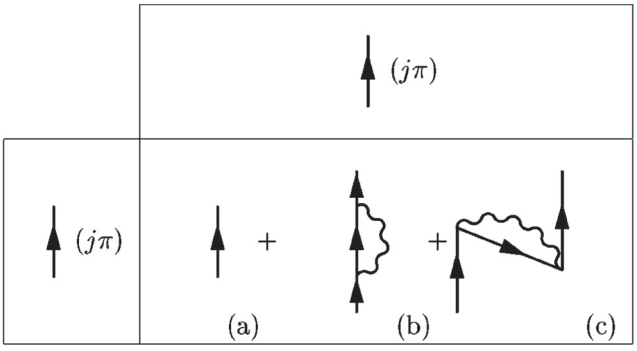

Figure 11.7. Schematic representation of the effective matrix used in the Bloch–Horowitz perturbation theory to calculate the eigenvalues of ^{11}Be (see Section 10.2). An arrowed line pointing upwards (downwards) indicates a particle (hole), while a wavy line indicates a collective vibrational state. Reprinted with permission from Gori *et al.*, *Phys. Rev.* **C69**: 041302 (R) (2004a). Copyright 2004 by the American Physical Society.

in a spherical box of radius equal to 30 fm so as to discretize the continuum states. The quantity m_k is the k-mass while $U'(r) = (m/m_k)U(r)$, $U(r)$ being a Saxon–Woods potential with a standard parametrization for the depth (Bohr and Mottelson (1969))

$$V = -50.5 + 33\frac{N-Z}{A}\,\text{MeV}. \tag{11.10}$$

In keeping with the fact that the k-mass is directly connected with non-locality effects (mainly exchange effects associated with the Fock potential), it is expected to strongly depend on the density of the system. In the case of nuclei along the stability valley, $m_k \approx 0.7m$, while in the case of halo nuclei like ^{11}Be, one expects $0.8m \leq m_k \leq m$. Calculations using both of the limiting values of m_k were carried out, with rather similar results, as explained below.

Making use of the associated particle–hole basis and of a separable multipole–multipole interaction, the $L^\pi = 2^+$ and 3^- vibrations were calculated in the QRPA (equation (8.47)). A self-consistent coupling constant k_L (see equation (10.27)), slightly adjusted to reproduce the energy of quadrupole vibrations, was used. The range of the associated deformation parameters β_L is consistent with observation (Iwasaki *et al.* (2000a,b), Raman *et al.* (1987)).

The eigenvalues of the dressed single-particle states were obtained by diagonalizing (energy-dependent) matrices of the order $10^2 \times 10^2$ whose elements connect a basis of unperturbed states containing both bound and continuum solutions of equation (11.9) with energies up to 350 MeV, with states containing a particle and a vibration (Fig. (11.7(b)) as well as two particles and a hole plus a collective mode (Fig. (11.7(c)). The calculations were carried out for states with quantum number $s_{1/2}$, $p_{1/2}$ and $d_{5/2}$. Similar results were obtained by making use

https://doi.org/10.1017/9781009401920 Published online by Cambridge University Press

Table 11.6. *Comparison of experimental binding energy and spectroscopic factors with those resulting from the NFT calculations (see Table 11.2, also referred to as particle-vibration $+v_{14}$ (see Table 11.1)) and from an independent particle (mean-field) model. The spectroscopic factors are those for the transfer of one particle on $s_{1/2}$ and $p_{1/2}$ states. They were measured for ^{11}Be and ^{12}Be by Navin et al. (2000) and Iwasaki et al. (2000a,b) respectively. For ^{12}Be, we also show the components of the resulting ground-state wavefunction (after Gori et al. (2004a)).*

			Theory	
		Exper.	Particle-vibration	Mean-field
$^{11}_{4}$Be$_7$	$E_{s_{1/2}}$	-0.504 MeV	-0.48 MeV	~ 0.14 MeV
	$E_{p_{1/2}}$	-0.18 MeV	-0.27 MeV	-3.12 MeV
	$E_{d_{5/2}}$	1.28 MeV(*)	~ 0 MeV	~ 2.4 MeV
	$S\left[1/2^+\right]$	0.77	0.87	1
	$S\left[1/2^-\right]$	0.96	0.86	1
	$S\left[5/2^+\right]$		0.72	1
$^{12}_{4}$Be$_8$	S_{2n}	-3.673 MeV	-3.58 MeV	-6.24 MeV
	s^2, p^2, d^2		23%, 29%, 48%	0%, 100%, 0%
	$S\left[1/2^+\right]$	0.42 ± 0.10	0.31	0
	$S\left[1/2^-\right]$	0.37 ± 0.10	0.57	1

* Tentative assignment.

of the unperturbed single-particle basis calculated solving equation (11.9) with $m_k/m = 1$ and $m_k/m = 0.8$, as the larger (absolute) values of the energies ϵ_j are compensated by the stronger particle-vibration coupling vertices proportional to β_L and to $\partial U'/\partial r$ (see equation (8.18)). In what follows we shall refer to the results obtained with $m_k/m = 1$, results which are displayed in Table 11.6, compared with the experimental findings. Theory provides an overall account of the experimental findings, also concerning the spectroscopic factors associated with the reaction ^{10}Be$(d, p)^{11}$Be (Zwieglinski *et al.* (1979)). The way these quantities were calculated is discussed below in connection with a shell model calculation carried out in connection with the reaction ^{12}Be$(^9$Be,^{9}Be $+n + \gamma)^{11}$Be (Navin *et al.* (2000)).

Note that there is experimental evidence of the existence of a resonant $d_{5/2}$ state at 1.28 MeV (Zwieglinski *et al.* (1979), Ajzenberg-Selove (1990)). A calculation was carried out following the steps discussed in Navin *et al.* (2000) but setting the unperturbed energy of the $d_{5/2}$ resonance at 4.1 MeV, so that the dressed resonance had an energy of 1.2 MeV. In this case the spectroscopic factors

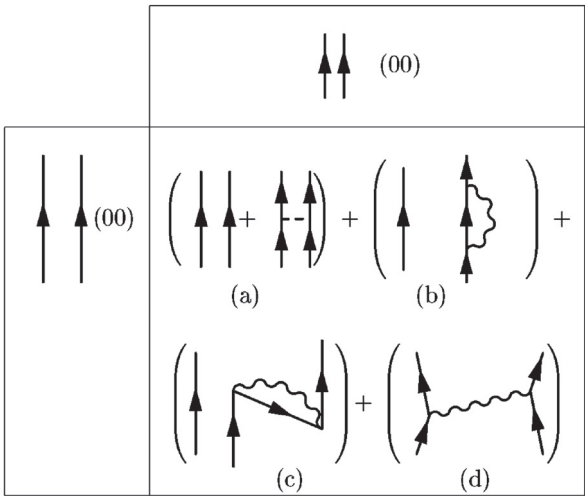

Figure 11.8. Schematic representation of the effective matrix used in the Bloch-Horowitz perturbation theory to calculate the eigenvalues of ^{12}Be. The dashed horizontal line represent the bare (Argonne v_{14}) nucleon–nucleon potential. Pairs of nucleons are coupled to angular momentum $L = 0$. Reprinted with permission from Gori *et al*., *Phys. Rev.* **C69**: 041302 (R) (2004). Copyright 2004 by the American Physical Society.

associated with ^{11}Be are 0.9, 0.96 and 0.73 respectively, while the ^{12}Be ground-state wavefunction becomes (s^2, p^2, d^2) 80%, 5%, 15%.

The self-energy (Fig. 11.7(b)) and Pauli principle correction (Fig. 11.7(c)) processes used to describe the dressed single-particle states of ^{11}Be, which eventually accounted for the parity inversion experimentally observed, have been included in the description of the ground state of ^{12}Be as can be seen from Fig. 11.8, which shows the effective matrix to be diagonalized in order to describe the ground-state properties of the correlated three-body system ^{12}Be (similar calculations carried out by Nuñez *et al*. (1996) did not include processes of type (c), Fig. 11.8). The Hilbert space used to describe ^{12}Be is made out of two-particle states (see Fig. 11.8(a)), two particles and one phonon (Fig. 11.8(b) and Fig. 11.8(d)), and three particles, one hole and one phonon states (Fig. 11.8(c)). All these configurations are coupled to zero angular momentum and display energies up to 500 MeV. The effects of v_{14} and of the particle-vibration coupling in ^{12}Be are determined by diagonalizing the effective, energy-dependent ($\approx 10^3 \times 10^3$) matrix. The lowest eigenvalue -3.58 MeV is to be compared with the experimental two-particle separation energy of -3.67 MeV. The main contribution to the nucleon–nucleon interaction arises from the induced interaction (Fig. 11.8(d)), that associated with the bare nucleon–nucleon potential (see Fig. 11.8(a)) being very small ($\approx$100 keV), a situation already encountered in the study of ^{11}Li and associated with the small l-content of the s, p, d-subspace.

https://doi.org/10.1017/9781009401920 Published online by Cambridge University Press

The squared amplitudes of the ^{12}Be ground-state wavefunction are shown in Table 11.6. The large $d^2_{5/2}(0)$-amplitude predicted for the ^{12}Be ground state (see also Navin *et al*. (2000)) compared with that calculated in the case of ^{11}Li can be understood in terms of the fact that the $d_{5/2}$ orbital is, in ^{10}Li, much less confined than in ^{11}Be, thus displaying much smaller overlaps with the $1s_{1/2}$ and $0p_{1/2}$ orbitals. Furthermore, this result is also connected with the fact that in ^{11}Li the dipole mode is much softer than in ^{12}Be (Iwasaki *et al*. (2000a,b)). Using the ^{12}Be ground-state wavefunction and that obtained for the ground state and the first excited state of ^{11}Be, one has calculated the spectroscopic factors associated with the knock-out reaction ^{12}Be (^{9}Be, ^{9}Be $+n+\gamma$) ^{11}Be. The results are compared in Table 11.6 with the experimental findings (Navin *et al*. (2000)).

https://doi.org/10.1017/9781009401920 Published online by Cambridge University Press

Appendix A
A brief résumé of second quantization

Second quantization provides an economic representation of quantum mechanics which includes automatically the statistics fulfilled by the particles composing the system. This appendix summarizes some of the basic results for fermions and bosons.

A.1 Fermions

Let us consider a system of n identical fermions and let $\Psi(\vec{r}_1, \vec{r}_2, \ldots, \vec{r}_n)$ denote the exact wavefunction of the system. Let us introduce the state $\Phi(\vec{r}_1, \vec{r}_2, \ldots, \vec{r}_n)$, a member of a complete set of n-particle wavefunctions. It is constructed as a properly symmetrized product of one-particle wavefunctions $\varphi_\nu(\vec{r})$, which form a complete orthonormal set

$$\int \varphi_\nu^*(\vec{r})\, \varphi_{\nu'}(\vec{r})\, \mathrm{d}^3 r = \delta(\nu, \nu'), \tag{A.1}$$

$$\sum_\nu \varphi_\nu^*(\vec{r}\,')\, \varphi_\nu(\vec{r}) = \delta(\vec{r} - \vec{r}\,'). \tag{A.2}$$

The function $\Phi(\vec{r}_1, \vec{r}_2, \ldots, \vec{r}_n)$, in the case of fermions, is given by the determinant of the single-particle wavefunctions

$$\Phi(\vec{r}_1, \vec{r}_2, \ldots, \vec{r}_n) = \frac{\det}{\sqrt{n!}}(\varphi_{\nu_1}(\vec{r}_1)\varphi_{\nu_2}(\vec{r}_2)\cdots\varphi_{\nu_n}(\vec{r}_n)). \tag{A.3}$$

The function Ψ is thus a linear combination of determinants.

We now introduce the creation and annihilation fermion operators $a_\nu^\dagger$ and a_ν respectively, acting on the fermion vacuum state $|0\rangle_\mathrm{F}$. These operators satisfy the anticommutation relations

$$\{a_\nu, a_{\nu'}^\dagger\} = a_\nu a_{\nu'}^\dagger + a_{\nu'}^\dagger a_\nu = \delta(\nu, \nu') \tag{A.4}$$

and

$$\{a_\nu, a_{\nu'}\} = \{a_\nu^\dagger, a_{\nu'}^\dagger\} = 0. \tag{A.5}$$

https://doi.org/10.1017/9781009401920 Published online by Cambridge University Press

This choice restricts the occupation number of the states ν to 0 or 1 as required by Fermi statistics and to antisymmetric normalized states. Acting with the creation operator $a_j^\dagger$ on the vacuum one creates a single-particle state

$$a_j^\dagger |0\rangle_{\mathrm{F}} = |j\rangle, \tag{A.6}$$

where the r-representation coincides with the single-particle wavefunction

$$\langle \vec{r}\,|\, j\rangle = \varphi_j(\vec{r}).$$

The orthonormalization condition

$$\begin{aligned}\langle j\,|\, j'\rangle &= {}_{\mathrm{F}}\langle 0|a_j a_{j'}^\dagger|0\rangle_{\mathrm{F}} = {}_{\mathrm{F}}\langle 0|\delta(j, j') - a_{j'}^\dagger a_j|0\rangle_{\mathrm{F}} \\ &= \delta(j, j') \equiv {}_{\mathrm{F}}\langle 0|\overbrace{a_j a_{j'}^\dagger}|0\rangle_{\mathrm{F}}\,,\end{aligned} \tag{A.7}$$

where the relation given by equation (A.4) has been used together with

$$a_j|0\rangle_{\mathrm{F}} = 0, \tag{A.8}$$

and

$${}_{\mathrm{F}}\langle 0|0\rangle_{\mathrm{F}} = 1. \tag{A.9}$$

The symbol in the last term of equation (A.7) denotes a contraction. According to Wick's theorem, to calculate overlaps or matrix elements involving $a^\dagger$ and a, one should carry out all possible contractions between creation and annihilation operators, introducing a minus sign each time that in the contraction one jumps over an odd number of operators, and a plus sign otherwise.

A two-particle state in this representation reads

$$a_j^\dagger a_{j'}^\dagger|0\rangle_{\mathrm{F}} = |j, j'\rangle. \tag{A.10}$$

Making use of the anticommutation relation (A.5) one can show that

$$|j, j'\rangle = -|j', j\rangle, \tag{A.11}$$

i.e. the two-particle state is antisymmetric. Consequently,

$$|j, j\rangle = 0, \tag{A.12}$$

i.e. no two fermions can occupy the same quantal state, as required by the Pauli principle.

The orthonormalization condition of the state $|j, j'\rangle$ is given by the relation

$$\langle j_1, j_2|j_1', j_2'\rangle = {}_{\mathrm{F}}\langle 0|\,\overbrace{a_{j_2}\overbrace{a_{j_1}a_{j_1'}^\dagger}a_{j_2'}^\dagger}|0\rangle_{\mathrm{F}} \tag{A.13}$$

$$= \delta(j_2, j_2')\,\delta(j_1, j_1') - \delta(j_1, j_2')\,\delta(j_1', j_2). \tag{A.14}$$

This result can also be obtained directly without using Wick's theorem by making repeated use of the anticommutation relation given in equation (A.4). Equations (A.11),

https://doi.org/10.1017/9781009401920 Published online by Cambridge University Press

(A.12) and (A.14) indicate that

$$\langle \vec{r}, \vec{r}\,' | j_1\, j_2 \rangle = \frac{1}{\sqrt{2}} \begin{vmatrix} \varphi_{j_1}(\vec{r}) & \varphi_{j_2}(\vec{r}) \\ \varphi_{j_1}(\vec{r}\,') & \varphi_{j_2}(\vec{r}\,') \end{vmatrix}. \tag{A.15}$$

Let us now calculate the matrix element of a two-body interaction

$$\begin{aligned} \langle j_1 j_2 | v | j_1' j_2' \rangle_a &= \frac{1}{2} \int \mathrm{d}^3 r\, \mathrm{d}^3 r' \begin{vmatrix} \varphi_{j_1}(\vec{r}) & \varphi_{j_2}(\vec{r}) \\ \varphi_{j_1}(\vec{r}\,') & \varphi_{j_2}(\vec{r}\,') \end{vmatrix}^* v(|\vec{r} - \vec{r}\,'|) \begin{vmatrix} \varphi_{j_1'}(\vec{r}) & \varphi_{j_2'}(\vec{r}) \\ \varphi_{j_1'}(\vec{r}\,') & \varphi_{j_2'}(\vec{r}\,') \end{vmatrix} \\ &= \int \mathrm{d}^3 r\, \mathrm{d}^3 r' \varphi^*_{j_1}(\vec{r})\, \varphi^*_{j_2}(\vec{r}\,') v(|\vec{r} - \vec{r}\,'|) \varphi_{j_1'}(\vec{r})\, \varphi_{j_2'}(\vec{r}\,') \\ &\quad - \int \mathrm{d}^3 r\, \mathrm{d}^3 r' \varphi^*_{j_1}(\vec{r})\, \varphi^*_{j_2}(\vec{r}\,') v(|\vec{r} - \vec{r}\,'|)\, \varphi_{j_2'}(\vec{r})\, \varphi_{j_1'}(\vec{r}\,'). \end{aligned} \tag{A.16}$$

Note that this matrix element changes sign each time two particles are exchanged either in the initial or in the final states. For example,

$$\begin{aligned} \langle j_2 j_1 | v | j_1' j_2' \rangle_a &= \int \mathrm{d}^3 r \mathrm{d}^3 r' \varphi^*_{j_2}(\vec{r}) \varphi^*_{j_1}(\vec{r}\,') v(|\vec{r} - \vec{r}\,'|) \varphi_{j_1'}(\vec{r}) \varphi_{j_2'}(\vec{r}\,') \\ &\quad - \int \mathrm{d}^3 r \mathrm{d}^3 r' \varphi^*_{j_2}(\vec{r}) \varphi^*_{j_1}(\vec{r}\,') v(|\vec{r} - \vec{r}\,'|) \varphi_{j_2'}(\vec{r}) \varphi_{j_1'}(\vec{r}\,') \\ &= \int \mathrm{d}^3 r \mathrm{d}^3 r' \varphi^*_{j_1}(\vec{r}) \varphi^*_{j_2}(\vec{r}\,') v(|\vec{r} - \vec{r}\,'|) \varphi_{j_2'}(\vec{r}) \varphi_{j_1'}(\vec{r}\,') \\ &\quad - \int \mathrm{d}^3 r \mathrm{d}^3 r' \varphi^*_{j_1}(\vec{r}) \varphi^*_{j_2}(\vec{r}\,') v(|\vec{r} - \vec{r}\,'|) \varphi_{j_1'}(\vec{r}) \varphi_{j_2'}(\vec{r}\,') \\ &= -\langle j_1 j_2 | v | j_1' j_2' \rangle_a, \end{aligned}$$

where in going from the first to the second expression one has exchanged $\vec{r}$ to $\vec{r}\,'$. Consequently,

$$\begin{aligned} \langle j_1 j_2 | v | j_1' j_2' \rangle_a &= -\langle j_1 j_2 | v | j_2' j_1' \rangle_a \\ &= -\langle j_2 j_1 | v | j_1' j_2' \rangle_a = \langle j_2 j_1 | v | j_2' j_1' \rangle_a. \end{aligned} \tag{A.17}$$

We now proceed to express operators in second quantization. Because a one-body operator can change, at most, the state of motion of a single particle it must be bilinear in the creation and destruction operators. Similarly, a two-body interaction which can change the state of motion of two particles simultaneously must be a quartic function of the creation and annihilation operators. In particular the Hamiltonian, sum of a kinetic term and a two-body interaction can be written in second quantization as

$$H = \sum_{j_1\, j_2} \langle j_1 | T | j_2 \rangle a^\dagger_{j_1} a_{j_2} + \frac{1}{4} \sum_{\substack{j_1\, j_2 \\ j_3\, j_4}} \langle j_1\, j_2 | v | j_3\, j_4 \rangle_a a^\dagger_{j_2} a^\dagger_{j_1} a_{j_3} a_{j_4}. \tag{A.18}$$

In Fig. A.1 we schematically display the action of the second term on a pair of particles. The matrix element $\langle j_1\, j_2 | v | j_3\, j_4 \rangle_a$ has been defined in equation (A.16).

We now proceed to derive the Hartree–Fock equation associated with H, which means to extract the one-body Hartree–Fock Hamiltonian. For this purpose we have to carry

https://doi.org/10.1017/9781009401920 Published online by Cambridge University Press

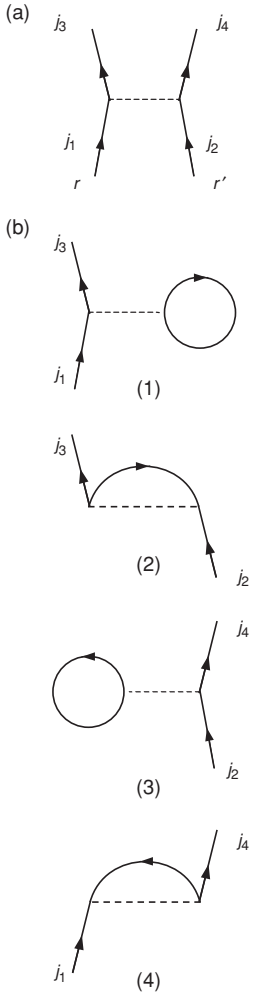

Figure A.1. (a) Scattering of two nucleons through the bare NN interaction. (b) (1) and (3): contributions to the (direct) Hartree potential (see equations (A.20) and (A.22) as well as (A.28)). (2) and (4): contributions to the (exchange) Fock potential (see equations (A.21), (A.23) and (A.30)).

out single contractions in the second term of H. The first term is already bilinear in the creation and annihilation operators. The four possible contractions are

$$\overset{\textcircled{2}}{\overset{\textcircled{1}}{a^\dagger_{j_2} a^\dagger_{j_1} a_{j_3} a_{j_4}}}, \qquad \overset{\textcircled{3}}{\textcircled{4}} \tag{A.19}$$

https://doi.org/10.1017/9781009401920 Published online by Cambridge University Press

leading to the four contributions (see Fig. A.1)

$$①= \frac{1}{4}\sum_{j_1\, j_3}\sum_{\substack{i\\(\varepsilon_i \le \varepsilon_F)}} \langle j_1\, i\,|v|\, j_3\, i\rangle_a\, a^\dagger_{j_1}\, a_{j_3}, \tag{A.20}$$

$$②= -\frac{1}{4}\sum_{j_1\, j_4}\sum_{\substack{i\\(\varepsilon_i \le \varepsilon_F)}} \langle j_1 i\,|v|\, i j_4\rangle_a\, a^\dagger_{j_1}\, a_{j_4}, \tag{A.21}$$

$$③= \frac{1}{4}\sum_{j_2\, j_4}\sum_{\substack{i\\(\varepsilon_i \le \varepsilon_F)}} \langle i j_2|v|i j_4\rangle_a\, a^\dagger_{j_2}\, a_{j_4}, \tag{A.22}$$

$$④= -\frac{1}{4}\sum_{j_2\, j_3}\sum_{\substack{i\\(\varepsilon_i \le \varepsilon_F)}} \langle i j_2|v|j_3 i\rangle_a\, a^\dagger_{j_2}\, a_{j_3}. \tag{A.23}$$

Making use of the relations given in equation (A.17), one notes that all the contributions are equal, their sum being

$$\sum_{j_1\, j_2}\sum_{\substack{i\\(\varepsilon_i \le \varepsilon_F)}} \langle j_1\, i\,|v|\, j_2\, i\rangle_a\, a^\dagger_{j_1} a_{j_2}\ . \tag{A.24}$$

Note that i runs only over occupied states, i.e. $\varepsilon_i \le \varepsilon_F$. This is because to annihilate a particle (e.g. in the contraction ① that is the state j_3) the corresponding quantal state should be occupied.

Equating the sum of the kinetic energy term (see equation in terms of (A.18)) and of the potential term (equation (A.24)) to a diagonal, single-particle energy, provides the mean-field Schrödinger equation

$$\sum_{j_1\, j_2}\left(\langle j_1|T|j_2\rangle + \sum_{\substack{i\\(\varepsilon_i \le \varepsilon_F)}} \langle j_1\, i\,|v|\, j_2\, i\rangle_a\right) a^\dagger_{j_1} a_{j_2} = \sum_{j_1\, j_2} \varepsilon_{j_1} a^\dagger_{j_1}\, a_{j_2}\delta(j_1, j_2), \tag{A.25}$$

that is

$$\begin{aligned}
&\int \mathrm{d}^3 r''\varphi^*_{j'}(\vec{r}\,'')T\varphi_j(\vec{r}\,'') \\
&\qquad + \sum_{\substack{i\\(\varepsilon_i \le \varepsilon_F)}} \int \mathrm{d}^3 r'\mathrm{d}^3 r''\varphi^*_{j'}(\vec{r}\,'')\varphi^*_i(\vec{r}\,')v(|\vec{r}\,'' - \vec{r}\,'|)\varphi_j(\vec{r}\,'')\varphi_i(\vec{r}\,') \\
&\qquad - \sum_{\substack{i\\(\varepsilon_i \le \varepsilon_F)}} \int \mathrm{d}^3 r'\mathrm{d}^3 r''\varphi^*_{j'}(\vec{r}\,'')\varphi^*_i(\vec{r}\,')v(|\vec{r}\,'' - \vec{r}\,'|)\varphi_j(\vec{r}\,')\varphi_i(\vec{r}\,'') \\
&\qquad = \varepsilon_j\delta(j, j')
\end{aligned} \tag{A.26}$$

https://doi.org/10.1017/9781009401920 Published online by Cambridge University Press

Multiplying from the left by $\Sigma_{j'}\varphi_{j'}(\vec{r})$, one obtains the Hartree–Fock equation in the r-representation,

$$\Big(T + U(r)\Big)\varphi_j(\vec{r}) + \int \mathrm{d}^3 r'\, U_x(|\vec{r} - \vec{r}\,'|)\varphi_j(\vec{r}\,') = \varepsilon_j \varphi_j(\vec{r}), \tag{A.27}$$

where

$$U(r) = \int \mathrm{d}^3 r'\, \rho(r)\, v(|\vec{r} - \vec{r}\,'|) \tag{A.28}$$

is the Hartree potential associated with processes depicted in graphs (1) and (3) of Fig. A.1 (see also equations (A.20) and (A.22)). In this expression

$$\rho(r) = \sum_{\substack{i \\ (\varepsilon_i \le \varepsilon_\mathrm{F})}} |\varphi_i(\vec{r})|^2, \tag{A.29}$$

is the density of the system. The term

$$U_x = - \sum_{\substack{i \\ (\varepsilon_i \le \varepsilon_\mathrm{F})}} \varphi_i^*(\vec{r}\,')\, v(|\vec{r} - \vec{r}\,'|)\, \varphi_i(\vec{r}) \tag{A.30}$$

is the Fock (exchange) potential and has its origin on the Pauli principle (graphs (2) and (4) of Fig. A.1 and equations (A.21) and (A.23)). This term eliminates contributions to the mean field arising from the interaction of a fermion with itself. To see this let us neglect for a moment the exchange potential. Then equation (A.26) can be written as

$$-\frac{\hbar^2}{2m}\varphi_j(\vec{r}) + \sum_{\substack{i \\ (\varepsilon_i \le \varepsilon_\mathrm{F})}} \int \mathrm{d}^3 r'\, \varphi_i^*(\vec{r}\,') v(|\vec{r} - \vec{r}\,'|)\, \varphi_i(\vec{r}\,')\, \varphi_j(\vec{r}) = \varepsilon_j\, \varphi_j(\vec{r}). \tag{A.31}$$

However, because we are dealing with fermions, the product wavefunction $\varphi_i(\vec{r}\,')\,\varphi_j(\vec{r})$ has to be replaced by $\varphi_i(\vec{r}\,')\,\varphi_j(\vec{r}) - \varphi_i(\vec{r}\,')\,\varphi_j(\vec{r})$, thus leading to equation (A.27). Consequently, all contributions to the mean field from terms with $j = i$ vanish.

Once diagonalized, the Hartree–Fock Hamiltonian can be written in second quantization as

$$H_\mathrm{sp} = \sum_{\nu'} \varepsilon_{\nu'}\, a_{\nu'}^\dagger\, a_{\nu'}. \tag{A.32}$$

where

$$N_\nu = a_\nu^\dagger a_\nu \tag{A.33}$$

When applied to the state

$$|\nu\rangle = a_\nu^\dagger |0\rangle_\mathrm{F}, \tag{A.34}$$

https://doi.org/10.1017/9781009401920 Published online by Cambridge University Press

one obtains

$$H_{\rm sp}|\nu\rangle = \sum_{\nu'} \varepsilon_{\nu'}\, a^{\dagger}_{\nu'}\, a_{\nu'}\, a^{\dagger}_{\nu}\, |0\rangle_{\rm F} = \sum_{\nu'} \varepsilon_{\nu'}\, a^{\dagger}_{\nu'} \left(\delta(\nu, \nu') - a^{\dagger}_{\nu}\, a_{\nu'}\right)|0\rangle_{\rm F}$$
$$= \varepsilon_{\nu}\, a^{\dagger}_{\nu}\, |0\rangle_{\rm F} = \varepsilon_{\nu}\, |\nu\rangle, \tag{A.35}$$

making use of the fact that

$$a_{\nu'}\, |0\rangle_{\rm F} = 0. \tag{A.36}$$

A.2 Particles and holes

The ground (vacuum) state of Hartree–Fock theory can be written, in second quantization, as

$$|0\rangle_{\rm HF} = \prod_{\substack{i \\ (\varepsilon_i \le \varepsilon_{\rm F})}} a^{\dagger}_i |0\rangle_{\rm F} \quad \left(\sum_{\substack{i \\ (\varepsilon_i \le \varepsilon_{\rm F})}} 1 = A\right), \tag{A.37}$$

where i runs over the quantum numbers of all the occupied states. Assuming the state $|0\rangle_{\rm HF}$ to have an even number of particles, in particular to correspond to a closed-shell system, the total magnetic quantum number is

$$M_{\rm F} = \sum_i m_i = 0. \tag{A.38}$$

If one annihilates a particle in the state i with magnetic quantum number m_i, the resulting hole state

$$a_i |0\rangle_{\rm HF} \tag{A.39}$$

has projection

$$M_i = \sum_{i' \neq i} m_{i'} = -m_i. \tag{A.40}$$

This is because adding a particle with projection m_i to this state, one obtains a state with zero projection, as expressed by the relation given in equation (A.40). Because the angular momentum projection of the hole state (A.39) is opposite to that of the angular momentum of the corresponding particle state and because the third component of the angular momentum changes sign under time reversal it is possible to relate the creation operator of a hole in a given quantal state to the annihilation operator of a particle in the corresponding time-reversal state.

To be more explicit, the time reversal operator τ acting on a single-particle state $|jm\rangle$ with angular momentum quantum numbers (j, m) changes the sign of the projection of the angular momentum leading to

$$\tau\, |jm\rangle = (-1)^{p-m}\, |j\, -m\rangle\, .$$

The m-dependence of the phase is necessary to maintain the correct angular momentum transformation properties but the phase p can be chosen in various ways. Bohr and

https://doi.org/10.1017/9781009401920 Published online by Cambridge University Press

Mottelson (1969) choose $p = j$ but other choices are possible. The operation

$$b^\dagger_{jm}|0\rangle_{\rm HF} = (-1)^{j-m}\, a_{j-m}|0\rangle_{\rm HF}$$

creates a hole state with angular momentum quantum numbers (j, m).

More generally, one can define the creation operator of a hole as

$$b^\dagger_i = a_{\tilde{\imath}}, \tag{A.41}$$

where $|\tilde{\imath}\rangle = \tau\,|i\rangle$ is the time reverse of the state $|i\rangle$. The associate hole state is

$$|i^{-1}\rangle = b^\dagger_i|0\rangle_{\rm HF} = a_{\tilde{\imath}}|0\rangle_{\rm HF} \quad (\varepsilon_i \le \varepsilon_{\rm F})\,. \tag{A.42}$$

Implicit in equations (A.41) and (A.42) is the requirement that the same phase factors should be used in the definition of the hole creation operator as for the time-reversal operator. Note that

$$b^\dagger_{\tilde{\nu}} = a_{\tilde{\tilde{\nu}}} = -a_\nu \tag{A.43}$$

because $\tau^2 = -1$.

The economy associated with the concepts of particles and holes is evident. Instead of having to explicitly describe the motion of all the $i' \neq i$ particles present in the Hartree–Fock ground states, one needs to concentrate on the degrees of freedom of the single one which is missing in describing the behaviour of the hole state $|i^{-1}\rangle$. Although not mentioned explicitly, this approach has already been used in dealing with particle states. In fact, in describing the state

$$|k\rangle = a^\dagger_k|0\rangle_{\rm HF} \quad (\varepsilon_k > \varepsilon_{\rm F}), \tag{A.44}$$

one does not talk about all the $A + 1$ nucleons participating in this state (A are packed in $|0\rangle_{\rm HF}$) but only about the single-particle state k.

Let us now write the single-particle operator $\hat{F}$ in terms of creation and annihilation operators of particles and of holes, i.e.

$$\begin{aligned}\hat{F} &= \sum_{\nu_1\nu_2}\langle\nu_1|F|\nu_2\rangle a^\dagger_{\nu_1}a_{\nu_2} \\ &= \sum_{\nu_1\nu_2>\nu_F}\langle\nu_1|F|\nu_2\rangle a^\dagger_{\nu_1}a_{\nu_2} + \sum_{\nu_1\nu_2\le\nu_F}\langle\nu_1|F|\nu_2\rangle(-b_{\tilde{\nu}_1})(-b^\dagger_{\tilde{\nu}_2}) + \cdots\,,\end{aligned} \tag{A.45}$$

where the relation (A.42) has been used. The sum $\nu_1\nu_2 > \nu_{\rm F}$ is over single-particle states with energies larger than $\varepsilon_{\rm F}$, while $\nu_1\nu_2 \le \nu_{\rm F}$ implies states lying below or at $\varepsilon_{\rm F}$. One can then write

$$\hat{F} = \sum_{\nu_1\nu_2>\nu_{\rm F}}\langle\nu_1|F|\nu_2\rangle a^\dagger_{\nu_1}a_{\nu_2} - \sum_{\nu_1\nu_2\le\nu_{\rm F}}\langle\tilde{\nu}_1|F|\tilde{\nu}_2\rangle b^\dagger_{\nu_2}b_{\nu_1} + \cdots\,. \tag{A.46}$$

The dots in equations (A.45) and (A.46) refer to terms which create or annihilate particle–hole states.

Consequently

$$\langle\nu_1|\hat{F}|\nu_2\rangle = \langle\nu_1|F|\nu_2\rangle = \int {\rm d}^3r\;\varphi^*_{\nu_1}(\vec{r})\,F(\vec{r})\,\varphi_{\nu_2}(\vec{r}), \tag{A.47}$$

https://doi.org/10.1017/9781009401920 Published online by Cambridge University Press

while

$$\langle \nu_1^{-1}|\hat{F}|\nu_2^{-1}\rangle = -\langle \tilde{\nu}_2|F|\tilde{\nu}_1\rangle = -\langle \nu_2|\tau^{-1}F\tau|\nu_1\rangle = -\langle \nu_1|(\tau^{-1}F\tau)^\dagger|\nu_2\rangle. \tag{A.48}$$

Many single-particle operators have the time-reversal transformation property (Bohr and Mottelson (1969), Section 3-1b)

$$(\tau^{-1}F\tau)^\dagger = -cF, \tag{A.49}$$

where $c = \pm 1$. For example, time-even operators like the coordinate operator $\hat{\mathbf{r}}$ transform according to equation (A.49) with $c = -1$ while time-odd operators like the momentum $\hat{\mathbf{p}}$ and angular momentum $\hat{\mathbf{l}}$ have $c = 1$ (see Bortignon *et al*. (1983)). If an operator has the time-reversal transformation property (A.49) then the hole and particle state matrix elements are related by

$$\langle \nu_1^{-1}|\hat{F}|\nu_2^{-1}\rangle = c\langle \nu_1|F|\nu_2\rangle. \tag{A.50}$$

As explained earlier, this result depends on a consistent definition of the phases in the time-reversal transformation and particle–hole conjugation (see discussions following equations (3.90) and (8.71)).

A.3 Bosons

In the case of particles fulfilling Bose–Einstein statistics we introduce the boson operators $\Gamma_\alpha^\dagger$, Γ_α which create and annihilate a boson in a state α, and respect the commutation relations

$$[\Gamma_\alpha, \Gamma_{\alpha'}^\dagger] = \Gamma_\alpha\Gamma_{\alpha'}^\dagger - \Gamma_{\alpha'}^\dagger\Gamma_\alpha = \delta(\alpha, \alpha') \tag{A.51}$$

and

$$[\Gamma_\alpha, \Gamma_{\alpha'}] = [\Gamma_\alpha^\dagger, \Gamma_{\alpha'}^\dagger] = 0. \tag{A.52}$$

Calling $|0\rangle_{\mathrm{B}}$ the normalized boson vacuum state, i.e.

$${}_{\mathrm{B}}\langle 0|0\rangle_{\mathrm{B}} = 1, \tag{A.53}$$

one obtains, by definition,

$$\Gamma_\alpha|0\rangle_{\mathrm{B}} = 0. \tag{A.54}$$

The one-phonon state is defined as

$$\Gamma_\alpha^\dagger|0\rangle_{\mathrm{B}} = |n_\alpha = 1\rangle, \tag{A.55}$$

where n_α indicates the number of phonons in the quantal state α. This state is normalized. In fact

$$\begin{aligned}\langle n_\alpha = 1|n_{\alpha'} = 1\rangle &= {}_{\mathrm{B}}\langle 0|\Gamma_\alpha\Gamma_{\alpha'}^\dagger|0\rangle_{\mathrm{B}} \\ &= {}_{\mathrm{B}}\langle 0|\big(\delta(\alpha, \alpha') + \Gamma_{\alpha'}^\dagger\Gamma_\alpha\big)|0\rangle_{\mathrm{B}} = {}_{\mathrm{B}}\langle 0|\underbrace{\Gamma_\alpha\Gamma_{\alpha'}^\dagger}|0\rangle = \delta(\alpha, \alpha').\end{aligned} \tag{A.56}$$

https://doi.org/10.1017/9781009401920 Published online by Cambridge University Press

The last step in equation (A.56) contains a contraction between the boson creation and annihilation operators. It is the analogue of the contraction between fermion operators in equation (A.7). There is the Wick theorem for bosons which is the same as the one for fermions except that there are no sign changes when operators are interchanged. The commutation relation given in equation (A.51) implies that

$$\Gamma_\alpha^\dagger \Gamma_\alpha^\dagger |0\rangle_{\mathrm{B}} \neq 0, \tag{A.57}$$

i.e. bosons can occupy the same quantal state. Let us now work out the orthonormalization of this two-phonon state by carrying out all contractions

$${}_{\mathrm{B}}\langle 0|\Gamma_{\alpha'}\Gamma_{\alpha'}\Gamma_\alpha^\dagger\Gamma_\alpha^\dagger|0\rangle_{\mathrm{B}} = \delta(\alpha,\alpha')\,\delta(\alpha,\alpha') + \delta(\alpha,\alpha')\,\delta(\alpha,\alpha') = 2\delta(\alpha,\alpha'). \tag{A.58}$$

Consequently, the two-boson state

$$|n_\alpha = 2\rangle = \frac{1}{\sqrt{2}}\Gamma_\alpha^\dagger\Gamma_\alpha^\dagger|0\rangle_{\mathrm{B}} \tag{A.59}$$

is a normalized state. Note that

$$\Gamma_\alpha^\dagger|n=1\rangle = \Gamma_\alpha^\dagger\Gamma_\alpha^\dagger|0\rangle_{\mathrm{B}} = \sqrt{2}\,|n_\alpha = 1\rangle \tag{A.60}$$

and, in general,

$$\Gamma_\alpha^\dagger|n_\alpha = N\rangle = \sqrt{N+1}\,|n_\alpha = N+1\rangle. \tag{A.61}$$

We will now write the harmonic oscillator Hamiltonian in second quantization as originally done by Dirac (1935),

$$H = \sum_{\alpha'} \hbar\omega_{\alpha'}\left(\Gamma_{\alpha'}^\dagger\Gamma_{\alpha'} + \tfrac{1}{2}\right). \tag{A.62}$$

The energy of the ground state (vacuum state) is

$$H|0\rangle_{\mathrm{B}} = E_0, \tag{A.63}$$

where

$$E_0 = \frac{1}{2}\sum_{\alpha'} \hbar\omega_{\alpha'}. \tag{A.64}$$

It receives a $\frac{1}{2}\hbar\omega_\alpha$ contribution (zero-point fluctuation) for each degree of freedom of the system.

The one-phonon state has an energy

$$\begin{aligned} H|n_\alpha = 1\rangle &= \sum_{\alpha'} \hbar\omega_{\alpha'}\left(\Gamma_{\alpha'}^\dagger\Gamma_{\alpha'} + \frac{1}{2}\right)\Gamma_\alpha^\dagger|0\rangle_{\mathrm{B}} = \sum_{\alpha} \hbar\omega_{\alpha'}\Gamma_{\alpha'}^\dagger\Gamma_{\alpha'}\Gamma_\alpha^\dagger\ |0\rangle_{\mathrm{B}} + E_0\Gamma_\alpha^\dagger|0\rangle_{\mathrm{B}} \\ &= \left(\hbar\omega_\alpha + E_0\right)|n_\alpha = 1\rangle. \end{aligned} \tag{A.65}$$

https://doi.org/10.1017/9781009401920 Published online by Cambridge University Press

We will now calculate the commutator

$$[H, \Gamma_\alpha^\dagger] = \sum_\alpha \hbar\omega_{\alpha'}[\Gamma_{\alpha'}^\dagger \Gamma_{\alpha'}, \Gamma_\alpha^\dagger]. \tag{A.66}$$

Making use of the relation

$$[AB, C] = A[B, C] + [A, C]B, \tag{A.67}$$

one obtains

$$[H, \Gamma_\alpha^\dagger] = \sum_{\alpha'} \hbar\omega_{\alpha'}\left(\Gamma_{\alpha'}^\dagger[\Gamma_{\alpha'}, \Gamma_\alpha^\dagger] + [\Gamma_{\alpha'}^\dagger, \Gamma_\alpha^\dagger]\Gamma_{\alpha'}\right) = \sum_{\alpha'} \hbar\omega_{\alpha'}\Gamma_{\alpha'}^\dagger\delta(\alpha, \alpha') = \hbar\omega_\alpha\Gamma_\alpha^\dagger. \tag{A.68}$$

That is, this expression provides a relation to determine the eigenvalues of a Hamiltonian H in the harmonic approximation. Of course this approximation becomes exact if H is the Hamiltonian describing a harmonic oscillator.

A.4 Quasi-bosons

Making use of the relations given in equation (A.67) and those relating commutators to anticommutators,

$$[A, BC] = -B\{A, C\} + \{A, B\}C, \tag{A.69}$$

one can calculate

$$\begin{aligned}
[a_{\bar\nu}a_\nu, a_{\nu'}^\dagger a_{\bar\nu'}^\dagger] &= a_{\bar\nu}[a_\nu, a_{\nu'}^\dagger a_{\bar\nu'}^\dagger] + [a_{\bar\nu}, a_{\nu'}^\dagger a_{\bar\nu'}^\dagger]a_\nu \\
&= a_{\bar\nu}\Big(-a_{\nu'}^\dagger\{a_\nu, a_{\bar\nu'}^\dagger\} + \{a_\nu, a_{\nu'}^\dagger\}a_{\bar\nu'}^\dagger \\
&\qquad -a_{\nu'}^\dagger\{a_{\bar\nu}, a_{\bar\nu'}^\dagger\} + \{a_{\bar\nu}, a_{\nu'}^\dagger\}a_{\bar\nu'}^\dagger\Big)a_\nu \\
&= a_{\bar\nu}\left(\delta(\nu, \nu')a_{\bar\nu}^\dagger - a_\nu^\dagger\delta(\nu, \nu')\right)a_\nu \\
&= \delta(\nu, \nu')\left(1 - N_\nu - N_{\bar\nu}\right),
\end{aligned} \tag{A.70}$$

where $N_\nu = a_\nu^\dagger a_\nu$, and where it has been assumed that ν and $\bar\nu\,'$ are two different quantal states, one of the class with positive angular momentum projection and the other with negative m-value. If this commutator is applied to the vacuum state one obtains

$$[a_{\bar\nu}a_\nu, a_{\nu'}^\dagger a_{\bar\nu'}^\dagger]|0\rangle = \delta(\nu, \nu')|0\rangle. \tag{A.71}$$

Consequently, under certain circumstances, a couple of fermions behave like a (quasi-) boson (see equation (5.12)). Making use of (A.70) one obtains

$$[P, P^\dagger] = \delta(\nu, \nu')\Omega\left(1 - \frac{\hat N}{\Omega}\right), \tag{A.72}$$

https://doi.org/10.1017/9781009401920 Published online by Cambridge University Press

where

$$P = \sum_{\nu>0} a_\nu^\dagger a_{\bar{\nu}}^\dagger,$$

2Ω is the number of degenerate single fermion states and $\hat{N} = \sum_\nu a_\nu^\dagger a_\nu = \sum_{\nu>0} \left(a_\nu' a_\nu + a_{\bar{\nu}}^\dagger a_{\bar{\nu}} \right)$ is the operator number of particles. It is then clear that the last factor in equation (A.72) arises from the Pauli principle acting between fermions.

https://doi.org/10.1017/9781009401920 Published online by Cambridge University Press

Appendix B
Single particle in a non-local potential

The exchange (Fock) term in the single-particle Hartree–Fock equation is non-local in the position coordinate $\vec{r}$ (see Fig. B.1, see also Fig. A1(4)). A short range non-locality can be approximated by a momentum dependence which can be included in the Schrödinger equation by defining a k-effective mass m_k. This k-mass approximation was introduced in Chapter 8. The effective interaction between nucleons due to phonon exchange has a time dependence, which can be incorporated in an ω-effective mass m_ω (Chapter 9). The purpose of this appendix is to discuss some of the properties of these effective masses.

Let us start with the time-dependent Hartree–Fock equation

$$\mathrm{i}\hbar\frac{\partial\varphi_\nu(\vec{r},t)}{\partial t} = \Big(-\frac{\hbar^2\nabla^2}{2m} + U(r)\Big)\varphi_\nu(\vec{r},t) + \int \mathrm{d}^3r'\, U_x(\vec{r},\vec{r}\,')\,\varphi_\nu(\vec{r}\,',t), \tag{B.1}$$

where $U_x(\vec{r},\vec{r}\,')$ is the Fock term in the single-particle potential. Let us assume an infinite system and $U(r) = V_0$ (constant) for simplicity. Consequently,

$$\varphi_\nu(\vec{r},t) = \mathrm{e}^{\mathrm{i}(\vec{k}_\nu\cdot\vec{r}-\omega t)}/\sqrt{V}, \tag{B.2}$$

where V is the volume of the system.

Replacing this wavefunction in equation (B.1) leads to

$$\hbar\omega\mathrm{e}^{\mathrm{i}(\vec{k}_\nu\cdot\vec{r}-\omega t)} = \left(\frac{\hbar^2k_\nu^2}{2m} + V_0\right)\mathrm{e}^{\mathrm{i}(\vec{k}_\nu\cdot\vec{r}-\omega t)} + \int \mathrm{d}^3r'\, U_x(\vec{r},\vec{r}\,')\mathrm{e}^{\mathrm{i}(\vec{k}_\nu\cdot\vec{r}\,'-\omega t)}.$$

Multiplying from the left by $\mathrm{e}^{-\mathrm{i}(\vec{k}_\nu\cdot\vec{r}-\omega t)}$ and making use of the fact that $U_x(\vec{r},\vec{r}\,')$ does not depend on the centre of mass coordinate $\vec{R} = (\vec{r}+\vec{r}\,')/2$ but only on the relative coordinate $\varrho = \vec{r}-\vec{r}\,'$ and that the Jacobian $\partial(\vec{\varrho},\vec{R})/\partial(\vec{r},\vec{r}\,') = 1$, one obtains

$$\varepsilon = \frac{\hbar^2k^2}{2m} + V_0 + U_x(k). \tag{B.3}$$

https://doi.org/10.1017/9781009401920 Published online by Cambridge University Press

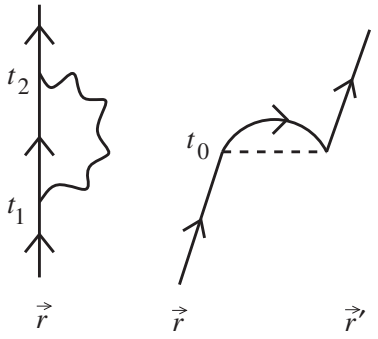

Figure B.1. Coupling of a particle to a vibration (left). Exchange diagram associated with the Fock potential (right).

Here $\varepsilon = \hbar\omega$ is the single-particle energy and

$$U_x(k) = \int \frac{\mathrm{d}^3R}{V} \int \mathrm{d}^3\varrho \mathrm{e}^{-\mathrm{i}(\vec{k}_v.\vec{r}-\omega t)} U_x(\vec{r},\vec{r}\,') \mathrm{e}^{\mathrm{i}(\vec{k}_v.\vec{r}\,'-\omega t)}$$
$$= \int \mathrm{d}^3\varrho \mathrm{e}^{-\mathrm{i}\vec{k}_v.\vec{\varrho}} U_x(\vec{r},\vec{r}\,')$$

is the Fourier transform of the Fock (exchange) potential. Let us force an independent single-particle dispersion relation by absorbing the non-local potential in an effective k-mass

$$\varepsilon = \frac{\hbar^2k^2}{2m_k} + \tilde{V}_0, \tag{B.4}$$

where $\tilde{V}_0$ is a constant. From the relation (note that we are determining an inertia, i.e. studying the reaction of the system to a change in its state of motion)

$$\frac{\mathrm{d}\varepsilon}{\mathrm{d}k} = \frac{\hbar^2k}{m} + \frac{\partial U_x}{\partial k} \approx \frac{\hbar^2k}{m_k}, \tag{B.5}$$

which assumes that m_k is approximately constant, we obtain

$$m_k = m\left(1 + \frac{m}{\hbar^2k}\frac{\partial U_x}{\partial k}\right)^{-1}. \tag{B.6}$$

The momentum dependence in equation (B.3) can be replaced by a dispersion relation for the energy

$$\varepsilon = \frac{\hbar^2k^2}{2m} + U(\varepsilon). \tag{B.7}$$

From equation (B.4) one can write

$$\frac{\hbar^2k^2}{2m} = \frac{m_k}{m}\left(\varepsilon - \tilde{V}_0\right).$$

https://doi.org/10.1017/9781009401920 Published online by Cambridge University Press

Replacing this relation in equation (B.7) one obtains

$$U(\varepsilon) = \varepsilon - \frac{m_k}{m}\left(\varepsilon - \tilde{V}_0\right)$$
$$= \frac{m_k}{m}\tilde{V}_0 + \left(1 - \frac{m_k}{m}\right)\varepsilon. \tag{B.8}$$

Inserting this relation in equation (B.7) and comparing with equation (B.3) one obtains

$$V_0 = \frac{m_k}{m}\tilde{V}_0.$$

Summing up

$$\varepsilon = \frac{\hbar^2 k^2}{2m_k} + \frac{m}{m_k}V_0. \tag{B.9}$$

In other words, equations (B.3) and (B.9) should provide an equivalent description of the system under consideration. Note that m_k may depend on r.

B.1 Single particle in a non-local, ω-dependent potential

The processes depicted in Fig. B.1 give rise to a non-local (k-dependent) and time-dependent (ω-dependent) potential. In what follows we shall discuss some of its consequences making use of a one-dimensional system. Equation (B.1) becomes

$$\mathrm{i}\hbar\frac{\partial\varphi_\nu(x,t)}{\partial t} = -\frac{\hbar^2}{2m}\nabla^2\varphi_\nu(x,t) + \int \mathrm{d}x'\,\mathrm{d}t'\,U(x'-x,t'-t)\,\varphi_\nu(x',t')\,. \tag{B.10}$$

Making use of wavefunctions like the one given in equation (B.2), but in one dimension, one obtains

$$\varepsilon = \frac{\hbar^2 k^2}{2m} + \int \mathrm{d}x'\,\mathrm{d}t'\,\mathrm{e}^{\mathrm{i}(k(x'-x)-\omega(t'-t))}U(x'-x,t'-t),$$

leading to

$$\hbar\omega = \varepsilon = \frac{\hbar^2 k^2}{2m} + V_0 + U(k,\omega), \tag{B.11}$$

where $U(k,\omega)$ is the Fourier transform of $U(x'-x,t'-t)$. Again, we impose the single-particle dispersion relation introducing an effective mass m^*, i.e.

$$\hbar\omega = \frac{\hbar^2 k^2}{2m^*} + \tilde{V}^0. \tag{B.12}$$

Taking the derivative of equation (B.11) with respect to k one obtains

$$\frac{\mathrm{d}\varepsilon}{\mathrm{d}k}\left(1 - \frac{\partial U}{\partial\varepsilon}\right) = \frac{\hbar^2 k}{m}\left(1 + \frac{m}{\hbar^2 k}\frac{\partial U}{\partial k}\right). \tag{B.13}$$

We now make the approximation

$$\frac{\mathrm{d}\varepsilon}{\mathrm{d}k} = \frac{\hbar^2 k}{m^*}. \tag{B.14}$$

https://doi.org/10.1017/9781009401920 Published online by Cambridge University Press

One can interpret the left-hand side of this equation as the rate of change in energy when the momentum changes or, equivalently, when the number of nodes per unit length changes. Since the latter can be used to label the single-particle states, the energy spacing between levels, i.e. the density of levels, changes as m^* changes. Note that this statement also applies to equation (B.5). Note also that m_w may depend on r.

Inserting the relation (B.14) in equation (B.13) one obtains

$$\frac{m^*}{m} = \frac{m_\omega}{m}\frac{m_k}{m}, \tag{B.15}$$

where

$$\frac{m_\omega}{m} = \left(1 - \frac{\partial U}{\partial(\hbar\omega)}\right) \tag{B.16}$$

and

$$\frac{m_k}{m} = \left(1 + \frac{m}{\hbar^2 k}\frac{\partial U}{\partial k}\right)^{-1}. \tag{B.17}$$

Assuming a dispersion relation of the form (B.7) for the energy we get

$$U(\varepsilon) = \frac{m^*}{m}\tilde{V}^0 + \left(1 - \frac{m^*}{m}\right)\varepsilon. \tag{B.18}$$

From the comparison of equations (B.7) and (B.8) with equation (B.11) one obtains

$$\widetilde{V}^0 = \frac{m}{m^*}V^0.$$

Summing up

$$\varepsilon = \frac{\hbar k^2}{2m^*} + \frac{m}{m^*}V_0. \tag{B.19}$$

To bridge the gap between infinite nuclear matter and the case of potential wells of finite range let us consider a particle of mass m in a one-dimensional harmonic potential (see Mahaux (1985)). The Hamiltonian describing its motion,

$$H = \frac{p^2}{2m} + \frac{C}{2}x^2, \tag{B.20}$$

leads to discrete energy levels with a constant spacing

$$\hbar\omega_0 = \hbar\sqrt{\frac{C}{m}}. \tag{B.21}$$

It follows from this expression that the density of states is proportional to the square root of m. We notice, however, that this result is derived by assuming that the potential remains unchanged if the bare mass is replaced by an effective mass. If this is the case, the ground-state wavefunction

$$\Psi_0 \sim \exp\left(-\frac{x^2}{2b^2}\right) \tag{B.22}$$

with

$$b = \sqrt{\frac{\hbar^2}{mC}} \tag{B.23}$$

for a particle of mass $m^* > m$ will shrink in space compared with the one of mass m and consequently the mean square radius of the system

$$\langle r^2 \rangle = \frac{\hbar}{m^* \omega_0} \left(N + \frac{3}{2} \right) = b^2 \left(N + \frac{3}{2} \right) \tag{B.24}$$

will decrease. This is of course not correct, and one has to impose the condition $b^2 =$ constant. This condition implies that the energy difference between levels is inversely proportional to the mass (or effective mass) of the system, in keeping with the fact that

$$\hbar\omega_0 = \frac{\hbar^2}{m^* b^2}, \tag{B.25}$$

see equations (B.5) and (B.14), as well as the discussion following equation (9.9).

Because the inverse of the level distance at the Fermi energy is proportional to the density of levels $\rho(\varepsilon_F)$ (see Eq. (2.1)), $\rho(\varepsilon_F) \sim m^*$. Within this context, one can interpret the left-hand side of Eq. (B.14) as the rate of change in energy when the momentum changes or, equivalently, when the number of nodes per unit length changes. Since the latter can be used to label the single-particle states, the energy spacing between levels decreases for increasing values of m^*. Thus, the density of single-particle levels at the Fermi energy is proportional to the effective mass. (To be noted that while $\rho(\varepsilon_F) = 3A/2\varepsilon_F$ ($\varepsilon_F = \hbar^2 k_F^2/2m^*$) is the total density of single-particle levels (i.e. spin-up and -down and both protons and neutrons), $\rho(\varepsilon_F)/4$ is the level density associated with a single spin orientation and with one type of nucleon (either protons or neutrons).)

https://doi.org/10.1017/9781009401920 Published online by Cambridge University Press

Appendix C
Useful relations in the treatment of collective modes

In this appendix we give some simple relations used in the treatment of collective surface vibrations in the harmonic approximation.

C.1 Limit on the multipolarity of collective surface vibrations

Collective surface vibrations can be self-sustained modes provided the ripples they produce on the surface contain many particles, so that the surface can be viewed as a continuous elastic medium. In other words (see Fig. C.1(a))

$$\frac{2\pi R}{2\lambda} \gg d, \tag{C.1}$$

where $R = 1.2A^{1/3}$ fm is the nuclear radius, λ is the multipolarity of the surface mode and

$$d = \left(\frac{\frac{4\pi}{3}R^3}{A}\right)^{1/3} \approx 2\,\text{fm} \tag{C.2}$$

is the mean distance between nucleons. From equations (C.1) and (C.2) one obtains (see Fig. C.1(b))

$$\lambda \ll 2A^{1/3} \approx 10 \tag{C.3}$$

for a nucleus with mass number $A \sim 120$. This result agrees well with the experimental fact that collective states in medium-heavy mass nuclei have multipolarities $\lambda \leq 5$.

C.2 The relation between $\hat{F}$ and $\hat{\alpha}$

The operator $\hat{F}$ defined in equation (8.29) is restricted, in the random phase approximation, to either create or destroy particle–hole excitations, i.e.

$$\hat{F} = \sum_{\nu_k\,\nu_i} \left\{ \langle \nu_k | F | \tilde{\nu}_i \rangle \Gamma^{\dagger}_{\nu_k\,\nu_i} + \langle \tilde{\nu}_i | F | \nu_k \rangle \Gamma_{\nu_k\,\nu_i} \right\}. \tag{C.4}$$

https://doi.org/10.1017/9781009401920 Published online by Cambridge University Press

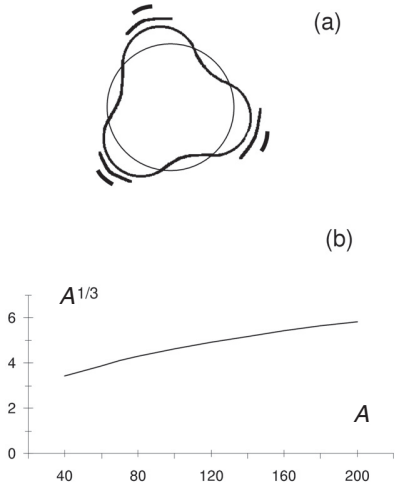

Figure C.1. (a) Schematic representation of an octupole surface wave. (b) The quantity $(A)^{1/3}$ as a function of A for medium-heavy nuclei.

Making use of equation (8.43) and the corresponding equation for $\Gamma_{\nu_k \nu_i}$ one can write equation (C.4) in terms of the RPA boson operators $\Gamma^{\dagger}_{\alpha}$ and Γ_{α}, according to

$$\begin{aligned}\hat{F} = \sum_{\substack{\nu_k \nu_i \\ \alpha'}} \Bigg\{ & \frac{\Lambda_{\alpha'} |\langle \tilde{\nu}_i | F | \nu_k \rangle|^2}{(\varepsilon_{\nu_k} - \varepsilon_{\nu_i}) - \hbar\omega_{\alpha'}} \Gamma^{\dagger}_{\alpha'} - \Big(- \frac{\Lambda_{\alpha'} |\langle \tilde{\nu}_i | F | \nu_k \rangle|^2}{(\varepsilon_{\nu_k} - \varepsilon_{\nu_i}) + \hbar\omega_{\alpha'}} \Big) \Gamma_{\alpha'} \\ & + \frac{\Lambda_{\alpha'} |\langle \tilde{\nu}_i | F | \nu_k \rangle|^2}{(\varepsilon_{\nu_k} - \varepsilon_{\nu_i}) - \hbar\omega_{\alpha'}} \Gamma_{\alpha'} - \Big(- \frac{\Lambda_{\alpha'} |\langle \tilde{\nu}_i | F | \nu_k \rangle|^2}{(\varepsilon_{\nu_k} - \varepsilon_{\nu_i}) + \hbar\omega_{\alpha'}} \Gamma^{\dagger}_{\alpha'} \Big) \Bigg\} \\ = & \sum_{\alpha'} \Lambda_{\alpha'} \sum_{\nu_k \nu_i} \frac{|\langle \tilde{\nu}_i | F | \nu_k \rangle|^2 \, 2(\varepsilon_{\nu_k} - \varepsilon_{\nu_i})}{(\varepsilon_{\nu_k} - \varepsilon_{\nu_i})^2 - (\hbar\omega_{\alpha'})^2} (\Gamma^{\dagger}_{\alpha'} + \Gamma_{\alpha'}) \\ = & \sum_{\alpha'} \frac{\Lambda_{\alpha'}}{\kappa} (\Gamma^{\dagger}_{\alpha'} + \Gamma_{\alpha'}) = \sum_{\alpha'} \sqrt{\frac{\hbar\omega_{\alpha'}}{2C_{\alpha'}}} (\Gamma^{\dagger}_{\alpha'} + \Gamma_{\alpha'}) = \hat{\alpha}, \end{aligned} \tag{C.5}$$

where use has been made of equation (8.39).

In other words, $\hat{F}$ and $\hat{\alpha}$ are the single-particle and the collective representations of the same operator.

https://doi.org/10.1017/9781009401920 Published online by Cambridge University Press

Appendix D
Particle-vibration coupling

The purpose of this appendix is to summarize results for particle-vibration coupling matrix elements, which are used in Chapters 8, 9 and 10. The particle-vibration interaction from equation (8.24) is

$$\delta U(r) = -R_0 \frac{\partial U}{\partial r} \sum_{LM} \alpha_{LM} Y^*_{LM}(\hat{r}) = -\kappa \sum_{LM} \alpha_{LM} F_{LM}, \tag{D.1}$$

where the collective coordinates α_{LM} are nuclear deformation parameters. The dimensionless quantity

$$F_{LM} = \frac{R_0}{\kappa} \frac{\partial U}{\partial r} Y^*_{LM}(\hat{r}) \tag{D.2}$$

is a single-particle field peaked at the nuclear surface and κ is a constant fixed by a self-consistency condition discussed in Section 8.3 (see also (10.27)). The coordinate α is related to phonon creation and annihilation operators by

$$\hat{\alpha}_{LM} = \sqrt{\frac{\hbar\omega_L}{2C_L}} (\hat{\Gamma}^\dagger_{LM} + (-1)^M \Gamma_{L-M}), \tag{D.3}$$

where $\hbar\omega_L$ is the energy of the phonon with multipolarity L and $C_L\hat{\alpha}^2/2$ is the potential energy associated with the collective coordinate. The matrix element of the collective coordinate between the phonon ground state and a one-phonon excited state is

$$\langle LM|\hat{\alpha}_{LM}|00\rangle = \sqrt{\frac{\hbar\omega_L}{2C_L}} = \frac{1}{\sqrt{2L+1}} \beta_L. \tag{D.4}$$

The quantity β_L is the reduced matrix element and is known as the multipole deformation parameter.

The particle-vibration interaction matrix element $V\left(jm, j'm', LM\right)$ from equations (D.1) and (D.4) is

$$V\left(jm, j'm', LM\right) = -\frac{\beta_L}{\sqrt{2L+1}} \langle j'|R_0 \frac{\partial U}{\partial r}|j\rangle \langle l'j'm'|Y_{LM}|ljm\rangle \ . \tag{D.5}$$

https://doi.org/10.1017/9781009401920 Published online by Cambridge University Press

The nucleon self energy and particle-vibration induced interaction involve sums over magnetic quantum numbers and can be expressed in terms of the quantity

$$\left|V\left(j,j',L\right)\right|^2=\sum_{mm'M}\frac{\beta_L^2}{2L+1}\langle j'|R_0\frac{\partial U}{\partial r}|j\rangle^2\left|\langle l'j'm'|Y_{LM}|ljm\rangle\right|^2 \tag{D.6}$$

which is symmetric in j and j'. Making use of the Wigner–Eckart theorem

$$\langle j'm'|Y_{LM}|jm\rangle=\frac{\langle jmLM|j'm'\rangle}{\sqrt{2j'+1}}\langle l'j'||Y||lj\rangle \tag{D.7}$$

and the normalization property

$$\sum_{mm'}\left|\langle jmLM|j'm'\rangle\right|^2=\frac{\left(2j'+1\right)}{(2L+1)} \tag{D.8}$$

of the Clebsch–Gordon coefficients, equation (D.6) simplifies to

$$V^2\left(j,j',L\right)=\frac{\beta_L^2}{2L+1}\langle j'|R_0\frac{\partial U}{\partial r}|j\rangle^2\langle l'j'||Y_L||lj\rangle^2, \tag{D.9}$$

which is equivalent to equation (10.3). The definition (D.7) of the reduced matrix element is the one used by Bohr and Mottelson (1969).

The self-energy of a nucleon in the single-particle state j is

$$\Sigma_j=\sum_{jL}\frac{1}{(2j+1)}\frac{V^2\left(j,j';L\right)}{\varepsilon_j-\left(\varepsilon_{j'}+\hbar\omega_L\right)}, \tag{D.10}$$

where ε_j and $\varepsilon_{j'}$ are single-particle energies and $\hbar\omega_L$ are phonon energies. The factor $1/(2j+1)$ appears because there is an average over the spin orientation m of the initial state j. The induced interaction matrix element $v_{jj'}$ in Chapter 10 involves a scattering between the normalized two-nucleon initial state $|(jj)_0\rangle$ with total angular momentum $J=0$ and the final state $|\left(j'j'\right)_0\rangle$ also with $J=0$,

$$\begin{aligned}v_{jj'}=\langle(jj)_0\,|v|\left(j'j'\right)_0\rangle&=\textstyle\sum_{mm'}\frac{1}{2\sqrt{(2j'+1)(2j+1)}}\langle jm,\widetilde{jm}|v|j'm',\widetilde{j'm'}\rangle_a\\&=\textstyle\sum_{mm'}\frac{1}{\sqrt{(2j'+1)(2j+1)}}\langle jm,\widetilde{jm}|v|j'm',\widetilde{j'm'}\rangle,\end{aligned} \tag{D.11}$$

where the general structure of the antisymmetrized matrix element $\langle|v|\rangle_a$ has been defined in equation (A.16).

The uncoupled phonon exchange matrix element has the angular momentum structure

$$\langle jm,\widetilde{jm}|v|j'm',\widetilde{j'm'}\rangle=\sum_{LM}\frac{\left|V\left(jm,j'm',LM\right)\right|^2}{D_\lambda}, \tag{D.12}$$

where D_λ is an energy denominator which can be approximated in various ways. The microscopic calculations reported in Section 10.2 use a Bloch–Horowitz expression for the energy denominator. In the following equation we substitute the simple estimate $D_\lambda\approx-\hbar\omega_L$ which is used in Section 10.1. The interaction matrix element reduces to

$$v_{jj'}=\sum_L v_{jj'}^L, \tag{D.13}$$

https://doi.org/10.1017/9781009401920 Published online by Cambridge University Press

where

$$v^{L}_{jj'} = -\frac{2}{\sqrt{(2j'+1)(2j+1)}}\frac{V^2\left(j, j', L\right)}{\hbar\omega_L}. \tag{D.14}$$

The factor 2 occurs because two perturbation diagrams (time orderings) contribute to the induced interaction.

The normalization in the microscopic calculations reported in Section 10.2 is the one used in Barranco *et al.* (1999). In their notation the suffix ν refers to a state with a pair of nucleons with quantum numbers $l_\nu j_\nu$ coupled to zero total angular momentum, and $v_{\nu\nu'}$ is defined by

$$G_{\nu\nu'} = -v_{\nu\nu'} = -\frac{2\langle (j_\nu j_\nu)_0 \,|v|\, (j_{\nu'} j_{\nu'})_0\rangle}{\sqrt{(2j_\nu+1)(2j_{\nu'}+1)}} = -\frac{2v_{j_\nu j_{\nu'}}}{\sqrt{(2j_\nu+1)(2j_{\nu'}+1)}}, \tag{D.15}$$

where the factor of 2 arises from the antisymmetry of the pairing matrix element (see equation (A.16)).

Thus the normalization and sign of $G_{\nu\nu'}$ is the same as that of the BCS coupling constant G and the values of $G_{\nu\nu'}$ in Tables 10.1, 10.2 and 10.3 can be compared directly with BCS G-values for ^{120}Sn, $G \approx 27/A = 0.22$, where $G = \overline{G_{\nu\nu'}}$.

D.1 Estimate of $\langle lj||Y_L||lj\rangle$

The interaction strengths $V^2\left(j, j', L\right)$ defined in equation (D.9) are proportional to squares of reduced matrix elements of spherical harmonics. These can be expressed in terms of Clebsch–Gordon coefficients and can be calculated using standard formulae. Some qualitative properties and simple asymptotic expressions are collected in this appendix.

The reduced matrix elements $\langle l'j'||Y_L||lj\rangle$ with $j = l + 1/2$, $j' = l' - 1/2$ or $j = l - 1/2$, $j' = l' + 1/2$ involve a spin-flip at the interaction vertex. There is no spin-flip in the other two reduced matrix elements. The spin-flip matrix elements are small compared with the no-spin-flip and become very small when j and j' are large. The spin-flip processes are essentially possible only because of quantal fluctuations, owing to the parity condition that the matrix elements of Y_L vanish unless $l + l' + L$ is even. The spin-flip character of the reduced matrix elements $\langle l'j'||Y_L||lj\rangle$ can be recognized because $j + j' + L$ is even for spin-flip matrix elements and odd for the non-spin-flip matrix elements.

The square of the reduced matrix element $\langle lj||Y_L||l'j'\rangle$ can be expressed in terms of a Wigner 3-j symbol as

$$\begin{aligned}\langle lj||Y_L||l'j'\rangle^2 &= \frac{(2j+1)\left(2j'+1\right)(2L+1)}{4\pi}\begin{pmatrix} j & j' & L \\ \frac{1}{2} & -\frac{1}{2} & 0\end{pmatrix}^2 \\ &= \frac{(2j+1)(2L+1)}{4\pi}\langle j\tfrac{1}{2}L0|j'\tfrac{1}{2}\rangle^2.\end{aligned} \tag{D.16}$$

Diagonal matrix elements have $j = j'$ and $l = l'$ and the parity condition requires L to be even. A useful asymptotic formula introduced in equation (10.5) expresses the

https://doi.org/10.1017/9781009401920 Published online by Cambridge University Press

Clebsch–Gordon coefficient in equation (D.16) in terms of a Legendre polynomial

$$\langle j\tfrac{1}{2}L0|j\tfrac{1}{2}\rangle \approx \; P_L(0)\,.$$

This formula is valid when L is even and $j \gg L$. Thus

$$\langle j||Y_L||j\rangle^2 \approx \frac{(2j+1)(2L+1)}{4\pi}\,(P_L(0))^2\,.$$

Introducing the numerical values of the Legendre polynomial we have

$$\langle j||Y_L||j\rangle^2 \approx 0.1(2j+1) \tag{D.17}$$

for $L = 2, 4$ and 6.

The following examples calculated with $L = 2$ show that this result is quite accurate. For this purpose, use is made of the relation (Varshalovich *et al.* (1988), Table 8.4)

$$\begin{pmatrix} j & j' & 2 \\ \frac{1}{2} & -\frac{1}{2} & 0 \end{pmatrix}^2 = \frac{4(\frac{3}{4} - j(j+1))^2}{(2j+3)(2j+2)(2j+1)(2j)(2j-1)}\,.$$

In the case of $j = 11/2$

$$\begin{pmatrix} \frac{11}{2} & \frac{11}{2} & 2 \\ \frac{1}{2} & -\frac{1}{2} & 0 \end{pmatrix}^2 = \frac{4(\frac{3}{4} - \frac{11}{2}\times\frac{13}{2})^2}{14\times13\times12\times11\times10} = 0.02040$$

and

$$\langle 11/2||Y_2||11/2\rangle = \frac{(12)^2\times5}{4\pi}\times 0.02040 = 1.17.$$

In the case $j = 7/2$,

$$\begin{pmatrix} 7/2 & 7/2 & 2 \\ \frac{1}{2} & -\frac{1}{2} & 0 \end{pmatrix}^2 = \frac{4(\frac{3}{4} - \frac{7}{2}\times\frac{9}{2})^2}{10\times9\times8\times7\times6} = 0.02976.$$

Thus

$$\langle 7/2||Y_2||7/2\rangle^2 = \frac{8^2\times5}{4\pi}\times 0.02976 \approx 0.76.$$

In Table D.1 we compare the exact results given in equation (D.16), with the results obtained from equation (D.17).

There is another approximate relation which is valid for $j,\, j' \gg L$ when the no-spin-flip condition is satisfied (when $j + j' + L$ is odd or equivalently when $j - j' + L$ is even). The asymptotic formula for the Clebsch coefficients gives (Varshalovich *et al.* (1988), Section 8.9)

$$\left|\langle j\tfrac{1}{2}L0|j'\tfrac{1}{2}\rangle\right|^2 \approx \frac{4\pi}{2L+1}\,(Y_{LM}(0,0))^2\,, \tag{D.18}$$

with $M = \left|j - j'\right|$. When L is large and $L + M$ is even Varshalovich *et al.* (1988, Section 5.12) give

$$(Y_{LM}(0,0))^2 \approx \frac{1}{\pi^2}.$$

https://doi.org/10.1017/9781009401920 Published online by Cambridge University Press

Table D.1. *Comparison of the results obtained using the approximate expression given in equation (D.17) with exact results obtained using equation (D.16).*

	$\langle j\|\|Y_2\|\|j\rangle^2$	
j	exact	$0.1(2j+1)$
7/2	0.76	0.8
11/2	1.17	1.2

Combining these results gives a simple approximate expression for the no-spin-flip reduced matrix elements

$$\langle j||Y_L||j'\rangle^2 \approx \frac{\sqrt{(2j+1)(2j'+1)}}{\pi^2} \approx 0.1\sqrt{(2j+1)(2j'+1)}. \tag{D.19}$$

This is equivalent to equation (D.17) when $j = j'$ and is quite accurate even for $L \geqslant 2$ and j and $j' > 1/2$. When $j' = 1/2$ and $j = L \pm 1/2$ then there is an exact formula

$$\langle j||Y_L||1/2\rangle^2 = \frac{2j+1}{4\pi}. \tag{D.20}$$

D.2 A simple estimate of $\langle R_0 \frac{\partial U}{\partial r}\rangle$

The average $\langle R_0 \partial U/\partial r\rangle$ will be estimated using a square well approximation for the Saxon–Woods potential

$$U(r) = \frac{U_0}{1+\exp(\frac{r-R_0}{a})} \approx U_0\Theta(r-R_0), \tag{D.21}$$

where

$$\Theta(r-R_0) = \begin{cases} 1 & r \leq R_0, \\ 0 & r > R_0. \end{cases} \tag{D.22}$$

Making use of the fact that

$$\frac{\partial\Theta(r-R_0)}{\partial r} = \delta(r-R_0), \tag{D.23}$$

one can write

$$\begin{aligned} \langle R_0 \frac{\partial U}{\partial r}\rangle &= R_0 U_0 \int r^2\,\mathrm{d}r\,\mathcal{R}^2(r)\,\delta(r-R_0) \\ &= U_0 R_0^3 \mathcal{R}^2(R_0), \end{aligned} \tag{D.24}$$

https://doi.org/10.1017/9781009401920 Published online by Cambridge University Press

where $\mathcal{R}(r)$ is the radial wavefunction. Making use of the fact that (see Bohr and Mottelson (1969) p. 326, equation (3.22))

$$R_0^3 \mathcal{R}^2(R_0) \approx 1.4, \tag{D.25}$$

one obtains

$$\langle R_0 \frac{\partial U}{\partial r} \rangle = U_0 \times 1.4 \approx -60\,\mathrm{MeV}, \tag{D.26}$$

where use was made of $U_0 \approx -45\,\mathrm{MeV}$. If one corrects this estimate for the spillout of the nucleons one has to divide the result shown above by a factor $(1 + a/R) \approx 1.1$ (see Bertsch and Broglia (1994), p. 87), in which case one obtains $\langle R_0 \frac{\partial U}{\partial r} \rangle \approx -50\,\mathrm{MeV}$.

https://doi.org/10.1017/9781009401920 Published online by Cambridge University Press

Appendix E
Model of the single-particle strength function

In the extreme single-particle model of nuclear structure, single-particle states are either occupied or empty. As explained in Chapter 9 the coupling of single-particle motion to vibrations changes this situation and single-particle states near the Fermi surface are partially occupied. The spectroscopic factor is a measure of the occupancy of a level. This appendix presents a simple model ('picket fence' model) which relates the spectroscopic factor to the ω-mass (see Bohr and Mottelson (1969), Mahaux *et al*. (1985)).

We consider a two-level model where the pure single-particle state $|a\rangle$ couples to a more complicated state $|\alpha\rangle$ of which a possible representation could be a single-particle state coupled to a vibration (see Fig. E.1). We want to diagonalize the Hamiltonian (see Bohr and Mottelson (1969)),

$$H = H_0 + v, \tag{E.1}$$

where

$$H_0|a\rangle = E_a|a\rangle \tag{E.2}$$

and

$$H_0|\alpha\rangle = E_\alpha|\alpha\rangle. \tag{E.3}$$

The interaction v couples these states. Assuming

$$\langle a|v|a\rangle = \langle \alpha|v|\alpha\rangle = 0, \tag{E.4}$$

and calling

$$v_{a\alpha} = \langle a|v|\alpha\rangle, \tag{E.5}$$

one can write the secular equation associated with H as

$$\begin{pmatrix} E_\alpha - E_i & v_{a\alpha} \\ v_{a\alpha} & E_a - E_i \end{pmatrix} \begin{pmatrix} c_\alpha(i) \\ c_a(i) \end{pmatrix} = 0, \tag{E.6}$$

https://doi.org/10.1017/9781009401920 Published online by Cambridge University Press

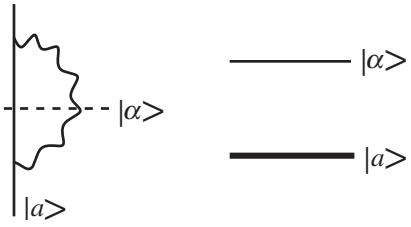

Figure E.1. The coupling between the state $|a\rangle$ and the intermediate state $|\alpha\rangle$ associated with the process in which a nucleon excites a vibrational mode to reabsorb it at a later time.

leading to the two equations

$$(E_\alpha - E_i)c_\alpha(i) + v_{a\alpha}c_a(i) = 0, \tag{E.7}$$

$$v_{a\alpha}c_\alpha(i) + (E_a - E_i)c_a(i) = 0. \tag{E.8}$$

From the first equation one obtains

$$c_\alpha(i) = -\frac{v_{a\alpha}}{E_\alpha - E_i}c_a(i). \tag{E.9}$$

From this relation and from

$$c_a^2(i) + c_\alpha^2(i) = 1, \tag{E.10}$$

one obtains

$$c_a^2(i) = \left(1 + \frac{v_{a\alpha}^2}{(E_\alpha - E_i)^2}\right)^{-1}. \tag{E.11}$$

Inserting equation (E.9) into equation (E.8) leads to

$$-\frac{v_{a\alpha}^2}{E_\alpha - E_i} + (E_a - E_i) = 0. \tag{E.12}$$

Thus

$$E_i = E_a - \frac{v_{a\alpha}^2}{E_\alpha - E_i}, \tag{E.13}$$

which is, within the present model, the self-consistent Dyson equation.

In other words, the single-particle self-energy is

$$\Delta E_a(E) = E - E_a = -\frac{v_{a\alpha}^2}{E_\alpha - E}\,. \tag{E.14}$$

Defining the ω-mass by

$$\frac{m_\omega}{m} = 1 - \left.\frac{\partial \Delta E_a}{\partial E}\right|_{E=E_i}, \tag{E.15}$$

https://doi.org/10.1017/9781009401920 Published online by Cambridge University Press

and making use of the above equation we get

$$\frac{m_\omega}{m} = 1 + \frac{v_{a\alpha}^2}{(E_\alpha - E_i)^2}. \tag{E.16}$$

Comparing with equation (E.11) for $c_a^2(i)$ we see that the spectroscopic factor associated with the quasi-pure single-particle state

$$|\tilde{a}\rangle = c_a(i)|a\rangle + c_\alpha(i)|\alpha\rangle \tag{E.17}$$

is

$$Z_\omega = c_a^2(i) = \left(\frac{m_\omega}{m}\right)^{-1}. \tag{E.18}$$

https://doi.org/10.1017/9781009401920 Published online by Cambridge University Press

Appendix F
Simple model of Pauli principle corrections

The induced interaction shown in Fig. F.1(a) leads to the contribution

$$v_{kk'} = \sum_{\alpha} \frac{V^2(k, k'\alpha)}{\varepsilon_k - (\varepsilon_{k'} + \hbar\omega_\alpha)},$$

while that shown in Fig. F.1(c) leads to

$$(v_{kk'})_{\text{Pauli}} = -\sum_{\alpha\alpha'} \sum_{ik''} \frac{V(k, k'\alpha')V(k, k''\alpha)}{(\varepsilon_k - (\varepsilon_{k'} + \hbar\omega_{\alpha'}))} \times \frac{V(k', i\alpha)V(k'', i\alpha')}{(\varepsilon_k - (\varepsilon_{k'} + \varepsilon_{k''} - \varepsilon_i))(\varepsilon_k - (\varepsilon_{k''} + \hbar\omega_\alpha)}. \tag{F.1}$$

In what follows we shall carry out an order of magnitude estimate of the ratio of $(v_{kk'})_{\text{Pauli}}/v_{kk'}$ making use of the schematic two-level model (see Fig. F.2) and nuclear field theory rules.

The Hamiltonian describing the system

$$H = H_{\text{sp}} + H_{\text{TB}}, \tag{F.2}$$

is composed of a single-particle Hamiltonian and a two-body interaction. The particle-vibration coupling matrix element is

$$V(k, k'\alpha) = -K_0\sqrt{\Omega}, \tag{F.3}$$

and the collective RPA solution of (F.2) has an energy

$$\hbar\omega = \varepsilon - K_0\Omega. \tag{F.4}$$

Let us assume $\hbar\omega \approx \frac{1}{2}\varepsilon$. Thus $K_0 = \frac{\varepsilon}{2\Omega}$ and

$$(v_{kk'})_{\text{Pauli}} \approx -v_{kk'}\frac{V^2(k, k'\alpha)}{\hbar\omega \times \varepsilon} \approx -\frac{v_{kk'}}{2\Omega}. \tag{F.5}$$

https://doi.org/10.1017/9781009401920 Published online by Cambridge University Press

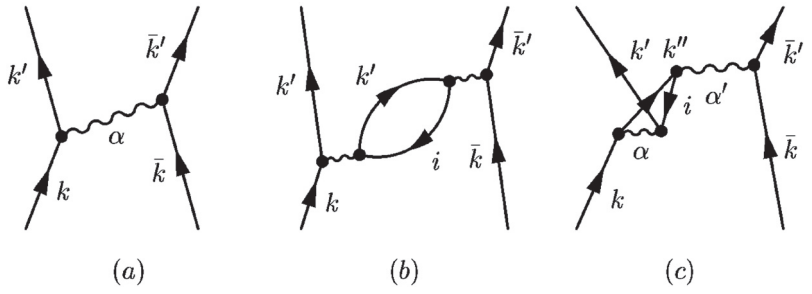

Figure F.1. (*a*) Induced interaction. (*b*) Schematic representation of the induced interaction showing one of the possible bubble contributions to the collective state (RPA). (*c*) Pauli principle contribution to the induced interaction arising from the exchange of the particle moving in the state k' in the bubble of graph (*b*) and in the final state. Note that graph (*b*) has been drawn only for the purpose of illustration as this process is forbidden by the rules of nuclear field theory (Bes *et al*. (1976a, 1976b)).

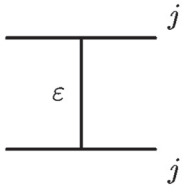

Figure F.2. Schematic model used in the estimates. The two orbitals have the same pair degeneracy $\Omega = (2\gamma + 1)/2$. The lowest level is assumed to be filled.

For ^{11}Li, where $\Omega = (2j + 1)/2 \approx 1$ ($s_{1/2}p_{1/2}$ single-particle space) one thus obtains

$$(v_{kk'})_{\text{Pauli}} \approx -0.5 v_{kk'}. \tag{F.6}$$

On the other hand, for nuclei lying along the stability valley, where

$$\Omega \approx A^{2/3}, \tag{F.7}$$

one obtains

$$(v_{kk'})_{\text{Pauli}} \approx \frac{v_{kk'}}{2A^{2/3}}. \tag{F.8}$$

For medium/heavy nuclei ($A^{1/3} \approx 5$) this expansion leads to the ratio

$$\frac{(v_{kk'})_{\text{Pauli}}}{v_{kk'}} \approx -2 \times 10^{-2}. \tag{F.9}$$

https://doi.org/10.1017/9781009401920 Published online by Cambridge University Press

Appendix G
Pairing mean-field solution

G.1 Solution of the pairing Hamiltonian

This appendix gives an alternative derivation of the pairing mean-field Hamiltonian and the BCS wavefunction to that provided in the text.

Let us start with the Hamiltonian

$$H = H_{\rm sp} + H_{\rm p},$$

which is the sum of a single-particle Hamiltonian

$$H_{\rm sp} = \sum_{\nu>0} (\varepsilon_\nu - \lambda)(a^\dagger_\nu a_\nu + a^\dagger_{\bar\nu} a_{\bar\nu})$$

and a pairing interaction with constant matrix elements

$$H_{\rm p} = -G \sum_{\substack{\nu\,>\,0 \\ \nu'\,>\,0}} a^\dagger_\nu a^\dagger_{\bar\nu} a_{\bar\nu'} a_{\nu'}. \tag{G.1}$$

In what follows we shall solve H in the mean-field approximation. For this purpose we introduce the pair-creation operator,

$$P^\dagger = \sum_{\nu>0} a^\dagger_\nu a^\dagger_{\bar\nu} = \alpha_0 + (P^\dagger - \alpha_0)$$

and add and subtract from it the mean-field value

$$\alpha_0 = \langle {\rm BCS}|P^\dagger|{\rm BCS}\rangle = \langle {\rm BCS}|P|{\rm BCS}\rangle$$

of the pair transfer operator in the, still unknown, mean-field ground state. This state is called the $|{\rm BCS}\rangle$ state, because this solution was first proposed by Bardeen, Cooper and Schrieffer. Note that $\langle {\rm BCS}|{\rm BCS}\rangle = 1$. We can now write

$$\begin{aligned} H_{\rm p} &= -G(\alpha_0 + (P^\dagger - \alpha_0))(\alpha_0 + (P - \alpha_0)) \\ &= -G(\alpha_0^2 + \alpha_0(P^\dagger + P - 2\alpha_0) + (P^\dagger - \alpha_0)(P - \alpha_0)). \end{aligned}$$

https://doi.org/10.1017/9781009401920 Published online by Cambridge University Press

Assuming that the matrix elements of the operators $(P^\dagger - \alpha_0)$ and $(P - \alpha_0)$ in the states near to the ground state are much smaller than α_0, one obtains the pairing field

$$V_\mathrm{p} = -\Delta(P^\dagger + P) + \frac{\Delta^2}{G}, \qquad \Delta = G\alpha_0\,. \tag{G.2}$$

The mean-field Hamiltonian then becomes

$$\begin{aligned} H_\mathrm{MF} &= H_\mathrm{sp} + V_\mathrm{p} \\ &= \sum_{\nu>0}(\varepsilon_\nu - \lambda)(a_\nu^\dagger a_\nu + a_{\bar\nu}^\dagger a_{\bar\nu}) - \Delta\sum_{\nu>0}(a_\nu^\dagger a_{\bar\nu}^\dagger + a_{\bar\nu}a_\nu) + \frac{\Delta^2}{G}\,. \end{aligned}$$

This is a bilinear expression in the creation and annihilation operators. Consequently, it can be diagonalized by a rotation in $(a^\dagger, a)$-space. This can be accomplished through the Bogoliubov–Valatin transformation

$$\alpha_\nu^\dagger = U_\nu a_\nu^\dagger - V_\nu a_{\bar\nu}.$$

From this definition one can anticipate that the BCS solution does not change the energies ε_ν of the single-particle levels or the associated wavefunction $\varphi_\nu(\vec{r})$, but the occupation probabilities for levels around the Fermi energy within an energy range 2Δ, a quantity much smaller than the Fermi energy ε_F. What is also changed is the mechanism by which the system can be excited, which implies, for nucleons moving around the Fermi energy, the breaking of Cooper pairs.

The creation operator of a quasiparticle $\alpha_\nu^\dagger$ creates a particle in the single-particle state ν with probability U_ν^2, while it creates a hole (annihilates a particle) with probability V_ν^2. To be able to create a particle, the state ν should be empty, while to create a hole it has to be filled, so U_ν^2 and V_ν^2 are the probabilities that the state ν is empty and is occupied respectively.

Expressing the creation and annihilation operators $(a_\nu^\dagger, a_\nu)$ in terms of the quasiparticle operators $(\alpha_\nu^\dagger, \alpha_\nu)$, and expressing H_MF in terms of quasiparticles, one has the parameters U_ν and V_ν for each level ν to make this Hamiltonian diagonal (in fact one, see equation (G.3)).

Making use of the anticommutation relations

$$\begin{aligned} \{a_\nu, a_{\nu'}^\dagger\} &= \delta(\nu, \nu') \\ \{a_\nu, a_{\nu'}\} &= \{a_\nu^\dagger, a_{\nu'}^\dagger\} = 0, \end{aligned}$$

one obtains

$$\begin{aligned} \{\alpha_\nu, \alpha_{\nu'}^\dagger\} &= \{(U_\nu a_\nu - V_\nu a_{\bar\nu}^\dagger), (U_{\nu'} a_{\nu'}^\dagger - V_{\nu'} a_{\bar\nu'})\} \\ &= (U_\nu U_{\nu'} + V_\nu V_{\nu'})\,\delta(\nu, \nu'). \end{aligned}$$

That is, for the quasiparticle transformation to be unitary, the U_ν, V_ν occupation factors have to fulfil the relation

$$U_\nu^2 + V_\nu^2 = 1, \tag{G.3}$$

https://doi.org/10.1017/9781009401920 Published online by Cambridge University Press

implying also that the one-quasiparticle states are orthonormal. In particular

$$\begin{aligned}\langle\nu|\nu\rangle = 1 &= \langle \mathrm{BCS}|\alpha_\nu\alpha_\nu^\dagger|\mathrm{BCS}\rangle = \langle \mathrm{BCS}|\{\alpha_\nu, \alpha_\nu^\dagger\}|\mathrm{BCS}\rangle \\ &= U_\nu^2 + V_\nu^2\end{aligned}$$

implies that the state

$$|\nu\rangle = \alpha_\nu^\dagger|\mathrm{BCS}\rangle$$

is normalized.

Note that $|\mathrm{BCS}\rangle$ is also the quasiparticle vacuum, i.e.

$$\alpha_\nu|\mathrm{BCS}\rangle = 0.$$

Let us now invert the quasiparticle transformation, i.e. express $a_\nu^\dagger$ in terms of $\alpha_\nu^\dagger$ and $\alpha_{\bar\nu}$. Multiplying $\alpha_\nu^\dagger$ by U_ν and $\alpha_{\bar\nu}$ by V_ν gives

$$\begin{aligned}U_\nu\alpha_\nu^\dagger &= U_\nu^2 a_\nu^\dagger - U_\nu V_\nu a_{\bar\nu}, \\ V_\nu\alpha_{\bar\nu} &= U_\nu V_\nu a_{\bar\nu} + V_\nu^2 a_\nu^\dagger.\end{aligned}$$

Adding these expressions one obtains

$$a_\nu^\dagger = U_\nu\alpha_\nu^\dagger + V_\nu\alpha_{\bar\nu}.$$

We shall now express $a_\nu^\dagger a_\nu$ in terms of quasiparticles, i.e.

$$\begin{aligned}a_\nu^\dagger a_\nu &= (U_\nu\alpha_\nu^\dagger + V_\nu\alpha_{\bar\nu})(U_\nu\alpha_\nu + V_\nu\alpha_{\bar\nu}^\dagger) \\ &= U_\nu^2\alpha_\nu^\dagger\alpha_\nu + U_\nu V_\nu\alpha_\nu^\dagger\alpha_{\bar\nu}^\dagger + U_\nu V_\nu\alpha_{\bar\nu}\alpha_\nu + V_\nu^2\alpha_{\bar\nu}\alpha_{\bar\nu}^\dagger \\ &= U_\nu^2\alpha_\nu^\dagger\alpha_\nu + U_\nu V_\nu(\alpha_\nu^\dagger\alpha_{\bar\nu}^\dagger + \alpha_{\bar\nu}\alpha_\nu) - V_\nu^2\alpha_{\bar\nu}^\dagger\alpha_{\bar\nu} + V_\nu^2. \qquad \text{(G.4)}\end{aligned}$$

The time reversal of this expression reads

$$a_{\bar\nu}^\dagger a_{\bar\nu} = U_\nu^2\alpha_{\bar\nu}^\dagger\alpha_{\bar\nu} + U_\nu V_\nu(\alpha_\nu^\dagger\alpha_{\bar\nu}^\dagger + \alpha_{\bar\nu}\alpha_\nu) - V_\nu^2\alpha_\nu^\dagger\alpha_\nu + V_\nu^2,$$

where the phase relation $|\tilde{\bar\nu}>= \tau^2|\nu>= -|\nu>$ and thus $a_{\tilde{\bar\nu}}^\dagger = -a_\nu^\dagger$ have been used. One can then write

$$\begin{aligned}(a_\nu^\dagger a_\nu + a_{\bar\nu}^\dagger a_{\bar\nu}) &= (U_\nu^2 - V_\nu^2)(\alpha_\nu^\dagger\alpha_\nu + \alpha_{\bar\nu}^\dagger\alpha_{\bar\nu}) \\ &\quad + 2U_\nu V_\nu(\alpha_\nu^\dagger\alpha_{\bar\nu}^\dagger + \alpha_{\bar\nu}\alpha_\nu) + 2V_\nu^2. \qquad \text{(G.5)}\end{aligned}$$

Note that

$$N = \langle \mathrm{BCS}|\hat{N}|\mathrm{BCS}\rangle = \langle \mathrm{BCS}|\sum_{\nu>0}(a_\nu^\dagger a_\nu + a_{\bar\nu}^\dagger a_{\bar\nu})|\mathrm{BCS}\rangle = 2\sum_{\nu>0} V_\nu^2 \qquad \text{(G.6)}$$

is the average number of particles in the pairing mean-field ground state (BCS state).

Let us now express the pair-creation field $a_\nu^\dagger a_{\bar\nu}^\dagger$ in terms of quasiparticles

$$\begin{aligned}a_\nu^\dagger a_{\bar\nu}^\dagger &= (U_\nu\alpha_\nu^\dagger + V_\nu\alpha_{\bar\nu})(U_\nu\alpha_{\bar\nu}^\dagger - V_\nu\alpha_\nu) \\ &= U_\nu^2\alpha_\nu^\dagger\alpha_{\bar\nu}^\dagger - U_\nu V_\nu\alpha_\nu^\dagger\alpha_\nu \\ &\quad + V_\nu U_\nu\alpha_{\bar\nu}^\dagger\alpha_{\bar\nu} - V_\nu^2\alpha_{\bar\nu}\alpha_\nu + U_\nu V_\nu. \qquad \text{(G.7)}\end{aligned}$$

https://doi.org/10.1017/9781009401920 Published online by Cambridge University Press

The Hermitian conjugate of this expression is then

$$a_{\bar{\nu}}a_\nu = U_\nu^2\alpha_{\bar{\nu}}\alpha_\nu - U_\nu V_\nu(\alpha_\nu^\dagger\alpha_\nu + \alpha_{\bar{\nu}}^\dagger\alpha_{\bar{\nu}}) - V_\nu^2\alpha_\nu^\dagger\alpha_{\bar{\nu}}^\dagger + U_\nu V_\nu. \tag{G.8}$$

Summing these expressions leads to

$$(a_\nu^\dagger a_{\bar{\nu}}^\dagger + a_{\bar{\nu}}a_\nu) = (U_\nu^2 - V_\nu^2)(\alpha_\nu^\dagger\alpha_{\bar{\nu}}^\dagger + \alpha_{\bar{\nu}}\alpha_\nu) - 2U_\nu V_\nu(\alpha_\nu^\dagger\alpha_{\bar{\nu}} + \alpha_{\bar{\nu}}^\dagger\alpha_\nu) + 2U_\nu V_\nu.$$

Note that

$$\alpha_0 = \langle \mathrm{BCS}|P^\dagger|\mathrm{BCS}\rangle = \sum_{\nu>0}\langle \mathrm{BCS}|a_\nu^\dagger a_{\bar{\nu}}|\mathrm{BCS}\rangle = \sum_{\nu>0} U_\nu V_\nu \tag{G.9}$$

and

$$\Delta = G\alpha_0 = G\sum_{\nu>0} U_\nu V_\nu. \tag{G.10}$$

Making use of the relations worked out above one can express H_{MF} in terms of quasiparticles, i.e.

$$H_{\mathrm{MF}} = U + H_{11} + H_{20}, \tag{G.11}$$

where

$$\begin{aligned}
U &= 2\sum_{\nu>0}(\varepsilon_\nu - \lambda)V_\nu^2 - \Delta\sum_{\nu>0} 2U_\nu V_\nu + \frac{\Delta^2}{G},\\
H_{11} &= \sum_{\nu>0}\left\{(\varepsilon_\nu - \lambda)(U_\nu^2 - V_\nu^2) + \Delta 2U_\nu V_\nu\right\}(\alpha_\nu^\dagger\alpha_\nu + \alpha_{\bar{\nu}}^\dagger\alpha_{\bar{\nu}}),\\
H_{20} &= \sum_{\nu>0}\left\{(\varepsilon_\nu - \lambda)2U_\nu V_\nu - \Delta(U_\nu^2 - V_\nu^2)\right\}(\alpha_\nu^\dagger\alpha_{\bar{\nu}}^\dagger + \alpha_{\bar{\nu}}\alpha_\nu).
\end{aligned}$$

In other words, the mean-field pairing Hamiltonian expressed in terms of quasiparticles is equal to the sum of three terms: one which is a constant, a second one which is diagonal in the quasiparticle basis, and a third one which, although bilinear in the operators $\alpha^\dagger$ and α, is not diagonal. Consequently, imposing the condition $H_{20} = 0$, i.e.

$$(\varepsilon_\nu - \lambda)2U_\nu V_\nu = \Delta(U_\nu^2 - V_\nu^2), \tag{G.12}$$

is equivalent to diagonalizing H_{MF}. This relation together with equation (G.3) allows us to calculate the corresponding coefficients U_ν and V_ν.

We start by taking the square of the above relation,

$$(\varepsilon_\nu - \lambda)^2 4U_\nu^2 V_\nu^2 = \Delta^2(U_\nu^2 - V_\nu^2)^2. \tag{G.13}$$

From the normalization relation one can write

$$(U_\nu^2 + V_\nu^2)^2 = 1 = U_\nu^4 + V_\nu^4 + 2U_\nu^2 V_\nu^2$$

and

$$U_\nu^4 + V_\nu^4 = 1 - 2U_\nu^2 V_\nu^2.$$

https://doi.org/10.1017/9781009401920 Published online by Cambridge University Press

Consequently,

$$(U_\nu^2 - V_\nu^2)^2 = U_\nu^4 + U_\nu^4 - 2U_\nu^2 V_\nu^2 = 1 - 4U_\nu^2 V_\nu^2.$$

Inserting this relation in equation (G.13) leads to

$$4U_\nu^2 V_\nu^2((\varepsilon_\nu - \lambda)^2 + \Delta^2) = \Delta^2,$$

a relation which can be rewritten as

$$2U_\nu V_\nu = \frac{\Delta}{E_\nu}, \tag{G.14}$$

where the + sign of the square root operation implies the minimization of the ground-state energy U. The quantity E_ν is given by

$$E_\nu = \sqrt{(\varepsilon_\nu - \lambda)^2 + \Delta^2}. \tag{G.15}$$

Making use again of the condition $H_{20} = 0$ one can write

$$(\varepsilon_\nu - \lambda)\frac{\Delta}{E_\nu} = \Delta(U_\nu^2 - V_\nu^2),$$

i.e.

$$(U_\nu^2 - V_\nu^2) = \frac{\varepsilon_\nu - \lambda}{E_\nu}, \tag{G.16}$$

$$U_\nu^2 - V_\nu^2 = 1 - 2V_\nu^2 = \frac{\varepsilon_\nu - \lambda}{E_\nu},$$

$$V_\nu^2 = \frac{1}{2}\left(1 - \frac{\varepsilon_\nu - \lambda}{E_\nu}\right),$$

leading to

$$V_\nu = \frac{1}{\sqrt{2}}\left(1 - \frac{\varepsilon_\nu - \lambda}{E_\nu}\right)^{1/2}, \tag{G.17}$$

$$U_\nu = \frac{1}{\sqrt{2}}\left(1 + \frac{\varepsilon_\nu - \lambda}{E_\nu}\right)^{1/2}. \tag{G.18}$$

Let us now substitute these expressions in the relation (G.10). One obtains

$$\Delta = \frac{G}{2}\sum_{\nu>0}\left(1 - \frac{(\varepsilon_\nu - \lambda)^2}{E_\nu^2}\right)^{1/2} = \frac{G}{2}\sum_{\nu>0}\frac{\Delta}{E_\nu}.$$

The above equation together with equation (G.6) are the BCS equations, i.e.

$$N = 2\sum_{\nu>0} V_\nu^2 \qquad \text{(number equation)}, \tag{G.19}$$

$$\frac{1}{G} = \sum_{\nu>0}\frac{1}{2E_\nu} \qquad \text{(gap equation)}. \tag{G.20}$$

These equations allow us to calculate the parameters λ and Δ from the knowledge of G and ε_ν, parameters which completely determine the occupation amplitudes U_ν and V_ν.

https://doi.org/10.1017/9781009401920 Published online by Cambridge University Press

One can now write U in terms of the parameters λ and Δ, i.e.

$$\begin{aligned} U &= 2\sum_{\nu>0}(\varepsilon_\nu - \lambda)V_\nu^2 - 2\frac{\Delta^2}{G} + \frac{\Delta^2}{G} \\ &= 2\sum_{\nu>0}(\varepsilon_\nu - \lambda)V_\nu^2 - \frac{\Delta^2}{G}. \end{aligned}$$

Making use of equations (G.14), (G.15) and (G.18) one can write H_{11} in terms of λ and Δ,

$$\begin{aligned} H_{11} &= \sum_{\nu>0}\left\{\frac{(\varepsilon_\nu - \lambda)^2}{E_\nu} + \frac{\Delta^2}{E_\nu}\right\}(\alpha_\nu^\dagger\alpha_\nu + \alpha_{\bar{\nu}}^\dagger\alpha_{\bar{\nu}}) \\ &= \sum_{\nu>0} E_\nu(\alpha_\nu^\dagger\alpha_\nu + \alpha_{\bar{\nu}}^\dagger\alpha_{\bar{\nu}}) = \sum_\nu E_\nu\alpha_\nu^\dagger\alpha_\nu \\ &= \sum_\nu E_\nu\hat{N}_\nu, \end{aligned} \tag{G.21}$$

where $\hat{N}_\nu = \alpha_\nu^\dagger\alpha_\nu$.

G.2 Two-quasiparticle excitations

In the case of a normal system, within the independent-particle model, the lowest excitations are of particle–hole character, i.e.

$$|ki\rangle = a_k^\dagger a_i|0\rangle_{\mathrm{HF}},$$

where

$$|0\rangle_{\mathrm{HF}} = \prod_{i=1}^{A} a_i^\dagger|0\rangle\ ,$$

($|0\rangle_{\mathrm{HF}}$: Hartree–Fock vacuum, $|0\rangle$: fermion vacuum).

Making use of the single-particle Hamiltonian

$$H_{\mathrm{sp}} = \sum_\nu \varepsilon_\nu a_\nu^\dagger a_\nu = \sum_\nu \varepsilon_\nu\hat{N}_\nu$$

one can calculate the energy of the particle–hole states. Let us start with the calculation of the ground-state energy,

$$\begin{aligned} H_{\mathrm{sp}}|0\rangle_{\mathrm{HF}} &= \sum_\nu \varepsilon_\nu N_\nu \prod_{i=1}^{A} a_i^\dagger|0\rangle \\ &= \sum_\nu \varepsilon_\nu \overbrace{a_\nu^\dagger a_\nu \quad a_1^\dagger a_2^\dagger \cdots a_A^\dagger}|0\rangle \\ &= (\varepsilon_{\nu_1} + \varepsilon_{\nu_2} + \cdots + \varepsilon_{\nu_A})|0\rangle_{\mathrm{HF}} = E_0|0\rangle_{\mathrm{HF}}. \end{aligned}$$

https://doi.org/10.1017/9781009401920 Published online by Cambridge University Press

Let us now calculate the energy of the particle–hole excitation referred to this energy, i.e.

$$(H_{\rm sp} - E_0)|ki\rangle = \sum_\nu (\varepsilon_\nu \hat{N}_\nu - E_0) a_k^\dagger a_i |0\rangle_{\rm HF}$$
$$= \sum_\nu \varepsilon_\nu (a_k^\dagger \left[\hat{N}_\nu, a_i\right] + \left[\hat{N}_\nu, a_k^\dagger\right] a_i)|0\rangle_{\rm HF}.$$

We have now to work out the commutation relations appearing in the above equations. They lead to

$$\left[\hat{N}_\nu, a_i\right] = \left[a_\nu^\dagger a_\nu, a_i\right] = -\{a_\nu^\dagger, a_i\} a_\nu = -\delta(\nu, i) a_\nu,$$
$$\left[N_\nu, a_k^\dagger\right] = \left[a_\nu^\dagger a_\nu, a_k^\dagger\right] = a_\nu^\dagger \{a_\nu, a_k^\dagger\} = \delta(\nu, k) a_\nu^\dagger,$$

where use was made of the relations

$$[AB, C] = A\,[B, C] + [A, C]\,B = ABC - ACB - ACB + CAB$$

and

$$[AB, C] = A\{B, C\} - \{A, C\}B = ABC + ACB - ACB - CAB.$$

One can then write

$$(H_{\rm sp} - E_0)|ki\rangle = \sum_\nu \varepsilon (a_k^\dagger(-\delta(\nu, i) a_\nu + \delta(\nu, k) a_\nu^\dagger a_i)|0\rangle_{\rm HF}$$
$$= (\varepsilon_k - \varepsilon_i) a_k^\dagger a_i |0\rangle_{\rm HF} = (\varepsilon_k - \varepsilon_i)|ki\rangle.$$

Summing up, the simplest excitation of the $|0\rangle_{\rm HF}$ vacuum is

$$a_k^\dagger a_i |0\rangle_{\rm HF},$$

i.e. a particle–hole excitation. The lowest of these excitations connects the last occupied and the first empty state.

In the case of quasiparticles

$$H_{\rm sp} \Rightarrow H_{11} + U; \quad |0\rangle_{\rm HF} \Rightarrow |{\rm BCS}\rangle$$
$$a_k^\dagger a_i \Rightarrow a_\nu^\dagger a_\nu = (U_\nu \alpha_\nu^\dagger + V_\nu \alpha_{\bar\nu})(U_\nu \alpha_\nu + V_\nu \alpha_{\bar\nu}^\dagger)$$
$$= U_\nu^2 \alpha_\nu^\dagger \alpha_\nu + U_\nu V_\nu \alpha_\nu^\dagger \alpha_{\bar\nu}^\dagger + V_\nu U_\nu \alpha_{\bar\nu} \alpha_\nu$$
$$- V_\nu^2 \alpha_{\bar\nu}^\dagger \alpha_\nu + V_\nu^2\,,$$

leading to

$$a_k^\dagger a_i |0\rangle_{\rm HF} \to U_\nu V_\nu \alpha_\nu^\dagger \alpha_{\bar\nu}^\dagger |{\rm BCS}\rangle \sim \alpha_\nu^\dagger \alpha_{\bar\nu}^\dagger |{\rm BCS}\rangle,$$

in that $V_\nu^2|{\rm BCS}\rangle$ is not an excitation. Thus, the simplest excitation of the $|{\rm BCS}\rangle$ vacuum is

$$\alpha_\nu^\dagger \alpha_{\bar\nu}^\dagger |{\rm BCS}\rangle = |\nu\bar\nu\rangle,$$

i.e. a two-quasiparticle state.

https://doi.org/10.1017/9781009401920 Published online by Cambridge University Press

The excitation energy associated with these states is

$$H_{11}|\nu_1\nu_2\rangle = \sum_\nu E_\nu \hat{N}_\nu \alpha^\dagger_{\nu_1}\alpha^\dagger_{\nu_2}|\text{BCS}\rangle$$
$$= \sum_\nu E_\nu [\hat{N}_{\nu_1}\alpha^\dagger_{\nu_1}\alpha^\dagger_{\nu_2}]|\text{BCS}\rangle,$$

in keeping with the fact that $\hat{N}_\nu|BCS\rangle = 0$. We now calculate

$$[\hat{N}_\nu, \alpha^\dagger_{\nu_1}\alpha^\dagger_{\nu_2}] = \alpha^\dagger_{\nu_1}[\hat{N}_\nu, \alpha^\dagger_{\nu_2}] + [\hat{N}_\nu, \alpha^\dagger_{\nu_1}]\alpha^\dagger_{\alpha_2},$$
$$\left[\hat{N}_\nu, \alpha^\dagger_{\nu_2}\right] = [\alpha^\dagger_\nu\alpha_\nu, \alpha^\dagger_{\nu_2}] = \alpha^\dagger_\nu\{\alpha_\nu, \alpha^\dagger_{\nu_2}\} - \{\alpha^\dagger_\nu, \alpha^\dagger_{\nu_2}\}\alpha_\nu$$
$$= \delta(\nu, \nu_2)\alpha^\dagger_\nu$$

and

$$\left[\hat{N}_\nu, \alpha^\dagger_{\nu_1}\right] = [\alpha^\dagger_\nu\alpha_\nu, \alpha^\dagger_{\nu_1}] = \alpha^\dagger_\nu\{\alpha_\nu, \alpha^\dagger_{\nu_1}\} - \{\alpha^\dagger_\nu, \alpha^\dagger_{\nu_1}\}\alpha_\nu$$
$$= \delta(\nu, \nu_1)\alpha^\dagger_\nu. \tag{G.22}$$

Consequently

$$\left[\hat{N}_\nu, \alpha^\dagger_{\nu_1}\alpha^\dagger_{\nu_2}\right] = \delta(\nu, \nu_2)\alpha^\dagger_{\nu_1}\alpha^\dagger_\nu + \delta(\nu, \nu_1)\alpha^\dagger_\nu\alpha^\dagger_{\nu_2}.$$

From these relations one can write

$$H_{11}|\nu_1\nu_2\rangle = \sum_\nu E_\nu\big(\delta(\nu, \nu_2)\alpha^\dagger_{\nu_1}\alpha^\dagger_\nu + \delta(\nu, \nu_1)\alpha^\dagger_\nu\alpha_{\nu_2})|\text{BCS}\rangle$$
$$= (E_{\nu_1} + E_{\nu_2})\alpha^\dagger_{\nu_1}\alpha^\dagger_{\nu_2}|\text{BCS}\rangle = (E_{\nu_1} + E_{\nu_2})|\nu_1\nu_2\rangle.$$

Because $(E_{\nu_1} + E_{\nu_2}) \geq 2\Delta$, the lowest excitation in the pairing correlated system lies at an energy $\geq 2\Delta$, i.e. the energy which it takes to break a pair. In fact, in the paired system, the only excitations possible are those associated with the breaking of pairs of particles moving in time-reversal states, an operation which takes an energy of the order of 2Δ.

G.3 Minimization

Writing the pairing Hamiltonian given in equation (G.1) in terms of quasiparticles one can calculate the average value in the $|\text{BCS}\rangle$ ground state, obtaining

$$\langle\text{BCS}|H_\text{p}|\text{BCS}\rangle = -G\sum_{\nu>0} V^4_\nu - G\sum_{\nu,\nu'>0} U_\nu V_\nu U_{\nu'} V_{\nu'}$$
$$= -G\big(\sum_{\nu>0} U_\nu V_\nu\big)^2 - G\sum_{\nu>0} V^4_\nu$$
$$= -\frac{\Delta^2}{G} - G\sum_{\nu>0} V^4_\nu.$$

Similarly,

$$\langle\text{BCS}|H_\text{sp}|\text{BCS}\rangle = 2\sum_{\nu>0}(\varepsilon_\nu - \lambda)V^2_\nu.$$

https://doi.org/10.1017/9781009401920 Published online by Cambridge University Press

Consequently

$$E_0 = \langle \text{BCS}|H|\text{BCS}\rangle = 2\sum_{\nu>0}(\varepsilon_\nu - \lambda)V_\nu^2 - \frac{\Delta^2}{G} - G\sum_{\nu>0}V_\nu^4$$
$$= 2\sum_{\nu>0}(\varepsilon_\nu - \lambda)V_\nu^2 - G(\sum_{\nu>0}U_\nu V_\nu)^2 - G\sum_{\nu>0}V_\nu^4$$
$$\approx 2\sum_{\nu>0}(\varepsilon_\nu - \lambda)V_\nu^2 - G\left(\sum_{\nu>0}U_\nu V_\nu\right)^2,$$

where we have neglected the mean-field pairing contribution to the single-particle energy (i.e. $\varepsilon'_\nu = \varepsilon_\nu - GV_\nu^2/2 \approx \varepsilon_\nu$), in keeping with the fact that $GV_\nu^2/2$ is small ($\approx \frac{G}{4} \approx \frac{6}{A}$ MeV ~ 0.05 MeV, with the ansatz $V_\nu^2 \approx \frac{1}{2}$ and for $A \approx 120$).

Let us minimize E_0 with respect to V_ν

$$\frac{\partial\langle \text{BCS}|H|\text{BCS}\rangle}{\partial V_\nu} = 0,$$

taking into account the normalization condition,

$$\frac{\partial U_\nu}{\partial V_\nu} = \frac{\partial}{\partial V_\nu}(1 - V_\nu^2)^{1/2} = \frac{1}{2}(1 - V_\nu^2)^{-1/2}(-2V_\nu)$$
$$= -\frac{V_\nu}{U_\nu}\,.$$

One thus obtains

$$\frac{\partial\langle \text{BCS}|H|\text{BCS}\rangle}{\partial V_{\nu'}} = 4(\varepsilon_{\nu'} - \lambda)V'_\nu - 2G\left(\sum_{\nu>0}U_\nu V_\nu)(U_{\nu'} - V_{\nu'}\frac{V_{\nu'}}{U_{\nu'}}\right)$$
$$= 4(\varepsilon_{\nu'} - \lambda)V_{\nu'} - 2\frac{\Delta}{U_{\nu'}}(U_{\nu'}^2 - V_{\nu'}^2) = 0,$$

i.e.

$$2(\varepsilon_{\nu'} - \lambda)U_{\nu'}V_{\nu'} = \Delta(U_{\nu'}^2 - V_{\nu'}^2), \tag{G.23}$$

which is the condition $H_{20} = 0$ (see (G.12)).

G.4 BCS wavefunction

The state $|\text{BCS}\rangle$ is the quasiparticle vacuum, i.e.

$$\alpha_\nu|\text{BCS}\rangle = 0.$$

Consequently, it can be written as

$$|\text{BCS}\rangle \sim \prod_\nu \alpha_\nu|0\rangle \sim \prod_{\nu>0}\alpha_\nu\alpha_{\overline{\nu}}|0\rangle.$$

Let us now calculate $\alpha_\nu\alpha_{\overline{\nu}}$, i.e. the product of

$$\alpha_\nu = U_\nu a_\nu - V_\nu a^\dagger_{\overline{\nu}}$$

https://doi.org/10.1017/9781009401920 Published online by Cambridge University Press

and

$$\alpha_{\overline{\nu}} = U_\nu a_{\overline{\nu}} + V_\nu a_\nu^\dagger.$$

It leads to

$$\begin{aligned}\alpha_\nu \alpha_{\overline{\nu}} &= U_\nu^2 a_\nu a_{\overline{\nu}} + U_\nu V_\nu a_\nu a_\nu^\dagger - U_\nu V_\nu a_{\overline{\nu}}^\dagger a_{\overline{\nu}} - V_\nu^2 a_{\overline{\nu}}^\dagger a_\nu^\dagger \\ &= U_\nu^2 a_\nu a_{\overline{\nu}} + U_\nu V_\nu (1 - a_\nu^\dagger a_\nu) - U_\nu V_\nu a_{\overline{\nu}}^\dagger a_{\overline{\nu}} + V_\nu^2 a_\nu^\dagger a_{\overline{\nu}}^\dagger.\end{aligned}$$

Consequently

$$\begin{aligned}|\mathrm{BCS}\rangle &= N \prod_{\nu>0} \Big(U_\nu^2 a_\nu a_{\overline{\nu}} + U_\nu V_\nu (1 - a_\nu^\dagger a_\nu) - U_\nu V_\nu a_{\overline{\nu}}^\dagger a_{\overline{\nu}} + V_\nu^2 a_\nu^\dagger a_{\overline{\nu}}^\dagger \Big) |0\rangle \\ &= N \prod_{\nu>0} \Big(U_\nu V_\nu + V_\nu^2 a_\nu^\dagger a_{\overline{\nu}}^\dagger \Big) |0\rangle \\ &= N \prod_{\nu>0} V_\nu \Big(U_\nu + V_\nu a_\nu^\dagger a_{\overline{\nu}}^\dagger \Big) |0\rangle,\end{aligned}$$

where N is a normalization constant, to be determined from the relation

$$\begin{aligned}1 &= \langle \mathrm{BCS} | \mathrm{BCS} \rangle \\ &= N^2 \langle 0 | \prod_{\nu>0} V_\nu \Big(U_\nu + V_\nu a_{\overline{\nu}} a_\nu \Big) \prod_{\nu'>0} V_{\nu'} \Big(U_{\nu'} + V_{\nu'} a_{\nu'}^\dagger a_{\overline{\nu}'}^\dagger \Big) |0\rangle \\ &= N^2 \langle 0 | \prod_{\nu>0} V_\nu^2 (U_\nu^2 + V_\nu^2) |0\rangle,\end{aligned}$$

$$N = \Big(\prod_{\nu>0} V_\nu^2 \Big)^{-\frac{1}{2}} = \Big(\prod_{\nu>0} V_\nu \Big)^{-1},$$

leading to

$$|\mathrm{BCS}\rangle = \prod_{\nu>0} \Big(U_\nu + V_\nu a_\nu^\dagger a_{\overline{\nu}}^\dagger \Big) |0\rangle.$$

https://doi.org/10.1017/9781009401920 Published online by Cambridge University Press

Appendix H
Pairing in a single *j*-shell

H.1 BCS solution

We shall discuss some of the consequences of pairing correlations in the case of particles moving in a single *j*-shell. The number of degenerate pair levels $(\nu, \bar{\nu})$ which can be accommodated in the shell is

$$\Omega = \frac{2j+1}{2}. \tag{H.1}$$

The value of the occupation numbers V_ν and U_ν must be the same for all the orbitals. In particular, the occupation probability of the level when the system is occupied with N particles is $N/2\Omega$. Consequently,

$$V_\nu = V = \sqrt{\frac{N}{2\Omega}} \tag{H.2}$$

and

$$U_\nu = U = \sqrt{1 - \frac{N}{2\Omega}}, \tag{H.3}$$

in keeping with the fact that $U_\nu^2 + V_\nu^2 = 1$. Making use of the above relation one finds

$$\begin{aligned} \Delta &= G \sum_{\nu>0} U_\nu V_\nu = G\Omega U V \\ &= \frac{G}{2}\sqrt{N(2\Omega - N)}. \end{aligned} \tag{H.4}$$

The pairing gap thus achieves its maximum value for the system with $N = \Omega$ particles (half-filled shell), in keeping with the fact that, owing to the degeneracy of the levels, pairs of particles and hole states are equivalent as far as pairing correlations are concerned (see Fig. H.1).

Making use of the condition $H_{20} = 0$, i.e.

$$2(\varepsilon_\nu - \lambda)U_\nu V_\nu = \Delta(U_\nu^2 - V_\nu^2), \tag{H.5}$$

https://doi.org/10.1017/9781009401920 Published online by Cambridge University Press

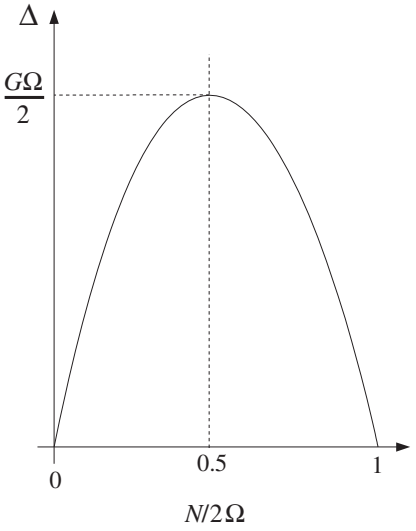

Figure H.1. Schematic representation of the pairing gap as a function of the number of particles (see equation (H.4)).

and assuming $\varepsilon_\nu = \varepsilon = 0$, one obtains

$$-\frac{2\lambda}{2\Omega}\sqrt{N(2\Omega - N)} = \frac{G}{2}\sqrt{N(2\Omega - N)}\frac{1}{\Omega}(\Omega - N), \tag{H.6}$$

thus leading to

$$\lambda = -\frac{G}{2}(\Omega - N). \tag{H.7}$$

Let us now calculate the ground-state energy

$$E_0 = U + \lambda N = 2\sum_{\nu>0}\varepsilon_\nu V_\nu^2 - \frac{\Delta^2}{G}.$$

Consequently,

$$\begin{aligned} E_0 &= -\frac{\Delta^2}{G} = -\frac{G^2}{4}\frac{1}{G}N(2\Omega - N) \\ &= -\frac{G\Omega}{2}N + \frac{G}{4}N^2. \end{aligned} \tag{H.8}$$

Assuming $\Omega \gg N$ one obtains from equation (H.7)

$$\lambda \approx -\frac{G\Omega}{2}$$

and equation (H.8) can be rewritten as

$$E_0 \approx \lambda N + \frac{G}{4}N^2. \tag{H.9}$$

https://doi.org/10.1017/9781009401920 Published online by Cambridge University Press

Interpreting the second term in equation (H.8) or (H.9) as that corresponding to a rotor in two dimensions with moment of inertia

$$\frac{\hbar^2}{2\mathcal{I}} = \frac{G}{4} \tag{H.10}$$

or

$$\frac{\mathcal{I}}{\hbar^2} = \frac{2}{G} \tag{H.11}$$

we finally write

$$E_0 \approx \lambda N + \frac{\hbar^2}{2\mathcal{I}} N^2, \tag{H.12}$$

$$\left.\frac{\partial E_0}{\partial N}\right|_{N=0} = \lambda, \tag{H.13}$$

$$\frac{\partial^2 E_0}{\partial N^2} = \frac{\hbar^2}{\mathcal{I}}. \tag{H.14}$$

Making use of the estimate given in equation (2.27) (see also end of Section 2.5) for G and $A \approx 100$ (Sn-isotopes), we obtain $\hbar^2/2\mathcal{I} \approx 0.07$ MeV. This result is very close to the value needed to fit the experimental data (see Fig. 4.2, where the pairing rotational band is fitted with a parabola whose quadratic term is 0.1 MeV N^2).

In the single f-shell model, the quasiparticle energy is given by

$$\begin{aligned} E_\nu &= \sqrt{(\varepsilon_\nu - \lambda)^2 + \Delta^2} \\ &= \left[\frac{G^2}{4}(\Omega - N)^2 + \frac{G^2}{4} N(2\Omega - N)\right]^{1/2} \\ &= \frac{G}{2}\left[\Omega^2 - 2\Omega N + N^2 + 2\Omega N - N^2\right]^{1/2}, \\ E_\nu &= E = \frac{G\Omega}{2}. \end{aligned} \tag{H.15}$$

H.2 Cranking moment of inertia

The cranking formula of the moment of inertia associated with pairing rotations (rotations in gauge space) is

$$\begin{aligned} \mathcal{I} &= 2\hbar^2 \sum_{\nu>0} \frac{|< \nu\bar{\nu}|N_\nu|\mathrm{BCS} >|^2}{2E_\nu} \\ &= \sum_{\nu} \frac{|< \nu\bar{\nu}|\hbar N_\nu|\mathrm{BCS} >|^2}{2E_\nu}. \end{aligned} \tag{H.16}$$

Making use of the relation

$$\begin{aligned} N_\nu &= a_\nu^\dagger a_\nu + a_{\bar{\nu}}^\dagger a_{\bar{\nu}} \\ &= (U_\nu^2 - V_\nu^2)(\alpha_\nu^\dagger \alpha_\nu + \alpha_{\bar{\nu}}^\dagger \alpha_{\bar{\nu}}) + 2U_\nu V_\nu (\alpha_\nu^\dagger \alpha_{\bar{\nu}}^\dagger + \alpha_{\bar{\nu}} \alpha_\nu) + 2V_\nu^2 \end{aligned}$$

https://doi.org/10.1017/9781009401920 Published online by Cambridge University Press

one obtains

$$\langle \nu\bar{\nu}\,|N_\nu|\,\mathrm{BCS}\rangle = 2U_\nu V_\nu$$

leading to

$$\frac{\mathcal{I}}{\hbar^2} = 4\sum_{\nu>0}\frac{U_\nu^2 V_\nu^2}{E_\nu} = \sum_{\nu>0}\frac{\Delta^2}{E_\nu^3}. \tag{H.17}$$

Inserting (H.2), (H.3) and (H.15) into equation (H.17) one obtains

$$\begin{aligned}\frac{\mathcal{I}}{\hbar^2} &= 4\Omega\frac{N}{2\Omega}\left(1-\frac{N}{2\Omega}\right)\\ &= \frac{4N}{G\Omega}\left(1-\frac{N}{2\Omega}\right).\end{aligned} \tag{H.18}$$

Setting $N = \Omega$,

$$\frac{\mathcal{I}}{\hbar^2} = \frac{2}{G}, \tag{H.19}$$

which coincides with the result shown in equation (H.11).

Note that

$$\frac{(\hbar^2/2\mathcal{I})}{(G\Omega/2)} = \frac{1}{2\Omega},$$

implying that collective pairing rotations have much lower energy than two-quasiparticle excitation.

H.3 Two-particle transfer

The transfer operator is

$$\begin{aligned}P^\dagger &= \sum_{\nu>0} a_\nu^\dagger a_{\bar{\nu}}^\dagger\\ &= \sum_{\nu>0}\left(U_\nu^2\alpha_\nu^\dagger\alpha_{\bar{\nu}}^\dagger - U_\nu V_\nu\left(\alpha_\nu^\dagger\alpha_\nu + \alpha_{\bar{\nu}}^\dagger\alpha_{\bar{\nu}}\right)\right.\\ &\quad \left. - V_\nu^2\alpha_{\bar{\nu}}\alpha_\nu + U_\nu V_\nu\right).\end{aligned} \tag{H.20}$$

Consequently

$$\left\langle \mathrm{BCS}\left|P^\dagger\right|\mathrm{BCS}\right\rangle = \sum_{\nu>0} U_\nu V_\nu = \frac{\Delta}{G}, \tag{H.21}$$

and the two-particle transfer cross-section can be written as

$$\sigma(\mathrm{gs}\to\mathrm{gs}) \approx \left(\frac{\Delta}{G}\right)^2 = \left(\frac{12}{\sqrt{A}}\frac{A}{28}\right)^2 \approx \frac{A}{4}. \tag{H.22}$$

https://doi.org/10.1017/9781009401920 Published online by Cambridge University Press

On the other hand

$$\left\langle \nu\bar{\nu} \left| P^{\dagger} \right| BCS \right\rangle = U_{\nu}^{2} \approx 1, \tag{H.23}$$

leading to

$$\sigma(\text{gs} \rightarrow \text{2qp}) \approx U_{\nu}^{4} \approx 1. \tag{H.24}$$

From the above equations one obtains

$$R = \frac{\sigma(\text{gs} \rightarrow \text{gs})}{\sigma(\text{gs} \rightarrow \text{2qp})} \approx \frac{A}{4}. \tag{H.25}$$

For Sn-isotopes ($A \approx 100$) one thus expects

$$R = 25 \qquad \text{(BCS model)}. \tag{H.26}$$

Making use of the experimental results displayed in Fig. 4.2 one can calculate the average value of the ten observed two-particle transfer cross-sections connecting the members of the Sn-ground-state pairing rotational band ($64 \leq N \leq 76$), normalized to the ${}^{116}_{50}\text{Sn(gs)} \leftrightarrow {}^{118}_{50}\text{Sn(gs)}$ (p, t) and (t, p) cross-sections. One obtains,

$$\begin{aligned} &\sigma(\text{gs} \rightarrow \text{gs})_{\text{exp}} \\ &= \frac{1.3 + 1.2 + 1.0 + 1.3 + 1.5 + 1.1 + 1.4 + 1.1 + 1.2 + 1.1}{10} = 1.22. \end{aligned} \tag{H.27}$$

Similarly, the calculation of the average of the six two-particle (relative) cross-sections connecting members of the ground-state pairing rotational band to members of the two-quasiparticle (2qp) pairing vibrational bands leads to

$$\sigma(\text{gs} \rightarrow \text{2qp})_{\text{exp}} = \frac{0.04 + 0.03 + 0.04 + 0.06 + 0.05 + 0.08}{6} = 0.05. \tag{H.28}$$

Consequently,

$$R_{\text{exp}} \approx \frac{1.22}{0.05} \approx 24.4, \tag{H.29}$$

essentially as predicted by theory (see also (2.58)).

H.4 Polarization effects

In the following we summarize in simple terms the results obtained in sub-section 10.4.1. The relation in equation (H.4) with $N = \Omega$ leads to

$$\Delta = \frac{1}{2} G\Omega. \tag{H.30}$$

We are particularly concerned with the role of polarization effects on the renormalization of the value of the pairing gap in a superfluid nucleus like e.g. ${}^{120}\text{Sn}$.

We shall call G_b and Ω_b the bare pairing strength and degeneracy (closely related to the density of levels) associated with an effective mass equal to the k-mass ($m_k \approx 0.7$ m) (see equations (8.20) and (8.21)). From the results displayed in Figs. 8.6, 8.9 and 10.1

https://doi.org/10.1017/9781009401920 Published online by Cambridge University Press

one can write

$$\frac{1}{2}G_b\Omega_b = 0.5\Delta_{\text{exp}}, \tag{H.31}$$

$$\frac{1}{2}G_b\Omega_d = 1.4\Delta_{\text{exp}}, \tag{H.32}$$

and

$$\frac{1}{2}g_{\text{p-v}}\Omega_d \approx 0.8\Delta_{\text{exp}}, \tag{H.33}$$

where Ω_d is the effective (dressed) degeneracy arising from the coupling of single-particle motion to collective vibrations (ω-effective mass, see Section 9.2), while $g_{\text{p-v}}$ is the induced pairing interaction due to the exchange of vibrations between pairs of nucleons moving in time-reversal states close to the Fermi energy (see Section 9.3).

In keeping with the results displayed in Fig. 10.16, one can also write

$$\frac{1}{2}G_d\Omega_d = \Delta_{\text{exp}}, \tag{H.34}$$

where G_d is the dressed pairing interaction. Because the density of levels is proportional to the ω-mass (see discussion end of Section 9.1.1 as well as equation (9.23)), one can write

$$\Omega_d \approx \frac{\Omega_b}{Z_\omega}, \tag{H.35}$$

where $Z_\omega = (m_\omega/m)^{-1}$ (see also Section 9.3).

Due to the coupling to vibrations, nucleons spend part of the time in more complicated configurations than pure single-particle states (see Fig. 9.2). The factor Z_ω measures the content of single-particle strength present in levels around the Fermi energy available to nucleons to interact through a (pairing) force and correlate, eventually giving rise to a superfluid system. In the case of the dressed pairing coupling constant, one then can write the expression

$$G_d = Z_\omega^2(G_b + g_{\text{p-v}}). \tag{H.36}$$

Making use of this relation and of equation (H.34) one can write

$$\frac{1}{2}G_d\Omega_d = Z_\omega\frac{1}{2}G_b\Omega_b + Z_\omega\frac{1}{2}g_{\text{p-v}}\Omega_b. \tag{H.37}$$

The above relation implies that, without considering the contribution of the induced pairing interaction to the dressed pairing gap, the increase of the density of levels arising from the coupling of nucleons to collective vibrations is overcompensated by the reduction in the single-particle content of these levels, the net result being a decrease of the pairing gap (from the minimum value it can have in the static mean-field approximation, i.e. $\frac{1}{2}G_b\Omega_b$). On the other hand, relations (H.32) and (H.33) imply

$$g_{\text{p-v}} \approx 0.6G_b. \tag{H.38}$$

Summing up, taking into account the renormalization effects leading to an ω-mass, and thus to an increase of the density of levels, one has to consider, at the same time, the actual single-particle strength in the levels lying close to the Fermi energy.

Note that a proper treatment of the dressing of single-particle states not only involves the Z_ω-coefficients (arising from $\Delta E = \mathrm{Re}\Sigma$), but also the splitting of the single-particle strength (arising from $-2\mathrm{Im}\Sigma$, see Section 9.1, equation (9.11), see also (9.14)). This last effect leads to a further reduction of the ability of time reversal single-particle states to participate in Cooper pair formation (see equation (9.41)).

https://doi.org/10.1017/9781009401920 Published online by Cambridge University Press

Appendix I
Fluctuations and symmetry restoration

This appendix contains some relations on spontaneous symmetry breaking which are used in Chapter 4.

I.1 Conjugate variables

The uncertainty relation

$$\Delta x \Delta p \geq \mathrm{i}\hbar \tag{I.1}$$

specifies the limits within which the particle picture can be applied. Any use of the word 'position' with an accuracy exceeding that given by the above equation is just meaningless, because quantum mechanical processes can be described equally well in terms of waves as particles.

Momentum and position are conjugate variables and satisfy commutation relations

$$[x, p] = \mathrm{i}\hbar. \tag{I.2}$$

In the coordinate representation the wavefunctions $\psi(x)$ are functions of position, and the momentum operator can be written as

$$p = -\mathrm{i}\hbar \frac{\partial}{\partial x}. \tag{I.3}$$

The relation

$$x = \mathrm{i}\hbar \frac{\partial}{\partial p} \tag{I.4}$$

is a valid form of the position operator in the momentum representation.

The Heisenberg equation of motion for an operator A which does not depend explicitly on the time is

$$\dot{A} = \frac{\mathrm{i}}{\hbar} [H, A], \tag{I.5}$$

https://doi.org/10.1017/9781009401920 Published online by Cambridge University Press

where H is the Hamiltonian. If $H(p)$ is a function of the momentum of a particle then the velocity

$$\dot{x} = \frac{\mathrm{i}}{\hbar}[H, x] = \frac{\partial H}{\partial p}, \tag{I.6}$$

where the first step follows from the Heisenberg equation and the second from the representation of the position operator. Choosing the special form $H = p^2/2m$ we have $\dot{x} = p/m$ and

$$\frac{\partial \dot{x}}{\partial p} = \frac{\partial^2 H}{\partial p^2} = \frac{1}{m}. \tag{I.7}$$

I.2 Rotation about an axis

The situation is similar for the angle and angular momentum of a rigid body rotating about an axis but there are important differences. This is because the angle is restricted to the range $-\pi < \varphi \leqslant \pi$ and the angular momentum L is quantized. In the angle representation the wavefunctions $\psi(\varphi)$ must be periodic functions with period 2π. The commutation relation $[\varphi, L] = \mathrm{i}\hbar$ must be used with care. The representation of the angular momentum operator

$$L = -\mathrm{i}\hbar\frac{\partial}{\partial \varphi} \tag{I.8}$$

is valid when applied to wavefunctions which have the correct periodicity properties but the representation

$$\varphi = \mathrm{i}\hbar\frac{\partial}{\partial L} \tag{I.9}$$

is correct only in a heuristic or semiclassical sense. This is because L is quantized and the derivative is not defined.

Suppose that the rotor has a Hamiltonian $H(L)$ which is a function of L. Heisenberg's equation of motion gives

$$\omega_{\mathrm{rot}} = \dot{\varphi} = \frac{\mathrm{i}}{\hbar}[H, \varphi] \tag{I.10}$$

where ω_{rot} is the rotational frequency. Making use of the semiclassical relation

$$\frac{\mathrm{i}}{\hbar}[H, \varphi]\,|\,\psi\,\rangle = \frac{\partial H}{\partial L}\,|\,\psi\,\rangle, \tag{I.11}$$

which follows from equation (I.9), we get

$$\hbar\omega_{\mathrm{rot}} = \hbar\frac{\partial H}{\partial L} = \frac{\partial H}{\partial I} = \frac{\hbar^2 I}{\mathcal{I}}. \tag{I.12}$$

https://doi.org/10.1017/9781009401920 Published online by Cambridge University Press

Here we have used $L = \hbar I$ so that L has the dimensions of angular momentum while I is dimensionless. Equation (I.12) defines a moment of inertia $\mathcal{I}$. Consequently

$$\frac{\partial \hbar\omega_{\text{rot}}}{\partial I} = \frac{\hbar^2}{\mathcal{I}} = \frac{\partial^2 H}{\partial I^2}, \tag{I.13}$$

a consequence of the structure of the Hamiltonian. If the moment of inertia is constant then

$$H = \frac{L^2}{2\mathcal{I}} = \frac{\hbar^2 I^2}{2\mathcal{I}}. \tag{I.14}$$

This last relation is the Hamiltonian of a rigid body. Equations (I.13) and (I.14) are used in the analysis the rotational spectra of deformed nuclei. As discussed in Chapter 6, equation (I.13) defines the first moment of inertia and equation (I.13) the second moment of inertia. For an even nucleus $I = 0, 2, 4, \ldots$, the quantities $\hbar\omega_{\text{rot}}$ are related to gamma ray energies and the derivatives are calculated as finite differences.

I.3 Rotations in gauge space

The above discussions concerning rotations about an axis carry over to rotations in gauge space.* In this case the particle number operator $\hat{N}$ plays the role of the angular momentum. The gauge angle ϕ and the particle number operator satisfy the commutation relation $[\phi, \hat{N}] = i$ and in the number representation

$$\phi = \mathrm{i}\frac{\partial}{\partial N}. \tag{I.15}$$

The Hamiltonian for the BCS pairing problem is

$$H = H_0 - \lambda\hat{N}, \tag{I.16}$$

where H_0 includes the kinetic energy of the nucleons and the pairing interaction, $\hat{N}$ is the particle number operator and λ is a Lagrange multiplier which is used to fix the number of nucleons. Physically it is the Fermi energy and is determined by measuring the energy change of the system when adding and subtracting particles. For example the change in energy of the nucleus when an even number δN of nucleons are added is

$$\delta\langle E\rangle = \lambda\delta N. \tag{I.17}$$

The time derivative of the gauge angle is given by Heisenberg's equation of motion

$$\dot{\phi} = \frac{\mathrm{i}}{\hbar}[H, \phi] = \frac{1}{\hbar}\frac{\partial H}{\partial N} = \frac{1}{\hbar}\lambda. \tag{I.18}$$

* The role of conjugate variables becomes very intuitive when viewed in terms of the corresponding unitary transformation leaving invariant the total Hamiltonian: Galilean (translational invariance homogeneity of space) $T = \exp(-\mathrm{i}p_x x)$, Rotation (rotational invariance, space isotropy) $R = \exp(-\mathrm{i}\varphi I)$, Gauge (conservation particle number) $G = \exp(-\mathrm{i}\phi N)$, etc. Nature breaks spontaneously all these symmetries. The fingerprints of the associated deformations are the families of states corresponding to the quantized rotation of the system as a whole (AGN modes).

https://doi.org/10.1017/9781009401920 Published online by Cambridge University Press

Thus the combination

$$2\hbar\dot{\phi} = 2\lambda = \delta \langle E \rangle \tag{I.19}$$

has the physical meaning of the change in energy of the nucleus when a pair ($\delta N = 2$) of nucleons is added to it. Taking the derivative with respect to N

$$\frac{\partial \dot{\phi}}{\partial N} = \frac{1}{\hbar}\frac{\partial \lambda}{\partial N} = \frac{1}{\hbar}\frac{\partial^2 H}{\partial N^2} = \frac{\hbar}{\mathcal{I}}. \tag{I.20}$$

This equation defines the pairing 'moment of inertia' $\mathcal{I}$ describing rotations in gauge space. It is analogous to the moment of inertia for rotations in ordinary space. The 'pairing moment of inertia' can also be written as

$$\frac{\mathcal{I}}{\hbar^2} = \frac{\partial N}{\partial \lambda}. \tag{I.21}$$

This expression is very general and depends only on λ being a Lagrange multiplier in a variational principle for the energy. If $E\,(N_0)$ is the energy of a nucleus with N_0 nucleons and if the pairing 'moment of inertia' is approximately constant then equation (I.21) can be integrated to give the energy of nearby nuclei with N nucleons

$$E\,(N) \approx E\,(N_0) + \lambda(N - N_0) + \frac{\hbar^2}{2\mathcal{I}}\,(N - N_0)^2\,. \tag{I.22}$$

This is the energy dependence of a 'pairing rotational band'. The importance of the quadratic term depends on the value of the moment of inertia. The simplest way to calculate the pairing moment of inertia in the BCS model is to use equation (I.21). The average number of particles is

$$N = 2\sum_{\nu>0} V_\nu^2 = \sum_{\nu>0}\left[1 - \frac{\varepsilon_\nu - \lambda}{E_\nu}\right], \tag{I.23}$$

where E_ν are the quasiparticle energies. Evaluating the derivative with respect to λ gives

$$\frac{\mathcal{I}}{\hbar^2} = \frac{\partial N}{\partial \lambda} = \sum_{\nu>0}\frac{\Delta^2}{E_\nu^3} + \Delta\frac{\mathrm{d}\Delta}{\mathrm{d}\lambda}\sum_{\nu>0}\frac{\varepsilon_\nu - \lambda}{E_\nu^3}. \tag{I.24}$$

The derivative $\mathrm{d}\Delta/\mathrm{d}\lambda$ in the second term can be calculated by differentiating the gap equation. The second term is expected to be small in a situation where the energy level distribution is more or less symmetrical above and below the Fermi level. It is more important near the beginning or end of a shell. Neglecting this term we obtain the cranking formula given in equation (H.17).

I.4 Symmetry restoring fluctuations and pairing rotations

Another method to obtain the pairing moment of inertia is to extract it from the zero frequency mode of the pairing RPA. The Hamiltonian is

$$H = H_{\mathrm{MF}} + H''_{\mathrm{p}} \tag{I.25}$$

https://doi.org/10.1017/9781009401920 Published online by Cambridge University Press

making the approximation of taking only the even part H_{p}'' of the fluctuating term $H_{\mathrm{p}}' + H_{\mathrm{p}}''$. Solving the RPA equation of motion

$$[H, {\Gamma_n}^{\dagger}] = W_n'' {\Gamma_n}^{\dagger}. \tag{I.26}$$

The discussion in Section 4.2.2 showed that equation (I.26) has a zero-frequency solution $\left(W_1'' = 0\right)$ related to the gauge invariance of the original Hamiltonian. The corresponding creation operator was related to the number operator by

$$\Gamma_1^{\dagger} = \frac{\Lambda_1''}{2\Delta}\left(\hat{N} - N_0\right), \tag{I.27}$$

where N_0 is the average number of nucleons in the BCS state, which is the eigenstate of the mean-field Hamiltonian H_{MF} and the normalization constant

$$\Lambda_1'' = \frac{1}{2}\left[\sum_{\nu>0} \frac{2E_\nu W_1''}{((2E_\nu)^2 - W_1''^2)^2}\right]^{-1/2}. \tag{I.28}$$

The normalization constant Λ_1'' (particle–vibration coupling) diverges for the zero-frequency mode, but for the moment we assume that $W_1'' > 0$ and then take the limit $W_n'' \to 0$ later in the calculation.

Now we make a comparison with an oscillator with Hamiltonian

$$H = \frac{p^2}{2D_1''} + \frac{1}{2} D_1'' \omega_1''^2 q^2, \tag{I.29}$$

and identify the momentum with the number operator, the coordinate with the gauge angle and the frequency with the RPA energy:

$$p = \hbar\left(\hat{N} - N_0\right), \qquad q = \phi, \qquad \hbar\omega_1'' = W_1''. \tag{I.30}$$

The phonon creation operator for the oscillator is

$$\Gamma^{\dagger} = \sqrt{\frac{\hbar^2}{2D_1''W_1''}}\left(\hat{N} - N_0\right) + \mathrm{i}\phi\sqrt{\frac{D_1''W_1''}{2\hbar^2}}. \tag{I.31}$$

Comparing the coefficients of $\left(\hat{N} - N_0\right)$ in equations (I.27) and (I.31) and noting that the coefficient of ϕ in equation (I.31) vanishes in the limit $W_1'' \to 0$, we get an expression for the mass parameter

$$\frac{\hbar^2}{2D_1''W_1''} = \left(\frac{\Lambda_1''}{2\Delta}\right)^2 \quad \text{or} \quad \frac{D_1''}{\hbar^2} = \frac{4\Delta^2}{2W_1''\Lambda_1''^2}. \tag{I.32}$$

Taking the limit $W_1'' \to 0$ we have

$$\frac{1}{W_1''\Lambda_1''^2} = \frac{4}{W_1''}\left[\sum_{\nu>0} \frac{2E_\nu W_1''}{((2E_\nu)^2 - W_1''^2)^2}\right] = \sum_\nu \frac{1}{2E_\nu^3} \tag{I.33}$$

https://doi.org/10.1017/9781009401920 Published online by Cambridge University Press

and the mass parameter reduces to

$$\frac{D_1''}{\hbar^2} = \sum_{\nu>0} \frac{\Delta^2}{E_\nu^3}. \tag{I.34}$$

This agrees with the previous approximate expressions for the pairing moment of inertia (see equations (4.47), (H.17)). A more accurate calculation which includes the effect of the odd part $H_{\rm p}'$ of the interaction modifies this result and leads to an expression equivalent to (I.24).

Making use of the above result, and the fact that $\lambda = \partial H/\partial N$, the energy of the members of the pairing rotational band can be written as

$$E = \lambda N + \frac{\hbar^2}{2\mathcal{I}} N^2, \tag{I.35}$$

where

$$\frac{\mathcal{I}}{\hbar^2} = \frac{D_1''}{\hbar^2} = \sum_{\nu>0} \frac{4U_\nu^2 V_\nu^2}{E_\nu} = 2\sum_{\nu>0} \frac{\langle \nu\overline{\nu}|\hat{N}|BCS\rangle^2}{2E_\nu}, \tag{I.36}$$

which is the cranking formula of the moment of inertia rotations in gauge space.

I.4.1 Demonstration that $[H_{\rm MF} + H_{\rm p}'', \tilde{N}] = 0$

In what follows we demonstrate that

$$[H_{\rm MF} + H_{\rm p}'', \tilde{N}] = 0, \tag{I.37}$$

where (see equations (G.11), (G.12) and (G.21))

$$H_{\rm MF} = U + H_{11}, \tag{I.38}$$

U being a constant and

$$H_{11} = \sum_\nu E_\nu \alpha_\nu^\dagger \alpha_\nu. \tag{I.39}$$

We do this within the harmonic approximation (RPA), where two-quasiparticle excitations are described in terms of the (quasi-boson) operators

$$\Gamma_\nu^\dagger = \alpha_\nu^\dagger \alpha_{\overline{\nu}}^\dagger, \quad \Gamma_\nu = \alpha_{\overline{\nu}} \alpha_\nu, \tag{I.40}$$

for which we impose the condition (see equation (A.71))

$$[\Gamma_\nu, \Gamma_{\nu'}^\dagger] = \delta(\nu, \nu'). \tag{I.41}$$

Within this approximation $H_{\rm MF}$ can be written as

$$H_{\rm MF} = \sum_\nu 2E_\nu \Gamma_\nu^\dagger \Gamma_\nu. \tag{I.42}$$

https://doi.org/10.1017/9781009401920 Published online by Cambridge University Press

Within the same approximation, the relation (G.5) is

$$a_\nu^\dagger a_\nu + a_{\bar{\nu}}^\dagger a_{\bar{\nu}} \approx 2U_\nu V_\nu \left(\Gamma_\nu^\dagger + \Gamma_\nu\right) + 2V_\nu^2,$$

and the operator number of particles is

$$\tilde{N} = \Delta \sum_{\nu>0} \frac{1}{E_\nu} \left(\Gamma_\nu^\dagger + \Gamma_\nu\right) + N_0. \tag{I.43}$$

Making use of the commutation relations

$$\begin{aligned}\left[\Gamma_\nu^\dagger \Gamma_\nu, \left(\Gamma_{\nu'}^\dagger + \Gamma_{\nu'}\right)\right] &= \Gamma_\nu \left[\Gamma_\nu, \left(\Gamma_{\nu'}^\dagger + \Gamma_{\nu'}\right)\right] + \left[\Gamma_\nu^\dagger, \left(\Gamma_{\nu'}^\dagger + \Gamma_{\nu'}\right)\right] \Gamma_\nu \\ &= \delta(\nu, \nu') \left(\Gamma_\nu^\dagger - \Gamma_{\nu'}\right)\end{aligned}$$

and

$$\left[\left(\Gamma_\nu^\dagger - \Gamma_{\nu'}\right), \left(\Gamma_{\nu'}^\dagger + \Gamma_{\nu'}\right)\right] = -2\delta(\nu, \nu'),$$

one obtains

$$\begin{aligned}[H_{\mathrm{MF}}, \tilde{N}] &= \sum_{\nu>0} 2E_\nu \sum_{\nu'>0} \frac{\Delta}{E_{\nu'}} \left[\Gamma_\nu^\dagger \Gamma_\nu, \left(\Gamma_{\nu'}^\dagger + \Gamma_\nu\right)\right] \\ &= 2\Delta \sum_{\nu>0} \left(\Gamma_\nu^\dagger - \Gamma_\nu\right)\end{aligned} \tag{I.44}$$

and

$$\begin{aligned}[H_{\mathrm{p}}'', \tilde{N}] &= \frac{G}{4} \sum_{\nu'>0} \frac{\Delta}{E_{\nu'}} \left[\sum_{\nu>0} \left(\Gamma_\nu^\dagger - \Gamma_\nu\right)^2, \left(\Gamma_\nu^\dagger + \Gamma_{\nu'}\right)\right] \\ &= \frac{G}{4} \sum_{\nu'>0} \frac{\Delta}{E_{\nu'}} 2 \left(\sum_{\nu>0} \left(\Gamma_\nu^\dagger - \Gamma_\nu\right)\right) \left[\sum_{\nu''} \left(\Gamma_{\nu''}^\dagger - \Gamma_{\nu''}\right) \left(\Gamma_{\nu'}^\dagger + \Gamma_{\nu'}\right)\right] \\ &= -G \sum_{\nu'>0} \frac{\Delta}{E_{\nu'}} \sum_{\nu>0} \left(\Gamma_\nu^\dagger - \Gamma_\nu\right) \\ &= -2\Delta \sum_{\nu>0} \left(\Gamma_\nu^\dagger - \Gamma_\nu\right),\end{aligned} \tag{I.45}$$

where in the last step use was made of the BCS gap equation.

From equations (I.44) and (I.45) one obtains

$$[H_{\mathrm{MF}} + H_{\mathrm{p}}'', \tilde{N}] = 0. \tag{I.46}$$

Because

$$\begin{aligned}\left[\left(\Gamma_\nu^\dagger + \Gamma_\nu\right), \left(\Gamma_{\nu'}^\dagger + \Gamma_{\nu'}\right)\right] &= -\delta(\nu, \nu') + \delta(\nu, \nu') = 0, \\ [H_{\mathrm{p}}', \tilde{N}] &= 0.\end{aligned} \tag{I.47}$$

Consequently, H_{p}'' is the term of the residual interaction among the quasiparticles which, within the quasi-boson approximation, restores gauge invariance to the symmetry-breaking BCS Hamiltonian H_{MF}.

https://doi.org/10.1017/9781009401920 Published online by Cambridge University Press

We now show the quasi-boson approximation is a good approximation provided the number of quasiparticles excited in the system is small. In fact,

$$\begin{aligned}[\alpha_{\bar{\nu}}\alpha_{\nu}, \alpha^{\dagger}_{\nu'}\alpha^{\dagger}_{\bar{\nu}'}] &= \alpha_{\bar{\nu}}[\alpha_{\nu}, \alpha^{\dagger}_{\nu'}\alpha^{\dagger}_{\bar{\nu}'}] + [\alpha_{\bar{\nu}}, \alpha^{\dagger}_{\nu'}\alpha_{\bar{\nu}'}]\alpha_{\nu} \\ &= \alpha_{\bar{\nu}}\left\{\alpha_{\nu}, \alpha^{\dagger}_{\nu'}\right\}\alpha^{\dagger}_{\bar{\nu}'} - \alpha^{\dagger}_{\nu'}\left\{\alpha_{\bar{\nu}}, \alpha^{\dagger}_{\bar{\nu}'}\right\}\alpha_{\nu} \\ &= \delta(\nu, \nu')(1 - N_{\nu} - N_{\bar{\nu}}), \end{aligned} \tag{I.48}$$

where

$$N_{\nu} = \alpha^{\dagger}_{\nu}\alpha_{\nu}. \tag{I.49}$$

Consequently, the last two terms in the parentheses in equation (I.48) are connected with the Pauli principle. Furthermore,

$$[\alpha_{\bar{\nu}}\alpha_{\nu}, \alpha^{\dagger}_{\nu'}\alpha^{\dagger}_{\bar{\nu}'}]|\text{BCS}\rangle = \delta(\nu, \nu')|\text{BCS}\rangle \tag{I.50}$$

Let us end this technical section with a physical image. Restoration of gauge symmetry arises, within the picture of deformation in gauge space developed in Chapter 4 (see Fig. 4.1), in terms of fluctuations in the orientation of the body-fixed system $\mathcal{K}'$ defining a privileged direction in gauge space. In the present case, this is also the orientation defined by the symmetry axis of the (static) deformation of the system.

In keeping with the analogies carried out in Section I.1 (Euler angle $\varphi \leftrightarrow$ gauge angle ϕ, rotational frequency $\omega_{\text{rot}} \leftrightarrow$ Fermi energy in units of Planck's constant $\lambda/\hbar$, angular momentum $I \leftrightarrow$ number of particles N), and the fact that quantum mechanically a spherical system cannot rotate, one can view the pairing gap Δ as the deformation in gauge space (or equivalently α_0, see equation (G.2)) corresponding to the static quadrupole moment Q_0 of a deformed nucleus in normal space (axial symmetry has been assumed for simplicity).

Let us now use this deformed system, which is easy to visualize, to develop the line of reasoning. For a fixed orientation this system violates rotational invariance. To restore this symmetry, the privileged orientation has to be averaged out. That is, the system has to rotate at given frequencies ($\omega_{\text{rot}} = \hbar I/\mathcal{I}$), tantamount to saying that it has to be in a state of definite angular momentum I.

Summing up, starting from a rotational invariant Hamiltonian the (mean-field) state of lowest energy describes a deformed system and thus a privileged orientation in space. A part of the residual interaction (corresponding to H''_{p} in gauge space) gives rise to a vibrational mode which, in the harmonic approximation, has zero frequency (i.e. its associated restoring force vanishes) and divergent zero-point fluctuations. Making an analogy with deformations in three-dimensional space: an axially symmetric quadrupole vibration defines dynamically a privileged orientation which, changing direction with time, is averaged out leaving the system in a state of angular momentum $L = 2$ (surface wave). As the restoring constant C tends to zero, the time in which a privileged direction in space is well defined increases. In the limit in which $C = 0$, one has a deformed system which rotates as a whole, the resulting lowest energy state having zero angular momentum.

Appendix J
RPA solution of the pairing Hamiltonian

In this appendix we shall derive in detail the properties of the collective modes associated with the pairing Hamiltonian

$$H = H_{\rm sp} + H_{\rm p},$$

where

$$H_{\rm sp} = \sum_{\nu} (\epsilon_\nu - \lambda) a^\dagger_\nu a_\nu$$

and

$$H_{\rm p} = -G \sum_{\nu,\nu'} a^\dagger_\nu a^\dagger_{\bar{\nu}}\, a_{\bar{\nu}'} a_{\nu'}.$$

This Hamiltonian becomes, in the quasiparticle basis (Högaasen–Feldman (1961), Bes and Broglia (1966)),

$$N = \sum_i E_i N_i - \frac{1}{4} G \left(\sum_i \sqrt{\Omega_i}\, f_i \left(\Gamma^\dagger_i + \Gamma_i \right) \right)^2 + \frac{1}{4} G \left(\sum_i \sqrt{\Omega_i} \left(\Gamma^\dagger_i - \Gamma_i \right) \right)^2 \quad \text{(J.1)}$$

neglecting terms of the order of 1 and of order $\sqrt{\Omega_i}$, where

$$\Omega_i = \frac{2j_i + 1}{2},$$

as well as terms proportional to the quasiparticle number operator

$$N_i = \sum_m \alpha^\dagger_{im} \alpha_{im}. \quad \text{(J.2)}$$

Consistent with this approximation we shall also neglect the Pauli principle among quasiparticles as expressed in the conmutation relation (see equations (A.72) and (I.50)),

$$\left[\Gamma_i, \Gamma^\dagger_j \right] = \delta(i, j) \left(1 - \frac{N_i}{\Omega_i} \right), \quad \text{(J.3)}$$

https://doi.org/10.1017/9781009401920 Published online by Cambridge University Press

i.e. assume that

$$\left[\Gamma_i, \Gamma_j^\dagger\right] = \delta(i, j). \tag{J.4}$$

This is a good approximation to the extent that the number of quasiparticle excitations is much smaller than Ω_i, the pair degeneracy of the system.

In the above equations the definitions and relations

$$E_i = \sqrt{(\epsilon_i - \lambda)^2 + \Delta^2}, \tag{J.5}$$

$$\Gamma_j^\dagger = \frac{1}{\sqrt{\Omega_j}} \sum_{m>0} (-1)^{j-m} \alpha_{j,m}^\dagger \alpha_{j,-m}^\dagger, \tag{J.6}$$

$$f_i = U_i^2 - V_i^2 \tag{J.7}$$

and

$$\left[N_i, \Gamma_j^\dagger\right] = \delta(i, j) 2\Gamma_j^\dagger \tag{J.8}$$

have been used.

In what follows we shall also use the phonon-creation operator

$$\Gamma_n^\dagger = \sum_i a_{ni} \Gamma_i^\dagger + \sum_i b_{ni} \Gamma_i. \tag{J.9}$$

We can separate the residual interaction into two parts, one with matrix elements which are odd with respect to the Fermi energy,

$$H_{\mathrm{p}}' = -\frac{1}{4} G \left(\sum_i \sqrt{\Omega_i} f_i \left(\Gamma_i^\dagger + \Gamma_i \right) \right)^2,$$

which give rise to pairing vibrations, and one which is even,

$$H_{\mathrm{p}}'' = \frac{1}{4} G \left(\sum_i \sqrt{\Omega_i} \left(\Gamma_i^\dagger - \Gamma_i \right) \right)^2,$$

and which is connected with the Anderson–Goldstone–Nambu mode of the system (see Chapther 4). We are first going to treat both parts separately and then later linearize the whole Hamiltonian.

J.1 Diagonalization of the $H_0 + H_{\mathrm{p}}'$ Hamiltonian (odd solution)

We shall diagonalize the Hamiltonian

$$H = \sum_i E_i N_i - \frac{1}{4} G \left(\sum_i \sqrt{\Omega_i} f_i \left(\Gamma_i^\dagger + \Gamma_i \right) \right)^2 = H_0 + H_{\mathrm{p}}', \tag{J.10}$$

in the harmonic approximation, thus requiring that (see equation (A.68))

$$\left[H, \Gamma_n^\dagger\right] = W_n \Gamma_n^\dagger.$$

https://doi.org/10.1017/9781009401920 Published online by Cambridge University Press

Let us first calculate the commutation with H_0,

$$\begin{aligned}\left[H_0, \Gamma_n^\dagger\right] &= \left[\sum_i E_i N_i \ , \ \left(\sum_j a_{nj}\Gamma_j^\dagger + \sum_j b_{nj}\Gamma_j\right)\right] \\ &= \sum_{i,j} E_i \ a_{nj} \ \delta(i,j)\, 2\Gamma_j^\dagger - \sum_{i,j} E_i \ b_{nj} \ \delta(i,j)\, 2\Gamma_j,\end{aligned}$$

leading to

$$\left[H_0, \Gamma_n^\dagger\right] = 2\sum_i E_i a_{ni}\Gamma_i^\dagger - 2\sum_i E_i b_{ni}\Gamma_i. \tag{J.11}$$

Making use of the Hamiltonian

$$\begin{aligned}H_{\rm p}' &= -\frac{1}{4}G\left(\sum_i \sqrt{\Omega}_i f_i(\Gamma_i^\dagger + \Gamma_i)\right)^2 \\ &= -\frac{1}{4}G\left(\sum_i \sqrt{\Omega}_i f_i(\Gamma_i^\dagger + \Gamma_i)\right)\left(\sum_j \sqrt{\Omega}_j f_j(\Gamma_j^\dagger + \Gamma_j)\right),\end{aligned}$$

we calculate the commutation relation

$$\begin{aligned}\left[H_{\rm p}', \Gamma_n^\dagger\right] &= -\frac{1}{4}G\left[\left(\sum_i \sqrt{\Omega}_i f_i(\Gamma_i^\dagger + \Gamma_i)\right)\right. \\ &\qquad \left.\times \left(\sum_j \sqrt{\Omega}_j f_j(\Gamma_j^\dagger + \Gamma_j)\right), \left(\sum_k a_{nk}\Gamma_k^\dagger + \sum_k b_{nk}\Gamma_k\right)\right] \\ &= -\frac{1}{4}G\left(\sum_i \sqrt{\Omega}_i f_i(\Gamma_i^\dagger + \Gamma_i)\right) \\ &\quad \times\left[\left(\sum_j \sqrt{\Omega}_j f_j(\Gamma_j^\dagger + \Gamma_j)\right), \left(\sum_k a_{nk}\Gamma_k^\dagger + \sum_k b_{nk}\Gamma_k\right)\right] \\ &\quad -\frac{1}{4}G\left[\left(\sum_i \sqrt{\Omega}_i f_i(\Gamma_i^\dagger + \Gamma_i)\right), \left(\sum_k a_{nk}\Gamma_k^\dagger + \sum_k b_{nk}\Gamma_k\right)\right] \\ &\quad \times\left(\sum_j \sqrt{\Omega}_j f_j(\Gamma_j^\dagger + \Gamma_j)\right) \\ &= -\frac{1}{4}G\left(\sum_i \sqrt{\Omega}_i f_i(\Gamma_i^\dagger + \Gamma_i)\right) \\ &\quad \times\sum_j \sqrt{\Omega}_j f_j\left\{\sum_k a_{nk}\left[\Gamma_j, \Gamma_k^\dagger\right] + \sum_k b_{nk}\left[\Gamma_j^\dagger, \Gamma_k\right]\right\} \\ &\quad -\frac{1}{4}G\sum_i \sqrt{\Omega}_i f_i\left\{\sum_k a_{nk}\left[\Gamma_i, \Gamma_k^\dagger\right] + \sum_k b_{nk}\left[\Gamma_i^\dagger, \Gamma_k\right]\right\}\left(\sum_j \sqrt{\Omega}_j f_j(\Gamma_j^\dagger + \Gamma_j)\right)\end{aligned}$$

https://doi.org/10.1017/9781009401920 Published online by Cambridge University Press

$$= -\frac{1}{4}G\left(\sum_i \sqrt{\Omega}_i f_i(\Gamma_i^\dagger + \Gamma_i)\right)\sum_j \sqrt{\Omega}_j f_j(a_{nj} - b_{nj})$$
$$-\frac{1}{4}G\sum_i \sqrt{\Omega}_i f_i(a_{ni} - b_{ni})\left(\sum_j \sqrt{\Omega}_j f_j(\Gamma_j^\dagger + \Gamma_j)\right).$$

Consequently,

$$\left[H'_{\rm p}, \Gamma_n^\dagger\right] = \frac{1}{2}G\sum_j \sqrt{\Omega}_j f_j(b_{nj} - a_{nj})\left(\sum_i \sqrt{\Omega}_i f_i(\Gamma_i^\dagger + \Gamma_i)\right). \tag{J.12}$$

From equations (J.11) and (J.12) we find

$$\begin{aligned}\left[H, \Gamma_n^\dagger\right] &= 2\sum_i E_i a_{ni}\Gamma_i^\dagger - 2\sum_i E_i b_{ni}\Gamma_i + \frac{1}{2}G\sum_j \sqrt{\Omega}_j f_j(b_{nj} - a_{nj}) \\ &\quad\times\left(\sum_i \sqrt{\Omega}_i f_i(\Gamma_i^\dagger + \Gamma_i)\right) \\ &= \sum_i \left\{2E_i a_{ni} + \frac{1}{2}G\left(\sum_j \sqrt{\Omega}_j f_j(b_{nj} - a_{nj})\right) f_i\sqrt{\Omega}_i\right\}\Gamma_i^\dagger \\ &\quad + \sum_i \left\{-2E_i b_{ni} + \frac{1}{2}G\left(\sum_j \sqrt{\Omega}_j f_j(b_{nj} - a_{nj})\right) f_i\sqrt{\Omega}_i\right\}\Gamma_i^\dagger \\ &= W_n\sum_i a_{ni}\Gamma_i^\dagger + W_n\sum_i b_{ni}\Gamma_i.\end{aligned}$$

Thus,

$$2E_i a_{ni} + \frac{G}{2}\left(\sum_j \sqrt{\Omega}_j f_j(b_{nj} - a_{nj})\right) f_i\sqrt{\Omega}_i = W_n a_{ni},$$
$$-2E_i b_{ni} + \frac{G}{2}\left(\sum_j \sqrt{\Omega}_j f_j(b_{nj} - a_{nj})\right) f_i\sqrt{\Omega}_i = W_n b_{ni}.$$

Defining

$$\Lambda_n = \frac{G}{2}\left(\sum_j \sqrt{\Omega}_j f_j(a_{nj} - b_{nj})\right), \tag{J.13}$$

one obtains

$$2E_i a_{ni} - \Lambda_n f_i\sqrt{\Omega}_i = W_n a_{ni},$$
$$-2E_i b_{ni} - \Lambda_n f_i\sqrt{\Omega}_i = W_n b_{ni},$$

which lead to

$$a_{ni} = \frac{\Lambda_n f_i\sqrt{\Omega}_i}{2E_i - W_n}, \qquad b_{ni} = -\frac{\Lambda_n f_i\sqrt{\Omega}_i}{2E_i + W_n}. \tag{J.14}$$

https://doi.org/10.1017/9781009401920 Published online by Cambridge University Press

Substituting equations (J.14) in (J.13) one can write

$$\Lambda_n = \frac{G}{2}\sum_j \sqrt{\Omega}_j f_j \left(\frac{\Lambda_n f_j \sqrt{\Omega}_j}{2E_j - W_n} + \frac{\Lambda_n f_j \sqrt{\Omega}_j}{2E_j + W_n}\right)$$
$$= G\sum_j \Omega_j f_j^2 \left(\frac{2E_j}{4E_j^2 - W_n^2}\right)\Lambda_n = G\sum_j \frac{2E_j\Omega_j f_j^2}{4E_j^2 - W_n^2}\Lambda_n,$$

leading to

$$\frac{1}{G} = \sum_j \frac{2E_j\Omega_j f_j^2}{4E_j^2 - W_n^2}. \tag{J.15}$$

The normalization condition

$$\left[\Gamma_n, \Gamma_n^\dagger\right] = \left[\left(\sum_i a_{ni}\Gamma_i + \sum_i b_{ni}\Gamma_i^\dagger\right), \left(\sum_j a_{mj}\Gamma_j^\dagger + \sum_j b_{mj}\Gamma_j\right)\right]$$

gives the relation

$$\sum_i a_{ni}a_{mi} - \sum_i b_{ni}b_{mi} = \delta(n,m). \tag{J.16}$$

Consequently

$$\sum_i (a_{ni}^2 - b_{ni}^2) = 1.$$

Inserting in this equation the amplitudes defined in equation (J.14) one obtains

$$\Lambda_n^2 \sum_i \left\{\frac{f_i^2\Omega_i}{(2E_i - W_n)^2} - \frac{f_i^2\Omega_i}{(2E_i + W_n)^2}\right\} = 1,$$

$$\Lambda_n^2 \sum_i \frac{4E_i^2 + 4E_iW_n + W_n^2 - 4E_i^2 + 4E_iW_n - W_n^2}{(2E_i - W_n)^2(2E_i + W_n)^2} f_i^2\Omega_i = 1,$$

leading to

$$\Lambda_n^2 \sum_i \frac{f_i^2\Omega_i 8E_iW_n}{(4E_i^2 - W_n^2)^2} = 1.$$

Thus

$$\Lambda_n = \frac{1}{2}\left[\sum_i \frac{f_i^2\Omega_i 2E_iW_n}{(4E_i^2 - W_n^2)^2}\right]^{-1/2}. \tag{J.17}$$

J.2 Diagonalization of the $H_0 + H_{\mathrm{p}}''$ Hamiltonian (even solution)

Let us now consider the Hamiltonian

$$H = H_0 + H_{\mathrm{p}}'' = \sum_i E_i N_i + \frac{1}{4}G\left(\sum_i \sqrt{\Omega}_i(\Gamma_i^\dagger - \Gamma_i)\right)^2,$$

https://doi.org/10.1017/9781009401920 Published online by Cambridge University Press

where

$$H''_{\rm p} = \frac{1}{4}G\left(\sum_i \sqrt{\Omega}_i(\Gamma_i^\dagger - \Gamma_i)\right)^2$$
$$= \frac{1}{4}G\left(\sum_i \sqrt{\Omega}_i(\Gamma_i^\dagger - \Gamma_i)\right)\left(\sum_j \sqrt{\Omega}_j(\Gamma_j^\dagger - \Gamma_j)\right).$$

We start by calculating the commutation relation

$$\left[H''_{\rm p}, \Gamma_n^\dagger\right] = \frac{1}{4}G\left[\left(\sum_i \sqrt{\Omega}_i(\Gamma_i^\dagger - \Gamma_i)\right)\left(\sum_j \sqrt{\Omega}_j(\Gamma_j^\dagger - \Gamma_j)\right), \Gamma_n^\dagger\right]$$
$$= \frac{1}{4}G\left(\sum_i \sqrt{\Omega}_i(\Gamma_i^\dagger - \Gamma_i)\right)\left[\left(\sum_j \sqrt{\Omega}_j(\Gamma_j^\dagger - \Gamma_j)\right), \Gamma_n^\dagger\right]$$
$$+ \frac{1}{4}G\left[\left(\sum_i \sqrt{\Omega}_i(\Gamma_i^\dagger - \Gamma_i)\right), \Gamma_n^\dagger\right]\left(\sum_j \sqrt{\Omega}_j(\Gamma_j^\dagger - \Gamma_j)\right)$$
$$= \frac{1}{4}G\left(\sum_i \sqrt{\Omega}_i(\Gamma_i^\dagger - \Gamma_i)\right)$$
$$\times\left[\left(\sum_j \sqrt{\Omega}_j(\Gamma_j^\dagger - \Gamma_j)\right), \left(\sum_k a_{nk}\Gamma_k^\dagger + \sum_k b_{nk}\Gamma_k\right)\right]$$
$$+ \frac{1}{4}G\left[\left(\sum_i \sqrt{\Omega}_i(\Gamma_i^\dagger - \Gamma_i)\right), \left(\sum_k a_{nk}\Gamma_k^\dagger + \sum_k b_{nk}\Gamma_k\right)\right]$$
$$\times\left(\sum_j \sqrt{\Omega}_j(\Gamma_j^\dagger - \Gamma_j)\right)$$
$$= \frac{1}{4}G\left(\sum_i \sqrt{\Omega}_i(\Gamma_i^\dagger - \Gamma_i)\right)$$
$$\times\sum_j \sqrt{\Omega}_j\left\{-\sum_k b_{n,k}\delta(j,k) - \sum_k a_{n,k}\delta(j,k)\right\}$$
$$+ \frac{1}{4}G\sum_i \sqrt{\Omega}_i\left\{-\sum_k \delta(i,k)b_{n,k} - \sum_k a_{n,k}\delta(i,k)\right\}$$
$$\times\left(\sum_j \sqrt{\Omega}_j(\Gamma_j^\dagger - \Gamma_j)\right)$$
$$= -\frac{G}{2}\left(\sum_i \sqrt{\Omega}_i(a_{n,i} + b_{n,i})\right)\left(\sum_j \sqrt{\Omega}_j(\Gamma_j^\dagger - \Gamma_j)\right).$$

https://doi.org/10.1017/9781009401920 Published online by Cambridge University Press

That is

$$\left[H''_{\mathrm{p}}, \Gamma_n^\dagger\right] = -\frac{G}{2}\left(\sum_i \sqrt{\Omega}_i(a_{n,i} + b_{n,i})\right)\left(\sum_j \sqrt{\Omega}_j(\Gamma_j^\dagger - \Gamma_j)\right). \tag{J.18}$$

Making use of this relation and equation (J.11), one can write

$$\begin{aligned}
\left[H, \Gamma_n^\dagger\right] &= 2\sum_i E_i a_{n,i}\Gamma_i^\dagger - 2\sum_i E_i b_{n,i}\Gamma_i \\
&\quad - \frac{1}{2}G\sum_j \sqrt{\Omega}_j(a_{n,j} + b_{n,j})\sum_i \sqrt{\Omega}_i\Gamma_i^\dagger \\
&\quad + \frac{1}{2}G\sum_j \sqrt{\Omega}_j(a_{n,j} + b_{n,j})\sum_i \sqrt{\Omega}_i\Gamma_i \\
&= \sum_i \left\{2E_i a_{n,i} - \frac{1}{2}G\sum_j \sqrt{\Omega}_j(a_{n,j} + b_{n,j})\right\}\sqrt{\Omega}_i\Gamma_i^\dagger \\
&\quad + \sum_i \left\{-2E_i b_{n,i} + \frac{1}{2}G\sum_j \sqrt{\Omega}_j(a_{n,j} + b_{n,j})\right\}\sqrt{\Omega}_i\Gamma_i \\
&= W_n\sum_i a_{n,i}\Gamma_i^\dagger + W_n\sum_i b_{n,i}\Gamma_i.
\end{aligned}$$

This relation implies that

$$\begin{aligned}
2E_i a_{n,i} - \left(\frac{1}{2}G\sum_j \sqrt{\Omega}_j(a_{n,j} + b_{n,j})\right)\sqrt{\Omega}_i &= W_n a_{n,i}, \\
-2E_i b_{n,i} + \left(\frac{1}{2}G\sum_j \sqrt{\Omega}_j(a_{n,j} + b_{n,j})\right)\sqrt{\Omega}_i &= W_n b_{n,i}.
\end{aligned}$$

Defining the quantity

$$\Lambda_n = \frac{1}{2}G\sum_j \sqrt{\Omega}_j(a_{n,j} + b_{n,j}), \tag{J.19}$$

the above equations can be written as

$$\begin{aligned}
2E_i a_{n,i} - \Lambda_n\sqrt{\Omega}_i &= W_n a_{n,i}, \\
-2E_i b_{n,i} + \Lambda_n\sqrt{\Omega}_i &= W_n b_{n,i},
\end{aligned}$$

leading to

$$\begin{aligned}
(2E_i - W_N)a_{n,i} &= \Lambda_n\sqrt{\Omega}_i, \\
(2E_i + W_N)b_{n,i} &= \Lambda_n\sqrt{\Omega}_i.
\end{aligned}$$

https://doi.org/10.1017/9781009401920 Published online by Cambridge University Press

The colletive phonon forwards-going and backwards-going amplitudes (see Fig. 8.11) are thus

$$a_{ni} = \frac{\Lambda_n \sqrt{\Omega_i}}{2E_i - W_n}, \qquad b_{ni} = \frac{\Lambda_n \sqrt{\Omega_i}}{2E_i + W_n}. \tag{J.20}$$

Replacing these amplitudes in equation (J.19) leads to the relation

$$\Lambda_n = \frac{1}{2} G \sum_i \sqrt{\Omega_i} \left\{ \frac{\Lambda_n \sqrt{\Omega_i}}{2E_i - W_n} + \frac{\Lambda_n \sqrt{\Omega_i}}{2E_i + W_n} \right\},$$
$$\Lambda_n = \frac{1}{2} G \Lambda_n \sum_i \frac{2E_i + W_n + 2E_i - W_n}{4E_i^2 - W_n^2} \Omega_i,$$

and thus to the dispersion relation

$$\frac{1}{G} = \sum_i \frac{2E_i \Omega_i}{4E_i^2 - W_n^2}. \tag{J.21}$$

It can be seen that this equation has, as the lowest root, $W_1 = 0$. In fact, in this case the above expression leads to

$$\frac{2}{G} = \sum_i \frac{\Omega_i}{E_i},$$

which is the BCS gap equation.

From the normalization condition,

$$1 = \sum_i (a_{n,i}^2 - b_{n,i}^2) = \Lambda_n^2 \sum_i \left\{ \frac{\Omega_i}{(2E_i - W_n)^2} - \frac{\Omega_i}{(2E_i + W_n)^2} \right\}$$
$$= \Lambda_n^2 \sum_i \frac{4E_i^2 + 4E_i W_n + W_n^2 - 4E_i^2 + 4E_i W_n - W_n^2}{(4E_i^2 - W_n^2)^2} \Omega_i$$
$$= \Lambda_n^2 \sum_i \frac{8E_i W_n \Omega_i}{(4E_i^2 - W_n^2)^2},$$

one obtains

$$\Lambda_n = \frac{1}{2} \left[\sum_i \frac{2E_i W_n \Omega_i}{(4E_i^2 - W_n^2)^2} \right]^{-1/2}. \tag{J.22}$$

https://doi.org/10.1017/9781009401920 Published online by Cambridge University Press

J.3 Diagonalization of the full Hamiltonian $H = H_0 + H'_{\rm p} + H''_{\rm p}$

We consider now the complete Hamiltonian

$$H = H_0 + H'_{\rm p} + H''_{\rm p} = \sum_i E_i N_i - \frac{1}{4} G \left(\sum_i \sqrt{\Omega}_i f_i (\Gamma_i^\dagger + \Gamma_i) \right)^2 + \frac{1}{4} G \left(\sum_i \sqrt{\Omega}_i (\Gamma_i^\dagger - \Gamma_i) \right)^2 ,$$

and linearize it, i.e. impose

$$[H, \Gamma_n^\dagger] = [H_0, \Gamma_n^\dagger] + [H'_{\rm p}, \Gamma_n^\dagger] + [H''_{\rm p}, \Gamma_n^\dagger] = W_n \sum_i a_{ni} \Gamma_i^\dagger + W_n \sum_i b_{ni} \Gamma_i .$$

From equations (J.11), (J.12) and (J.18) we get,

$$\begin{aligned} &\sum_i 2E_i a_{ni} \Gamma_i^\dagger - \sum_i 2E_i b_{ni} \Gamma_i \\ &\quad + \frac{G}{2} \sum_j \sqrt{\Omega}_j f_j (b_{nj} - a_{nj}) \left(\sum_i \sqrt{\Omega}_i f_i (\Gamma_i^\dagger + \Gamma_i) \right) \\ &\quad - \frac{G}{2} \sum_j \sqrt{\Omega}_i (a_{nj} + b_{nj}) \left(\sum_i \sqrt{\Omega}_i (\Gamma_i^\dagger - \Gamma_i) \right) \\ &\quad = W_n \sum_i a_{ni} \Gamma_i^\dagger + W_n \sum_i b_{ni} \Gamma_i . \end{aligned}$$

That is,

$$\begin{aligned} &\sum_i \left\{ 2E_i a_{ni} + \frac{1}{2} G \left(\sum_j \sqrt{\Omega}_j f_j (b_{nj} - a_{nj}) \right) \sqrt{\Omega}_i f_i \right. \\ &\left. - \frac{1}{2} G \left(\sum_j \sqrt{\Omega}_j (a_{nj} + b_{nj}) \right) \sqrt{\Omega}_i \right\} \Gamma_i^\dagger \\ &+ \sum_i \left\{ -2E_i a_{ni} + \frac{1}{2} G \left(\sum_j \sqrt{\Omega}_j f_j (b_{nj} - a_{nj}) \right) \sqrt{\Omega}_i f_i \right. \\ &\left. + \frac{1}{2} G \left(\sum_j \sqrt{\Omega}_j (a_{nj} + b_{nj}) \right) \sqrt{\Omega}_i \right\} \Gamma_i \\ &= W_n \sum_i a_{ni} \Gamma_i^\dagger + W_n \sum_i b_{ni} \Gamma_i . \end{aligned}$$

https://doi.org/10.1017/9781009401920 Published online by Cambridge University Press

This relation leads to

$$2E_i a_{ni} + \frac{1}{2}G\left(\sum_j \sqrt{\Omega}_j f_j (b_{nj} - a_{nj})\right)\sqrt{\Omega}_i f_i$$
$$-\frac{1}{2}G\left(\sum_j \sqrt{\Omega}_j (a_{nj} + b_{nj})\right)\sqrt{\Omega}_i = W_n a_{ni}$$

and

$$-2E_i b_{ni} + \frac{1}{2}G\left(\sum_j \sqrt{\Omega}_j f_j (b_{nj} - a_{nj})\right)\sqrt{\Omega}_i f_i$$
$$+\frac{1}{2}G\left(\sum_j \sqrt{\Omega}_j (a_{nj} + b_{nj})\right)\sqrt{\Omega}_i = W_n b_{ni}.$$

Defining the quantities

$$\Lambda_{1n} = -\frac{1}{2}G\left(\sum_j \sqrt{\Omega}_j f_j (b_{nj} - a_{nj})\right),$$

and (J.23)

$$\Lambda_{2n} = \frac{1}{2}G\left(\sum_j \sqrt{\Omega}_j (a_{nj} + b_{nj})\right),$$

one can rewrite the above equations as

$$2E_i a_{ni} - \Lambda_{1n}\sqrt{\Omega}_i f_i - \Lambda_{2n}\sqrt{\Omega}_i = W_n a_{ni},$$
$$-2E_i b_{ni} - \Lambda_{1n}\sqrt{\Omega}_i f_i + \Lambda_{2n}\sqrt{\Omega}_i = W_n b_{ni},$$

leading to

$$(2E_i - W_n)a_{ni} = \Lambda_{1n}\sqrt{\Omega}_i f_i + \Lambda_{2n}\sqrt{\Omega}_i,$$
$$(2E_i + W_n)b_{ni} = -\Lambda_{1n}\sqrt{\Omega}_i f_i + \Lambda_{2n}\sqrt{\Omega}_i,$$

from which the RPA amplitudes

$$a_{ni} = \frac{\Lambda_{1n} f_i + \Lambda_{2n}}{(2E_i - W_n)}\sqrt{\Omega}_i,$$
$$b_{ni} = \frac{-\Lambda_{1n} f_i + \Lambda_{2n}}{(2E_i + W_n)}\sqrt{\Omega}_i, \quad \text{(J.24)}$$

are determined.

https://doi.org/10.1017/9781009401920 Published online by Cambridge University Press

Replacing the amplitudes in equations (J.23) one gets

$$\begin{aligned}
\Lambda_{1n} &= -\tfrac{1}{2}G\sum_i \sqrt{\Omega_i}\, f_i \sqrt{\Omega_i}\left\{\frac{-\Lambda_{1n}f_i+\Lambda_{2n}}{2E_i+W_n} - \frac{\Lambda_{1n}f_i+\Lambda_{2n}}{2E_i-W_n}\right\} \\
&= -\tfrac{1}{2}G\sum_i \Omega_i f_i \left\{\frac{(-\Lambda_{1n}f_i+\Lambda_{2n})(2E_i-W_n)-(\Lambda_{1n}f_i+\Lambda_{2n})(2E_i+W_n)}{(4E_i^2-W_n^2)}\right\} \\
&= -\tfrac{1}{2}G\sum_i \Omega_i f_i \\
&\quad\times\left\{\frac{-\Lambda_{1n}f_i 2E_i+\Lambda_{1n}f_i W_n+\Lambda_{2n}2E_i-\Lambda_{2n}W_n-\Lambda_{1n}f_i 2E_i-\Lambda_{1n}f_i W_n-\Lambda_{2n}2E_i-\Lambda_{2n}W_n}{(4E_i^2-W_n^2)}\right\} \\
&= -\tfrac{1}{2}G\sum_i \frac{\Omega_i f_i}{(4E_i^2-W_n^2)}\{-4\Lambda_{1n}f_i E_i - 2\Lambda_{2n}W_n\} \\
&= G\sum_i \frac{\Omega_i f_i}{(4E_i^2-W_n^2)}\{2E_i f_i\Lambda_{1n} + W_n\Lambda_{2n}\} \\
&= \left(G\sum_i \frac{\Omega_i f_i^2 2E_i}{(4E_i^2-W_n^2)}\right)\Lambda_{1n} + \left(G\sum_i \frac{\Omega_i f_i W_n}{(4E_i^2-W_n^2)}\right)\Lambda_{2n},
\end{aligned}$$

$$\left(\sum_i \frac{\Omega_i f_i^2 2E_i}{(4E_i^2-W_n^2)} - \frac{1}{G}\right)\Lambda_{1n} + \left(W_n\sum_i \frac{\Omega_i f_i}{(4E_i^2-W_n^2)}\right)\Lambda_{2n} = 0 \tag{J.25}$$

and

$$\begin{aligned}
\Lambda_{2n} &= \tfrac{1}{2}G\sum_i \sqrt{\Omega_i}\sqrt{\Omega_i}\left\{\frac{\Lambda_{1n}f_i+\Lambda_{2n}}{2E_i-W_n} + \frac{-\Lambda_{1n}f_i+\Lambda_{2n}}{2E_i+W_n}\right\} \\
&= \tfrac{1}{2}G\sum_i \Omega_i \\
&\quad\times\left\{\frac{\Lambda_{1n}f_i(2E_i+W_n)+\Lambda_{2n}(2E_i+W_n)-\Lambda_{1n}f_i(2E_i-W_n)+\Lambda_{2n}(2E_i-W_n)}{(4E_i^2-W_n^2)}\right\} \\
&= \tfrac{1}{2}G\sum_i \frac{\Omega_i}{(4E_i^2-W_n^2)}\{\Lambda_{1n}f_i 2W_n + 4E_i\Lambda_{2n}\} \\
&= \left(G\sum_i \frac{\Omega_i f_i W_n}{(4E_i^2-W_n^2)}\right)\Lambda_{1n} + \left(G\sum_i \frac{\Omega_i 2E_i}{(4E_i^2-W_n^2)}\right)\Lambda_{2n}
\end{aligned}$$

$$\left(W_n\sum_i \frac{\Omega_i f_i}{(4E_i^2-W_n^2)}\right)\Lambda_{1n} + \left(\sum_i \frac{\Omega_i 2E_i}{(4E_i^2-W_n^2)} - \frac{1}{G}\right)\Lambda_{2n} = 0. \tag{J.26}$$

In order that the system of equations (J.25), (J.26) has a solution we set the determinant of the coefficients to be zero, i.e.

$$\begin{vmatrix}
\left(\sum_i \frac{\Omega_i f_i^2 2E_i}{(4E_i^2-W_n^2)} - \frac{1}{G}\right) & W_n\left(\sum_i \frac{\Omega_i f_i}{(4E_i^2-W_n^2)}\right) \\
W_n\left(\sum_i \frac{\Omega_i f_i}{(4E_i^2-W_n^2)}\right) & \left(\sum_i \frac{\Omega_i 2E_i}{(4E_i^2-W_n^2)} - \frac{1}{G}\right)
\end{vmatrix} = 0. \tag{J.27}$$

https://doi.org/10.1017/9781009401920 Published online by Cambridge University Press

Taking into account that we have previously solved the BCS equations, (in particular $\frac{2}{G} = \sum_i \frac{\Omega_i}{E_i}$), the element $\left(\sum_i \frac{\Omega_i 2E_i}{(4E_i^2 - W_n^2)} - \frac{1}{G}\right)$ of the determinant can be written as

$$\left(\sum_i \frac{\Omega_i 2E_i}{(4E_i^2 - W_n^2)} - \frac{1}{G}\right) = \sum_i \frac{\Omega_i 2E_i}{(4E_i^2 - W_n^2)} - \sum_i \frac{\Omega_i}{2E_i}$$

$$= \sum_i \frac{\Omega_i(4E_i^2 - 4E_i^2 + W_n^2)}{2E_i(4E_i^2 - W_n^2)} = W_n^2 \sum_i \frac{\Omega_i}{2E_i(4E_i^2 - W_n^2)},$$

i.e.

$$\left(\sum_i \frac{\Omega_i 2E_i}{(4E_i^2 - W_n^2)} - \frac{1}{G}\right) = W_n^2 \sum_i \frac{\Omega_i}{2E_i(4E_i^2 - W_n^2)}. \tag{J.28}$$

In the same way

$$\left(\sum_i \frac{\Omega_i 2E_i f_i^2}{(4E_i^2 - W_n^2)} - \frac{1}{G}\right) = \sum_i \frac{\Omega_i f_i^2 2E_i}{(4E_i^2 - W_n^2)} - \sum_i \frac{\Omega_i}{2E_i}$$

$$= \sum_i \frac{\Omega_i(f_i^2 4E_i^2 - 4E_i^2 + W_n^2)}{2E_i(4E_i^2 - W_n^2)} = \sum_i \frac{4E_i^2(f_i^2 - 1) + W_n^2}{2E_i(4E_i^2 - W_n^2)} \Omega_i.$$

We shall now rewrite the expression

$$4E_i^2(f_i^2 - 1) = 4E_i^2((U_i^2 - V_i^2)^2 - 1) = 4E_i^2(U_i^4 + V_i^4 - 2U_i^2 V_i^2 - 1),$$

making use of the BCS relations

$$(U_i^2 + V_i^2)^2 = 1, \quad U_i^4 + V_i^4 + 2U_i^2 V_i^2 = 1,$$

$$U_i^4 + V_i^4 - 2U_i^2 V_i^2 = 1 - 4U_i^2 V_i^2,$$
$$U_i^4 + V_i^4 - 2U_i^2 V_i^2 - 1 = -4U_i^2 V_i^2 = (f_i^2 - 1).$$

Because

$$2U_i V_i = \frac{\Delta}{E_\nu}$$

one can write

$$(f_i^2 - 1) = -\frac{\Delta^2}{E_\nu^2},$$

and thus

$$4E_i^2(f_i^2 - 1) = -4\Delta^2.$$

Consequently,

$$\left(\sum_i \frac{\Omega_i 2E_i f_i^2}{(4E_i^2 - W_n^2)} - \frac{1}{G}\right) = (W_n^2 - 4\Delta^2) \sum_i \frac{\Omega_i}{2E_i(4E_i^2 - W_n^2)}. \tag{J.29}$$

https://doi.org/10.1017/9781009401920 Published online by Cambridge University Press

Making use of equations (J.28) and (J.29) the determinant (J.27) can be written as

$$\begin{vmatrix} (W_n^2 - 4\Delta^2)\sum_i \frac{\Omega_i}{2E_i(4E_i^2 - W_n^2)} & W_n\left(\sum_i \frac{\Omega_i f_i}{(4E_i^2 - W_n^2)}\right) \\ W_n\left(\sum_i \frac{\Omega_i f_i}{(4E_i^2 - W_n^2)}\right) & W_n^2 \sum_i \frac{\Omega_i}{2E_i(4E_i^2 - W_n^2)} \end{vmatrix} = 0, \tag{J.30}$$

$$W_n^2\left[(W_n^2 - 4\Delta^2)\left(\sum_i \frac{\Omega_i}{2E_i(4E_i^2 - W_n^2)}\right)^2 - \left(\sum_i \frac{\Omega_i f_i}{(4E_i^2 - W_n^2)}\right)^2\right] = 0. \tag{J.31}$$

Introducing

$$\mathcal{Y}_n^2 = W_n^2 - 4\Delta^2,$$

one can write

$$4E_i^2 - W_n^2 = 4(\epsilon_i - \lambda)^2 + 4\Delta^2 - W_n^2 = 4(\epsilon_i - \lambda)^2 - \mathcal{Y}_n^2.$$

Consequently, equation (J.31) becomes

$$\mathcal{Y}_n^2\left(\sum_i \frac{\Omega_i}{2E_i(4(\epsilon_i - \lambda)^2 - \mathcal{Y}_n^2)}\right)^2 = \left(\sum_i \frac{\Omega_i f_i}{4(\epsilon_i - \lambda)^2 - \mathcal{Y}_n^2}\right)^2,$$

which, making use of the relation

$$f_i = U_i^2 - V_i^2 = \frac{\epsilon_i - \lambda}{E_i},$$

leads to

$$\mathcal{Y}_n \sum_i \frac{\Omega_i}{2E_i(4(\epsilon_i - \lambda)^2 - \mathcal{Y}_n^2)} = \sum_i \frac{\Omega_i(\epsilon_i - \lambda)}{(4(\epsilon_i - \lambda)^2 - \mathcal{Y}_n^2)E_i},$$

and finally to

$$\sum_i \frac{(\mathcal{Y}_n - 2(\epsilon_i - \lambda))\Omega_i}{2E_i\{(2(\epsilon_i - \lambda) + \mathcal{Y}_n)(2(\epsilon_i - \lambda) - \mathcal{Y}_n)\}} = 0.$$

Consequently,

$$\sum_i \frac{\Omega_i}{E_i(\mathcal{Y}_n + 2(\epsilon_i - \lambda))} = 0. \tag{J.32}$$

From equation (J.26)

$$\frac{\Lambda_{2n}}{\Lambda_{1n}} = -\frac{W_n \sum_i \frac{\Omega_i f_i}{(4E_i^2 - W_n^2)}}{\sum_i \frac{\Omega_i 2E_i}{(4E_i^2 - W_n^2)} - \frac{1}{G}}$$

https://doi.org/10.1017/9781009401920 Published online by Cambridge University Press

and equation (J.28)

$$\frac{\Lambda_{2n}}{\Lambda_{1n}} = -\frac{W_n \sum_i \frac{\Omega_i f_i}{(4E_i^2 - W_n^2)}}{W_n^2 \sum_i \frac{\Omega_i}{2E_i(4E_i^2 - W_n^2)}},$$

one obtains

$$\frac{\Lambda_{2n}}{\Lambda_{1n}} = -\frac{\sum_i \frac{\Omega_i f_i}{(4E_i^2 - W_n^2)}}{W_n \sum_i \frac{\Omega_i}{2E_i(4E_i^2 - W_n^2)}}. \tag{J.33}$$

Making use of the normalization condition,

$$\begin{aligned}
1 &= \sum_i (a_{ni}^2 - b_{ni}^2) \\
&= \sum_i \left\{ \left(\frac{\Lambda_{1n} f_i + \Lambda_{2n}}{2E_i - W_n} \sqrt{\Omega_i} \right)^2 - \left(\frac{-\Lambda_{1n} f_i + \Lambda_{2n}}{2E_i + W_n} \sqrt{\Omega_i} \right)^2 \right\} \\
&= \sum_i \Omega_i \left\{ \frac{\Lambda_{1n}^2 f_i^2 + 2\Lambda_{1n}\Lambda_{2n} f_i + \Lambda_{2n}^2}{(2E_i - W_n)^2} - \frac{\Lambda_{1n}^2 f_i^2 - 2\Lambda_{1n}\Lambda_{2n} f_i + \Lambda_{2n}^2}{(2E_i + W_n)^2} \right\} \\
&= \sum_i \frac{f_i^2 W_n 8E_i \Lambda_{1n}^2 + 4f_i(4E_i^2 + W_n^2)\Lambda_{1n}\Lambda_{2n} + 8E_i W_n \Lambda_{2n}^2}{(4E_i^2 - W_n^2)^2} \Omega_i,
\end{aligned}$$

which leads to

$$\begin{aligned}
\frac{1}{\Lambda_{1n}^2} = 4 \Bigg[&\left(\sum_i \frac{f_i^2 2E_i W_n \Omega_i}{(4E_i^2 - W_n^2)^2} \right) + \left(\sum_i \frac{f_i(4E_i^2 + W_n^2)\Omega_i}{(4E_i^2 - W_n^2)^2} \right) \left(\frac{\Lambda_{2n}}{\Lambda_{1n}} \right) \\
&+ \left(\sum_i \frac{2E_i W_n \Omega_i}{(4E_i^2 - W_n^2)^2} \right) \left(\frac{\Lambda_{2n}}{\Lambda_{1n}} \right)^2 \Bigg].
\end{aligned}$$

That is,

$$\begin{aligned}
\Lambda_{1n} = \frac{1}{2} \Bigg[&W_n \left(\sum_i \frac{f_i^2 2E_i \Omega_i}{(4E_i^2 - W_n^2)^2} \right) + \left(\sum_i \frac{f_i(4E_i^2 + W_n^2)\Omega_i}{(4E_i^2 - W_n^2)^2} \right) \left(\frac{\Lambda_{2n}}{\Lambda_{1n}} \right) \\
&+ W_n \left(\sum_i \frac{2E_i \Omega_i}{(4E_i^2 - W_n^2)^2} \right) \left(\frac{\Lambda_{2n}}{\Lambda_{1n}} \right)^2 \Bigg]^{-1/2}.
\end{aligned} \tag{J.34}$$

https://doi.org/10.1017/9781009401920 Published online by Cambridge University Press

Appendix K
Vortices in nuclei

In this appendix we follow the argument presented in Bertsch *et al*. (1988).

K.1 Simple estimates

Nuclei in their ground state can be viewed, in general, as a condensate of pairs of nucleons coupled to angular momentum zero. Evidence for the existence of multipole (non-zero J) pairing has also been found in a variety of nuclear properties (see Section 5.3). Empirically, d-state pairing correlation of a single pair is about half that of a monopole pair. The reduction is due to the decrease in phase space for valence pairs with higher J. This is shown schematically in Fig. K.1.

This situation may be rather different for rapidly rotating nuclei. In this case, large values of the angular momentum can be built by using a coupling scheme where both valence and core particles couple pairwise to angular momentum J. The lowest multipolarity different from zero to which pairs of particles can couple is $J = 1$. Under these circumstances, Galilean invariance allows one to redefine the phase space where dipole pairing acts, so that the resulting phase space is nearly the same as for $J = 0$ pairing. To be able to carry out analytically the different estimates we shall approximate the nucleus by a cylinder of the same radius as that of the nucleus, and a height such that the volume is conserved (see Fig. K.2). That is,

$$v = \frac{4\pi}{3} R^3 = \pi R^2 H, \tag{K.1}$$

leading to

$$H = \tfrac{4}{3} R. \tag{K.2}$$

In this way we also conserve density,

$$\rho_0 = \frac{mA}{v} = \frac{M}{v}, \tag{K.3}$$

where m is the nucleon mass and M the total mass of the system.

https://doi.org/10.1017/9781009401920 Published online by Cambridge University Press

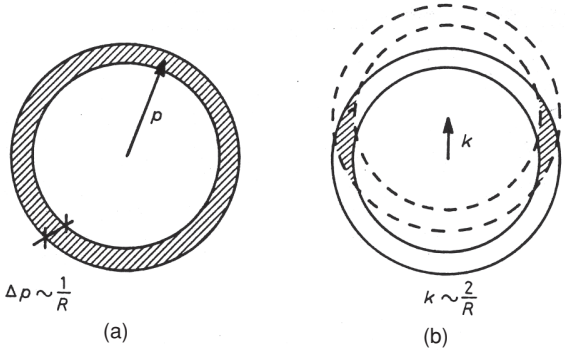

Figure K.1. Phase space for particles in paired wavefunctions. The available momenta for valence particles in a Fermi system are shown in (a). All momenta are allowed for a particle in a pair with total momentum zero. When the pair momentum is non-zero, the valence phase space is reduced as indicated in (b) (after Bertsch *et al*. (1988)). Copyright © Società italiana di Fisica.

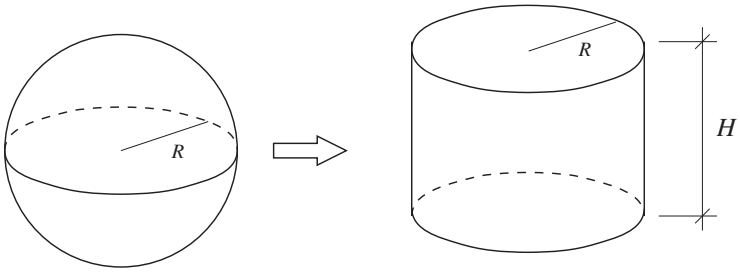

Figure K.2. Approximation used to describe vortex motion. The height H is defined such that $\pi R^2 H = (4/3)\pi R^3$.

Because of $J \neq 0$ superfluidity, a vortex forms with a cylindrical hole along the axis of rotation. The velocity field of the fluid in the vortex can be written as

$$V_0 = \frac{g}{r}, \tag{K.4}$$

where

$$g = \frac{\hbar}{2m}, \tag{K.5}$$

for $J = 1$ vorticity (i.e. each Cooper pair carries angular momentum $J = 1$). In this case the total angular momentum of the system is

$$I \approx \frac{A}{2}. \tag{K.6}$$

The energy of the vortex consists of a rotational part and a part associated with the surface created to generate the hole compatible with the velocity field given in equation

https://doi.org/10.1017/9781009401920 Published online by Cambridge University Press

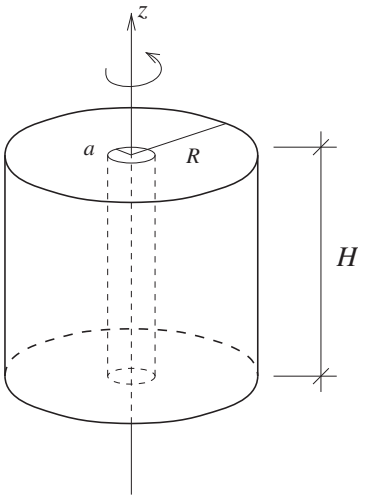

Figure K.3. Atomic nucleus with a vortex, i.e. in a condensed phase of pairs $a^+_{j,m}a^+_{j,-m+1}$, and $I_z = A/2$.

(K.4). The rotational energy is estimated as

$$E_{\text{vortex}} = \int \mathrm{d}\tau \frac{\rho_0 V_0^2}{2} = \frac{\rho_0}{2}\int_0^{2\pi}\mathrm{d}\phi\int_0^H \mathrm{d}z\int_a^R V_0^2 r\mathrm{d}r$$
$$= \frac{\rho_0}{2}2\pi H g^2\int_a^R \mathrm{d}\ln r = \frac{1}{R^2M}L^2\ln\frac{R}{a}\,, \tag{K.7}$$

where

$$L = \int \mathrm{d}\tau\rho_0 r V_0 = \rho_0\int_0^{2\pi}\mathrm{d}\phi\int_0^H \mathrm{d}z\int_a^R V_0 r^2\mathrm{d}r$$
$$\approx \rho_0 2\pi H g\int_a^R r\mathrm{d}r \approx \rho_0\pi H g R^2 \tag{K.8}$$

is the angular momentum of the system.

Note that the above relation implies (see Fig. K.3) that

$$L = \frac{M}{\nu}\pi R^2 H\frac{\hbar}{2m} = \hbar\frac{A}{2}, \tag{K.9}$$

as assumed. The extra energy needed to create the hole of radius a is

$$E_{\text{surf}} = 2\pi a H\sigma, \tag{K.10}$$

where σ is the surface tension (cf. equation (7.32)).

To determine a we minimize the total energy

$$\frac{\partial}{\partial a}(E_{\text{vortex}} + E_{\text{surf}}) = -\frac{1}{R^2M}L^2\frac{1}{a} + 2\pi H\sigma = 0, \tag{K.11}$$

https://doi.org/10.1017/9781009401920 Published online by Cambridge University Press

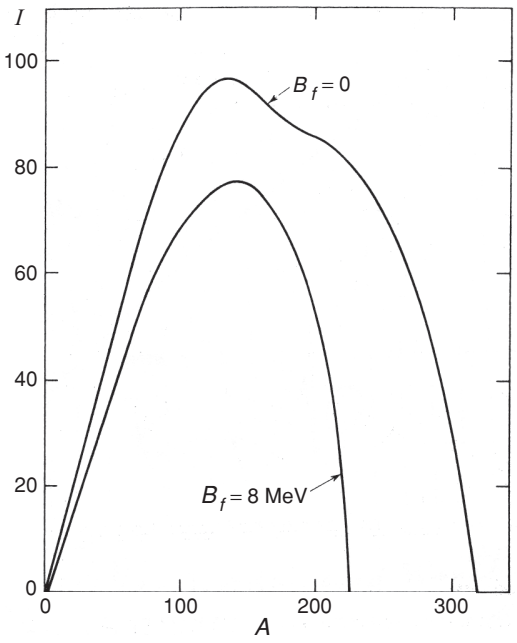

Figure K.4. Stability against fission for a rotating nucleus. The critical angular momentum I for which the nucleus becomes unstable against fission has been calculated in the liquid-drop model as a function of the mass number of the nucleus, and the corresponding curve is labelled $B_f = 0$. The curve labelled $B_f = 8$ MeV shows the angular momentum for which the fission barrier is found at an energy of 8 MeV above the ground state corresponding to the average neutron separation energy. The figure is based on Cohen *et al.* (1974) (see also Bohr and Mottelson (1974)). Reprinted from *Annals of Physics*, Vol. 82, Cohen *et al.*, 'Equilibrium configurations of rotating charged or gravitating liquid masses, II', page 557, Copyright 1974, with permission from Elsevier.

thus obtaining

$$a = \frac{1}{2\pi H\sigma}\frac{L^2}{R^2 M} = \frac{1}{8\sigma}\frac{A}{v}\frac{\hbar^2}{m}. \tag{K.12}$$

This now poses the following questions.

1. Does the nucleus allows spins as high as $I \sim A/2$?
2. How does the energy cost in forming a vortex compare with the energy gain of pairing?

Making use of the liquid-drop model with a surface tension $\sigma(= 1\,\text{MeV fm}^{-1})$, one obtains the curves given in Fig. K.4. Thus, a nucleus of $A \approx 150$ can, in principle, sustain about 80 units of angular momentum, i.e. of the order of $A/2 \approx 75$ as required to make a vortex.

https://doi.org/10.1017/9781009401920 Published online by Cambridge University Press

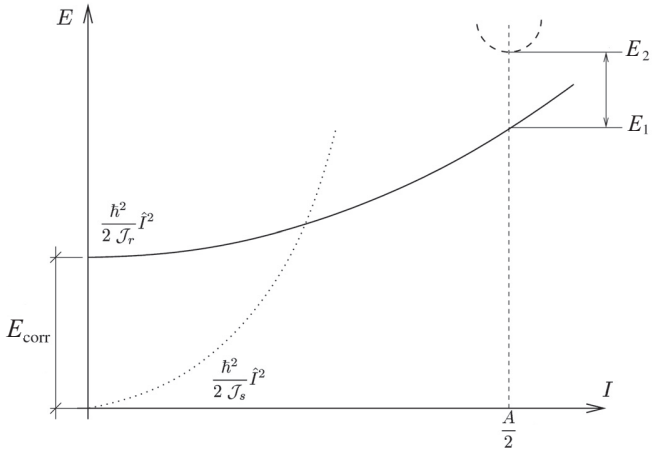

Figure K.5. Schematic representation of rotational bands with superfluid moment of inertia ($\mathcal{J}_s$, dotted curve) and rigid moment of inertia ($\mathcal{J}_r$, continuous curve) as well as roton minimum (dashed curve). Also shown is the summed pairing correlation energy (protons plus neutrons) $\approx \Delta^2/d$ (see Section 3.5).

The answer to question 2 is schematically given in Fig. K.5, where

$$E_1 = E_{\text{rigid}}(L = 75) + |E_{\text{corr}}|, \tag{K.13}$$

and

$$E_2 = E_{\text{vortex}} + E_{\text{surf}}. \tag{K.14}$$

The quantity E_{corr} is the pairing correlation energy. In other words, question 2 is equivalent to asking whether E_1 is smaller or larger than E_2.

The pairing correlation energy is given by (see equation (3.60))

$$E_{\text{corr}} = -\frac{\Delta_n^2 + \Delta_p^2}{2d}, \tag{K.15}$$

with

$$\Delta_n \approx \Delta_p \approx \frac{12}{\sqrt{A}}\,\text{MeV} \tag{K.16}$$

and

$$d \approx 0.4\,\text{MeV}. \tag{K.17}$$

Thus

$$E_{\text{corr}} \approx -\frac{\Delta^2}{d} \approx -\frac{360}{A}\,\text{MeV}\,. \tag{K.18}$$

https://doi.org/10.1017/9781009401920 Published online by Cambridge University Press

Making use of the fact that

$$E_{\text{rigid}} = \frac{L^2}{MR^2}, \tag{K.19}$$

one obtains for the energy of the vortex measured with respect to $E_{\text{rigid}} + E_{\text{corr}}$

$$\delta E = E_2 - E_1 = \frac{L^2}{MR^2}\left(\ln\frac{R}{a} - 1\right) + 2\pi H\sigma a - \frac{360\,\text{MeV}}{A}. \tag{K.20}$$

Assuming $A = 150$ and making use of the parameters

$$R = 1.2A^{1/3}\ \text{fm} = 6.4\ \text{fm}, \tag{K.21}$$

$$H = \tfrac{4}{3}R \approx 8.5\ \text{fm}, \tag{K.22}$$

$$a = \frac{1}{8 \times \frac{1\,\text{MeV}}{\text{fm}^2}} \times \frac{150}{\pi(6.4\ \text{fm})^2 8.5\ \text{fm}} 40\ \text{MeV fm}^2 \approx 0.7\ \text{fm} \tag{K.23}$$

and

$$\begin{aligned}\frac{L^2}{MR^2} &= \left(\frac{A}{2}\right)^2 \frac{\hbar^2}{Am}\frac{1}{R^2} = (75)^2 \times \frac{40\,\text{MeV fm}^2}{150 \times (6.4\ \text{fm})^2} \\ &= 36.6\,\text{MeV},\end{aligned} \tag{K.24}$$

$$\begin{aligned}\delta E &= 36.6\ \text{MeV}\left(\ln\frac{6.4}{0.7} - 1\right) + 2\pi 8.5\ \text{fm}\frac{1\ \text{MeV}}{\text{fm}^2}0.7\ \text{fm} - \frac{360}{150}\ \text{MeV} \\ &= 36.6\ \text{MeV} \times 1.2 + 37.4\ \text{MeV} - 2.4\ \text{MeV} \\ &\approx 79\ \text{MeV}.\end{aligned} \tag{K.25}$$

Thus

$$E_2 > E_1\ . \tag{K.26}$$

Consequently, a vortex can, in principle, exist in an atomic nucleus. However, its statistical weight is likely to be too small to be observed, because of its high excitation energy above the yrast state with the same angular momentum (see, however Section 3.10.1). One reason for this is that the vortex kinetic energy is about twice the kinetic energy of rigid rotation ($E_{\text{vortex}} \approx 2.2E_{\text{rigid}}$). The other is the large surface energy of the vortex core ($E_{\text{surf}} \approx 37\,\text{MeV}$).

K.2 Critical velocity for the excitation of rotons

From the value of the vortex angular momentum

$$L = p_0 R = \hbar k_0 R = \hbar I, \tag{K.27}$$

$$I \approx \frac{A}{2}, \tag{K.28}$$

https://doi.org/10.1017/9781009401920 Published online by Cambridge University Press

one can determine the associated momentum

$$k_0 = \frac{A}{2R} \approx \frac{A^{2/3}}{2.4 \times \text{fm}}, \tag{K.29}$$

$$k_0 \approx 0.4 \times A^{2/3} \text{fm}^{-1}. \tag{K.30}$$

Making use of the excitation energy of the roton (see equations (1.6), (K.25) as well as Figs. 1.6 and K.5)

$$\Delta = \delta E \approx 79 \text{ MeV}, \tag{K.31}$$

$$(V_{\text{cr}})_{\text{vortex}} = \frac{\Delta}{\hbar k_0} = \frac{79 \text{ MeV}}{(\hbar c) \times 0.4 A^{2/3} \text{ fm}^{-1}} c \tag{K.32}$$

$$\approx \frac{79 \text{ MeV}}{200 \text{ MeV fm} \times 0.4 A^{2/3} \text{ fm}^{-1}} c \approx \frac{c}{A^{2/3}}, \tag{K.33}$$

consequently,

$$(V_{\text{cr}})_{\text{vortex}} \approx \frac{c}{A^{2/3}} \approx \frac{c}{25} \approx 12 \times 10^6 \text{ m s}^{-1} . \tag{K.34}$$

which is the lowest velocity needed to excite a vortex, i.e. one of the elementary modes of excitation of the system.

K.3 Critical velocity for superfluidity

$$(V_{\text{cr}})_{\text{sup}} \approx \frac{\Delta}{\hbar k_{\text{F}}} = \frac{12}{\sqrt{A}} \text{ MeV} \times \left(\frac{1}{200 \text{ MeV fm} \times 1.36 \text{ fm}^{-1}} \right) c$$

$$\approx \frac{4 \times 10^{-2}}{\sqrt{A}} c , \tag{K.35}$$

where c is the velocity of light. Thus, when $A = 150$,

$$(V_c)_{\text{sup}} \approx 1.1 \times 10^6 \text{ ms}^{-1} , \tag{K.36}$$

which is the critical velocity to excite quasiparticles, in other words, the lowest velocity needed to excite one of the elementary modes of the system.

As already stated above, we note that in equation (K.32) Δ is the gap at the roton minimum ($= \delta E$, equation (K.31)) while in equation (K.35) it is the BCS superfluid pairing gap of a nucleus (see equation (1.17) as well as (1.21)) (see also the last paragraph of Section 1.5).

While one does not expect supercurrents to take place in nuclei, the phenomenon may be realized in neutron stars (see Sections 1.10 and 10.5). In any case, the estimates given in equations (K.34) and (K.36) can be viewed as an excercise concerning orders of magnitude within the framework of the discussion carried out in Sections 1.4 and 1.5.

https://doi.org/10.1017/9781009401920 Published online by Cambridge University Press

Appendix L
Josephson effect

Josephson (1962) proposed that there should be a contribution to the current through an insulating barrier between two superconductors which would behave like direct tunnelling of condensed pairs from one condensed gas of bound pairs at the Fermi surface to the other. The measurement of such an effect has provided a beautiful scenario where the collective rotational degree of freedom in gauge space manifests itself, let alone some of the most accurate measurements of the electron charge (Anderson (1964)).

Before proceeding further let us briefly discuss a technical detail which, aside from being essential to microscopically understanding the mechanism which is at the basis of the effect, also clarifies the long-range order induced by pairing correlations. Because one is interested in calculating the tunnelling of Cooper pairs across the barrier separating the two superconductors, it is natural to start by assuming that it is the pairing interaction that is the source of this transfer, by annihilating a pair in superconductor 2 and creating a pair in superconductor 1 (see Fig. L.1). Although this is what effectively happens, it can be shown that the pairing interaction leads to a negligible contribution to pair transfer, and that essentially all the transfer proceeds through the single-particle mean field acting twice. Note that this reaction mechanism leading to a (successive) two-particle tunnelling does not destroy the correlation existing between the pair of fermions of a Cooper pair participating in the condensate. In fact, aside from the fact that ξ is much larger than typical particle distances (see equation (1.32) and (1.39)), successive transfer mediated by the single-particle field is essentially equivalent to simultaneous transfer, being only one of the different choices of representations used to describe the process to properly take into account the non-orthogonality of the wavefunctions describing the motion of the fermions in each of the superconductors: prior-prior, post-prior, post-post representations (see Cohen *et al*. (1962), Prange (1963), Anderson and Rowell (1963), Götz *et al*. (1975), Broglia and Winther (1991)). Let us now come back to the main subject of this appendix, i.e. the Josephson effect.

Owing to the macroscopic number of paired electrons which are present in a superconductor, it is not possible to observe so directly as in the case of a finite system like the nucleus the individual states of the (pairing) rotational spectrum (in gauge space) shown, for example, in Fig. 4.2. The so-called Josephson junction consists of two

https://doi.org/10.1017/9781009401920 Published online by Cambridge University Press

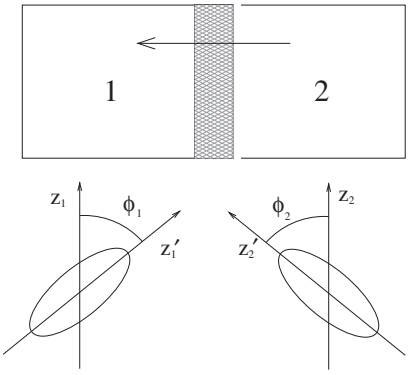

Figure L.1. Schematic representation of a Josephson junction.

superconductors which are separated by a thin dioxide (insulating) layer, through which the electrons can penetrate. Each of the superconductors can, because of the analogy discussed in connection with Fig. 4.1 (see also Sections 1.2, 3.8, 4.2, equation (4.14), as well as Appendix I), be thought of as a rotor (see Fig. L.1). These two rotors are coupled together through the exchange of pairs

$$P_1^\dagger P_2 = \mathrm{e}^{2\mathrm{i}\phi_1} P_1'^\dagger \mathrm{e}^{-2\mathrm{i}\phi_2} P_2', \tag{L.1}$$

where

$$a_\nu'^\dagger = \mathcal{G}(\phi) a_\nu^\dagger \mathcal{G}^{-1}(\phi) = \mathrm{e}^{-\mathrm{i}\phi} a_\nu^\dagger, \tag{L.2}$$

and thus

$$a_\nu^\dagger = \mathrm{e}^{\mathrm{i}\phi} a_\nu'^\dagger. \tag{L.3}$$

This implies

$$P_1^\dagger = \sum_{\nu_1>0} a_{\nu_1}^\dagger a_{\bar{\nu}_1}^\dagger = \mathrm{e}^{2\mathrm{i}\phi} P_1'^\dagger, \tag{L.4}$$

and similarly for P_2.

Consequently, the coupling between the superconductors is

$$\begin{aligned} H_{\mathrm{coupl}} &\sim \mathrm{e}^{2\mathrm{i}\phi_1} \mathrm{e}^{-2\mathrm{i}\phi_2} \mathrm{e}^{\mathrm{i}\delta} + \mathrm{h.c.} \\ &\sim \cos(2(\phi_1 - \phi_2) + 2\delta), \end{aligned} \tag{L.5}$$

where ϕ_1 and ϕ_2 are the gauge phases of the superconductors and δ a phase shift, associated with barrier penetration. The rate at which the quanta are exchanged between the two superconductors is thus given by

$$\begin{aligned} \dot{N}_1 = (-\dot{N}_2) = \frac{\mathrm{i}}{\hbar}[H, N_1] = \frac{\mathrm{i}}{\hbar}\left(\mathrm{i}\frac{\partial H}{\partial \phi}\right) = -\frac{1}{\hbar}\frac{\partial H}{\partial \phi} \\ \sim \sin\left(2(\phi_1 - \phi_2) + 2\delta\right). \end{aligned} \tag{L.6}$$

https://doi.org/10.1017/9781009401920 Published online by Cambridge University Press

The rotational frequency of the rotors corresponds to the chemical potential of the superconductors (see Appendix I, Section I.3)

$$\dot{\phi_1} = \frac{1}{\hbar}\frac{\partial H}{\partial N_1} = \frac{1}{\hbar}\lambda_1 \tag{L.7}$$

and

$$\dot{\phi_2} = \frac{1}{\hbar}\frac{\partial H}{\partial N_2} = \frac{1}{\hbar}\lambda_2. \tag{L.8}$$

Introducing $\phi = \dot{\phi}t = \frac{\lambda}{\hbar}t$ in equation (L.6) one obtains

$$\dot{N}_1 \sim \sin\left(\frac{2}{\hbar}(\lambda_1 - \lambda_2)\,t + 2\delta\right). \tag{L.9}$$

This means that if there is a difference in chemical potential between the two superconductors, which can be obtained by applying an external voltage, there will be an oscillating current running between the superconductors. In terms of the voltage differential $V_1 - V_2$, equation (L.9) can be written as

$$\dot{N}_1 \sim \sin\left(\frac{2e}{\hbar}(V_1 - V_2)\,t + 2\delta\right). \tag{L.10}$$

This shows that the frequency of the oscillating current is determined by the applied voltage, the carriers having charge $2e$. Note that to make this point evident we have used the function $\mathcal{G}(\phi) = \mathrm{e}^{-\mathrm{i}\hat{N}\phi}$ to induce a gauge transformation (see equation (L.2)), and not $\mathrm{e}^{\mathrm{i}\frac{\hat{N}}{2}\phi}$ as introduced in equation (4.12).

The remarkable confirmation of the picture of deformation and of rotation in gauge space provided by the Josephson effect is an example of the general fact that, arguably, the most successful approach to physics is a combination of phenomenology with microscopic theory, and of experiment with both. From this kind of approach one can arrive at a degree of understanding of phenomena which essentially amounts to certainty. Superconductivity and superfluidity are likely to belong to this category of phenomena, of whose basic nature one is virtually certain, primarily because of the large variety of phenomena which can be correlated by one form or another of BCS theory.

In general, a condensation phenomenon is characterized by a new parameter in the condensed phase leading to emergent properties which were not present in the original system nor in the particles which compose it. For example, below its Curie point a ferromagnet has magnetization in the absence of a field. The long-range order of a solid is not present in the liquid. The order parameter of a superconductor is the energy gap itself.

All these systems and their order parameters have an important feature in common: the condensed system does not have the full symmetry of the Hamiltonian describing it. Superfluidity and superconductivity can be considered particular examples of this general theory, letting the order parameter be $\langle \mathrm{BCS}|G\,P^{\dagger}|\mathrm{BCS}\rangle = \mathrm{e}^{2\mathrm{i}\phi}\Delta$ and fixing the magnitude and the phase ϕ. Then, it is gauge invariance which is violated in the superconductor.

https://doi.org/10.1017/9781009401920 Published online by Cambridge University Press

Clearly, general gauge invariance is not violated, but from the point of view of individual fermions it is, in the sense that the phase of the field operator with which we insert additional particles is relevant.

It is of course physically obvious that the full symmetry of the original Hamiltonian still governs the system, in the sense that it is only the state of the system which is taken to be non-invariant, and one considers all other states to which the assumed state can be carried by symmetry operations as degenerate with a given one (see Section 4.2.1, in particular equation (4.14)).

These ideas seem rather evident and general. Now, however, one comes to the real distinction among the different situations. In a few cases – ferromagnetism being an obvious example – the order parameter is a constant of motion. Then, of course, the non-invariant states are, rigorously, degenerate eigenstates of H, and no serious questions of principle arise: all the consequences of the true symmetry of H can be retained in the most direct fashion.

More common is the opposite case: the order parameter is not a quantum-mechanical constant of the motion. The orientation of the solid in space, for instance, and its position, are not constants of the motion; the correct constants are total momentum and angular momentum. In the superconductor we find the phase variable is not only not a constant of motion, but is normally assumed to be meaningless.

In the cases of the solid or the ferroelectric one can understand the physics of the situation. What happens is that the condensation has given the system one form or another of long-range order, so that $\approx 10^{23}$ different atoms must move as a unit rather than individually. Under such circumstances the system is so large that its behaviour is essentially classical, and one may fix the value of the order parameter even though it is not a constant of motion – the coordinate or orientation of the solid, for instance. There is indeed zero-point motion of a macroscopic solid, but it is so small that one does not need to deal with it.

Another aspect of the situation is that in general the usual type of condensed system finds itself in the presence of external fields which fix the order parameter at some preferred value. Because of the long-range order, only a very small external force is necessary to do this. A small external field can align a ferromagnet, a small external force pin down the orientation and position of a crystal (see final paragraph of Section 4.2.4, Weinberg's chair).

In actual fact one seldom deals with condensed systems in the absence of external fields, so that one is accustomed to think of such systems as having definite values of such order parameters as the orientation. But this is because we are accustomed to working with measuring instruments which are themselve rigid, i.e. have a long-range positional order. Thus it does not seem extraordinary that a solid has a fixed position and orientation. In the case of magnets, again one is used to instruments which violate time-reversal symmetry themselves, and thus we do not find it unusual for a system to have a definite value of ferromagnetic order.

In the case of superconducting systems things are quite different. The internal long-range order parameter – the phase – is not a parameter for which suitable measurement instruments exist. A superconductor, or a superfluid, has rather perfect internal phase order, but as has been shown in Section 4.2.1 (equation (4.39)) (see also Appendix I),

the zero-point motion of the total order parameter of an isolated superconductor is large and rather rapid.

The importance of the Josephson effect is that it provides for the first time an instrument which can act like a clamp for a solid: it can pin down the order parameter, making superfluidity and superconductivity one more example of condensation phenomena.

Summing up, condensation is a self-consistent choice by the system of a state – and a corresponding mean self-consistent field – which does not have the full symmetry of the Hamiltonian. Fluctuations of the order parameter will, in the absence of asymmetric external forces, restore the original symmetry. The external forces needed to 'pin down' the quantum fluctuations can only come from systems which themselves violate the given symmetry: in the case of a superconductor, another superconductor.

The possibility to study the transfer of Cooper pairs between superfluid nuclei in a heavy ion collision (transient Josephson junction), has been extensively discussed (see e.g. von Oertzen (1994), Broglia and Winther (1991) and references therein)

References

Åberg, S. (1987). In *Proceedings of the XXV International Winter Meeting on Nuclear Physics, Bormio, Italy*, Iori, I., ed., Milan: Ricerca Scientifica ed Educazione Permanente, Supplemento, Universitá di Milano, page 661.

Åberg, S. (1999). *Phys. Rev. Lett*. **82**:299.

Ainsworth, T. L., Wambach, J., and Pines, D. (1989). *Phys. Lett.*, **B222**:173.

Ajzenberg-Selove, F. (1988). *Nucl. Phys.*, **A490**:1.

Ajzenberg-Selove, F. (1990). *Nucl. Phys.*, **A506**:1.

Alberico, W.M., Kirson, M., Molinari, A., and Broglia, R. A. (1976). *Phys. Rev.* **B13**:1080.

Alexandrov, A. S. (2003). *Theory of Superconductivity*, Institute of Physics, Bristol.

Al-Khalili, J. S. and Tostevin, J. A. (1996). *Phys. Rev. Lett.*, **76**:3903.

Alpar, M. A. (1977). *Astrophys.*, **213**:527.

Alpar, M. A. (1998). *Phys. World*, **11**:25.

Ambegaokar, V. and Mermin, N.D. (1973). *Phys. Rev. Lett*. **30**:81.

Anderson, P. W. (1952). *Phys. Rev.*, **86**:694.

Anderson, P. W. (1958). *Phys. Rev.*, **112**:1900.

Anderson, P. W. (1959). *J. Phys. Chem. Solids*, **11**:26.

Anderson, P. W. (1963). *Phys. Rev.*, **130**:439.

Anderson, P. W. (1964). *Lectures on the Many-body Problem*, Caianiello, E.R., ed. Volume 2. New York: Academic Press, page 113.

Anderson, P. W. (1972). *Science*, **177**:393.

Anderson, P. W. (1984). *Basic Notions of Condensed Matter Physics,* Benjamin, California: Advanced Book Programme Menlo Park.

Anderson, P. W. and Brinkman, W.F. (1973). *Phys. Rev. Lett*., **30**:1108.

Anderson, P.W. and Brinkman, W.F. (1975). *Proceedings of 15th Scottish Universities Summer School in Physics*, Armitage, J.G.M and Farquhar, I.E., eds. New York: Academic Press.

Anderson, P. W. and Itoh, N. (1975). *Nature*, **256**:25.

Anderson, P.W. and Morel, P. (1961). *Phys. Rev.*, **123**:1911.

Anderson, P. W. and Rowell, J. M. (1963). *Phys. Rev. Lett.*, **10**:230.

Anderson, P. W., Alpar, M. A., Pines, D., and Shaham, J. (1982). *Phil. Mag. A*, **45**:227.
Andreoiu, C., Døssing, T., Fahlander, C. *et al.* (2003). *Phys. Rev. Lett*, **91**:232502–1.
Aoi, N., Yoneda, K., Miyatake, H., *et al*. (1997). *Nucl. Phys.*, **616**:181.
Arndt, R. A. and Roper, L. D. (1985). *Phys. Rev.*, **D31**:2230.
Atkins, K. R. (1959). *Liquid Helium*. London: Cambridge University Press.
Audi, G. and Wapstra, A. H. (1995). *Nucl. Phys.*, **A595**:409.
Baldo, M., Cugnon, J., Lejeune, A., and Lombrado, U. (1990). *Nucl. Phys.*, **A550**:409.
Baldo, M., Cugnon, J., Lejeune, A., and Lombrado, U. (1991). *Nucl. Phys.*, **A556**:545.
Baldo, M., Lombardo, U., Schulze, H.J., and Wei, Z. (2002). *Phys. Rev.* **C66**:054304.
Balian, R. and Werthamer, N.R. (1963). *Phys. Rev*., **131**:1553.
Bardeen, J., Cooper, L. N., and Schrieffer, J. R. (1957a). *Phys. Rev.*, **106**:162.
Bardeen, J., Cooper, L. N., and Schrieffer, J. R. (1957b). *Phys. Rev.*, **108**:1175.
Barnett, R.N., Landman, U., and Rajagopal, G. (1991). *Phys. Rev. Lett*., **67**:3058.
Baroni, S., Armati, M., Barranco, F., Broglia, R. A., Coló, G., Gori, G., and Vigezzi, E. (2004). *J. Phys. G*, **30**:1353.
Barranco, F., Gallardo, M., and Broglia, R. A. (1987). *Phys. Lett*., **B198**:19.
Barranco, F., Broglia, R. A., and Bertsch, G. F. (1988a). *Phys. Rev. Lett.*, **60**:507.
Barranco, F., Vigezzi, E., Broglia, R. A., and Bertsch, G. F. (1988b). *Phys. Rev.*, **C38**:1523.
Barranco, F., Vigezzi, E., and Broglia, R. A. (1988c). In *Proceedings of the Conference on High-Spin Nuclear Structure and Novel Nuclear Shapes*, Volume ANL-PHY-88-2, Argonne Natl. Lab., page 130.
Barranco, F., Vigezzi, E., and Broglia, R. A. (1989). *Phys. Rev.*, **C39**:2101–2104.
Barranco, F., Bertsch, G., Broglia, R. A., and Vigezzi, E. (1990). *Nucl. Phys.*, **A512**: 253.
Barranco, F., Broglia, R. A., Esbensen, H., and Vigezzi, E. (1997). *Phys. Lett.*, **390B**:13.
Barranco, F., Broglia, R. A., Esbensen, H., and Vigezzi, E. (1998). *Phys. Rev.*, **C58**:1257.
Barranco, F., Broglia, R. A., Gori, G., Vigezzi, E., Bortignon, P. F., and Terasaki, J. (1999). *Phys. Rev. Lett.*, **83**:2147.
Barranco, F., Bortignon, P. F., Broglia, R. A., Coló, G., and Vigezzi, E. (2001). *Eur. Phys. J. A*, **11**:385–392.
Barranco, F. *et al*. (2004). *Eur. Phys. J.*, **A21**:57.
Barranco, M., Hernandez, E. S., Lombard, R., and Serra, L. (1992). *Z. Phys. (Atoms, Molecules and Clusters)*, **D22**:659.
Bartel, J., Quentin, P., Brack, M., Guet, C., and Hakansson, H. B. (1982). *Nucl. Phys.*, **A386**:79.
Bauer, M., Hernandez-Saldana, E., Hodgson, P. E., and Quintillame, J. (1982). *J. Phys.*, **G8**, no. 525.
Bayman, B. (1960). Lectures on seniority, quasi-particles and collective vibrations. Princeton, New Jersey (unpublished).
Bayman, B., Bes, D. R., and Broglia, R. A. (1969). *Phys. Rev. Lett.*, **23**:1299.
Beer, O., el Behay, A., Lopato, P., Terrien, Y., Vellois, G., and Seth, K.K. (1970). *Nucl. Phys.* **A147** (326):246.
Belyaev, T. (1958a). *Sov. Phys. JETP*, **7**:289.
Belyaev, T. (1958b). *Sov. Phys. JETP*, **7**:299.

Belyaev, S. T. (1959). *Mat. Fys. Medd. Dan. Vid. Selsk.*, **31**, no.11.
Belyaev, S. T. (1961). *Nucl. Phys*., **24**:322.
Belyaev, S. T. (1972). In *Proceedings of the International School of Physics 'E. Fermi'*, *Course L II*, Morinaga, H., ed. New York: Academic Press, page 234.
Bender, M., Bertsch, G. F., and Heenen, P. H. (2004). *Phys. Rev*., **C69**:034340.
Bengtsson, T., Broglia, R. A., Vigezzi, E., Barranco, F., Dönau, F., and Jing-ye Zhang (1989). *Phys. Rev. Lett.*, **62**:2448.
Bertsch, G. F. (1980). *Phys. Lett.*, **B95**:157.
Bertsch, G. F. (1988). In *Proceedings of the International School of Physics 'E. Fermi'*, *Course CIV*, Broglia, R. A. and Schrieffer, J., eds, Amsterdam: North Holland, page 41.
Bertsch, G. F. (1994). *Proceedings of the International School of Physics 'E. Fermi' Course CXXI*, Broglia, R.A., Schrieffer, J.R., and Bortignon, P.F., eds. Amsterdam: North Holland, p. 127.
Bertsch, G. F. and Broglia, R. A. (1994). *Oscillations in Finite Quantum Systems*. Cambridge: Cambridge University Press.
Bertsch, G. F. and Esbensen, H. (1991). *Ann. Phys.*, **209**:327.
Bertsch, G. F. and Esbensen, H. (1985). *Phys. Lett*., **161B**:248.
Bertsch, G. F. and Hagino, K. (2001). *Phys. Atom. Nucl.*, **64**:533.
Bertsch, G. F. and Kuo, T. T. S. (1968). *Nucl. Phys.*, **A112**:204.
Bertsch, G. F., Bortignon, P. F., and Broglia, R. A. (1983). *Rev. Mod. Phys.*, **55**:287.
Bertsch, G. F., Broglia, R. A., and Schrieffer, J. R. (1988). *Nuov. Cim.*, **100**:283.
Bes, D. R. and Broglia, R. A. (1966). *Nucl. Phys.*, **80**:289.
Bes, D. R. and Broglia, R. A. (1971). *Phys. Rev.*, **C3**:2349.
Bes, D. R. and Broglia, R. A. (1977). In *Proceedings of the International School of Physics 'E. Fermi'*, *Course LXIX*, Bohr, A. and Broglia, R. A., eds, Amsterdam: North Holland, page 55.
Bes, D.R. and Sorensen, R. A. (1969). *Adv. Nucl. Phys.*, **2**:129.
Bes, D. R., Broglia, R. A., Perazzo, R., and Kumar, K. (1970). *Nucl. Phys.*, **A143**:1.
Bes, D. R., Broglia, R. A., and Nilsson, B. S. (1972). *Phys. Lett.*, **B40**:338.
Bes, D. R., Broglia, R. A., Dussel, G. G., Liotta, R. J., and Perazzo, R. P. J. (1976a). *Nucl. Phys.*, **A260**:77.
Bes, D. R., Broglia, R. A., Dussel, G. G., Liotta, R. J., and Sofia, H. M. (1976b). *Nucl. Phys.*, **A260**:1, 27.
Bes, D. R., Broglia, R. A., Hansen, D., and Nathan, O. (1977). *Phys. Rep.*, **B40**:338.
Bes, D. R. and Kurchan, J. (1990). *The Treatment of Collective Coordinates*. Singapore: World Scientific.
Bes, D. R., Civitarese, O., Maqueda, E. E., and Scoccola, N. N. (2000). *Phys. Rev.*, **61**:024315.
Bjerregaard, J.H., Hansen, O., Nathan, N., and Hinds, S. (1966a). *Nucl. Phys.*, **89**:147.
Bjerregaard, J.H., Hansen, O., Nathan, N., and Hinds, S. (1966b). *Nucl. Phys.*, **86**:145.
Bjerregaard, J. H., Hansen, O., Nathan, O., Chapman, R., and Hinds, S. (1969). *Nucl. Phys.*, **A131**:481.
Bjerregaard, J. H., Hansen, O., Nathan, O., Vistisen, L., Chapman, R., and Hinds, S. (1968). *Nucl. Phys.*, **A110**:1.

Black, C. T., Ralph, D. C., and Tinkham, M. (1996). *Phys. Rev. Lett.*, **76**:688.
Blaizot, J. P. and Gogny, D. (1977). *Nucl. Phys.*, **A284**:429.
Blatt, J.M. and Butler, S.J. (1995). *Phys. Rev.*, **100**:476.
Bloch, B. and Horowitz, J. (1958). *Nucl. Phys.*, **8**:91.
Block, C. and Feshbach, H. (1963). *Ann. Phys. (NY)*, **23**:17.
Bogoliubov, N. N. (1958a). *J. Exp. Theor. Phys. USSR*, **34**:58.
Bogoliubov, N. N. (1958b). *Nuov. Cim.*, **7**:794.
Bogoliubov, N. N., Tolmachov, V. V., and Sirkov, V. (1958). *Fortschr. Phys.*, **6**:605.
Bohr, A. (1968). In *Nuclear Structure*, Vienna: IAEA, page 179.
Bohr, A. (1977) In *Proceedings of the International School of Physics 'E. Fermi'*, *Course LXIX*, Bohr, A. and Broglia, R., eds. Amsterdam: North Holland, page 3.
Bohr, A. and Mottelson, B. R. (1953). *Mat. Fys. Medd. Dan. Vid. Selsk.*, **27**, no.16.
Bohr, A. and Mottelson, B. R. (1969). *Nuclear Structure*, Volume 1. New York: Benjamin.
Bohr, A. and Mottelson, B. R. (1973). *Ann. Rev. Nucl. Part. Sci.*, **23**:363.
Bohr, A. and Mottelson, B. R. (1974). *Phys. Scripta*, **10A**:13.
Bohr, A. and Mottelson, B. R. (1975). *Nuclear Structure*, Volume 2. Reading, Mass: Benjamin.
Bohr, A. and Mottelson, B. R. (1981). *Phys. Scripta*, **24**:171.
Bohr, A., Mottelson, B. R., and Pines, D. (1958). *Phys. Rev.*, **110**:936.
Bonetti, R., Fioretto, E., Migliorino, C., Pasinetti, A., Barranco, F., Vigezzi, E., and Broglia, R. A. (1990). *Phys. Lett.*, **B241**:179.
Bonetti, R., Guglielmetti, A., Mikheev, V., Tretyakova, S. R., Cesana, A., and Terrani, M. (2000). *Phys. Rev.*, **C62**:047304.
Bortignon, P. F., Bracco, A., and Broglia, R. A. (1998). *Giant Resonances: Nuclear Structure at Finite Temperature*. New York: Harwood Academic Press.
Bortignon, P. F. and Broglia, R. A. (1981). *Nucl. Phys.*, **A371**:405.
Bortignon, P. F., Broglia, R. A., Bertsch, G. F., and Pacheco, J. (1986). *Nucl. Phys.*, **A460**:149.
Bortignon, P. F., Broglia, R. A., Bes, D. R., and Liotta, R. (1977). *Phys. Rep.*, **30C**:305.
Bortignon, P. F., Broglia, R. A., and Dasso, C. H. (1983). *Nucl. Phys.*, **A398**:221.
Brink, D.M. (1994). *Proceedings of the International School of Physics 'E. Fermi' Course CXXI*, Broglia, R. A., Schrieffer, J. R., and Bortignon, P.-F., eds. Amsterdam: North Holland, page 255.
Brink, D.M. and Satchler, R. (1968, 1993). *Angular Momentum*. Oxford: Clarendon Press.
Broglia, R. A. (1981). In *Workshop on Interacting Bosons and Fermions in Nuclei*, Iachello, F., ed. New York: Plenum Press, page 95.
Broglia, R. A. (1985). In *Proceeding of the 2nd La Rábida Summer School on Nuclear Physics*, Lozano, M. and Madurga, G., eds. Singapore: World Scientific, page 133.
Broglia, R. A. and Sørensen, B. (1968). *Nucl. Phys.*, **A110**:241.
Broglia, R. A. and Winther, A. (1991). *Heavy Ion Reactions*, Volume 1. New York: Addison Wesley; (2004), Boulder: Westview Press.
Broglia, R. A. and Riedel, C. (1967a). *Nucl. Phys.*, **A92**:145.
Broglia, R. A. and Riedel, C. (1967b). *Nucl. Phys.*, **A92**:241.

Broglia, R. A., Riedel, C., Sørensen, B., and Udagawa, T. (1968a). *Nucl. Phys.*, **A115**:273.
Broglia, R. A., Riedel, C., and Sørensen, B. (1968b). *Nucl. Phys.*, **A107**:1.
Broglia, R. A., Riedel, C., and Udagawa, T. (1969). *Nucl. Phys*., **A135**:561.
Broglia, R. A., Paar, V., and Bes, D. R. (1971a). *Phys. Lett.*, **37B**:159.
Broglia, R. A., Paar, V., and Bes, D. R. (1971b). *Phys. Lett.*, **37B**:257.
Broglia, R. A., Riedel, C., and Udagawa, T. (1971c). *Nucl. Phys*., **A169**:225.
Broglia, R. A., Riedel, C., and Udagawa, T. (1972). *Nucl. Phys*., **A184**:23.
Broglia, R. A., Riedel, C., and Hansen, O. (1973). *Adv. Nucl. Phys.*, **6**:287.
Broglia, R. A., Molinari, A., Pollarolo, G., and Regge, T. (1974a). *Phys. Lett.*, **50B**:295.
Broglia, R. A., Bes, D. R., and Nilsson, B. S. (1974b). *Phys. Lett.*, **B50**:213.
Broglia, R. A., Molinari, A., Pollarolo, G., and Regge, T. (1975). *Phys. Lett.*, **57B**:113.
Broglia, R. A., Molinari, A., and Regge, T. (1977). *Ann. Phys.*, **109**:349.
Broglia, R. A., Diebel, M., Barranco, F., and Frauendorf, S. (1985a). In *Proceedings of the XXIII International Winter Meeting on Nuclear Physics, Bormio, Italy*, Iori, I., ed., Ricerca Scientifica ed Educazione Permanente, Supplemento, Milan: Universitá di Milano, page 320.
Broglia, R. A., Barranco, F., and Gallardo, M. (1985b). In *Nuclear Structure 985*, Broglia, R. A., Hagemann, G., and Herskind, B., eds. Amsterdam: North Holland, page 193.
Broglia, R. A., Diebel, M., Frauendorf, S., and Gallardo, M. (1986). *Phys.Lett.*, **B166**:252.
Broglia, R. A., Barranco, F., and Vigezzi, E. (1993). In *Foundation of Quantum Mechanics*. Tokyo: Japanese Journal of Applied Physics.
Broglia, R.A., Barranco, F., Bertsch, G.F., and Vigezzi, E. (1994). *Phys. Rev.*, **C49**:552.
Broglia, R. A., Terasaki, J., and Giovanardi, N. (2000). *Phys. Rep*., **335**:1.
Broglia, R. A., Barranco, F., Bortignon, P. F., Gori, G., Terasaki, J., and Vigezzi, E. (2001). In *The Nuclear Many-Body Problem*, Volume 53 of *NATO Science Series*. London: Kluwer.
Broglia, R. A., Barranco, F., Coló, G., Vigezzi, E., Bortignon, P. F., Gori, G., and Terasaki, J. (2002). In *INCP 2001*. New York: American Institute of Physics.
Broglia, R. A., Coló, G., Onida, G., and Roman, H. E. (2004). *Solid State Physics of Finite Systems: Metal Clusters, Fullerenes, Atomic Wires*. Berlin, Heidelberg: Springer.
Brueckner, K. A. and Sawada, K. (1957a). *Phys. Rev.*, **106**:1117.
Brueckner, K. A. and Sawada, K. (1957b). *Phys. Rev.*, **106**:1128.
Bruus, H. and Flensberg, K. (2004). *Many-Body Quantum Theory in Condensed Matter Physics*. Oxford: Oxford University Press.
Buck, B. and Merchant, A. C. (1989). *Phys. Rev.*, **C39**:2097.
Buck, B., Merchant, A. C., Horner, M. J., and Peres, S. M. (2000). *Phys. Rev.*, **C61**:024314.
Casten, R. F., Flynn, E. R., Garrett, J. D., *et al*. (1972). *Phys. Lett*., **40B**:333.
Chen, J. M. C., Clark, J. W., Davé, R. D., and Khodel, V. V. (1993). *Nucl. Phys.*, **A555**:59.
Chen, J. M. C., Clark, J. W., Krotscheck, E., and Smith, R. A. (1986). *Nucl. Phys.*, **A451**:509.
Cohen, M. H., Falicov, L. M., and Phillips, J. C. (1962). *Phys. Rev. Lett.*, **8**:316.

Cohen, S., Plasil, F., and Swiatecki, W. J. (1974). *Ann. Phys.*, **82**:557.
Coló, G. L. and Bortignon, P. F. (2001). *Nucl. Phys.*, **A696**:427.
Combescot, R. (1999). *Phys. Rev. Lett.*, **83**:3766.
Cooper, L. N. (1956). *Phys. Rev.*, **104**:1189.
Dang, N. D. and Arima, A. (1998). *Phys. Rev. Lett.*, **80**:4145.
Dang, N. D. and Arima, A. (2003). *Phys. Rev.*, **C68**:014318.
de Gennes, P. (1966). *Superconductivity of Metals and Alloys*. New York: Addison Wesley.
de Heer, W. A. and Knight, W. D. (1988). In *Elemental and Molecular Clusters*, Benedek, G., Martin, T., and Pacchioni, G., eds, Berlin: Springer-Verlag, page 45.
de Shalit, A. and Talmi, I. (1963). *Nuclear Shell Theory*. New York: Academic Press.
Delion, D. S., Baldo, M., and Lomdardo, U. (1995). *Nucl. Phys.*, **A593**:151.
Dirac, P. A. M. (1935). *The Principles of Quantum Mechanics*, 2nd edn. Oxford: Clarendon Press.
Dobaczewski, J. and Nazarewicz, W. (1998). *Phil. Trans. R. Soc. Lond.*, **A356**:2007.
Dobaczewski, J., Nazarewicz, W., and Stoitsov, M. V. (2002). In *The Nuclear Many-Body Problem 2001*, Nazarewicz, W. and Vretener, D., eds. Dordrecht: Kluwer Academic Publishers.
Donati, P., Døssing, T., Shimizu, Y. R., Bortignon, P. F., and Broglia, R. A. (1999a). *Nucl. Phys.*, **A653**:27.
Donati, P., Døssing, T., Shimizu, Y. R., Bortignon, P. F., and Broglia, R. A. (1999b). *Nucl. Phys.*, **A653**:225.
Donati, P., Giovanardi, N., Bortignon, P. F., and Broglia, R. A. (1996). *Phys. Lett.*, **B383**:15.
Donati, P. and Pizzochero, P. M. (2003). *Phys. Rev. Lett.*, **90**:211101.
Dönau, F., Almehed, D., and Nazmitdinov, R. G. (1999). *Phys. Rev. Lett.*, **83**:280.
Dukelsky, J., Esebagg, C., and Pittel, S. (2002). *Phys. Rev. Lett.*, **88**:062501.
Dussel, G. G., Maqueda, E., and Perazzo, R. P. J. (1970). *Nucl. Phys.*, **A153**:469.
Eckardt, W. (1984). *Phys. Rev.*, **B29**:1558.
Eguchi, T. and Nishijima, K., eds. (1995). *Broken Symmetry, Selected Papers of Y. Nambu*. Singapore: World Scientific.
Engel, J., Pittel, S., Stoitsov, M., Vogel, P., and Dukelsky, J. (1997). *Phys. Rev.*, **C55**:1781.
Epstein, R. I. and Baym, G. (1988). *Astrophys. J.*, **328**:680.
Esbensen, H. and Bertsch, G. F. (1984a). *Ann. Phys.*, **157**:255.
Esbensen, H. and Bertsch, G. F. (1984b). *Phys. Rev. Lett.*, **52**:2257.
Esbensen, H., Bertsch, G. F., and Henckean, K. (1997). *Phys. Rev.*, **C56**:3054.
Faessler, A. (1968). *Fortschr. Phys.*, **16**:309.
Farine, M. and Schuck, P. (2002). In *The Nuclear Many-Body Problem 2001*, Nazarewicz, W. and Vretener, D., eds. Dordrecht: Kluwer Academic Publishers.
Feshbach, H. (1974). *Rev. Mod. Phys.*, **46**:1.
Fetter, A. L. and Walecka, J. D. (1971). *Quantum Theory of Many-Particle Systems*. New York: McGraw-Hill.
Feynman, R. R. (1972). *Statistical Mechanics,* Reading, MA: Benjamin.
File, J. and Mills, R. G. (1963). *Phys. Rev. Lett.*, **10**:93.
Flanagan, C. (1990). *Nature*, **345**:416.

Fleming, D. G., Blann, M., Fulbright, H. W., and Robbins, J. A. (1970). *Nucl. Phys.*, **A157**:1.
Flynn, E. R., Beery, J. G., and Blair, A. G. (1970). *Nucl. Phys.*, **A154**:225.
Flynn, E. R., Igo, G. J., and Broglia, R. A. (1972). *Phys. Lett.*, **41B**, 397.
Frascaria, N., Gales, S., and Van Giai, N., eds. (2004). *Proceedings of the International Conference on Collective Motion in Nuclei under Extreme Conditions. Nucl. Phys.*, A731.
Frauendorf, S. and Sheikh, J. A. (2000). *Phys. Scripta*, **T88**:162.
Furry, W. H. (1937). *Phys. Rev.*, **51**:125.
Garrett, J. D., Hagemann, G. B., Herskind, B. *et al*. (1982). *Phys. Lett.* **B118**:297.
Garrett, J., Hagemann, G. B., and Herskind, B. (1983). *Nucl. Phys. A*, **400**:113c.
Garrett, J., Hagemann, G., and Herskind, B. (1986). *Ann. Rev. Nucl.Part. Sci.*, **36**:419.
Garrett, J. D., Nyberg, J. Yu, C. H., Espino, J. M., Gofrey, M. J. (1988). *Proceedings on the International Conference on Contemporary Topics in Nuclear Structure Physics,* Casten, R.F., Frank, A., Moshinsky, M., and Pittel, S., eds. Singapore: World Scientific, page 699.
Garrido, E., Sarriguren, P., Moya de Guerra, E., and Schuck, P. (1999). *Phys. Rev.*, **C60**:064312.
Ginzburg, V. L. and Landau, L. D. (1950). *Zh Eksp. Teor. Fiz.*, **20**:1064.
Giovanardi, N., Barranco, F., Broglia, R. A., and Vigezzi, E. (2002). *Phys. Rev. C*, **65**:041304–1.
Gogny, D. (1975). *Nucl. Phys.*, **A237**:399.
Gold, T. (1969). *Nature*, **218**:731.
Goldstone, J. (1961). *Nuov. Cim.*, **19**:154.
Goldstone, J., Salam, A., and Weinberg, S. (1962). *Phys. Rev.*, **127**:965.
Goodman, A. L. (1998). *Phys. Rev.*, **C58**:R3051.
Gori, G. (2002). Dynamical correlation effects in deformed nuclei and in nuclei far from the stability valley, PhD Thesis, University of Milan, (unpublished).
Gori, G., Barranco, F., Vigezzi, E., and Broglia, R. A. (2004a). *Phys. Rev.*, **C69**:041302(R).
Gori, G., Ramponi, F., Barranco, F., Broglia, R. A., Coló, G., Sarchi, D., and Vigezzi, E. (2004b). *Nucl. Phys.*, **A731**:401.
Goriely, S., Samyn, M., Heenen, P. H., Pearson, J. M., and Tondeur, F. (2002). *Phys. Rev.*, **C66**:024326–1.
Goriely, S., Tondeur, F., and Pearson, J. M. (2001). *At. Data Nucl. Data Tables*, **77**:311.
Gor′kov, L. P. (1960a). *JETP*, **9**:1364.
Gor′kov, L. P. (1960b). *JETP*, **10**:593.
Gor′kov, L. P. and Melik-Barkhudarov, T. K. (1961). *Sov. Phys. JETP*, **13**, 1018.
Goswami, A., Lin, L., and Strube, G. (1967). *Phys. Lett.*, **B25**:451.
Götz, U., Ichimura, M., Broglia, R. A., and Winther, A. (1975). *Phys. Rep.*, **16**:111.
Green, I. and Mozkowski, S. A. (1965). *Phys. Rev.*, **139B**:790.
Greiner, M., Regal, C. A., and Jin, D. S. (2003). *Nature*, **426**:537.
Gunnarsson, O. (1997). *Rev. Mod. Phys.*, **69**:575.
Gunnarsson, O. (2004). *Alkali-doped Fullerides: Narrow-band Solids with Unusual Properties*. Singapore: World Scientific.

Hamamoto, I. (1977). In *Proceedings of the International School of Physics 'E. Fermi', Course LXIX*, Bohr, A. and Broglia, R. A., eds. Amsterdam: North-Holland, page 234.
Hamamoto, I. and Mottelson, B. F. (2003). *Phys. Rev.*, **C68**, 034312.
Hansen, P. G. (1996). *Nature*, **384**:413.
Herskind, B., Lauritzen, B., Schiffer, K., Broglia, R. A., Barranco, F., Gallardo, M., Dudek, J., and Vigezzi, E. (1988). *Phys. Rev. Lett.*, **59**:2416–19.
Hewish, A., Bell, S. J., Pilkingston, J. D. H., Scott, P. F., and Collins, R. A. (1968). *Nature*, **217**:709.
Heyde, K. L. G. H. (1990). *The Nuclear Shell Model*. Berlin and Heidelberg: Springer Verlag.
Högaasen-Feldman, J. (1961). *Nucl. Phys.*, **28**:258.
Hugenholtz, N. and Pines, D. (1959). *Phys. Rev*., **116**: 489.
Ichimura, M. (1964). *Prog. Theor. Phys.*, **32**. 757.
Igo, G., Barnes, P. D., and Flynn, E. R. (1971). *Ann. Phys.*, **66**:60.
Iwasaki, H., Motobayashi, T., Akiyoshi, H. *et al*. (2000a). *Phys. Lett.*, **B481**:7.
Iwasaki, H., Motobayashi, T., Akiyoshi, H. *et al*. (2000b). *Phys. Lett.*, **B491**:8.
Jochim, S., Bartenstein, M., Altmeyer, A. *et al.* (2003). *Science,* **302**:2101.
Jonsson, N. G., Backlin, A., Kantele, J., Julin, R., Luontama, M., and Passoja, A. (1981). *Nucl. Phys.*, **A371**:333.
Josephson, B. D. (1962). *Phys. Lett.*, **1**:251.
Kennedy, R. G. (1968). *Nucl. Phys*, **A118**:189.
Kerman, A. K., Lawson, R. D., and Macfarlane, M. H. (1961). *Phys. Rev.*, **124**:162.
Kisslinger, L.S. and Sorensen, R. (1963). *Rev. Mod. Phys.*, **35**:853.
Kittel, C. (1968). *Introduction to Solid State Physics*. New York: Wiley.
Kobayashi, T. (1993). *Nucl. Phys.*, **A553**:465c.
Kobayashi, T., Shimoura, S., Tanihata, I., *et al*. (1989). *Phys. Lett.*, **B232**:51.
Kubo, R. (1962). *J. Phys. Soc. Jap.*, **17**:975.
Kuo, T. T. S., Krmpotić, F., and Tzeng, Y. (1997). *Phys. Rev. Lett.*, **78**:2708.
Landau, L. D. (1941). *J. Phys. USSR*, **5**,**11**:71,592.
Landau, L. D. (1947). *J. Phys. USSR*, **11**:91.
Landau, L. D. (1959). *JEPT*, **3**:920.
Landford, W. A. and McGrory, J. (1973). *Phys. Lett.*, **45B**:238.
Lane, A. (1964). *Nuclear Theory*. New York: Benjamin.
Lauritzen, B., Anselmino, A., Bortignon, P., and Broglia, R. (1993). *Ann. Phys.*, **223**:216.
Lawson, R. D. (1980). *Theory of the Nuclear Shell Model*. Oxford: Clarendon Press.
Lee, D. M. (1997). *Rev. Mod. Phys.*, **69**:645.
Leggett, A. J. (1972). *Phys. Rev. Lett.*, **29**:1227.
Leggett, A. J. (1980). *Modern Trends in the Theory of condensed Matter*, Pekalski, A. and Przystawa, R., eds. Berlin: Springer.
Leggett, A. J. (1989). *The New Physics*. Cambridge: Cambridge University Press.
Lesher, S. R., Aprahamian, A., Trache, L., Oros-Peusquens, A., Gollwitzer, A., Hertenberger, R. *et al*. (2002). *Phys. Rev.*, **C65**:031301.
Link, B. and Epstein, R. (1991). *Astrophys. J.*, **373**:592.
Lipkin, H. (1960). *Ann. Phys.* **9**:272; *Ann. Phys*. **12**:425.

Nogami, Y. (1963). *Prog. Theoret. Phys*. **29**:938.
Nogami, Y. (1964). *Phys. Rev.* **B134**:313.
Lipparini, E. (2003). *Modern Many-Particle Physics*. Singapore: World Scientific.
Lombardo, U. and Schulze, H. J. (2001). Superfluidity in neutron star matter. In *Physics of Neutron Star Interiors*, Blaschke, D., Glendenning, N. K., and Sedrakian, A., eds. Berlin: Springer, page 30.
London, F. (1954). *Superfluids* Vols. I, II, New York: Dover, Reprinted 1964.
Mahan, G.D. (1981). *Many Particle Physics*. New York: Plenum Press.
Mahaux, C., Bortignon, P. F., Broglia, R. A., and Dasso, C. H. (1985). *Phys. Rep.*, **120**:1.
Maher, J. V., Erskine, J. R., Friedman, A. M., Schiffer, J. P., and Siemssen, R. H. (1970). *Phys. Rev. Lett.*, **25**:302.
Mayer M. G. and Jensen, J. H. D. (1955). *Elementary Theory of Nuclear Shell Structure*. New York: Wiley.
McCullough, P. M., Hamilton, P. A., McConnell, D., and King, E. A. (1990). *Nature*, **346**:822.
McKenna, J. and Lyne, A. (1990). *Nature*, **343**:349.
Meissner, W. and Ochsenfeld, R. (1933). *Naturwiss.*, **21**:787.
Mercerau, J. E. (1969) In *Superconductivity*, Parks, R. D. and Dekker, M., eds. New York: Marcel Dekker, Inc., page 393.
Michaudon, A. (1973). *Adv. Nucl. Phys.*, **6**:1.
Migdal, A.B. (1959). *Nucl. Phys.* **13**: 655.
Migdal, A. B. (1967). *Theory of Finite Fermi Systems and Applications to Atomic Nuclei*. New York: John Wiley.
Morel, P. and Nozières, P. (1962). *Phys. Rev.* **126**: 1909.
Mottelson, B. R. (1962) In *Proceedings of the International School of Physics 'E. Fermi', Course XV*, Racah, G., ed. New York: Academic Press, page 44.
Mottelson, B. R. (1977). *Proceedings of the International School of Physics 'E. Fermi' Course LXIX*, Bohr, A., Broglia, R.A., eds. Amsterdam: North Holland, page 31.
Mottelson, B. R. (1992). In *Clustering Phenomena in Atoms and Nuclei*, Brenner, M., Lönnroth, T., and Malik, F. B., eds. Berlin: Springer-Verlag, page 571.
Mottelson, B. R. (1996). *Trends in Nuclear Physics, 100 Years Later, UJFG, Les Houches, session LXVI*. Amsterdam: Elsevier, page 25.
Mottelson, B. R. and Valatin, J. G. (1960). *Phys. Rev. Lett.*, **5**:511.
Mühlschlegel, B., Scalapino, D. J., and Denton, R. (1972). *Phys. Rev.*, **B6**:1767.
Nambu, Y. (1959). *Phys. Rev.*, **117**:648.
Nambu, Y. (1960). *Phys. Rev. Lett.*, **4**:380.
Nambu, Y. and Jona-Lasinio, G. (1961a). *Phys. Rev.*, **122**:345.
Nambu, Y. and Jona-Lasinio, G. (1961b). *Phys. Rev.*, **124**:246.
Nathan, O. (1968). In *Nuclear Structure*, Vienna: IAEA, page 191.
Nathan, O. and Nilsson, S. G. (1965). *Alpha- Beta- and Gamma-Ray Spectroscopy*, Volume I. Amsterdam: North-Holland, page 601.
Navin, A., Anthony, D. W., Aumann, T., Baumann, T., Bazin, D., Blumenfeld, Y. *et al*. (2000). *Phys. Rev. Lett.*, **85**:266.
Negele, J. and Vautherin, D. (1973). *Nucl. Phys.*, **A207**:298.
Nikam, R. S. and Ring, P. (1987). *Phys. Rev. Lett.*, **58**:980.

Nikam, R. S., Ring, P., and Canto, C. F. (1986). *Z. Phys. A.*, **324**:241.
Nikam, R. S., Ring, P., and Canto, C. F. (1987). *Phys. Lett.*, **B185**:269.
Nilsson, S. G. (1955). *Mat. Fys. Medd. Dan. Vid. Selsk.*, **29**, no.16.
Nilsson, S. G. and Ragnarsson, I. (1995). *Shapes and Shells in Nuclear Structure*. Cambridge: Cambridge University Press.
Nogami, Y. (1963). *Prog. Theor. Phys.*, **29**:938.
Nogami, Y. (1964). *Phys. Rev.*, **134**:B313.
Nolan, P. and Twin, P. (1988). *Ann. Rev. Nucl. Part. Sci.*, **38**:533.
Nuñes, F. M., Christley, J. A., Thompson, I. J., Johnson, R. C., and Efros, V. D. (1996). *Nucl. Phys.*, **A609**:4.
Ogg, Jr., R.A. (1946). *Phys. Rev.*, **69**:243.
Osheroff, D. D. (1997). *Rev. Mod. Phys.*, **69**:667.
Osheroff, D. D., Gully, W. J., Richardson, R. C., and Lee, D. M. (1972a). *Phys. Rev. Lett.*, **29**:920.
Osheroff, D. D., Richardson, R. C., and Lee, D. M. (1972b). *Phys. Rev. Lett.*, **28**:885.
Parikh, J. P. (1965). *Nucl. Phys.*, **63**:214.
Parks, R. D. and Little, W. A. (1964). *Phys. Rev.*, **133**:A97.
Patashinskii, A. Z. and Pokrovskii, V. L. (1979), *Fluctuation Theory of Phase Transitions*. Oxford: Pergamon Press.
Perenboom, J. A. A. J., Wyder, P., and Meier, F. (1981). *Phys. Rep.*, **78**:173.
Pethick, C. J. and Smith, H. (2002). *Bose-Einstein Condensation in Dilute Gases*. Cambridge: Cambridge University Press.
Pines, D. (1963). *Elementary Excitations in Solids*. New York: Benjamin.
Pines, D. (1980). *J. Phys. Colloq.*, **41**:C2/111.
Pines, D., Shaham, A., Alpar, M. A., and Anderson, P. W. (1980). *Prog. Theo. Phys. Supp.*, **69**:376.
Pines, D., Tamagaki, R., and Tsuruta, S., eds. (1992). *The Structure and Evolution of Neutron Stars*. Menlo Park, California: Addison-Wesley.
Pitaevskii, L. and Stringari, S. (2003). *Bose-Einstein Condensation*. Oxford: Oxford University Press.
Pizzochero, P. M., Barranco, F., Vigezzi, E., and Broglia, R. A. (2002). *Astrophys. J.*, **591**:381–394.
Pizzochero, P. M., Viverit, L., and Broglia, R. A. (1997). *Phys. Rev. Lett.*, **79**:3347.
Prange, R. E. (1963). *Phys. Rev.*, **131**:1083.
Pudliner, B. S., Pandharipande, V. R., Carlson, J., and Wiringa, R. B. (1995). *Phys. Rev. Lett.*, **74**:4396.
Quentin, P. and Flocard, H. (1978). *Ann. Rev. Nucl. Sci.*, **28**:523.
Racah, G. (1942). *Phys. Rev.*, **62**:438.
Racah, G. (1943). *Phys. Rev.*, **63**:367.
Ragnarsson, I. and Åberg, S. (1986). *Phys. Lett. B*, **180**:191.
Ragnarsson, I. and Broglia, R. A. (1976). *Nucl. Phys. A*, **263**:315.
Ralph, D. C., Black, C. T., and Tinkham, M. (1997). *Phys. Rev. Lett.*, **78**:4087.
Raman, S., Malarkey, C. H., Milner, W. T., Nestor, C. W., and Stelson, P. H. (1987). *At. Data Nucl. Data Tables*, **36**:1.
Regal, C.A., Greiner, M., and Jin, D.S. (2004), *Phys. Rev. Lett.*, **92**, 083201.

Reinhardt, P.G. and Otten, E.W. (1984). *Nucl. Phys.*, **A420**:173.
Reppy, J. D. and Depatie, D. (1964). *Phys. Rev. Lett.*, **12**:187.
Richardson, R. W. (1963). *Phys. Lett.*, **3**:277.
Richardson, R. W. (1965). *Phys. Rev.*, **141**:949.
Richardson, R. W. (1977). *J. Math. Phys.*, **18**:1802.
Richardson, R. W. and Sherman, N. (1964). *Nucl. Phys.*, **52**:221.
Ring, P. and Schuck, P. (1980). *The Nuclear Many-Body Problem*. Heidelberg: Springer.
Rombouts, S., Van Neck, D., and Dukelsky, J. (2004). *Phys. Rev.* C**69**:061303
Rose, H. J. and Jones, G. A. C. (1984). *Nature*, **307**:245.
Rowe, D. J. (1970). *Nuclear Collective Motion: Models and Theory*. London: Methuen and Co.
Ruderman, M. (1972). *Ann. Rev. Astron. Astrophys.*, **10**:427.
Rutz, K., Bender, M., Reinhard, P. G., and Mahrun, J. A. (1999). *Phys. Lett.*, **B468**:1.
Sachdev, S. (1999). *Quantum Phase Transitions*. Cambridge: Cambridge University Press.
Sagawa, H., Brown, B. A., and Esbensen, H. (1993). *Phys. Lett.*, **B309**:1.
Sandulescu, N., VanGiai, N., and Liotta, R. J. (2004). *Phys. Rev.*, **C69**:045802–1.
Satchler, G. R. (1977) In *Proceedings of the International School of Physics 'E. Fermi', Course LXIX*, Bohr, A. and Broglia, R. A., eds. Amsterdam: North Holland, page 271.
Satula, W., Dean, D. J., Gary, J., Mizutori, S., and Nazariewicz, W. (1997a). *Phys. Lett.*, **B407**:103.
Satula, W., Dobaczewski, J., and Nazariewicz, W. (1998). *Phys. Rev. Lett.*, **81**:3599.
Satula, W. and Wyss, R. (1997b). *Phys. Lett.*, **B393**:1.
Satula, W. and Wyss, R. (2001a). *Phys. Rev. Lett.*, **86**:4488.
Satula, W. and Wyss, R. (2001b). *Phys. Rev. Lett.*, **87**:052504–1.
Sauls, J. A. (1989) In *NATO ASI Series, Mathematical and Physical Sciences*, Ögelman, H. and van den Heuvel, E. P. J., eds. Volume 262, page 457.
Saunders, E. (1990). *Phys. Rev. Lett.*, **64**:3046.
Scadron, M. D. (1985). *Ann. Phys.*, **159**:184.
Schafroth, M. R. (1955). *Phys. Rev.*, **100**, 463.
Schmidt, H. (1972) In *Proceedings of the International School of Physics 'E. Fermi'*, *Course LII*, Morinaga, H., ed., New York: Academic Press, page 144.
Schrieffer, J. R. (1964). *Theory of Superconductivity*. Reading, Mass.: Benjamin.
Schrieffer, J. R. (1994). *Proceedings of the International School of Physics 'E. Fermi' Course CXXI*, Broglia, R. A., Schrieffer, J. R., and Bortignon, P.-F. Amsterdam: North Holland, page 231.
Schulze, H. J., Cugnon, J., Lejeune, A., Baldo, M., and Lomdardo, U. (1996). *Phys. Lett.*, **B375**:1.
Sergeant, A. J., Hussein, M. S., Pato, M. P., and Ueda, M. (2002). *Phys. Rev.*, **C65**: 024302.
Shaham, A. (1980). *J. Phys.*, **C2**:9.
Shapiro, S. L. and Teukolsky, S. A. (1983). *Black Holes, White Dwarfs and Neutron Stars*. New York: Wiley.
Shimizu, Y. R. and Broglia, R. A. (1990). *Nucl. Phys.*, **A515**:38.

Shimizu, Y. R., Donati, P., and Broglia, R. A. (2000). *Phys. Rev. Lett.*, **85**:2260.
Shimizu, Y. R., Garrett, J. D., Broglia, R. A., Gallardo, M., and Vigezzi, E. (1989). *Rev. Mod. Phys.*, **61**:131.
Shimizu, Y. R., Vigezzi, E., and Broglia, R. A. (1987). *Phys. Lett.*, **B198**:33.
Sierra, G., Dukelsky, J., Dussel, G. G., van Delft, J., and Braun, F. (2000). *Phys. Rev.*, **B61**, **R11**:890.
Simon, H., Aleksandrov, D., Aumano, T., Axelsson, L., Baumann, T., Borge, M. J. G. *et al*. (1999). *Phys. Rev. Lett.*, **83**:496.
Skyrme, T. H. R. (1959). *Nucl. Phys.*, **9**:615.
Snider, D. R. and Sorbello, R. S. (1984). *Surface Sci.*, **143**.
Stelson, P. H., McGowan, F. K., Robinson, R. L., and Milner, W. T. (1970). *Phys. Rev.*, **C2**:2015.
Stephens, F. (1985) In *Frontiers in Nuclear Dynamics*, Broglia, R. A. and Dasso, C. H., eds. New York: Plenum Press, number 25 in Ettore Majorana, International Science Series, page 73.
Stephens, F. and Simon, R. S. (1972). *Nucl. Phys.*, **A183**:257.
Stetcu, I. and Johnson, C. W. (2002). *Phys. Rev.*, **C66**:034301.
Szymanski, Z. (1985). *Nuclear Structure*. Amsterdam: Elsevier, page 343.
Takahara, S., Onishi, N., and Tagima, N. (1994). *Phys. Lett.*, **B331**:261.
Takahashi, H. (1957). *Nuov. Cim.*, **6**:370.
Takatsuka, T. (1984). *Progr. Theor. Phys.*, **71**:1432.
Talmi, I. (1972). *Nucl. Phys.*, **A172**:1.
Tanihata, I. (1996). *J. Phys. G*, **22**:157.
Terasaki, J., Barranco, F., Broglia, R. A., Vigezzi, E., and Bortignon, P. F. (2002a). *Nucl. Phys.*, **A697**:127.
Terasaki, J., Barranco, F., Vigezzi, E., Broglia, R. A., and Bortignon, P. F. (2002b). *Prog. Theor. Phys.*, **108**:495.
Thouless, D. J. (1961a). *Nucl. Phys.*, **22**, 78.
Thouless, D.J. (1961b). *The Quantum Mechanics of Many-Body Systems*, New York: Academic Press.
Tilley, D. R. and Tilley, J. (1974). *Superfluidity and Superconductivity*. New York: Van Nostrand Reinhold.
Tinkham, M. (1996). *Introduction to Superconductivity*. New York: Mc-Graw Hill.
Tonozuka, I. and Arima, A. (1979). *Nucl. Phys.*, **A323**:45.
Tsuboi, T. and Suzuki, T. (1977). *J. Phys. Soc. Japan*, **42**:437.
Twin, P., Nyako, B. M., Nelson, A. H., Simpson, J., Bentley, M. A., Crammer-Gordon, H. W. *et al*. (1986). *Phys. Rev. Lett.*, **57**:811.
Valatin, D. G. (1958). *Nuov. Cim.*, **7**:843.
Van der Sluys, V., van Neck, D., Waroquier, M., and Ryckebusch, J. (1993). *Nucl. Phys.*, **A551**:210.
Van Rij, W. and Kahana, S. (1972). *Phys. Rev. Lett.*, **28**:50.
Varshalovich, D. A., Moskalev, A. N., and Khersonskii, V. K. (1988). *Quantum Theory of Angular Momentum*. Singapore: World Scientific.
Vigezzi, E., Bes, D. R., Broglia, R. A., and Frauendorf, S. (1988). *Phys. Rev.*, **C38**:1448.
Vinh Mau, N. (1995). *Nucl. Phys.*, **A592**:33.

Vollhardt, D. and Wölfle, P. (1990). *The Superfluid Phases of Helium 3*. London: Taylor and Francis.
Volya, A., Brown, B. A., and Zelevinsky, V. (2001). *Phys. Lett.*, **B509**:37.
Volya, A., Zelevinsky, V., and Brown, B. A. (2002). *Phys. Rev.*, **C65**:054312.
von Oertzen, W. (1994). *Proceedings of the International School of Heavy Ion Physics*, 3rd Course: Probing the Nuclear Paradigm with Heavy Ion Reactions, Broglia, R. A., Kienle, P., and Bortignon, P. F. eds. Singapore: Word Sientific, page 29.
Wambach, J., Ainsworth, T. L., and Pines, D. (1993). *Nucl. Phys.*, **A555**:128.
Wapstra, A. H. and Gove, N. B. (1971). *Nucl. Data Tables*, **9**:265.
Ward, J. C. (1950). *Phys. Rev.*, 78:182.
Weinberg, S. (1996). *The Quantum Theory of Fields*, Volume II, Chapter 19. Cambridge: Cambridge University Press.
Wiringa, R. B., Smith, R. A., and Ainsworth, T. L. (1984). *Phys. Rev.*, **C29**:1207.
Wölfle, P. (1972). *Rep. Prog. Phys.*, **42**:265.
Wölfle, P. (1978). *Prog. Low Temp. Phys.*, **7A**:191.
Yakovlev, D. G. and Pethick, C. J. (2004). *Ann. Rev. Astron. Astrophys.*, **42**:169.
Zamfir, N. V., Zhang, J., and Casten, R. F. (2002). *Phys. Rev.*, **C66**:057303.
Zeldes, N., Grill, A., and Simievic, A. (1967). *Mat. Fys. Skr. Dan. Vid. Selsk.*, **3**:5.
Zelevinsky, V. and Volya, A. (2004). *Nucl. Phys.*, **A731**:299.
Zhukov, M. V. (1991). *Phys. Lett.*, **B265**:19.
Zhukov, M. V. (1993). *Phys. Rep.*, **231**:151.
Zinser, M., Humbert, F., Nilsson, T., Schwab, W., Blaich, T., Borge, M. J. G. *et al.* (1995). *Phys. Rev. Lett.*, **75**:1719.
Zinser, M., Humbert, F., Nilsson, T., Schwab, W., Blaich, T., Borge, M. J. G. *et al.* (1997). *Nucl. Phys.*, **A619**:151.
Zwieglinski, B., Benenson, W., Robertson, R. G. H., and Coker, W. R. (1979). *Nucl. Phys.*, **A315**:124.
Zwierlein, M. W., Stau, C. A., Schunck, C. H. *et al.* (2003). *Phys. Rev. Lett.*, **91**:250401.

Index

https://doi.org/10.1017/9781009401920 Published online by Cambridge University Press

https://doi.org/10.1017/9781009401920 Published online by Cambridge University Press